

Dissertation zur Erlangung des Doktorgrades  
der Fakultät für Chemie und Pharmazie  
der Ludwig-Maximilians-Universität München

---

**Structure and Stability of Radicals  
and  
Quantification of Electrophilic Reactivity**

---

von  
**Harish Harish**  
aus  
Deoli, Delhi, India

**2018**



## **Erklärung**

Diese Dissertation wurde im Sinne von §7 der Promotionsordnung vom 28. November 2011 von Herrn Prof. Dr. Hendrik Zipse betreut.

## **Eidesstattliche Versicherung**

Diese Dissertation wurde eigenständig und ohne unerlaubte Hilfe bearbeitet.

München, 13.02.2019

.....  
Harish Harish

Dissertation eingereicht am: 27.12.2018

1. Gutachter: Prof. Dr. Hendrik Zipse
2. Gutachter: Prof. Dr. Herbert Mayr

Mündliche Prüfung am: 08.02.2019



Dedicated to

**My Family**

**Har Har Har Mahadev**



## Acknowledgement

---

First of all, I would like to convey my deepest gratitude to Prof. Dr. Hendrik Zipse for accepting me in his research group and supervising my doctoral study. Over the last five years, he has helped me in countless ways and taught me numerous things. I thank him for his guidance, unending patience, constant support and encouragement. Every single time, I feel amazed and inspired, by his ability to see the value in my work that I failed to see myself, thank you for believing in me. I really appreciate all the time and efforts he devoted to the valuable discussions we had, it means a lot to me.

Second, I wholeheartedly thank Prof. Dr. Herbert Mayr not only for kindly accepting to be “Zweitgutachter” but also for providing extensive collaboration opportunities. I extend my sincere thanks to all the members of the review committee. I’m very grateful for their time and efforts.

I would also like to thank Dr. Armin R. Ofial, Prof. Ruth M. Gschwind, Prof. Ulrick Jahn, Prof. Philippe Renaud and Prof. Massimo Bietti, for the fruitful collaborations. In addition, special thanks to Michael H. Haindl, Quan Chen, Tynchtyk Amatov and Zhen Li for being excellent research partners and making substantial contributions to this work.

My words of thanks to my old and new colleagues in the Zipse group. They have been very helpful to me, irrespective of the nature of my problems. Raman Tandon, for encouraging words. Christoph Lindner, for helping me to navigate bureaucracies. Florian Achrainger, Sandhiya Lakshmana, Julian Helberg and Marta Marin Luna for being more friends than colleagues. Florian Barth, Cong Zhang, Pascal Patschinski, Jutta Tumpach, Ieva Teikmane, Stefanie Mayr, Benjamin Pölloth, Heena Ugale, Salavat Ashirbaev, Vasily Korotenko and Fabian Zott for lending me a helping hand in an hour of need and making me feel welcome. I want to express special thanks to my friend Johnny Hioe, for all of his support and cooperation in the early days of my doctoral study.

I thankfully acknowledge financial support by Deutsche Forschungsgemeinschaft (SFB 749, project C6). Furthermore, I thank Mrs. Birgit Carell, she was exceptionally kind to me, and Mr. Christoph Singer, who was always more than willing to help. I also gratefully acknowledge the compute and data resources provided by the Leibniz Supercomputing Centre ([www.lrz.de](http://www.lrz.de)).

At this moment, I would also like to recall and thank all my former teachers. I am particularly thankful to Prof. Prasad V. Bharatam. I always believe that their guidance and encouragement have helped me get to where I am today.

I am deeply thankful to my family for their infinite love and support. As always, it is hard for me to put in words how grateful I am for all of the things they have done for me. My loving parents, Late Sh. Ram Niwas & Smt. Kamlesh, my caring uncle and aunty, Sh. Ved Prakash & Smt. Kanta, my dear brothers and sisters, Sapna, Gaurav, Hitesh and Sourav and my partner for life, Preeti. They all have made great sacrifices, and I do not doubt that without them, this thesis would never have been possible. This work is dedicated to you all.

My final words of gratitude and prayer to Lord Shiva, Har Har Har Mahadev.

Thank you  
Harish



## LIST OF PUBLICATIONS

---

Parts of this thesis have been published as follows:

H. Jangra, M. H. Haindl, F. Achrainer, J. Hioe, R. M. Gschwind, H. Zipse, “**Conformational Preferences in Small Peptide Models: The Relevance of *cis/trans*-Conformations**” *Chem. Eur. J.* **2016**, *22*, 13328-13335.

D. S. Allgäuer, H. Jangra, H. Asahara, Z. Li, Q. Chen, H. Zipse, A. R. Ofial, H. Mayr, “**Quantification and Theoretical Analysis of the Electrophilicities of Michael Acceptors**” *J. Am. Chem. Soc.* **2017**, *139*, 13318-13329.

Z. Li, H. Jangra, Q. Chen, P. Mayer, A. R. Ofial, H. Zipse, H. Mayr, “**Kinetics and Mechanism of Oxirane Formation by Darzens Condensation of Ketones: Quantification of the Electrophilicities of Ketones**” *J. Am. Chem. Soc.* **2018**, *140*, 5500-5515.

T. Amatov, H. Jangra, R. Pohl, I. Cisařová, H. Zipse, U. Jahn, “**Unique Stereoselective Homolytic C–O Bond Activation in Diketopiperazine-Derived Alkoxyamines by Adjacent Amide Pyramidalization**” *Chem. Eur. J.* **2018**, *24*, 15336-15345.

H. Jangra, H. Zipse, “**Electrostatic Effects on the Stability of Peptide Radicals**” *J. Phys. Chem. B* **2018**, *122*, 8880-8890.

D. Meyer, H. Jangra, F. Walther, H. Zipse, P. Renaud, “**A Third Generation of Radical Fluorinating Agents Based on *N*-fluoro-*N*-arylsulfonamides**” *Nat. Commun.* **2018**, *9*, 1-10.

H. Jangra, Q. Chen, E. Fuks, I. Zenz, P. Mayer, A. R. Ofial, H. Zipse, H. Mayr “**Nucleophilicity and Electrophilicity Parameters for Predicting Absolute Rate Constants of Highly Asynchronous 1,3-Dipolar Cycloadditions of Aryldiazomethanes**” *J. Am. Chem. Soc.* **2018**, *140*, 16758–16772.



## Table of Contents

---

<b>Abstract</b>	<b>1</b>
<b>Chapter 1. Introduction</b>	<b>5</b>
1.1 Structure and Stability of Radicals .....	5
1.2 Quantification of Electrophilic Reactivity .....	12
<b>Chapter 2. Conformational Preferences in Small Peptide Models: The Relevance of <i>cis/trans</i>-Conformations</b>	<b>19</b>
2.1 Supporting Information.....	29
<b>Chapter 3. Electrostatic Effects on The Stability of Peptide Radicals</b>	<b>39</b>
3.1 Supporting Information.....	52
<b>Chapter 4. Stability of Peptide Radicals: Thermodynamics vs. Kinetics</b>	<b>79</b>
4.1 Introduction.....	81
4.2 Results and Discussion .....	81
4.3 Supporting Information.....	91
<b>Chapter 5. Unique Stereoselective Homolytic C-O Bond Activation in Diketopiperazine-Derived Alkoxyamines by Adjacent Amide Pyramidalization</b>	<b>95</b>
5.1 Supporting Information.....	107
<b>Chapter 6. A Third Generation of Radical Fluorinating Agents Based on <i>N</i>-Fluoro-<i>N</i>-Arylsulfonamides</b>	<b>115</b>
6.1 Supporting Information.....	127
<b>Chapter 7. Quantification and Theoretical Analysis of the Electrophilicities of Michael Acceptors</b>	<b>137</b>
7.1 Supporting Information.....	151
<b>Chapter 8. Kinetics and Mechanism of Oxirane-Formation by Darzens Condensation of Ketones: Quantification of the Electrophilicities of Ketones</b>	<b>167</b>
8.1 Supporting Information.....	185
<b>Chapter 9. Nucleophilicity and Electrophilicity Parameters for Predicting Absolute Rate Constants of Highly Asynchronous 1,3-Dipolar Cycloadditions of Aryldiazomethanes</b>	<b>197</b>
9.1 Supporting Information.....	214
<b>Curriculum Vitae</b>	<b>230</b>



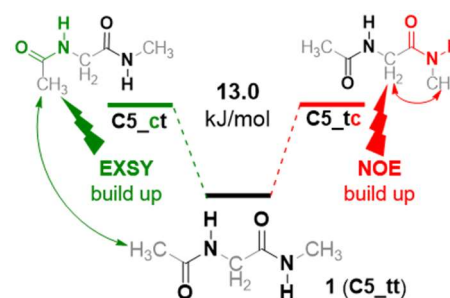
## Abstract

This work comprises two different aspects of chemical reactivity. In the first part of the thesis, we investigated different factors that influence the structure and stability of radicals. The second part of the work involves quantification of electrophilic reactivity.

### Structure and Stability of Radicals:

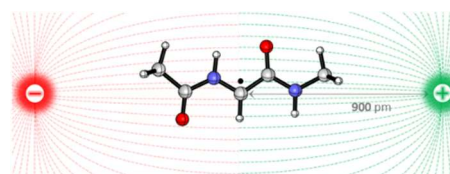
#### *Conformational Preferences in Small Peptide Models - the Relevance of Cis/Trans Conformations<sup>i</sup>*

The accurate description of *cis/trans* peptide structures is of fundamental relevance for the field of protein modelling and protein structure determination. QM-derived thermochemical data and detailed NMR studies predict an extended **C5<sub>tt</sub>** conformation for dipeptide model Ace-Gly-NMe **1** as the preferred conformation in DMSO solution. Isomerization of the N- or C-terminal amide bonds are both found to be endergonic by 12 kJ/mol at 300 K, leading to the occurrence of the *trans-cis* (**tc**) and *cis-trans* (**ct**) conformations as detectable species by NMR measurements in DMSO-*d*<sub>6</sub>. Supported by theoretical chemical shift calculations, this allowed for the complete assignment of <sup>1</sup>H and <sup>13</sup>C chemical shift data for these *cis/trans* isomers. Temperature-dependent <sup>1</sup>H NMR measurements indicate that the *cis-trans* energy differences are mainly of enthalpic origin, which is again in line with theoretical predictions. The ability to reproduce the conformational preferences of **1** with common protein force fields is limited.



#### *Electrostatic Effects on The Stability of Peptide Radicals<sup>ii</sup>*

An external electric field (EEF) to tune the chemical and biological (re)activity of open-shell species attracted significant attention recently. Using high-level quantum chemical methods, we explored the influence of EEFs on the stability of a C<sub>α</sub>-glycine dipeptide model radical (**r1**). Remotely located ions (Cl<sup>-</sup>/Na<sup>+</sup>) were used to implement EEF effects. The ions have a significant influence on the stability of **r1**. The charge and orientation of the ion determine its interaction with radical **r1**. The Cl<sup>-</sup> and Na<sup>+</sup> at 180° in the XY-plane stabilise (-9.7 kJ/mol) and destabilise (8.8 kJ/mol) **r1**, respectively. Suitable point charges and EEFs can be used to reproduce these effects. Effects of charge on the stability of **r1** are stronger in the XY-plane compared to the XZ- and YZ-planes. The (de)protonated side chain functional groups in acidic (asp & glu) and basic (lys & his) amino acids destabilise their corresponding peptide radicals except in the case of arginine (arg), where protonation stabilises the cation radical by -16.6 kJ/mol.



#### *Stability of Peptide Radicals: Thermodynamic vs Kinetics*

Thermodynamics and kinetics of hydrogen atom transfer (HAT) from dipeptide model Ace-Gly-NMe **1** by cumyloxy radical (CumO•) were investigated using quantum chemical computations and laser flash photolysis (LFP). Absolute rate constants for HAT measured by LFP indicates that the CumO• radical predominantly abstracts hydrogen atoms from the N-methylamide (NMe) protecting group in Ace-Gly-NMe. These results are consistent with previous experimental observations of structurally related systems. Thermodynamic favourability of HAT from different carbon centres of Ace-Gly-NMe by CumO• was quantified at different levels of theory, and C<sub>α</sub> of Ace-Gly-NMe was found to be the thermodynamically most favourable site. HAT from The C-terminal methyl

<sup>i</sup> Reprinted with permission from *Chem. Eur. J.*, **2016**, *22*, 13328-13335 © 2016 WILEY-VCH Verlag GmbH & Co. KGaA.

<sup>ii</sup> Reprinted with permission from *J. Phys. Chem. B*, **2018**, *122*, 8880-8890 © 2018 American Chemical Society.

group of Ace-Gly-NMe by CumO• was found to have the lowest activation barrier in acetonitrile and is the kinetically preferred site for hydrogen atom abstraction. Solvation effects play an important role in the stabilization of transition states and thus significantly influence the reaction kinetics.

### Unique Stereoselective Homolytic C-O Bond Activation in Diketopiperazine-derived Alkoxyamines via Adjacent Amide Pyramidalization<sup>iii</sup>

Simple monocyclic diketopiperazine (DKP)-derived alkoxyamines exhibit an unprecedented activation of a remote C-O bond for homolysis by amide distortion. The combination of strain release-driven amide planarization and the persistent radical effect (PRE) enable a unique, irreversible and quantitative *trans*→*cis* isomerization under much milder conditions than typically observed for such homolysis-limited reactions. This isomerization is shown to be general and independent of the steric and electronic nature of both amino acid side chains and substituents at the DKP nitrogen atoms. Homolysis rate constants have been determined and they significantly differ for both, the labile *trans*-diastereomers and the stable *cis*-diastereomers. To reveal the factors influencing this unusual process, structural features of the kinetically preferred *trans*- and the more stable *cis*-diastereomers were investigated in the solid state and in solution. X-ray crystallographic analysis and computational studies indicate a substantial distortion of the amide bond from planarity in the *trans*-alkoxyamines, which is the cause for the facile and quantitative isomerization. Thus, these amino acid-derived alkoxyamines are the first examples that exhibit a large thermodynamic preference for one diastereomer over the other upon thermal homolysis, which allows controlled switching of configurations and configurational cycling.

### A Third Generation of Radical Fluorinating Agents Based on *N*-fluoro-*N*-arylsulfonamides<sup>iv</sup>

Radical fluorination has been known for a long time, but synthetic applications were severely limited by the hazardous nature of the first generation of reagents such as F<sub>2</sub> and the strongly electrophilic nature of the second generation of reagents such as *N*-fluorobenzenesulfonimide (NFSI) and Selectfluor<sup>®</sup>. Here, we report the preparation, use, and properties of *N*-fluoro-*N*-arylsulfonamides (NFASs), a class of fluorinating reagents suitable for radical fluorination under mild conditions. Their N-F bond dissociation energies (BDE) are 30–45 kJ/mol lower than the N-F BDE of the reagents of the second generation. This favors clean radical fluorination processes over undesired side reactions. The utility of NFASs is demonstrated by a metal-free radical hydrofluorination of alkenes including an efficient remote C-H fluorination via a 1,5-hydrogen atom transfer. NFASs have the potential to become the reagents of choice in many radical fluorination processes.

### Quantification of Electrophilic Reactivity:

#### Quantification and Theoretical Analysis of the Electrophilicities of Michael Acceptors<sup>v</sup>

To quantify the electrophilic reactivities of common Michael acceptors, we measured the kinetics of the reactions of mono-acceptor-substituted ethylenes (**1**) and styrenes (**2**) with pyridinium ylides (**3**), a sulfonium ylide (**4**), and a sulfonyl substituted chloromethyl anion (**5**). From the second-order rate constants *k*, we have calculated by using the Mayr-Patz equation [ $\log k = s_N(N + E)$ ] the electrophilicity parameters *E* of the MACs. Kinetic investigations show that the reactions of **1** or **2**

<sup>iii</sup> Reprinted with permission from *Chem. Eur. J.*, **2018**, *24*, 15336-15345 © 2018 Wiley-VCH Verlag GmbH & Co. KGaA.

<sup>iv</sup> Reprinted with permission from *Nat. Commun.*, **2018** (DOI: 10.1038/s41467-018-07196-9) © The Author(s) 2018.

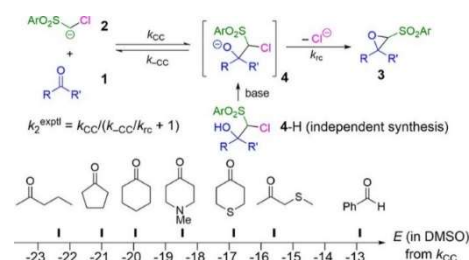
<sup>v</sup> Reprinted with permission from *J. Am. Chem. Soc.*, **2017**, *139*, 13318-13329 © 2017 American Chemical Society.

with **3-5** follow the Mayr-Patz equation, indicating stepwise processes with a common rate-determining step. It is further confirmed by PES calculations. The electrophilic parameters  $E$  correlate poorly with frontier orbital energies or with global and local electrophilicity indices ( $\omega$  &  $\omega_\beta$ ). Good correlations were found between  $E$  and their calculated methyl anion affinities, particularly when solvation by DMSO was taken into account.



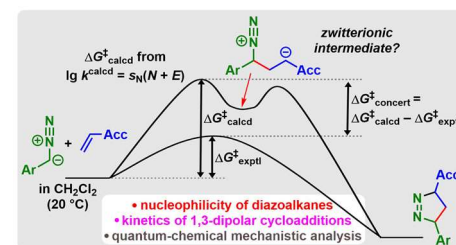
### Kinetics and Mechanism of Oxirane-Formation by Darzens Condensation of Ketones: Quantification of the Electrophilicities of Ketones<sup>vi</sup>

The kinetics of epoxide formation by Darzens condensation of aliphatic ketones **1** with arylsulfonyl-substituted chloromethyl anions **2** have been determined photometrically. DFT calculations of the intrinsic reaction pathways showed that the reactions of the ketones **1** with the chloromethyl anions **2** yield two rotational isomers of the intermediate halohydrin anions **4**, only one of which can cyclize while the other undergoes retroaddition because the barrier for rotation is higher than that for reversal to the reactants **1** and **2**. The rate constants  $k_{CC}$  for the initial nucleophilic attack are accessible by combination of the directly measured gross rate constants for the formation of the epoxides **3** from the reactants **1** and **2** ( $k_2^{\text{exp}}$ ) with the degree of reversibility of the initial step ( $k_{-CC}/k_{CC}$ ). From  $k_{CC}$  and previously reported  $N$  and  $s_N$  parameters for **2**, we have calculated by using  $\log k = s_N(N + E)$  the electrophilicity parameters  $E$ . They correlate moderately with the LUMO energies of the carbonyl groups, very poorly with Parr's electrophilicity indices, and best with the methyl anion affinities calculated for DMSO solution.



### Nucleophilicity and Electrophilicity Parameters for Predicting Absolute Rate Constants of Highly Asynchronous 1,3-Dipolar Cycloadditions of Aryldiazomethanes<sup>vii</sup>

Kinetics of the reactions of aryldiazomethanes ( $\text{ArCHN}_2$ ) with benzhydrylium ions ( $\text{Ar}_2\text{CH}^+$ ) have been measured photometrically in dichloromethane. The resulting second-order rate constants correlate linearly with the electrophilicities  $E$  of the benzhydrylium ions which allowed us to use the correlation  $\log k = s_N(N + E)$  (eq. 1) for determining the nucleophile-specific parameters  $N$  and  $s_N$  of the diazo compounds. UV-Vis spectroscopy was analogously employed to measure the rates of the 1,3-dipolar cycloadditions of these aryldiazomethanes with acceptor-substituted ethylenes of known electrophilicities  $E$ . The measured rate constants for the reactions of the diazoalkanes with highly electrophilic Michael acceptors ( $E > -11$ , for example 2-benzylidene Meldrum's acid or 1,1-bis(phenylsulfonyl)ethylene) agreed with those calculated by eq. 1 from the one-bond nucleophilicities  $N$  and  $s_N$  of the diazo compounds and the one-bond electrophilicities of the dipolarophiles, indicating that the incremental approach of eq. 1 may also be applied to predict the rates of highly asynchronous cycloadditions. Weaker electrophiles, e.g., methyl acrylate, react faster than calculated from  $E$ ,  $N$ , and  $s_N$ , and the ratio of experimental to calculated rate constants was suggested to be a measure for the energy of concert  $\Delta G^\ddagger_{\text{concert}} = RT \ln(k_2^{\text{exptl}}/k_2^{\text{calcd}})$ . Quantum chemical calculations indicated that all products isolated from the reactions of the aryldiazomethanes with acceptor substituted ethylenes ( $\Delta^2$ -pyrazolines, cyclopropanes, and



<sup>vi</sup> Reprinted with permission from *J. Am. Chem. Soc.*, **2018**, 140, 5500–5515 © 2018 American Chemical Society.

<sup>vii</sup> Reprinted with permission from *J. Am. Chem. Soc.*, **2018** © 2018 American Chemical Society.

substituted ethylenes) arise from intermediate  $\Delta^1$ -pyrazolines, which are formed through concerted 1,3-dipolar cycloadditions with transition states, in which the C–N bond formation lags behind the C–C bond formation. The Gibbs activation energies for these cycloadditions calculated at the PCM(UA0,CH<sub>2</sub>Cl<sub>2</sub>)/(U)B3LYP-D3/6-31+G(d,p) level of theory agree within 5 kJ mol<sup>-1</sup> with the experimental numbers showing the suitability of the applied polarizable continuum model (PCM) for considering solvation.

## Chapter 1. Introduction

### 1.1 Structure and Stability of Radicals

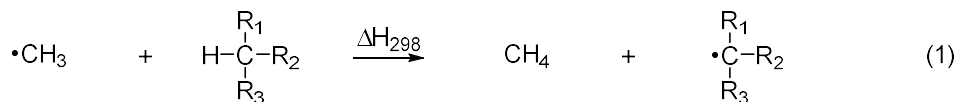
In theoretical organic chemistry, a radical (molecular entity with an unpaired electron) comes under the umbrella category of open-shell systems: atomic or molecular systems in which all electrons are not entirely paired in orbitals.<sup>1</sup> The presence of an unpaired electron make radicals highly reactive and short-lived species with few exceptions. Historically, radicals were considered as uncontrollable, unstable, and useless species with a little practical application. In 1955, C. K. Ingold had jokingly said:<sup>2</sup>

*“Homolysis, even between consenting adults, is grounds for instant dismissal from this Department.”*

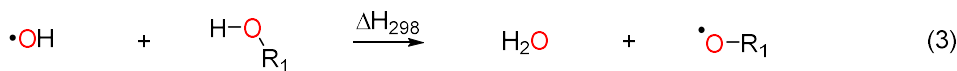
Regardless of the bleak outset, the current overview of the role of radicals in chemistry and biology reveals its astonishing impact on the polymer, pharmaceutical, agricultural, atmospheric, natural product, and organic synthesis. The Zipse group has been working toward developing understanding about the roles of radicals in biological and chemical processes using the tools and techniques of theoretical chemistry.

#### 1.1.1 Radicals in Biology

In biology, radicals of proteins and peptides are of fundamental importance and have been implicated to play a crucial role in various biochemical and physiological processes.<sup>3</sup> Recent times have seen a large increase in the number of reports on radical-mediated enzymatic catalysis, and it is now a well-established fact that enzymatic catalysis often involve open-shell intermediates.<sup>4</sup> In previous work, Zipse and co-workers used the radical stabilization energy (**RSE**), as defined in eq. 1, to quantify the thermodynamics of hydrogen atom transfer steps in enzymatic reactions.<sup>5</sup>



The RSE defined here using the isodesmic hydrogen transfer reaction shown in eq. 1 is a measure of the thermodynamic stability of carbon-centred radicals. Negative RSE values indicate that the radical ( $\text{R}^1\text{R}^2\text{R}^3\text{C}\bullet$ ) under consideration is more stable than the reference methyl radical ( $\text{CH}_3\bullet$ ) and vice-versa. A similar approach is used to define thermodynamic stabilities of nitrogen-, oxygen-, and sulfur-centred radicals as shown in eqs. 2, 3 and 4.



Combining calculated RSE values with the experimentally determined bond dissociation energies (**BDEs**) of the corresponding reference systems yields calculated BDEs for the systems under investigation. For example, The C-H bond dissociation energy in methane amounts to  $\text{BDE}(\text{CH}_3\text{-H}) = +439.3 \pm 0.4 \text{ kJ/mol}$ .<sup>6</sup> The BDE value for the C-H bond in ethane ( $\text{CH}_3\text{CH}_3\text{-H}$ ) can be calculated by adding the RSE of the ethyl radical ( $\text{CH}_3\text{CH}_2\bullet$ ) to the reference  $\text{BDE}(\text{CH}_3\text{-H})$ . [ $\text{BDE}(\text{CH}_3\text{CH}_3\text{-H}) = \text{BDE}(\text{CH}_3\text{-H}) + \text{RSE}(\text{CH}_3\text{CH}_2\bullet)$ ]

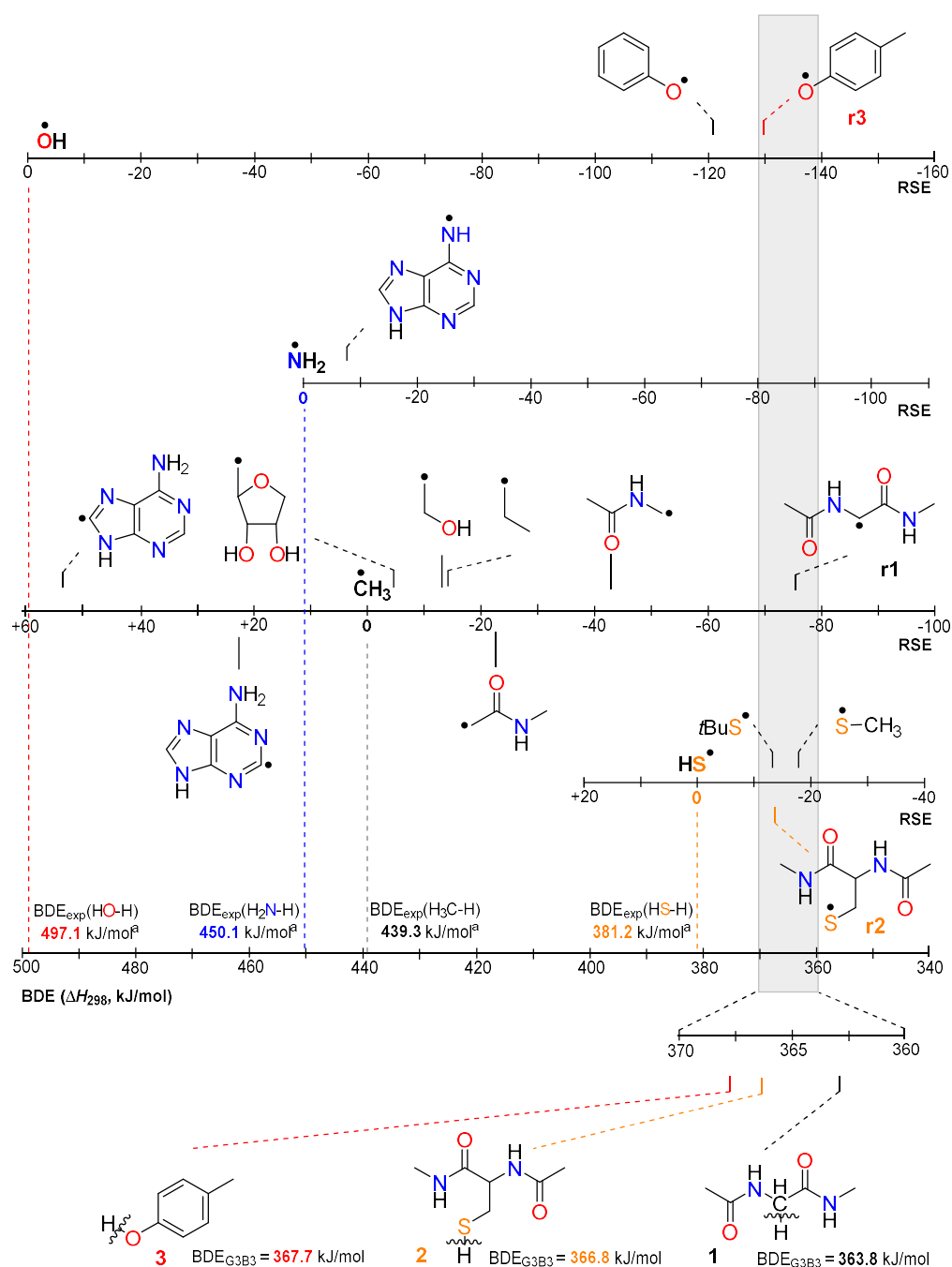


**Figure 1-1.** A unified scale of thermodynamic stability of C-, N-, O-, and S-centered radicals based on the RSE and BDE data calculated at G3B3 and IMOMO(G3B3,G3(MP2)-RAD) level of theory. RSE values were collected from Ref. 5d and literature cited therein. <sup>a</sup> BDE values were taken from Ref. 6.

Using concepts explained in the previous paragraphs, a unifying scale of thermodynamic stability can be obtained by plotting  $BDE_{\text{exp}}$  of the reference systems on the universal BDE scale and then placing systems of interest using their calculated RSE values with respect to their system of reference as shown in Figure 1-1. This type of graphical representation provides a convenient way of comparing the stability of structurally different radicals. For example, The  $C_{\alpha}$ -H BDE for glycine dipeptide **1** (363.8 kJ/mol), the S-H BDE for cysteine **2** (366.8 kJ/mol) and the O-H BDE for tyrosine [modelled using *p*-cresol **3**, 367.7 kJ/mol] were found to be very similar, with glycyl radical dipeptide **r1** having the largest intrinsic thermodynamic stability. In previous studies the data shown in Figure 1-1 has effectively been employed for quantifying the HAT reactions for selected S-adenosylmethionine (SAM)-dependent enzymes.<sup>7</sup>

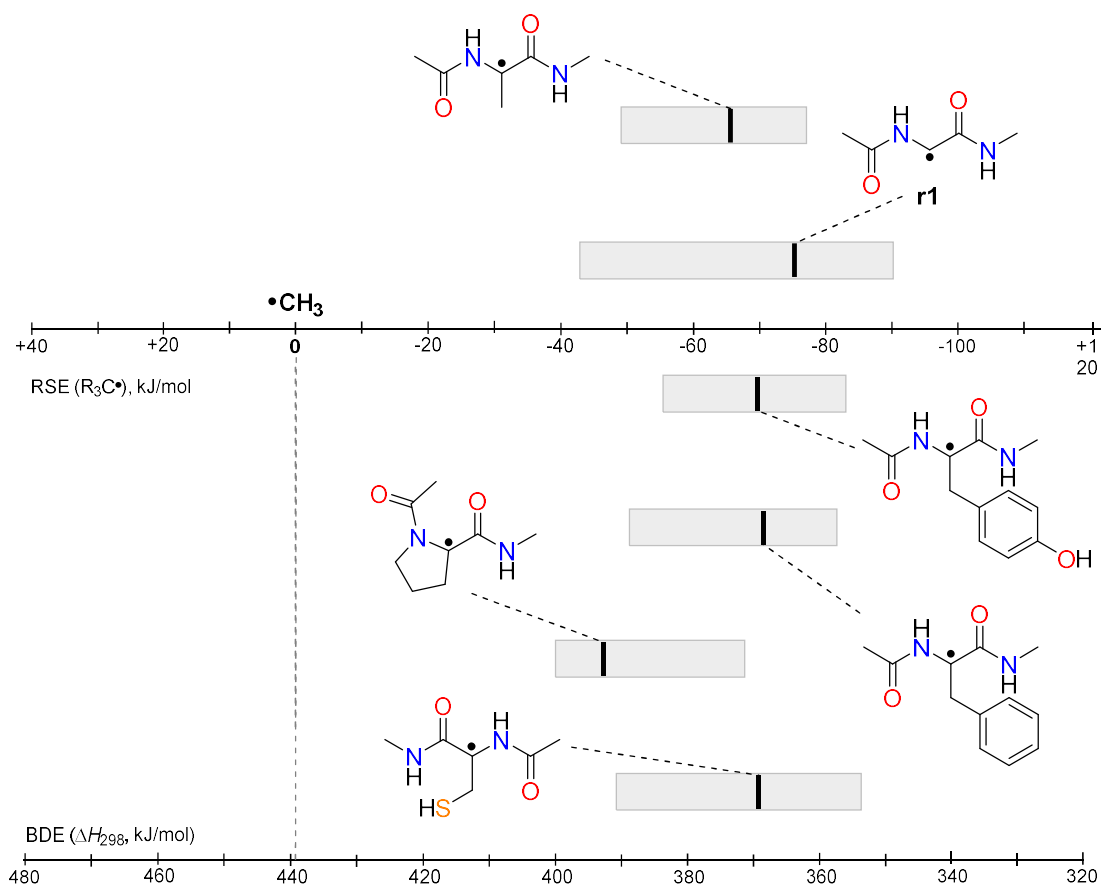


**Figure 1-2.** The effect of conformational variation on the RSE and BDE ( $\Delta H_{298}$ , kJ/mol, highlighted using a grey bar) of selected dipeptide radicals calculated at the G3(MP2)-RAD level of theory. Bold lines are used to indicate the Boltzmann-averaged RSE values.<sup>5c</sup>

The conformational analysis reveals some interesting properties of these peptide radicals. The stability of peptide radicals and their corresponding closed-shell parents is highly sensitive toward the backbone geometry.

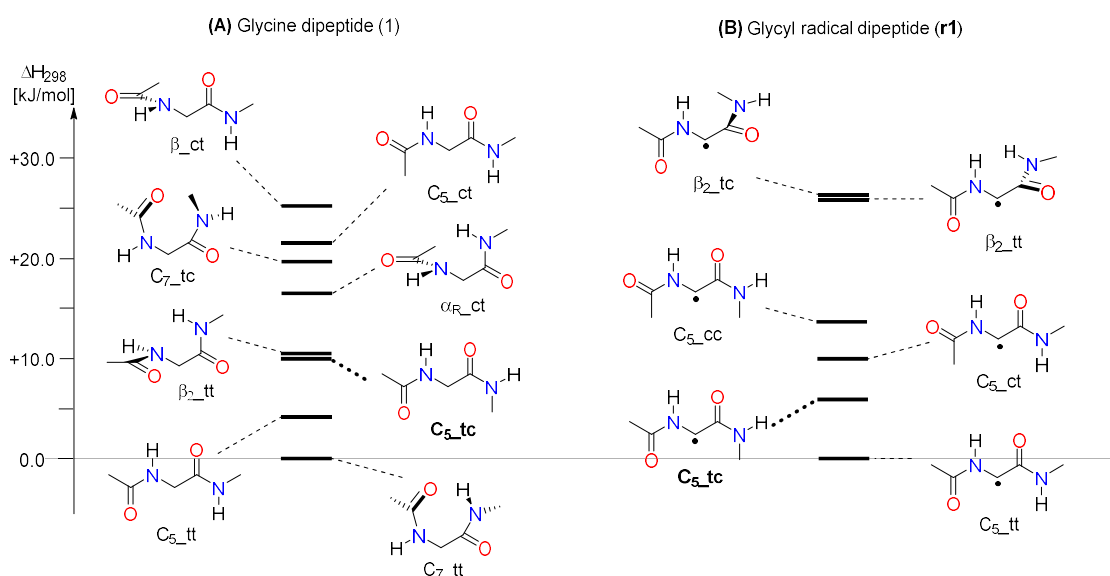


**Figure 1-3.** The gas phase enthalpy-based conformational distribution ( $\Delta H_{298}$ , kJ/mol) of (A) glycine dipeptide **1** and the corresponding (B) radical  $r_1$  calculated at the G3(MP2)-RAD level of theory. Only conformers with relative  $\Delta H_{298}$  values below 30 kJ/mol are shown.<sup>5c</sup>

The largest variation of radical stability was found to be associated with the glycy radical dipeptide **r1** as shown in Figure 1-2 as the length of a grey bar). These properties of glycine, cysteine and tyrosine, up to a certain extent explain why they serve as a source of peptide radicals in enzymatic catalysis. Further analysis of conformational space of closed-shell glycine dipeptide **1**, show that the conformer with one *cis*-peptide orientation (**C5, tc**) occurs just above 10 kJ/mol and the more surprising, for the corresponding radical **r1**, the *cis*-peptide (**C5, tc**) appears just 7 kJ/mol above the global minimum (Figure 1-3). With the largest thermodynamic radical stability and its highest conformation based tuning potential, glycine dipeptide **1** warrants further investigation of structural preference and other factors that can be employed by an enzyme to alter its reactivity.

In the second chapter of this thesis, we present the findings of our investigation on the conformational preference in small-peptide models with a particular focus devoted to the *cis* orientation of peptide bonds.<sup>8</sup> This study employed a combination of theoretical and experimental approaches to evaluate the relevance of *cis*-peptide conformers of glycine dipeptide **1**. The relative solution phase (DMSO) free energies ( $\Delta G_{\text{sol}}$ , in kJ/mol at 298.15 K) for glycine dipeptide **1** conformers reveal that N- and C-terminal *trans/cis* isomerization are similarly endergonic and lead to almost isoenergetic **C5\_ct** and **C5\_tc** conformers roughly  $\sim 12$  kJ/mol above the global **C5\_tt** minimum (Figure 1-4). These conformers are further investigated by NMR measurement in DMSO- $d_6$ . The QM-derived structural and chemical shift information is employed in the complete assignment of experimentally measured  $^1\text{H}$  and  $^{13}\text{C}$  chemical shift data for these conformers. The  $\Delta G_{300\text{K}}$  difference of  $\sim 13$  kJ/mol for *cis/trans* conformers with respect to the global minimum were calculated based on the temperature-dependent population changes followed by  $^1\text{H}$  NMR. These observations are close to the calculated solvation phase free energy difference of roughly  $\sim 12$  kJ/mol.

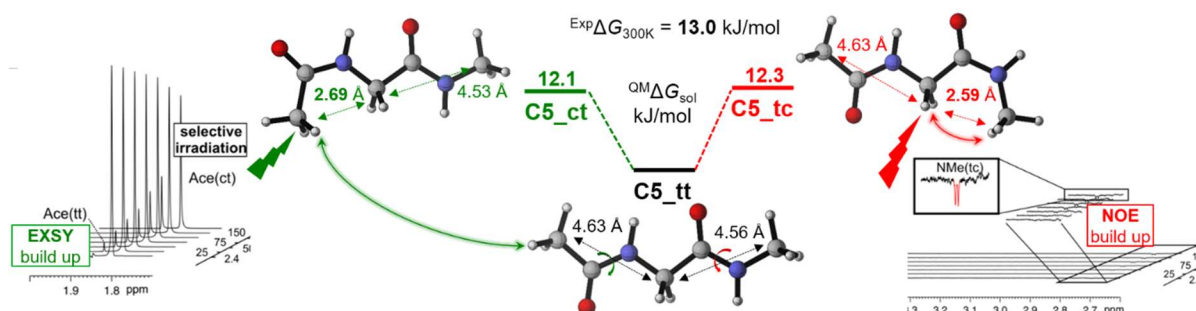


**Figure 1-4.** Graphical summary from the 2<sup>nd</sup> chapter of this thesis.

Our work shows, how high-level quantum chemical modelling complements advanced NMR techniques to characterize the sparsely populated *cis/trans* conformers of small peptide models such as glycine dipeptide **1**. We also investigated the commonly used forcefields (**FFs**) to recapitulate the occurrence to *cis*-peptide conformations and reveal their limited performance in describing such structural features.

Following this detailed investigation of structural preferences of glycine dipeptide **1**, we shifted our focus to the thermodynamic stability of glycy radical dipeptide **r1**. As mentioned earlier, **r1** has the largest range for conformation-based tuning of its thermodynamic stability. It is quite possible that enzymes use these structural features of **r1** to alter its reactivity in catalytic processes. Active site analysis of selected members of the glycy radical enzyme (**GRE**) family shows the presence of functional groups that can bear charge on de/protonation close to the glycine residue (Figure 1-5). Upon bearing charge, these functional groups have the potential to influence the reactivity of glycine residue toward HAT reactions.<sup>9</sup> The idea that enzymes use pre-organized structural features, such as the charge on selected side chain residues for catalysis is not new and is quickly gaining more and more acceptance.<sup>10</sup> Following this lead, we investigated the influence of external charge on the stability of glycy radical **r1**.



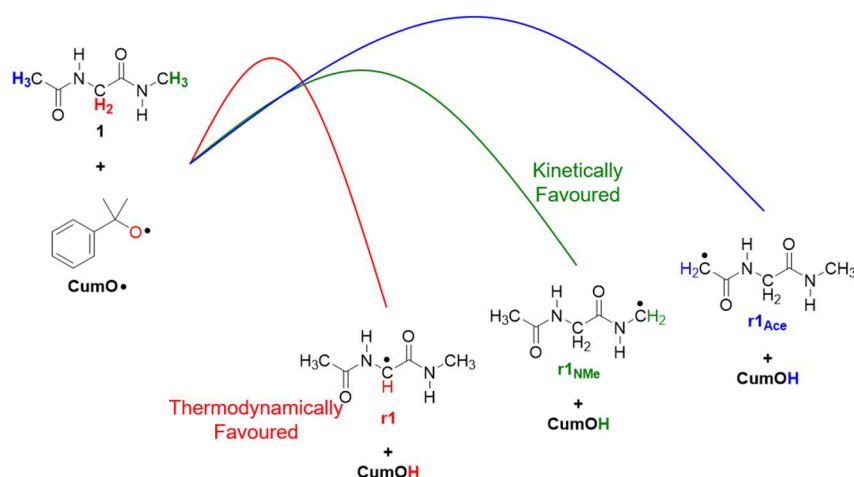


**Figure 1-7.** The qualitative depiction of calculated thermodynamics and kinetics profiles of HAT from glycine dipeptide **1** by cumyloxyl radical **CumO•**.

The C-H bonds at the C<sub>α</sub> position were found to be the weakest C-H bonds in glycine dipeptide **1** in terms of quantum chemically calculated thermodynamic driving force, due to the formation of captodatively stabilized radical **r1**. However, calculated solution phase free energy barriers support the experimental observation, where hydrogen abstraction from the C terminal methyl of glycine dipeptide **1** is having the lowest barrier among all C-H bonds.

### 1.1.2 Radicals in Organic Synthesis

Application of theoretical chemistry concepts to further enhance our understanding of the experimental observations saw a remarkable increase. In collaboration with Prof. Ullrich Jahn, we investigated the stereoselective activation of the C-O bond by amide pyramidalization in diketopiperazine (DKP)-derived alkoxyamines.<sup>12</sup>

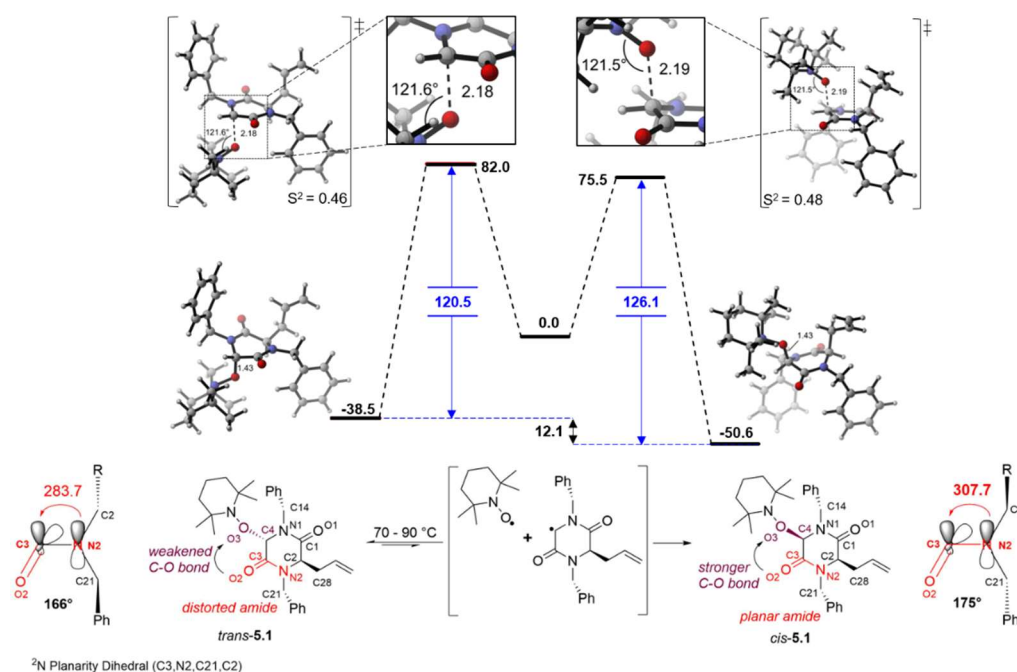


**Figure 1-8.** Solvation-corrected Gibbs energy (in kJ/mol) profile for *trans-cis* isomerization of DKP-derived alkoxyamines **5.1** calculated at the (U)B2PLYP/G3MP2Large//((U)B3LYP/6-31G(d)) level of theory. Single-point solvation energies were calculated for DMSO at the SMD(DMSO)/(U)B3LYP/6-31G(d) level of theory. The hyperconjugation interactions (in kJ/mol, NBO) in *trans-5.1* and *cis-5.1* have been calculated at the (U)B3LYP/6-31G(d) level of theory.

Results have been presented in the fifth chapter of this thesis. The investigation started with the surprising observation of quantitative and unidirectional *trans-cis* isomerization of DKP-derived alkoxyamines **5.1** at temperatures as low as 80 °C. Heating (80 °C) of a *trans/cis* mixture of **5.1** yields pure *cis*-**5.1**. The stereochemistry of both isomers has been confirmed using X-ray crystallography. The preference for *cis* configuration is a common feature in all other DKP-derived alkoxyamines studied, regardless of the steric and electronic features at the amino acid side chains or the DKP nitrogen atoms. Structural data derived from X-ray crystallography and quantum chemical calculations show that the distortion of the amide bond from planarity is significantly higher in *trans*-**5.1** compared to *cis*-**5.1** and thus appears to be the reason for higher thermodynamically facility for homolysis in the former stereoisomer as compared to the latter. Natural bond orbital (NBO) analysis for DKP-derived alkoxyamines **5.1** also confirms that higher amide distortion in *trans*-**5.1** leads to weaker amide resonance interaction than in *cis*-**5.1**. The kinetic investigation reveals that the homolysis rate constant for *trans*-**5.1** is higher than for *cis*-**5.1** and isomerization of *trans*-**5.1** into the more stable *cis*-**5.1** is faster than any other follow-up transformation like cyclization. The same is true for the other DKP-derived alkoxyamines that we studied. Quantum chemical calculations verified these experimental findings. The solvation-corrected Gibbs energy profile for *trans-cis* isomerization of DKP-derived alkoxyamines **5.1** reveals that *cis*-**5.1** is more stable than *trans*-**5.1** and that the reaction barrier for homolysis of *trans*-**5.1** to a radical pair is lower than for *cis*-**5.1** (Figure 1-8). These results are consistent with the experimental observations and proved to be a valuable support in rationalizing the structural and reactivity parameters governing the chemical transformations discussed here.

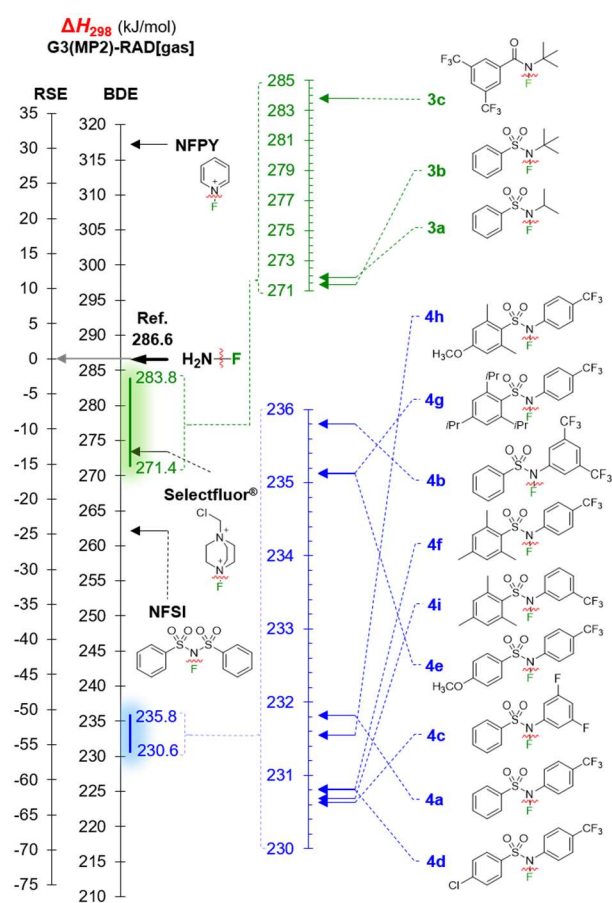


**Figure 1-9.** Gas phase ( $\Delta H_{298}$ ) F—NR<sub>2</sub> bond dissociation energies (BDEs) and radical stabilization energies (RSEs) calculated at the G3(MP2)-RAD level of theory.

Organofluorine compounds have great importance in the field of pharmaceuticals, agrochemicals and materials science. Introduction of fluorine atoms into an existing complex organic molecule under compatible conditions is highly desirable.<sup>13</sup> We collaborated with the group of Prof. Philippe Renaud at the University of Bern for developing a new class of radical fluorinating agents called *N*-Fluoro-*N*-Arylsulfonamides (NFASs) for fluorine atom transfer reactions under mild conditions.<sup>14</sup> Details are provided in the sixth chapter of this thesis. The N-F BDE values of these reagents were found to be significantly lower than in previously used reagents like *N*-fluorobenzenesulfonimide (NFSI) and Selectfluor® (Figure 1-9). The weaker N-F bond enables clean radical fluorination reactions over more complex side reactions. The advantage of NFASs over NFSI and Selectfluor® as radical fluorinating agents is demonstrated by their successful use in the metal-free deboronofluorination of alkylboronates, decarboxylative fluorination of tert-butyl peresters, and the asymmetric hydrofluorination of alkenes.

## 1.2 Quantification of Electrophilic Reactivity

Nucleophile-electrophile combinations are among the most important reactions in organic synthesis. In the past, numerous experimental and theoretical attempts were made to develop a general method to qualitatively/quantitatively predict the reactivity and selectivity for such reactions.

To quantify the relative reactivity, Mayr and co-workers developed one of the most comprehensive scales of nucleophilicity and electrophilicity from experimental kinetic data.<sup>15</sup> It has been shown that the second order rate constants ( $k_2$ ) for a broad range of polar organic reactions can be described by a linear free energy relationship-based eq. 5, where the electrophile reactivity is characterized by one parameter,  $E$  (electrophilicity) and nucleophiles by two solvent dependent parameters  $N$  (nucleophilicity) and  $s_N$  (susceptibility).

$$\log k_2(20^\circ\text{C}) = s_N(N + E) \quad (5)$$

In collaboration with Prof. Herbert Mayr and Dr. Armin Ofial, we screened various commonly used quantum chemical reactivity descriptors against the experimentally measured electrophilicity ( $E$ ) of a structurally diverse set of electrophiles. This collaboration resulted in three publications that are presented as three chapters of this thesis (Chapters 7-9). Experimental parts of these projects are entirely performed by the group of Prof. Mayr and Dr. Ofial. The computational parts are performed by the author of this thesis under the guidance of Prof. Hendrik Zipse. The second half of this thesis documents our efforts in this direction with a focus on the computational part of these studies.

Some of the most widely employed theoretical approaches that are relevant in this regard include the frontier molecular orbital (FMO) theory,<sup>16</sup> reaction energy models based on the Bell-Evans-Polanyi (BEP) principle<sup>17</sup>/Marcus theory,<sup>18</sup> and the distortion-interaction model<sup>19</sup>. FMO theory uses the electronic properties of isolated reactants [energies of the highest occupied molecular orbital (HOMO) and the lowest unoccupied molecular orbital (LUMO)] to estimate the energy change in the early state of a reaction and extrapolate it to the TS region [Figure 1-10(A)].<sup>20</sup> As two molecules approach each other and their orbitals start to overlap, larger stabilization of the interacting molecules occur with larger overlap and smaller energy gap between the interacting orbitals. FMO theory only considers the contribution of the HOMO-LUMO interactions and accordingly assume, at least initially, that the course of the reaction will be guided by the nuclear configuration that leads to the most favourable HOMO-LUMO overlap. In the context of quantification of electrophilic reactivity, several studies have shown that within a smaller group of structurally similar electrophiles, often their relative reactivities correlate with the corresponding LUMO energies [Figure 1-10(B)].<sup>21</sup>

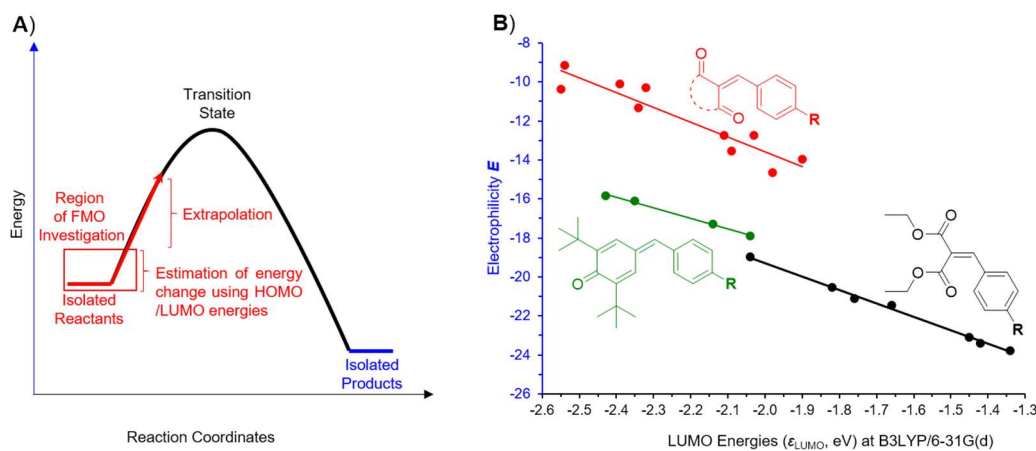


**Figure 1-10.** (A) Graphical representation of qualitative FMO theory. (B) Correlation between experimental electrophilicity ( $E$ ) and the LUMO energies of Michael acceptors calculated at the B3LYP/6-31G(d) level of theory from Zhuo *et al.*<sup>21c</sup>

Parr's global electrophilicity index ( $\omega$ ) for molecules is obtained from "division of the square of its chemical potential ( $\mu$ ) by its chemical hardness ( $\eta$ )", as expressed in eq. 6.<sup>22</sup> The latter two quantities ( $\mu$  and  $\eta$ ) can be obtained from frontier orbital energies, as shown in eqs. 7 and 8. For an electrophilic (electron-deficient) molecular system, Parr's electrophilicity index  $\omega$  is a measure of its energetic stabilization at fixed nuclear configuration upon receiving an additional amount of electronic charge from the environment. The  $\mu^2$  (also defined as the square of electronegativity) quantifies the tendency of a molecule to acquire an additional charge, while the resistance to the same is measured in terms of  $\eta$ .

$$\omega = \mu^2/2\eta \quad (6)$$

$$\mu = \frac{1}{2} (\epsilon_{\text{HOMO}} + \epsilon_{\text{LUMO}}) \quad (7)$$

$$\eta = (\epsilon_{\text{LUMO}} - \epsilon_{\text{HOMO}}) \quad (8)$$

It is possible to project global electrophilicity  $\omega$  at the specific site of interest in the molecule (atom  $k$ ) using Fukui functions ( $f_k^\alpha$ ,  $\alpha = +, -, 0$ ) to obtain the regional variant called local electrophilicity index ( $\omega_k$ ) (eq. 9).<sup>22c</sup> The electrophilic Fukui function ( $f_k^+$ , for nucleophilic attack) is defined as the change of partial charge  $q$  at atom  $k$  upon adding an electron to the corresponding molecule (eq. 10, where  $N =$  a total number of electrons in the neutral molecule).<sup>23</sup>

$$\omega_k = \omega \cdot f_k^+ \quad (9)$$

$$f_k^+ = q(k, N+1) - q(k, N) \quad (10)$$

Parr's global electrophilicity index ( $\omega$ ) and its partial atomic charge-derived variant, local electrophilicity index ( $\omega_k$ ), have been reported to be a better measure of relative electrophilic reactivities in structurally constrained chemical space. These indices usually work well, when the difference in the reactivity is predominantly controlled by the electronic effect of the substituent far away from the site of reactivity. These electrophilicity indices have been employed extensively as a measure of relative electrophilic reactivity with varying degrees of success.<sup>24</sup>

FMO theory and associated indices based on it use properties of reactant(s). In more comprehensive approaches, relative reactivity prediction models - that are based on reactivity-thermodynamic relationships like the BEP principle<sup>17</sup>/Marcus theory<sup>18</sup> - employ properties of both reactant(s) and product(s). According to the BEP principle, in a set of similar reactions, the more exothermic reaction takes place at a faster rate than the less exothermic ones. For two similar reactions, the difference in the activation energies is thus proportional to the difference in the reaction energies.

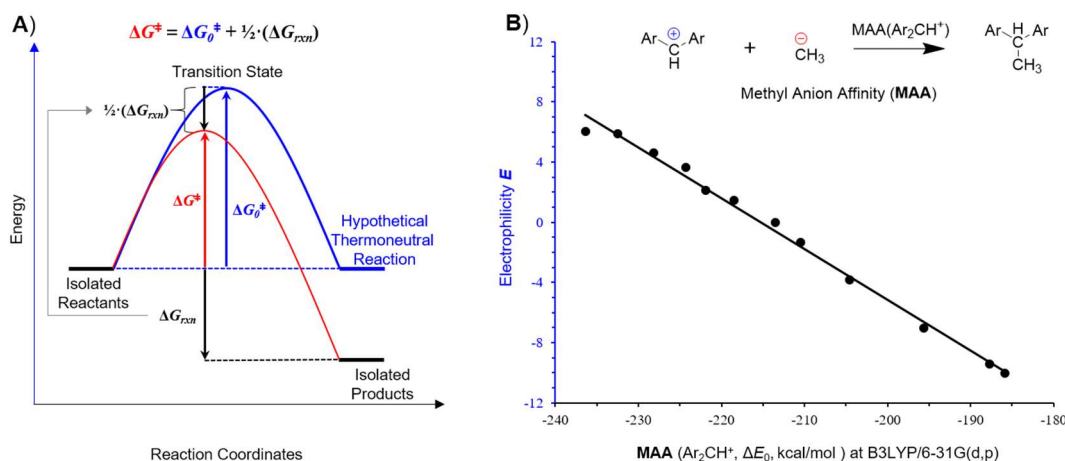


**Figure 1-11.** (A) Reactivity ( $\Delta G^\ddagger$ )-thermodynamics ( $\Delta G_{rxn}$ ) relationship based on the simplified Marcus equation. (B) Correlation between experimentally determined electrophilicities ( $E$ ) of various benzhydryl cation ( $\text{Ar}_2\text{CH}^+$ ) with gas phase methyl anion affinities [ $\text{MAA}(\text{Ar}_2\text{CH}^+)$ ] calculated at B3LYP/6-31G(d,p) from Ref. 25.

The Marcus equation (eq. 11) represents a more quantitative form of the same principle, relating the thermodynamics of a reaction to its activation free energy.<sup>18</sup> In eq. 11, the activation barrier ( $\Delta G^\ddagger$ ) of a reaction is expressed in terms of the intrinsic barrier ( $\Delta G_0^\ddagger$ ) for a hypothetical thermoneutral reaction and the reaction thermodynamic driving force ( $\Delta G_{rxn}$ ). Neglecting the second-order term of eq. 11 [ $(\Delta G_{rxn}^2)/(16 \cdot \Delta G_0^\ddagger)$ ], roughly half of the reaction energy enters into the activation barrier for reactions within the same family [Figure 1-11(A)].<sup>20</sup>

$$\Delta G^\ddagger = \Delta G_0^\ddagger + \frac{1}{2} \cdot (\Delta G_{rxn}) + (\Delta G_{rxn}^2)/(16 \cdot \Delta G_0^\ddagger) \quad (11)$$

The Marcus equation was derived for electron-transfer reactions, but it has been shown that similar quantitative reactivity-thermodynamics relationships can be derived for quantifying electrophilic reactivity [Figure 1-11(B)].<sup>26a, 25, 26b</sup>

More insight into chemical reactivity can be gained from transition state (TS) calculations for the reaction under consideration. Characterization of the transition state in terms of the evolution of bond-order, charge transfer, and distortion-interaction type analysis further augment and deepen our understanding of the origin of chemical reactivity. In the following, we highlight that computational chemistry tools and techniques not only provide an independent method to review experimental observations, but are a complementary approach that goes hand in hand with experimental methods.

Chapter 7 of this thesis discusses the combined experimental and quantum mechanics based theoretical investigation of the electrophilic reactivities of common Michael acceptors.<sup>27</sup> The kinetics of the reactions of mono-acceptor-substituted ethylenes and styrenes with pyridinium ylides, a sulfonium ylide, and a sulfonyl-substituted chloromethyl anion were measured for the quantification of electrophilicities of Michael acceptors, to further extend the application of the Mayr-Patz equation (eq. 5). The empirical electrophilicity parameters  $E$  of the Michael acceptors, were calculated from the second-order rate constants ( $\log k$ ) measured in this work and the previously published  $N$  and  $s_N$  parameters of the nucleophiles,<sup>28</sup> using eq. 5.

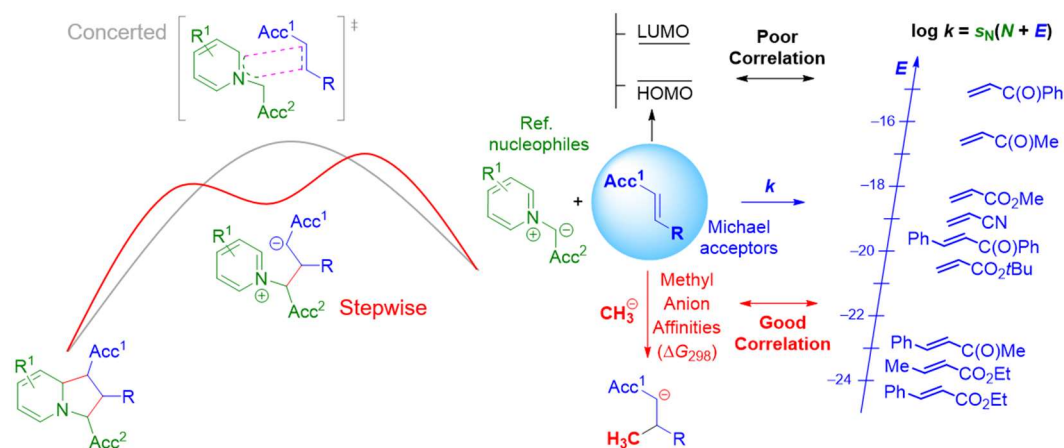


**Figure 1-12.** Summary of the 7<sup>th</sup> chapter of this thesis.

Density function theory (DFT)-based investigation of the energy profiles for the cycloaddition reactions of reference nucleophiles with a representative set of Michael acceptors of different reactivity were performed to confirm the proposed reaction mechanism and to elucidate the origin of the electrophilic reactivities. This investigation reveals that the barriers for stepwise and concerted cycloadditions are energetically quite close, and that the concerted TSs show high asynchronicity with similar structural and electronic features as stepwise TSs. Correlations between electrophilicity of Michael acceptors ( $E$ ) and various QM-based reactivity descriptors were investigated in order to develop a model that allows prediction of electrophilic reactivities of Michael acceptors that are not yet experimentally characterized. Taking a lead from previous studies,<sup>21</sup> we attempted to characterize the electrophilic reactivities of Michael acceptors ( $E$ ) using

frontier molecular orbital energies and associated reactivity indices. Empirical electrophilicity parameter  $E$  correlate poorly with frontier molecular orbital energies or with global and local electrophilicity indices ( $\omega$  &  $\omega_\beta$ ). Moreover, our study highlights the inherent discrepancy in these indices. A more comprehensive electrophilic reactivity measure, methyl anion affinities, was found to be an excellent descriptor for the experimentally observed electrophilic reactivities of Michael acceptors ( $E$ ). The good correlations between  $E$  and methyl anion affinities were found, particularly when solvation by DMSO was considered. The QM calculations also show that methyl anion affinities allow the prediction of relative electrophilic reactivities of structurally diverse Michael acceptors.

Chapter 8 of this thesis describes the quantification of the electrophilicities of ketones using a combination of experimental kinetic data and computational analysis.<sup>29</sup> We studied the formation of epoxides **8.3** by Darzens condensation of electrophilic aliphatic ketones **8.1** with arylsulfonyl-substituted chloromethyl anions **8.2**<sup>28c</sup> in DMSO solution at 20 °C. The reactions proceed via nucleophilic attack of the carbanions **8.2** at the carbonyl carbon of the ketones **8.1** to give intermediate halohydrin anions **8.4**, which subsequently cyclize with formation of epoxides **8.3** (Figure 1-13). The kinetics ( $k_2^{\text{exptl}}$ ) of these reactions were determined photometrically following the disappearance of the UV/Vis absorption of anions **8.2**. The intermediate halohydrins **8.4-H** were prepared independently and subjected to cross-over experiments to determine the rate limiting step. Deprotonation of halohydrins **8.4-H** in the presence of trapping reagents for the regenerated carbanions **8.2** provided the relative rates of backward retroaddition ( $k_{-CC}$ , to starting ketones **8.1** and carbanions **8.2**) and ring closure ( $k_{rc}$ , with formation of epoxide **8.3**) reactions from the intermediates halohydrin anions **8.4**. These rate constant values were used to calculate the second order rate constants ( $k_{CC}$ ) for the nucleophilic attack to carbanions **8.2** at the carbonyl carbon of ketones **8.1**, that are subsequently employed along with previously published reactivity parameters  $N$  and  $s_N$  for the reference nucleophiles<sup>28c</sup> to obtain the electrophilicity parameters  $E$  for aliphatic ketones **8.1**.

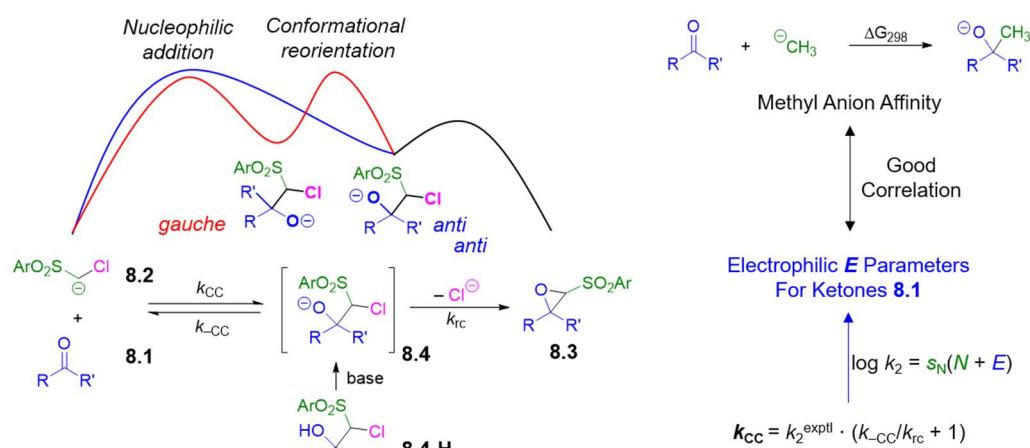


**Figure 1-13.** Summary of the results from chapter 8 of this thesis.

The QM based potential energy surface (PES) investigations for the reactions between carbanions **8.2** and ketones **8.1** show that two rotamers of intermediate halohydrin anions **8.4** are formed as the result of initial nucleophilic attack (Figure 1-13). Rotamers with *anti* C-Cl and C-O<sup>-</sup> bonds orientation cyclize directly to epoxide **8.3**, but isomers with a *gauche* orientation between C-Cl and C-O<sup>-</sup> bonds, have to undergo rotation around the newly formed C-C bond to attain a conformation where cyclization is feasible. The calculations explain that the reversibility observed in the cross-over experiments is a result of a lower barrier for retroaddition as compared to the barrier for conformational re-orientation for intermediate halohydrin anions **8.4**. QM-based conformational analysis of halohydrin **8.4-H** shows that *gauche*- and *anti*-conformers are energetically close, and

**8.4-H** possibly exists as a mixture of these conformers in solution. Theoretical mechanistic investigation into nucleophilic addition of carbanions **8.2** to Michael acceptor as dimethyl maleate shows that the initial step of the reaction is similar to that with ketones, but irreversible in nature. The experimental electrophilicity  $E$  of ketones was found to be moderately correlated with their calculated the LUMO energies, which is in contrast to the very poor correlations found for Michael acceptors as described previously. The quality of correlation degraded significantly as we employed global and local electrophilicity indices ( $\omega$  &  $\omega_\beta$ ) as a theoretical measure of electrophilic reactivity. The experimental electrophilicities  $E$  of ketones correlate well with the computationally predicted methyl anion affinities of the ketones, in which the solvation effect plays an important role.

In the final ninth chapter of this thesis, we present a combination of experimental and theoretical studies of 1,3-dipolar cycloaddition reactions of nucleophilic diazomethanes with acceptor-substituted ethylenes of a wide range of electrophilicities.<sup>30</sup> Photometrically monitored kinetics of the aryldiazomethanes ( $\text{ArCHN}_2$ ) with a set of colored benzhydrylium ions ( $\text{Ar}_2\text{CH}^+$ ) of known electrophilicities  $E$ <sup>31</sup> were studied first to determine the nucleophile-specific parameters ( $S_N$  and  $N$ ) for the diazo compounds using eq. 5. The second order rate constants ( $k_2^{\text{exptl}}$ ) of the 1,3-dipolar cycloaddition reactions between the diazo compounds characterized in this work and a set of acceptor-substituted ethylenes of known electrophilicities  $E$  were then determined using previously published methods.<sup>27</sup> We found that for highly electrophilic acceptor-substituted alkenes (with  $E$  values more than -11), their reaction rates with diazo compounds could be accurately predicted with the reactivity parameters  $E$ ,  $S_N$  and  $N$  using eq. 5. Their calculated rate constants  $k_2^{\text{calcd}}$  from eq. 5 correlate well with the experimentally measured  $k_2^{\text{exptl}}$ , while the faster rates were observed for weaker electrophiles ( $E < -11$ ) than predicted using the reactivity parameters ( $k_2^{\text{calcd}} > k_2^{\text{exptl}}$ ). These deviations are the result of higher degree of concertedness during cycloaddition reactions between the diazo compounds and weaker electrophiles that lower the activation barrier by stabilization of the transition state.

$$\Delta G^\ddagger_{\text{concert}} = RT \ln(k_2^{\text{exptl}}/k_2^{\text{calcd}}) \quad (12)$$

The magnitude of the barrier reduction [also called energy of concert ( $\Delta G^\ddagger_{\text{concert}}$ )] could be obtained by the ratio of experimental to calculated rate constants, as shown by eq. 12.

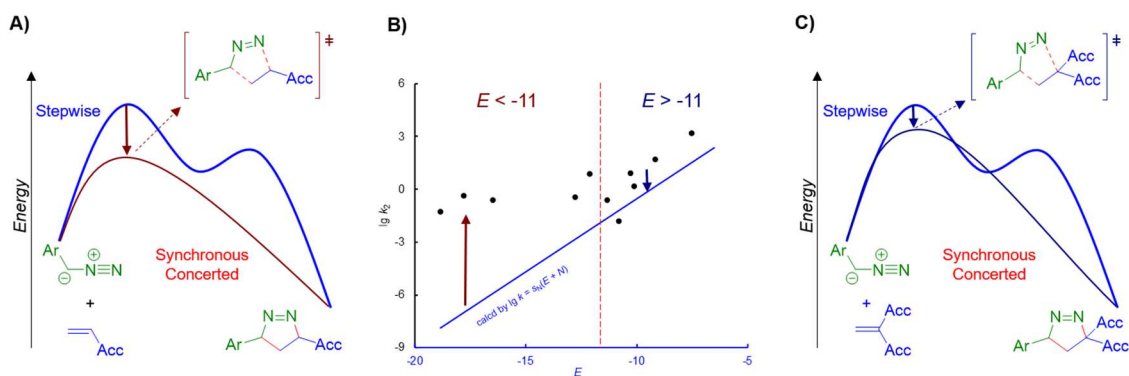


**Figure 1-14.** Qualitative potential energy surface of the 1,3-dipolar cycloaddition reactions between the diazo compound and acceptor-substituted alkenes with low (A) and high (C) electrophilicity ( $E$ ). (B) Correlation of electrophilicity parameter ( $E$ ) of acceptor-substituted alkenes versus  $\lg k_2$  for their reactions with phenyldiazomethane.

Quantum chemically investigated 1,3-dipolar cycloaddition reactions of phenyldiazomethane **9.1a** with a set of representative acceptor-substituted alkenes show that these reactions proceed through concerted and asynchronous transition states to form intermediate  $\Delta^1$ -pyrazolines that subsequently transforms into  $\Delta^2$ -pyrazolines, cyclopropanes, and substituted alkenes. These findings are in excellent agreement with experimental observations. The calculated reaction barriers also agree very well with the experimental activation energies. Analysis of structural parameters, the charge

distribution and the evolution of bond orders of transition states was used to quantify the asynchronicity of these cycloaddition reactions. QM-based analysis confirms that highly electrophilic acceptor-substituted alkenes react through highly asynchronous 1,3-dipolar cycloadditions with phenyldiazomethane as compared to weaker electrophiles, which supports the interpretations of experimental investigations. The higher asynchronicity with higher electrophilicity means the C-C bond formation is much more advanced than the C-N bond formation at the transition state (the C-N bond effectively contributes very little to the TS stabilization) and that is why the reactivity parameters  $E$ ,  $s_N$  and  $N$  are well suited to predict experimental reactivity values, as these reactivity parameters were derived from reactions, where only one bond is formed in the rate-determining step.

## References

- (1) Minkin, V. I., *Pure Appl. Chem.* **1999**, *71*, 1919-1981.
- (2) Ingold, K., *Pure Appl. Chem.* **1997**, *69*, 241-244.
- (3) (a) Stadtman, E. R., *Science* **1992**, *257*, 1220-1224. (b) Droge, W., *Physiol. Rev.* **2002**, *82*, 47-95. (c) Valko, M.; Leibfritz, D.; Moncol, J.; Cronin, M. T.; Mazur, M.; Telser, J., *Int. J. Biochem. Cell Biol.* **2007**, *39*, 44-84.
- (4) Stubbe, J.; Van Der Donk, W. A., *Chem. Rev.* **1998**, *98*, 705-762.
- (5) (a) Hioe, J.; Zipse, H., *Faraday Discuss.* **2010**, *145*, 301-313. (b) Hioe, J.; Zipse, H., *Org. Biomol. Chem.* **2010**, *8*, 3609-3617. (c) Hioe, J.; Savasci, G.; Brand, H.; Zipse, H., *Chem. Eur. J.* **2011**, *17*, 3781-3789. (d) Hioe, J.; Zipse, H., Radical Stability—Thermochemical Aspects. In *Encyclopedia of Radicals in Chemistry, Biology and Materials*, Chrystostomos, C.; Armido, S., Eds. John Wiley & Sons Ltd: Chichester, UK, 2012; pp 449-476. (e) Hioe, J.; Mosch, M.; Smith, D. M.; Zipse, H., *RSC Adv.* **2013**, *3*, 12403-12408.
- (6) Luo, Y.-R., *Comprehensive Handbook of Chemical Bond Energies*. CRC press: **2007**.
- (7) Hioe, J.; Zipse, H., *Chem. Eur. J.* **2012**, *18*, 16463-16472.
- (8) Jangra, H.; Haindl, M. H.; Achraimer, F.; Hioe, J.; Gschwind, R. M.; Zipse, H., *Chem. Eur. J.* **2016**, *22*, 13328-13335.
- (9) (a) Gryn'ova, G.; Marshall, D. L.; Blanksby, S. J.; Coote, M. L., *Nat. Chem.* **2013**, *5*, 474-481. (b) Gryn'ova, G.; Coote, M. L., *J. Am. Chem. Soc.* **2013**, *135*, 15392-15403. (c) Shaik, S.; Mandal, D.; Ramanan, R., *Nat. Chem.* **2016**, *8*, 1091-1098.
- (10) (a) Shaik, S.; de Visser, S. P.; Kumar, D., *J. Am. Chem. Soc.* **2004**, *126*, 11746-11749. (b) Lai, W.; Chen, H.; Cho, K.-B.; Shaik, S., *J. Phys. Chem. Lett.* **2010**, *1*, 2082-2087. (c) Fried, S. D.; Bagchi, S.; Boxer, S. G., *Science* **2014**, *346*, 1510-1514. (d) Wu, Y.; Boxer, S. G., *J. Am. Chem. Soc.* **2016**, *138*, 11890-11895. (e) Fried, S. D.; Boxer, S. G., *Annu. Rev. Biochem.* **2017**, *86*, 387-415. (f) Maji, R.; Wheeler, S. E., *J. Am. Chem. Soc.* **2017**, *139*, 12441-12449.
- (11) Jangra, H.; Zipse, H., *J. Phys. Chem. B* **2018**, *122*, 8880-8890.
- (12) Amatov, T.; Jangra, H.; Pohl, R.; Cisařová, I.; Zipse, H.; Jahn, U., *Chem. Eur. J.* **2018**, *24*, 15336-15345.
- (13) (a) Müller, K.; Faeh, C.; Diederich, F., *Science* **2007**, *317*, 1881-1886. (b) O'Hagan, D., *Chem. Soc. Rev.* **2008**, *37*, 308-319. (c) Purser, S.; Moore, P. R.; Swallow, S.; Gouverneur, V., *Chem. Soc. Rev.* **2008**, *37*, 320-330.
- (14) Meyer, D.; Jangra, H.; Walther, F.; Zipse, H.; Renaud, P., *Nat. Commun.* **2018**, *9*, 1-10.
- (15) (a) Mayr, H.; Patz, M., *Angew. Chem. Int. Ed.* **1994**, *33*, 938-957. (b) Mayr, H.; Kempf, B.; Ofial, A. R., *Acc. Chem. Res.* **2003**, *36*, 66-77. (c) Mayr, H.; Ofial, A. R., *Pure Appl. Chem.* **2005**, *77*, 1807-1821. (d) Mayr, H.; Ofial, A. R., *J. Phys. Org. Chem.* **2008**, *21*, 584-595.
- (16) (a) Houk, K.; Sims, J.; Watts, C. R.; Luskus, L., *J. Am. Chem. Soc.* **1973**, *95*, 7301-7315. (b) Fukui, K., *Angew. Chem. Int. Ed.* **1982**, *21*, 801-809. (c) Fleming, I., *Molecular Orbitals and Organic Chemical Reactions*. John Wiley & Sons: **2011**.

- (17) (a) Bell, R., *Proc. R. Soc. London, Ser. A* **1936**, *154*, 414. (b) Evans, M.; Polanyi, M., *Trans. Faraday Society* **1936**, *32*, 1333-1360.
- (18) (a) Marcus, R. A., *J. Chem. Phys.* **1956**, *24*, 966-978. (b) Marcus, R. A., *J. Phys. Chem.* **1968**, *72*, 891-899.
- (19) (a) Ess, D. H.; Houk, K., *J. Am. Chem. Soc.* **2008**, *130*, 10187-10198. (b) Bickelhaupt, F. M.; Houk, K. N., *Angew. Chem. Int. Ed.* **2017**, *56*, 10070-10086.
- (20) Jensen, F., *Introduction to Computational Chemistry*. John Wiley & Sons: **2017**.
- (21) (a) Sustmann, R., *Pure Appl. Chem.* **1974**, *40*, 569-593. (b) Houk, K. N., *Acc. Chem. Res.* **1975**, *8*, 361-369. (c) Zhuo, L. G.; Liao, W.; Yu, Z. X., *Asian J. Org. Chem.* **2012**, *1*, 336-345.
- (22) (a) Parr, R. G.; Szentpaly, L. v.; Liu, S., *J. Am. Chem. Soc.* **1999**, *121*, 1922-1924. (b) Domingo, L. R.; Pérez, P.; Contreras, R., *Tetrahedron* **2004**, *60*, 6585-6591. (c) Chattaraj, P. K.; Roy, D. R., *Chem. Rev.* **2007**, *107*, PR46-PR74. (d) Chattaraj, P. K.; Giri, S.; Duley, S., *Chem. Rev.* **2011**, *111*, PR43-PR75.
- (23) Yang, W.; Mortier, W. J., *J. Am. Chem. Soc.* **1986**, *108*, 5708-5711.
- (24) (a) Contreras, R. R.; Fuentealba, P.; Galván, M.; Pérez, P., *Chem. Phys. Lett.* **1999**, *304*, 405-413. (b) Aizman, A.; Contreras, R.; Pérez, P., *Tetrahedron* **2005**, *61*, 889-895. (c) Moraleda, D.; El Abed, D.; Pellissier, H.; Santelli, M., *J. Mol. Struct.: THEOCHEM* **2006**, *760*, 113-119. (d) Pérez, P.; Domingo, L. R.; Aizman, A.; Contreras, R., The electrophilicity index in organic chemistry. In *Theoretical and Computational Chemistry*, Elsevier: 2007; Vol. 19, pp 139-201. (e) Domingo, L. R.; Chamorro, E.; Pérez, P., *Eur. J. Org. Chem.* **2009**, *2009*, 3036-3044. (f) Wondrousch, D.; Böhme, A.; Thaens, D.; Ost, N.; Schüürmann, G., *J. Phys. Chem. Lett.* **2010**, *1*, 1605-1610. (g) Domingo, L. R.; Ríos-Gutiérrez, M.; Pérez, P., *Molecules* **2016**, *21*, 748.
- (25) Schindele, C.; Houk, K.; Mayr, H., *J. Am. Chem. Soc.* **2002**, *124*, 11208-11214.
- (26) (a) Böttger, G. M.; Fröhlich, R.; Würthwein, E. U., *Eur. J. Org. Chem.* **2000**, *2000*, 1589-1593. (b) Mayr, H.; Ammer, J.; Baidya, M.; Maji, B.; Nigst, T. A.; Ofial, A. R.; Singer, T., *J. Am. Chem. Soc.* **2015**, *137*, 2580-2599.
- (27) Allgäuer, D. S.; Jangra, H.; Asahara, H.; Li, Z.; Chen, Q.; Zipse, H.; Ofial, A. R.; Mayr, H., *J. Am. Chem. Soc.* **2017**, *139*, 13318-13329.
- (28) (a) Appel, R.; Hartmann, N.; Mayr, H., *J. Am. Chem. Soc.* **2010**, *132*, 17894-17900. (b) Allgäuer, D. S.; Mayer, P.; Mayr, H., *J. Am. Chem. Soc.* **2013**, *135*, 15216-15224. (c) Li, Z.; Chen, Q.; Mayer, P.; Mayr, H., *J. Org. Chem.* **2017**, *82*, 2011-2017.
- (29) Li, Z.; Jangra, H.; Chen, Q.; Mayer, P.; Ofial, A. R.; Zipse, H.; Mayr, H., *J. Am. Chem. Soc.* **2018**, *140*, 5500-5515.
- (30) Jangra, H.; Chen, Q.; Fuks, E.; Zenz, I.; Mayer, P.; Ofial, A. R.; Zipse, H.; Mayr, H., *J. Am. Chem. Soc.* **2018**, *140*, 16758-16772.
- (31) (a) Mayr, H.; Bug, T.; Gotta, M. F.; Hering, N.; Irrgang, B.; Janker, B.; Kempf, B.; Loos, R.; Ofial, A. R.; Remennikov, G., *J. Am. Chem. Soc.* **2001**, *123*, 9500-9512. (b) Mayer, R. J.; Hampel, N.; Mayer, P.; Ofial, A. R.; Mayr, H., *Eur. J. Org. Chem.* **2018**, *2018*, 6010-6017.

## **Chapter 2. Conformational Preferences in Small Peptide Models: The Relevance of *cis/trans*-Conformations**

Harish Jangra, Michael H. Haindl, Florian Achraimer, Johnny Hioe, Ruth M. Gschwind and Hendrik Zipse  
*Chem. Eur. J.* **2016**, 22, 13328-13335.

---

### ***Authors contribution***

H.Z. conceive the project. The computational research strategy was designed by H.Z. and H.H., and performed by H.H with the assistance of H.J. The experimental work was designed by R.M.G. and performed by M.H.H. Substrates for experimental studies were synthesised by F.A. The manuscript was jointly written by H.H., M.H.H., R.M.G., and H.Z.

### ***Copyright***

This research was originally published in the *Chemistry – A European Journal* and is reprinted here as the 2<sup>nd</sup> chapter of this thesis from *Chem. Eur. J.* **2016**, 22, 13328-13335 © 2016 WILEY-VCH Verlag GmbH & Co. KGaA, Weinheim.

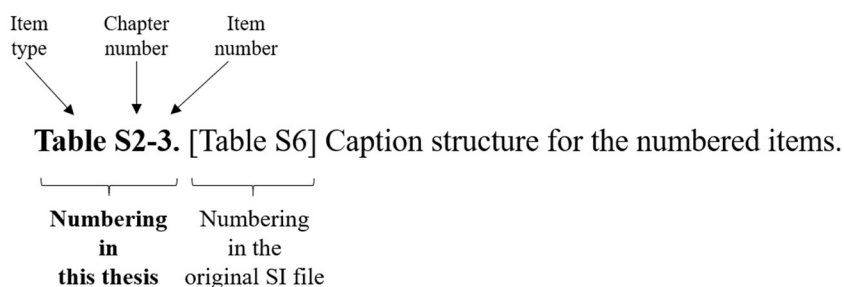
(Link to article: <https://onlinelibrary.wiley.com/doi/full/10.1002/chem.201601828>)

Selected supporting material for the computational part of this work is provided at the end of this chapter. For complete supporting information (SI), please follow the link below:

[https://onlinelibrary.wiley.com/action/downloadSupplement?doi=10.1002%2Fchem.201601828&file=chem201601828-sup-0001-misc\\_information.pdf](https://onlinelibrary.wiley.com/action/downloadSupplement?doi=10.1002%2Fchem.201601828&file=chem201601828-sup-0001-misc_information.pdf)

### ***Additional information***

The accompanying SI is the shorter and altered version of the original content. The items (Tables, Figure, Schemes etc.) may have a different number than what was originally assigned. To make it easier to locate the SI content referred to in the following reprint, the original numbering is also provided in the caption of the numbered items as described below:



## Conformation Analysis

Conformational Preferences in Small Peptide Models:  
The Relevance of *cis/trans*-ConformationsHarish Jangra,<sup>[a]</sup> Michael H. Haindl,<sup>[b]</sup> Florian Achraimer,<sup>[a]</sup> Johnny Hioe,<sup>[b]</sup>  
Ruth M. Gschwind,<sup>\*[b]</sup> and Hendrik Zipse<sup>\*[a]</sup>

**Abstract:** The accurate description of *cis/trans* peptide structures is of fundamental relevance for the field of protein modeling and protein structure determination. A comprehensive conformational analysis of dipeptide model Ace-Gly-NMe (**1**) has been carried out by using a combination of theoretical calculations and experimental (<sup>1</sup>H and <sup>13</sup>C NMR and NOESY) spectroscopic measurements to assess the relevance of *cis*-peptide conformers. NMR measurements in dimethyl sulfoxide (DMSO) solution and calculations employing a continuum solvation model both point to the extended *trans*-

*trans* conformer **C5\_tt** as the global minimum. The *cis*-peptide structures **C5\_ct** and **C5\_tc**, with the N- or C-terminal amide group in *cis*-conformation, are observed separately and located  $13.0 \pm 2$  kJ mol<sup>-1</sup> higher in energy. This is in close agreement with the theoretical prediction of around 12 kJ mol<sup>-1</sup> in DMSO. The ability of common protein force fields to reproduce the energies of the *cis*-amide conformers **C5\_ct** and **C5\_tc** in **1** is limited, making these methods unsuitable for the description of *cis*-peptide structures in protein simulations.

## Introduction

Intrinsically disordered but functional proteins as well as sparsely populated conformational states of proteins providing a key role in molecular recognition, self-assembly or conformational selection are hot topics in structural biology.<sup>[1–4]</sup> In both fields, the lowly populated and often transient states cannot be detected directly by classical structural methods such as conventional NMR or X-ray analysis, but require advanced NMR techniques for example, relaxation dispersion or saturation transfer methods and rely strongly on the reliable computation of the energetics of the conformational space to calculate the structural ensembles. The correct prediction of the conformational preferences including high free-energy states by molecular mechanics-based theoretical approaches is thus of fundamental importance for the applicability of these methods. Several recently developed force fields for peptide and protein modeling have therefore been derived with reference to accurate structural and energetic data obtained from ab initio studies on small peptide models.<sup>[5–16]</sup> Similarly, a large number of theoretical studies have been performed on small (di)peptide

models, again often aiding the development of more accurate protein force fields. However, in practically all of these studies, *cis*-peptide conformations have been excluded on the basis of their unfavorable stability.<sup>[17–19]</sup> The *cis/trans* isomerization occurs quite frequently at proline residues and this issue has already been addressed in a number of previous studies.<sup>[20]</sup> Nevertheless, *cis*-peptide structures also occur at other residues at a low rate.<sup>[4,21–29]</sup> In addition, numerous surveys and statistical analyses of the PDB database revealed that *cis*-peptide conformations occur as much as 50 times less than expected (for non-proline residues) and a systematic increase is observed with increasing resolution of the protein structures.<sup>[20–25,27]</sup> Some of the very recent analyses of PDB structures concern the potentially incorrect assignment of peptide conformations.<sup>[28]</sup> These findings, together with the debate on *cis/trans* isomerism in side-chain amide bonds,<sup>[30]</sup> are in line with the typical features of spectroscopically invisible “dark” states characterized by relative high free energies in combination with short lifetimes. As a result, *cis*-peptide conformations in large proteins are usually not detectable by conventional NMR or X-ray analysis of large proteins.<sup>[1–2]</sup>

Small peptide models have therefore to be used to provide accurate experimental and theoretical data for *cis*-peptide conformations in systems other than those containing proline. One important reference compound for *cis*-conformations is *N*-methylacetamide (NMA), the *cis/trans* energy difference of which has been studied extensively by experimental and theoretical means (see Figure 1 A). Almost irrespective of the choice of solvent, the *trans* conformation (**NMA\_t**) is preferred over the *cis* conformation (**NMA\_c**) by 8.5–10.5 kJ mol<sup>-1</sup>, corresponding to *cis* populations of between 2.8 and 0.8% (see Figure 1 A).<sup>[31–33]</sup> Experimental studies are challenged by both the

[a] H. Jangra, Dr. F. Achraimer, Prof. Dr. H. Zipse  
Department of Chemistry, LMU München  
Butenandstrasse 5–14, 81377 München (Germany)  
E-mail: zipse@cup.uni-muenchen.de

[b] M. H. Haindl, Dr. J. Hioe, Prof. Dr. R. M. Gschwind  
Institut für Organische Chemie, Universität Regensburg  
93053 Regensburg (Germany)  
E-mail: ruth.gschwind@ur.de

Supporting information for this article and ORCID from one of the authors are available on the WWW under <http://dx.doi.org/10.1002/chem.201601828>.

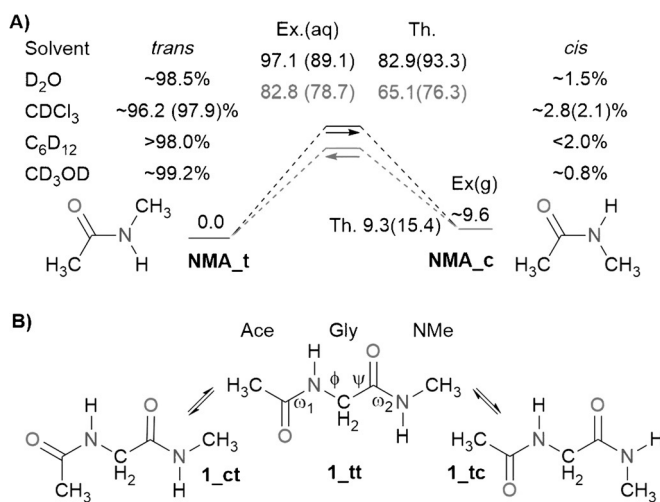


**Figure 1.** A) *N*-Methylacetamide (NMA): known experimental and theoretical data (in  $\text{kJ mol}^{-1}$ ) on the relative stability and *trans/cis* isomerization barrier shown in terms of  $\Delta H$  ( $\Delta G$ );<sup>[31–40]</sup> and B) the most relevant *cis/trans* conformational isomers of 2-acetamino-*N*-methylacetamide (1).

low population of the *cis*-conformer NMA\_c as well as by the high *trans/cis* isomerization barrier of more than  $80 \text{ kJ mol}^{-1}$ .<sup>[34–40]</sup> That the *cis/trans* energy difference shows little solvent dependence is surprising in light of the large absolute solvation energies of peptides in polar media.<sup>[40]</sup> Glycine derivative 2-acetamino-*N*-methylacetamide (1) represents the smallest dipeptide model featuring peptide-like conformational properties and has therefore been studied repeatedly in the past.<sup>[7–8, 12, 29, 41–44]</sup> In a recent exploration of the stability of peptide radicals, we calculated a gas-phase enthalpy difference of  $10.7 \text{ kJ mol}^{-1}$  between the global minimum (*C<sub>7</sub>*) and the lowest lying *cis* amide conformer of 1 (Figure 1B). Unfortunately, conformational energies for *cis*-amide conformers have not been reported in other theoretical studies of 1, and experimental results on this energy difference also appear not to exist. To study the relevance of *cis*-peptide conformations other than proline and to provide reliable energetic differences, we use in the present work an array of different quantum chemical methods combined with detailed NMR spectroscopic data. The conformational preferences of 1 are explored including the energetics of the sparsely populated *cis/trans* (*tc* and *ct*) conformers and their chemical exchange rates with the more favorable all-*trans* conformers.

## Results and Discussion

### Theoretical results

#### Gas-phase conformational distribution of glycine dipeptide (1)

The conformational space of 1 was explored by using a systematic search with defined variations in the four most relevant dihedral angles ( $\Phi$ ,  $\Psi$ ,  $\omega_1$  and  $\omega_2$ ) as shown in a Figure 1B to obtain starting geometries that were subsequently optimized at B3LYP/6-

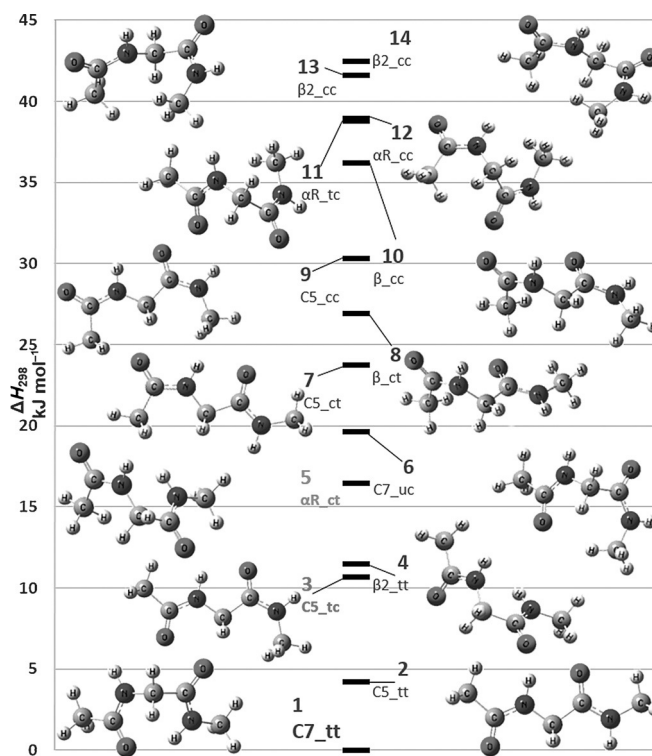


**Figure 2.** The structures of gas-phase minima obtained at B3LYP/6-31G(d) level and  $\Delta H_{298}$  calculated at G3(MP2)-RAD level.

31G(d) level of theory (see the Supporting Information for further details). This strategy locates the 14 structures shown in Figure 2. Conformational ordering as reflected in relative enthalpies at 298.15 K ( $\Delta H_{298}$ ) shows little dependence on the particular theoretical method used and is practically identical to that calculated with the previously used G3(MP2)-RAD and the slightly more elaborate G3B3 and CCSD(T)/CBS methods

**Table 1.** Relative enthalpies  $\Delta H_{298}$  ( $\text{kJ mol}^{-1}$ ) for conformers of glycine dipeptide model (1) at different QM theoretical levels.

SI	Conf. <sup>[a]</sup>	B3LYP/ 6-31G(d)	B2PLYP/ G3M2LARGE	G3(MP2)-RAD	G3B3	CCSD(T)/ CBS
1	C7_tt	0.0	0.0	0.0	0.0	0.0
2	C5_tt	2.0	1.3	4.2	4.7	2.7
3	C5_tc	9.8	8.5	10.7	11.2	9.7
4	β2_tt	10.1	9.7	11.5	11.8	10.9
5	αR_ct	17.9	16.2	16.5	16.9	16.1
6	C7_uc <sup>[b]</sup>	20.1	19.6	19.6	19.8	19.6
7	C5_ct	20.7	21.0	23.7	24.3	22.2
8	β_ct	26.2	26.7	26.9	27.3	26.4
9	C5_cc	28.5	28.4	30.3	30.9	29.4
10	β_cc	37.0	36.9	36.2	36.6	36.0
11	αR_tc	42.7	40.1	38.8	39.0	39.7
12	αR_cc	40.9	40.0	39.0	39.4	39.4
13	β2_cc	44.5	42.3	41.6	42.1	42.4
14	β2_cc	44.2	42.8	42.5	43.0	43.1

[a] Refer to the Supporting Information Table S1 for conformational nomenclature. [b] "u" indicates a peptide bond conformation deviating more than 15 degrees from the idealized dihedral angles of 0.0 (*cis*, *c*) and 180.0 (*trans*, *t*) degrees. For C7\_uc, the dihedral angle amounts to 164.4 degrees.

(Table 1). We will therefore continue to discuss the G3(MP2)-RAD results, if not noted otherwise. Perusal of the gas-phase enthalpy data in Figure 2 shows that the best conformation for **1** corresponds to **C7\_tt**, which is very much in line with most of the previous theoretical studies of this system. The extended **C5\_tt** structure is located only 4.2 kJ mol<sup>-1</sup> higher in energy and thus represents the 2<sup>nd</sup> best conformation. Rotation around the C-terminal amide bond leads to the **C5\_tc** conformer, which is located +10.7 kJ mol<sup>-1</sup> above the global minimum and represents the 3<sup>rd</sup> best conformation overall. This is followed by the all-*trans* conformation **β2\_tt** at +11.5 kJ mol<sup>-1</sup>. The first N-terminal *cis*-conformer **αR\_ct** is found as the 5<sup>th</sup> best conformer at +16.5 kJ mol<sup>-1</sup>. The most stable di-*cis* amide conformer **C5\_cc** occurs at 30.3 kJ mol<sup>-1</sup> relative to the global minimum, which implies that the energetic effort of rotating the amide bonds on the N- or C-terminal side of **1** into the *cis*-conformation is quite independent of other conformational settings.

In free energy terms ( $\Delta G_{298}$ ), the extended **C5\_tt** conformation represents the global minimum, followed by **C7\_tt** at +2.7 kJ mol<sup>-1</sup> (1<sup>st</sup> column in Figure 3). This flip can be understood in terms of the entropic cost of the internal hydrogen bond present in **C7\_tt** as compared with the extended **C5\_tt** structure. The order and relative stability for the rest of the conformers is not changed much: the **C5\_tc** structure remains the 3<sup>rd</sup> best conformer and appears at 8.8 kJ mol<sup>-1</sup>, whereas the first conformation with a *cis*-amide on the N-terminal side **αR\_ct** occurs at 18.8 kJ mol<sup>-1</sup>; that is, 10 kJ mol<sup>-1</sup> higher than

**C5\_tc**. In summary all gas-phase results predict a close competition of **C5\_tt** and **C7\_tt** conformations, followed by the **C5\_tc** conformation as the lowest lying *cis*-amide structure. The best conformation of **ct** type is, at all levels, significantly less stable than that of **tc** type.

### Solvation energies

The effects of solvation were explored for dimethyl sulfoxide (DMSO) as one of the most often used polar solvents for NMR spectroscopy. Building on the gas-phase geometries and energies shown in Figure 2, solvation free-energies were calculated by using the IEFPCM, SMD, and COSMO-SAC continuum solvation models. Subsequent combination with the gas-phase free-energies then yields the conformational distribution shown in Figure 3. IEFPCM and SMD predict almost identical conformational ordering for **1** in DMSO solution, hence only the IEFPCM results are displayed (refer to the Supporting Information for SMD results). Irrespective of the solvation model, the **C5\_tt** conformation is predicted as the global minimum, followed by **β2\_tt** as the 2<sup>nd</sup> best and the **C7\_tt** conformation as the 3<sup>rd</sup> best *trans-trans* conformer. This change in conformational preferences relative to those in the gas phase is due to a comparatively low solvation energy for the **C7\_tt** conformation, which is an effect also predicted in earlier theoretical studies.<sup>[44]</sup> The differential solvation energies mean that the **C5\_ct** and **C5\_tc** conformations are almost isoenergetic, now located ca. 12 kJ mol<sup>-1</sup> above the global minimum using COSMO-SAC solvation energies. This is in close agreement with the experimental measurements predicting energy differences of 13.0 ± 2 kJ mol<sup>-1</sup> (2<sup>nd</sup> column in Figure 3).

### Experimental results

The four characteristic regions of the <sup>1</sup>H NMR spectrum of **1** (NH, H<sub>α</sub>, Ace, and NMe see Figure 4A) reveal signal sets of the main conformer **1\_tt** as well as of the two very low populated *cis*-conformers **1\_ct** and **1\_tc**. At 600 MHz, some of the *cis*-conformer signals partially overlap with the large resonances of the main conformer, but several signals of **1\_ct** and **1\_tc** are baseline separated and enable a highly reliable integration. In Figure 4B, the <sup>1</sup>H chemical shifts of **1\_tt**, **1\_ct**, and **1\_tc** in [D<sub>6</sub>]DMSO at 305 K are depicted (for 2D assignment spectra and <sup>13</sup>C chemical shift assignments refer to the Supporting Information). Signal intensities for the two *cis* conformers are similar to those of the <sup>13</sup>C satellites of the main conformer **1\_tt** (see Figure 1B), indicating a population of about 0.5% each. The amide protons of the *cis*-conformers (H<sub>N<sub>Ace</sub></sub> and H<sub>N<sub>Me</sub></sub> of **1\_ct** and **1\_tc**) were identified unambiguously by using magnetization transfer via chemical exchange (EXSY) in 1D-selective NOESY experiments. Selective irradiation of H<sub>N<sub>Ace</sub></sub> or H<sub>N<sub>Me</sub></sub> in **1\_tt** results in an EXSY signal build-up of the corresponding signals in **1\_ct** and **1\_tc** (for details see the Supporting Information) and thus differentiates these signals from possible impurities. Intramolecular NOE contacts of H<sub>α</sub> (tc) and NMe (tc) as well as H<sub>α</sub> (ct) and Ace (ct) detected by 1D-selective NOESY experiments prove *cis*-conformations in **1\_ct** and **1\_tc** (see

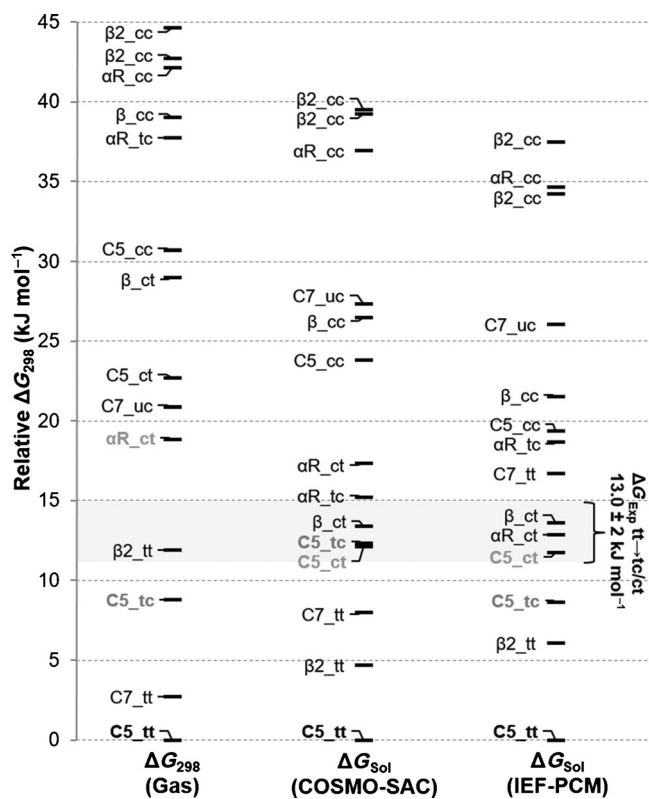
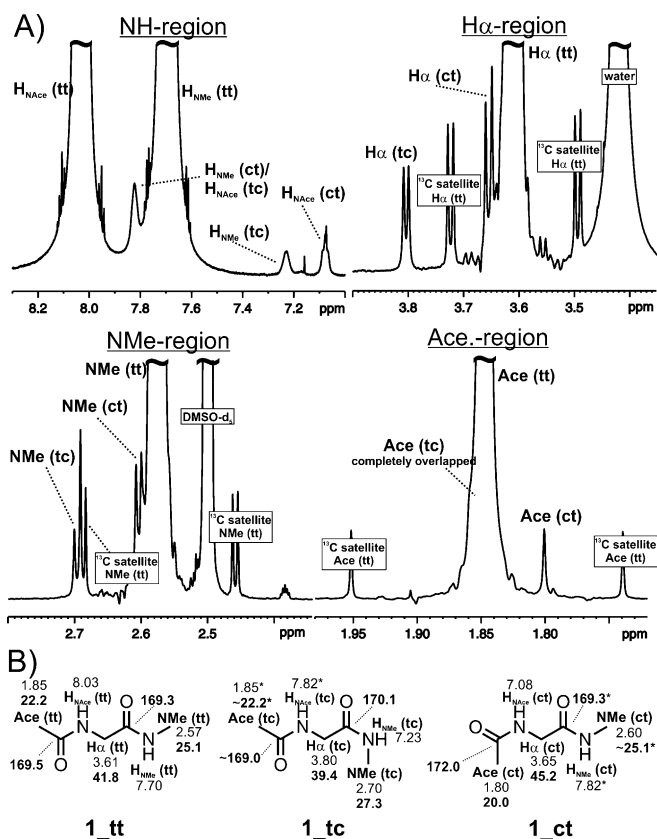
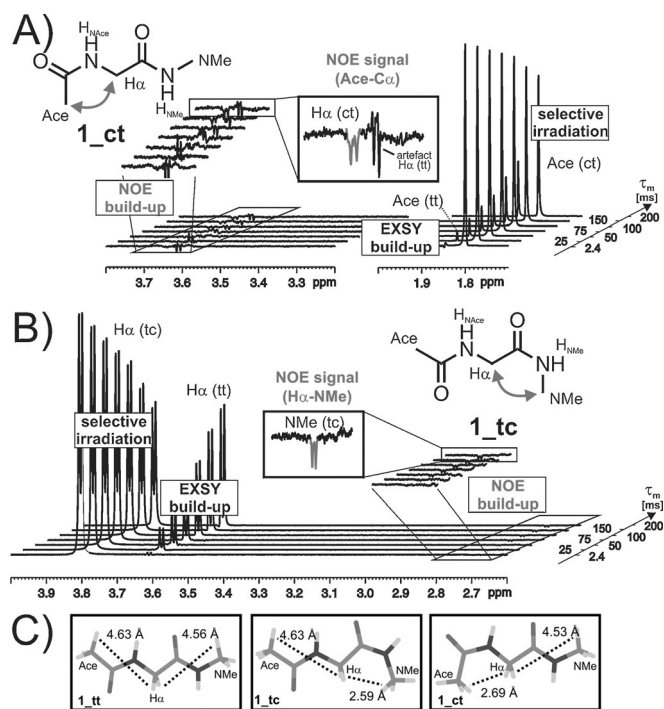


Figure 3. Gas-phase and solution-phase (DMSO) free-energy differences ( $\Delta G_{298}$ , kJ mol<sup>-1</sup>) for conformers of glycine dipeptide model **1**.



**Figure 4.** A) The <sup>1</sup>H NMR spectrum of **1** (600 MHz, 380 mm, [D<sub>6</sub>]DMSO) shows several baseline separated signals of the two *cis* conformers **1<sub>tc</sub>** and **1<sub>ct</sub>** with populations of around 0.5% relative to the main conformer **1<sub>tt</sub>**. B) <sup>1</sup>H and <sup>13</sup>C chemical shift assignments of **1<sub>tt</sub>**, **1<sub>tc</sub>**, and **1<sub>ct</sub>** [ppm]. Strongly overlapping signals are marked with “\*”, and ambiguous assignments with “-”.

Figure 5). The intensity of the Nuclear Overhauser Effect (NOE) is directly proportional to the inverse 6<sup>th</sup> power of the corresponding, weighted proton-proton distance. In sufficiently concentrated samples, modern NMR equipment allows for NOE detection up to a distance of roughly 5 Å. In samples of lower concentration or in the case of minor conformers such as **1<sub>ct</sub>** and **1<sub>tc</sub>**, the individual cut-off distance can be significantly shorter because of sensitivity problems. Thus, in the applied setup for the *cis*-conformer **1<sub>tc</sub>**, even a distance of 3.69 Å (H<sub>α</sub>-H<sub>NMe</sub>) was not detected by NOESY experiments (see the Supporting Information). As a result, the detected NOE contacts of H<sub>α</sub> (tc) and NMe (tc) as well as H<sub>α</sub> (ct) and Ace (ct) indicate considerably shorter distances, which is in agreement with the theoretical H<sub>α</sub>-Ace and H<sub>α</sub>-NMe distances of **1<sub>tc</sub>** and **1<sub>ct</sub>** (2.69 and 2.59 Å). In contrast, in all theoretically calculated *trans*-isomer geometries, these distances are larger than 4.5 Å (see Figure 5C). Thus, the detected NOE contacts shown in Figure 5 fully support the population of *cis*-conformers of peptide **1** in DMSO. Additionally, a comparison of the assigned structures (see Figure 5C) shows that only in the **ct** conformer is the N-terminal carbonyl group pointing away from the C<sub>α</sub> group and therefore exclusively in this conformer the C<sub>α</sub> carbon should sense a significant shielding effect of the



**Figure 5.** Assignment and structure determination of *cis* conformers based on 1D-selective/EXSY spectra. Stacked plots of 1D-selective NOESY spectra of **1** with increasing mixing time (τ<sub>m</sub>) reveal both unambiguous assignments by EXSY signals as well as distance information within the *cis* conformers by NOESY signals. This is shown for selective irradiation of Ace (ct) in (A) and for H<sub>α</sub> (tc) in (B). C) Selected geometries for dipeptide model **1** optimized at B3LYP/6-31G(d) together with distances between C<sub>α</sub> and methyl group protons.

carbonyl π-system. If the assignments of **1<sub>tt</sub>**, **1<sub>tc</sub>**, and **1<sub>ct</sub>** are correct, this must result in a considerably higher <sup>13</sup>C chemical shift of C<sub>α</sub> (ct) compared with those of the C<sub>α</sub> (tt) and C<sub>α</sub> (tc) conformers. Indeed, the experimental <sup>13</sup>C chemical shift of C<sub>α</sub> (ct) (45.2 ppm) is more than 3 ppm higher than in conformers **tt** (41.8 ppm) and **tc** (39.4 ppm), which further supports the conformer assignments. Signal overlap meant that the *cis-cis* conformations cannot be excluded experimentally (for details refer to the Supporting Information). However, theoretical considerations make the population of double *cis* peptide structure **1<sub>cc</sub>** very unlikely.

The thermodynamic constants ΔG<sub>T</sub> (change in Gibbs free energy), ΔH (change in enthalpy) and ΔS (change in entropy) of the equilibrium between the conformers **tt** and **ct** as well as **tt** and **tc** of peptide **1** (see Figure 6) were then calculated

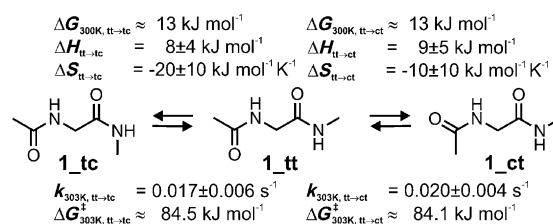


**Figure 6.** Conformer equilibria and NMR spectroscopically determined thermodynamic and kinetic constants.

based on the temperature-dependent population changes monitored by proton NMR spectroscopy (for details refer to the Supporting Information). To check the reliability of the data originating from a combination of very small and very large integrals for each of the two equilibria, two independent sets of signals were chosen (amide protons:  $H_{NAce}$  (tt),  $H_{NMe}$  (tc),  $H_{NAce}$  (ct); aliphatic protons:  $^{13}C$  satellite of  $H_{\alpha}$  (tt),  $H_{\alpha}$  (tc), Ace. (ct)). The temperature dependence of  $\Delta G_T$  for  $1_{tt} \rightarrow 1_{tc}$  is presented in Figure 7, and the thermodynamic and kinetic con-

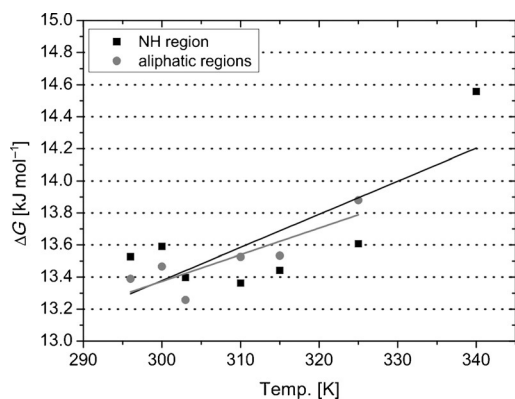


**Figure 7.** Plots of  $\Delta G$  against  $T$  for two signal sets (NH, aliphatic) of the equilibrium  $1_{tt} \rightarrow 1_{tc}$ .  $R^2$  values are 0.51 (NH) and 0.66 (aliphatic).

stants are summarized in Figure 6. For both *cis*-conformers, the experimentally determined  $\Delta H$  values are very similar ( $\Delta H_{tt \rightarrow tc} = 8 \pm 4 \text{ kJ mol}^{-1}$  and  $\Delta H_{tt \rightarrow ct} = 9 \pm 5 \text{ kJ mol}^{-1}$ ) and the  $\Delta S$  values are small ( $\Delta S_{tt \rightarrow tc} = -20 \pm 10 \text{ J mol}^{-1} \text{ K}^{-1}$ ,  $\Delta S_{tt \rightarrow ct} = -10 \pm 10 \text{ J mol}^{-1} \text{ K}^{-1}$ ), as expected for a conformer equilibrium. The experimentally determined  $\Delta G_{300K}$  values for both equilibria (ca.  $13 \text{ kJ mol}^{-1}$ ) are rather similar to the theoretical values for  $C5_{ct}$  and  $C5_{tc}$  ( $\Delta G_{sol}$ , COSMO-SAC).

The rate constants  $k$  were determined based on 1D-selective NOESY/EXSY spectra in combination with the initial rate approximation as applied recently for investigations on the formation mechanism of the central organocatalytic enamine intermediate.<sup>[45]</sup> This method is based on the work of Perrin and Dwyer<sup>[46–47]</sup> and makes use of the NOESY experiment and the chemical exchange during the chosen mixing time  $\tau_m$  (for details, additional results applying a 2D NOESY approach as well as a rate constant cross check, see the Supporting Information). Peptide **1** *cis*-conformer formation rate constants determined by 1D-selective NOESY and the initial rate approximation in  $[D_6]DMSO$  at  $303 \text{ K}$ <sup>[48]</sup> are  $k_{tt \rightarrow tc} = 0.017 \pm 0.006 \text{ s}^{-1}$  and  $k_{tt \rightarrow ct} = 0.020 \pm 0.004 \text{ s}^{-1}$ , respectively. This corresponds to activation free energies for *trans/cis* isomerization of  $\Delta G_{303}^\ddagger$  of  $+84 \text{ kJ mol}^{-1}$  in DMSO, which is a value slightly lower than the barrier of  $+89.1 \text{ kJ mol}^{-1}$  measured for NMA in water.<sup>[34]</sup> In the actual sample at a total concentration of peptide **1** of  $380 \text{ mM}$ , this translates into *cis*-conformer formation rates of approximately  $0.008 \text{ mol}/(\text{L}^{-1} \text{ s}^{-1})$ . In other words, within 1 min reaction time, a number of molecules exceeding the whole population of the main conformer  $1_{tt}$  reacts once to a minor *cis*-

conformer. Therefore, even if the populations of the *cis*-conformers  $1_{tc}$  and  $1_{ct}$  are extremely low, they are kinetically very much accessible.

## Collective analysis of experimental and theoretical data

### Structural preferences within the $1_{tt}$ , $1_{ct}$ and $1_{tc}$ conformers

The NMR data discussed in the previous section provide separated sets of signals for  $1_{tt}$ ,  $1_{ct}$ , and  $1_{tc}$  because of the high isomerization barrier of peptide bonds. The additional conformations due to rotations around  $C_{\alpha}$  ( $\Phi$  and  $\Psi$ ) postulated by the theoretical calculations (see Figure 2) cannot be resolved spectroscopically and appear as population-weighted means in the NMR spectra. To address these additional structural preferences of  $1_{tt}$ ,  $1_{ct}$ , and  $1_{tc}$  in solution, Boltzmann-weighted averages of proton–proton distances as well as  $^1H$  and  $^{13}C$  chemical shifts were calculated from the theoretical models and compared with the experimental data.

**A) The best conformation for  $1_{tt}$ :** In terms of  $\Delta G_{sol}$  (COSMO-SAC),  $C5_{tt}$  is predicted to be the best conformer, followed by  $\beta 2_{tt}$  (see Figure 3). To investigate this further, structural information was extracted from proton–proton NOE integrals in 2D-NOESY spectra between the corresponding protons (see Figure 8A). The NOE integral between  $H_{\alpha}$  protons to amide

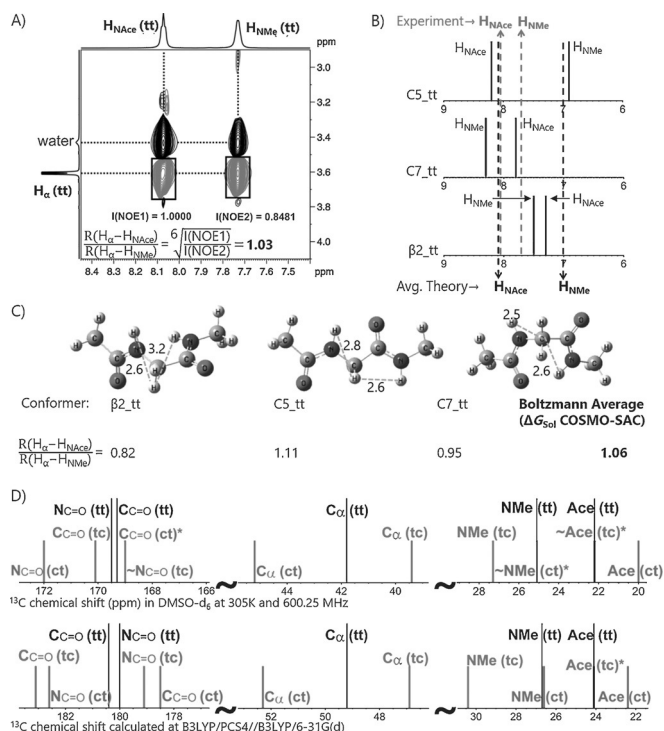


**Figure 8.** A) Section of the 2D NOESY spectrum of **1** ( $380 \text{ mM}$ ) in  $[D_6]DMSO$  at  $300 \text{ K}$  and a mixing time of  $250 \text{ ms}$ . B) Comparison of experimentally measured and theoretically calculated  $^1H$  chemical shifts [PCM/DMSO/B3LYP/PSC4/B3LYP/6-31G(d)] for the amide protons in the all-*trans* conformer of **1**. C) Boltzmann-averaged ( $\Delta G_{sol}$  COSMO-SAC, Figure 3) distance ratios  $[R(H_{\alpha}-H_{NAce})/R(H_{\alpha}-H_{NMe})]$  for all-*trans* conformers of **1**. D) Comparison of experimentally measured and theoretically calculated  $^{13}C$  chemical shifts for **1**.

protons ( $H_{\text{NAce}}$  and  $H_{\text{NMe}}$ ) were used to determine a distance ratio of 1.03 [ $R(H_{\alpha}-H_{\text{NMe}})/R(H_{\alpha}-H_{\text{NAce}})$ ]. A very similar value of 1.06 was obtained by using the Boltzmann-averaged distance ratio calculated over **C7\_tt**,  **$\beta$ 2\_tt**, and **C5\_tt** gas-phase geometries using weighted distances between  $H_{\alpha}$  and amide protons ( $H_{\text{NAce}}$  and  $H_{\text{NMe}}$ , see Figure 8C). An individual conformer analysis reveals that **C5\_tt** has a distance ratio of 1.11, whereas  **$\beta$ 2\_tt** and **C7\_tt** have distance ratios of 0.82 and 0.95, respectively. A very similar conclusion can be drawn from analysis of the  $^1\text{H}$  chemical shifts of the amide protons of **1\_tt**. These can be observed experimentally for the all-*trans* conformer at 8.03 ppm ( $H_{\text{NAce}}$  proton), 0.33 ppm downfield from the  $H_{\text{NMe}}$  proton at 7.7 ppm. Calculated  $^1\text{H}$  chemical shifts (B3LYP/PCS4/DMSO//B3LYP/6-31G(d), gas) for the all-*trans* conformers indicate that only for the **C5\_tt** conformer does the  $H_{\text{NAce}}$  signals occur downfield from the  $H_{\text{NMe}}$  signals, whereas the reverse order is predicted for the  **$\beta$ 2\_tt** and **C7\_tt** conformers (Figure 8B). Taken together, the energetics, structural, and chemical shift analyses indicates that **C5\_tt** is the preferred conformation for **1\_tt** in DMSO.

**B) The  $^{13}\text{C}$  spectral trends in 1:** The experimental  $^{13}\text{C}$  signals for the **tt**, **tc**, and **ct** conformers strongly overlap in a number of instances, which complicates the assignments for the low-abundant **tc** and **ct** isomers. By using the theoretically calculated  $^{13}\text{C}$  chemical shifts shown in Figure 8D, the assignment of the *cis*-peptide conformers can be aided substantially. Calculated absolute  $^{13}\text{C}$  shifts deviate from the experimental values by 2–10 ppm, and the three most relevant regions of the calculated  $^{13}\text{C}$  NMR spectrum for **1** in Figure 8D with signals for the carbonyl carbon (C=O),  $C_{\alpha}$  and terminal methyl carbon (Ace and NMe) are therefore shifted such that the best alignment is obtained for the **1\_tt** signals. The theoretical prediction of  $^{13}\text{C}$  shifts for Ace, NMe, and  $C_{\alpha}$  carbon of **tt**, **tc** and **ct** conformers relative to each other matches the experimentally observed trends. The calculated values verify the overlapping behavior of Ace (tc→tt) and NMe(ct→tt) carbon signals. The  $C_{\alpha}$  shifts for **1\_tc** and **1\_ct** relative to that of **1\_tt** is also supported by the theoretical results. The  $^{13}\text{C}$  shifts calculated for carbonyl carbon atoms show slightly less satisfactory agreement in an absolute sense, but again show the same relative order of signals for each individual conformer.

### Force-field based modeling

With accurate gas- and solution-phase information on the conformational ordering in dipeptide model **1** in hand, it is possible to validate the performance of commonly used force fields developed for the description of polypeptides. We here consider the AMBER94 force field as implemented in MacroModel 10.8,<sup>[49]</sup> and the AMBER99SB, CHARMM22, CHARMM22-CMAP, and AMOEAPRO13 force fields implemented in Tinker 7.1.<sup>[50]</sup>

Results for the five best conformations of **1** are collected in Table 2 together with relative gas-phase enthalpies obtained at G3(MP2)-RAD level (see the Supporting Information for a full conformational list). Whereas all force fields reproduce the **C7\_**

**Table 2.** Relative conformational energies (in  $\text{kJ mol}^{-1}$ ) for the five best conformers of **1** calculated with different force fields and the G3(MP2)-RAD compound method.

Theoretical method	<b>C7_tt</b>	<b>C5_tt</b>	<b>C5_tc</b>	<b><math>\beta</math>2_tt</b>	<b><math>\alpha</math>R_ct</b>
QM <sup>[a]</sup>	0.0	+4.2	+10.7	+11.5	+16.5
AMBER94	0.0	+8.0	+18.0	–	+22.6
AMBER99SB	0.0	+5.1	+15.8	–	+23.8
AMOBAPRO13	0.0	+15.6	+25.6	–	+12.4
CHARMM22	0.0	+3.9	+8.4	–	+26.8
CHARMM22CMAP	0.0	+7.8	+10.6	+15.6	+6.8

[a]  $\Delta H_{298}$  at G3(MP2)-RAD level.

**tt** conformation as the global minimum in the gas phase, the energy separation to the next best (**C5\_tt**) conformation is quite variable, with AMBER99SB and CHARMM22 being the most accurate methods. Energies predicted for the two *cis*-peptide conformations (**C5\_tc** and  **$\alpha$ R\_ct**) are highly variable, with the two AMBER force fields considered here being systematically too unfavorable. Predictions for the **C5\_tc** structure are quite good with both CHARMM variants, but energies for the  **$\alpha$ R\_ct** structure are either too high (CHARMM22) or too low (CHARM22CMAP) by  $10 \text{ kJ mol}^{-1}$ . A somewhat surprising finding is that all force fields (except CHARM22CMAP) fail to locate the  **$\beta$ 2\_tt** structure as a minimum on the potential energy surface. In conclusion, the performance of the force fields selected here in reproducing energies of *cis*-amide structures in dipeptide model **1** is less than optimal, and the utility of these approaches in modeling *cis* peptide structures in proteins is thus quite uncertain.

### Conclusion

QM-derived thermochemical data and detailed NMR studies predict an extended **C5\_tt** conformation for dipeptide model **1** as the preferred conformation in DMSO solution. Isomerization of the N- or C-terminal amide bond are both found to be endergonic by  $12 \text{ kJ mol}^{-1}$  at 300 K, leading to the occurrence of the *trans-cis* (**tc**) and *cis-trans* (**ct**) conformations as detectable species by NMR measurements in  $[\text{D}_6]\text{DMSO}$ . Supported by theoretical chemical shift calculations, this allowed for the complete assignment of  $^1\text{H}$  and  $^{13}\text{C}$  chemical shift data for these *cis/trans* isomers. Temperature-dependent  $^1\text{H}$  NMR measurements indicate that the *cis-trans* energy differences are mainly of enthalpic origin, which is again in line with theoretical predictions. Experimentally measured *trans/cis* isomerization rate constants show that, irrespective of their low absolute population, *cis* peptide conformers are easily accessible kinetically at 300 K. The ability to reproduce the conformational preferences of dipeptide model **1** with common protein force fields is limited, showing particular problems with the description of the *cis*-peptide conformations. This is likely to negatively impact the accurate description of protein folding processes as well as the description of unfolded protein regions with these force fields.

## Experimental Section

**Experimental details:** Dipeptide **1** (2-acetamino-*N*-methylacetamide, 380 mM) was prepared inside a melt-sealed standard 5 mm NMR tube in [D<sub>6</sub>]DMSO. NMR spectra were recorded with a Bruker Avance DRX 600 (600.13 MHz) and with a Bruker Avance III 600 (600.25 MHz) spectrometer, with the latter being equipped with a TCI cryoprobe with z-gradient. All spectra were referenced to the DMSO residual peaks (<sup>1</sup>H: 2.50 ppm, <sup>13</sup>C: 39.5 ppm).

**Computational details:** The geometries of all the conformers of **1** were optimized at the B3LYP/6–31G(d) level of theory in the gas phase.<sup>[51–52]</sup> The frequency calculations were performed at the same level of theory and all minima were confirmed with all-positive frequencies. Single-point calculations were performed at double hybrid B2-PLYP/G3MP2LARGE,<sup>[53]</sup> and composite methods G3(MP3)-RAD,<sup>[54]</sup> G3B3,<sup>[55]</sup> and CCSD(T)/CBS.<sup>[56–57]</sup> For CCSD(T)/CBS, extrapolations to the complete-basis-set (CBS) limit were carried out based on the MP2 single-point energies by the two-point extrapolation scheme using cc-pVTZ and cc-pVQZ basis set (see the Supporting Information for a detailed description).<sup>[58]</sup> The energies were calculated for a temperature of 298.15 K in the gas phase and the thermal corrections to the enthalpy and Gibb's free energy were obtained at the B3LYP/6–31G(d) level of theory. Solvent corrections for ΔG<sub>soln</sub> were calculated by using the IEFPCM,<sup>[59]</sup> SMD,<sup>[60]</sup> and COSMO-SAC<sup>[61]</sup> models in DMSO and subsequently added to the single-point energy. To calculate nuclear magnetic shielding values, the specifically optimized pcS-n (PCS2 and PCS4) type basis sets developed by Jensen were used with the B3LYP, OPBE, OLYP, and MP2 methods in the gas phase and in DMSO.<sup>[62–64]</sup> The IEFPCM is used to model implicit DMSO. The solvation energies using COSMO-SAC were calculated by using the COSMO-RS module implemented<sup>[65–66]</sup> in ADF2014 with Gaussian09 generated COSMO potential and all other calculations were performed by using Gaussian09, Rev. D.01.<sup>[67]</sup>

## Acknowledgements

Financial support by the Deutsche Forschungsgemeinschaft (SFB 749, project C6) is gratefully acknowledged.

**Keywords:** conformation analysis · density functional calculations · peptides · protein folding · protein structures

- [1] G. M. Clore, *Protein Sci.* **2011**, *20*, 229–246.
- [2] N. J. Anthis, G. M. Clore, *Q. Rev. Biophys.* **2015**, *48*, 35–116.
- [3] M. R. Jensen, M. Zweckstetter, J.-r. Huang, M. Blackledge, *Chem. Rev.* **2014**, *114*, 6632–6660.
- [4] G. Pappenberger, H. Aygün, J. W. Engels, U. Reimer, G. Fischer, T. Kiefhaber, *Nat. Struct. Mol. Biol.* **2001**, *8*, 452–458.
- [5] M. D. Beachy, D. Chasman, R. B. Murphy, T. A. Halgren, R. A. Friesner, *J. Am. Chem. Soc.* **1997**, *119*, 5908–5920.
- [6] W. D. Cornell, P. Cieplak, C. I. Bayly, I. R. Gould, K. M. Merz, D. M. Ferguson, D. C. Spellmeyer, T. Fox, J. W. Caldwell, P. A. Kollman, *J. Am. Chem. Soc.* **1995**, *117*, 5179–5197.
- [7] W. D. Cornell, I. R. Gould, P. A. Kollman, *J. Mol. Struct.* **1997**, *392*, 101–109.
- [8] H. Fujitani, A. Matsuura, S. Sakai, H. Sato, Y. Tanida, *J. Chem. Theory Comput.* **2009**, *5*, 1155–1165.
- [9] I. R. Gould, W. D. Cornell, I. H. Hillier, *J. Am. Chem. Soc.* **1994**, *116*, 9250–9256.
- [10] I. R. Gould, P. A. Kollman, *J. Phys. Chem.* **1992**, *96*, 9255–9258.
- [11] T. A. Halgren, *J. Comput. Chem.* **1996**, *17*, 490–519.
- [12] T. Head-Gordon, M. Head-Gordon, M. J. Frisch, C. L. Brooks III, J. A. Pople, *J. Am. Chem. Soc.* **1991**, *113*, 5989–5997.
- [13] a) J. Hioe, G. Savasci, H. Brand, H. Zipse, *Chem. Eur. J.* **2011**, *17*, 3781–3789; b) J. Hioe, M. Mosch, D. M. Smith, H. Zipse, *RSC Adv.* **2013**, *3*, 12403–12408.
- [14] H. Hu, M. Elstner, J. Hermans, *Proteins Struct. Funct. Bioinf.* **2003**, *50*, 451–463.
- [15] J. Jiang, Y. Wu, Z.-X. Wang, C. Wu, *J. Chem. Theory Comput.* **2010**, *6*, 1199–1209.
- [16] J. Kaminsky, F. Jensen, *J. Chem. Theory Comput.* **2007**, *3*, 1774–1788.
- [17] R. C. Neuman, V. Jonas, K. Anderson, R. Barry, *Biochem. Biophys. Res. Commun.* **1971**, *44*, 1156–1161.
- [18] S. Mathieu, R. Poteau, G. Trinquier, *J. Phys. Chem. B* **2008**, *112*, 7894–7902.
- [19] K. Nguyen, M. Iskandar, D. L. Rabenstein, *J. Phys. Chem. B* **2010**, *114*, 3387–3392.
- [20] U. Doshi, D. Hamelberg, *J. Phys. Chem. B* **2009**, *113*, 16590–16595.
- [21] D. E. Stewart, A. Sarkar, J. E. Wampler, *J. Mol. Biol.* **1990**, *214*, 253–260.
- [22] M. S. Weiss, A. Jabs, R. Hilgenfeld, *Nat. Struct. Mol. Biol.* **1998**, *5*, 676–676.
- [23] X.-L. He, H.-M. Li, Z.-H. Zeng, X.-Q. Liu, M. Wang, D.-C. Wang, *J. Mol. Biol.* **1999**, *292*, 125–135.
- [24] A. Jabs, M. S. Weiss, R. Hilgenfeld, *J. Mol. Biol.* **1999**, *286*, 291–304.
- [25] M. S. Weiss, R. Hilgenfeld, *Biopolymers* **1999**, *50*, 536–544.
- [26] C. Dugave, *cis-trans Isomerization in Biochemistry*, Wiley-VCH, Weinheim, **2006**.
- [27] D. Pal, P. Chakrabarti, *J. Mol. Biol.* **1999**, *294*, 271–288.
- [28] W. G. Touw, R. P. Joosten, G. Vriend, *Acta Crystallogr. Sect. A* **2015**, *71*, s270.
- [29] J. Zhang, M. W. Germann, *Biopolymers* **2011**, *95*, 607.
- [30] A. Genshaft, J. A. S. Moser, E. L. D'Antonio, C. M. Bowman, D. W. Christianson, *Proteins Struct. Funct. Bioinf.* **2013**, *81*, 1051–1057.
- [31] S. Ataka, H. Takeuchi, M. Tasumi, *J. Mol. Struct.* **1984**, *113*, 147–160.
- [32] A. Radzicka, L. Pedersen, R. Wolfenden, *Biochemistry* **1988**, *27*, 4538–4541.
- [33] A. G. Martínez, E. T. Vilar, A. G. Fraile, P. Martínez-Ruiz, *J. Phys. Chem. A* **2002**, *106*, 4942–4950.
- [34] T. Drakenberg, S. Forsén, *J. Chem. Soc. D* **1971**, 1404–1405.
- [35] W. L. Jorgensen, J. Gao, *J. Am. Chem. Soc.* **1988**, *110*, 4212–4216.
- [36] V. Villani, G. Alagona, C. Ghio, *Mol. Eng.* **1998**, *8*, 135–153.
- [37] Y. K. Kang, H. S. Park, *J. Mol. Struct.* **2004**, *676*, 171–176.
- [38] Y. A. Mantz, H. Gerard, R. Iftimie, G. J. Martyna, *J. Am. Chem. Soc.* **2004**, *126*, 4080–4081.
- [39] Y. A. Mantz, H. Gerard, R. Iftimie, G. J. Martyna, *J. Phys. Chem. B* **2006**, *110*, 13523–13538.
- [40] Y. A. Mantz, D. Branduardi, G. Bussi, M. Parrinello, *J. Phys. Chem. B* **2009**, *113*, 12521–12529.
- [41] L. Schäfer, C. VanAlsenoy, J. N. Scarsdale, *J. Chem. Phys.* **1982**, *76*, 1439–1444.
- [42] K. Bisetty, J. G. Catalan, H. G. Kruger, J. J. Perez, *J. Mol. Struct.* **2005**, *731*, 127–137.
- [43] G. Pohl, A. Perczel, E. Vass, G. Magyarfalvi, G. Tarczay, *Phys. Chem. Chem. Phys.* **2007**, *9*, 4698–4708.
- [44] R. A. Cormanich, R. Rittner, M. Bühl, *RSC Adv.* **2015**, *5*, 13052–13060.
- [45] M. H. Haindl, J. Hioe, R. M. Gschwind, *J. Am. Chem. Soc.* **2015**, *137*, 12835–12842.
- [46] C. L. Perrin, R. K. Gipe, *J. Am. Chem. Soc.* **1984**, *106*, 4036–4038.
- [47] C. L. Perrin, T. J. Dwyer, *Chem. Rev.* **1990**, *90*, 935–967.
- [48] Rate constants were determined at elevated temperature (303 K) to increase the exchange rates and thereby improve the signal to noise ratios.
- [49] Schrödinger Release 2015–2: MacroModel, version 10.8, Schrödinger, LLC, New York, NY, USA, 2015.
- [50] J. W. Ponder, Tinker Software Tools for Molecular Design, version 7.1, Dept. of Chemistry, Washington University, Missouri, USA, 2015.
- [51] A. D. Becke, *J. Chem. Phys.* **1993**, *98*, 5648–5652.
- [52] P. C. Hariharan, J. A. Pople, *Theor. Chim. Acta.* **1973**, *28*, 213–222.
- [53] D. C. Graham, A. S. Menon, L. Goerigk, S. Grimme, L. Radom, *J. Phys. Chem. A* **2009**, *113*, 9861–9873.
- [54] D. J. Henry, C. J. Parkinson, L. Radom, *J. Phys. Chem. A* **2002**, *106*, 7927–7936.
- [55] A. G. Baboul, L. A. Curtiss, P. C. Redfern, K. Raghavachari, *J. Chem. Phys.* **1999**, *110*, 7650.

- [56] A. Halkier, T. Helgaker, P. Jørgensen, W. Klopper, H. Koch, J. Olsen, A. K. Wilson, *Chem. Phys. Lett.* **1998**, *286*, 243–252.
- [57] L. Goerigk, A. Karton, J. M. Martin, L. Radom, *Phys. Chem. Chem. Phys.* **2013**, *15*, 7028–7031.
- [58] T. H. Dunning Jr, *J. Chem. Phys.* **1989**, *90*, 1007–1023.
- [59] S. Miertuš, E. Scrocco, J. Tomasi, *Chem. Phys.* **1981**, *55*, 117–129.
- [60] A. V. Marenich, C. J. Cramer, D. G. Truhlar, *J. Phys. Chem. B* **2009**, *113*, 6378–6396.
- [61] R. Xiong, S. I. Sandler, R. I. Burnett, *Ind. Eng. Chem. Res.* **2014**, *53*, 8265–8278.
- [62] F. Jensen, *J. Chem. Theory Comput.* **2008**, *4*, 719–727.
- [63] T. Zhu, X. He, J. Z. Zhang, *Phys. Chem. Chem. Phys.* **2012**, *14*, 7837–7845.
- [64] T. Zhu, J. Z. Zhang, X. He, *J. Chem. Theory Comput.* **2013**, *9*, 2104–2114.
- [65] C. C. Pye, T. Ziegler, E. Van Lenthe, J. N. Louwen, *Can. J. Chem.* **2009**, *87*, 790–797.
- [66] ADF2014 COSMO-RS, SCM, Theoretical Chemistry, Vrije Universiteit, Amsterdam, The Netherlands, <http://www.scm.com>.
- [67] M. J. Frisch, G. W. Trucks, H. B. Schlegel, G. E. Scuseria, M. A. Robb, J. R. Cheeseman, G. Scalmani, V. Barone, B. Mennucci, G. A. Petersson, H. Nakatsuji, M. Caricato, X. Li, H. P. Hratchian, A. F. Izmaylov, J. Bloino, G. Zheng, J. L. Sonnenberg, M. Hada, M. Ehara, K. Toyota, R. Fukuda, J. Hasegawa, M. Ishida, T. Nakajima, Y. Honda, O. Kitao, H. Nakai, T. Vreven, J. A. Montgomery Jr., J. E. Peralta, F. Ogliaro, M. J. Bearpark, J. Heyd, E. N. Brothers, K. N. Kudin, V. N. Staroverov, R. Kobayashi, J. Normand, K. Raghavachari, A. P. Rendell, J. C. Burant, S. S. Iyengar, J. Tomasi, M. Cossi, N. Rega, N. J. Millam, M. Klene, J. E. Knox, J. B. Cross, V. Bakken, C. Adamo, J. Jaramillo, R. Gomperts, R. E. Stratmann, O. Yazyev, A. J. Austin, R. Cammi, C. Pomelli, J. W. Ochterski, R. L. Martin, K. Morokuma, V. G. Zakrzewski, G. A. Voth, P. Salvador, J. J. Dannenberg, S. Dapprich, A. D. Daniels, Ö. Farkas, J. B. Foresman, J. V. Ortiz, J. Cioslowski, D. J. Fox, Gaussian, Inc., Wallingford, CT, USA, **2009**.

Received: April 19, 2016

Published online on August 18, 2016

## 2.1 Supporting Information

For: Conformational Preferences in Small Peptide Models: The Relevance of *cis/trans*-Conformations

---

### 2.1.1 Technical Details

**Force field-based calculation:** Maestro 10.2, MacroModel<sup>1</sup> and Tinker 7.1<sup>2</sup> were employed for molecular mechanics (MM)-based conformational searches using the AMBER94, AMBER99SB, MM3\*, OPLS\_2005, MMFFs, AMOBAPRO13, CHARMM22, and CHARMM22CMAP force field (FF) parameters.

**Quantum mechanics calculations:** The geometries of all conformers of 2-acetamino-N-methylacetamide (**1**) were optimized at the B3LYP/6-31G(d) level of theory in the gas phase.<sup>3</sup> The frequency calculations were performed at the same level of theory and all minima were confirmed with all positive frequencies. Single point calculations were done at double hybrid B2-PLYP/G3MP2LARGE,<sup>4</sup> composite methods G3(MP3)-RAD,<sup>5</sup> G3B3<sup>6</sup> and CCSD(T)/CBS<sup>7</sup> on B3LYP/6-31G(d) optimized geometries.

#### G3(MP2)-RAD scheme:

$$E(\text{G3(MP2)-RAD}) = E(\text{CCSD(T)/6-31G(d)}) + (\text{MP2/G3MP2large} - \text{MP2(FC)/6-31G(d)}) \quad (1)$$

#### G3B3 scheme:

$$E(\text{G3B3}) = E(\text{QCISD/6-31G(d)}) + \text{DE}(+) + \text{DE}(2\text{df,p}) + \text{DE}(\text{G3large}) \quad (2)$$

$$\text{DE}(+) = E(\text{MP4/6-31+G(d)}) - E(\text{MP4/6-31G(d)}) \quad (3)$$

$$\text{DE}(2\text{df,p}) = E(\text{MP4/6-31G}(2\text{df,p})) - E(\text{MP4/6-31G(d)}) \quad (4)$$

$$\text{DE}(\text{G3large}) = E(\text{MP2/G3large}) - E(\text{MP2/6-31G}(2\text{df,p})) - E(\text{MP2/6-31+G(d)}) + E(\text{MP2/6-31G(d)}) \quad (5)$$

#### CCSD(T)/CBS scheme:

Extrapolations to the complete-basis-set (CBS) limit for CCSD(T) were carried out via separate extrapolation of HF and MP2 correlation energies by the two-point extrapolation scheme using cc-pVTZ and cc-pVQZ basis set.<sup>8</sup>

$$E(\text{HF}\backslash\text{CBS}) = \frac{E(\text{HF}\backslash\text{cc-pVTZ}) 3^5 - E(\text{HF}\backslash\text{cc-pVQZ}) 4^5}{3^5 - 4^5} \quad (6)$$

$$E_c(\text{MP2}\backslash\text{CBS}) = \frac{E_c(\text{MP2}\backslash\text{cc-pVTZ} - \text{HF}\backslash\text{cc-pVTZ}) 3^3 - E_c(\text{MP2}\backslash\text{cc-pVQZ} - \text{HF}\backslash\text{cc-pVQZ}) 4^3}{3^3 - 4^3} \quad (7)$$

$$E(\text{MP2}\backslash\text{CBS}) = E_c(\text{MP2}\backslash\text{CBS}) + E(\text{HF}\backslash\text{CBS}) \quad (8)$$

$$E(\text{CCSD(T)}\backslash\text{CBS}) = E(\text{MP2}\backslash\text{CBS}) + E(\text{CCSD(T)}\backslash\text{cc-pVDZ}) - E(\text{MP2}\backslash\text{cc-pVDZ}) \quad (9)$$

The energies were calculated for a temperature of 298.15 K in the gas phase and the thermal corrections to the enthalpy and Gibb's free energy were obtained at the B3LYP/6-31G(d) level of theory. ZPE corrections were scaled by a factor of 0.9806 and 0.960 for G3(MP2)-RAD and G3B3 respectively. For isotropic chemical shieldings, the specifically optimized pcS-4 basis set developed by Jensen was used with B3LYP in the gas phase and in DMSO.<sup>9</sup> The IEFPCM<sup>10</sup> model is used for modelling implicit DMSO. The solvent correction for  $\Delta G_{\text{solv}}$  was calculated at using IEFPCM and COSMO-RS<sup>11</sup> models in DMSO and subsequently added to the single point energy. The solvation energies using COSMO-SAC were calculated using COSMO-RS module implemented in ADF2014<sup>12</sup> with Gaussian09 generated COSMO potential and all other calculations are performed using Gaussian09, Rev. D.01.<sup>13</sup>

## 2.1.2 Procedure for Conformational Search

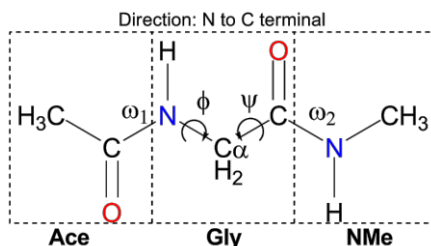


**Figure S2-1.** [Figure S1] The systematic diagram of 2-acetamino-N-methylacetamide, referred to as glycine dipeptide (**1**) in the text.

**Table S2-1.** [Table S1] Definitions and markers used for the nomenclature in classifying the peptide geometry.

PHI ( $\phi$ )	PSI ( $\psi$ )	Backbone C alpha( $C_\alpha$ ) geometry marker
0.0 – 120.0	0.0 – 120.0	$\alpha_L$
120.0 – 240.0	0.0 – 120.0	$\beta_2$
240.0 – 360.0	0.0 – 120.0	$C_{7,eq}$
0.0 – 120.0	120.0 – 240.0	$\alpha_D$
120.0 – 240.0	120.0 – 240.0	$C_5$
240.0 – 360.0	120.0 – 240.0	$\beta$
0.0 – 120.0	240.0 – 360.0	$C_{7,ax}$
120.0 – 240.0	240.0 – 360.0	$\alpha$
240.0 – 360.0	240.0 – 360.0	$\alpha_R$

In case of glycine dipeptide  $C_{7,eq} = C_{7,ax} = C_7$ ,  $\alpha' = \beta_2$ ,  $\alpha_D = \beta$ ,  $\alpha_L = \alpha_D$ ; Peptide bond conformation marker: *trans* (t) =  $180^\circ \pm 15^\circ$  & *cis* (c) =  $0^\circ \pm 15^\circ$

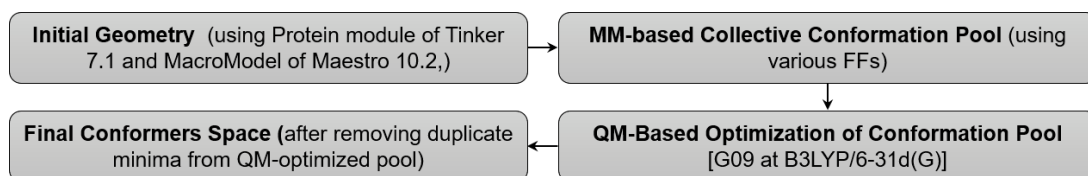
### 2.1.2.1 Systematic search (SS) procedure

To explore the conformational space of glycine dipeptide **1** in a systematic manner, four dihedral angles mentioned in Figure S2-1 i.e.  $\Phi$  (phi,  $CNC_\alpha C$ ),  $\Psi$  (psi,  $NCC_\alpha N$ ),  $\omega_1$  (N terminal peptide bond) and  $\omega_2$  (C terminal peptide bond) were varied in a systematic way. To obtain initial geometries, dihedral angle  $\Phi$  is varied from 0 to 180 with a 10 degree interval, for each value of  $\Phi$  the dihedral angle  $\Psi$  is varied from 0 to 180 with a 10 degree interval and finally for each combination of  $\Phi$  and  $\Psi$ , four combinations of  $\omega_1$  and  $\omega_2$  were used [(180, 180), (180,0), (0, 180) and (0, 0)]. All other distances, angles, and dihedrals needed to define the geometry of **1** have been taken from its extended  $C_5$ , all *trans* conformer that is optimized at B3LYP/6-31G(d) level in the gas phase. The above specified systematic variations generated 1444 ( $\Phi * \Psi * \omega_1 * \omega_2$ ,  $19 * 19 * 2 * 2$ ) initial geometries. These structures were subject to optimization at B3LYP/6-31G(d) level in the gas phase. This leads to 30 unique conformers, after removing duplicates and other modified structures resulted from different bond formation during optimization. These 30 structures were further screened using frequencies calculated at B3LYP/6-31G(d) level, to characterize these stationary points as true minima, transitional states and saddle points of different order. Finally, this exercise leads to 14 unique true minima on the PES of glycine dipeptide **1** (Table S2-2) and 16 other stationary points.

### 2.1.2.2 Force field-based approach

Maestro 10.2.011, MacroModel, and Tinker 7.1 were employed for molecular mechanics (MM)-based conformational searches using the AMBER94, AMBER99SB, MM3\*, OPLS\_2005, MMFFs, AMOBAPRO13, CHARMM22 and CHARMM22CMAP force field (FF) parameters. For MacroModel the mixed torsional/low-mode sampling method with extended torsion sampling options were chosen for conformational sampling. An energy window of 63 kJ/mol (~15 kcal/mol) was used for exploring the potential energy surface of glycine dipeptide **1**. Scheme S2-1 depicts the strategy to explore the conformation space using force field based molecular mechanics. For Tinker,

the protein module is used to generate initial structures that were later subjected to conformational searches using the scan module with an energy window of 20 kcal/mol. Other criteria are set as follows: automatic selection of torsion angle (0), search direction is set to 5 with a convergence criterion of 0.0001 kcal/mol. A collective pool of different structures was obtained with the AMBER94, MM3\*, OPLS\_2005 and MMFFs force fields-based conformation search. All conformers were then subjected to optimization with the B3LYP/6-31G(d) hybrid functional in the gas phase. To get the final conformational space, duplicate minima were removed from the optimized conformation pool obtained in the last step.



**Scheme S2-1.** [Scheme S1] Strategy for force field-based conformation search.

## 2.1.3 Energies and Structural Parameters for Glycine Dipeptide 1

### 2.1.3.1 Gas phase calculations

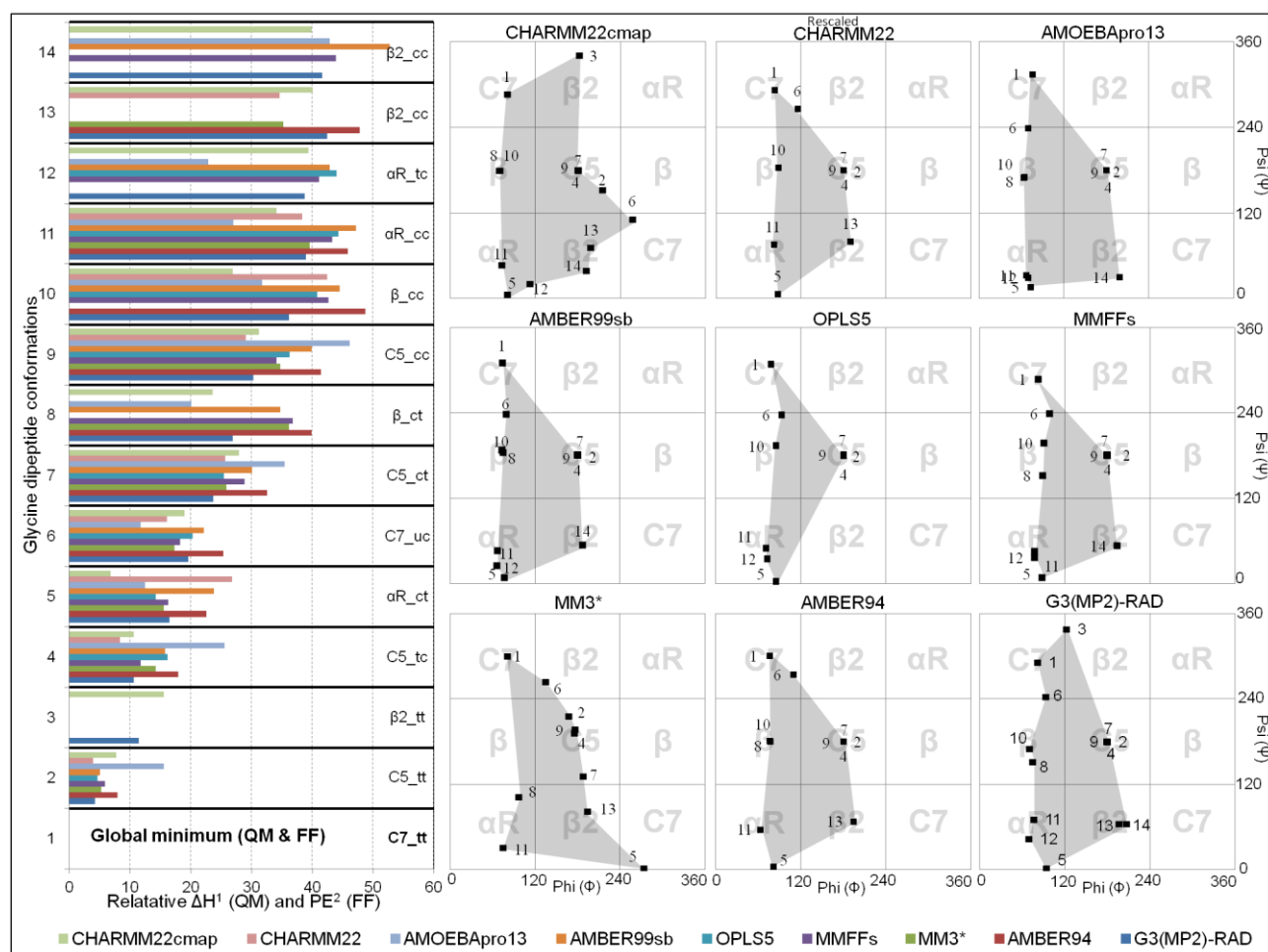


**Figure S2-2.** [Figure S2] A comparison of relative energies [ $^1\Delta H_{298}$  at G3(MP2)-RAD for QM and  $^2$ Potential Energy (PE) for FF] and structural information ( $\phi$  and  $\psi$ ) of conformational space of glycine dipeptide 1.

**Table S2-2.** [Table S2] List of minima for **1** at B3LYP/6-31G(d) level in the gas phase, located by a systematic conformational search.

Marker	Molecule <sup>1</sup>	Low Frequency			Cor. $\delta H$	Cor. $\delta G$	B3LYP/6-31G(d)	$\Phi$	$\Psi$	$\omega_1$	$\omega_2$	$C_\alpha$	Peptide	Rel. $\Delta E$
1	Gly_0_30_180_180	-8	-6	0	0.170862	0.122111	-456.5375163	82	292	174	184	C7	tt	0.0
2	Gly_20_160_180_180	-10	-3	-3	0.170286	0.118913	-456.5361652	180	180	180	180	C5	tt	3.5
3	Gly_0_40_180_180	0	0	0	0.170546	0.120943	-456.5333573	123	338	188	176	$\beta_2$	tt	10.9
4	Gly_0_160_180_0	-5	0	0	0.170278	0.119786	-456.5331903	180	180	180	4	C5	tc	11.4
5	Gly_20_40_0_180	-4	0	0	0.170461	0.121583	-456.5302838	94	2	6	182	$\alpha R$	ct	19.0
6	Gly_50_0_180_0	-9	-5	-3	0.170901	0.121606	-456.5298830	94	243	164	1	C7	uc	20.0
7	Gly_180_90_0_180	0	0	0	0.170076	0.119908	-456.5288423	180	180	360	180	C5	ct	22.8
8	Gly_20_180_0_180	-8	-4	0	0.170384	0.121386	-456.5270436	75	152	349	178	$\beta$	ct	27.5
9	Gly_180_130_0_0	-12	-11	-2	0.169940	0.120317	-456.5257541	180	180	360	4	C5	cc	30.9
10	Gly_40_170_0_0	-9	-8	0	0.170227	0.121536	-456.5227786	71	170	347	3	$\beta$	cc	38.7
11	Gly_20_60_0_0	-12	0	0	0.170463	0.121897	-456.5215423	77	71	358	6	$\alpha R$	cc	41.9
12	Gly_20_40_180_0	-14	-2	0	0.170221	0.120072	-456.5206067	70	43	186	4	$\alpha R$	tc	44.4
13	Gly_180_60_0_0	-4	0	0	0.170490	0.121543	-456.5203164	197	64	350	356	$\beta_2$	cc	45.2
14	Gly_170_20_0_0	-10	-3	0	0.170403	0.121061	-456.5200926	208	65	351	4	$\beta_2$	cc	45.7

<sup>1</sup>Notation specifies the starting geometry in the following manner, Gly\_  $\Phi$ \_  $\Psi$ \_  $\omega_1$ \_  $\omega_2$ .

**Table S2-3.** [Table S4] Starting conformations and relative energies (in kJ/mol) for conformers of **1** calculated with different force fields and the G3(MP2)-RAD compound method.

G3(MP2)-RAD			AMBER94			AMBER99SB			AMOBAPRO13			CHARMM22			CHARMM22CMAP		
Marker	Conf.	Rel. $\Delta H_{298}$	No.	Conf.	Rel. Pot. $E$	No.	Conf.	Rel. Pot. $E$	No.	Conf.	Rel. Pot. $E$	No.	Conf.	Rel. Pot. $E$	No.	Conf.	Rel. Pot. $E$
1	C7_tt	0.0	1	C7_tt	0.0	4	C7_tt	0.0	3	C7_tt	0.0	4	C7_tt	0.0	6	C7_tt	0.0
2	C5_tt	4.2	2	C5_tt	8.0	1	C5_tt	5.1	5	C5_tt	15.6	1	C5_tt	3.9	1	C5_tt	7.8
3	$\beta_2$ _tt	11.5	-	-	-	-	-	-	-	-	-	-	-	-	19	$\beta_2$ _tt	15.6
4	C5_tc	10.7	3	C5_tc	18.0	3	C5_tc	15.8	13	C5_tc	25.6	3	C5_tc	8.4	3	C5_tc	10.6
5	$\alpha R$ _ct	16.5	4	$\alpha R$ _ct	22.6	7	$\alpha R$ _ct	23.8	7	$\alpha R$ _ct	12.4	6	$\alpha R$ _ct	26.8	27	$\alpha R$ _ct	6.8
6	C7_tc	19.6	5	C7_tc	25.3	9	$\beta$ _tc	22.1	18	$\beta$ _tc	11.7	7	C7_tc	16.1	22	C7_tc	19.0
7	C5_ct	23.7	6	C5_ct	32.6	2	C5_ct	30.1	16	C5_ct	35.4	2	C5_ct	25.6	2	C5_ct	27.9
8	$\beta$ _ct	26.9	7	$\beta$ _ct	39.9	6	$\beta$ _ct	34.8	2	$\beta$ _ct	20.1	-	-	-	11	$\beta$ _ct	23.6
9	C5_cc	30.3	8	C5_cc	41.4	5	C5_cc	39.8	12	C5_cc	46.2	5	C5_cc	29.0	9	C5_cc	31.3
10	$\beta$ _cc	36.2	11	$\beta$ _cc	48.7	10	$\beta$ _cc	44.5	6	$\beta$ _cc	31.7	10	$\beta$ _cc	42.5	15	$\beta$ _cc	26.9
11	$\alpha R$ _cc	39.0	9	$\alpha R$ _cc	45.9	11	$\alpha R$ _cc	47.2	14	$\alpha R$ _cc	27.0	11	$\alpha R$ _cc	38.4	30	$\alpha R$ _cc	34.1
12	$\alpha R$ _tc	38.8	-	-	-	8	$\alpha R$ _tc	42.9	17	$\alpha R$ _tc	22.9	-	-	-	24	$\alpha R$ _tc	39.3
13	$\beta_2$ _cc	42.5	10	$\beta_2$ _cc	47.8	-	-	-	-	-	-	9	$\beta_2$ _cc	34.6	49	$\beta_2$ _cc	40.1
14	$\beta_2$ _cc	41.6	-	-	-	12	$\beta_2$ _cc	52.8	15	$\beta_2$ _cc	42.9	-	-	-	32	$\beta_2$ _cc	39.8

## 2.1.3.2 Effects of solvent on the conformational preference

**Table S2-4.** [Table S7] Rel.  $\Delta G_{298}$  plus solvation energies (kJ/mol) for **1** in DMSO using the COSMO-SAC, IEFPCM and SMD solvation models.

SI	Conf.	Rel. $\Delta G_{298}$	Rel. $\Delta G_{Sol}$		
		G3(MP2)-RAD (kJ/mol)	B3LYP/6-31G(d), COSMO-SAC	HF/6-31G(d), IEFPCM, UAHF	HF/6-31G(d), SMD
1	C7_tt	2.7	8.0	16.7	15.7
2	C5_tt	0.0	0.0	0.0	0.0
3	C5_tc	8.8	12.3	8.6	9.1
4	$\beta$ 2_tt	11.9	4.7	6.1	7.2
5	$\alpha$ R_ct	18.8	17.3	12.9	14.2
6	C7_uc	20.9	27.3	26.1	25.3
7	C5_ct	22.7	12.1	11.7	13.1
8	$\beta$ _ct	29.0	13.4	13.6	15.2
9	C5_cc	30.7	23.8	19.4	20.5
10	$\beta$ _cc	39.0	26.5	21.5	24.2
11	$\alpha$ R_tc	42.1	37.0	34.6	36.2
12	$\alpha$ R_cc	37.8	15.2	18.7	20.9
13	$\beta$ 2_cc	42.7	39.2	34.2	35.9
14	$\beta$ 2_cc	44.6	39.5	37.5	38.8

**Table S2-5.** [Table S8] A list of **1** conformers obtained through optimization in implicit DMSO using the IEFPCM model at B3LYP/6-31G(d) level and solvation energies ( $\Delta G_{solv}$ ) calculated at HF/6-31G(d) level using UAHF radii.

SI.	Marker	$\Phi$	$\Psi$	$\omega_1$	$\omega_2$	C $\alpha$	Peptide	Rel. $\Delta E$	$\Delta G_{solv}$ DMSO
1	2	176.0	190.1	182.1	178.8	C5	tt	0.0	-161.4
2	1	103.4	355.8	181.8	178.0	C7	tt	2.0	-172.8
3	29	289.6	158.7	184.7	179.1	$\beta$	tt	3.7	-175.6
4	21	75.8	161.2	351.8	180.0	$\beta$	ct	9.4	-180.9
5	20	178.1	190.6	2.5	181.8	C5	ct	10.8	-173.8
6	19	94.4	357.7	359.5	181.5	C7	ct	11.2	-170.8
7	5	95.4	356.4	359.3	180.4	C7	ct	11.8	-168.5
8	30	272.2	186.3	186.4	359.4	$\beta$	tc	11.9	-178.7
9	12	64.8	49.4	178.8	2.8	$\alpha$ R	tc	24.3	-182.1
10	11	81.5	72.2	357.5	4.9	$\alpha$ R	cc	31.8	-168.2
11	14	213.3	56.9	354.4	2.8	$\beta$ 2	cc	37.1	-169.4

30 conformers that are located using the systematic search approach as described in the previous section, were subject to re-optimization at B3LYP/6-31G(d) level under implicit solvent conditions. DMSO is used as a solvent with the IEFPCM model and UAHF radii. Only true minima are reported and marker entries in the tables can be used to trace the starting gas phase stationary point that later converged to the respective minima under implicit solvation re-optimization.

## 2.1.4 Calculated Isotropic Shielding

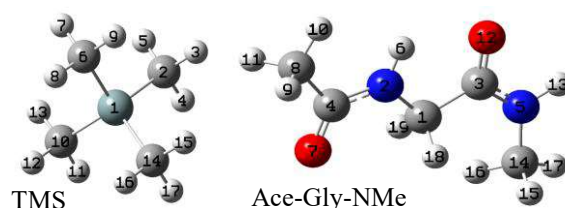


**Figure S2-3.** [Figure S4] Diagram of tetramethylsilane (TMS) and Ace-Gly-NMe (**1**), atoms are marked with numeric label. TMS is used as the reference for the calculation of chemical shifts.

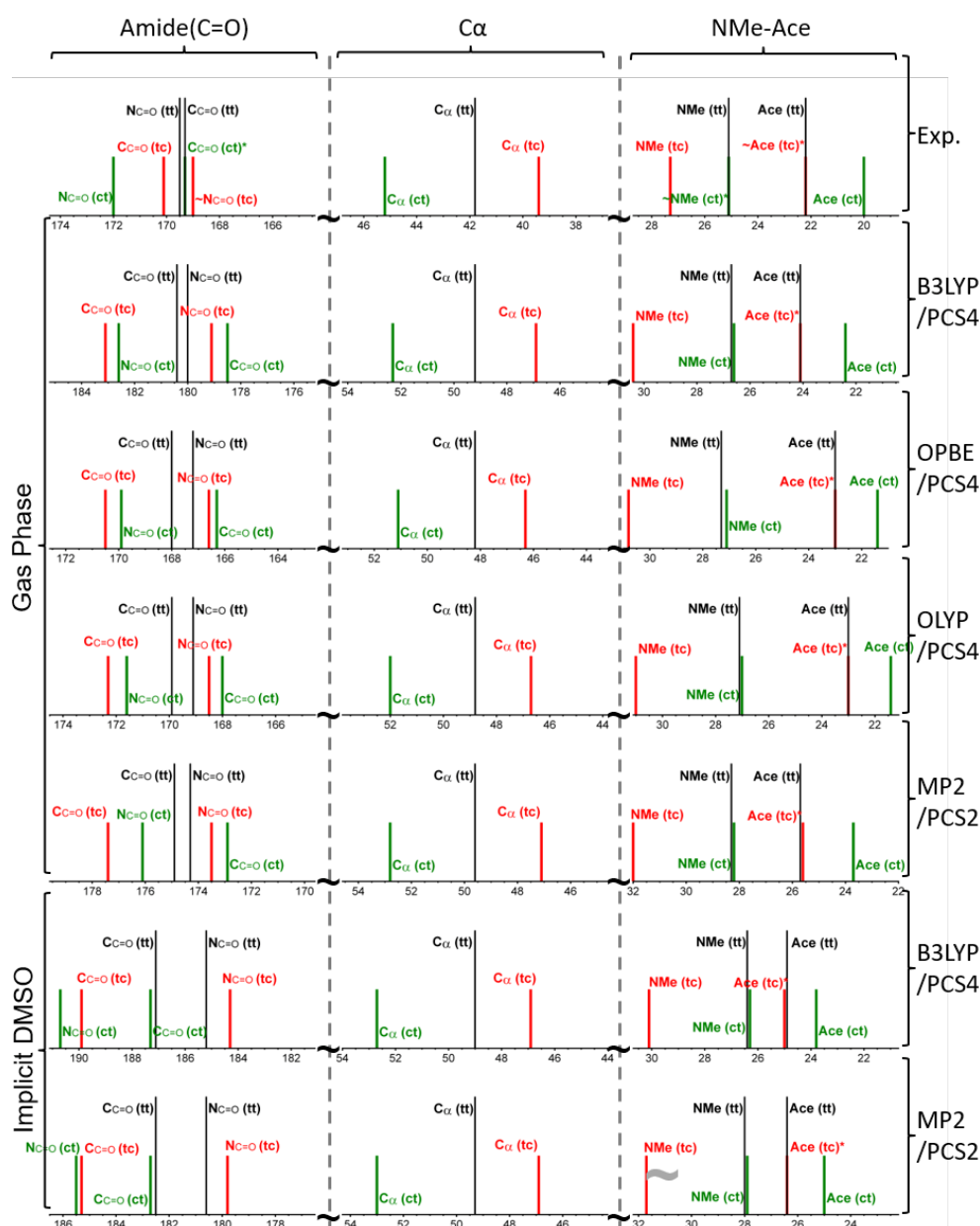


**Figure S2-4.** [Figure S5] Comparison of the experimentally measured and theoretically calculated  $^{13}\text{C}$  chemical shifts for **1** at different levels of theory using geometries optimized at B3LYP/6-31G(d) level in the gas phase. The conformers are weighted using Boltzmann avg. populations based on  $\Delta G_{298}$  energies at G3(MP2)-RAD level.

**Table S2-6.** [Table S15] Isotropic shielding values for TMS at different levels of theory using the gas phase B3LYP/6-31G(d) geometry. See Figure S2-3 for labels.

Label	1	2	6	10	14	3	4	5	7	8	9	11	12	13	15	16	17	Avg. Signal	
Symbol	Si	C	C	C	C	H	H	H	H	H	H	H	H	H	H	H	H	C	H
B3LYP/PCS4, Gas	321.9	179.6	179.6	179.6	179.6	31.5	31.5	31.4	31.4	31.5	31.5	31.4	31.5	31.4	31.5	31.4	31.4	179.6	31.4
B3LYP/PCS4, DMSO	321.6	180.9	180.8	180.8	180.8	31.4	31.4	31.4	31.4	31.4	31.4	31.4	31.4	31.4	31.4	31.4	31.4	180.8	31.4
MP2/PCS2, Gas	358.4	196.2	196.1	196.2	196.2	31.4	31.4	31.4	31.4	31.4	31.4	31.4	31.4	31.4	31.4	31.4	31.4	196.2	31.4
MP2/PCS2, DMSO	358.1	197.3	197.3	197.3	197.3	31.3	31.3	31.3	31.3	31.3	31.3	31.3	31.3	31.3	31.3	31.3	31.3	197.3	31.3
OPBE/PCS4, Gas	351.4	184.7	184.7	184.7	184.7	31.3	31.3	31.3	31.3	31.3	31.3	31.3	31.3	31.3	31.3	31.3	31.3	184.7	31.3
OLYP/PCS4, Gas	337.2	180.8	180.8	180.8	180.7	31.4	31.4	31.4	31.4	31.4	31.4	31.4	31.4	31.4	31.4	31.4	31.4	180.8	31.4

**Table S2-7.** [Table S16] Isotropic shielding values for **1** calculated at B3LYP/PCS4//B3LYP/6-31G(d) level in the gas phase. See Figure S2-3 for labels.

Label->	1	2	3	4	5	6	7	8	9	10	11	12	13	14	15	16	17	18	19	
FileName	Conf.	C	N	C	C	N	H	O	C	H	H	H	O	H	C	H	H	H	H	
Gly_0_30_180_180	C7_tt	126.8	115.2	-1.3	-3.7	127.8	25.6	-74.3	155.1	29.4	30.0	29.4	-81.3	24.0	153.4	27.3	29.2	29.2	28.5	27.0
Gly_0_40_180_180	$\beta$ 2_tt	131.0	117.9	0.1	-0.5	138.0	26.2	-94.0	154.9	29.3	30.0	29.4	-70.7	25.7	153.2	27.1	29.2	29.2	28.3	26.4
Gly_20_160_180_180	C5_tt	131.6	125.4	-0.6	0.7	136.2	24.7	-94.4	155.6	29.8	29.5	29.5	-60.5	26.7	152.7	29.1	27.0	29.1	27.6	27.6
Gly_0_160_180_0	C5_tc	132.7	124.1	-3.5	0.5	137.5	24.5	-94.3	155.5	29.5	29.8	29.5	-72.2	26.5	149.2	28.6	28.5	28.8	27.6	27.5
Gly_20_40_180_0	$\alpha$ R_tc	128.0	122.1	-0.3	0.1	138.3	26.1	-112.7	155.9	29.4	30.0	29.5	-106.4	26.7	146.2	28.3	28.5	28.8	28.1	27.3
Gly_50_0_180_0	C7_uc	136.6	116.9	-4.9	-2.4	134.4	25.5	-86.0	154.9	29.5	29.9	29.5	-74.6	26.7	147.6	27.1	28.9	28.6	28.7	26.6
Gly_180_90_0_180	C5_ct	129.7	131.6	1.6	1.2	137.3	25.3	-109.3	155.4	29.6	29.6	29.6	-68.5	26.9	152.4	27.0	29.1	29.1	27.6	27.6
Gly_20_180_0_180	$\beta$ _ct	127.4	125.7	-1.2	-5.5	137.5	26.8	-127.0	157.7	29.0	29.7	29.6	-77.9	26.7	152.5	27.1	29.1	29.1	28.2	27.6
Gly_20_40_0_180	$\alpha$ R_ct	126.8	124.0	1.0	-3.9	135.8	26.4	-123.0	157.5	29.6	29.5	29.6	-59.6	25.2	153.1	29.1	27.1	29.1	27.9	27.6
Gly_170_20_0_0	$\beta$ 2_cc	125.6	125.5	-1.2	-2.0	134.3	26.8	-120.9	156.7	29.5	29.5	29.5	-113.7	26.6	146.6	28.3	28.5	28.8	27.3	27.7
Gly_180_130_0_0	C5_cc	130.7	130.0	-1.2	1.0	139.4	25.2	-110.4	155.3	29.5	29.5	29.5	-81.0	26.5	149.3	28.6	28.6	28.7	27.6	27.5
Gly_180_60_0_0	$\beta$ 2_cc	125.4	125.3	-2.1	-2.8	133.7	26.7	-125.8	156.7	29.6	29.5	29.5	-119.9	26.7	148.5	27.9	28.6	28.8	27.5	27.8
Gly_20_60_0_0	$\alpha$ R_cc	128.3	126.8	-2.7	-3.9	135.4	26.4	-117.4	156.6	28.8	29.5	29.7	-111.2	26.7	147.1	28.3	28.5	28.7	27.7	27.6
Gly_40_170_0_0	$\beta$ _cc	129.8	130.7	-2.9	-5.5	140.5	26.8	-127.9	158.0	29.4	29.7	29.6	-97.1	26.6	148.5	28.5	28.5	28.7	27.8	27.6

**Table S2-8.** [Table S17] Isotropic shielding values for **1** calculated at B3LYP/PCS4, DMSO//B3LYP/6-31G(d) level using gas phase geometries. IEFPCM is used to model implicit DMSO. See Figure S2-3 for labels.

Label->	1	2	3	4	5	6	7	8	9	10	11	12	13	14	15	16	17	18	19	
FileName	Conf.	C	N	C	C	N	H	O	C	H	H	H	O	H	C	H	H	H	H	
Gly_0_30_180_180	C7_tt	128.7	107.4	-8.5	-7.7	120.7	23.6	-27.1	155.8	29.4	29.5	29.4	-22.2	23.1	154.9	27.6	28.9	29.0	27.5	26.1
Gly_0_40_180_180	$\beta$ 2_tt	131.6	108.6	-7.5	-6.5	129.4	24.1	-26.6	155.4	29.3	29.4	29.5	-2.4	23.9	154.7	27.4	29.0	28.9	27.3	25.8
Gly_20_160_180_180	C5_tt	132.9	113.2	-5.5	-3.2	130.5	23.2	-26.8	155.9	29.4	29.5	29.5	-6.0	24.5	154.2	28.9	27.3	28.9	26.6	26.6
Gly_0_160_180_0	C5_tc	133.9	112.6	-9.0	-3.5	128.6	23.1	-27.6	155.8	29.5	29.4	29.5	-11.5	24.8	150.7	28.5	28.3	28.5	26.5	26.4

Gly_20_40_180_0	$\alpha$ R_tc	129.0	109.5	-9.7	-6.6	125.5	23.8	-35.3	156.2	29.4	29.4	29.5	-24.0	25.0	148.0	28.3	28.2	28.6	26.5	26.8
Gly_50_0_180_0	C7_uc	137.8	110.3	-11.2	-7.2	125.7	23.7	-37.8	155.4	29.5	29.4	29.4	-11.0	25.0	148.3	27.4	28.6	28.3	27.5	25.8
Gly_180_90_0_180	C5_ct	131.3	117.8	-4.8	-5.5	132.1	24.2	-28.3	155.4	29.2	29.2	29.8	-6.1	24.6	154.1	27.4	28.9	28.9	26.4	26.4
Gly_20_180_0_180	$\beta$ _ct	129.6	112.4	-7.6	-13.5	130.8	25.1	-52.4	157.0	28.9	29.0	29.9	-12.0	24.5	154.2	27.4	28.9	28.9	26.7	26.4
Gly_20_40_0_180	$\alpha$ R_ct	127.4	111.2	-6.8	-10.7	128.2	24.6	-45.9	157.3	29.3	29.1	29.9	9.2	23.6	154.7	28.9	27.4	28.9	26.8	26.6
Gly_170_20_0_0	$\beta$ 2_cc	127.1	113.8	-9.0	-9.0	123.2	25.1	-43.6	156.5	29.2	28.9	29.8	-35.7	24.9	148.4	28.4	28.2	28.5	26.0	27.0
Gly_180_130_0_0	C5_cc	132.1	117.0	-8.2	-5.8	130.2	24.1	-29.5	155.3	29.1	29.1	29.8	-11.3	24.8	150.8	28.5	28.4	28.5	26.3	26.2
Gly_180_60_0_0	$\beta$ 2_cc	126.9	113.5	-10.1	-9.8	123.5	25.1	-47.5	156.5	29.2	29.0	29.8	-42.0	25.0	149.6	27.8	28.4	28.6	26.2	27.1
Gly_20_60_0_0	$\alpha$ R_cc	130.4	112.5	-9.8	-10.0	124.3	24.5	-44.0	156.6	28.7	29.0	29.9	-42.0	25.0	148.8	28.4	28.1	28.5	26.3	26.8
Gly_40_170_0_0	$\beta$ _cc	131.3	116.6	-10.4	-13.9	130.9	25.1	-52.5	157.3	29.3	29.1	29.9	-20.0	24.9	150.1	28.4	28.3	28.5	26.4	26.3

**Table S2-9.** [Table S18] Isotropic shielding values for **1** calculated at OPBE/PCS4//B3LYP/6-31G(d) level in the gas phase for tt, tc and ct conformers. See Figure S2-3 for labels.

FileName	Label-> Conf.	1 C	2 N	3 C	4 C	5 N	6 H	7 O	8 C	9 H	10 H	11 H	12 O	13 H	14 C	15 H	16 H	17 H	18 H	19 H
Gly_0_30_180_180	C7_tt	133.7	121.6	16.7	14.8	132.2	25.3	-53.3	161.4	29.3	29.8	29.3	-62.0	23.8	158.0	27.2	29.1	29.1	28.3	26.8
Gly_0_40_180_180	$\beta$ 2_tt	137.3	124.3	17.5	17.1	142.9	25.9	-71.4	161.2	29.2	29.7	29.3	-50.0	25.5	157.8	27.0	29.1	29.1	28.1	26.2
Gly_20_160_180_180	C5_tt	137.5	131.1	16.7	18.4	141.4	24.4	-75.2	161.8	29.6	29.4	29.4	-39.6	26.4	157.2	29.0	26.9	29.0	27.4	27.4
Gly_0_160_180_0	C5_tc	138.4	130.0	14.2	18.1	141.9	24.3	-75.1	161.7	29.4	29.6	29.4	-53.4	26.3	153.9	28.4	28.3	28.6	27.4	27.3
Gly_20_40_180_0	$\alpha$ R_tc	134.7	128.4	17.4	17.7	142.4	25.7	-89.6	162.2	29.3	29.7	29.4	-85.5	26.6	151.6	28.2	28.4	28.7	27.9	27.1
Gly_50_0_180_0	C7_uc	143.1	123.0	13.5	15.7	139.0	25.2	-66.5	161.2	29.4	29.7	29.4	-59.4	26.5	152.7	27.0	28.8	28.5	28.5	26.4
Gly_180_90_0_180	C5_ct	135.5	135.8	18.6	18.8	142.3	25.1	-87.5	161.5	29.5	29.5	29.5	-45.9	26.5	157.0	26.9	28.9	28.9	27.4	27.4
Gly_20_180_0_180	$\beta$ _ct	134.3	130.8	16.3	12.2	142.8	26.6	-105.1	163.9	28.9	29.5	29.6	-57.7	26.4	157.2	27.0	29.0	29.0	27.9	27.3
Gly_20_40_0_180	$\alpha$ R_ct	133.2	129.1	18.5	14.0	140.8	26.2	-100.5	163.7	29.5	29.4	29.5	-39.8	24.9	157.7	29.0	27.0	29.0	27.7	27.4

**Table S2-10.** [Table S19] Isotropic shielding values for **1** calculated at OLYP/PCS4//B3LYP/6-31G(d) level in the gas phase for tt, tc and ct conformers. See Figure S2-3 for labels.

FileName	Label-> Conf.	1 C	2 N	3 C	4 C	5 N	6 H	7 O	8 C	9 H	10 H	11 H	12 O	13 H	14 C	15 H	16 H	17 H	18 H	19 H
Gly_0_30_180_180	C7_tt	128.5	117.3	10.6	9.0	128.6	25.3	-56.9	157.4	29.4	29.8	29.4	-64.6	23.9	154.2	27.3	29.1	29.2	28.5	26.9
Gly_0_40_180_180	$\beta$ 2_tt	132.6	119.3	11.9	11.4	139.1	26.0	-73.2	157.2	29.3	29.8	29.4	-52.6	25.6	153.9	27.1	29.1	29.1	28.2	26.3
Gly_20_160_180_180	C5_tt	133.1	126.8	11.0	12.6	137.0	24.6	-77.3	157.9	29.7	29.5	29.5	-42.6	26.5	153.4	29.0	27.0	29.0	27.5	27.5
Gly_0_160_180_0	C5_tc	134.1	125.6	8.5	12.3	137.3	24.5	-77.3	157.7	29.5	29.7	29.5	-55.4	26.4	149.8	28.5	28.4	28.7	27.5	27.4
Gly_20_40_180_0	$\alpha$ R_tc	129.8	123.8	11.7	11.9	137.9	25.8	-91.6	158.3	29.4	29.8	29.5	-87.7	26.7	147.2	28.2	28.4	28.7	27.9	27.2
Gly_50_0_180_0	C7_uc	138.5	118.5	7.5	9.9	134.8	25.3	-68.9	157.2	29.5	29.8	29.5	-60.2	26.6	148.5	27.1	28.9	28.5	28.6	26.5
Gly_180_90_0_180	C5_ct	130.9	131.1	12.9	13.2	138.0	25.2	-89.1	157.5	29.5	29.5	29.6	-49.4	26.7	153.2	27.0	29.0	29.0	27.5	27.5
Gly_20_180_0_180	$\beta$ _ct	129.5	125.3	10.4	6.5	138.9	26.7	-107.2	160.0	28.9	29.6	29.7	-60.4	26.6	153.3	27.0	29.0	29.1	28.0	27.5

Gly 20 40 0 180     $\alpha$ R\_ct    128.2 123.8 12.8 8.3 137.0 26.3 -102.3 159.8 29.6 29.4 29.6 -42.4 25.1 153.9 29.0 27.1 29.0 27.8 27.5

**Table S2-11.** [Table S20] Isotropic shielding values for **1** calculated at MP2/PCS2//B3LYP/6-31G(d) level in the gas phase for tt, tc and ct conformers. See Figure S2-3 for labels.

Label->	1	2	3	4	5	6	7	8	9	10	11	12	13	14	15	16	17	18	19
Conf.	C	N	C	C	N	H	O	C	H	H	H	O	H	C	H	H	H	H	H
C7_tt	142.4	143.6	20.6	18.8	157.7	25.7	-26.0	170.2	29.4	30.1	29.4	-27.6	24.3	168.4	29.1	27.4	29.2	28.5	27.1
C5_tt	148.0	154.3	21.5	22.9	165.7	25.0	-41.7	170.6	29.9	29.5	29.5	-10.4	26.7	167.7	29.0	27.1	29.0	27.8	27.8
B2_tt	147.2	147.6	22.4	22.5	167.6	26.5	-41.3	170.1	29.4	29.3	30.1	-19.0	25.9	168.2	29.1	29.1	27.2	28.3	26.5
C5_tc	149.1	153.1	18.8	22.7	166.8	24.9	-41.5	170.5	29.5	29.9	29.5	-22.1	26.5	164.2	28.7	28.5	28.6	27.7	27.6
C7_tc	151.9	146.2	17.1	20.1	164.1	25.6	-35.9	170.1	29.5	30.0	29.5	-24.3	26.8	162.5	28.9	27.2	28.6	26.7	28.7
aR_tc	143.8	150.9	22.2	23.0	168.3	26.4	-57.8	170.9	30.1	29.4	29.4	-53.2	26.8	161.2	28.4	28.8	28.5	28.0	27.4
aR_ct	142.8	154.2	23.1	19.3	165.7	26.5	-69.4	172.8	29.6	29.5	29.7	-8.6	25.4	168.1	29.1	27.2	29.0	28.0	27.7
C5_ct	146.1	161.6	23.8	23.6	167.0	25.5	-56.6	170.7	29.6	29.6	29.6	-16.3	26.9	167.5	29.0	29.0	27.1	27.8	27.8
B_ct	143.2	155.7	21.3	17.8	166.9	26.9	-73.8	172.8	29.7	29.6	29.1	-24.6	26.9	167.6	29.1	29.1	27.1	27.7	28.3

**Table S2-12.** [Table S21] Isotropic shielding values for **1** calculated at MP2/PCS2,DMSO//B3LYP/6-31G(d) level using gas phase geometries for tt, tc and ct conformers. See Figure S2-3 for labels.

Label->	1	2	3	4	5	6	7	8	9	10	11	12	13	14	15	16	17	18	19
Conf.	C	N	C	C	N	H	O	C	H	H	H	O	H	C	H	H	H	H	H
C7_tt	144.3	135.6	12.6	13.8	150.0	23.7	14.9	170.9	29.4	29.5	29.4	20.7	23.3	169.7	28.8	27.6	28.9	27.4	26.2
C5_tt	149.3	142.1	15.6	17.7	159.1	23.4	16.6	171.0	29.5	29.5	29.5	36.1	24.5	169.1	28.8	27.3	28.8	26.7	26.7
B2_tt	147.8	138.1	13.8	15.1	158.2	24.3	15.8	170.5	29.5	29.3	29.5	38.7	24.0	169.5	28.9	28.8	27.4	27.3	25.9
C5_tc	150.3	141.7	12.1	17.5	157.3	23.4	16.1	170.9	29.4	29.5	29.4	30.3	24.8	165.6	28.4	28.3	28.5	26.6	26.4
C7_tc	153.1	139.6	9.8	14.3	154.5	23.8	4.5	170.6	29.5	29.5	29.4	30.7	25.0	163.2	28.5	27.5	28.3	25.9	27.5
aR_tc	144.9	138.2	11.4	14.9	155.2	24.0	8.0	171.2	29.5	29.4	29.5	16.7	25.0	162.8	28.3	28.5	28.2	26.4	26.9
aR_ct	143.6	141.6	14.3	11.1	157.1	24.6	-4.8	172.7	29.8	29.1	29.3	49.9	23.7	169.5	28.8	27.4	28.8	26.8	26.7
C5_ct	147.6	147.9	16.3	15.5	160.7	24.4	12.3	170.8	29.8	29.1	29.1	36.3	24.6	169.0	28.8	28.8	27.4	26.5	26.5
B_ct	145.4	142.8	13.6	8.4	159.1	25.1	-11.7	172.3	29.0	29.8	28.9	31.9	24.6	169.1	28.9	28.8	27.4	26.5	26.8

### 2.1.5 References

- (1) *Schrödinger Release 2015–2: MacroModel*, Version 10.8; Schrödinger: LLC, New York, USA, **2015**.
- (2) Ponder, J. W. *Tinker Software Tools for Molecular Design*, version 7.1; Dept. of Chemistry, Washington University: Missouri, USA, **2015**.
- (3) (a) Hariharan, P. C.; Pople, J. A., *Theor. Chim. Acta.* **1973**, *28*, 213-222. (b) Becke, A. D., *J. Chem. Phys.* **1993**, *98*, 5648-5652.
- (4) Graham, D. C.; Menon, A. S.; Goerigk, L.; Grimme, S.; Radom, L., *J. Phys. Chem. A* **2009**, *113*, 9861-9873.
- (5) Henry, D. J.; Parkinson, C. J.; Radom, L., *J. Phys. Chem. A* **2002**, *106*, 7927-7936.
- (6) Baboul, A. G.; Curtiss, L. A.; Redfern, P. C.; Raghavachari, K., *J. Chem. Phys.* **1999**, *110*, 7650.
- (7) (a) Halkier, A.; Helgaker, T.; Jørgensen, P.; Klopper, W.; Koch, H.; Olsen, J.; Wilson, A. K., *Chem. Phys. Lett.* **1998**, *286*, 243-252. (b) Goerigk, L.; Karton, A.; Martin, J. M.; Radom, L., *Phys. Chem. Chem. Phys.* **2013**, *15*, 7028-7031.
- (8) Dunning Jr, T. H., *J. Chem. Phys.* **1989**, *90*, 1007-1023.
- (9) Jensen, F., *J. Chem. Theory Comput.* **2008**, *4*, 719-727.
- (10) Miertuš, S.; Scrocco, E.; Tomasi, J., *Chem. Phys.* **1981**, *55*, 117-129.
- (11) Xiong, R.; Sandler, S. I.; Burnett, R. I., *Ind. Eng. Chem. Res.* **2014**, *53*, 8265-8278.
- (12) (a) Pye, C. C.; Ziegler, T.; Van Lenthe, E.; Louwen, J. N., *Can. J. Chem.* **2009**, *87*, 790-797. (b) Louwen, J.; Pye, C.; van Lenthe, E.; McGarrity, E.; Xiong, R.; Sandler, S.; Burnett, R. *ADF2014 COSMO-RS, Software for Chemistry & Materials*, Vrije Universiteit: Amsterdam, **2014**.
- (13) Frisch, M. J. T., G. W.; Schlegel, H. B.; Scuseria, G. E.; Robb, M. A.; Cheeseman, J. R.; Scalmani, G.; Barone, V.; Mennucci, B.; Petersson, G. A.; Nakatsuji, H.; Caricato, M.; Li, X.; Hratchian, H. P.; Izmaylov, A. F.; Bloino, J.; Zheng, G.; Sonnenberg, J. L.; Hada, M.; Ehara, M.; Toyota, K.; Fukuda, R.; Hasegawa, J.; Ishida, M.; Nakajima, T.; Honda, Y.; Kitao, O.; Nakai, H.; Vreven, T.; Montgomery, Jr., J. A.; Peralta, J. E.; Ogliaro, F.; Bearpark, M.; Heyd, J. J.; Brothers, E.; Kudin, K. N.; Staroverov, V. N.; Keith, T.; Kobayashi, R.; Normand, J.; Raghavachari, K.; Rendell, A.; Burant, J. C.; Iyengar, S. S.; Tomasi, J.; Cossi, M.; Rega, N.; Millam, J. M.; Klene, M.; Knox, J. E.; Cross, J. B.; Bakken, V.; Adamo, C.; Jaramillo, J.; Gomperts, R.; Stratmann, R. E.; Yazyev, O.; Austin, A. J.; Cammi, R.; Pomelli, C.; Ochterski, J. W.; Martin, R. L.; Morokuma, K.; Zakrzewski, V. G.; Voth, G. A.; Salvador, P.; Dannenberg, J. J.; Dapprich, S.; Daniels, A. D.; Farkas, O.; Foresman, J. B.; Ortiz, J. V.; Cioslowski, J.; Fox, D. J.; *Gaussian 09 Revision D. 01*, Gaussian, Inc., Wallingford CT: **2013**.

## **Chapter 3. Electrostatic Effects on The Stability of Peptide Radicals**

Harish Jangra and Hendrik Zipse  
*J. Phys. Chem. B* **2018**, *122*, 8880-8890.

---

### ***Authors contribution***

H.Z. conceive and supervised the study. All the calculations were designed by H.H. and H.Z., and performed by H.H. The manuscript was jointly written by H.H. and H.Z.

### ***Copyright***

This research was originally published in the *Journal of Physical Chemistry B* and reprinted with permission from *J. Phys. Chem. B* **2018**, *122*, 8880-8890 © 2018 American Chemical Society as the 3<sup>rd</sup> chapter of this thesis.

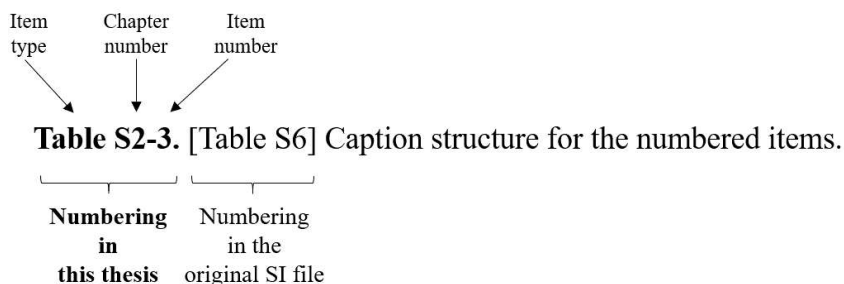
(Link to article: <https://pubs.acs.org/doi/abs/10.1021/acs.jpccb.8b07485>)

Selected supporting material for the computational part of this work is provided at the end of this chapter. For complete supporting information (SI), please follow the link below:

<https://pubs.acs.org/doi/suppl/10.1021/acs.jpccb.8b07485>

### ***Additional information***

The accompanying SI is the shorter and altered version of the original content. The items (Tables, Figure, Schemes etc.) may have a different number than what was originally assigned. To make it easier to locate the SI content referred to in the following reprint, the original numbering is also provided in the caption of the numbered items as described below:



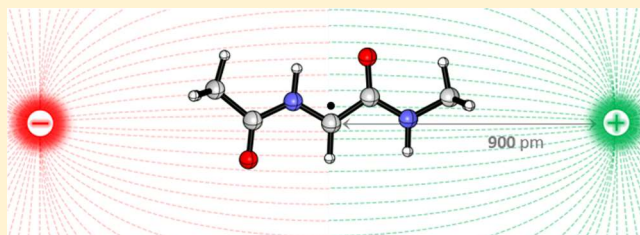
# Electrostatic Effects on the Stability of Peptide Radicals

Harish Jangra and Hendrik Zipse\*<sup>1</sup>

Department of Chemistry, LMU München, Butenandtstrasse 5-13, 81377 München, Germany

## Supporting Information

**ABSTRACT:** We explored the influence of external electric fields (EEFs) on the stability of a glycine dipeptide model radical using high-level quantum chemical methods. Remotely located ions ( $\text{Cl}^-/\text{Na}^+$ ) are used to implement EEF effects. The effects of these ions are reproduced using background point charges and oriented EEFs. Remote charges as far as 900 pm from the  $\text{C}_\alpha$  radical center can be significantly stabilizing or destabilizing as a function of their relative orientation. The magnitude of these effects is also strongly dependent on the distance between the radical center and the charge location. After examining the strengths and weaknesses of some frequently used quantum mechanics methods in describing these effects properly, a comparison is made on the stability of dipeptide radicals bearing protonable or deprotonable side chains. In this group, the stability of the respective  $\text{C}_\alpha$  radicals mainly depends on the preferred orientation of the charge-carrying side chain.



## INTRODUCTION

The concentration and physical state of reactant(s), temperature, solvent, and catalysts are the established factors that influence chemical reactivity almost universally. The concept of employing external electric fields (EEFs) to modulate the properties of molecular systems beyond the redox domain is relatively new. Taking the lead from theoretical work of Shaik et al.,<sup>1</sup> Aragonès et al. recently reported a new way to accelerate the Diels–Alder reaction by an oriented EEF, further expanding the scope of EEF-guided chemical reactivity.<sup>2</sup> Multiple reports were published recently to highlight the potential application<sup>3–7</sup> and actual implementation<sup>8–13</sup> of EEFs as smart reagents of the future. Attempts were also made to develop a more scalable solution to adjust the relative orientation of EEFs and reactants for electrostatic chemical catalysis.<sup>14–16</sup> This may be particularly relevant for biomolecular systems whose structural features can impose highly oriented EFs on bound substrates in enzyme active sites.<sup>17–19</sup> Theoretical work by Shaik et al. demonstrated that EEFs have a significant effect on the catalytic cycle of P450 enzymes.<sup>20,21</sup> Fried et al. and others have shown that enzymes have the ability to generate extreme EFs in an organized environment which results in large electrostatic stabilization of the bound substrate.<sup>22–25</sup> In solution-phase chemical synthesis, the scope of EEF-induced control is limited due to the absence of an organized environment. However, recent theoretical reports from Coote et al. demonstrate for a broad selection of delocalized radicals that their stabilities can be significantly increased via generation of a negatively charged site in the vicinity of (but not in direct resonance with) the formal radical center.<sup>26–30</sup> Subsequent experimental studies by several groups have shown that the electrostatic stabilization of radicals remains significant in low-polarity solvents, but vanishes in more polar media.<sup>31,32</sup> Radical stability was quantified in these studies through X–H bond dissociation energies (BDEs) for neutral or

anionic radical precursors. Wavefunction (WF) analysis for neutral and charged radical species also indicated conversion of singly occupied molecular orbital (SOMO) and highest occupied molecular orbital energy levels for systems displaying strong stabilization effects. Selecting alcohols as a protonable/deprotonable substrate class, Radom et al. have confirmed the finding of systematically smaller C–H bond energies in anionic systems compared to their respective neutral (or protonated) versions.<sup>33</sup>

These studies conclude that variations in the stabilities are mainly due to electrostatic effects. We have recently calculated C–H bond energies of dipeptide model systems as a measure of the stabilities of the respective peptide radicals.<sup>34–38</sup> We explore here the possible influence of remote negatively or positively charged sites on the stabilities of these biochemically important species.

## RESULTS

**Methodological Considerations.** Initial studies have been performed for glycine dipeptide model system **1/r1**, for which the radical stabilization energy [RSE(1a)] can be defined as the isodesmic hydrogen exchange reaction with methane (**2**) (eqn 1a, Figure 1A). Similarly, RSE(1b) is calculated as stated in eqn 1b, where **1** and **r1** are complexed with an external anion. The net effects of external charge on the stability of **1/r1** are then calculated as the charge-induced radical stabilization energy (ciRSE) that is the difference between RSE values obtained from eqn 1a,b, as defined in eqn 1c. The ciRSE can also be expressed as the difference in the complexation energies of  $\text{Cl}^-$  with radical **r1** (radical complexation energy, RCE) and the corresponding

Received: August 2, 2018

Revised: September 10, 2018

Published: September 10, 2018

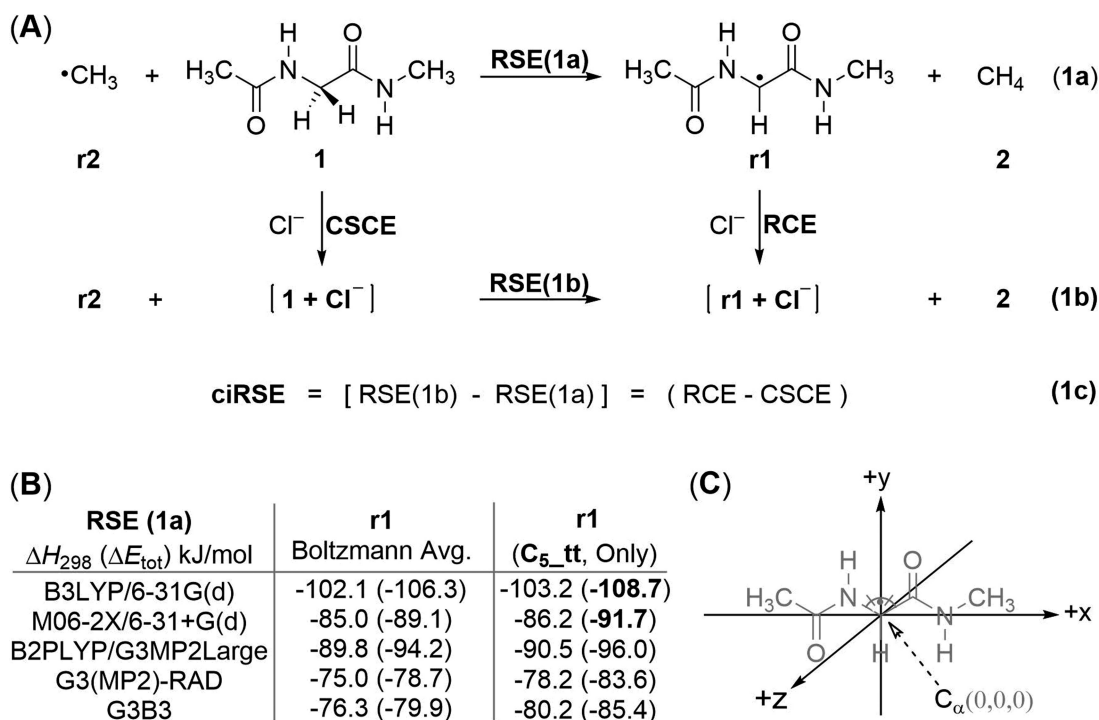


**Figure 1.** (A) Isodesmic reactions used to calculate the stability of radical **r1** and its chloride anion-complexed derivative [**r1**+Cl<sup>-</sup>]. (B) Gas phase RSE(1a) values calculated for **r1**. (C) The coordinate system used for positioning the external charge. C<sub>α</sub> is located at the center, and all non-hydrogen atoms lie in the *xy*-plane, where the +*y*-axis bisects the N–C<sub>α</sub>–C angle (see the SI for more details).

**Table 1.** ciRSEs ( $\Delta E_{\text{tot}}$ , kJ/mol) for Radical **r1** in the Presence of an External Cl<sup>-</sup> at the B3LYP/6-31G(d) Level Using Different Convergence Procedures<sup>a</sup>

system 1/r1+Cl <sup>-</sup>		the position of Cl <sup>-</sup> around 1/r1				
		-x	+x	-y	+y	+z
SCF = DIIS default	ciRSE	-18.5	<sup>c</sup>	-7.0 <sup>b</sup>	-5.8 <sup>b</sup>	-1.8
	Cl <sup>-</sup> (q)	-0.8		-0.9	-0.9	-0.9
	C <sub>α</sub> (S)	+0.6		+0.6	+0.6	+0.6
SCF = QC	ciRSE	-9.4 <sup>b</sup>	+6.2 <sup>b</sup>	-1.4 <sup>b</sup>	+1.2 <sup>b</sup>	-1.8
	Cl <sup>-</sup> (q)	-1.0	-1.0	-1.0	-1.0	-0.9
	C <sub>α</sub> (S)	+0.7	+0.7	+0.7	+0.7	+0.6
stable = opt	ciRSE	-18.6	-2.1	-7.1	-6.1	-1.8
	Cl <sup>-</sup> (q)	-0.8	-0.9	-0.9	-0.9	-0.9
	C <sub>α</sub> (S)	+0.6	+0.6	+0.6	+0.6	+0.6

<sup>a</sup>RSE (1/r1, C<sub>5</sub> only) of 108.7 kJ/mol ( $\Delta E_{\text{tot}}$ ) is used as a reference. <sup>b</sup>WF with internal instability. <sup>c</sup>SCF not converged.

closed-shell parent **1** (closed-shell complexation energy, CSCE). To limit the influence of conformational effects, the following analysis will restrict itself to the extended C<sub>5</sub> conformation of these systems, for which RSE values are listed in Figure 1B along with Boltzmann averaged values over a range of conformations (see Supporting Information (SI)). The stability values for the C<sub>5</sub> conformation are closely similar to those obtained after conformational averaging, and it can thus be used as an effective model for studying the influence of external charges.

The effect of remote charges on the stability of 1/r1 was first explored by positioning a Cl<sup>-</sup> 500 pm away from (and thus far outside the vdW radius of) the nearest atom of the respective systems in -/+x, y, and z-direction(s) using the coordinate conventions shown in Figure 1C. Due to the C<sub>5</sub> symmetry of radical **r1** and closed-shell parent **1**, positioning in +z and -z-direction(s) produces identical results. The same Cl<sup>-</sup> positions were used for both **r1** and **1**. The ciRSEs were calculated for these five orientations of Cl<sup>-</sup> in its complex with 1/r1 to identify

suitable theoretical methods. Due to the frozen coordinates used in placing the ion at defined positions, the ciRSE values are calculated from total energies ( $\Delta E_{\text{tot}}$ , i.e., without thermal corrections). The results obtained at the (U)B3LYP/6-31G(d)<sup>39,40</sup> level as one of the more commonly used hybrid density functional theory (DFT) methods are presented in Table 1. It is important to highlight the peculiar behavior of self consistent field (SCF) algorithms at this level as different choices lead to different electronic states for the **r1**+Cl<sup>-</sup> complexes. The default SCF procedure (DIIS) in Gaussian 09<sup>41</sup> converges to a wavefunction (WF) that may best be described as “delocalized” in that some negative charge is transferred from Cl<sup>-</sup> to **r1** and unpaired spin is delocalized over all atoms of the system. Perusal of the default SCF results in Table 1 indicates that the presence of Cl<sup>-</sup> stabilizes radical **r1** in all orientations, albeit to different degrees. For example, Cl<sup>-</sup> placed in the -x-direction produces a large stabilization of -18.5 kJ/mol. The quadratically convergent (QC) SCF method leads to an energetically less

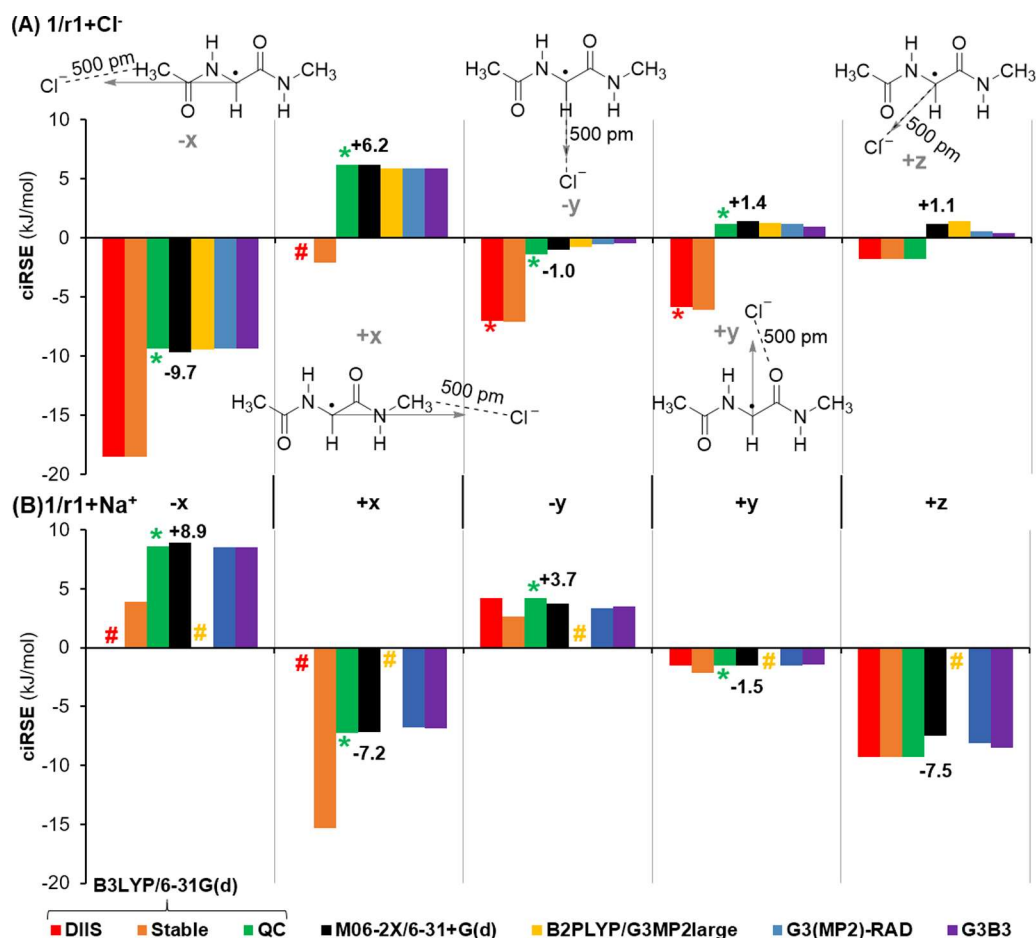


**Figure 2.** ciRSE (kJ/mol) for radical  $r1$  in the presence of an external  $\text{Cl}^-$  (A) and  $\text{Na}^+$  (B) calculated at different levels of theory. \*marked the internal instability in WF. #non-convergent SCF cases.

stable radical (ciRSE of  $-9.4$  kJ/mol for  $-x$ ) and a more “localized” WF in that  $\text{Cl}^-$  retains an integral negative charge, and the unpaired spin density is fully localized on radical  $r1$ . Further analysis indicates that this latter wavefunction contains an internal instability, and reoptimization of such an unstable WF (stable = opt) leads to the same solution obtained already with DIIS. The stable WF is accompanied by the orbital conversion phenomenon, where the SOMO of the  $r1+\text{Cl}^-$  complex is located below the orbitals describing the lone pairs of  $\text{Cl}^-$  (see the SI).

The appearance of two close-lying electronic states for the B3LYP functional also persists with larger basis sets (see the Supporting Information) and this phenomenon was therefore tested with other theoretical approaches including other commonly used hybrid DFT methods [(U)M06-2X<sup>42,43</sup>/6-31+G(d)], the (RO)B2-PLYP<sup>44</sup>/G3MP2large double hybrid method, the G3(MP2)-RAD<sup>45</sup> compound scheme optimized for open-shell systems, and the more sophisticated G3B3<sup>46</sup> compound scheme. These four methods converge to the stable localized states exclusively (Figure 2A). The calculations were repeated with  $\text{Na}^+$  replacing  $\text{Cl}^-$ , where both (U)B3LYP/6-31G(d) and (RO)B2-PLYP/G3MP2large were found to suffer from convergence problems and unstable WFs, Figure 2B. All other methods converge to stable localized electronic states with practically no unpaired spin density on the sodium cation. Because serious convergence problems were encountered in (U)B3LYP and (RO)B2-PLYP calculations, these methods were eliminated from further consideration. From the results

compiled in Figure 2, we can see that values obtained from relatively low-cost (U)M06-2X/6-31+G(d) calculations show very good agreement with the more expensive methods [i.e., G3(MP2)-RAD and G3B3] for both systems, without any convergence problem. All results shown in the following for glycine dipeptide **1** were therefore calculated at the (U)M06-2X/6-31+G(d) level, if not mentioned otherwise. For the  $1/r1+\text{Cl}^-$  system, positioning  $\text{Cl}^-$  in the  $-x$ -direction leads to a stabilization with ciRSE of  $-9.7$  kJ/mol, while  $+6.2$  kJ/mol (destabilization) is obtained for the  $+x$ -orientation. These ciRSE values are larger than those obtained when positioning  $\text{Cl}^-$  in  $+/-y$  and  $+z$ -orientation(s) where  $\text{Cl}^-$  is positioned directly on top of the  $\text{C}_\alpha$  position in  $1/r1$ . Replacing  $\text{Cl}^-$  with  $\text{Na}^+$  reverses the nature of ciRSE in  $xyz$  orientations. This supports the assumption made by Coote et al. that remote charge-induced radical stabilizations are mainly electrostatic in nature.<sup>2,27–30</sup> For all orientations of  $\text{Cl}^-$  around  $r1$ , whether stabilizing or destabilizing, the  $r1+\text{Cl}^-$  complex exhibits orbital conversion (OC). This implies that OC is an associated, but not causative phenomenon. The stabilization/destabilization of radical  $r1$  through a sodium cation described in Figure 2 is not accompanied by an OC phenomenon simply due to the absence of high-lying occupied MOs in the sodium cation. The fact that the ciRSE of radical  $r1$  is a highly directional effect is easily seen from the results in Figure 2. These factors are further investigated in the next section, where using the coordinate conventions defined in Figure 1C, a remote charge ( $\text{Cl}^-/\text{Na}^+$  ion) is placed around  $1/r1$  in  $xy$ ,  $xz$ , and  $yz$ -plane(s) with varying

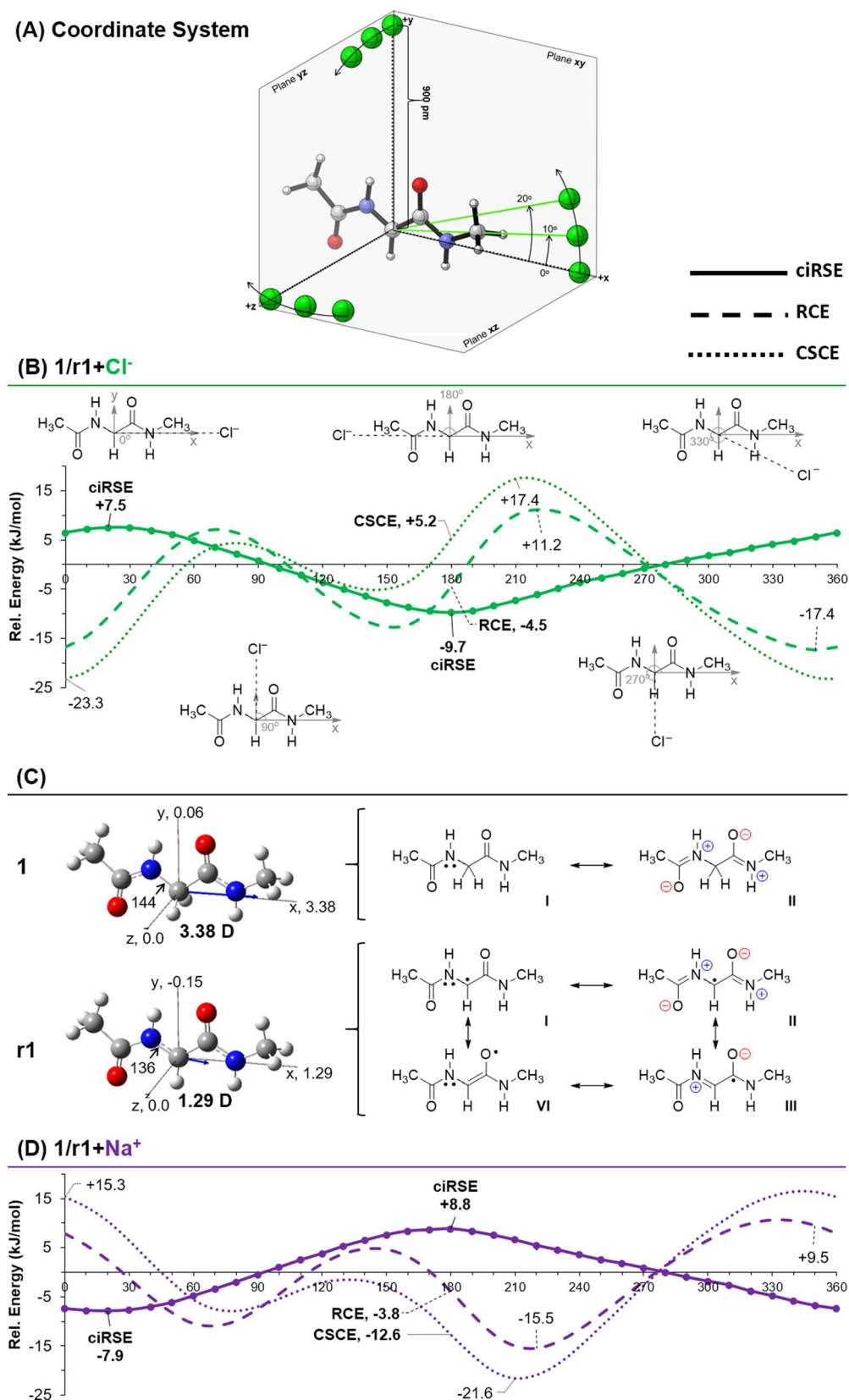


**Figure 3.** (A) Coordinate system used for the placement of external ions around  $1/r1$  in the  $xy$ ,  $xz$ , and  $yz$ -plane(s). The ciRSE, RCE, and CSCE are plotted as a function of ion orientation around  $1/r1$  in the  $xy$ -plane at 900 pm distance from  $C_\alpha$  for (B)  $Cl^-$  and (D)  $Na^+$ . (C) The molecular dipole moment (MDM, Debye) vector of  $1/r1$  calculated at (U)M06-2X/6-31+G(d) and selected resonance structures.

distances from its  $C_\alpha$ . The effects of ions are reproduced using point charges (PCs) and EEFs.

**Orientalional Dependence of Radical Stabilization.**  
Figure 3A describes the  $r1+Cl^-$  system with a portion of the

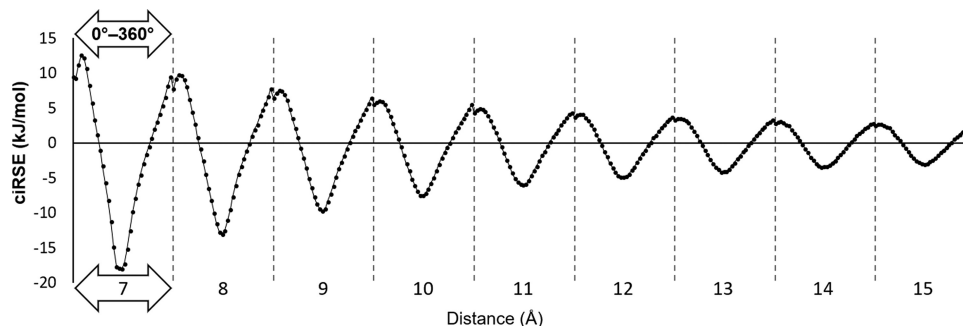


**Figure 4.** ciRSE values as a function of  $\text{Cl}^-$  orientation in the  $xy$ -plane at distances from the radical center ranging from 700 to 1500 pm. Each segment has a ciRSE curve plotted as a function of  $\text{Cl}^-$ - $\text{C}_\alpha$ - $x$ -axis angle at a fixed distance between  $\text{Cl}^-$  and  $\text{C}_\alpha$ .

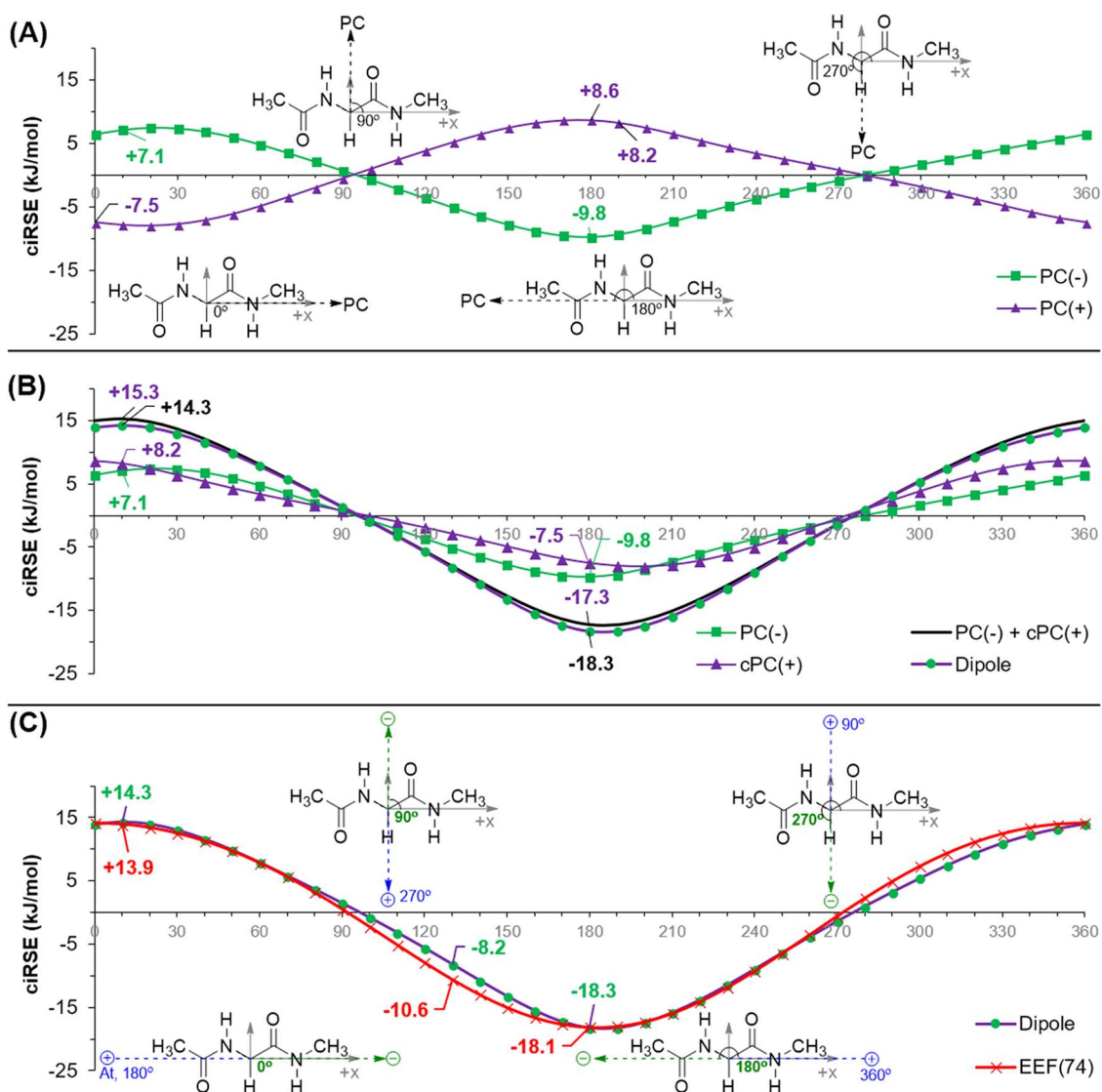


**Figure 5.** (A) Dependence of the ciRSE on the angle between point charges (PC) and the  $+x$ -axis in the  $xy$ -plane at 900 pm from  $\text{C}_\alpha$  of  $1/\mathbf{r}1$ . (B) The curve of ciRSE for estimated dipole [ $\text{PC}(+) + \text{cPC}(-)$ ] and its comparison with ciRSE values for an actual dipole. (C) A comparative plot of ciRSE for the unit charge dipole to ciRSE calculated in the presence of an EEF of  $74 \times 10^{-4}$  au.

associated  $xy$ ,  $xz$ , and  $yz$ -plane(s) used for ion positioning. In the following sections, the results from each plane will be discussed separately.

**Plane  $xy$ .** The ciRSE, CSCE, and RCE values for  $1/\mathbf{r}1 + \text{Cl}^-$  complexes are plotted as a function of the angle  $\text{Cl}^-$  makes with the  $x$ -axis, where it is revolving around  $1/\mathbf{r}1$  in the  $xy$ -plane at a

distance of 900 pm from the  $\text{C}_\alpha$  position (see the SI for more details). As shown in Figure 3B, the most negative (stabilizing) ciRSE values are calculated for  $\text{Cl}^-$  orientations along the  $-x$ -axis, with the largest stabilization of  $-9.7$  kJ/mol found at  $180^\circ$ , while the largest positive (destabilizing) ciRSE values result from chloride orientations along the  $+x$ -axis with the largest

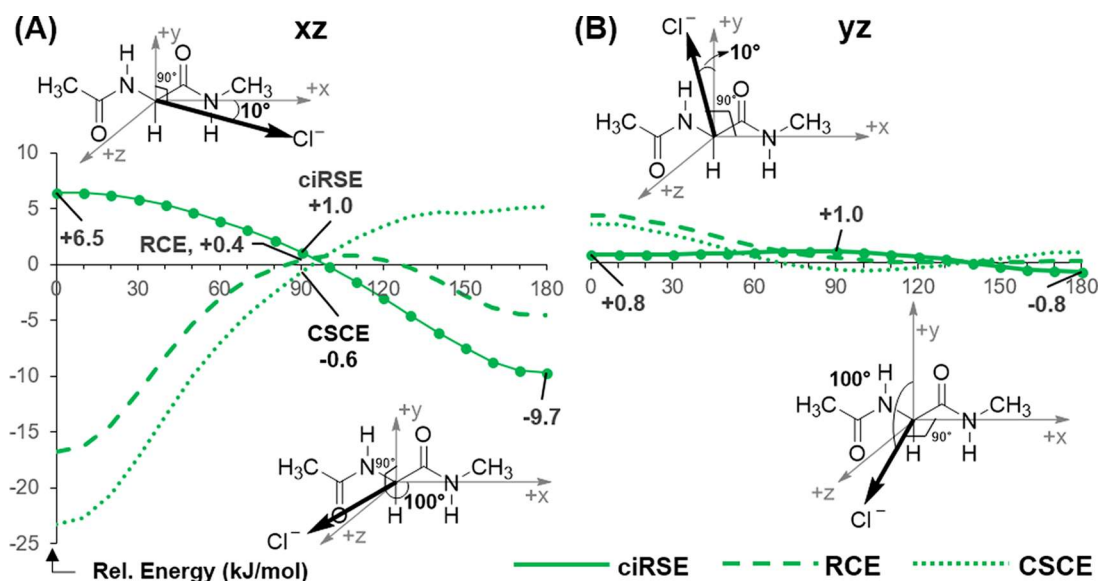


**Figure 6.** ciRSE curves plotted as function of Cl<sup>-</sup> orientations in (A) *xz*- and (B) *yz*-planes at 900 pm from C<sub>α</sub> of 1/r1. For the *xz*-plane, the Cl<sup>-</sup>-C<sub>α</sub>-*x*-axis angle is plotted on the *x*-axis of the plot and Cl<sup>-</sup>-C<sub>α</sub>-*y*-axis angle is fixed at 90° in the *xyz*-coordinates system for 1/r1, *visa-versa* for the *yz*-plane. Because of the symmetrical nature of 1/r1, only the orientations of chloride from 0 to 180° are shown.

value of +7.5 kJ/mol found at 20°. The external charge placed at 90 and 270°, *i.e.*, along the +*y* and -*y*-axis, has only a minimal effect on the C<sub>α</sub> bond strength (ciRSE < 1 kJ/mol). These trends fully agree with the data shown earlier in Figure 2A. As mentioned before the ciRSE can also be expressed as the difference in complexation energies of Cl<sup>-</sup> with radical r1 (RCE) and its closed-shell parent 1 (CSCE). For example, at 180° (see Figure 3B) Cl<sup>-</sup> interaction with radical r1 is stabilizing by -4.5 kJ/mol (RCE), while interaction with 1 is destabilizing by +5.2 kJ/mol (CSCE). The resulting ciRSE of -9.7 kJ/mol (RCE-CSCE) is the combination of both of these effects. Interestingly, for the orientation of Cl<sup>-</sup> that leads to maximum overall destabilization (ciRSE = +7.5 kJ/mol at 20°) the complexation energies for both 1 and r1 are negative, but larger for 1 than for radical r1 (CSCE > RCE), which leads to an overall increase in C<sub>α</sub>-H BDE by +7.5 kJ/mol. The most positive and most negative CSCE values (located at 210 and 0°, respectively) are numerically larger than those found in the RCE curve, which indicates that closed-shell 1 reacts more strongly to external charge than radical r1. This can be better understood by examining the charge distribution in 1/r1 without a complexation partner. As shown through the resonance structures in Figure 3C, the radical center positioned between the polar amide units in radical r1 leads to better charge delocalization and hence a lower molecular dipole moment (MDM) compared to closed-shell parent 1. The higher MDM makes 1 more sensitive to external charges than r1. The ciRSE curve shown in Figure 3B for chloride can be divided into a region of net destabilization (ND) ranging from 0–90 + 270–360° and a region of net stabilization ranging from 90 to 270°. For most part of the ND region, chloride aligns favorably with the MDM vector of 1/r1, which leads to favorable complexation energies, and thus, stabilization of both 1 and r1, as reflected by the negative RCE and CSCE values (Figure 3B).

The fact that the combination of these effects leads to radical destabilization (positive ciRSE values) is simply due to higher complexation energies for parent 1 than for radical r1. The region of maximum radical destabilization seen in the range of 350–0–20° thus falls together with the location of maximum

chloride complexation energies for parent 1 (-23.3 kJ/mol at 0°) and radical r1 (-17.4 kJ/mol at 350°). The situation is less clear in the region of net radical stabilization ranging from 90 to 270°, where chloride interactions with 1 and its radical r1 can be positive or negative. The large positive complexation energies of +17.4 (CSCE) and +11.2 kJ/mol (RSE) can be seen in the region around 210 and 220° where Cl<sup>-</sup> is oriented toward the partially negatively charged oxygen atom in the N-terminal amide group. The fact that the repulsion in this region is smaller for radical r1 than for parent 1 results from smaller partial charges for the amide oxygen atom as a consequence of better charge equilibration as expressed through the resonance structures shown in Figure 3C. These may also be responsible for the fact that the chloride complexation energies are actually slightly attractive in the 120–170° range due to Cl<sup>-</sup> interactions with the positively polarized amide and methyl hydrogens at the N-terminal amide group.

**Nature of Charge.** The Na<sup>+</sup> ion is used to study the effect of positive charge on 1/r1. The cation is placed using the same strategy adopted for Cl<sup>-</sup> and the results are depicted in Figure 3D. By comparing the ciRSE, CSCE, and RCE curves of Na<sup>+</sup> with those for Cl<sup>-</sup>, the electrostatic nature of the interactions between these ions and 1/r1 is evident. ciRSE and complexation energies are almost identical in magnitude and opposite in sign for Na<sup>+</sup> compared to Cl<sup>-</sup>. One interesting point to note is that the electrostatically most favorable orientation of these ions to 1/r1 results in anion and cation positions for 1 of around 0 and 210°, respectively. This leads to an increase in C<sub>α</sub>-H BDE as marked by +ciRSE at 0° for the Cl<sup>-</sup> and 210° for the Na<sup>+</sup>.

**Distance.** To analyze the relationship between ciRSE and the distance between the charge and C<sub>α</sub> of 1/r1, Cl<sup>-</sup> is circularly placed in the *xy*-plane (as explained previously) at varying distances ranging from 700 to 1500 pm with 100 pm intervals. The results are shown in Figure 4. The ciRSE decreases with an increasing distance between C<sub>α</sub>-Cl<sup>-</sup>, as expected, indicating an inverse non-linear relationship between ciRSE and the C<sub>α</sub>-Cl<sup>-</sup> distance.

**Effects of Point Charges (PCs) and EEFs.** The effects of ions (Cl<sup>-</sup>/Na<sup>+</sup>) on ciRSE of r1 can be reproduced using suitable

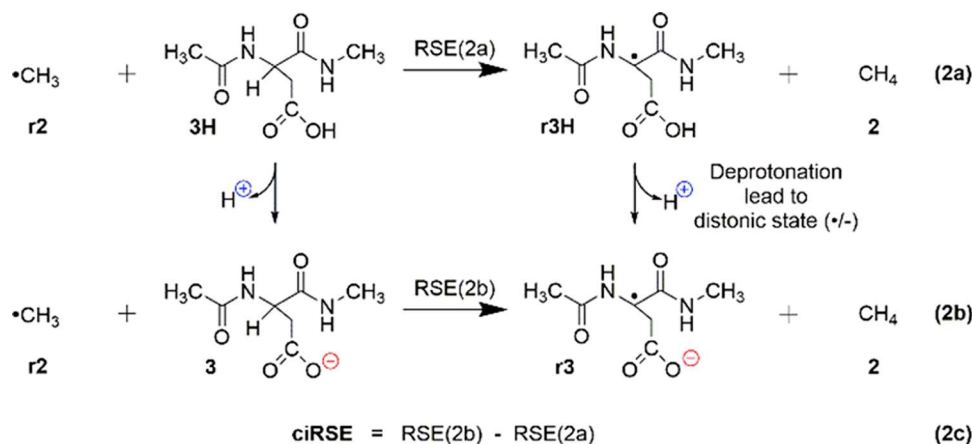


Figure 7. Reaction schemes employed to study the effects of charge on the stability of  $C_{\alpha}$  radicals of acidic and basic amino acids (AAs).

background point charges (PC)s. Figure 5A shows the ciRSE curves for positive(+) and negative(−) PCs, which are almost identical to the curves obtained for  $\text{Na}^+$  and  $\text{Cl}^-$ , respectively, in Figures 3D and 3B. The PCs are a more suitable probe for the theoretical investigation of long-range electrostatic interactions between radical and external charge, as at the lower limit of the distance between reacting species, PCs do not suffer from charge or spin transfer effects. Oriented external electric fields (EEFs) represent another tool for such an investigation. In the Gaussian program, EEFs are implemented as a dipole, and the proper comparison between the effects of ions or PCs to those of EEFs on the ciRSE require the organization of external charges as a dipole and comparison with the results obtained for an EEF of appropriate strength. In our case, we combine the ciRSE values calculated for individual charges to obtain the effects of the dipole. For this, we added the ciRSE curve for  $\text{PC}(-)$  to the  $180^\circ$ -shifted ciRSE curve for  $\text{PC}(+)$  designated by  $\text{cPC}(+)$ , where c stands for corrected, as shown in Figure 5B. The shift by  $180^\circ$  facilitates summation of the effects of both charges as it puts the value of  $\text{PC}(+)$  along with the corresponding value of  $\text{PC}(-)$  like they were reflecting the contribution of individual components in a dipole. The summation of  $\text{PC}(+)$  and  $\text{cPC}(-)$  yields an estimated value for a dipole of unit charge, the estimated values are close to the calculated values for actual dipole implementations as shown in Figure 5B (see the SI file for more details). There is a small systematic overestimation of ciRSE values for dipoles obtained by summation of unit charge effects compared to the calculated values for an actual dipole. The maximum deviation of 1.1 kJ/mol occurs at orientations with maximum  $\pm$ ciRSE values, as can be noted in the ciRSE curves for estimated and calculated ciRSE at 0 and  $180^\circ$  in Figure 5B. Analyzing the influence of EEFs on the stability of **r1** we find that the presence of an EEF of  $74 \times 10^{-4}$  au strength affects the C–H bond strength at  $C_{\alpha}$  of **1** in a manner similar to that of a unit charge dipole (Figure 5C). The ciRSE curve obtained in the presence of an EEF is slightly more symmetrical than that obtained for the unit dipole model, the maximum deviations amounting to ca. 2 kJ/mol in the region around  $130^\circ$ .

**Planes  $xz$  and  $yz$ .** Following the same strategy described above for the  $xy$ -plane, the effects of external charges on the ciRSE were investigated by placing ions in the  $xz$ - and  $yz$ -planes. Since the effects of  $\text{Cl}^-/\text{Na}^+$  ions, of PCs and of EEFs on the ciRSE of **r1** in the  $xz$  and  $yz$ -planes are quite comparable, only the results for  $\text{Cl}^-$  are discussed here, and the remaining results are reported in the SI file. The ciRSE, CSCE, and RCE curves for

$\text{Cl}^-$  are plotted as a function of its orientation in the  $xz$ -plane in Figure 6A and in the  $yz$ -plane in Figure 6B. Looking at the complexation energy curves, as  $\text{Cl}^-$  moves out of the  $xy$ -plane either into the  $xz$ - or  $yz$ -plane, its strength of interaction with **1/r1** decreases. The chloride complexation energies with **1/r1** near the  $+z$ -axis are actually less than 1.0 kJ/mol, which is well in line with the negligible component of the MDM for **1/r1** in this direction (see Figure 3C).

Similarly, the MDM component is very small in the direction of the  $y$ -axis, which causes equally small complexation energy values at the positive and negative end of this axis. The fact that the complexation energies are slightly larger (positive) at angles around  $0^\circ$  than at  $180^\circ$  is likely due to repulsive interactions with the oxygen atom of the C-terminal amide group. However, the overall effect of  $\text{Cl}^-$  on the stability of radical **r1** remains small for all orientations in the  $yz$ -plane. As with any electrostatic effect between the two molecular entities, the presence of a polarizable environment is expected to moderate the magnitude of the resulting interaction energies, and thus the size of the resulting radical stabilization energies.<sup>26–30</sup> How much of the gas phase effects reported here will be retained in a particular experiment will thus depend on the particular properties of the respective reaction medium (see the SI for further information).

#### Effects of Charged Side Chains in Peptide Radicals.

The most relevant situation where charged sites impact the stability of  $C_{\alpha}$  peptide radicals concerns peptides with (de)protonable side chains. As shown for the example of aspartate radical **r3** in Figure 7,  $C_{\alpha}$  radical formation in these peptides generates “dystonic” radical ions,<sup>47</sup> where the formal center of unpaired spin density ( $C_{\alpha}$ ) is separated from the charge-carrying residues through a non-resonant bridge. As before, our interest here is to study the effect of terminal charge on the strength of the  $C_{\alpha}$ –H bond, which will be reported in terms of the “charge-induced RSE” (ciRSE) calculated as the difference between the RSE values of neutral and charged radicals as expressed by eqn 2c in Figure 7.

Table 2 presents the ciRSE values for acidic and basic AA dipeptide models calculated at different levels of theory to facilitate comparison to the glycine dipeptide results. In the discussion we will focus on the conformationally averaged results derived from enthalpy values  $\Delta H_{298}$  calculated at the G3B3 level. For the sake of reference, Figure 8 also includes an RSE scale for each of the participating neutral/ionic radicals and glycyl radical **1r** as the reference located at  $\text{RSE}(\mathbf{1r}) = -76.3$  kJ/mol. Relative to this value, introduction of the aspartic acid side

**Table 2.** Boltzmann Averaged ciRSE Values ( $\Delta H_{298}$ , kJ/mol) for  $C_\alpha$  Centered Radicals for Acidic and Basic AA Dipeptide Models at Different Levels of Theory ( $\Delta E_{\text{tot}}$  Values are Given in Parenthesis)<sup>a</sup>

Dipeptide Model (distonic state)	B3LYP /sb	M06-2X /mb	B2PLYP /lb	G3(MP2)-RAD	G3B3
r3	0.0	-2.9 (-3.8)	+2.3	+0.6	+1.7
r4	-1.5	+8.6 (+13.8)	+3.2	+7.1	+7.5
r5H	+10.7	+10.5 (+15.1)	+13.9	+9.7	+9.0
r6H	+5.3	-20.8 (-20.0)	+1.4	-15.1	-16.8
r7H	+3.2	+7.5 (+7.5)	+3.5	+6.5	+7.6

<sup>a</sup>sb = 6-31G(d), mb = 6-31+G(d), lb = G3MP2large.

chain leads to a small increase in stability with  $\text{RSE}(\text{r3H}) = -77.3$  kJ/mol. Deprotonation of the terminal carboxylic acid group leads to destabilization of radical r3 with  $\text{RSE}(\text{r3}) = -75.7$  kJ/mol, and thus an overall small destabilization of the radical through anion formation of  $\text{ciRSE} = +1.7$  kJ/mol. Although it is tempting to interpret this change as the result of electrostatic interactions between the radical center and the carboxylate side chain, the inspection of the preferred conformations for closed-shell parents and their radical forms shows that direct hydrogen bonding interactions between the side chain residue and the dipeptide backbone are likely to be more relevant (Figure 9).

In agreement with earlier theoretical studies of this system,<sup>48–52</sup> the closed-shell neutral parent 3H prefers a local  $C_7$  conformation stabilized by hydrogen bonds between the carboxylic acid side chain and the amide backbone. A largely similar structure based on a  $C_5$  backbone conformation is only marginally less stable, and actually preferred for the corresponding  $C_\alpha$  radical r3H.<sup>53</sup>

In contrast, the deprotonated carboxylate serves as a hydrogen-bond acceptor to the dipeptide backbone N–H bonds in both the closed-shell parent 3 as well as is radical r3. We may thus conclude that the charge-induced stabilization/destabilization of dipeptide radicals must be seen as the result of various factors, the accurate size of which is difficult to assess. A similarly complex interplay of hydrogen bonding interactions and charge effects is at work in the other systems studied here. For glutamate, these effects appear to be larger compared to aspartate in that deprotonation of the carboxylate group leads to a destabilization of the radical center by 7.5 kJ/mol (Figure 8).

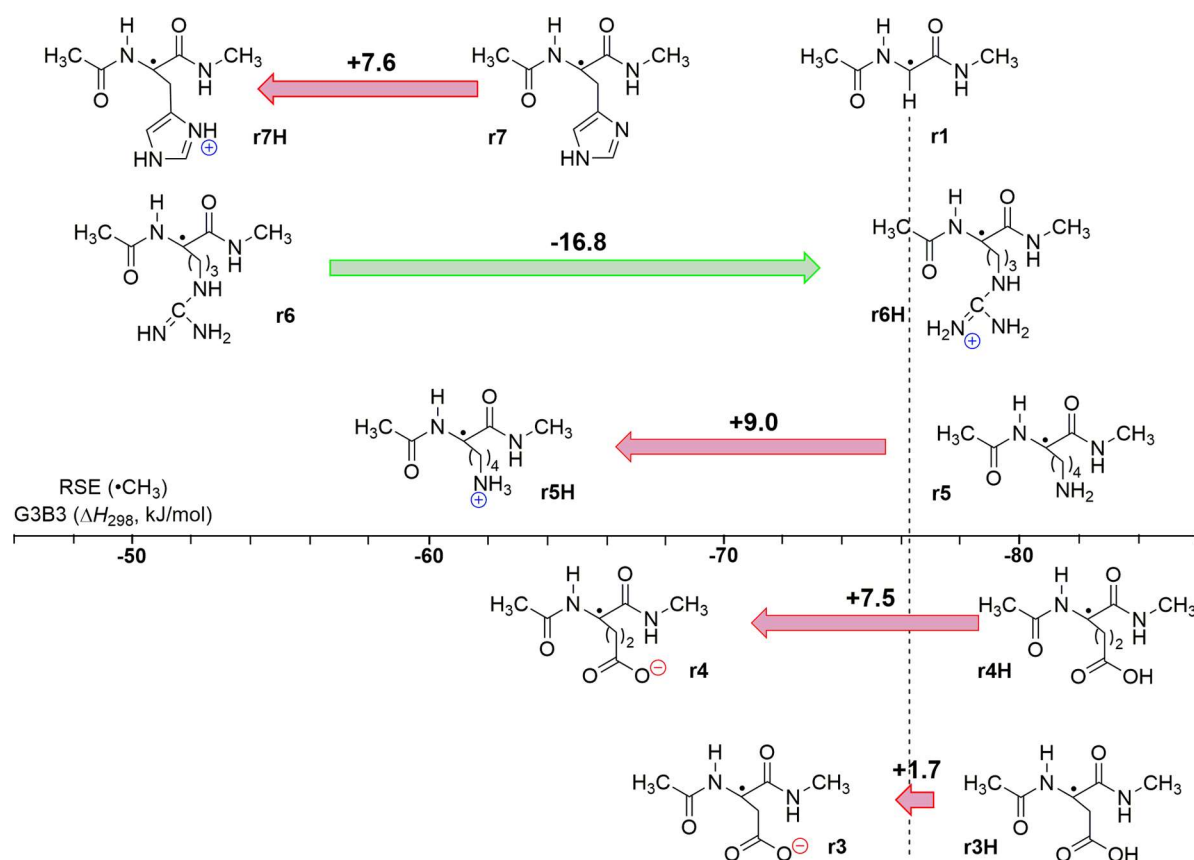


**Figure 8.** RSE values for neutral and charged  $C_\alpha$  radicals of acidic and basic AAs calculated at the G3B3 level (Boltzmann averaged,  $\Delta H_{298}$ , kJ/mol). The length of the bar and numerical values above shows the magnitude of ciRSE for the respective systems.

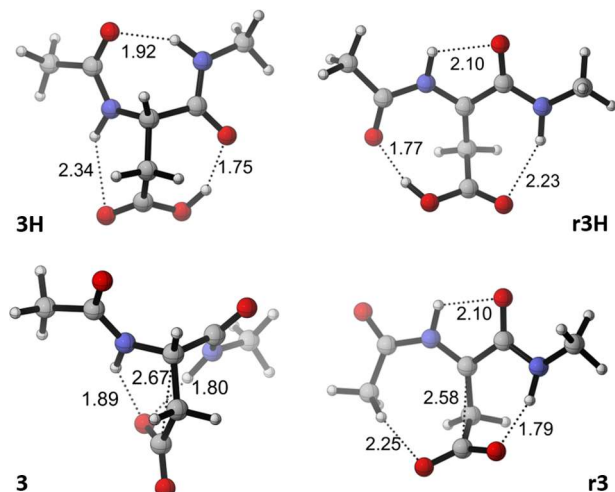


**Figure 9.** Preferred conformations for aspartic acid dipeptide model **3H**, its deprotonated form **3**, and the respective  $C_{\alpha}$  radicals **r3H** and **r3**.

An effect of similar magnitude is seen for lysine and histidine radicals, where protonation of the basic side chains leads to distonic radical cations destabilized by 9.0 and 7.6 kJ/mol, respectively, relative to their neutral counterparts. The only case of charge-induced radical stabilization occurs for arginine, where the  $C_{\alpha}$  radical cation **r6H** is more stable than neutral radical **r6** by 16.8 kJ/mol. Analysis of the energetically best conformations in all of these systems (see the *SI*) indicates the presence of hydrogen bonding interactions between the neutral and charged side chain residues and the dipeptide amide groups. It is only for lysine dipeptide model **5** that remote charge effects on radical stability can be analyzed in some more detail. This is due to the fact that local minima with fully extended side chains can be located for neutral parent **5** and its radical **r5**. These conformers are much less stable than the respective folded alternatives with hydrogen bonding contacts to the backbone amide groups, but can be utilized to construct extended conformers for the protonated parent **5H** and its radical **r5H**. Analysis of these results obtained at the (U)M06-2X/6-31+G(d) level used before shows that protonation of radical **r5** reduces its stability by 7.2 kJ/mol (see *SI* for details), a value closely similar to that shown in *Figure 8* for the conformationally averaged systems. Elimination of the covalent bridge between the  $C_{\alpha}$  radical center and the side chain amino group reduces this value to only 2.5 kJ/mol, which implies that the external charge effects on the stabilities of the neutral and ionic dipeptide models shown in *Figure 8* are quite small and that other effects such as variations in the hydrogen bond energies between side chain functional groups and backbone amide units as well as through-bond interactions between the same entities dominate. It should be added here that the RSE values reported in *Figure 8* and *Table 2* for fully conformationally averaged radicals and closed-shell parents differ significantly from those reported earlier by Rauk et al.<sup>48</sup> In this latter study dipeptide models and their radicals were conformationally biased such that they reflect the situation in disordered regions of proteins. This implies that experimental validation of the charge effects shown in *Figure 8* depends on the conformational freedom accessible under the respective experimental conditions.

## CONCLUSIONS

Remotely located monovalent ions such as chloride ( $\text{Cl}^-$ ) and sodium cation ( $\text{Na}^+$ ) have a significant influence on the stability of glycine dipeptide radical **r1**. The charge and orientation of the ion determine its interactions with the radical center. Positioning  $\text{Cl}^-$  and  $\text{Na}^+$  ions at  $180^\circ$  in the  $xy$ -plane leads to stabilizing ( $-9.7$  kJ/mol) and destabilizing ( $+8.8$  kJ/mol) effects on radical **r1**, respectively. Appropriately positioned point charges (PCs) and external electric fields (EEFs) reproduce these effects. Charge stabilizing effects for **r1** are stronger in the  $xy$ -plane compared to the  $xz$ - and  $yz$ -plane(s). The (de)protonated side chain functional groups in acidic and basic AAs destabilize the corresponding peptide radicals except for the case of arginine, where protonation stabilizes cation-radical (**r6H**) by  $-16.8$  kJ/mol. These latter variations in peptide radical stability are, however, more a consequence of direct interactions (such as hydrogen bonding contacts) between charged side chains and the peptide backbone than a reflection of external electric field effects.

## ASSOCIATED CONTENT

### Supporting Information

The Supporting Information is available free of charge on the ACS Publications website at DOI: 10.1021/acs.jpccb.8b07485.

Methodology; stabilization of radical; glycine radical enzyme; methodology consideration; glycine dipeptide and its complexation with  $\text{Cl}^-$  and  $\text{Na}^+$ ; distonic peptide system (PDF)  
Coordinate files (ZIP)

## AUTHOR INFORMATION

### Corresponding Author

\*E-mail: zipse@cup.uni-muenchen.de.

### ORCID

Hendrik Zipse: 0000-0002-0534-3585

### Notes

The authors declare no competing financial interest.

## ACKNOWLEDGMENTS

Financial support by the Deutsche Forschungsgemeinschaft (DFG) through the SFB 749 on “Dynamics and Intermediates of Molecular Transformations” (project C6) and COST action CM1201 are gratefully acknowledged. The authors also acknowledge the generous allocation of computational resources by the LRZ computing center.

## ABBREVIATIONS

EEF, external electric field; PC, point charge; RSE, radical stabilization energy; ciRSE, charge-induced radical stabilization energy; CSCE, closed-shell complexation energy; RCE, radical complexation energy

## REFERENCES

- (1) Meir, R.; Chen, H.; Lai, W.; Shaik, S. Oriented Electric Fields Accelerate Diels–Alder Reactions and Control the endo/exo Selectivity. *ChemPhysChem* **2010**, *11*, 301–310.
- (2) Aragonès, A. C.; Haworth, N. L.; Darwish, N.; Ciampi, S.; Bloomfield, N. J.; Wallace, G. G.; Diez-Perez, I.; Coote, M. L. Electrostatic catalysis of a Diels–Alder reaction. *Nature* **2016**, *531*, 88–91.
- (3) Shaik, S.; Mandal, D.; Ramanan, R. Oriented electric fields as future smart reagents in chemistry. *Nat. Chem.* **2016**, *8*, 1091–1098.

- (4) Xiang, L.; Tao, N. Reactions triggered electrically. *Nature* **2016**, *531*, 38–39.
- (5) Aitken, H. M.; Coote, M. L. Can electrostatic catalysis of Diels–Alder reactions be harnessed with pH-switchable charged functional groups? *Phys. Chem. Chem. Phys.* **2018**, *20*, 10671–10676.
- (6) Ramanan, R.; Danovich, D.; Mandal, D.; Shaik, S. Catalysis of Methyl Transfer Reactions by Oriented External Electric Fields: Are Gold-Thiolate Linkers Innocent? *J. Am. Chem. Soc.* **2018**, *140*, 4354–4362.
- (7) Che, F.; Gray, J. T.; Ha, S.; Kruse, N.; Scott, S. L.; McEwen, J.-S. Elucidating the Roles of Electric Fields in Catalysis: A Perspective. *ACS Catal.* **2018**, *8*, 5153–5174.
- (8) Lari, G. M.; Puértolas, B.; Shahrokhi, M.; López, N.; Pérez-Ramírez, J. Hybrid Palladium Nanoparticles for Direct Hydrogen Peroxide Synthesis: The Key Role of the Ligand. *Angew. Chem.* **2017**, *129*, 1801–1805.
- (9) Zhang, L.; Vogel, Y. B.; Noble, B. B.; Gonçalves, V. R.; Darwish, N.; Brun, A. L.; Gooding, J. J.; Wallace, G. G.; Coote, M. L.; Ciampi, S. TEMPO Monolayers on Si(100) Electrodes: Electrostatic Effects by the Electrolyte and Semiconductor Space-Charge on the Electroactivity of a Persistent Radical. *J. Am. Chem. Soc.* **2016**, *138*, 9611–9619.
- (10) Borca, B.; Michnowicz, T.; Pétuya, R.; Pristl, M.; Schendel, V.; Pentegov, I.; Kraft, U.; Klauk, H.; Wahl, P.; Gutzler, R.; et al. Electric-Field-Driven Direct Desulfurization. *ACS Nano* **2017**, *11*, 4703–4709.
- (11) Cassone, G.; Pietrucci, F.; Saija, F.; Guyot, F.; Saitta, A. M. One-step electric-field driven methane and formaldehyde synthesis from liquid methanol. *Chem. Sci.* **2017**, *8*, 2329–2336.
- (12) Geng, C.; Li, J.; Weiske, T.; Schlangen, M.; Shaik, S.; Schwarz, H. Electrostatic and Charge-Induced Methane Activation by a Concerted Double C–H Bond Insertion. *J. Am. Chem. Soc.* **2017**, *139*, 1684–1689.
- (13) Zhang, L.; Laborda, E.; Darwish, N.; Noble, B. B.; Tyrell, J. H.; Pluczyk, S.; Le Brun, A. P.; Wallace, G. G.; Gonzalez, J.; Coote, M. L.; et al. Electrochemical and Electrostatic Cleavage of Alkoxyamines. *J. Am. Chem. Soc.* **2018**, *140*, 766–774.
- (14) Gorin, C. F.; Beh, E. S.; Kanan, M. W. An electric field-induced change in the selectivity of a metal oxide-catalyzed epoxide rearrangement. *J. Am. Chem. Soc.* **2011**, *134*, 186–189.
- (15) Che, F.; Gray, J. T.; Ha, S.; McEwen, J.-S. Improving Ni Catalysts Using Electric Fields: A DFT and Experimental Study of the Methane Steam Reforming Reaction. *ACS Catal.* **2016**, *7*, 551–562.
- (16) Akamatsu, M.; Sakai, N.; Matile, S. Electric-Field-Assisted Anion- $\pi$  Catalysis. *J. Am. Chem. Soc.* **2017**, *139*, 6558–6561.
- (17) Warshel, A.; Sharma, P. K.; Kato, M.; Xiang, Y.; Liu, H.; Olsson, M. H. Electrostatic Basis for Enzyme Catalysis. *Chem. Rev.* **2006**, *106*, 3210–3235.
- (18) Fried, S. D.; Boxer, S. G. Electric Fields and Enzyme Catalysis. *Annu. Rev. Biochem.* **2017**, *86*, 387–415.
- (19) Morgenstern, A.; Jaszai, M.; Eberhart, M. E.; Alexandrova, A. N. Quantified electrostatic preorganization in enzymes using the geometry of the electron charge density. *Chem. Sci.* **2017**, *8*, 5010–5018.
- (20) Shaik, S.; de Visser, S. P.; Kumar, D. External electric field will control the selectivity of enzymatic-like bond activations. *J. Am. Chem. Soc.* **2004**, *126*, 11746–11749.
- (21) Lai, W.; Chen, H.; Cho, K.-B.; Shaik, S. External Electric Field Can Control the Catalytic Cycle of Cytochrome P450<sub>cam</sub>: A QM/MM Study. *J. Phys. Chem. Lett.* **2010**, *1*, 2082–2087.
- (22) Fried, S. D.; Bagchi, S.; Boxer, S. G. Extreme electric fields power catalysis in the active site of ketosteroid isomerase. *Science* **2014**, *346*, 1510–1514.
- (23) Fried, S. D.; Boxer, S. G. Measuring Electric Fields and Noncovalent Interactions Using the Vibrational Stark Effect. *Acc. Chem. Res.* **2015**, *48*, 998–1006.
- (24) Wu, Y.; Boxer, S. G. A Critical Test of the Electrostatic Contribution to Catalysis with Noncanonical Amino Acids in Ketosteroid Isomerase. *J. Am. Chem. Soc.* **2016**, *138*, 11890–11895.
- (25) Maji, R.; Wheeler, S. E. Importance of Electrostatic Effects in the Stereoselectivity of NHC-Catalyzed Kinetic Resolutions. *J. Am. Chem. Soc.* **2017**, *139*, 12441–12449.
- (26) Forbes, M. D. Radicals with multiple personalities. *Nat. Chem.* **2013**, *5*, 447–449.
- (27) Gryn'ova, G.; Coote, M. L. Origin and Scope of Long-Range Stabilizing Interactions and Associated SOMO–HOMO Conversion in Distonic Radical Anions. *J. Am. Chem. Soc.* **2013**, *135*, 15392–15403.
- (28) Gryn'ova, G.; Marshall, D. L.; Blanksby, S. J.; Coote, M. L. Switching radical stability by pH-induced orbital conversion. *Nat. Chem.* **2013**, *5*, 474–481.
- (29) Gryn'ova, G.; Smith, L. M.; Coote, M. L. Computational design of pH-switchable control agents for nitroxide mediated polymerization. *Phys. Chem. Chem. Phys.* **2017**, *19*, 22678–22683.
- (30) Gryn'ova, G.; Coote, M. L. Directionality and the Role of Polarization in Electric Field Effects on Radical Stability. *Aust. J. Chem.* **2017**, *70*, 367–372.
- (31) Franchi, P.; Mezzina, E.; Lucarini, M. SOMO–HOMO Conversion in Distonic Radical Anions: An Experimental Test in Solution by EPR Radical Equilibration Technique. *J. Am. Chem. Soc.* **2014**, *136*, 1250–1252.
- (32) Klinska, M.; Smith, L. M.; Gryn'ova, G.; Banwell, M. G.; Coote, M. L. Experimental demonstration of pH-dependent electrostatic catalysis of radical reactions. *Chem. Sci.* **2015**, *6*, 5623–5627.
- (33) Morris, M.; Chan, B.; Radom, L. Effect of Protonation State and Interposed Connector Groups on Bond Dissociation Enthalpies of Alcohols and Related Systems. *J. Phys. Chem. A* **2014**, *118*, 2810–2819.
- (34) Hioe, J.; Zipse, H. Radicals in enzymatic catalysis — a thermodynamic perspective. *Faraday Discuss.* **2010**, *145*, 301–313.
- (35) Hioe, J.; Zipse, H. Radical stability and its role in synthesis and catalysis. *Org. Biomol. Chem.* **2010**, *8*, 3609–3617.
- (36) Hioe, J.; Savasci, G.; Brand, H.; Zipse, H. The Stability of C $\alpha$  Peptide Radicals: Why Glycyl Radical Enzymes? *Chem. Eur. J.* **2011**, *17*, 3781–3789.
- (37) Hioe, J.; Zipse, H. Hydrogen Transfer in SAM-Mediated Enzymatic Radical Reactions. *Chem. - Eur. J.* **2012**, *18*, 16463–16472.
- (38) Hioe, J.; Mosch, M.; Smith, D. M.; Zipse, H. Dissociation energies of C $\alpha$ –H bonds in amino acids — a re-examination. *RSC Adv.* **2013**, *3*, 12403–12408.
- (39) Hariharan, P. C.; Pople, J. A. The influence of polarization functions on molecular orbital hydrogenation energies. *Theor. Chim. Acta* **1973**, *28*, 213–222.
- (40) Becke, A. D. Density-functional thermochemistry. III. The role of exact exchange. *J. Chem. Phys.* **1993**, *98*, 5648–5652.
- (41) Frisch, M. J.; Trucks, G. W.; Schlegel, H. B.; Scuseria, G. E.; Robb, M. A.; Cheeseman, J. R.; Scalmani, G.; Barone, V.; Mennucci, B.; Petersson, G. A.; et al. *Gaussian 09*; Gaussian, Inc.: Wallingford, CT, 2009.
- (42) Zhao, Y.; Truhlar, D. G. The M06 suite of density functionals for main group thermochemistry, thermochemical kinetics, noncovalent interactions, excited states, and transition elements: two new functionals and systematic testing of four M06-class functionals and 12 other functionals. *Theor. Chem. Acc.* **2008**, *120*, 215–241.
- (43) Zhao, Y.; Truhlar, D. G. Density Functionals with Broad Applicability in Chemistry. *Acc. Chem. Res.* **2008**, *41*, 157–167.
- (44) Graham, D. C.; Menon, A. S.; Goerigk, L.; Grimme, S.; Radom, L. Optimization and Basis-Set Dependence of a Restricted-Open-Shell Form of B2-PLYP Double-Hybrid Density Functional Theory. *J. Phys. Chem. A* **2009**, *113*, 9861–9873.
- (45) Henry, D. J.; Parkinson, C. J.; Radom, L. An Assessment of the Performance of High-Level Theoretical Procedures in the Computation of the Heats of Formation of Small Open-Shell Molecules. *J. Phys. Chem. A* **2002**, *106*, 7927–7936.
- (46) Baboul, A. G.; Curtiss, L. A.; Redfern, P. C.; Raghavachari, K. Gaussian-3 theory using density functional geometries and zero-point energies. *J. Chem. Phys.* **1999**, *110*, 7650–7657.
- (47) Yates, B. F.; Bouma, W. J.; Radom, L. Detection of the Prototype Phosphonium (CH<sub>2</sub>PH<sub>3</sub>), Sulfonium (CH<sub>2</sub>SH<sub>2</sub>), and Chloronium (CH<sub>2</sub>C<sub>1</sub>H) Ylides by Neutralization-Reionization Mass Spectrometry: A Theoretical Prediction. *J. Am. Chem. Soc.* **1984**, *106*, 5805–5808.
- (48) Rauk, A.; Yu, D.; Taylor, J.; Shustov, G. V.; Block, D. A.; Armstrong, D. A. Effects of Structure on <sup>o</sup>C–H Bond Enthalpies of

Amino Acid residues: relevance of H Transfers in Enzyme Mechanisms and in Protein Oxidation. *Biochemistry* **1999**, *38*, 9089–9096.

(49) Herrmann, K. A.; Wysocki, V. H.; Vorpapel, E. R. Computational investigation and hydrogen/deuterium exchange of the fixed charge derivative tris(2,4,6-Trimethoxyphenyl) phosphonium: Implications for the aspartic acid cleavage mechanism. *J. Am. Soc. Mass Spectrom.* **2005**, *16*, 1067–1080.

(50) Rozman, M. Aspartic acid side chain effect—Experimental and theoretical insight. *J. Am. Soc. Mass Spectrom.* **2007**, *18*, 121–127.

(51) Yuan, Y.; Mills, M. J. L.; Popelier, P. L. A.; Jensen, F. Comprehensive Analysis of Energy Minima of the Natural Amino Acids. *J. Phys. Chem. A* **2014**, *118*, 7876–7891.

(52) Chan, B.; Karton, A.; Easton, C. J.; Radom, L.  $\alpha$ -Hydrogen Abstraction by  $\bullet$ OH and  $\bullet$ SH Radicals from Amino Acids and Their Peptide Derivatives. *J. Chem. Theory Comput.* **2016**, *12*, 1606–1613.

(53) Which of the energetically close lying minima is preferred appears to depend on the particular choice of Hamiltonian and basis set, the preference of enthalpies or Gibbs free energies, and, most notably, on additional assumptions made for conformational selection.

## 3.1 Supporting Information

### For: Electrostatic Effects on The Stability of Peptide Radicals

---

#### 3.1.1 Introduction

##### 3.1.1.1 Naming conventions used in the SI

- 1) Glycine dipeptide (Gly, **1**) and its C<sub>α</sub> radical (rGly, **r1**)
- 2) Methane (CH<sub>4</sub>, **2**) and methyl radical (CH<sub>3</sub>, **r2**)
- 3) Complex of **1/r1** with ions is denoted as **1/r1+Cl<sup>-</sup>** and **1/r1+Na<sup>+</sup>**
- 4) External Electric Field (**EEF**)
- 5) Point Charge (**PC**)
- 6) Radical Stabilization Energy (**RSE**)
- 7) Charge-induced Radical Stabilization Energy (**ciRSE**)
- 8) Closed Shell Complexation Energy (**CSCE**)
- 9) Radical Complexation Energy (**RCE**)
- 10) Total Electronic Energy (**ΔE<sub>tot</sub>**)
- 11) Gibbs free energy (**ΔG<sub>298</sub>**)
- 12) Enthalpy (**ΔH<sub>298</sub>**)
- 13) Thermal correction of enthalpy (**corr. ΔH**) and for Gibbs free energy (**corr. ΔG**)

##### 3.1.1.2 Methodology

Force field-based calculations: MacroModel<sup>1</sup> module of Maestro 10.2, was employed for molecular mechanics (MM)-based conformational search using the OPLS 2005 force field.

Quantum mechanics calculations: The geometries of the C<sub>5</sub> conformer of **1/r1** were optimized at the (U)B3LYP/6-31G(d)<sup>2</sup> level of theory in the gas phase. Single point calculations were done at (U)B3LYP/6-31G(d), (U)M06-2X/6-31+G(d)<sup>3</sup>, double hybrid (RO)B2-PLYP/G3MP2Large<sup>4</sup>, composite methods G3(MP3)-RAD<sup>5</sup>, and G3B3<sup>6</sup> on the frozen coordinates of **1/r1** in the presence of an external ion, point charge and electric field. The initial investigation is conducted on the **1/r1** + ion (Cl<sup>-</sup>/Na<sup>+</sup>) system for selected ion orientations along the ± xyz axes as explained in section 3.1.3, to identify a suitable level of theory for further exploring the effects of remote charge on the stability of C<sub>α</sub> radicals in dipeptides. The energies were calculated for a temperature of 298.15 K in the gas phase and the thermal corrections to the enthalpy and Gibb's free energy were obtained at the (U)B3LYP/6-31G(d) level of theory. ZPE corrections were scaled by factors of 0.9806 and 0.960 for G3(MP2)-RAD and G3B3 calculations, respectively. All calculations were performed using Gaussian09, Rev. D.01.<sup>7</sup>

##### 3.1.1.3 Stabilization of radical **r1**

The stability of C<sub>α</sub> radical of 2-acetamino-N-methylacetamide (glycine dipeptide radical, **r1**) is measured in reference to a methyl radical (**r2**) using the isodesmic hydrogen exchange reaction shown in eq. 1a, and the reaction energy is termed as the radical stabilization energy (**RSE**). In case of Boltzmann averaged RSE values, the conformationally avg. energy values of **1/r1** are used to determine the RSE.<sup>1</sup> For the purpose of this study, only all-*trans* extended C<sub>5</sub> conformations were chosen for both **1** and **r1**. The symmetrical nature of C<sub>5</sub> is very helpful for this study. To determine the influence of external charges on the stability of the C<sub>α</sub> radical, both **1** and **r1** are complexed with an external ions and the RSE is calculated using these complexed system as shown in eq. 1b in Figure S3-1.



**Table S3-1.** [Table S1] Geometrical details of the active site glycine residue in GREs.

SI	Enzyme	Database	ID	Radical site sequence	In PDB			After Opt. at B3LYP/6-31G(d,p)		
					$\Phi$	$\Psi$	$C_\alpha$ Conf.	$\Phi$	$\Psi$	$C_\alpha$ Conf.
1	Pfl	RPDB	1H16	SER-GLY734( <b>R</b> )-TYR	135.6	9.3	$\beta_2$	122.6	338.2	$\beta_2$
2	Gdh	RPDB	1R8W	ALA-GLY763( <b>R</b> )-TYR	92.1	353.7	$C_7$	122.5	338.3	$\beta_2$
3	Pfl-2	RPDB	2F3O	ALA-GLY752( <b>R</b> )-TRP	158.0	356.6	$\beta_2$	122.6	338.2	$\beta_2$
4	Hpd	RPDB	2Y8N	ALA-GLY873( <b>R</b> )-PHE	77.0	3.5	$\alpha_R$	82.4	291.8	$C_7$
5	CutC	Uniprot	S6ZPB0	ALA-GLY1103( <b>R</b> )-TYR	-	-	-	-	-	-
6	Bss	Uniprot	087943	SER-GLY825( <b>R</b> )-PHE	-	-	-	-	-	-
7	Nrd III	Uniprot	P07071	CYS-GLY580( <b>R</b> )-TYR	-	-	-	-	-	-
8	Nrd III	RPDB	1HK8	CYS-ALA580( <b>R</b> )-TYR	-	-	-	-	-	-

### 3.1.2 Glycine Dipeptide (1)

**Table S3-2.** [Table S2] Radical stabilization energies (RSEs, in kJ/mol) calculated at different levels of theory for the  $C_\alpha$  radical of glycine dipeptide **r1** shown in eq. 1a, Figure S3-1.

	(U)B3LYP \6-31G(d) <sup>a</sup>			(U)M062X \6-31+G(d) <sup>b</sup>			(RO)B2PLYP \GTMP2large <sup>b</sup>			G3(MP2)-RAD <sup>b</sup>			G3B3 <sup>b</sup>			(U)M062X \6-31+G(d) <sup>a</sup>		
	$\Delta E$	$\Delta H_{298}$	$\Delta G_{298}$	$\Delta E$	$\Delta H_{298}$	$\Delta G_{298}$	$\Delta E$	$\Delta H_{298}$	$\Delta G_{298}$	$\Delta E$	$\Delta H_{298}$	$\Delta G_{298}$	$\Delta E$	$\Delta H_{298}$	$\Delta G_{298}$	$\Delta E$	$\Delta H_{298}$	$\Delta G_{298}$
Best Conf.	-105.2	-101.3	-96.9	-88.1	-84.1	-79.8	-93.2	-89.3	-84.1	-77.9	-74.1	-74.6	-79.2	-75.5	-76.5	-87.8	-83.3	-79.7
<b>C5_tt (CS Sym)</b>	<b>-108.7</b>	-103.2	-94.2	<b>-91.7</b>	-86.2	-77.2	<b>-96.0</b>	-90.5	-81.4	<b>-83.6</b>	-78.2	-71.9	<b>-85.4</b>	-80.2	-73.8	<b>-92.5</b>	-87.0	-79.7
Boltzmann Avg.	-106.3	-102.1	-96.6	-89.1	-85.0	-79.4	-94.2	-89.8	-83.7	-78.7	-75.0	-74.2	-79.9	-76.3	-76.1	-88.0	-83.6	-79.4

<sup>a</sup>Level of geometry optimization. <sup>b</sup>Single point energy calculations over (U)B3LYP/6-31G(d) optimized geometries.

### 3.1.3 Methodology Consideration

#### 3.1.3.1 Coordinate system convention

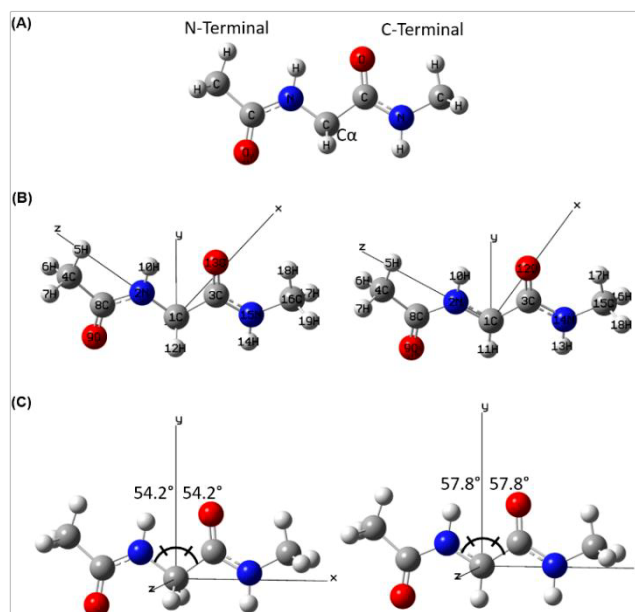


**Figure S3-3.** [Figure S5] (A) Extended C<sub>5</sub> conformation for **1**. (B) Default xyz coordinate system obtained from the Z-matrix of the B3LYP/6-31G(d) optimized geometries. (C) Reoriented **1/r1** and associated coordinate system.

The coordinate system used for glycine dipeptide **1** and the corresponding C<sub>α</sub> radical **r1** plays a very important role in this study, as it involves the external charges, ions and electric fields. The relative orientation of the external charges, ions and electric fields with respect to **1/r1** is among the major factors that influence the stability of **1/r1**. The study restricts itself to the extended C<sub>5</sub> conformation (CSSym) for **1/r1**, where all non-hydrogen atoms lie in a plane and both peptide bonds are in *trans* configuration as shown in Figure S3-3 (A). The geometry optimization of **1/r1** is carried out at (U)B3LYP/6-31G(d) level in the gas phase. The default xyz coordinates obtained from the Z-matrix of the optimized geometry has the C<sub>α</sub>(1) at the origin, while that +z axis passes through the C<sub>α</sub>(1)-N(2) bond and the +x axis lies in the same plane as all non-hydrogen atoms of **1/r1** [see Figure S3-3 (B)]. The structure is oriented such that C<sub>α</sub> remains the centre of the coordinate system (0,0,0) for both **1/r1**. The +y axis is a bisector of the angle made by atoms N(2)-C<sub>α</sub>(1)-C(3), and the x axis lies in the plane of all non-hydrogen atoms as shown in Figure S3-3 (C). Ghost atoms were used to reorient the molecule in the above-said manner from its default orientation.

#### 3.1.3.2 Placement of external ions (Cl<sup>-</sup>/Na<sup>+</sup>) along the ± xyz axes for the initial investigation

The initial investigation involves an ion placed along the ± xyz axes away from the central C<sub>α</sub> in such a way that the ion is 5 Å away from the nearest atom(s) in **1/r1**. In the following, we show the calculation for placing Cl<sup>-</sup> anion along the +y axis, 5 Å away from the nearest atom in **1** and the same strategy is used for all other directions.

**Placing Cl<sup>-</sup> along the +y axis:** First, we have to determine the atom in **1** that is going to be the closest to the ion Cl<sup>-</sup> placed along the +y axis. In this case, the C-terminal carbonyl oxygen (O<sub>c</sub>) lies nearest to Cl<sup>-</sup>. The Cl<sup>-</sup> thus has to be moved along the +y axis away from C<sub>α</sub> (centre of our coordinate system) till the distance between Cl<sup>-</sup> and O<sub>c</sub> becomes 5 Å. In this system, Cl<sup>-</sup>, C<sub>α</sub> and O<sub>c</sub> form a triangle, where we know the length of two sides (C<sub>α</sub>-O<sub>c</sub> = 2.4 Å and O<sub>c</sub>-Cl<sup>-</sup> = 5.0 Å) and one angle (O<sub>c</sub>-C<sub>α</sub>-Cl = 28.6°) as depicted in Figure S3-4. The side, side, angle (SSA) theorem is used to solve this triangle to determine the other necessary geometrical parameters. Figure S3-4 lists the different

steps of calculation along with a geometrical description for the  $\mathbf{1}+\text{Cl}^-$  system along the  $+y$  axis. As mentioned earlier, the exact same calculation is used for placing  $\text{Cl}^-$  in other directions.

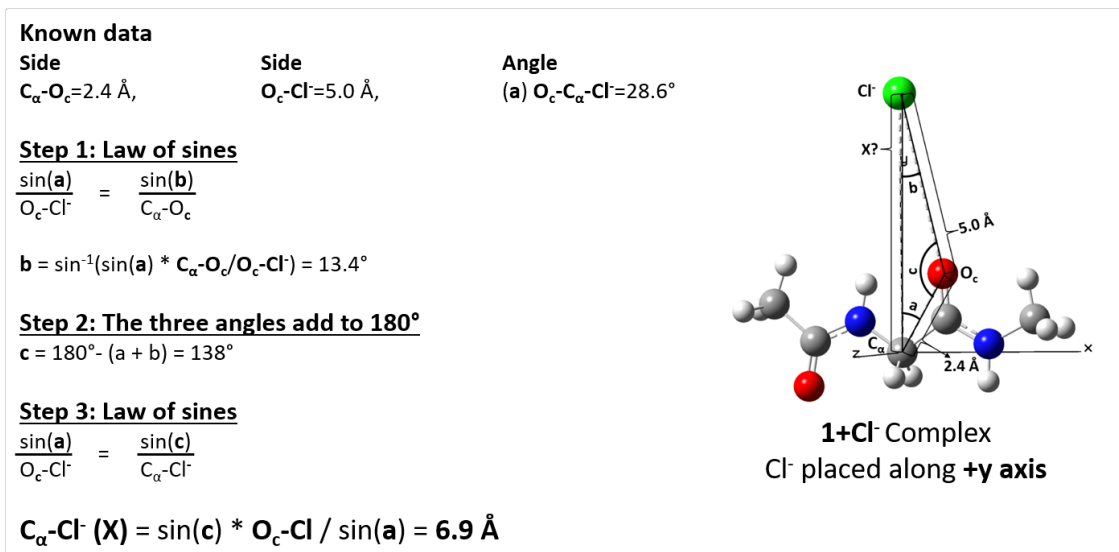


**Figure S3-4.** [Figure S6] Calculation for placing  $\text{Cl}^-$  along  $+y$  axis at  $5 \text{ \AA}$  away from the nearest atom in  $\mathbf{1}$  using the coordinate conventions defined in the previous section.

Similarly, coordinates for the ion are determined for the other directions. Placing an ion along the  $\pm z$  axes leads to an identical arrangements, so we limit ourselves here to the  $+z$  axis.

### 3.1.3.3 $\text{Cl}^-$ along $\pm xyz$ axes, $5 \text{ \AA}$ from $\mathbf{1}/\mathbf{r1}$ .

In this section, we discuss (U)B3LYP/6-31G(d) results from our initial investigation on  $\mathbf{1}/\mathbf{r1}+\text{Cl}^-$  systems for selected  $\text{Cl}^-$  orientations along the  $\pm xyz$  axes around  $\mathbf{1}/\mathbf{r1}$  using different convergence procedures. An isolated  $\mathbf{1}$ ,  $\mathbf{r1}$ ,  $\text{CH}_4$ ,  $\text{CH}_3$  and  $\text{Cl}^-$  ion are relatively easy to calculate using (U)B3LYP (a commonly used hybrid DFT method) with the 6-31G(d) basis set, compared to the  $\mathbf{r1}+\text{Cl}^-$  complex that has both unpaired spin and charge. In case of the former isolated systems, SCF calculations converge to stable wave function irrespective of the SCF algorithm (DIIS or QC), which is contrast to the behaviour of the complex systems ( $\mathbf{r1}+\text{Cl}^-$ ).

**Default convergent SCF procedure (DIIS):** In G09, The DIIS procedure is the default and uses a combination of the energy-direct inversion in the iterative subspace (EDIIS) and commutator-DIIS (CDIIS) extrapolation methods. In case of the  $\mathbf{r1}+\text{Cl}^-$  complex, The default SCF procedure has convergence problems at the (U)B3LYP/6-31G(d) level of theory, when  $\text{Cl}^-$  is placed along the  $+x$  axis. For the  $-x$  and  $+z$  directions the SCF converges and gives a stable wavefunction, while for the  $\pm y$  axes the SCF converges to a wavefunction with internal instability (see Table S3-3 for more details). The wavefunction obtained from the default convergence procedure can be described as delocalized and it is energetically favourable, see Figure S3-5. The presence of an external  $\text{Cl}^-$  always leads to a decrease in  $\text{C}_\alpha\text{-H}$  bond strength at  $\text{C}_\alpha$  of  $\mathbf{1}$ , as indicated by negative  $\text{ciRSE}$  values. The magnitude of the effect is strongly influenced by the relative orientation of  $\text{Cl}^-$  relative to  $\mathbf{1}/\mathbf{r1}$  ( $>-18 \text{ kJ/mol}$  for  $-x$  axis, while  $<-2 \text{ kJ/mol}$  for  $+z$  axis), but the nature of the effect remains the same, i.e. a decrease in  $\text{C}_\alpha\text{-H}$  bond strength. The delocalized nature of the wavefunction (obtained using DIIS) is apparent when we look at the spin density surfaces of the  $\mathbf{r1}+\text{Cl}^-$  complex (see Figure S3-5). For all orientations of  $\text{Cl}^-$  where the SCF converge, there is spin transfer from  $\mathbf{r1}$  to  $\text{Cl}^-$ , and charge transfer occurs vice-versa.

**Quadratically convergent SCF procedure (QC):** It is slower than the default DIIS extrapolation, but more reliable. The SCF converges to a wavefunction with internal instability with the QC algorithm for the  $\mathbf{r1+Cl}^-$  complexes at (U)B3LYP/6-31G(d) level for all orientations of  $\text{Cl}^-$ . The wavefunction obtained with the QC algorithm can be described as localized, where  $\text{Cl}^-$  is having almost a unit negative charge while the spin density is localized on  $\mathbf{r1}$  for all orientations except the +z direction [see Figure S3-5(B)]. The wavefunction is energetically less favourable than that obtained from DIIS [see Figure S3-5(A)] and after re-optimization (stable=opt), it converges back to the energetically more favourable delocalized state. The wavefunctions from both DIIS and QC converged to the same stable wavefunction after re-optimization. The ciRSE values calculated at (U)B3LYP/6-31G(d) level using QC indicates that both the magnitude and the nature of effect produced by the presence of an external charge is influenced by its relative orientation to the radical centre. The C-H bond strength at  $\text{C}_\alpha$  of  $\mathbf{1}$  is reduced in case where  $\text{Cl}^-$  is placed at along the -x, -y and +z axes. An increase in the  $\text{C}_\alpha$ -H bonds strength occur in case of the +x and +y axes orientations. See Figure S3-5 and Table S3-3 for more details.

**Table S3-3.** [Table S7-S8] The RSE, ciRSE, CSCE, and RCE values ( $\Delta E_{\text{tot}}$ , kJ/mol) for  $\mathbf{1/r1}$  in the presence of an external  $\text{Cl}^-$  placed along the  $\pm$  xyz axes, calculated at (U)B3LYP/6-31G(d) level using DIIS, QC and confirmed with stable=opt. The RSE for  $\mathbf{1/r1}$  (-108.7 kJ/mol) in the absence of an external charge is used as a reference.

DIIS		$\mathbf{r1+Cl}^-$				QC		$\mathbf{r1+Cl}^-$			
Axis	RSE	ciRSE	CSCE	RCE	Wavefunction	RSE	ciRSE	CSCE	RCE	Wavefunction	
-x	-127.3	-18.5	6.6	-12.0	Stable	-118.1	-9.4	6.6	-2.8	Unstable	
+x	-	-	-	-	No conversion	-102.6	6.2	-20.2	-14.0	Unstable	
-y	-115.7	-7.0	-1.3	-8.3	Unstable	-110.2	-1.4	-1.3	-2.7	Unstable	
+y	-114.6	-5.8	6.8	0.9	Unstable	-107.6	1.2	6.8	7.9	Unstable	
+z	-110.6	-1.8	-3.4	-5.2	Stable	-110.6	-1.8	-3.4	-5.2	Stable	
Opt=Stable						Opt=Stable					
-x	-127.3	-18.5	6.6	-12.0	Stable	-127.3	-18.6	6.6	-12.0	Stable	
+x	-	-	-	-	No conversion	-110.8	-2.1	-20.2	-22.3	Stable	
-y	-115.9	-7.1	-1.3	-8.5	Stable	-115.9	-7.1	-1.3	-8.5	Stable	
+y	-114.8	-6.1	6.8	0.7	Stable	-114.8	-6.1	6.8	0.7	Stable	
+z	-110.6	-1.8	-3.4	-5.2	Stable	-110.6	-1.8	-3.4	-5.2	Stable	

When converged wavefunction (DIIS) subjected to re-optimization (stable=opt). The stable wavefunction obtained as result of re-optimization is remain delocalized and even become energetically more favourable. The results from reoptimized wavefunction will be discussed shortly after QC results.

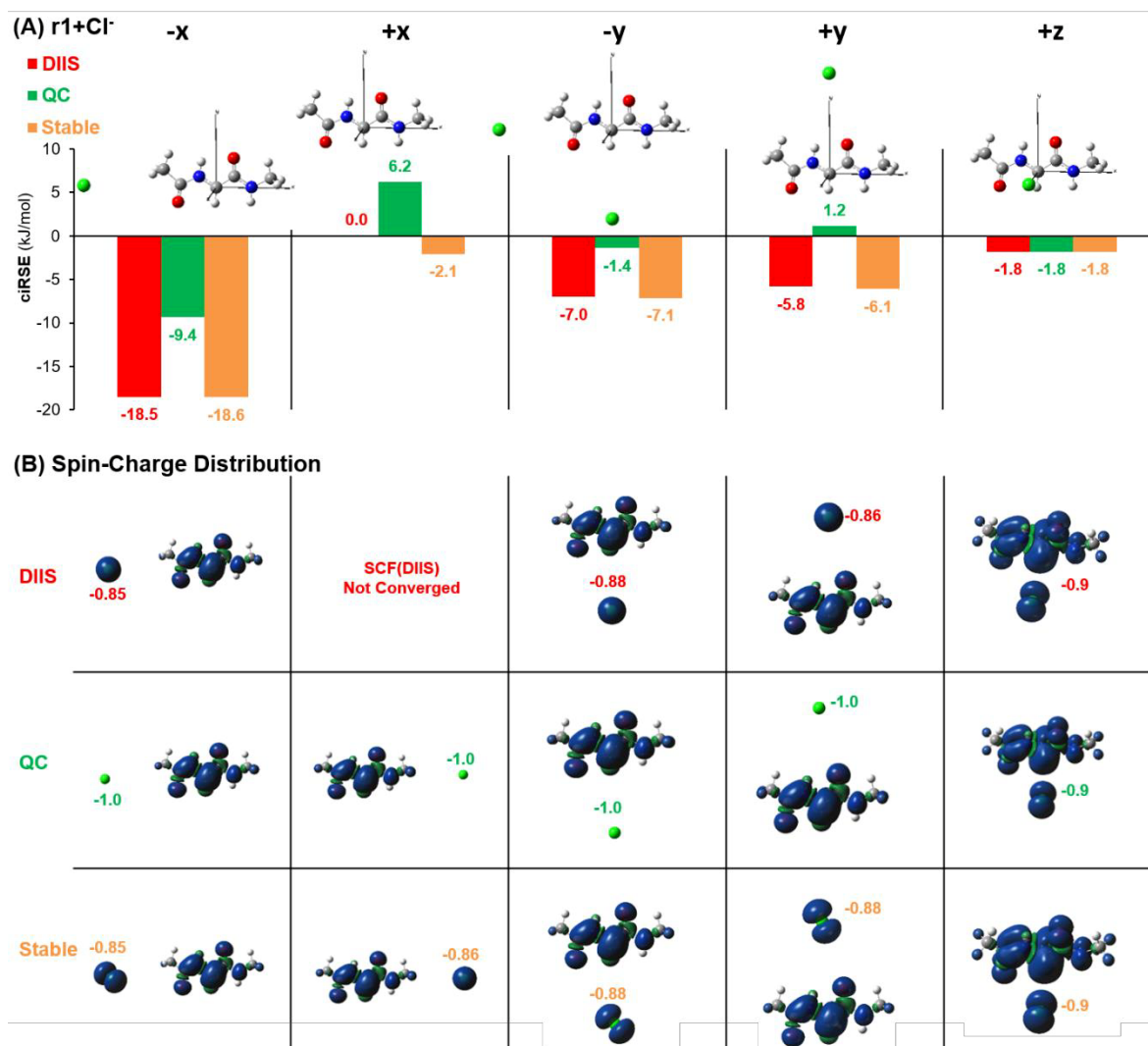


**Figure S3-5.** [Figure S7] Comparative plot of cIRSE (A) and the spin density surface along with the Mulliken charge on Cl<sup>-</sup> (B) for the  $r1+Cl^-$  complex for  $\pm xyz$  axes orientations calculated at the (U)B3LYP/6-31G(d) level of theory using the different convergent procedures.

**Table S3-4.** [Table S9] Spin density on  $C_\alpha$  of  $r1$  and partial charge on Cl<sup>-</sup> in the  $r1+Cl^-$  complex at (U)B3LYP/6-31G(d) level using different convergence procedures. For reference, the spin density on  $C_\alpha$  of  $r1$  in the absence of an external the charge is 0.70 and the charge on Cl<sup>-</sup> is -1.0.

Axis	Spin ( $C_\alpha$ )			Charge on Cl <sup>-</sup>		
	DIIS	QC	Opt=Stable	DIIS	QC	Opt=Stable
$r1$	0.70					
-x	0.58	0.68	0.58	-0.85	-1.00	-0.85
+x	-	0.72	0.62	-	-1.00	-0.86
-y	0.61	0.69	0.61	-0.88	-1.00	-0.88
+y	0.61	0.71	0.61	-0.86	-1.00	-0.86
+z	0.63	0.63	0.63	-0.90	-0.90	-0.90

## 3.1.3.4 Orbital analysis

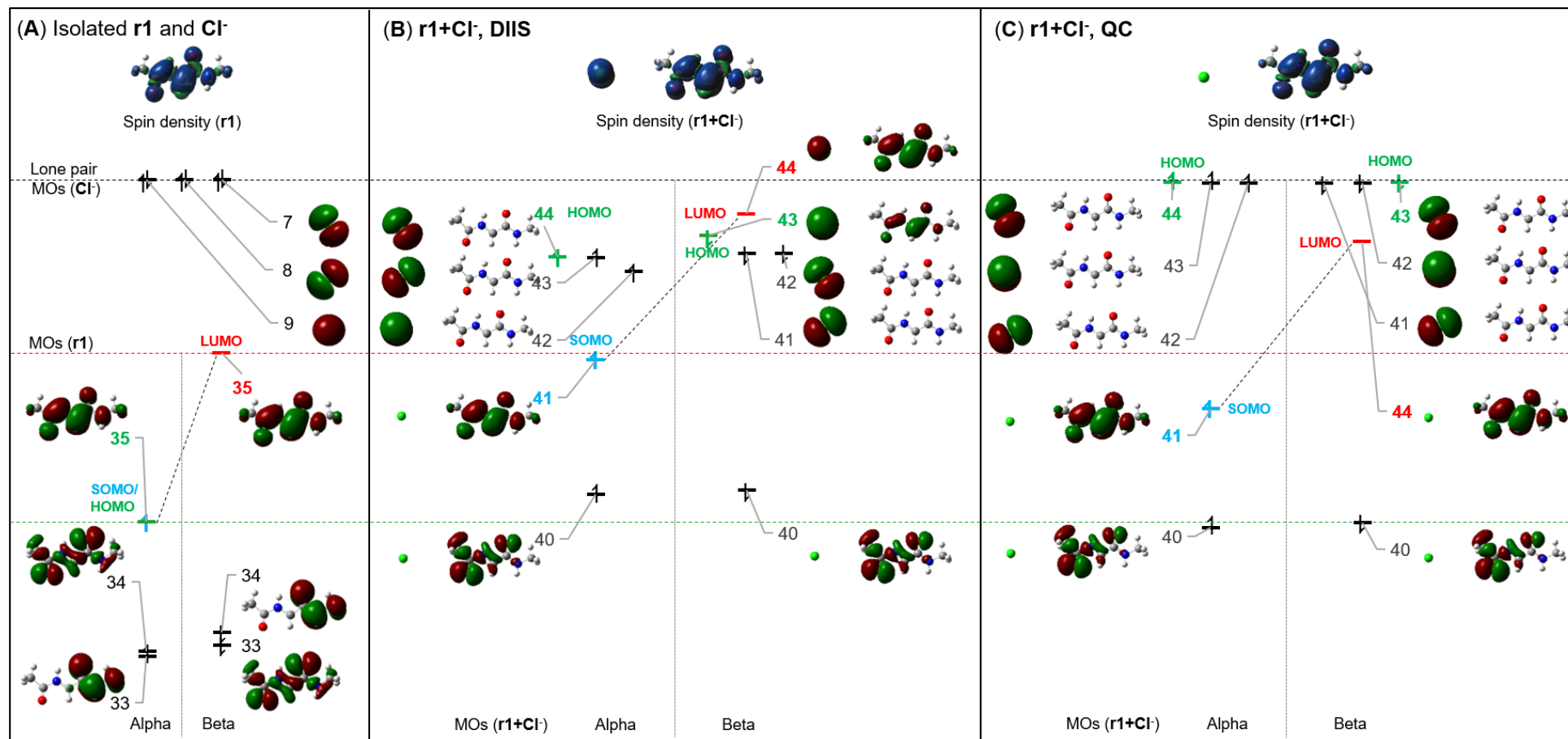


**Figure S3-6.** [Figure S8] (A) An orbital analysis for glycine dipeptide radical  $r1$  and isolated  $Cl^-$ . For the  $r1+Cl^-$  complex, where  $Cl^-$  is placed along  $-x$  axis, 5 Å away from the nearest atom(s), molecular orbitals and spin densities are calculated at (U)B3LYP/6-31G(d) level using different convergence procedure (B) DIIS and (C) QC.

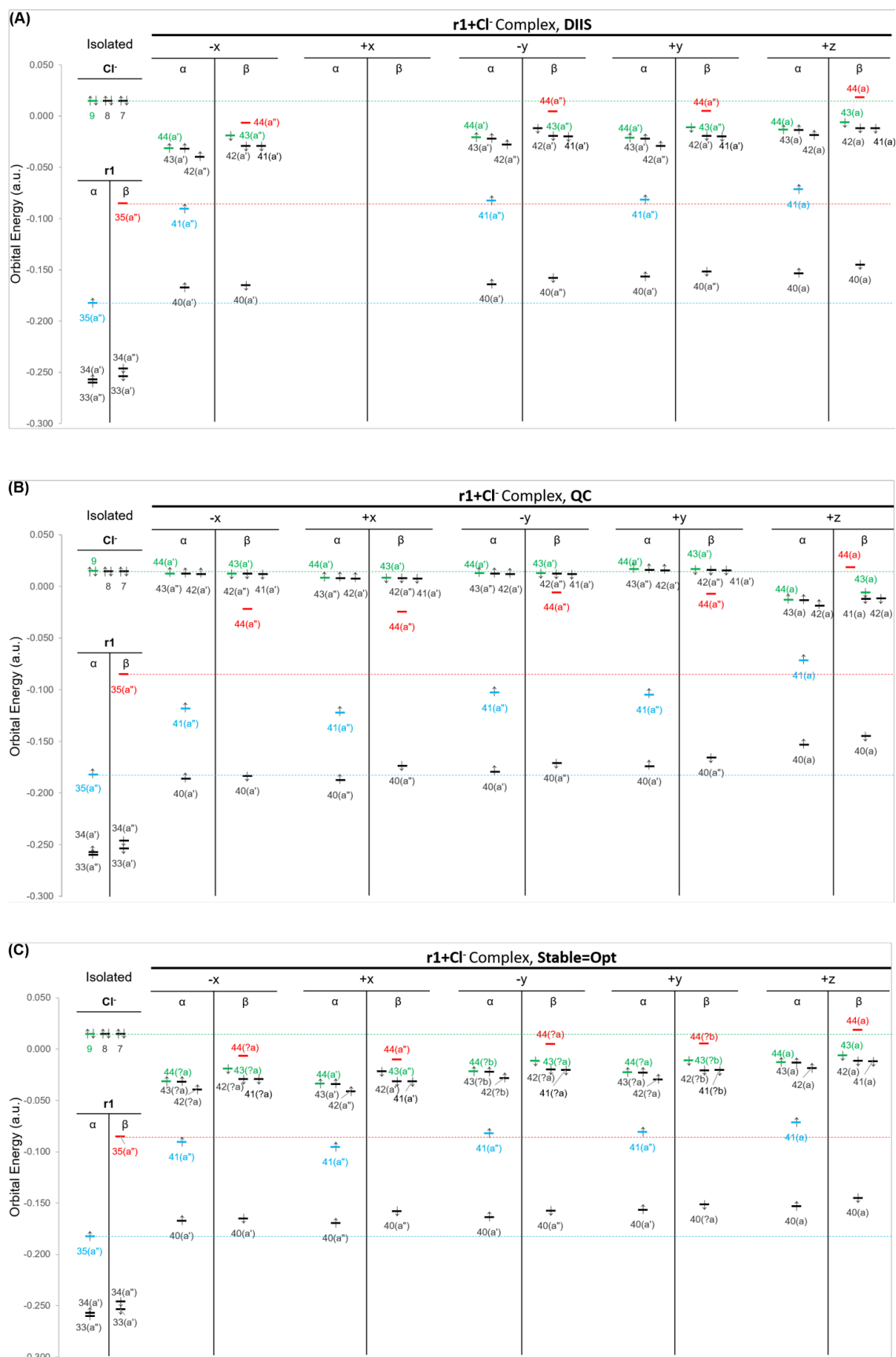


**Figure S3-7.** [Figure S9-S11] Orbital energy plots for the  $r1+Cl^-$  complex for different relative orientations of  $Cl^-$  w.r.t  $r1$ , calculated at (U)B3LYP/6-31G(d) level using (A) DIIS (B) QC for SCF and (C) stable=opt.

**Table S 3-5.** [Table S10-S11] RSE and ciRSE values ( $\Delta E_{\text{tot}}$ , kJ/mol) for **1/r1** in the presence of an external Cl<sup>-</sup> placed along the  $\pm xyz$  axes, calculated at different levels of theory and confirmed with stable=opt. The C<sub>5</sub> conformations of **1/r1** used were optimized at (U)B3LYP/6-31G(d) level.

Ref.	(U)B3LYP/6-31+G(d)					(U)B3LYP/6-311++G(3df,2pd)				
	RSE	Spin (C <sub>α</sub> )				RSE	Spin (C <sub>α</sub> )			
<b>1/r1</b>	-102.6	0.74								
DIIS	<b>r1+Cl<sup>-</sup></b>					<b>r1+Cl<sup>-</sup></b>				
Axis	RSE	ciRSE	Wave-function	Spin (C <sub>α</sub> )	Charge on Cl <sup>-</sup>	RSE	ciRSE	Wave-function	Spin (C <sub>α</sub> )	Charge on Cl <sup>-</sup>
-x	-114.5	-11.9	Stable	0.66	-0.91	-	-	#		
+x	-	-	#			-	-	#		
-y	-104.3	-1.7	Stable	0.69	-0.96	-104.6	-1.8	Stable	0.66	-0.93
+y	-102.5	0.0	Unstable	0.70	-0.94	-103.2	-0.4	Unstable	0.66	-0.91
+z	-101.1	1.4	Stable	0.72	-0.97	-102.0	0.8	Stable	0.67	-0.96
QC										
-x	-112.0	-9.5	Unstable	0.71	-1.00	-112.2	-9.4	Unstable	0.68	-0.99
+x	-96.7	5.9	Unstable	0.75	-1.00	-97.0	5.8	Unstable	0.72	-0.98
-y	-103.7	-1.1	Unstable	0.72	-1.00	-103.6	-0.8	Unstable	0.70	-0.98
+y	-101.3	1.3	Unstable	0.74	-1.00	-101.6	1.2	Unstable	0.71	-0.99
+z	-101.1	1.4	Stable	0.72	-0.97	-102.0	0.8	Stable	0.67	-0.96
Opt=Stable										
-x	-114.5	-11.9	Stable	0.66	-0.91	-115.1	-12.3	stable	0.62	-0.89
+x	-98.5	4.1	Stable	0.70	-0.92	-99.3	3.5	stable	0.67	-0.90
-y	-104.3	-1.7	Stable	0.69	-0.96	-104.6	-1.8	stable	0.66	-0.93
+y	-102.6	0.0	Stable	0.70	-0.93	-	-	#	-	-
+z	-101.1	1.4	Stable	0.72	-0.97	-102.0	0.8	stable	0.67	-0.96

**Table S3-6.** [Table S12] RSE, ciRSE, CSCE, and RCE values ( $\Delta E_{\text{tot}}$ , kJ/mol) for **1/r1** in the presence of an external Cl<sup>-</sup> placed along the  $\pm xyz$  axes, calculated at (U)M06-2X/6-31+G(d) level. The RSE for **1/r1** (-91.7 kJ/mol) in the absence of an external charge is used as a reference.

Direction	RSE	ciRSE	CSCE	RCE	<b>r1+Cl<sup>-</sup></b>		
					Wave-function	Charge on Cl <sup>-</sup>	Spin C <sub>α</sub>
-x	-101.4	-9.7	5.2	-4.5	Stable	-1.00	0.71
+x	-85.5	6.2	-21.8	-15.6	Stable	-1.00	0.75
-y	-92.7	-1.0	-2.6	-3.7	Stable	-1.00	0.72
+y	-90.3	1.4	6.1	7.5	Stable	-1.00	0.74
+z	-90.6	1.1	-4.8	-3.6	Stable	-0.99	0.72

**Table S3-7.** [Table S13] RSE and ciRSE values ( $\Delta E_{\text{tot}}$ , kJ/mol) for **1/r1** in the presence of an external Cl<sup>-</sup> placed along the  $\pm xyz$  axes, calculated at different levels of theory.

Reference	(RO)B2PLYP-FC\GTMP2Large		G3(MP2)-RAD		G3B3		
RSE ( <b>1/r1</b> )	-96.0		-83.6		-85.4		
Direction	RSE	ciRSE	RSE	ciRSE	RSE	ciRSE	
-x		-105.6	-9.6	-92.9	-9.4	-94.7	-9.4
+x		-89.9	6.1	-77.7	5.9	-79.5	5.9
-y		-96.8	-0.8	-84.2	-0.6	-85.8	-0.5
+y		-94.8	1.2	-82.4	1.2	-84.4	1.0
+z		-94.5	1.5	-83.0	0.6	-84.9	0.4

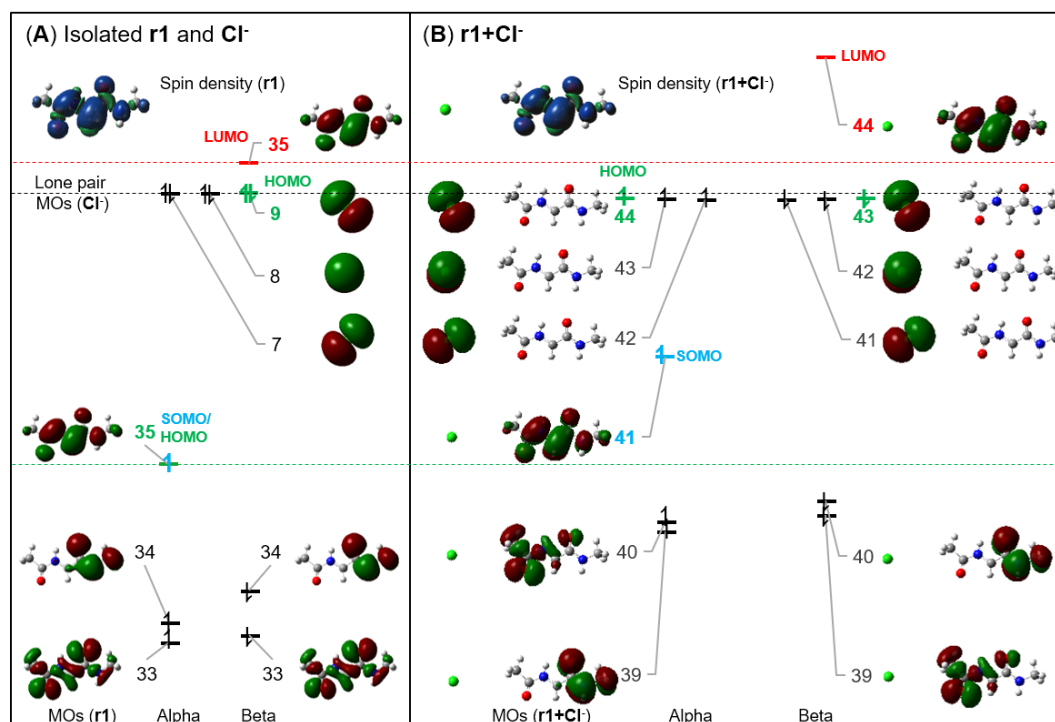


**Figure S3-8.** [Figure S12] An orbital analysis for (A) isolated glycine dipeptide radical **r1** and  $\text{Cl}^-$  and (B) the **r1+Cl<sup>-</sup>** complex, where  $\text{Cl}^-$  is placed along the  $-x$  axis, 5 Å away from the nearest atom(s). Molecular orbitals and spin densities have been calculated at (U)M06-2X/6-31+G(d) level.

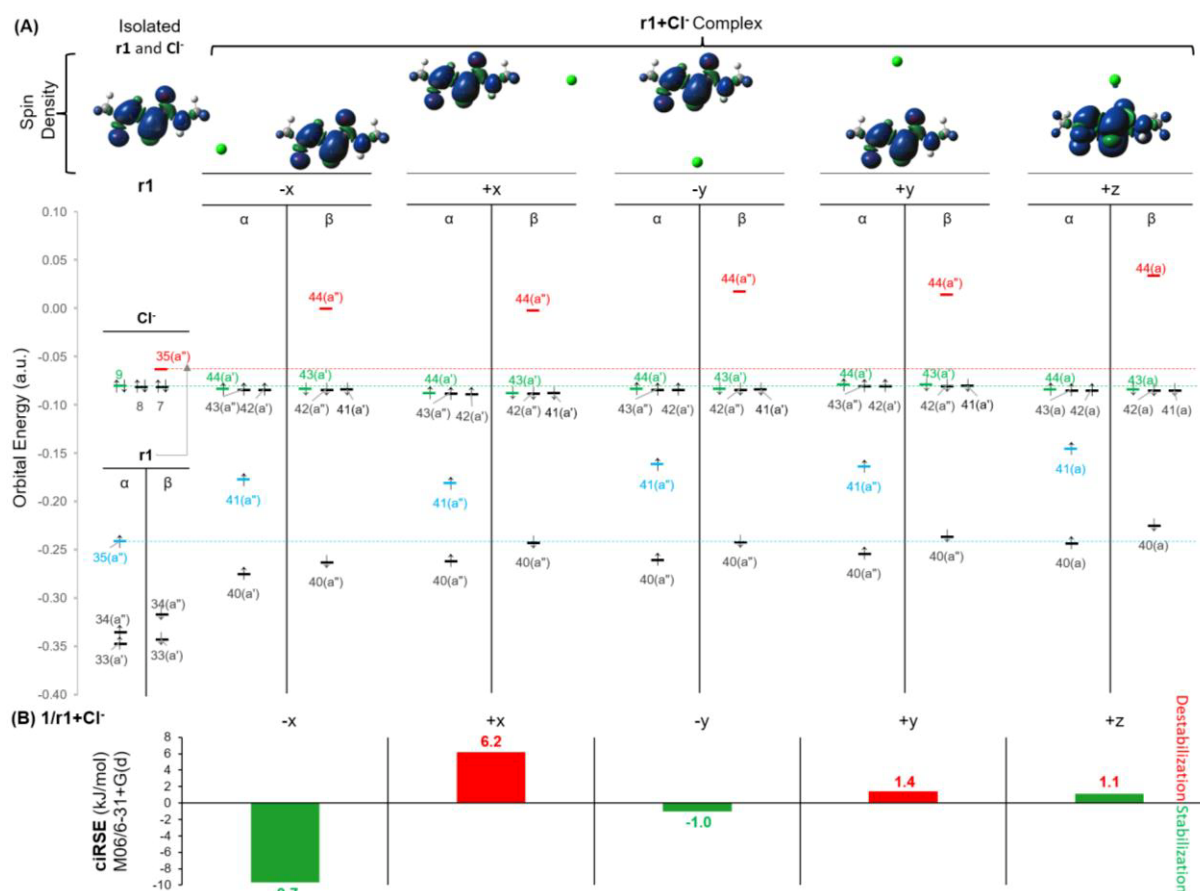
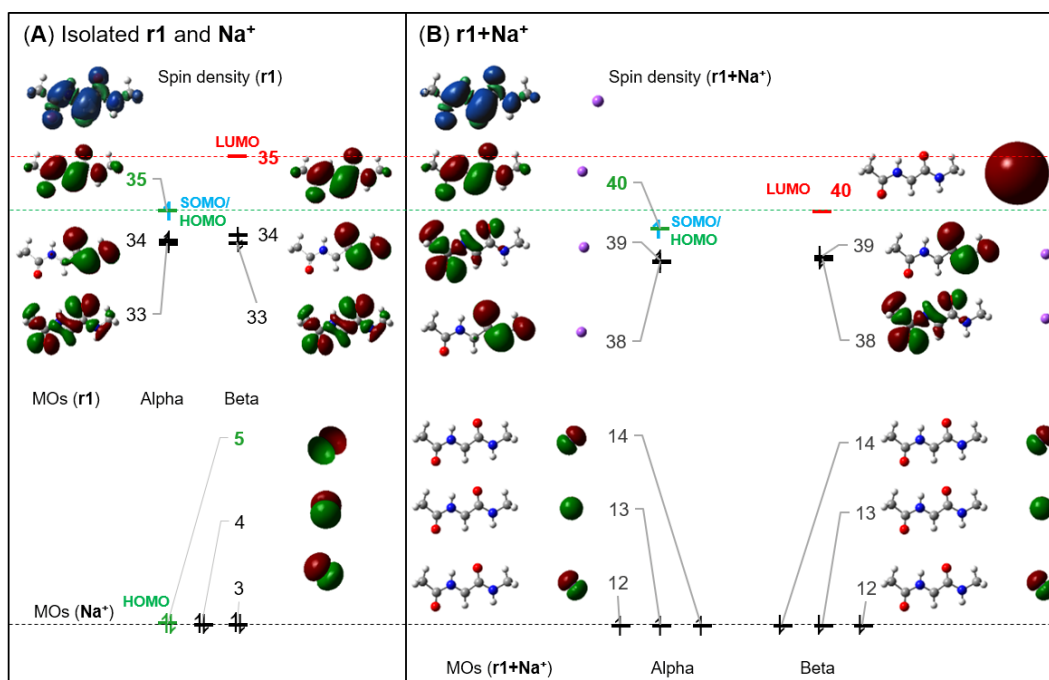


**Figure S3-9.** [Figure S13] (A) Spin density and orbital energy plot and (B) ciRSE values ( $\Delta E_{\text{tot}}$ , kJ/mol) for the **r1+Cl<sup>-</sup>** complexes for different relative orientations of  $\text{Cl}^-$  w.r.t **r1** calculated at the (U)M06-2X/6-31+G(d) level of theory.

### 3.1.3.5 Na<sup>+</sup> along the $\pm xyz$ axes, 5 Å from 1/r1.

**Table S3-8.** [Table S15] RSE, ciRSE, CSCE, and RCE values ( $\Delta E_{\text{tot}}$ , kJ/mol) for 1/r1 in the presence of an external Na<sup>+</sup> placed along the  $\pm xyz$  axes, calculated at (U)B3LYP/6-31G(d) level using DIIS, QC and confirmed with stable=opt.

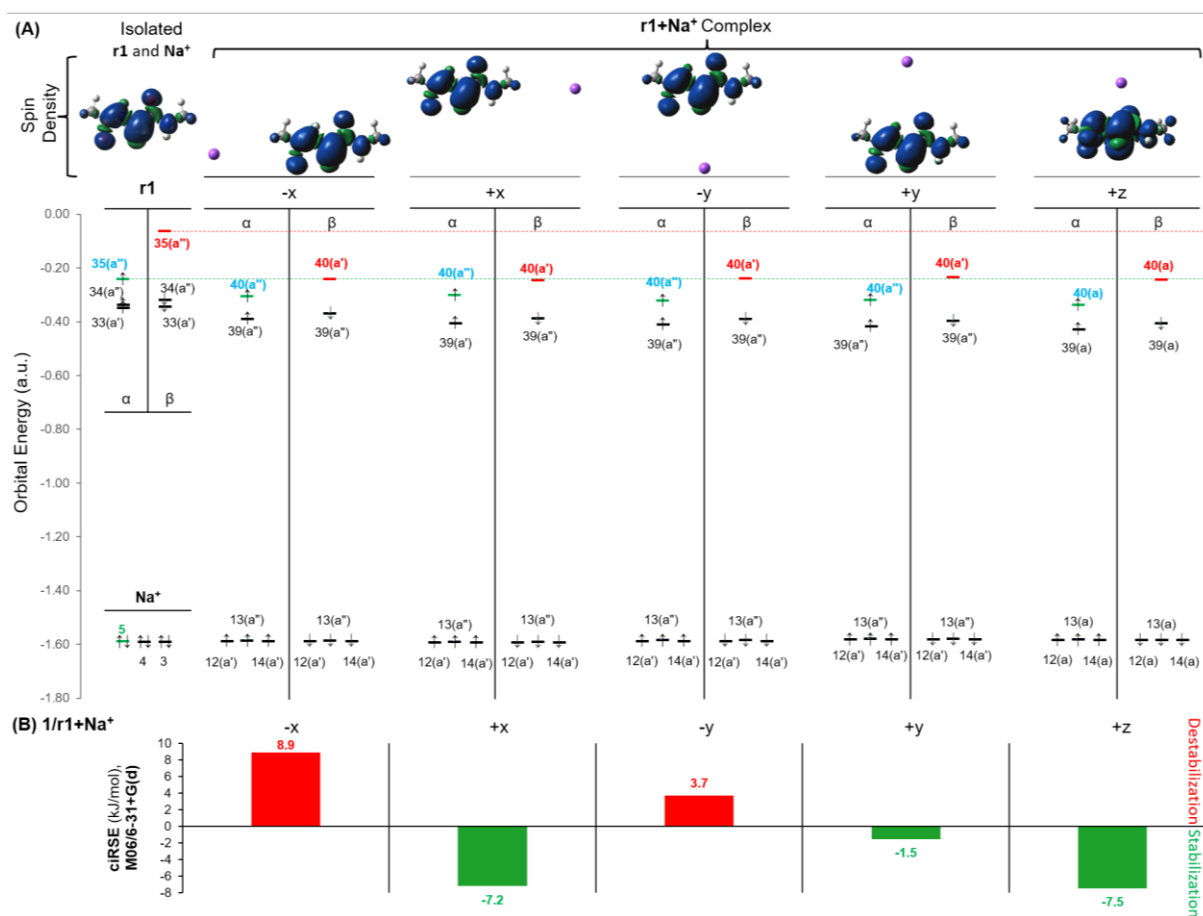
DIIS		r1+Na <sup>+</sup>				QC					r1+Na <sup>+</sup>
Direction	RSE	ciRSE	CSCE	RCE	Wavefunction	RSE	ciRSE	CSCE	RCE	Wavefunction	
-x	-	-	-14.5	-	No conversion	-100.2	8.6	-14.5	-5.9	Instable	
+x	-	-	13.7	-	No conversion	-116.0	-7.3	13.7	6.4	Instable	
-y	-104.5	4.2	-10.4	-6.2	Instable	-104.5	4.2	-10.4	-6.2	Instable	
+y	-110.3	-1.5	-18.2	-19.7	Instable	-110.3	-1.5	-18.2	-19.7	Instable	
+z	-118.0	-9.2	-4.0	-13.3	Stable	-118.0	-9.2	-4.0	-13.3	Stable	
Opt=Stable						Opt=Stable					
-x	-	-	-14.5	-	No conversion	-104.8	3.9	-14.5	-10.6	stable	
+x	-	-	13.7	-	No conversion	-124.1	-15.3	13.7	-1.6	stable	
-y	-106.1	2.6	-10.4	-7.7	Stable	-106.1	2.6	-10.4	-7.7	stable	
+y	-110.9	-2.1	-18.2	-20.3	Stable	-110.9	-2.1	-18.2	-20.3	stable	
+z	-118.0	-9.2	-4.0	-13.3	Stable	-118.0	-9.2	-4.0	-13.3	Stable	



**Figure S3-10.** [Figure S14.] An orbital analysis for (A) isolated glycine dipeptide radical **r1** and Na<sup>+</sup> and (B) the **r1+Na<sup>+</sup>** complex, where Na<sup>+</sup> is placed along the +x-axis 5 Å away from the nearest atom(s). Molecular orbitals and spin densities have been calculated at the (U)M06-2X/6-31+G(d) level of theory.

**Table S3-9.** [Table S18] RSE, ciRSE, CSCE, and RCE values ( $\Delta E_{\text{tot}}$ , kJ/mol) for **1/r1** in the presence of an external  $\text{Na}^+$  is placed along the  $\pm xyz$  axes calculated at different levels of theory.

Direction	(U)M06-2X/6-31+G(d)				Wave-function <b>r1+Na<sup>+</sup></b>	ROB2PLYP-FC \GTMP2Large		G3(MP2)-RAD		G3B3	
	RSE	ciRSE	CSCE	RCE		RSE	ciRSE	RSE	ciRSE	RSE	ciRSE
-x	-82.8	8.9	-12.7	-3.8	Stable	-	-	-75.1	8.5	-76.9	8.5
+x	-98.9	-7.2	14.8	7.6	Stable	-	-	-90.3	-6.7	-92.2	-6.8
-y	-88.0	3.7	-8.8	-5.1	Stable	-	-	-80.2	3.4	-81.9	3.5
+y	-93.2	-1.5	-17.2	-18.8	Stable	-	-	-85.1	-1.5	-86.8	-1.4
+z	-99.2	-7.5	-3.8	-11.3	Stable	-	-	-91.7	-8.1	-93.8	-8.5

**Figure S3-11.** [Figure S15] (A) Spin density and orbital energy plot and (B) ciRSE values ( $\Delta E_{\text{tot}}$ , kJ/mol) for **1/r1+Na<sup>+</sup>** complexes for different relative orientations of  $\text{Na}^+$  w.r.t **r1** calculated at the (U)M06-2X/6-31+G(d) level of theory.

### 3.1.4 Glycine Dipeptide and Its Complexation with Cl<sup>-</sup> and Na<sup>+</sup>

#### 3.1.4.1 Plane xy

##### Nature of charge (positive/negative)

**Table S3-10.** [Table S20-S21] RSE, ciRSE, CSCE, and RCE values ( $\Delta E_{\text{tot}}$ , kJ/mol) for **1/r1** in the presence of Cl<sup>-</sup>/Na<sup>+</sup> placed in the xy-plane at 900 pm distance from C<sub>α</sub>, calculated at (U)M06-2X/6-31+G(d) level. The position of Cl<sup>-</sup>/Na<sup>+</sup> w.r.t **1/r1** is indicated by the angle between the ion, C<sub>α</sub> and the +x axis (first column).

Angle	<b>1/r1+Cl<sup>-</sup></b>				<b>1/r1+Na<sup>+</sup></b>			
	RSE	ciRSE	CSCE	RCE	RSE	ciRSE	CSCE	RCE
0	-85.2	6.5	-23.3	-16.8	-99.1	-7.4	15.3	7.8
10	-84.5	7.2	-21.8	-14.6	-99.5	-7.8	13.2	5.4
20	-84.2	7.5	-18.2	-10.7	-99.6	-7.9	10.4	2.5
30	-84.2	7.5	-13.3	-5.9	-99.4	-7.7	6.5	-1.3
40	-84.8	6.9	-7.9	-0.9	-98.8	-7.1	2.0	-5.0
50	-85.6	6.1	-2.8	3.3	-97.9	-6.2	-2.0	-8.2
60	-86.9	4.8	1.3	6.1	-96.5	-4.8	-5.6	-10.4
70	-88.2	3.5	3.6	7.1	-95.1	-3.4	-7.5	-11.0
80	-89.6	2.1	4.3	6.4	-93.7	-2.0	-7.9	-9.9
90	-90.9	0.8	3.5	4.3	-92.2	-0.5	-7.1	-7.5
100	-92.4	-0.8	1.9	1.1	-90.8	0.9	-5.5	-4.5
110	-93.8	-2.1	-0.3	-2.4	-89.3	2.4	-3.7	-1.2
120	-95.3	-3.6	-2.4	-6.0	-87.9	3.8	-2.1	1.6
130	-96.7	-5.0	-4.1	-9.1	-86.5	5.2	-1.6	3.7
140	-98.1	-6.4	-5.1	-11.5	-85.2	6.4	-1.8	4.7
150	-99.4	-7.7	-5.0	-12.7	-84.1	7.6	-3.0	4.6
160	-100.5	-8.8	-3.6	-12.3	-83.3	8.3	-5.2	3.2
170	-101.2	-9.5	0.0	-9.5	-83.1	8.6	-8.3	0.3
180	-101.4	-9.7	5.2	-4.5	-82.9	8.8	-12.6	-3.8
190	-101.1	-9.4	10.7	1.3	-83.4	8.3	-16.8	-8.5
200	-100.1	-8.4	15.0	6.6	-84.2	7.5	-20.1	-12.6
210	-99.0	-7.3	17.4	10.0	-85.1	6.6	-21.6	-15.0
220	-97.8	-6.1	17.3	11.2	-86.3	5.4	-20.9	-15.5
230	-96.5	-4.8	15.5	10.7	-87.2	4.5	-18.7	-14.2
240	-95.3	-3.6	12.5	8.9	-88.2	3.5	-15.2	-11.7
250	-94.4	-2.7	8.9	6.2	-89.2	2.5	-11.2	-8.7
260	-93.5	-1.8	5.0	3.2	-89.9	1.8	-7.1	-5.3
270	-92.5	-0.8	1.0	0.2	-90.8	0.9	-2.8	-2.0
280	-91.6	0.0	-3.0	-2.9	-91.7	0.0	1.2	1.2
290	-90.7	1.0	-6.9	-5.9	-92.7	-1.0	4.9	3.9
300	-89.9	1.8	-10.5	-8.7	-93.5	-1.8	8.3	6.4
310	-89.3	2.4	-13.6	-11.2	-94.3	-2.6	11.2	8.5
320	-88.4	3.3	-16.7	-13.3	-95.6	-3.9	13.7	9.9
330	-87.6	4.1	-19.3	-15.2	-96.5	-4.8	15.4	10.6
340	-86.9	4.8	-21.5	-16.7	-97.6	-5.9	16.3	10.4
350	-86.1	5.6	-23.0	-17.4	-98.5	-6.8	16.3	9.5

## Solvent effects

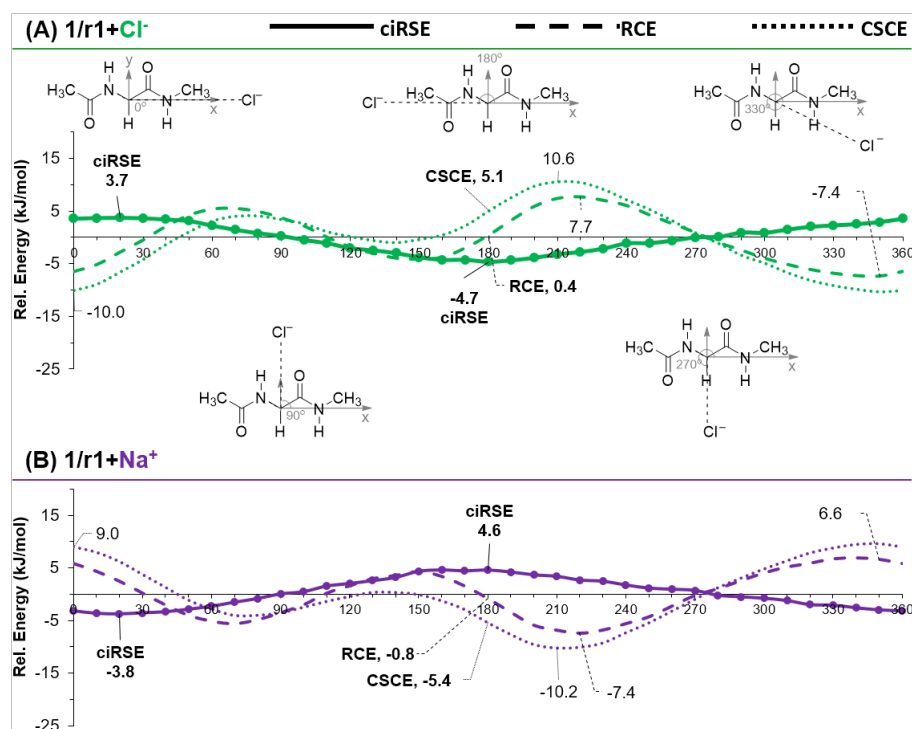


**Figure S 3-12.** [Figure S16] ciRSE, RCE, and CSCE values are plotted as a function of ion's orientation around  $1/r1$  in the  $xy$ -plane at 900 pm distance from  $C_\alpha$  for (A)  $Cl^-$  and (B)  $Na^+$  calculated at SMD(toluene)/(U)M06-2X/6-31+G(d) level.

**Table S3-11.** [Table S22-S23] RSE, ciRSE, CSCE and RCE values ( $\Delta E_{tot}$ , kJ/mol) for  $1/r1$  in the presence of  $Cl^-/Na^+$  placed in the  $xy$ -plane at 900 pm distance from  $C_\alpha$ , calculated at SMD(toluene)/(U)M06-2X/6-31+G(d) level. The position of  $Cl^-/Na^+$  w.r.t  $1/r1$  is indicated by an angle between the ion,  $C_\alpha$  and the  $+x$  axis (first column). The RSE for  $1/r1$  (-94.4 kJ/mol) is used as a reference.

Angle	$1/r1+Cl^-$				$1/r1+Na^+$			
	RSE	ciRSE	CSCE	RCE	RSE	ciRSE	CSCE	RCE
0	-90.8	3.5	-10.0	-6.5	-97.5	-3.2	9.0	5.8
10	-90.7	3.7	-8.8	-5.2	-98.0	-3.6	7.9	4.3
20	-90.7	3.7	-6.5	-2.8	-98.1	-3.8	6.2	2.4
30	-90.8	3.6	-4.1	-0.5	-97.9	-3.5	3.7	0.2
40	-91.0	3.4	-1.3	2.1	-97.7	-3.3	1.3	-2.0
50	-91.3	3.1	1.1	4.2	-97.2	-2.9	-1.1	-4.0
60	-92.2	2.2	3.2	5.4	-96.7	-2.3	-2.8	-5.1
70	-92.9	1.4	4.1	5.5	-95.9	-1.5	-4.0	-5.6
80	-93.6	0.7	4.2	4.9	-95.2	-0.8	-4.0	-4.8
90	-94.1	0.3	3.5	3.7	-94.3	0.1	-3.6	-3.5
100	-94.9	-0.5	2.7	2.1	-93.9	0.5	-2.5	-2.0
110	-95.5	-1.1	1.1	0.0	-92.8	1.5	-1.4	0.2
120	-96.4	-2.1	0.2	-1.8	-92.3	2.0	-0.5	1.6
130	-96.9	-2.5	-0.5	-3.0	-91.8	2.6	0.3	2.9
140	-97.4	-3.0	-0.9	-4.0	-91.2	3.2	0.3	3.5
150	-98.2	-3.8	-0.3	-4.2	-90.0	4.4	-0.1	4.3
160	-98.7	-4.3	0.5	-3.8	-89.7	4.6	-1.3	3.4
170	-98.7	-4.3	2.3	-2.0	-89.9	4.5	-2.9	1.5
180	-99.0	-4.7	5.1	0.4	-89.8	4.6	-5.4	-0.8
190	-98.7	-4.4	7.7	3.3	-90.1	4.2	-7.6	-3.4
200	-98.3	-3.9	9.8	5.9	-90.7	3.7	-9.6	-5.9
210	-97.6	-3.2	10.6	7.4	-91.0	3.4	-10.2	-6.8

220	-97.2	-2.8	10.5	7.7	-91.7	2.7	-10.1	-7.4
230	-96.5	-2.2	9.2	7.0	-91.9	2.5	-9.3	-6.8
240	-95.5	-1.2	7.2	6.0	-92.6	1.8	-7.3	-5.6
250	-95.5	-1.1	5.4	4.3	-93.2	1.2	-5.5	-4.3
260	-95.0	-0.6	3.2	2.6	-93.4	0.9	-3.2	-2.3
270	-94.4	0.0	0.9	0.9	-93.6	0.7	-1.0	-0.3
280	-94.3	0.1	-1.1	-1.0	-94.6	-0.2	1.2	1.0
290	-93.5	0.9	-3.3	-2.5	-94.9	-0.5	3.0	2.5
300	-93.5	0.8	-4.8	-4.0	-95.1	-0.8	4.8	4.0
310	-92.9	1.5	-6.7	-5.2	-95.6	-1.2	6.3	5.1
320	-92.4	2.0	-8.1	-6.1	-96.3	-2.0	7.8	5.8
330	-92.1	2.3	-9.1	-6.8	-96.5	-2.1	8.7	6.7
340	-91.9	2.5	-9.8	-7.3	-96.9	-2.6	9.4	6.8
350	-91.5	2.9	-10.3	-7.4	-97.3	-3.0	9.6	6.6

## Distance dependence

**Table S3-12.** [Table S24] ciRSE values ( $\Delta E_{\text{tot}}$ , kJ/mol) for **1/r1** in the presence of  $\text{Cl}^-$  placed in the xy-plane at varying distances from  $\text{C}_\alpha$  (7-15Å), calculated at (U)M06-2X/6-31+G(d) level. The position of  $\text{Cl}^-$  w.r.t **1/r1** is indicated by the angle between the ion,  $\text{C}_\alpha$  and the +x axis (first column) together with the distance between the ion and  $\text{C}_\alpha$  (first row).

Angle	7 Å	8 Å	9 Å	10 Å	11 Å	12 Å	13 Å	14 Å	15 Å
0	9.5	7.7	6.5	5.5	4.3	3.8	3.3	2.8	2.5
10	9.2	9.2	7.2	5.9	4.8	4.0	3.5	3.0	2.8
20	11.2	9.8	7.5	6.0	5.0	4.2	3.6	3.1	2.7
30	12.6	9.7	7.5	5.9	4.8	4.1	3.4	2.9	2.6
40	12.2	9.1	6.9	5.5	4.5	3.7	3.2	2.6	2.3
50	10.7	8.0	6.1	4.8	3.9	3.3	2.9	2.5	2.2
60	8.3	6.2	4.8	3.8	3.2	2.6	2.3	1.9	1.7
70	5.8	4.4	3.5	2.8	2.3	2.0	1.7	1.4	1.2
80	3.3	2.7	2.1	1.7	1.5	1.2	1.1	0.9	0.8
90	1.2	0.8	0.8	0.6	0.6	0.4	0.3	0.4	0.4
100	-1.0	-0.8	-0.8	-0.5	-0.5	-0.3	-0.3	-0.2	-0.2
110	-3.3	-2.6	-2.1	-1.8	-1.5	-1.2	-1.0	-0.8	-0.7
120	-5.7	-4.5	-3.6	-2.9	-2.5	-2.0	-1.6	-1.4	-1.2
130	-8.2	-6.4	-5.0	-4.0	-3.4	-2.9	-2.4	-2.0	-1.7
140	-11.3	-8.2	-6.4	-5.1	-4.2	-3.5	-2.9	-2.5	-2.1
150	-14.9	-10.0	-7.7	-6.0	-5.0	-4.1	-3.4	-2.9	-2.5
160	-17.7	-11.5	-8.8	-6.9	-5.5	-4.6	-3.8	-3.3	-2.8
170	-17.9	-12.7	-9.5	-7.5	-5.9	-4.8	-4.1	-3.4	-2.9
180	-18.0	-13.0	-9.7	-7.5	-6.0	-4.9	-4.1	-3.4	-3.0
190	-17.3	-12.5	-9.4	-7.2	-5.9	-4.8	-4.1	-3.3	-3.0
200	-15.2	-11.1	-8.4	-6.6	-5.4	-4.5	-3.7	-3.2	-2.7
210	-12.5	-9.5	-7.3	-5.8	-4.7	-3.9	-3.2	-2.8	-2.5
220	-9.8	-7.7	-6.1	-4.9	-4.0	-3.4	-2.8	-2.5	-2.2
230	-7.9	-6.1	-4.8	-4.0	-3.3	-2.7	-2.3	-2.1	-1.8
240	-5.9	-4.5	-3.6	-3.1	-2.6	-2.1	-1.8	-1.7	-1.3
250	-4.5	-3.4	-2.7	-2.1	-1.8	-1.5	-1.3	-1.2	-1.0
260	-3.0	-2.2	-1.8	-1.4	-1.2	-1.1	-0.9	-0.8	-0.6
270	-1.7	-1.1	-0.8	-0.6	-0.4	-0.3	-0.3	-0.2	-0.2
280	-0.5	-0.1	0.0	0.0	0.2	0.1	0.1	0.1	0.1
290	0.7	1.0	1.0	0.8	0.9	0.8	0.6	0.6	0.6
300	2.0	1.9	1.8	1.6	1.4	1.1	1.1	1.1	0.8
310	3.0	2.6	2.4	2.2	1.9	1.7	1.5	1.4	1.2
320	4.1	3.9	3.3	2.9	2.6	2.2	2.0	1.7	1.6
330	5.4	4.7	4.1	3.6	3.1	2.6	2.3	2.1	1.9
340	6.6	5.6	4.8	4.2	3.7	3.1	2.8	2.3	2.1
350	8.2	6.7	5.6	4.8	4.1	3.4	3.0	2.7	2.5

**Table S3-13.** [Table S25] ciRSE values ( $\Delta E_{\text{tot}}$ , kJ/mol) for  $\mathbf{1/r1}$  in the presence of  $\text{Na}^+$  placed in the xy-plane at varying distances from  $\text{C}_\alpha$  (7-15 Å), calculated at (U)M06-2X/6-31+G(d) level. The position of  $\text{Na}^+$  w.r.t  $\mathbf{1/r1}$  is indicated by the angle between the ion,  $\text{C}_\alpha$  and the +x axis (first column) together with the distance between the ion and  $\text{C}_\alpha$  (first row).

Angle	7 Å	8 Å	9 Å	10 Å	11 Å	12 Å	13 Å	14 Å	15 Å
0	-13.6	-9.8	-7.4	-5.9	-4.8	-3.9	-3.5	-2.9	-2.7
10	-13.4	-10.2	-7.8	-6.3	-5.0	-4.3	-3.5	-3.0	-2.6
20	-13.0	-10.2	-7.9	-6.3	-5.2	-4.3	-3.6	-3.1	-2.7
30	-12.8	-9.8	-7.7	-6.1	-4.9	-4.1	-3.5	-2.8	-2.5
40	-11.9	-9.2	-7.1	-5.7	-4.6	-3.8	-3.2	-2.7	-2.4
50	-10.2	-8.0	-6.2	-4.9	-4.0	-3.2	-2.6	-2.4	-2.0
60	-8.0	-6.2	-4.8	-3.9	-3.2	-2.7	-2.2	-1.9	-1.6
70	-5.5	-4.4	-3.4	-2.8	-2.3	-1.9	-1.6	-1.4	-1.2
80	-2.9	-2.5	-2.0	-1.7	-1.3	-1.2	-1.0	-0.8	-0.7
90	-0.5	-0.6	-0.5	-0.4	-0.5	-0.2	-0.3	-0.3	-0.2
100	1.9	1.3	0.9	0.8	0.6	0.5	0.4	0.4	0.3
110	4.3	3.2	2.4	2.0	1.6	1.3	1.1	1.0	0.9
120	7.0	5.1	3.8	3.2	2.5	2.1	1.8	1.5	1.3
130	9.7	6.9	5.2	4.2	3.4	2.8	2.4	2.2	1.8
140	12.5	8.6	6.4	5.2	4.1	3.5	2.9	2.6	2.2
150	14.3	10.1	7.6	5.9	4.9	4.0	3.4	3.0	2.5
160	15.0	10.9	8.3	6.6	5.3	4.5	3.8	3.3	2.8
170	15.0	11.3	8.6	6.9	5.7	4.7	3.9	3.3	3.0
180	14.8	11.2	8.8	6.9	5.7	4.7	4.0	3.4	3.0
190	13.9	10.6	8.3	6.7	5.4	4.6	3.8	3.3	2.9
200	12.1	9.5	7.5	6.1	5.0	4.3	3.7	3.0	2.8
210	9.8	8.0	6.6	5.3	4.5	3.8	3.2	2.9	2.5
220	7.8	6.4	5.4	4.6	3.8	3.2	2.7	2.4	2.1
230	6.2	5.3	4.5	3.7	3.1	2.7	2.4	2.1	1.8
240	5.0	4.0	3.5	2.9	2.6	2.3	2.0	1.7	1.3
250	3.8	3.1	2.5	2.0	1.8	1.6	1.3	1.3	1.2
260	2.5	2.2	1.8	1.5	1.2	1.0	0.9	0.8	0.7
270	1.4	1.1	0.9	0.7	0.6	0.5	0.4	0.4	0.4
280	0.2	0.0	0.0	-0.2	-0.1	-0.1	-0.1	-0.2	-0.1
290	-1.0	-1.0	-1.0	-0.8	-0.7	-0.6	-0.5	-0.5	-0.4
300	-2.5	-2.3	-1.8	-1.5	-1.3	-1.1	-0.9	-0.9	-0.7
310	-4.1	-3.3	-2.6	-2.3	-2.1	-1.9	-1.6	-1.3	-1.2
320	-5.8	-4.7	-3.9	-3.2	-2.7	-2.2	-2.0	-1.7	-1.5
330	-7.9	-6.1	-4.8	-4.0	-3.3	-2.8	-2.3	-2.0	-1.8
340	-10.4	-7.5	-5.9	-4.7	-3.9	-3.4	-2.9	-2.4	-2.2
350	-12.8	-8.8	-6.8	-5.4	-4.5	-3.7	-3.2	-2.7	-2.4

## Point charges (PCs)

**Table S3-14.** [Table S26] RSE, ciRSE, CSCE, and RCE values ( $\Delta E_{\text{tot}}$ , kJ/mol) for  $1/r\mathbf{1}$  in the presence of an external point charge (PC) placed in the xy-plane at 900 pm distance from  $C_{\alpha}$ , calculated at (U)M06-2X/6-31+G(d) level. The position of PC w.r.t  $1/r\mathbf{1}$  is indicated by the angle between the PC,  $C_{\alpha}$  and the +x axis (first column).

Angle	$1/r\mathbf{1}+\text{PC}(-)$				$1/r\mathbf{1}+\text{PC}(+)$			
	RSE	ciRSE	CSCE	RCE	RSE	ciRSE	CSCE	RCE
0	-85.3	6.4	-22.4	-16.0	-99.2	-7.5	15.4	7.9
10	-84.6	7.1	-20.8	-13.7	-99.6	-7.9	13.5	5.6
20	-84.3	7.4	-17.3	-9.8	-99.7	-8.0	10.6	2.5
30	-84.4	7.3	-12.5	-5.2	-99.5	-7.8	6.7	-1.1
40	-84.9	6.8	-7.3	-0.5	-98.9	-7.2	2.2	-4.9
50	-85.8	5.9	-2.4	3.6	-97.9	-6.2	-2.1	-8.3
60	-86.9	4.8	1.5	6.3	-96.6	-4.9	-5.5	-10.4
70	-88.2	3.4	3.8	7.2	-95.2	-3.5	-7.4	-10.9
80	-89.6	2.1	4.4	6.5	-93.7	-2.0	-7.8	-9.9
90	-91.0	0.7	3.7	4.3	-92.2	-0.5	-7.0	-7.5
100	-92.5	-0.8	2.0	1.2	-90.8	0.9	-5.4	-4.5
110	-93.9	-2.2	-0.1	-2.3	-89.3	2.4	-3.6	-1.3
120	-95.4	-3.7	-2.1	-5.8	-87.9	3.8	-2.2	1.6
130	-96.8	-5.1	-3.6	-8.7	-86.5	5.2	-1.5	3.7
140	-98.2	-6.5	-4.3	-10.9	-85.3	6.4	-1.7	4.7
150	-99.5	-7.8	-4.1	-11.9	-84.2	7.5	-2.8	4.6
160	-100.5	-8.8	-2.5	-11.4	-83.5	8.2	-5.0	3.2
170	-101.2	-9.6	0.9	-8.7	-83.1	8.6	-8.2	0.4
180	-101.4	-9.8	5.9	-3.9	-83.1	8.6	-12.4	-3.8
190	-101.1	-9.4	11.3	1.9	-83.4	8.2	-16.7	-8.5
200	-100.2	-8.5	15.4	6.9	-84.2	7.5	-20.1	-12.6
210	-99.0	-7.3	17.5	10.2	-85.2	6.5	-21.5	-15.0
220	-97.8	-6.1	17.5	11.4	-86.3	5.4	-20.9	-15.5
230	-96.6	-4.9	15.7	10.8	-87.3	4.3	-18.6	-14.3
240	-95.5	-3.8	12.7	8.9	-88.3	3.4	-15.2	-11.8
250	-94.4	-2.7	9.0	6.3	-89.2	2.5	-11.2	-8.7
260	-93.5	-1.8	5.1	3.3	-90.1	1.6	-7.0	-5.3
270	-92.6	-0.9	1.0	0.1	-90.9	0.8	-2.8	-2.0
280	-91.7	0.0	-3.0	-3.0	-91.8	-0.1	1.2	1.1
290	-90.9	0.8	-6.8	-6.0	-92.7	-1.0	5.0	4.0
300	-90.0	1.7	-10.4	-8.7	-93.6	-1.9	8.4	6.5
310	-89.2	2.5	-13.6	-11.2	-94.5	-2.8	11.3	8.5
320	-88.4	3.3	-16.5	-13.2	-95.5	-3.8	13.7	9.9
330	-87.6	4.1	-19.0	-14.9	-96.6	-4.9	15.5	10.6
340	-86.8	4.9	-21.0	-16.1	-97.6	-5.9	16.4	10.5
350	-86.1	5.6	-22.2	-16.6	-98.5	-6.8	16.4	9.6

## External dipole (eDP)

**Table S3-15.** [Table S27] RSE, ciRSE, CSCE, and RCE values ( $\Delta E_{\text{tot}}$ , kJ/mol) for  $1/r1$  in the presence of an external dipole (eDP) placed in the xy-plane at 900 pm distance from  $C_\alpha$ , calculated at (U)M06-2X/6-31+G(d) level. The position of the eDP w.r.t  $1/r1$  is indicated by the angle between the eDP-axis,  $C_\alpha$  and the +x axis (first column). The RSE for  $1/r1$  (91.7 kJ/mol) in the absence of an external charge is used as a reference. The estimated ciRSE for the dipole [ $1/r1+PC(-)+cPC(+)$ ] (last column) is summation of the ciRSE for external PC(+) and cPC(-) values, where c stand for the correction through shifting the PC(+) by 180°.

Angle	$1/r1+eDP$				ciRSE	ciRSE	ciRSE	cPC(+)	Angle	ciRSE
	RSE	ciRSE	CSCE	RCE	$1/r1+PC(-)$	$1/r1+PC(+)$	$1/r1+cPC(+)$	$1/r1+PC(-)+cPC(+)$		
0	-77.8	13.9	-115.8	-101.8	6.4	-7.5	8.6	180	15.0	
10	-77.4	14.3	-118.4	-104.1	7.1	-7.9	8.2	190	15.3	
20	-77.7	14.0	-117.9	-104.0	7.4	-8.0	7.5	200	14.9	
30	-78.7	13.0	-114.3	-101.3	7.3	-7.8	6.5	210	13.8	
40	-80.1	11.6	-108.1	-96.5	6.8	-7.2	5.4	220	12.2	
50	-81.9	9.8	-100.6	-90.7	5.9	-6.2	4.3	230	10.3	
60	-83.8	7.9	-93.1	-85.2	4.8	-4.9	3.4	240	8.2	
70	-85.9	5.8	-86.6	-80.8	3.4	-3.5	2.5	250	5.9	
80	-88.1	3.6	-81.7	-78.0	2.1	-2.0	1.6	260	3.7	
90	-90.3	1.4	-78.2	-76.8	0.7	-0.5	0.8	270	1.4	
100	-92.5	-0.8	-75.9	-76.7	-0.8	0.9	-0.1	280	-0.8	
110	-94.9	-3.2	-74.3	-77.5	-2.2	2.4	-1.0	290	-3.2	
120	-97.4	-5.7	-73.1	-78.7	-3.7	3.8	-1.9	300	-5.5	
130	-99.9	-8.2	-71.9	-80.1	-5.1	5.2	-2.8	310	-8.0	
140	-102.5	-10.8	-70.5	-81.3	-6.5	6.4	-3.8	320	-10.4	
150	-105.0	-13.3	-68.9	-82.2	-7.8	7.5	-4.9	330	-12.7	
160	-107.2	-15.5	-66.7	-82.3	-8.8	8.2	-5.9	340	-14.7	
170	-109.0	-17.3	-63.6	-80.9	-9.6	8.6	-6.8	350	-16.4	
180	-110.0	-18.3	-59.6	-77.9	-9.8	8.6	-7.5	360	-17.3	
190	-110.0	-18.3	-56.0	-74.3	-9.4	8.2	-7.9	10	-17.3	
200	-109.1	-17.4	-54.6	-72.0	-8.5	7.5	-8.0	20	-16.5	
210	-107.6	-15.9	-56.1	-72.0	-7.3	6.5	-7.8	30	-15.1	
220	-105.6	-13.9	-60.2	-74.1	-6.1	5.4	-7.2	40	-13.3	
230	-103.2	-11.5	-66.0	-77.5	-4.9	4.3	-6.2	50	-11.1	
240	-100.7	-9.0	-72.1	-81.2	-3.8	3.4	-4.9	60	-8.7	
250	-98.1	-6.4	-77.6	-84.0	-2.7	2.5	-3.5	70	-6.3	
260	-95.6	-3.9	-81.9	-85.8	-1.8	1.6	-2.0	80	-3.8	
270	-93.1	-1.4	-85.1	-86.5	-0.9	0.8	-0.5	90	-1.4	
280	-90.8	0.9	-87.5	-86.6	0.0	-0.1	0.9	100	0.9	
290	-88.5	3.2	-89.6	-86.5	0.8	-1.0	2.4	110	3.2	
300	-86.4	5.3	-91.9	-86.6	1.7	-1.9	3.8	120	5.5	
310	-84.3	7.4	-94.8	-87.4	2.5	-2.8	5.2	130	7.7	
320	-82.4	9.3	-98.2	-88.9	3.3	-3.8	6.4	140	9.7	
330	-80.8	10.9	-102.2	-91.3	4.1	-4.9	7.5	150	11.5	
340	-79.5	12.2	-106.6	-94.4	4.9	-5.9	8.2	160	13.1	
350	-78.5	13.2	-111.4	-98.2	5.6	-6.8	8.6	170	14.2	

**External electric field (EEF)**

**Table S3-16.** [Table S29] ciRSE values ( $\Delta E_{\text{tot}}$ , kJ/mol) for **1/r1** in the presence of an external electric field of varying strengths (EEF,  $72 \times 10^{-4}$  to  $82 \times 10^{-4}$  au with  $4 \times 10^{-4}$  interval) in the xy-plane, calculated at (U)M06-2X/6-31+G(d) level. The orientation of EEF w.r.t. **1/r1** is indicated by the angle the electric field vector makes with the +x axis having an origin at  $C_{\alpha}$ . The RSE for **1/r1** (91.7 kJ/mol) in the absence of an external charge is used as a reference. The  $C_5$  conformations of **1/r1** used were optimized at the (U)B3LYP/6-31G(d) level of theory.

Angle/EEF	72	74	76	78	80	82
0	13.8	14.1	14.4	14.7	15.1	15.4
10	13.6	13.9	14.2	14.5	14.9	15.2
20	13.1	13.4	13.7	14.0	14.3	14.6
30	12.2	12.5	12.8	13.1	13.3	13.6
40	11.0	11.2	11.5	11.8	12.0	12.3
50	9.4	9.7	9.9	10.1	10.4	10.6
60	7.6	7.8	8.0	8.2	8.3	8.5
70	5.5	5.6	5.7	5.9	6.0	6.2
80	3.1	3.2	3.2	3.3	3.4	3.5
90	0.5	0.5	0.5	0.5	0.6	0.6
100	-2.2	-2.3	-2.3	-2.4	-2.5	-2.5
110	-5.0	-5.1	-5.3	-5.4	-5.5	-5.7
120	-7.7	-7.9	-8.1	-8.4	-8.6	-8.8
130	-10.3	-10.6	-10.9	-11.2	-11.5	-11.8
140	-12.6	-13.0	-13.4	-13.7	-14.1	-14.5
150	-14.6	-15.0	-15.5	-15.9	-16.4	-16.8
160	-16.1	-16.6	-17.1	-17.6	-18.1	-18.6
170	-17.1	-17.7	-18.2	-18.7	-19.3	-19.8
180	-17.6	-18.1	-18.7	-19.2	-19.8	-20.3
190	-17.5	-18.0	-18.5	-19.1	-19.6	-20.2
200	-16.7	-17.3	-17.8	-18.3	-18.8	-19.4
210	-15.5	-15.9	-16.4	-16.9	-17.4	-17.9
220	-13.7	-14.1	-14.5	-15.0	-15.4	-15.8
230	-11.5	-11.9	-12.2	-12.6	-12.9	-13.3
240	-9.0	-9.3	-9.5	-9.8	-10.1	-10.4
250	-6.3	-6.5	-6.6	-6.8	-7.0	-7.2
260	-3.4	-3.5	-3.6	-3.7	-3.8	-3.9
270	-0.6	-0.6	-0.6	-0.6	-0.7	-0.7
280	2.2	2.2	2.3	2.3	2.4	2.5
290	4.7	4.9	5.0	5.1	5.2	5.4
300	7.1	7.3	7.4	7.6	7.8	8.0
310	9.1	9.3	9.6	9.8	10.0	10.3
320	10.8	11.0	11.3	11.6	11.9	12.1
330	12.1	12.4	12.7	13.0	13.3	13.6
340	13.0	13.3	13.7	14.0	14.3	14.6
350	13.6	13.9	14.2	14.6	14.9	15.2

## 3.1.4.2 Plane xz

**Table S3-17.** [Table S30] ciRSE values ( $\Delta E_{\text{tot}}$ , kJ/mol) for  $1/r\mathbf{1}$  in the presence of  $\text{Cl}^-$  placed in the xz-plane at varying distances from  $C_\alpha$ , calculated at (U)M06-2X/6-31+G(d) level. The position of  $\text{Cl}^-$  w.r.t  $1/r\mathbf{1}$  in the xz-plane is indicated by the angle between the ion,  $C_\alpha$  and the +x axis (first column) together with the distance between the ion and  $C_\alpha$  (first row). The angle between the ion,  $C_\alpha$  and the y axis is fixed at  $90^\circ$ .

Angle	7 Å	8 Å	9 Å	10 Å	11 Å	12 Å	13 Å	14 Å	15 Å
0	9.5	7.7	6.5	5.5	4.3	3.8	3.3	2.8	2.5
10	9.6	7.7	6.4	5.3	4.5	3.8	3.3	2.9	2.5
20	9.2	7.6	6.2	5.1	4.3	3.7	3.1	2.7	2.4
30	8.8	7.1	5.8	4.8	4.0	3.4	3.0	2.6	2.3
40	8.2	6.6	5.3	4.4	3.7	3.1	2.7	2.3	2.1
50	7.4	5.8	4.7	3.9	3.3	2.8	2.4	2.1	1.8
60	6.5	5.0	3.9	3.2	2.6	2.2	1.9	1.6	1.4
70	5.2	3.9	3.1	2.5	2.1	1.8	1.5	1.3	1.1
80	3.9	2.9	2.2	1.7	1.4	1.1	0.9	0.8	0.7
90	2.2	1.5	1.0	0.8	0.6	0.5	0.4	0.3	0.3
100	0.3	0.0	-0.2	-0.2	-0.3	-0.3	-0.3	-0.2	-0.2
110	-2.0	-1.8	-1.6	-1.3	-1.2	-1.0	-0.9	-0.7	-0.7
120	-4.6	-3.7	-3.0	-2.5	-2.1	-1.8	-1.6	-1.4	-1.2
130	-7.4	-5.7	-4.5	-3.7	-3.0	-2.5	-2.1	-1.8	-1.6
140	-10.3	-7.8	-6.1	-4.9	-4.0	-3.4	-2.9	-2.5	-2.1
150	-13.5	-9.8	-7.4	-5.9	-4.8	-4.0	-3.3	-2.8	-2.4
160	-16.1	-11.5	-8.7	-6.8	-5.4	-4.5	-3.8	-3.2	-2.7
170	-17.7	-12.7	-9.5	-7.4	-5.9	-4.8	-4.0	-3.4	-2.9
180	-18.0	-13.0	-9.7	-7.5	-6.0	-4.9	-4.1	-3.4	-3.0

**Table S3-18.** [Table S31] ciRSE values ( $\Delta E_{\text{tot}}$ , kJ/mol) for  $1/r\mathbf{1}$  in the presence of  $\text{Na}^+$  placed in the xz-plane at varying distances from  $C_\alpha$ , calculated at (U)M06-2X/6-31+G(d) level. The position of  $\text{Na}^+$  w.r.t  $1/r\mathbf{1}$  in the xz-plane is indicated by the angle between the ion,  $C_\alpha$  and the +x axis (first column) together with the distance between the ion and  $C_\alpha$  (first row). The angle between the ion,  $C_\alpha$  and the y axis is fixed at  $90^\circ$ .

Angle	7 Å	8 Å	9 Å	10 Å	11 Å	12 Å	13 Å	14 Å	15 Å
0	-13.6	-9.8	-7.4	-5.9	-4.8	-3.9	-3.5	-2.9	-2.7
10	-13.5	-9.7	-7.3	-5.8	-4.7	-4.0	-3.3	-2.9	-2.5
20	-13.0	-9.3	-7.0	-5.6	-4.6	-3.8	-3.3	-2.8	-2.4
30	-11.5	-8.4	-6.5	-5.1	-4.2	-3.5	-3.0	-2.6	-2.2
40	-9.7	-7.2	-5.6	-4.5	-3.7	-3.1	-2.7	-2.3	-2.0
50	-8.1	-6.2	-4.9	-3.9	-3.2	-2.7	-2.2	-1.9	-1.7
60	-6.7	-5.0	-3.9	-3.2	-2.6	-2.2	-1.9	-1.6	-1.4
70	-5.1	-3.9	-3.1	-2.4	-2.0	-1.6	-1.3	-1.1	-1.0
80	-3.6	-2.6	-1.9	-1.5	-1.2	-1.0	-0.8	-0.7	-0.6
90	-1.8	-1.2	-0.8	-0.6	-0.4	-0.3	-0.2	-0.2	-0.1
100	0.1	0.3	0.4	0.4	0.4	0.4	0.4	0.3	0.3
110	2.2	2.0	1.6	1.4	1.2	1.1	1.0	0.9	0.8
120	4.4	3.6	3.1	2.6	2.2	1.8	1.6	1.4	1.2
130	6.8	5.3	4.3	3.6	3.0	2.6	2.3	2.0	1.8
140	9.0	7.1	5.7	4.6	3.8	3.2	2.7	2.3	2.0
150	11.1	8.5	6.9	5.6	4.6	3.9	3.3	2.8	2.5
160	12.8	9.9	7.8	6.3	5.2	4.3	3.6	3.1	2.8
170	14.2	10.8	8.4	6.8	5.5	4.6	3.9	3.4	2.9
180	14.8	11.2	8.8	6.9	5.7	4.7	4.0	3.4	3.0

## 3.1.4.3 Plane yz

**Table S3-19.** [Table S32] ciRSE values ( $\Delta E_{\text{tot}}$ , kJ/mol) for  $\mathbf{1/r1}$  in the presence of  $\text{Cl}^-$  placed in the yz-plane at varying distances from  $C_\alpha$ , calculated at (U)M06-2X/6-31+G(d) level. The position of  $\text{Cl}^-$  w.r.t  $\mathbf{1/r1}$  in the yz-plane is indicated by the angle between the ion,  $C_\alpha$  and the y axis (first column) together with the distance between the ion and  $C_\alpha$  (first row). The angle between the ion,  $C_\alpha$  and the x axis is fixed at  $90^\circ$ .

Angle	5 Å	6 Å	7 Å	8 Å	9 Å	10 Å	11 Å	12 Å	13 Å	14 Å	15 Å
0	0.0	1.3	1.2	0.8	0.8	0.6	0.6	0.4	0.3	0.4	0.4
10	0.4	1.4	1.3	0.9	0.7	0.6	0.5	0.5	0.4	0.4	0.3
20	1.2	1.5	1.2	0.9	0.7	0.6	0.5	0.5	0.4	0.4	0.3
30	1.9	1.5	1.3	1.0	0.8	0.7	0.6	0.5	0.4	0.4	0.3
40	2.5	1.8	1.4	1.1	0.9	0.7	0.6	0.5	0.5	0.4	0.4
50	3.2	2.1	1.5	1.1	0.9	0.7	0.6	0.5	0.4	0.3	0.3
60	3.8	2.5	1.8	1.3	1.0	0.7	0.6	0.5	0.4	0.4	0.3
70	4.4	2.8	2.0	1.4	1.0	0.8	0.6	0.5	0.4	0.4	0.3
80	5.1	3.2	2.0	1.4	1.0	0.8	0.6	0.5	0.4	0.3	0.3
90	5.6	3.4	2.2	1.5	1.0	0.8	0.6	0.5	0.4	0.3	0.3
100	5.8	3.4	2.1	1.3	0.9	0.7	0.5	0.4	0.3	0.2	0.2
110	5.7	3.2	1.8	1.1	0.7	0.5	0.4	0.3	0.2	0.2	0.1
120	5.0	2.6	1.5	0.9	0.6	0.4	0.3	0.2	0.1	0.1	0.1
130	3.5	1.8	1.0	0.5	0.3	0.2	0.1	0.1	0.1	0.0	0.0
140	1.5	0.6	0.3	0.1	0.0	0.0	-0.1	-0.1	-0.1	0.0	0.0
150	-0.7	-0.5	-0.4	-0.3	-0.3	-0.2	-0.2	-0.2	-0.1	-0.1	-0.1
160	-2.7	-1.7	-1.1	-0.8	-0.6	-0.5	-0.4	-0.3	-0.3	-0.2	-0.2
170	-4.2	-2.4	-1.5	-1.0	-0.7	-0.6	-0.4	-0.3	-0.3	-0.2	-0.2
180	-4.7	-2.6	-1.7	-1.1	-0.8	-0.6	-0.4	-0.3	-0.3	-0.2	-0.2

**Table S3-20.** [Table S33] ciRSE values ( $\Delta E_{\text{tot}}$ , kJ/mol) for  $\mathbf{1/r1}$  in the presence of  $\text{Na}^+$  placed in the yz-plane at varying distance from  $C_\alpha$ , calculated at (U)M06-2X/6-31+G(d) level. The position of  $\text{Na}^+$  w.r.t  $\mathbf{1/r1}$  in the yz-plane is indicated by the angle between the ion,  $C_\alpha$  and the y axis (first column) together with the distance between the ion and  $C_\alpha$  (first row). The angle between the ion,  $C_\alpha$  and the x axis is fixed at  $90^\circ$ .

Angle	5 Å	6 Å	7 Å	8 Å	9 Å	10 Å	11 Å	12 Å	13 Å	14 Å	15 Å
0	0.8	-0.2	-0.5	-0.6	-0.5	-0.4	-0.5	-0.2	-0.3	-0.3	-0.2
10	0.5	-0.4	-0.6	-0.4	-0.5	-0.4	-0.4	-0.3	-0.2	-0.2	-0.2
20	-0.3	-0.8	-0.7	-0.6	-0.6	-0.5	-0.4	-0.3	-0.3	-0.2	-0.2
30	-1.2	-1.2	-1.0	-0.7	-0.6	-0.5	-0.4	-0.3	-0.3	-0.2	-0.2
40	-2.0	-1.5	-1.2	-0.9	-0.7	-0.5	-0.4	-0.3	-0.2	-0.2	-0.2
50	-2.6	-1.8	-1.3	-1.0	-0.7	-0.6	-0.5	-0.4	-0.3	-0.3	-0.2
60	-3.1	-2.0	-1.5	-1.0	-0.8	-0.6	-0.5	-0.4	-0.3	-0.3	-0.2
70	-3.9	-2.5	-1.5	-1.1	-0.8	-0.6	-0.5	-0.4	-0.3	-0.2	-0.2
80	-4.6	-2.7	-1.7	-1.2	-0.9	-0.6	-0.5	-0.4	-0.3	-0.2	-0.2
90	-5.2	-3.0	-1.8	-1.2	-0.8	-0.6	-0.4	-0.3	-0.2	-0.2	-0.1
100	-5.2	-2.9	-1.8	-1.1	-0.8	-0.5	-0.4	-0.3	-0.2	-0.2	-0.1
110	-4.7	-2.6	-1.6	-1.0	-0.7	-0.5	-0.3	-0.2	-0.2	-0.1	-0.1
120	-3.8	-2.0	-1.2	-0.7	-0.4	-0.3	-0.2	-0.1	-0.1	0.0	0.0
130	-2.4	-1.2	-0.6	-0.3	-0.1	0.0	0.0	0.1	0.1	0.1	0.1
140	-0.8	-0.3	-0.1	0.0	0.1	0.2	0.2	0.2	0.2	0.2	0.2
150	0.8	0.6	0.5	0.5	0.5	0.4	0.4	0.3	0.3	0.3	0.3
160	2.1	1.3	0.9	0.7	0.6	0.5	0.4	0.4	0.3	0.3	0.3
170	3.0	2.0	1.4	1.0	0.8	0.7	0.6	0.5	0.4	0.4	0.3
180	3.2	2.2	1.4	1.1	0.9	0.7	0.6	0.5	0.4	0.4	0.4

### 3.1.5 Distonic Peptide System

#### 3.1.5.1 Procedure for obtaining conformers to determine conformationally avg. energies.

Step 1. The MacroModel module of Maestro 10.2,<sup>1</sup> is used to generate a conformational pool. The Amber 94 force field was employed with an 50 kJ/mol energy window.

Step 2. The molecular mechanics-based conformational pool is optimized using QM-based methods. Duplicate conformers are removed from the list.

Step 3. Only conformers with an energy (Rel.  $\Delta E$ ) less than 20 kJ/mol relative to the global minima (conformer with the lowest energy) were considered. In case there is a large number of conformers (>15) in this energy window, the first 15 conformers with the lowest energy were selected for determining conformationally average energies.

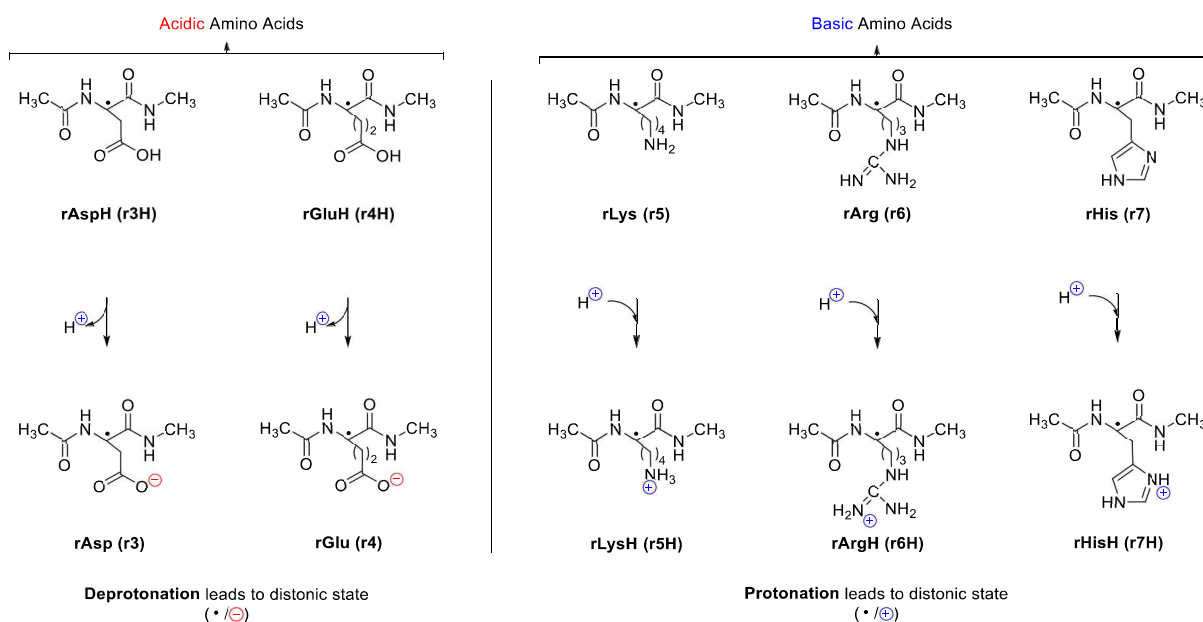


**Figure S3-13.** [Figure S17] Acidic and basic amino acids (AAs) investigated for the effect of deprotonation and protonation on the stability of their  $C_\alpha$  radicals.

**Table S3-21.** [Table S34, S39, S44, S52 and S57] ciRSE values (in kJ/mol) calculated at different levels of theory for the systems shown in Figure S3-13.

System	(U)B3LYP \6-31G(d) <sup>a</sup>			(U)M062X \6-31+G(d) <sup>b</sup>			(RO)B2PLYP \GTMP2large <sup>b</sup>			G3(MP2)-RAD <sup>b</sup>			G3B3 <sup>b</sup>			(U)M062X \6-31+G(d) <sup>a</sup>		
	$\Delta E_{\text{tot}}$	$\Delta H_{298}$	$\Delta G_{298}$	$\Delta E_{\text{tot}}$	$\Delta H_{298}$	$\Delta G_{298}$	$\Delta E_{\text{tot}}$	$\Delta H_{298}$	$\Delta G_{298}$	$\Delta E_{\text{tot}}$	$\Delta H_{298}$	$\Delta G_{298}$	$\Delta E_{\text{tot}}$	$\Delta H_{298}$	$\Delta G_{298}$	$\Delta E_{\text{tot}}$	$\Delta H_{298}$	$\Delta G_{298}$
<b>r3</b>																		
Boltzmann Avg.	-1.0	<b>0.0</b>	5.2	<b>-3.8</b>	<b>-2.9</b>	1.6	1.3	<b>2.3</b>	6.7	-0.2	<b>0.6</b>	6.0	0.8	<b>1.7</b>	7.0	-3.2	<b>-2.4</b>	-3.6
Best Conf.	-1.1	-0.2	4.8	-3.6	-3.3	0.8	1.6	2.3	6.0	0.5	0.9	4.9	1.6	2.3	6.3	-2.6	-2.4	-2.6
<b>r4</b>																		
Boltzmann Avg.	3.5	<b>-1.5</b>	-1.6	<b>13.8</b>	<b>8.6</b>	8.2	8.4	<b>3.2</b>	2.7	12.1	<b>7.1</b>	6.6	12.3	<b>7.5</b>	6.9	9.6	<b>2.1</b>	-4.0
Best Conf.	2.8	-1.9	-1.6	12.9	8.0	7.9	7.5	2.7	2.6	11.0	6.3	6.2	11.2	6.5	6.4	9.2	2.1	-3.5
<b>r5H</b>																		
Boltzmann Avg.	15.1	<b>10.7</b>	9.1	<b>15.1</b>	<b>10.5</b>	8.4	16.8	<b>13.9</b>	11.8	13.5	<b>9.7</b>	9.8	12.9	<b>9.0</b>	8.9	12.7	<b>8.6</b>	9.2
Best Conf.	14.5	9.9	8.2	14.9	10.6	8.9	16.0	13.6	12.1	14.1	9.9	10.1	13.3	9.3	9.0	12.0	8.3	9.7
<b>r6H</b>																		
Boltzmann Avg.	5.1	<b>5.3</b>	3.4	<b>-20.0</b>	<b>-20.8</b>	-13.4	0.3	<b>1.4</b>	1.3	-14.3	<b>-15.1</b>	-7.5	-16.2	<b>-16.8</b>	-8.7	-19.6	<b>-16.4</b>	-11.6
Best Conf.	4.3	4.5	2.7	-17.5	-18.7	-12.3	-0.2	-1.5	3.0	-12.3	-13.5	-6.8	-14.1	-15.2	-8.1	-17.7	-14.9	-8.2
<b>r7H</b>																		
Boltzmann Avg.	1.1	<b>3.2</b>	4.5	<b>7.5</b>	<b>7.5</b>	6.0	2.1	<b>3.5</b>	4.5	6.4	<b>6.5</b>	5.0	7.6	<b>7.6</b>	6.1	9.1	<b>6.5</b>	9.7
Best Conf.	0.3	3.1	4.5	7.1	6.8	5.5	1.9	3.8	5.2	5.9	6.2	5.0	7.1	7.1	5.8	8.2	5.7	9.4

<sup>a</sup>Level of geometry optimization. <sup>b</sup>Single point energy calculations over (U)B3LYP/6-31G(d) optimized geometries.

### 3.1.5.2 Extended Lysine (Lys, 5)

Conformational analysis of all distonic systems as listed in Figure S3-13 indicates the presence of hydrogen bonding interactions between the neutral and charged side chain residues and the dipeptide amide groups. It is only for lysine dipeptide model **5a** that remote charge effects on radical stability can be analyzed. This is due to the fact that conformational minima with fully extended side chains exist for all four relevant species [neutral and protonated forms of closed-shell parents and their radicals, see Figure S3-14 (B)]. In the discussion, we will focus on results derived from total free energy ( $\Delta E_{\text{tot}}$ ) and enthalpy values ( $\Delta H_{298}$ ) calculated at (U)M06-2X\6-31+G(d)//(U)B3LYP\6-31G(d) level.

#### Fully Optimized *cis/trans* Lysine Optimize (**5a**)

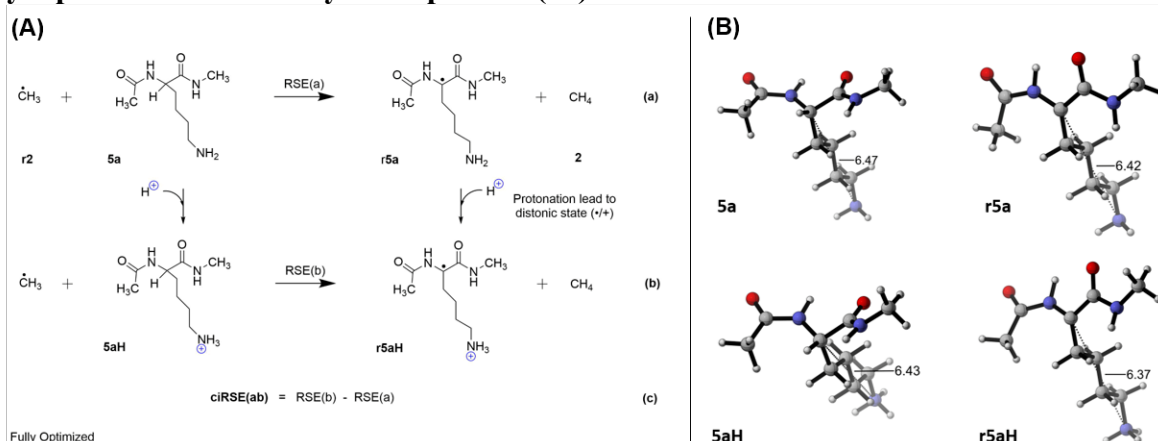


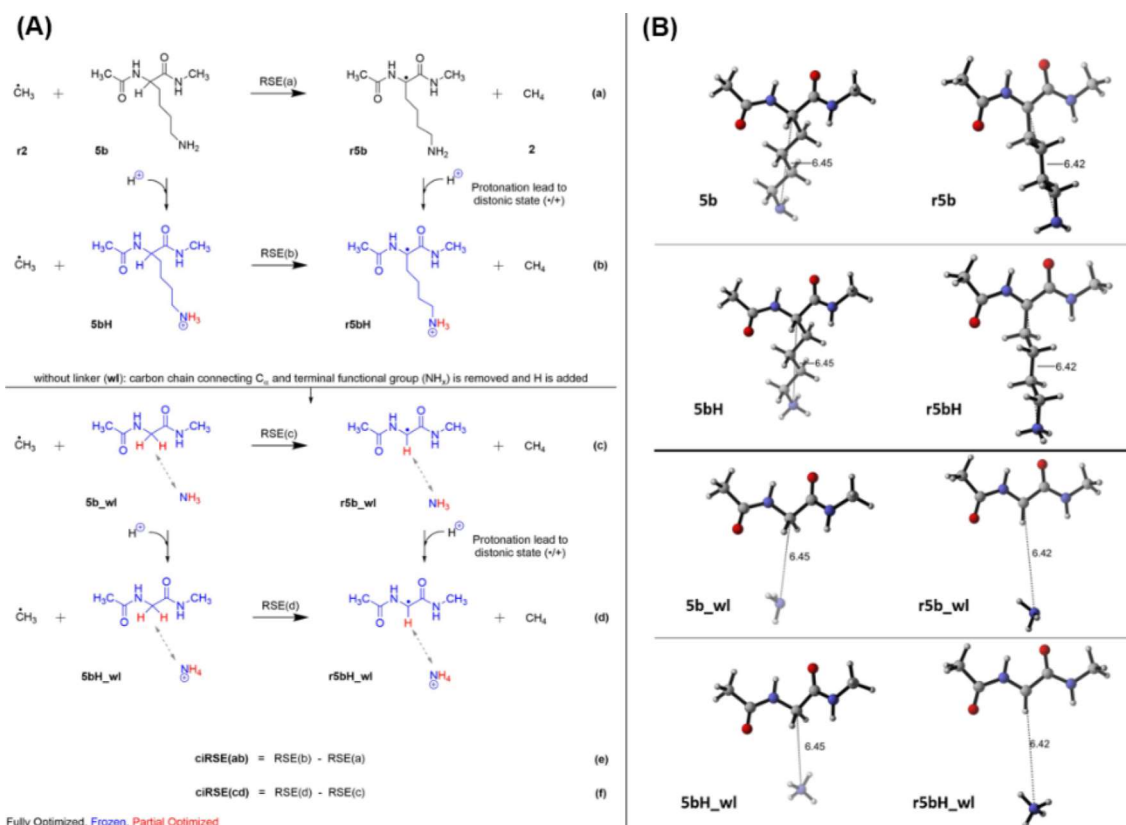
**Figure S3-14.** (A) [Scheme S5] Reaction system to study the effect of charge on the stability of the  $\text{C}_\alpha$  radical of extended *cis/trans* lysine (**5a**). (B) [Figure S24] Structures obtained from geometry optimization at the (U)B3LYP/6-31G(d) level of theory in the gas phase.

All four structures are energetically much less stable than the most favourable conformers with direct side chain-backbone interactions but can be assumed to be similarly biased through the extended side chain. Focusing on enthalpy values  $\Delta H_{298}$ , neutral radical **r5a** is strongly stabilized by  $\text{RSE(a, r5a)} = -80.6$  kJ/mol (Table S3-22), which is mainly due to the amide *s-cis* conformations as noted in earlier studies.<sup>6</sup> This value is reduced through protonation to cation radical **r5aH** to  $\text{RSE(b, r5aH)} = -60.6$  kJ/mol. The difference of 20.0 kJ/mol is very similar to that calculated using  $\Delta E_{\text{tot}}$  energy values (21.0 kJ/mol). The ciRSE of 20 kJ/mol for the lysine dipeptide model **5a** described in Table S3-22 is likely a consequence of multiple factors that include the through space charge/spin interactions, additional through bond interactions between side chain and radical center and conformational changes as the result of optimization after protonation. This makes the direct comparison with the stabilizing/destabilizing effects of  $\text{Na}^+$  on glyceryl dipeptide radical **r1** very difficult.

**Table S3-22.** [Table S49] RSEs and ciRSE values (in kJ/mol) calculated at different levels of theory for the systems shown in Figure S3-14 (A).

Cis Trans Lysine Optimized	RSE (a, <b>r5a</b> )	RSE (b, <b>r5aH</b> )	ciRSE (ab, <b>5a</b> )	RSE (a, <b>r5a</b> )	RSE (b, <b>r5aH</b> )	ciRSE (ab, <b>5a</b> )
	(U)B3LYP\6-31G(d) <sup>a</sup>			(U)M06-2X\6-31+G(d) <sup>b</sup>		
$\Delta E_{\text{tot}}$	-106.0	-83.8	<b>22.2</b>	-87.5	-66.5	<b>21.0</b>
$\Delta H_{298}$	-99.1	-77.8	<b>21.3</b>	-80.6	-60.6	<b>20.0</b>
$\Delta G_{298}$	-93.6	-71.4	<b>22.1</b>	-75.0	-54.2	<b>20.9</b>

<sup>a</sup>Level of geometry optimization. <sup>b</sup>Single point energy calculations over (U)B3LYP/6-31G(d) optimized geometries.

Partially Optimized All *trans* Lysine (**5b**)

**Figure S3-15.** (A) [Scheme S6] Reaction system to study the effect of charge on the stability of the  $\text{C}_\alpha$  radical of extended all *trans* lysine (**5b**) (B) [Figure S25] Structures for the system shown in Scheme S6. **5b** and **r5b** were obtained from geometry optimization at (U)B3LYP/6-31G(d) level of theory in the gas phase. For the remaining structures, only the added hydrogens are optimized (see Scheme S6 for more details).

Below describes the procedure we employed to limit the influence of conformational changes and to estimate through bond interactions between the side chain and the radical center on the ciRSE for the lysine dipeptide model. We are using all *trans* lysine (**5b**) as an example [Figure S3-15 (A)]. The same procedure is used for the other cases.

Step 1: The RSE(a) is calculated using a fully extended conformation of neutral closed-shell lysine (**5b**) and its  $\text{C}_\alpha$  radical (**r5b**). We paired structurally similar closed and open-shell systems [Figure S3-15 (B)].

Step 2: A remote charge is introduced via protonation at the terminal  $\text{NH}_2$  group of **5b** and **r5b**, which yield the starting structures for charged **5bH** and **r5bH**, respectively. Freezing the rest of the molecule, all hydrogens at the  $\text{NH}_3$  group of **5bH** and **r5bH** are relaxed during optimization. The RSE(b) is then calculated from partially optimized **5bH** and **r5bH**. The ciRSE(ab) obtained in this way has a very limited contribution from the change in conformations of the involved species.

Step 3: To estimate the contribution of through bond interactions between the terminal functional group and the radical center on the ciRSE, the carbon chain connecting  $\text{C}_\alpha$  and the terminal function group ( $\text{NH}_x$ ) is removed from all species of lysine [see eqs. c and d in Figure S3-15 (A)]. One hydrogen atom is added at  $\text{C}_\alpha$  and  $\text{NH}_x$  in this process. All the hydrogens at  $\text{C}_\alpha$  and  $\text{NH}_x$  are selectively relaxed by freezing the rest of the molecule during optimization. The ciRSE(cd) obtained this way is mainly the result of through space charge/spin interactions.

Table S3-23 lists the result on all *trans* lysine (**5b**) computed using the above-defined procedure. Here we discuss the results in terms of total free energy ( $\Delta E_{\text{tot}}$ ) calculated at (U)M06-2X/6-31+G(d) level. For all *trans* lysine (**5b**), ciRSE(ab) is 7.2 kJ/mol and charge effect is further reduced by 4.7 kJ/mol once we removed the carbon chain (linker). Thus, the ciRSE(cd) only amounts to 2.5 kJ/mol.

It is very small effect, but it is possible to make a rough direct comparison of ciRSE(cd) to the stabilizing/destabilizing effects of Na<sup>+</sup> on the glyceryl dipeptide radical **r1**. In **5bH\_wl**, the NH<sub>4</sub><sup>+</sup> group is located at 645 pm away from C<sub>α</sub> [Figure S3-15 (B)] and has a position equivalent to Na<sup>+</sup> at the angle of 270-280° in the yz-plane (at a distance of 600-700 pm).

**Table S3-23.** [Table S50] RSEs and ciRSE values (in kJ/mol) calculated at different levels of theory for the systems shown in Figure S3-15 (A).

$\Delta E_{\text{tot}}$	With Linker			Without Linker (wl)		
	RSE(a)	RSE(b)	ciRSE(ab)	RSE(c)	RSE(d)	ciRSE(cd)
			(U)B3LYP\6-31G(d)			
<b>5b</b>	-112.7	-105.5	<b>7.2</b>	-104.8	-101.9	<b>3.0</b>
			(U)M06-2X\6-31+G(d)			
<b>5b_wl</b>	-92.9	-85.7	<b>7.2</b>	-88.3	-85.8	<b>2.5</b>

Similarly, in **r5bH\_wl**, the NH<sub>4</sub><sup>+</sup> position is equivalent in terms of distance and direction to Na<sup>+</sup> at the angle of 150-160° in the yz-plane (at a distance of 600-700 pm). CSCE and RCE values for **1/r1+Na<sup>+</sup>** complexes in the yz-plane at a varying distances are listed in Table S3-20. CSCE for **1+Na<sup>+</sup>** at a distance of 600-700 pm and orientation of 270-280° in the yz-plane lies in a range of -2.2 to -4.7 kJ/mol. RCE for **r1+Na<sup>+</sup>** at a distance of 600-700 pm and orientation of 150-160° in the yz-plane lies in a range of -3.7 to -5.4 kJ/mol. The ciRSE (= RCE - CSCE) calculated using the **1/r1+Na<sup>+</sup>** complexes in the geometries described above yield stabilization energies of -0.5 to -1 kJ/mol relative to neutral **1/r1**. It is important to note that in case of glyceryl dipeptide both radical and closed shell systems have planar C<sub>5</sub> conformations, while the all *trans* lysine **5bH\_wl** has a non-planar C<sub>5</sub> conformation.

### 3.1.6 References

- (1) *Schrödinger Release 2015–2: MacroModel*, Version 10.8; Schrödinger: LLC, New York, USA, **2015**.
- (2) (a) Hariharan, P. C.; Pople, J. A., *Theor. Chim. Acta.* **1973**, *28*, 213-222. (b) Becke, A. D., *J. Chem. Phys.* **1993**, *98*, 5648-5652.
- (3) (a) Zhao, Y.; Truhlar, D. G., *Acc. Chem. Res.* **2008**, *41*, 157-167. (b) Zhao, Y.; Truhlar, D. G., *Theor. Chem. Acc.* **2008**, *120*, 215-241.
- (4) Graham, D. C.; Menon, A. S.; Goerigk, L.; Grimme, S.; Radom, L., *J. Phys. Chem. A* **2009**, *113*, 9861-9873.
- (5) Henry, D. J.; Parkinson, C. J.; Radom, L., *J. Phys. Chem. A* **2002**, *106*, 7927-7936.
- (6) Baboul, A. G.; Curtiss, L. A.; Redfern, P. C.; Raghavachari, K., *J. Chem. Phys.* **1999**, *110*, 7650.
- (7) Frisch, M. J. T., G. W.; Schlegel, H. B.; Scuseria, G. E.; Robb, M. A.; Cheeseman, J. R.; Scalmani, G.; Barone, V.; Mennucci, B.; Petersson, G. A.; Nakatsuji, H.; Caricato, M.; Li, X.; Hratchian, H. P.; Izmaylov, A. F.; Bloino, J.; Zheng, G.; Sonnenberg, J. L.; Hada, M.; Ehara, M.; Toyota, K.; Fukuda, R.; Hasegawa, J.; Ishida, M.; Nakajima, T.; Honda, Y.; Kitao, O.; Nakai, H.; Vreven, T.; Montgomery, Jr., J. A.; Peralta, J. E.; Ogliaro, F.; Bearpark, M.; Heyd, J. J.; Brothers, E.; Kudin, K. N.; Staroverov, V. N.; Keith, T.; Kobayashi, R.; Normand, J.; Raghavachari, K.; Rendell, A.; Burant, J. C.; Iyengar, S. S.; Tomasi, J.; Cossi, M.; Rega, N.; Millam, J. M.; Klene, M.; Knox, J. E.; Cross, J. B.; Bakken, V.; Adamo, C.; Jaramillo, J.; Gomperts, R.; Stratmann, R. E.; Yazyev, O.; Austin, A. J.; Cammi, R.; Pomelli, C.; Ochterski, J. W.; Martin, R. L.; Morokuma, K.; Zakrzewski, V. G.; Voth, G. A.; Salvador, P.; Dannenberg, J. J.; Dapprich, S.; Daniels, A. D.; Farkas, O.; Foresman, J. B.; Ortiz, J. V.; Cioslowski, J.; Fox, D. J.; *Gaussian 09 Revision D. 01*, Gaussian, Inc., Wallingford CT: **2013**.

## Chapter 4. Stability of Peptide Radicals: Thermodynamics vs. Kinetics

Harish Jangra<sup>1</sup>, Ieva Teikmane<sup>1</sup>, Salavat Ashirbaev<sup>1</sup>, Massimo Bietti<sup>2</sup> and Hendrik Zipse<sup>1</sup>

1. Department of Chemistry, LMU Munich, Germany

2. Department of Chemical Science and Technology, University of Rome, Italy

---

***Authors contribution***

H.Z. conceptualized the study and provided direction. All the calculations were designed by H.H. and H.Z., and performed by H.H. Laser Flash Photolysis (LFP) experiments were conducted in the lab of M.B.. I.T. synthesized substrates for LFP. S.A. is currently working on this project. This chapter was written by H.H. and approved by H.Z..



shell systems).<sup>8</sup> Thermal corrections have been scaled by a factor of 0.9806 for G3(MP2)-RAD. All the results that we are going to discuss were calculated at G3(MP2)-RAD level if not mentioned otherwise. For the solvation effect, G3(MP2)-RAD values were corrected with solvation energies obtained at the PCM(acetonitrile)/HF/6-31G(d)//(U)B3LYP/6-31G(d) level of theory.<sup>9</sup> The program MacroModel 10.8 was employed for molecular mechanics (MM)-based conformational searches with the OPLS\_2005 force field (FF)<sup>10</sup> parameters. All other calculations were performed by using Gaussian09, Rev. D.01.<sup>11</sup>

## 4.2.2 Conformational Preferences

The gas phase lowest enthalpy ( $\Delta H_{298}$ ) conformer of closed-shell parent compound **1** and open-shell systems  $\mathbf{r1}_{\text{Ace}}$  and  $\mathbf{r1}_{\text{NMe}}$  has a  $C_7$  conformation, while  $\mathbf{r1}_{\text{C}\alpha}$  prefers the extended  $C_5$  conformation (see Figure 4-2). The enthalpic conformational preference is the same for the level of optimization [(U)B3LYP/6-31G(d)] and for single point calculations at the G3(MP2)-RAD level of theory. In terms of the gas phase free energy ( $\Delta G_{298}$ ), the all-*trans* extended  $C_5$  conformer becomes the lowest energy conformer for closed-shell **1** and open-shell  $\mathbf{r1}_{\text{C}\alpha}$  (see SI for more details).

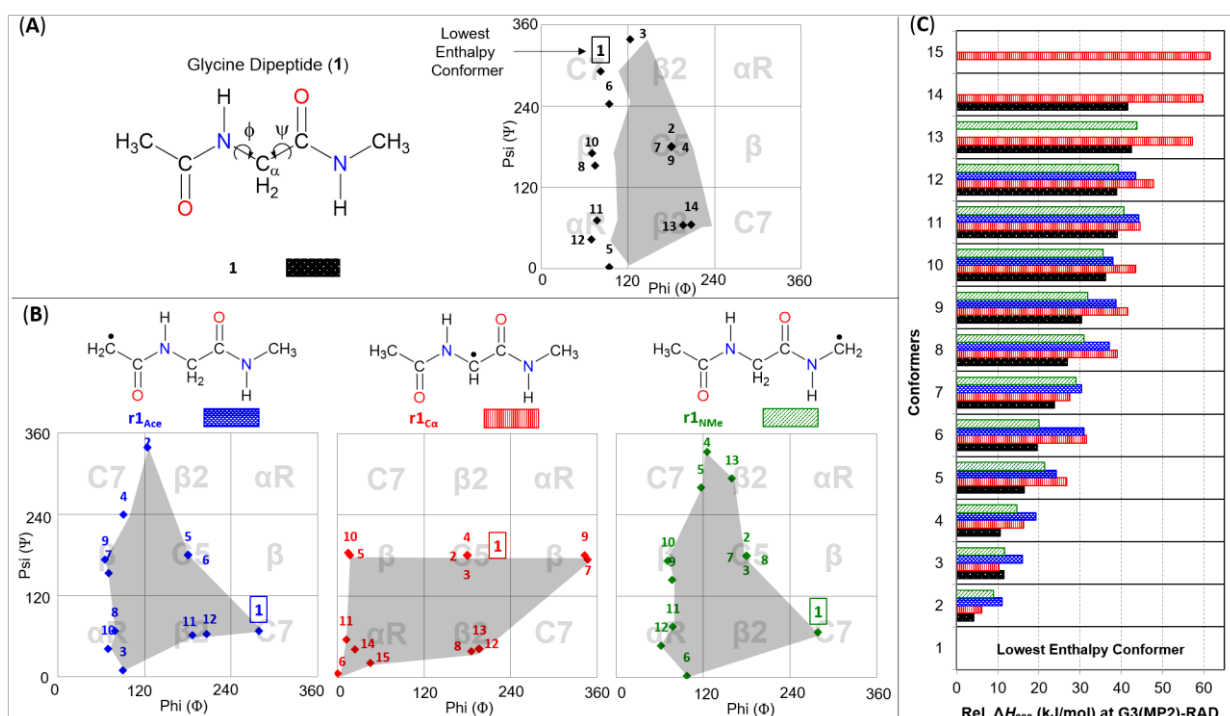


**Figure 4-2.** (A) Systematic diagram of glycine dipeptide (**1**) and its conformational distribution. (in terms of backbone  $\Psi$  and  $\Phi$  angles) (B) Conformational distribution of carbon-centered radicals ( $\mathbf{r1}_{\text{Ace}}$ ,  $\mathbf{r1}_{\text{C}\alpha}$  and  $\mathbf{r1}_{\text{NMe}}$ ) of **1**. Refer to **Table S2-1** for the details of the nomenclature in classifying the peptide geometry. (C) Gas phase rel.  $\Delta H_{298}$  values for **1**,  $\mathbf{r1}_{\text{Ace}}$ ,  $\mathbf{r1}_{\text{C}\alpha}$  and  $\mathbf{r1}_{\text{NMe}}$  calculated at G3(MP2)-RAD level of theory.

## 4.2.3 Thermodynamic Stability

### 4.2.3.1 Radical stabilization energies (RSEs)

We have recently calculated C–H bond energies of dipeptide model systems as a measure of the thermodynamic stabilities of the respective peptide radicals.<sup>12</sup> In the third chapter of this thesis, we have reported radical stabilization energy (RSE) values for the  $C_{\alpha}$  radical of glycine dipeptide ( $\mathbf{r1}_{\text{C}\alpha}$ ) in reference to methyl radical ( $\bullet\text{CH}_3$ ) calculated using equation 1 (Figure 4-3).<sup>6b</sup>

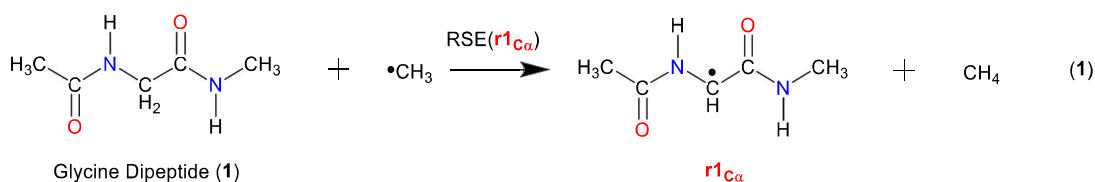


**Figure 4-3.** Isodesmotic reaction used to calculate the RSE of  $C_{\alpha}$  radical of glycine dipeptide ( $r1_{C\alpha}$ ).

We can use similar isodesmotic reactions for calculating RSE values for radicals  $r1_{Ace}$  and  $r1_{NMe}$  generated through a HAT process from the terminal methyl C-H bonds of **1** to methyl radical as employed for  $r1_{C\alpha}$  (Figure 4-4).

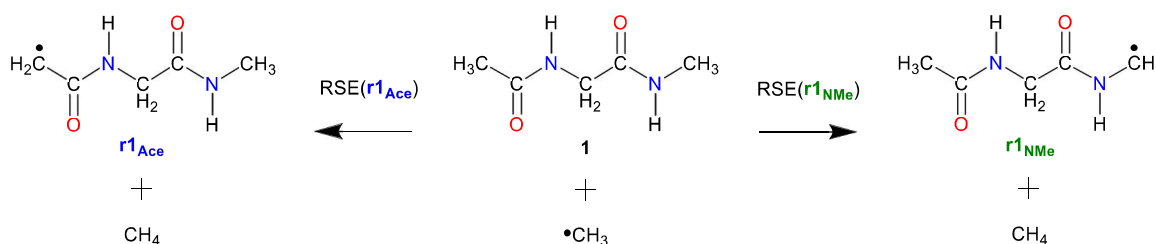


**Figure 4-4.** Isodesmotic reactions used to calculate RSE values for radicals  $r1_{Ace}$  and  $r1_{NMe}$ .

Figure 4-5 depicts gas phase RSE values for radicals  $r1_{Ace}$ ,  $r1_{C\alpha}$ , and  $r1_{NMe}$  calculated at the G3(MP2)-RAD level of theory. For the sake of simplicity, we use enthalpy ( $\Delta H_{298}$ )-based RSE values, as the relative order of stability for these radicals remains the same for free energies ( $\Delta G_{298}$ ) or enthalpies. The  $r1_{C\alpha}$  radical is the most stable among the three carbon-centred radicals of glycine dipeptide **1** with a best conformer-based gas phase stability value of  $RSE(r1_{C\alpha}) = -74.1$  kJ/mol that is followed by  $r1_{NMe}$  and  $r1_{Ace}$  with  $RSE(r1_{NMe}) = -45.7$  kJ/mol and  $RSE(r1_{Ace}) = -23.3$  kJ/mol respectively (see Figure 4-5). The stability trend remains the same with Boltzmann-averaged RSE values (see SI).

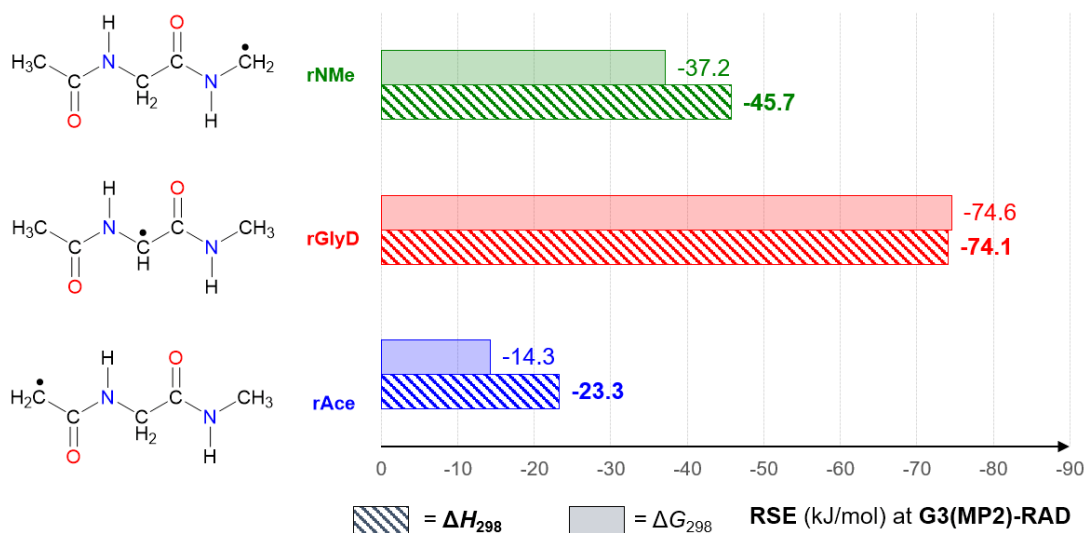


**Figure 4-5.** The best conformer-based gas phase RSE (kJ/mol) values for radicals  $r1_{Ace}$ ,  $r1_{C\alpha}$ , and  $r1_{NMe}$  calculated at the G3(MP2)-RAD level of theory, using equations defined in Figure 4-3 and Figure 4-4.

We can understand the order of stability in these radicals ( $r1_{Ace}$ ,  $r1_{C\alpha}$ , and  $r1_{NMe}$ ) using the concepts of resonance and frontier orbital theory. Relative to the  $\bullet CH_3$  radical,  $r1_{Ace}$  is  $-23.3$  kJ/mol (RSE) more stable. The RSE value reported here is in excellent agreement with previously reported values by our group and others for closely similar systems at the same or comparable levels of theory (see Figure 4-6). Radom et al. previously reported a RSE value of  $-23.0$  kJ/mol for carbonyl-substituted methyl radicals such as  $N$ -methylacetaminyll [ $\bullet CH_2-C(=O)-NH-CH_3$ ] calculated at G3(MP2)-RAD

level of theory.<sup>8b</sup> We previously reported RSE values of  $-22.7$  kJ/mol<sup>12d</sup> for the methyl-centred radical of acetic acid [ $\bullet\text{CH}_2\text{-C(=O)-OH}$ ] at G3(MP2)-RAD level, The Radom group also calculated a closely similar value ( $-22.1$  kJ/mol<sup>13</sup> at the G3X(MP2)-RAD level). The  $\mathbf{r1}_{\text{Ace}}$  radical is more stable than methyl because of resonance stabilization through the C-O double bond [ $\text{-C(=O)-NH-R}$ ]. Figure 4-7(A) shows the stabilizing interactions between the radical centre and the neighbouring  $\pi$ -acceptor in terms of a two orbital/one electron interaction between the radical SOMO and the acceptor LUMO, which leads to spin delocalization into the C-O double bond.

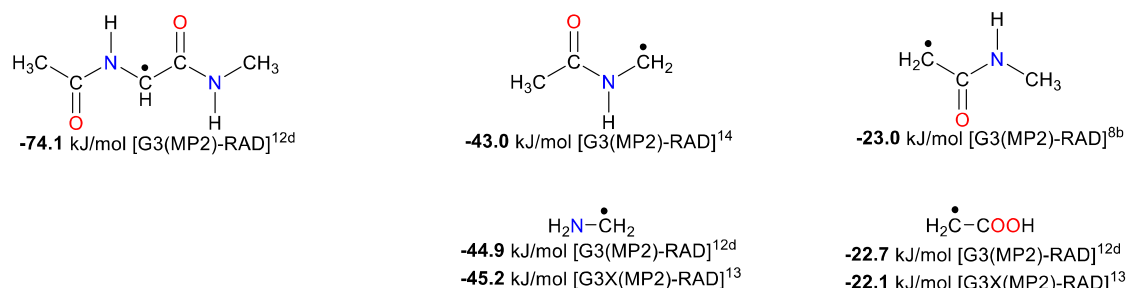


**Figure 4-6.** Previously reported RSE values ( $\Delta H_{298}$ , kJ/mol) for selected systems of interest.

The RSE value for radical  $\mathbf{r1}_{\text{NMe}}$  amounts to  $-45.7$  kJ/mol, which is close to the RSE values of  $-43.0$  kJ/mol<sup>14</sup> and  $-44.9$  kJ/mol<sup>12d</sup> for the structurally similar *N*-methyl radicals of *N*-methylacetamide [ $\bullet\text{CH}_2\text{-NH-C(=O)-CH}_3$ ] and aminomethyl radical [ $\bullet\text{CH}_2\text{-NH}_2$ ], respectively (see Figure 4-6).

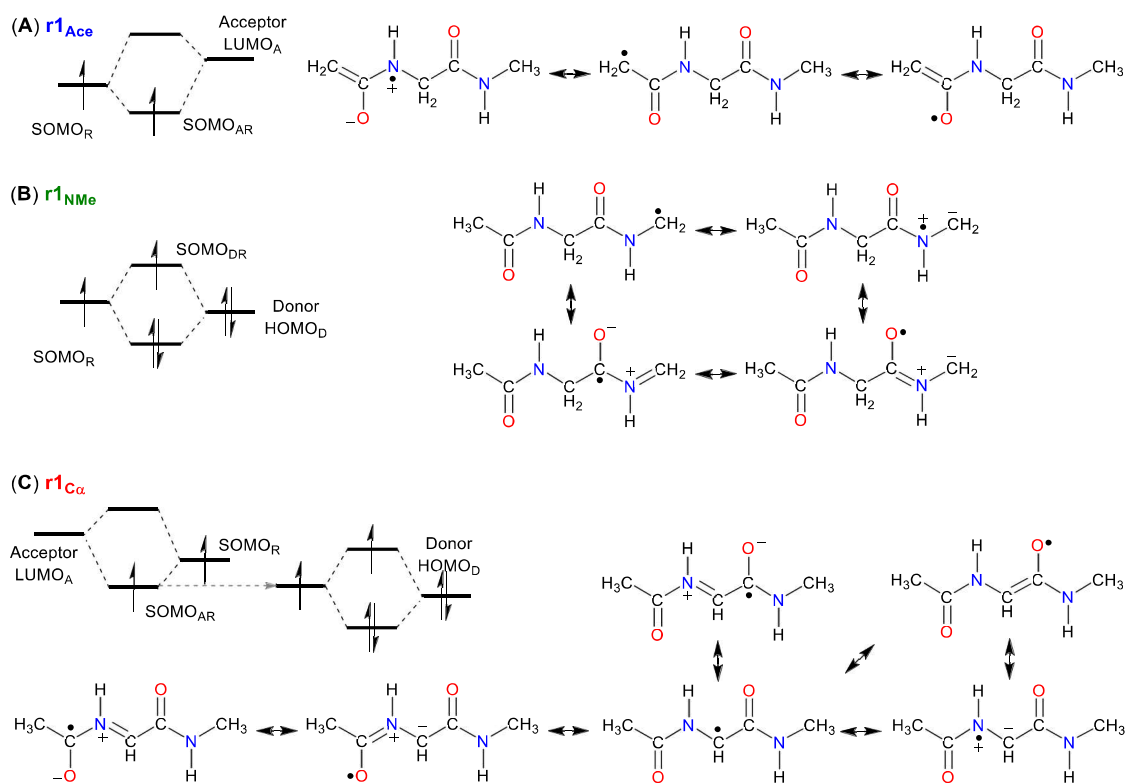


**Figure 4-7.** Orbital interaction and resonance structures for (A)  $\mathbf{r1}_{\text{Ace}}$  (B)  $\mathbf{r1}_{\text{NMe}}$  and (C)  $\mathbf{r1}_{\text{Ca}}$  radicals.

Radical  $\mathbf{r1}_{\text{NMe}}$  is more stable than methyl radical because of the presence of an adjacent lone pair donor group [ $\text{-NH-C(=O)-R}$ ]. The stabilizing effect of the lone pair donor substituent can be described by a two orbital/three electron interaction [between the radical SOMO and the lone pair HOMO], which leads to resonance-induced spin delocalization as shown in Figure 4-7(B). The nitrogen of the amide donor group [ $\text{-NH-C(=O)-R}$ ] destabilizes the radical centre by an electron-withdrawing inductive effect due to its higher electronegativity compared to carbon, but this destabilizing effect is outweighed by its stabilizing lone pair donor ability. Radical  $\mathbf{r1}_{\text{NMe}}$  is more

stable than  $\mathbf{r1}_{Ace}$  because the function of the lone pair donor substituent  $[-NH-C(=O)-R]$  in the former is more effective for spin delocalization. In  $\mathbf{r1}_{NMe}$  spin delocalization involves four centres compared to three in  $\mathbf{r1}_{Ace}$  [see resonance structures in Figure 4-7(A and B)]. Radical  $\mathbf{r1}_{C\alpha}$  is substituted by both electron donor and -acceptor groups. The total additive stabilizing effect of both groups is  $-69.0$  kJ/mol [ $RSE(\mathbf{r1}_{NMe}) = -45.7$  kJ/mol +  $RSE(\mathbf{r1}_{Ace}) = -23.3$  kJ/mol]. However, the  $RSE(\mathbf{r1}_{C\alpha}) = -74.1$  kJ/mol, that is  $5.1$  kJ/mol more than the additive value. This indicates that  $\pi$ -donor and -acceptor groups have a synergetic interaction. This synergetic behaviour is sometimes referred to as “*captodative effect*”. In FMO theory, orbitals interact more effectively as the energy difference between them decreases. We can understand the captodative effect in  $\mathbf{r1}_{C\alpha}$  using a stepwise perturbation approach, where interaction between radical  $SOMO_R$  and acceptor  $LUMO_A$  result into a  $SOMO_N$  that is lower in energy than  $SOMO_R$ . The energy difference between  $SOMO_{AR}$  and donor  $HOMO_D$  is lower than a difference of the later with the unperturbed  $SOMO_R$  and this leads to better stabilization by a donor substituent for disubstituted  $\mathbf{r1}_{C\alpha}$  as compare to  $\mathbf{r1}_{NMe}$ , where the  $HOMO_D$  interacts with the unperturbed  $SOMO_R$  (see Figure 4-7C). A similar argument can be framed for first analysing the  $SOMO_R$  and  $HOMO_D$  interaction that leads to a higher energy  $SOMO_{DR}$  [see orbital interaction in  $\mathbf{r1}_{NMe}$  Figure 4-7(B), the energy of new  $SOMO_{DR}$  is higher than  $SOMO_R$ ]. Now, the energy difference between  $SOMO_{DR}$  and  $LUMO_A$  is lower, and that leads to stronger stabilizing interaction. Thus, when a carbon radical is substituted by both  $\pi$ -donor and -acceptor groups then this results into extra stabilization as compare to monosubstituted radicals.

#### 4.2.3.2 Thermodynamics of HAT from **1** to $CumO\bullet$

The experimental investigation described in the next section for HAT from glycine dipeptide **1** is conducted using  $CumO\bullet$  as the hydrogen atom acceptor. The thermodynamics of HAT processes from different C-H bonds of **1** to  $CumO\bullet$  can be described using reaction equations that are similar as those shown in Figure 4-3 and Figure 4-4, except now the reference system has been changed from  $CH_4/\bullet CH_3$  to  $CumOH/CumO\bullet$ . The thermodynamic preference for a HAT from different sites of **1** is shown in Figure 4-8. The order of stability for the resultant radicals is  $\mathbf{r1}_{C\alpha} > \mathbf{r1}_{NMe} > \mathbf{r1}_{Ace}$  as expected, identical to the order indicated by RSE. The reaction energies for  $CumO\bullet$  are higher than those for  $\bullet CH_3$  because the former is less stable by  $12.0$  kJ/mol and  $9.0$  kJ/mol in terms of enthalpy and free energy, respectively.

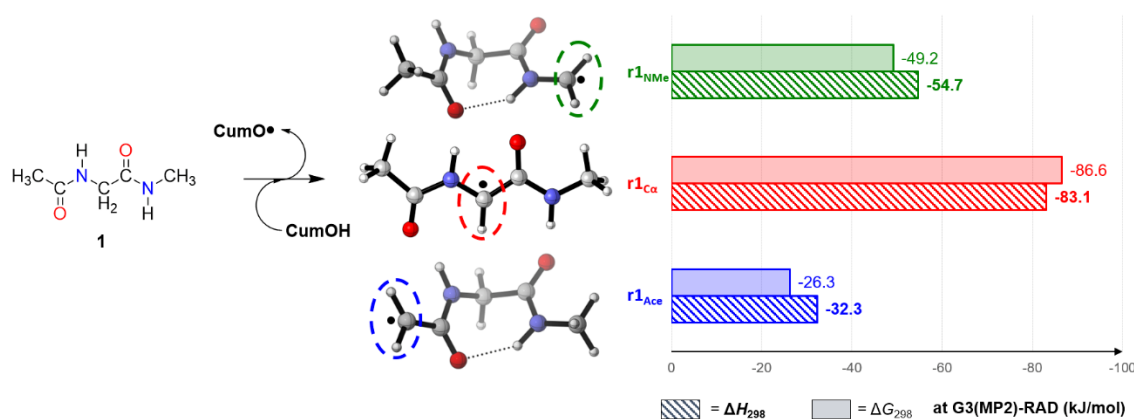


**Figure 4-8.** The best conformer-based gas phase reaction energies (kJ/mol) for a HAT to  $CumO\bullet$  from different carbon centres of **1** (that result in the formation of  $\mathbf{r1}_{Ace}$ ,  $\mathbf{r1}_{C\alpha}$ , and  $\mathbf{r1}_{NMe}$  radicals) calculated at G3(MP2)-RAD level of theory.

#### 4.2.4 Reaction Rates for HAT Processes

Bietti et al. recently measured the absolute rate constant for HAT from Boc-(*tert*-butyloxycarbonyl)-protected amino acids to  $CumO\bullet$  radical using laser flash photolysis.<sup>15, 4a</sup> The  $C\alpha$ -H was found to be the most reactive for a HAT to  $CumO\bullet$  for most of the amino acids. Here, we have studied the reaction of the cumyloxyl radical ( $CumO\bullet$ ) with *N*-methylacetamide (NMA),

glycine dipeptide (**1**) and alanine dipeptide (**2**). All the kinetic were performed in argon-saturated acetonitrile and DMSO solutions of dicumyl peroxide at  $25 \pm 0.5$  °C under magnetic stirring by following the visible absorption (490 nm) of **CumO•** radical. We have used a 10 mM concentration of dicumyl peroxide when employing 266 nm laser flash photolysis (LFP) for **CumO•** radical generation and a 1.0 M concentration when employing 355 nm LFP. In the kinetics experiments, the substrate concentration has been varied between 0.1 and 2.0 M depending on the reactivity towards **CumO•** radical. The observed rate constants ( $k_{obs}$ ) were derived following the decay of **CumO•** at different concentrations of substrate. A linear correlation is obtained between  $k_{obs}$  and the substrate concentration. The second-order rate constants for HAT to **CumO•** ( $k_H$ ) were obtained from the slope of this linear relationship (Figure 4-9).

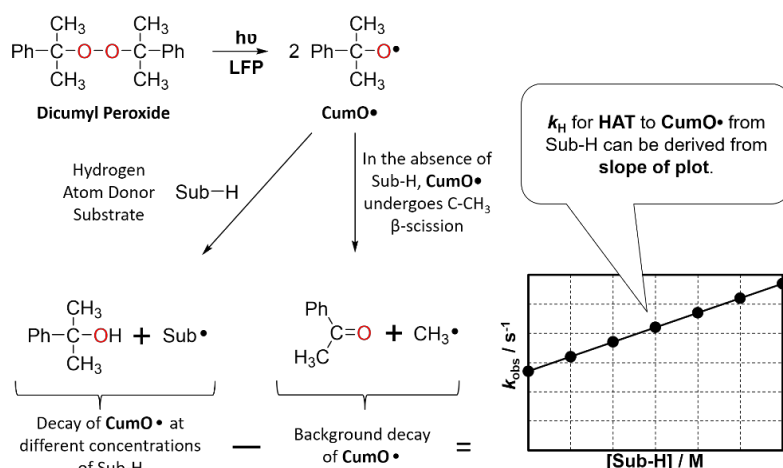


**Figure 4-9.** Procedural depiction of kinetic investigations to obtain the second-order rate constant ( $k_H$ ) for HAT reaction between **CumO•** and the substrate (**Sub-H**) under investigation using laser flash photolysis (LFP).

In DMSO, the measured second-order rate constants ( $k_H$ ) for the **CumO•** radical with **1** and **2** are  $2.9 \times 10^5$  and  $3.2 \times 10^5 \text{ M}^{-1}\text{s}^{-1}$  respectively (Figure 4-10). The measured  $k_H$  value of **1** is very close to the previously studied **Boc-Gly-OH** [ $k_H = (2.8 \pm 0.1) \times 10^5 \text{ M}^{-1}\text{s}^{-1}$ , DMSO]<sup>4a</sup> toward HAT with **CumO•**. The measured  $k_H$  values for **1** and **2** indicate that HAT predominantly occurs from the C-H bonds of the *N*-methylamide group that represents the most activated (or least deactivated) site for reaction with the electrophilic **CumO•**. This observation is supported by the similar values of  $k_H$  for both **1** and **2**, as in case of **Boc-Gly-OH** and **Boc-Ala-OH**, Salamone et al. found a 1.4–2-fold increase in  $k_H$  for **Boc-Gly-OH** as compare to **Boc-Ala-OH** (Figure 4-10).<sup>4a</sup> The similarity of the  $k_H$  values measured (in MeCN) for a HAT from *N*-methylacetamide (**NMA**) to **CumO•** ( $k_H = 3.2 \times 10^5 \text{ M}^{-1}\text{s}^{-1}$ ) with  $k_H$  values of **1** and **2** (in DMSO) further support the conclusion that hydrogen atom abstraction occurs mainly from the *N*-methylamide group in **1** and **2**, although it is important to note that the measurements are in different solvents and that makes the direct less reliable. Alternatively, the  $k_H$  values (in MeCN) are very similar for **NMA** and **Boc-Gly-OH**. Similarly, The  $k_H$  values (in DMSO) are similar for **Boc-Gly-OH** and **1**. It is also possible that C-H bonds at *N*-methylamide and C<sub>α</sub> have comparable reactivity for HAT to the **CumO•** radical.

Preferred Site	NMA	Boc-Gly-OH <sup>4a</sup>	Boc-Ala-OH <sup>4a</sup>	<b>1</b>	<b>2</b>
$k_H$ ( $\text{M}^{-1}\text{s}^{-1}$ )	$3.2 \times 10^5$ (MeCN)	$4.0 \times 10^5$ (MeCN) $5.5 \times 10^5$ ( $\text{CH}_2\text{Cl}_2$ ) $2.8 \times 10^5$ (DMSO)	$2.8 \times 10^5$ (MeCN) $2.7 \times 10^5$ ( $\text{CH}_2\text{Cl}_2$ )	$2.9 \times 10^5$ (DMSO)	$3.2 \times 10^5$ (DMSO)

**Figure 4-10.** Second-order rate constants ( $k_H$ ) for the reaction of **CumO•** with **NMA**, **Boc-Gly-OH**, **Boc-Ala-OH**, **1** and **2**.

Predominant hydrogen atom abstraction from the *N*-methyl group of **1** by **CumO•** instead of the weaker  $C_{\alpha}$ -H bonds is contrary to the thermodynamic preference reflected by the RSE values mentioned previously, and the resulting radical  $r1_{NMe}$  is less stable than radical  $r1_{C\alpha}$ . Previous reports by Watts and Easton on protonated  $[NH_3^+-CH_2-C(=O)-OH]$  and *N*-acetylated  $[CH_3-C(=O)-NH-CH_2-C(=O)-OH]$  AAs highlight the peculiar reaction profiles of their side chain C-H bonds (instead of the weaker  $C_{\alpha}$ -H bond) towards radical hydrogen abstraction by  $Cl\bullet$  and  $\bullet OH$ .<sup>2c</sup> Later studies explained this behaviour as a combined manifestation of several factors.<sup>16</sup> First, by kinetic deactivation of  $C_{\alpha}$ -H bonds through steric effects caused by the presence of adjacent carboxyl, protonated amino and acetamido groups that repel the attacking electronegative chlorine- and oxygen-based radicals. This causes a general kinetic deactivation of  $C_{\alpha}$ -H bonds towards radical reactions. Second, these electron withdrawing substituents deactivate the  $C_{\alpha}$ -H bonds electronically and slow down reaction with electrophilic radicals such as  $Cl\bullet$  and  $\bullet OH$  through “polar effects”.<sup>17</sup> The third important factor is the occurrence of comparatively early transition states, which implies that the thermodynamic preference for captodative stabilization in radical  $r1_{C\alpha}$  is not much reflected in the reaction barrier. Although these studies employed different AA models, their findings are highly relevant to the current system under investigation. In order to understand the contrathermodynamic behaviour of HAT between **CumO•** and **1**, we studied the potential energy surface (PES) for this process. Figure 4-11 depicts the key results of this exercise in terms of gas and solution phase free energies ( $\Delta G$ ). It is important to mention that the formation of reactant complexes (RC) is unfavourable entropically and thus plays no important role in determining the reaction barrier for HAT from **1** to **CumO•**. The barriers reported here are thus in reference to the isolated reactants **1** and **CumO•**.

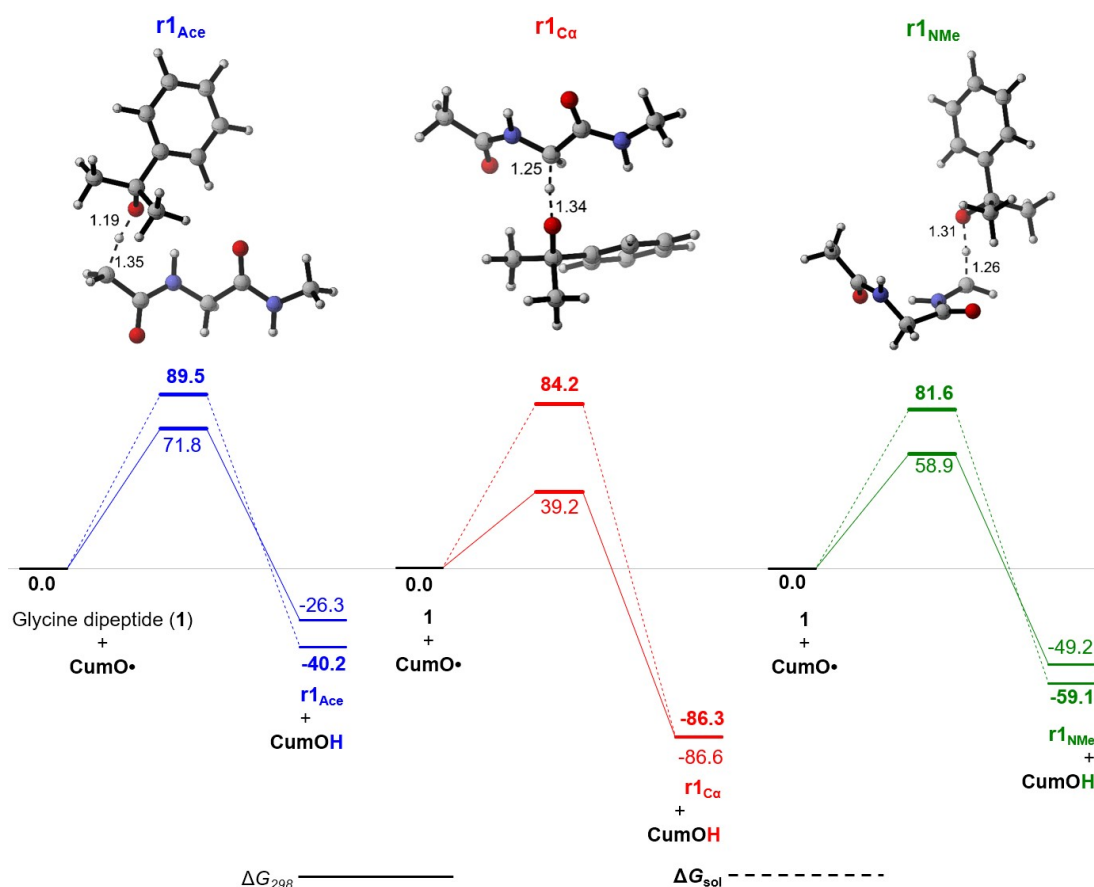


**Figure 4-11.** Gas ( $\Delta G_{298}$ ) and solution phase ( $\Delta G_{sol}$ ) free energy surfaces (in kJ/mol) for hydrogen abstraction reaction from different carbon centres of **1** by **CumO•** calculated at G3(MP2)-RAD level of theory. Solvation energies are obtained at the PCM(acetonitrile)/HF/6-31G(d)/(U)B3LYP/6-31G(d) level of theory. Distances are given in Å.

Gas phase free energy barriers ( $\Delta G_{298}$ ) for hydrogen atom abstraction correlate well with the exergonicity of the reactions (Figure 4-11). Hydrogen abstraction from N-terminal methyl is least exergonic (-26.3 kJ/mol) and has the highest barrier of +71.8 kJ/mol, followed by HAT from the C-terminal methyl group with a reaction free energy of -49.2 kJ/mol and a barrier of +58.9 kJ/mol. The hydrogen abstraction from the C(alpha) position has the lowest reaction barrier and is also most exergonic (Figure 4-11) that is also reflected by the RSE values (Figure 4-8) discussed in the previous section. Again, these gas phase reaction barriers indicate that the C $\alpha$ -H bond in **1** is the weakest C-H bond in the system and should thus be the preferred site for hydrogen abstraction by **CumO•**. This finding is contrary to the interpretation of currently available experimental reaction rates, where the C-terminal methyl group is assumed to be more reactive towards **CumO•**. In a case like ours, where the electrophilic **CumO•** radical abstracts hydrogen from aliphatic C-H bonds of **1**, the transition state (TS) is expected to be polar in nature. It is generally expected that the polarity of the medium has a significant influence on such a polar TS.<sup>18, 4b</sup> Solvation effects may be particularly relevant for our system (**1**) as the three sites of interest have different substitution patterns that may result in different polar effects in the TSs. Most of the experimental data that we have are calculated for reaction in acetonitrile and DMSO solutions. So, to estimate the effects of solvation in a polar organic medium, the gas phase free energy surfaces for hydrogen atom transfer have been corrected by single point solvation energy calculations at the PCM(acetonitrile)/HF/6-31G(d)//(U)B3LYP/6-31G(d) level of theory. The solution phase free energy surfaces ( $\Delta G_{sol}$ ) show that the polar aprotic solvent acetonitrile as described by the polarizable continuum model (PCM) destabilizes all transition states relative to the corresponding isolated reactants and products (Figure 4-11). The solvation-induced destabilization effect is largest for the TS for hydrogen abstraction from carbon alpha (+45 kJ/mol), where the barrier in solution ( $\Delta G_{sol}$ ) increases to 84.2 kJ/mol from 39.2 kJ/mol in the gas phase ( $\Delta G_{298}$ ). More importantly, hydrogen abstraction from the C-terminal methyl group is predicted to face the lowest free energy barrier of +81.6 kJ/mol in acetonitrile solution. This trend in solution phase barriers agrees well with the experimental observation that the C-terminal methyl group **1** is the preferential site of attack by **CumO•** for hydrogen abstraction.

#### 4.2.5 Conclusions

The results obtained in this investigation to understand the reactivity pattern for HAT from aliphatic carbons of glycine dipeptide **1** to cumyloxy radical **CumO•** shows the following. The C-H bonds of the N-terminal acetyl group, due to the presence of an electron withdrawing substituent, are deactivated for hydrogen abstraction by **CumO•**. The reaction path for this process is the least exergonic and has the highest reaction barrier in both gas and solution phase. The hydrogen atom abstraction from carbon alpha is the most exergonic in glycine dipeptide **1**, because of the generation of captodatively stabilized radical **r1Ca•**. This position is also the most favourable for hydrogen abstraction in terms of gas phase reaction barriers. Perhaps the most important conclusion so far is that the neighbouring lone pair donor-activated C-H bonds at the C-terminal methyl group has the lowest solution phase free energy barrier for radical hydrogen abstraction by **CumO•** among all C-H bonds in glycine dipeptide **1**. The polarity of the medium thus plays a crucial role in such a polar HAT processes.

#### 4.2.6 Outlook

Going further, we will investigate the reaction of glycine dipeptide **1** with di-tert-butylhyponitrite (**t-BuON=NOBu-t**), which can generate alkoxy radicals (**t-BuO•**) under mild conditions. Investigation includes synthesis of initial compounds: radical source **t-BuON=NOBu-t**, glycine dipeptide **1** and possible products of the reaction. Figure 4-12 depicted the calculated classical

deuterium kinetic isotope effects (KIE) on the reaction barrier for hydrogen abstraction reaction from different carbon centres of **1** by the **CumO•** radical calculated at G3(MP2)-RAD level.

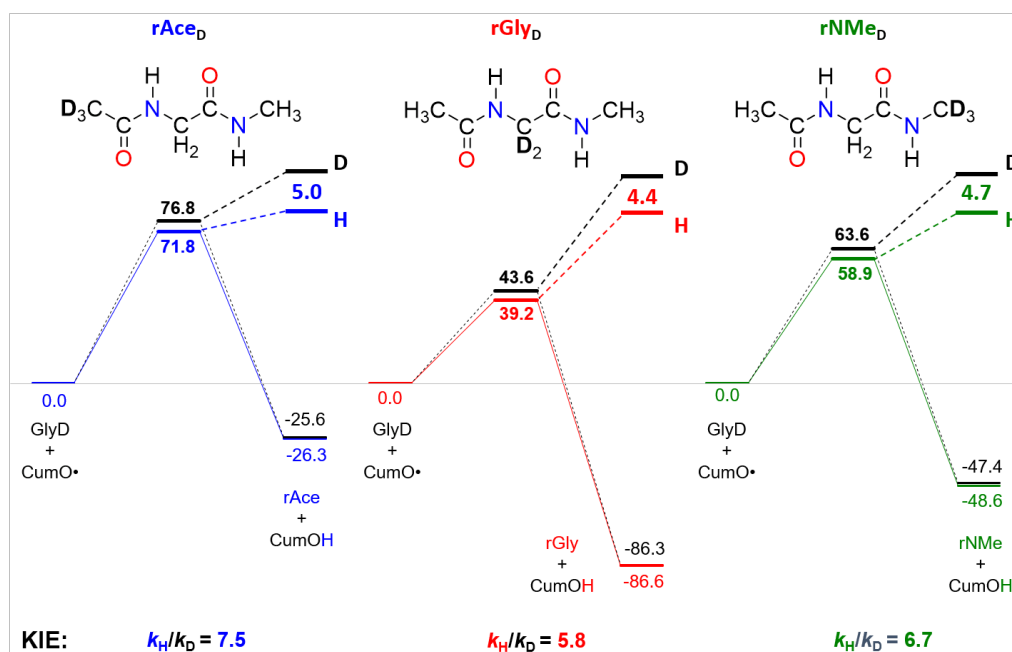


**Figure 4-12.** Classical deuterium kinetic isotope effects (KIE) on gas phase free energy surfaces ( $\Delta G_{298}$ , in kJ/mol) for hydrogen abstraction reaction from different carbon centres of **1** by **CumO•** calculated at G3(MP2)-RAD level.

The calculated KIE for **1** indicate a that its deuterated analogues react 5.5-7.5 times slower. The synthesis of site-specific isotopically labelled analogues of glycine dipeptide **1** is planned to exploit the KIE for investigating HAT reaction from glycine dipeptide **1** to the *t*-BuO• radical. To see the HAT dependence, the kinetics of the reactions will be measured in various solvents and different conditions (temperature, concentration).

#### 4.2.7 References

- (1) (a) Frey, P. A.; Hegeman, A. D.; Reed, G. H., *Chem. Rev.* **2006**, *106*, 3302-3316. (b) Hawkins, C. L.; Morgan, P. E.; Davies, M. J., *Free Radical Biol. Med.* **2009**, *46*, 965-988. (c) Frey, P. A., *Acc. Chem. Res.* **2013**, *47*, 540-549. (d) Halliwell, B.; Gutteridge, J. M., *Free Radicals in Biology and Medicine*. Oxford University Press, USA: **2015**.
- (2) (a) Easton, C. J., *Chem. Rev.* **1997**, *97*, 53-82. (b) Hawkins, C. L.; Davies, M. J., *Biochim. Biophys. Acta, Bioenerg.* **2001**, *1504*, 196-219. (c) Watts, Z. I.; Easton, C. J., *J. Am. Chem. Soc.* **2009**, *131*, 11323-11325. (d) Scheiner, S.; Kar, T., *J. Am. Chem. Soc.* **2010**, *132*, 16450-16459. (e) Chan, B.; Karton, A.; Easton, C. J.; Radom, L., *J. Chem. Theory Comput.* **2016**, *12*, 1606-1613. (f) Chan, B.; Easton, C. J.; Radom, L., *J. Phys. Chem. A* **2018**, *122*, 1741-1746.
- (3) (a) Burgess, V.; Easton, C.; Hay, M.; Steel, P., *Aust. J. Chem.* **1988**, *41*, 701-710. (b) Burgess, V. A.; Easton, C. J.; Hay, M. P., *J. Am. Chem. Soc.* **1989**, *111*, 1047-1052.
- (4) (a) Salamone, M.; Basili, F.; Bietti, M., *J. Org. Chem.* **2015**, *80*, 3643-3650. (b) Salamone, M.; Bietti, M., *Acc. Chem. Res.* **2015**, *48*, 2895-2903. (c) Pipitone, L. M.; Carboni, G.; Sorrentino, D.; Galeotti, M.; Salamone, M.; Bietti, M., *Org. Lett.* **2018**, *20*, 808-811.
- (5) Hioe, J.; Zipse, H., *Org. Biomol. Chem.* **2010**, *8*, 3609-3617.
- (6) (a) Jangra, H.; Haindl, M. H.; Achraimer, F.; Hioe, J.; Gschwind, R. M.; Zipse, H., *Chem. Eur. J.* **2016**, *22*, 13328-13335. (b) Jangra, H.; Zipse, H., *J. Phys. Chem. B* **2018**, *122*, 8880-8890.
- (7) (a) Hariharan, P. C.; Pople, J. A., *Theor. Chim. Acta* **1973**, *28*, 213-222. (b) Becke, A. D., *J. Chem. Phys.* **1993**, *98*, 5648-5652.

- (8) (a) Henry, D. J.; Parkinson, C. J.; Radom, L., *J. Phys. Chem. A* **2002**, *106*, 7927-7936. (b) Henry, D. J.; Sullivan, M. B.; Radom, L., *J. Chem. Phys.* **2003**, *118*, 4849-4860.
- (9) Miertuš, S.; Scrocco, E.; Tomasi, J., *Chem. Phys.* **1981**, *55*, 117-129.
- (10) *Schrödinger Release 2015–2: MacroModel Version 10.8*, Schrödinger, LLC, New York, NY, USA 2015.
- (11) Frisch, M. J. T., G. W.; Schlegel, H. B.; Scuseria, G. E.; Robb, M. A.; Cheeseman, J. R.; Scalmani, G.; Barone, V.; Mennucci, B.; Petersson, G. A.; Nakatsuji, H.; Caricato, M.; Li, X.; Hratchian, H. P.; Izmaylov, A. F.; Bloino, J.; Zheng, G.; Sonnenberg, J. L.; Hada, M.; Ehara, M.; Toyota, K.; Fukuda, R.; Hasegawa, J.; Ishida, M.; Nakajima, T.; Honda, Y.; Kitao, O.; Nakai, H.; Vreven, T.; Montgomery, Jr., J. A.; Peralta, J. E.; Ogliaro, F.; Bearpark, M.; Heyd, J. J.; Brothers, E.; Kudin, K. N.; Staroverov, V. N.; Keith, T.; Kobayashi, R.; Normand, J.; Raghavachari, K.; Rendell, A.; Burant, J. C.; Iyengar, S. S.; Tomasi, J.; Cossi, M.; Rega, N.; Millam, J. M.; Klene, M.; Knox, J. E.; Cross, J. B.; Bakken, V.; Adamo, C.; Jaramillo, J.; Gomperts, R.; Stratmann, R. E.; Yazyev, O.; Austin, A. J.; Cammi, R.; Pomelli, C.; Ochterski, J. W.; Martin, R. L.; Morokuma, K.; Zakrzewski, V. G.; Voth, G. A.; Salvador, P.; Dannenberg, J. J.; Dapprich, S.; Daniels, A. D.; Farkas, O.; Foresman, J. B.; Ortiz, J. V.; Cioslowski, J.; Fox, D. J.; *Gaussian 09 Revision D. 01*, Gaussian, Inc., Wallingford CT: **2013**.
- (12) (a) Coote, M. L.; Lin, C. Y.; Zipse, H., *The stability of carbon-centered radicals*. Wiley: Hoboken, NJ: **2010**. (b) Hioe, J.; Zipse, H., *Faraday Discuss.* **2010**, *145*, 301-313. (c) References. (d) Hioe, J.; Zipse, H., Radical Stability—Thermochemical Aspects. In *Encyclopedia of Radicals in Chemistry, Biology and Materials*, Chrysosostomos, C.; Armido, S., Eds. John Wiley & Sons Ltd: Chichester, UK, 2012; pp 449-476. (e) Hioe, J.; Mosch, M.; Smith, D. M.; Zipse, H., *RSC Adv.* **2013**, *3*, 12403-12408.
- (13) Menon, A. S.; Henry, D. J.; Bally, T.; Radom, L., *Org. Biomol. Chem.* **2011**, *9*, 3636-3657.
- (14) Henry, D. J.; Parkinson, C. J.; Radom, L., *J. Phys. Chem. A* **2002**, *106*, 7927-7936.
- (15) Salamone, M.; Milan, M.; DiLabio, G. A.; Bietti, M., *J. Org. Chem.* **2014**, *79*, 7179-7184.
- (16) (a) Taylor, M. S.; Ivanic, S. A.; Wood, G. P.; Easton, C. J.; Bacskey, G. B.; Radom, L., *J. Phys. Chem. A* **2009**, *113*, 11817-11832. (b) O'Reilly, R. J.; Chan, B.; Taylor, M. S.; Ivanic, S.; Bacskey, G. B.; Easton, C. J.; Radom, L., *J. Am. Chem. Soc.* **2011**, *133*, 16553-16559.
- (17) (a) Giese, B.; He, J.; Mehl, W., *Chem. Ber.* **1988**, *121*, 2063-2066. (b) Roberts, B., *Chem. Soc. Rev.* **1999**, *28*, 25-35.
- (18) (a) Mitroka, S.; Zimmeck, S.; Troya, D.; Tanko, J. M., *J. Am. Chem. Soc.* **2010**, *132*, 2907-2913. (b) Bietti, M.; Salamone, M.; DiLabio, G. A.; Jockusch, S.; Turro, N. J., *J. Org. Chem.* **2012**, *77*, 1267-1272.

### 4.3 Supporting Information

For: Stability of Peptide Radicals: Thermodynamics vs. Kinetics

#### 4.3.1 Conformational Preferences

**Table S4-1.** List of minima for glycine dipeptide (**1, Gly**) and its radicals [**r1<sub>Ace</sub> (rAce)**, **r1<sub>C $\alpha$</sub>  (rGly)** and **r1<sub>NMe</sub> (rNMe)**] obtained from geometry optimization at (U)B3LYP/6-31G(d) level of theory in the gas phase using systematic conformational search.

SI	Molecule	(U)B3LYP\6-31G(d)									G3(MP2)-RAD		
		$\Phi$	$\Psi$	$\omega_1$	$\omega_2$	$C_\alpha$	Peptide	$\Delta E$	$\Delta H_{298}$	$\Delta G_{298}$	$\Delta E$	$\Delta H_{298}$	$\Delta G_{298}$
<b>Glycine dipeptide (1)</b>													
1	Gly_0_30_180_180	82	291	173	183	C7	tt	0.0	0.0	4.8	0.0	0.0	2.7
2	GlyD_C5_CSSym <sup>1</sup>	180	180	180	180	C5	tt	3.5	2.0	0.1	5.7	4.2	0.1
3	Gly_20_160_180_180	180	180	180	180	C5	tt	3.5	2.0	0.0	5.7	4.2	0.0
4	Gly_0_40_180_180	123	338	188	176	$\beta_2$	tt	10.9	10.1	12.7	12.3	11.5	11.9
5	Gly_0_160_180_0	180	180	180	4	C5	tc	11.4	9.8	10.1	12.2	10.7	8.8
6	Gly_20_40_0_180	94	2	6	182	$\alpha R$	ct	19.0	17.9	22.5	17.5	16.5	18.8
7	Gly_50_0_180_0	94	243	164	1	C7	tc	20.0	20.1	23.6	19.5	19.6	20.9
8	Gly_180_90_0_180	180	180	360	180	C5	ct	22.8	20.7	21.8	25.7	23.7	22.7
9	Gly_20_180_0_180	75	152	349	178	$\beta$	ct	27.5	26.2	30.4	28.2	26.9	29.0
10	Gly_180_130_0_0	180	180	360	3	C5	cc	30.9	28.5	31.0	32.7	30.3	30.7
11	Gly_40_170_0_0	71	170	347	3	$\beta$	cc	38.7	37.0	42.0	37.8	36.2	39.0
12	Gly_20_60_0_0	77	71	358	6	$\alpha R$	cc	41.9	40.9	46.2	40.0	39.0	42.1
13	Gly_20_40_180_0	70	43	186	4	$\alpha R$	tc	44.4	42.7	43.9	40.4	38.8	37.8
14	Gly_180_60_0_0	197	64	350	356	$\beta_2$	cc	45.2	44.2	48.5	43.4	42.5	44.6
15	Gly_170_20_0_0	208	64	351	4	$\beta_2$	cc	45.7	44.5	47.8	42.7	41.6	42.7
<b>r1<sub>C<math>\alpha</math></sub> (rGly)</b>													
1	rGlyD_C5_CSSym <sup>1</sup>	180	180	180	180	C5	tt	0.0	0.1	2.8	0.0	0.1	2.8
2	rGly_170_110_180_180	180	180	180	180	C5	tt	0.0	0.0	0.0	0.0	0.0	0.0
3	rGly_110_160_180_0	180	179	180	357	C5	tc	7.7	7.9	8.9	5.9	6.1	7.2
4	rGly_160_120_0_180	180	180	360	180	C5	ct	11.3	10.7	17.1	10.8	10.3	16.7
5	rGly_160_90_0_0	180	179	0	356	C5	cc	18.7	18.3	24.9	16.7	16.3	22.9
6	rGly_170_20_180_180	184	15	176	216	$\beta_2$	tt	31.5	31.2	38.8	27.1	26.8	34.4
7	rGly_40_0_180_180	5	1	181	174	$\alpha R$	tt	31.6	32.1	36.5	30.9	31.4	35.8
8	rGly_130_0_0_180	174	346	2	147	$\beta_2$	ct	32.8	32.4	41.2	27.9	27.5	36.3
9	rGly_40_180_0_180	38	186	9	183	$\beta$	ct	43.1	42.3	48.6	39.7	38.9	45.2
10	rGly_120_10_180_0	180	343	183	355	$\beta_2$	tc	45.1	45.5	53.7	41.1	41.5	49.7
11	rGly_140_50_0_0	181	18	358	4	$\beta_2$	cc	47.9	48.2	57.8	43.1	43.4	53.0
12	rGly_30_20_0_180	56	12	14	202	$\alpha R$	ct	53.6	52.3	60.2	45.8	44.5	52.4
13	rGly_20_170_180_180	42	196	195	197	$\beta$	tt	59.4	57.4	62.9	49.7	47.7	53.2
14	rGly_20_150_180_0	42	197	195	357	$\beta$	tc	68.5	66.5	71.2	59.1	57.2	61.9
15	rGly_0_40_0_0	41	25	13	356	$\alpha R$	cc	69.8	69.1	78.0	60.4	59.8	68.7
16	rGly_20_50_180_0	21	46	190	9	$\alpha R$	tc	72.9	71.9	78.5	62.6	61.6	68.2
<b>r1<sub>Ace</sub> (rAce)</b>													
1	rAce_0_180_180_180	278	68	189	177	C7	tt	0.0	0.0	0.0	0.0	0.0	0.0
2	rAce_0_40_180_180	124	339	191	177	$\beta_2$	tt	11.3	10.4	7.5	11.8	11.0	8.1
3	rAce_10_90_0_180	90	10	9	181	$\alpha R$	ct	19.1	18.4	16.3	16.6	16.0	13.8
4	rAce_50_0_180_0	91	240	160	0	$\beta$	uc	20.3	20.5	20.0	19.1	19.3	18.8
5	rAce_130_140_0_180	181	180	0	180	C5	ct	23.6	21.6	13.5	26.0	24.1	16.0
6	rAce_180_130_0_0	180	180	360	3	C5	cc	31.5	29.5	25.0	32.9	30.9	26.4
7	rAce_20_180_0_180	70	153	347	178	$\beta$	ct	31.6	30.4	25.3	31.4	30.2	25.1
8	rAce_20_60_0_0	79	68	7	6	$\alpha R$	cc	39.7	39.2	38.6	37.4	37.0	36.4
9	rAce_40_170_0_0	66	174	345	5	$\beta$	cc	42.2	40.6	37.1	40.2	38.7	35.2
10	rAce_20_40_180_0	70	42	189	4	$\alpha R$	tc	44.6	42.8	39.7	39.6	37.9	34.8
11	rAce_180_60_0_0	187	62	348	355	$\beta_2$	cc	46.4	45.7	42.6	44.9	44.3	41.1
12	rAce_170_20_0_0	206	63	350	4	$\beta_2$	cc	47.3	46.3	40.7	44.4	43.4	37.8

<b>r1<sub>NMe</sub> (rNMe)</b>													
1	rNMe_0_0_180_180	279	67	187	178	C7	tt	0.0	0.0	0.4	0.0	0.0	0.0
2	rNMe_180_180_180_180	180	180	180	180	C5	tt	9.7	8.0	0.0	10.6	8.9	0.6
3	rNMe_0_160_180_0	180	180	180	360	C5	tc	11.6	10.0	0.2	13.1	11.6	1.5
4	rNMe_0_40_180_180	125	334	190	180	$\beta$ 2	tt	14.5	13.7	9.0	15.4	14.6	9.5
5	rNMe_50_0_180_0	116	280	179	1	C7	tc	20.7	20.9	18.8	21.2	21.4	19.0
6	rNMe_20_40_0_180	97	3	8	181	$\alpha$ R	ct	23.1	22.0	21.1	21.1	20.0	18.7
7	rNMe_130_140_0_180	180	180	0	180	C5	ct	29.5	27.2	21.6	31.2	28.9	23.0
8	rNMe_180_130_0_0	180	180	360	359	C5	cc	30.6	28.4	24.2	33.0	30.9	26.2
9	rNMe_0_180_0_180	77	144	349	179	$\beta$	ct	33.0	31.8	30.0	33.1	31.9	29.7
10	rNMe_40_170_0_0	71	173	348	2	$\beta$	cc	36.8	35.5	35.1	36.7	35.5	34.7
11	rNMe_20_60_0_0	78	75	352	3	$\alpha$ R	cc	41.1	40.6	41.0	41.1	40.6	40.6
12	rNMe_20_40_180_0	62	47	189	3	$\alpha$ R	tc	42.0	41.0	35.1	40.2	39.3	32.9
13	rNMe_180_0_0_0	160	294	9	2	$\beta$ 2	cc	44.4	43.8	42.9	44.3	43.7	42.4

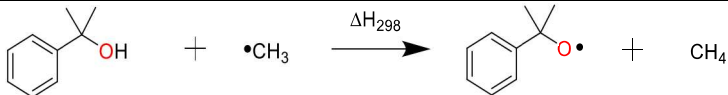
<sup>†</sup>\* C5 conformation with CS framework group.

### 4.3.2 Thermodynamic Stability

**Table S4-2.** RSE values (in kJ/mol) for radicals **r1<sub>Ace</sub>**, **r1<sub>Ca</sub>**, and **r1<sub>NMe</sub>** calculated at different levels of theory using equations defined in Figure 4-3 and Figure 4-4 (CH<sub>4</sub>/•CH<sub>3</sub> reference system).

	<b>r1<sub>Ace</sub></b>			<b>r1<sub>Ca</sub></b>			<b>r1<sub>NMe</sub></b>		
	$\Delta E$	$\Delta H_{298}$	$\Delta G_{298}$	$\Delta E$	$\Delta H_{298}$	$\Delta G_{298}$	$\Delta E$	$\Delta H_{298}$	$\Delta G_{298}$
(U)B3LYP/6-31G(d)									
Best Conf.	-39.8	-37.3	-23.4	-105.2	-101.3	-96.9	-58.7	-56.9	-43.9
Bolz. Avg.	-41.0	-38.2	-23.5	-106.3	-102.1	-96.6	-59.7	-57.5	-44.1
G3(MP2)-RAD									
Best Conf.	-25.7	<b>-23.3</b>	<b>-14.3</b>	-77.9	<b>-74.1</b>	<b>-74.6</b>	-47.4	<b>-45.7</b>	<b>-37.2</b>
Bolz. Avg.	-26.7	-24.4	-14.5	-78.7	-75.0	-74.2	-48.3	-46.6	-37.1

**Table S4-3.** Reaction energies (in kJ/mol) for HAT between **CumOH** and •CH<sub>3</sub> calculated at different levels of theory.

									
	(U)B3LYP/6-31G(d)			G3(MP2)-RAD					
	$\Delta E$	$\Delta H_{298}$	$\Delta G_{298}$	$\Delta E$	$\Delta H_{298}$	$\Delta G_{298}$			
Best Conf.	-43.9	-39.4	-33.7	4.7	9.0	12.0			

**Table S4-4.** Reaction energies (kJ/mol) for a HAT to **CumO•** from different carbon centres of **1** (that result in the formation of **r1<sub>Ace</sub>**, **r1<sub>Ca</sub>**, and **r1<sub>NMe</sub>** radicals) calculated at different levels of theory.

	<b>r1<sub>Ace</sub></b>			<b>r1<sub>Ca</sub></b>			<b>r1<sub>NMe</sub></b>		
	$\Delta E$	$\Delta H_{298}$	$\Delta G_{298}$	$\Delta E$	$\Delta H_{298}$	$\Delta G_{298}$	$\Delta E$	$\Delta H_{298}$	$\Delta G_{298}$
(U)B3LYP/6-31G(d)									
Best Conf.	4.1	2.1	10.3	-61.4	-61.9	-63.2	-14.9	-17.6	-10.2
Bolz. Avg.	2.9	1.1	10.2	-62.4	-62.8	-62.9	-15.8	-18.2	-10.4
G3(MP2)-RAD									
Best Conf.	-30.4	-32.3	-26.3	-82.6	-83.1	-86.6	-52.1	-54.7	-49.2
Bolz. Avg.	-31.4	-33.4	-26.5	-83.3	-84.0	-86.2	-53.0	-55.6	-49.2

### 4.3.3 Potential Energy Surface

**Table S4-5.** Transition state (TS), reactant complex (RC) and product complex (PC) energies ( $\Delta H$ , kJ/mol) relative to separate reactants for hydrogen abstraction reaction from different carbon centres of **1** by **CumO•** obtained at different levels of theory.

System Filename	(U)B3LYP/6-31G(d), $\Delta H_{298}$			G3(MP2)-RAD, $\Delta H_{298}$			G3(MP2)-RAD + PCM, $\Delta H_{sol}$		
	RC	TS	PC	RC	TS	PC	RC	TS	PC
<b>r1<sub>Ace</sub> (rAce)</b>									
ace_1	-33.6	33.8	-24.4	-	14.3	-	-	45.7	-
ace_co_ts_3	-33.6	35.4	-45.0	-39.7	21.6	-84.6	16.9	35.1	-41.2
ace_co_ts_9	-33.6	33.7	-30.1	-39.7	20.2	-74.6	16.9	48.8	-46.1
Isolated Product			2.1			-32.3			-58.3
<b>r1<sub>Ca</sub> (rGly)</b>									
ca_co_ts_7	-22.9	-5.5	-79.0	-35.3	-12.8	-116.2	-2.1	28.0	-82.7
Isolated Product			-61.9			-83.1			-94.9
<b>r1<sub>NMe</sub> (rNMe)</b>									
nme_14	-15.8	16.8	-37.5	-18.4	8.9	-86.3	6.2	27.3	-55.1
nme_19	-33.6	17.0	-40.1	-	-4.7	-	-	32.9	-
Isolated Product			-17.6			-54.7			-78.5

**Table S4-6.** Transition state (TS), reactant complex (RC), product complex (PC) and isolated products (IP) energies ( $\Delta G$ , kJ/mol) for hydrogen abstraction reaction from different carbon centres of **1** by **CumO•** obtained at different levels of theory.

System Filename	(U)B3LYP/6-31G(d), $\Delta G_{298}$			G3(MP2)-RAD, $\Delta G_{298}$			G3(MP2)-RAD + PCM, $\Delta G_{sol}$		
	RC	TS	PC	RC	TS	PC	RC	TS	PC
<b>r1<sub>Ace</sub> (rAce)</b>									
ace_1	18.9	95.7	28.5		73.7			109.3	
ace_co_ts_3	18.8	88.0	10.1	10.3	71.8	-31.9	71.2	89.5	15.7
ace_co_ts_9	18.9	89.0	21.8	10.4	73.0	-25.1	71.2	105.8	7.7
Isolated Product			10.3			-26.3			-48.1
<b>ca_co_ts_7</b>									
ca_co_ts_7	21.0	48.8	-38.7	6.2	39.2	-78.4	43.5	84.2	-40.7
Isolated Product			-63.2			-86.6			-94.2
<b>nme_14</b>									
nme_14	36.5	69.3	11.0	31.6	58.9	-40.3	60.3	81.6	-4.9
nme_19	18.9	83.2	18.3		59.1			100.9	
Isolated Product			-10.2			-49.2			-77.2



## **Chapter 5. Unique Stereoselective Homolytic C-O Bond Activation in Diketopiperazine-Derived Alkoxyamines by Adjacent Amide Pyramidalization**

Tynchtyk Amatov, Harish Jangra, Radek Pohl, Ivana Cisarova, Hendrik Zipse and Ullrich Jahn

*Chem. Eur. J.* **2018**, *24*, 15336-15345.

---

### ***Authors contribution***

T.A. and U.J. conceived the project. Experimental work was designed by T.A. and U.J and carried out by T.A. with the help of R.P., who assisted with the  $^1\text{H}$  NMR measurements and data analysis. The X-ray crystallography was conducted by I.C. Computational research strategy was designed by H.Z. and H.J., and performed by H.J. The manuscript was jointly written by T.A., H.J., H. Z. and U. J.

### ***Copyright***

This research was originally published in the *Chemistry – A European Journal* and is reprinted here as the 5<sup>th</sup> chapter of this thesis from *Chem. Eur. J.* **2018**, 24, 15336-15345 © 2018 Wiley-VCH Verlag GmbH & Co. KGaA, Weinheim.

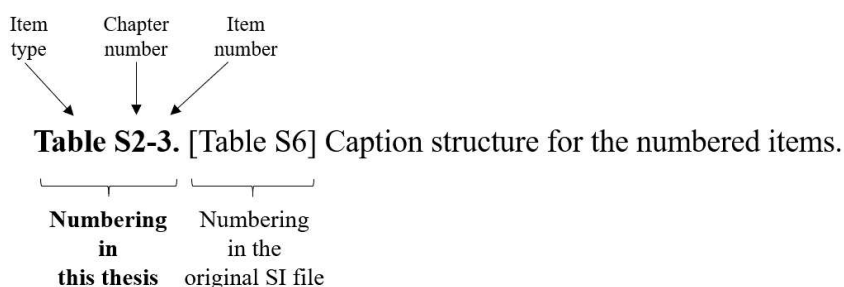
(Link to article: <https://onlinelibrary.wiley.com/doi/full/10.1002/chem.201803284>)

Selected supporting material for the computational part of this work is provided at the end of this chapter. For complete supporting information (SI), please follow the link below:

[https://onlinelibrary.wiley.com/action/downloadSupplement?doi=10.1002%2Fchem.201601828&file=chem201601828-sup-0001-misc\\_information.pdf](https://onlinelibrary.wiley.com/action/downloadSupplement?doi=10.1002%2Fchem.201601828&file=chem201601828-sup-0001-misc_information.pdf)

### ***Additional information***

The accompanying SI is the shorter and altered version of the original content. The items (Tables, Figure, Schemes etc.) may have a different number than what was originally assigned. To make it easier to locate the SI content referred to in the following reprint, the original numbering is also provided in the caption of the numbered items as described below:



## Isomerization | Very Important Paper |

## VIP Unique Stereoselective Homolytic C–O Bond Activation in Diketopiperazine-Derived Alkoxyamines by Adjacent Amide Pyramidalization

Tynchtyk Amatov,<sup>[a, b]</sup> Harish Jangra,<sup>[b]</sup> Radek Pohl,<sup>[a]</sup> Ivana Cisařová,<sup>[c]</sup> Hendrik Zipse,<sup>\*,[b]</sup> and Ullrich Jahn<sup>\*,[a]</sup>

**Abstract:** Simple monocyclic diketopiperazine (DKP)-derived alkoxyamines exhibit unprecedented activation of a remote C–O bond for homolysis by amide distortion. The combination of strain-release-driven amide planarization and the persistent radical effect (PRE) enables a unique, irreversible, and quantitative *trans*→*cis* isomerization under much milder conditions than typically observed for such homolysis-limited reactions. This isomerization is shown to be general and independent of the steric and electronic nature of both the amino acid side chains and the substituents at the DKP nitrogen atoms. Homolysis rate constants are determined, and they significantly differ for both the labile *trans* diastereomers and the stable *cis* diastereomers. To reveal the factors

influencing this unusual process, structural features of the kinetic *trans* diastereomers and thermodynamic *cis* diastereomers are investigated in the solid state and in solution. X-ray crystallographic analysis and computational studies indicate substantial distortion of the amide bond from planarity in the *trans*-alkoxyamines, and this is believed to be the cause for the facile and quantitative isomerization. Thus, these amino-acid-derived alkoxyamines are the first examples that exhibit a large thermodynamic preference for one diastereomer over the other upon thermal homolysis, and this allows controlled switching of configurations and configurational cycling.

## Introduction

The amide bond is one of the best-studied linkages because of its profound implications on the structure and functions of biomolecules as well as organo- and biocatalysts.<sup>[1]</sup> A strong  $n_N \rightarrow \pi^*_{C=O}$  interaction, which is responsible for its planar nature, and hydrogen-bonding abilities are central to making the amide unit a powerful conformation-controlling element.<sup>[2,3]</sup> Deviation from the planar geometry greatly alters both the physical and chemical properties of amide-containing molecules.<sup>[4,5]</sup> Lukeš proposed the structures of a bridgehead-nitrogen-bearing lactam, 2-quinolidone, and its one-carbon

shorter homologue<sup>[6]</sup> as early as 1938 and pointed out the disruption of the amide resonance in such twisted amides for the first time because of violation of Bredt's rule.<sup>[7]</sup> Since then, the chemistry of distorted amides, mostly incorporated into medium-sized bridged lactam architectures, has captured the imagination of chemists.<sup>[8]</sup> The unambiguous synthesis of 2-quinolidonium tetrafluoroborate by Stoltz et al.<sup>[9,10]</sup> was a landmark achievement more than 68 years after Lukeš's publication.<sup>[11]</sup> Significant weakening of the N–C(O) bond is the most important consequence of amide nitrogen pyramidalization. The  $\beta$ -lactam antibiotic penicillin is a prime example of a distorted amide, making it the warhead against harmful bacteria and saving countless human lives.<sup>[12]</sup> Very recently, considerable interest in applications of nonplanar amides **I**, which are not part of bridged lactam motifs,<sup>[13]</sup> in transition-metal-catalyzed N–C(O) bond activation by oxidative addition and coupling via acylmetal species **II** has emerged; its facility is a result of ground-state destabilization of the distorted amide bond (Figure 1).<sup>[14–16]</sup> This strategy can also be diverted to the decarbonylation of acylmetal species and subsequent cross-coupling, thus formally activating the C–C(O) bond as a consequence of N–C(O) insertion.<sup>[17]</sup> Amide bond pyramidalization may also affect the strength of adjacent bonds. Scattered examples document C–N  $\sigma$  bond-cleavage reactions in twisted amides of types **V** and **VI** under reductive, oxidative, and alkylative conditions, as reported by the Aube<sup>[18,19]</sup> and Szostak<sup>[20,21]</sup> groups. The  $pK_a$  of the  $\alpha$ C–H bond to the carbonyl group is

[a] Dr. T. Amatov, Dr. R. Pohl, Dr. U. Jahn  
Institute of Organic Chemistry and Biochemistry  
Academy of Sciences of the Czech Republic  
Flemingovo náměstí 2, 16610 Prague (Czech Republic)  
E-mail: ullrich.jahn@uochb.cas.cz

[b] Dr. T. Amatov, H. Jangra, Prof. Dr. H. Zipse  
Ludwig Maximilian University, Department of Chemistry  
Butenandstrasse 5–13, 81377 München (Germany)  
E-mail: zipse@cup.uni-muenchen.de

[c] Dr. I. Cisařová  
Department of Inorganic Chemistry, Faculty of Science,  
Charles University in Prague  
Hlavova 2030/8, 12843 Prague (Czech Republic)

Supporting Information and the ORCID identification number(s) for the author(s) of this article can be found under:  
<https://doi.org/10.1002/chem.201803284>

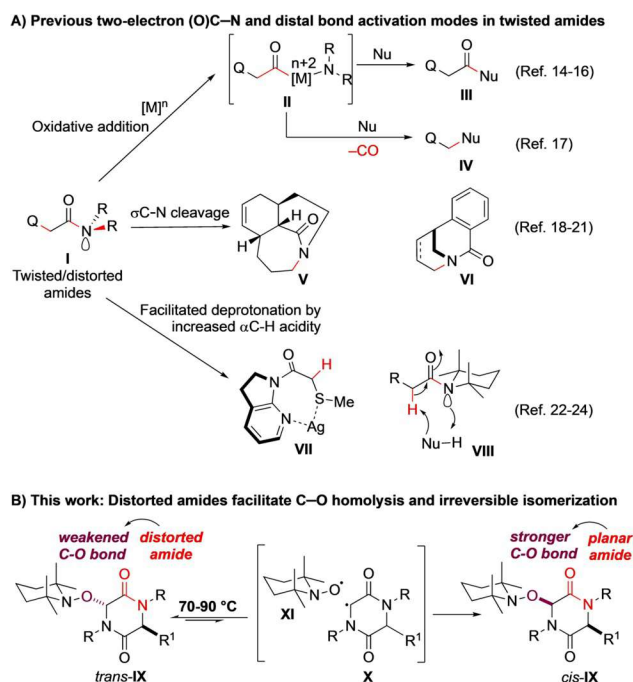


**Figure 1.** a) Known examples of amide-twisting-mediated bond-activation modes. b) Proposed selective homolytic cleavage of an adjacent C–O bond controlled by amide-bond distortion.

dramatically lowered, and as a result of amide nitrogen pyramidalization in **VII**, its use in aldol additions is enabled.<sup>[22,23]</sup> Similar effects were observed by Lloyd-Jones and Booker-Milburn in sterically hindered amides such as **VIII**,<sup>[24]</sup> which undergo rapid proton switch via a twisted conformer because of their enhanced  $\alpha$ C–H acidity.

The strain associated with disrupting the geometry of the amide bond should, in principle, also have significant implications for the strengths of C–Q bonds other than C–H bonds in **I** and enable their activation. This has so far widely been neglected; no studies exist. However, this principle may lay out new avenues for the design of catalytic and thermal reactions for the selective functionalization of amide-containing natural products and feedstock materials. We recently introduced alkoxyamines **IX** as diketopiperazine (DKP)-radical surrogates and applied them in the synthesis of diverse bridged DKP motifs that are present in numerous biologically active alkaloids.<sup>[25–27]</sup> This transformation is controlled by the persistent radical effect (PRE),<sup>[28–31]</sup> a powerful principle that governs the selective radical coupling between transient and persistent radical species **X** and **XI**. The homolysis of alkoxyamines is a well-appreciated phenomenon that is applied in nitroxide-mediated polymerization (NMP),<sup>[32–34]</sup> tin-free radical transformations,<sup>[35]</sup> and in materials research, which is a testament to the power of PRE. However, the vast majority of these transformations require temperatures beyond 100 °C to proceed, which prohibits their application under milder conditions. Thus, enormous interest exists in designing more labile alkoxyamines,<sup>[36]</sup> the homolysis of which can be triggered by external stimuli under controlled conditions.<sup>[37,38]</sup> Such labile alkoxyamines have been suggested as novel theranostic agents, applying transient and highly reactive alkyl radicals to irreversibly

damaging unhealthy cells and using the simultaneously formed persistent nitroxide radicals as diagnostic tools.<sup>[39,40]</sup> For such biological applications, the structures of alkoxyamines should play an important role; ideally they should be biocompatible and assist binding to desired biological targets, a feature that is not given in current compounds of this type. Given that DKPs constitute a large class of biologically active medicinally privileged scaffolds,<sup>[41–43]</sup> we hypothesized that a combination of amino-acid-derived DKPs with nitroxides may prove attractive for potential biomedical applications as theranostic agents.

Herein we report that *trans*-substituted diketopiperazine-derived alkoxyamines *trans*-**IX** are indeed a step on the way to this goal, as homolysis surprisingly starts at temperatures as low as 70 °C for tertiary alkoxyamines and even below room temperature for quaternary alkoxyamines. Preparative, structural, and computational studies demonstrate that deviation of the amide bonds from planarity is the cause for the significant weakening of the adjacent C–O bond. This effect can be used as a steering element for configurational switching to *cis*-**IX** by a radical mechanism.

## Results

### Preparative *trans*→*cis* isomerization reactions

During a temperature screening to find optimum conditions for PRE-mediated cyclization reactions, a *trans*–*cis* isomerization of DKP alkoxyamines was discovered. Heating a 5:1 *trans*/*cis* mixture of **1**<sup>[44]</sup> in *t*BuOH at 80 °C for 2 h provided pure *cis*-**1**, the spectral data of which matched the minor component in the original mixture (Figure 2A). Both isomers of **1** were individually crystallized, and their configurations were confirmed by X-ray crystallography (Figure 3). Similarly, an inseparable 11:1 *trans*-**2**/*cis*-**2** mixture with a benzyl group converged into pure *cis*-**2**. Enantiomerically pure tryptophan-derived DKP *trans*-**3**, bearing *N*-Me groups, also isomerized cleanly into the *cis* isomer upon heating without compromising the residing stereocenter. It is noteworthy that the isomerization proceeded quantitatively regardless of the steric features of the nitrogen substituents.

Hybridization and steric bulk of the C-substituent also did not influence the direction of the isomerization, as a 1:1 *trans*/*cis* mixture of aliphatic L-leucine-derived alkoxyamine **4** cleanly and quantitatively isomerized on heating at 90 °C, as revealed by <sup>1</sup>H NMR spectroscopy (Figure 2B). These results show that the radical coupling during isomerization occurs with exclusive diastereoselectivity, and thus, the isomerization of diketopiperazine alkoxyamines is unidirectional toward the *cis* isomers regardless of the steric and electronic features of the nitrogen and carbon substituents.

### Solid-state and solution structures of *trans*- and *cis*-DKP alkoxyamines

X-ray crystallographic investigation of DKP alkoxyamines *cis*-**1**/*trans*-**1**, *cis*-**2**, *cis*-**3**/*trans*-**3**, *cis*-**4**, and *trans*-**5** unambiguously

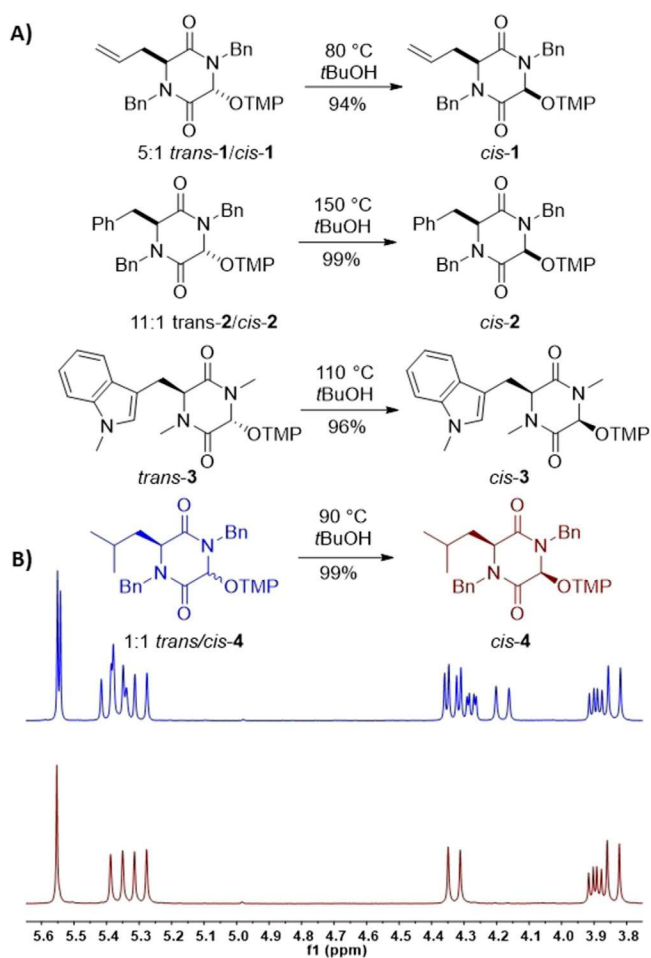


**Figure 2.** A) Thermal *trans*→*cis* isomerization of DKP-derived alkoxyamines. B) Comparison of the  $^1\text{H}$  NMR spectra of a 1:1 *trans/cis*-4 mixture before heating (blue) and after heating (maroon). TMP = 2,2,6,6-tetramethylpiperidin-1-yl.

confirmed the relative *trans* configuration of the alkyl and alkoxyamine substituents in the starting DKP alkoxyamines and their *cis* configuration in the products (Figure 3). None of the crystallographically determined structures reveals significant steric interactions of the substituents. An immediately recognizable feature in all molecular structures is that the alkoxyamine unit always occupies a pseudoaxial position in both the *trans* and *cis* diastereomers. NOE experiments for the *cis*-1/*trans*-1 and *cis*-2/*trans*-2 pairs also support a strong bias for axial orientation of the alkoxyamine unit in solution (see the Supporting information, Figure S1). The large difference in thermodynamic stability and dramatic difference in the C–ON bond strengths of the *cis* and *trans* diastereomers of alkoxyamines 1–4 should have a significant stereoelectronic origin.

It has been noted in the literature that simple alkoxyamines having a heteroatom in the  $\alpha$  position, such as  $\alpha$ -alkoxy,  $\alpha$ -ethylaminy, and  $\alpha$ -phenylsulfanyl substituents, have small homolysis rate constants ( $k_d$ ) and, consequently, high carbon–oxygen bond dissociation energies, BDE(C–ON), which, however, poorly correlate with the BDE(C–H) of the corresponding non-alkoxyamine-substituted precursors.<sup>[45–48]</sup> The common rationalization for these observations invokes the anomeric effect as the origin of unusually strong C–ON bonds in those cases, as also supported by computational studies, revealing the importance of hyperconjugative interactions between the lone pair of electrons of the oxygen atom of the alkoxyamine and the antibonding  $\sigma^*$  orbital of the neighboring  $\alpha\text{C}$ –heteroatom bond.<sup>[49]</sup>

Several features of the solid-state structures are noteworthy (Table 1). The bond lengths of the C4–OTMP unit vary over a rather small range of 0.01 Å (atom numbering of X-ray structures in Figure 3) and are somewhat shorter than those in comparable simpler cyclic  $\alpha$ -carbonyl-substituted alkoxyamines (cyclic ketones<sup>[50]</sup> 1.454 Å, esters<sup>[51]</sup> 1.435 Å) but are longer than those of  $\alpha$ -amino-substituted alkoxyamines. Surprisingly, the

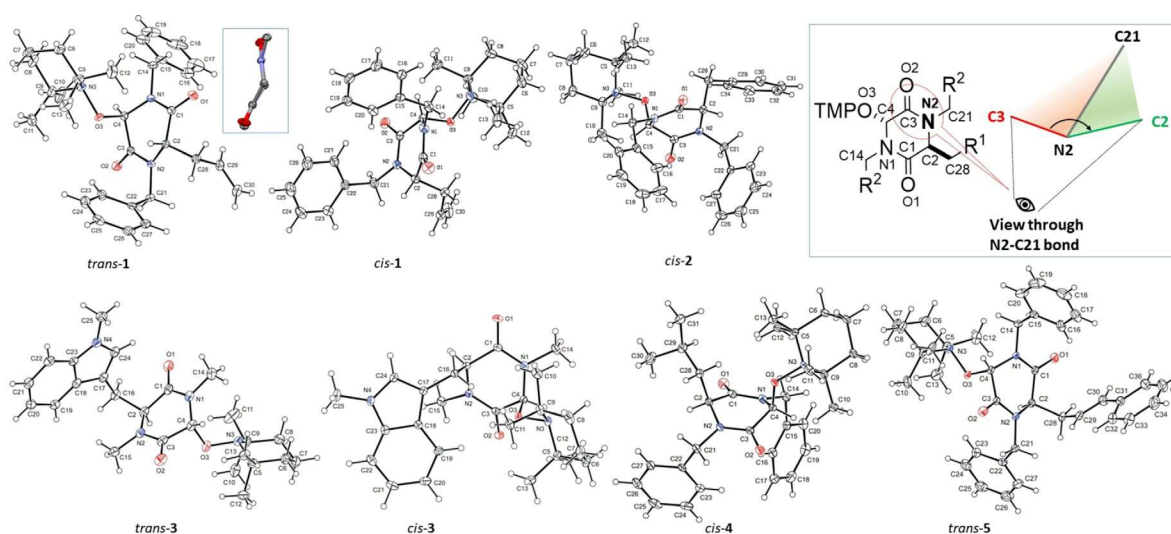


**Figure 3.** X-ray structures of alkoxyamines *cis/trans*-1, *cis*-2, *cis/trans*-3, *cis*-4, and *trans*-5. The insets show the Newman projection of the DKP core along the N2–C(O) and N1–C(O) bonds for *trans*-1, the common numbering scheme of the DKP skeleton, and the definition of the important C3–N2–C21–C2 dihedral angle. For *trans*-5, R<sup>1</sup> = *trans*-CH=CHPh, R<sup>2</sup> = Ph.

Parameter	<i>trans</i> -1	<i>cis</i> -1	<i>cis</i> -2	<i>trans</i> -3	<i>cis</i> -3	<i>cis</i> -4	<i>trans</i> -5
$d(\text{C4}-\text{OTMP}) [\text{\AA}]$	1.436	1.429	1.428	1.429	1.433	1.426	1.429
$d(\text{C3}-\text{N2}) [\text{\AA}]$	1.355	1.341	1.344	1.344	1.340	1.345	1.351
$d(\text{C1}-\text{N1}) [\text{\AA}]$	1.351	1.354	1.355	1.354	1.352	1.363	1.350
dihedral angle C3–N2–C21–C2 [°]	157.9	178.3	171.9	165.0	177.0	178.1	165.0
dihedral angle C1–N1–C14–C4 [°]	169.0	174.7	179.2	174.4	174.9	178.2	170.9
sum of angles at N2 (at N1) [°]	356 (359)	360 (360)	360 (360)	358 (360)	360 (360)	360 (360)	358 (359)
twist angle ( $\tau$ ) at N2 (at N1) [°]	9.1 (0.5)	2.7 (8.2)	3.0 (10.1)	3.3 (7.4)	1.8 (1.6)	3.4 (8.6)	9.8 (5.1)
$\chi_{\text{N2}} [^\circ]$	22.1	1.8	8.2	14.6	3.1	1.8	15.0
$\chi_{\text{N1}} [^\circ]$	11.3	5.3	0.7	5.5	5.1	1.8	9.2

C3–N2 distance varies and is, except for *trans*-3, longer than in the corresponding *cis* isomers, whereas the C1–N1 bond lengths do not differ very much in both isomers.

The C3–N2–C21–C2 dihedral angles of the *trans*-DKP units, as visualized in Figure 3, surprisingly show with 157–165° a strong deviation from planarity, whereas the same dihedral angles amount to 172–178° in the corresponding *cis* isomers. At the same time, the dihedral angles involving the N1 atom also deviate, but not that strongly. Notable twisting of the N2–C(O) amide bond is also observed in *trans*-1 and *trans*-5 with twist angles of  $\tau = 9.1$  and  $9.8^\circ$ , respectively. The twist angles go in opposite directions for both nitrogen atoms, in that they are larger at N2 in the *trans* isomers but are larger at N1 in the *cis* isomers, except for *cis*-3.

Pyramidalization of the N2 atom is significant, as determined by calculation of the classical Winkler–Dunitz distortion parameters  $\chi_{\text{N2}}$  and  $\chi_{\text{N1}}$ .<sup>[52]</sup> In all characterized *trans*-alkoxyamines, significant pyramidalization of N2 with  $\chi_{\text{N2}} = 14.6$ – $22.1^\circ$  is found, and N1 is also distorted, though less strongly with  $\chi_{\text{N1}} = 5.5$ – $11.3^\circ$ . In contrast, deviation from planarity of both amide nitrogen atoms is small in the *cis* isomers, except for *cis*-2. These data collectively demonstrate significant amide-bond twisting and pyramidalization in all *trans*-alkoxyamine diastereomers, whereas the distortion is much less marked in all *cis* isomers.

### Computational study of the structural effects in alkoxyamines 1

The relative importance of the anomeric effect and amide pyramidalization for the observed reactivity of DKP-derived alkoxyamines *cis*-1 and *trans*-1 was first evaluated by optimizing their structures at the B3LYP/6-31G(d) level of theory and comparing them with the X-ray crystallographic results, which are in good agreement (see Figure S7). Subsequently, the magnitude of these interactions was quantified by using natural bond orbital (NBO) analysis at the B3LYP/6-31G(d) level of theory (Figures 4 and S21, Table S3). Indeed, the lone pair of electrons of the alkoxyamine oxygen atom interacts favorably with the neighboring C–N, C–C, and C–H bonds, confirming the presence of an anomeric effect.

However, the cumulative energies for these interactions as well as their individual components are essentially identical for both isomers ( $-75 \text{ kJ mol}^{-1}$  for *cis*-1 vs.  $-74 \text{ kJ mol}^{-1}$  for *trans*-

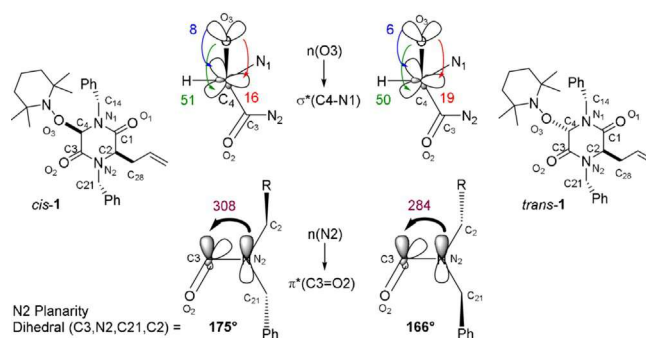


**Figure 4.** Important hyperconjugation interactions [ $\text{kJ mol}^{-1}$ ] (NBO) in *cis*-1 and *trans*-1 calculated at the B3LYP/6-31G(d) level of theory.

1), which implies that the stability difference between the *trans* and *cis* diastereomers must have other origins than the anomeric effect. The strongest donor–acceptor interactions in these systems concern the C3/N2 amide resonance interaction, which amounts to  $308 \text{ kJ mol}^{-1}$  in *cis*-1 but to only  $284 \text{ kJ mol}^{-1}$  in *trans*-1. This difference is accompanied by larger differences in amide bond planarity in these two stereoisomers, for which the calculated (O)C3–N2–C21–C2 dihedral angles amount to  $166^\circ$  in *trans*-1 and  $175^\circ$  in *cis*-1. These values differ somewhat from the experimentally obtained values of  $157.9$  and  $178.3^\circ$ , respectively, but show the trend very well.

### Kinetics of isomerization, reductive radical quenching, and cyclization of alkoxyamines 1 and 2

With solid structural information at hand, DKP alkoxyamines 1 and 2 were studied with respect to their potential for radical generation under mild conditions by determination of their homolysis, reduction, and cyclization kinetics.

The homolysis rate constants ( $k_d$ ) of the *trans* and *cis* diastereomers of alkoxyamines 1 and 2 were found to be dramatically different. The isomerization of *trans*-1 was monitored by  $^1\text{H}$  NMR spectroscopy at four different temperatures, and the experimental data fit to first-order kinetics (Figure 5A,B). Homolysis of *trans*-1 was reasonably fast and is rate determining, as no observable cyclization took place compared to the formation of *cis*-1 upon heating in the  $75$ – $85^\circ\text{C}$  temperature range, which allowed determination of its kinetics (Table 2,

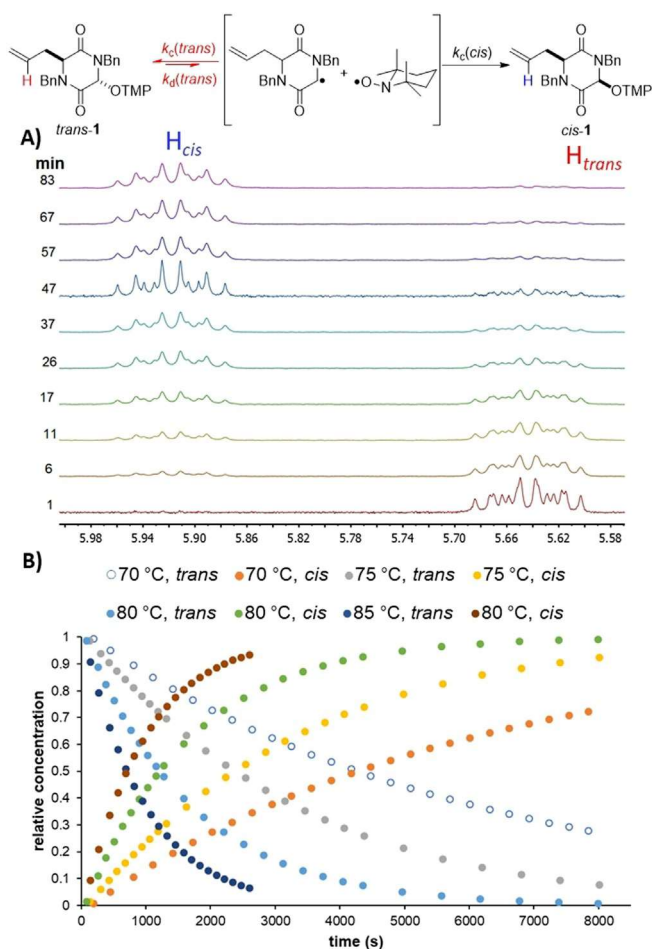


Figure 5. A) A typical  $^1\text{H}$  NMR spectrum of the vinylic proton region at  $80^\circ\text{C}$ . B) Kinetic traces for the isomerization of *trans*-1 between  $70$  and  $85^\circ\text{C}$ .

Table 2. Kinetic data for the thermal isomerization of <i>trans</i> -1 and <i>trans</i> -2.			
<i>trans</i> -1			
$T$ [K]	$k_d$ [ $10^{-4} \text{ s}^{-1}$ ]	$t_{1/2}$ [min]	$\Delta G^\ddagger$ [ $\text{kJ mol}^{-1}$ ]
343.15	1.6	72	109.3
348.15	3.3	35	109.0
353.15	6.1	19	108.8
358.15	11	11	108.5
$A^{[a]}$ [ $\text{s}^{-1}$ ]	$E_a$ [ $\text{kJ mol}^{-1}$ ]	$\Delta H^\ddagger$ [ $\text{kJ mol}^{-1}$ ]	$\Delta S^\ddagger$ [ $\text{J K}^{-1} \text{ mol}^{-1}$ ]
$13.5 \times 10^{15}$	131	128	54
<i>trans</i> -2			
$T$ [K]	$k_d$ [ $10^{-4} \text{ s}^{-1}$ ]	$t_{1/2}$ [min]	$\Delta G^\ddagger$ [ $\text{kJ mol}^{-1}$ ]
343.15	2.9	40	107.7
353.15	10	11	107.2
358.15	19	6	106.9
$A^{[a]}$ [ $\text{s}^{-1}$ ]	$E_a$ [ $\text{kJ mol}^{-1}$ ]	$\Delta H^\ddagger$ [ $\text{kJ mol}^{-1}$ ]	$\Delta S^\ddagger$ [ $\text{J K}^{-1} \text{ mol}^{-1}$ ]
$9.83 \times 10^{15}$	128	125	52
[a] $A$ = Arrhenius factor.			

Figures 5 and S2). The activation enthalpy was determined to be  $\Delta H^\ddagger = 128 \text{ kJ mol}^{-1}$ , and the corresponding activation entro-

py was determined to be  $\Delta S^\ddagger = 54 \text{ J K}^{-1} \text{ mol}^{-1}$ ; the activation energy amounts to  $E_a = 131 \text{ kJ mol}^{-1}$  by using the Arrhenius equation.

The isomerization of *trans*-2, bearing a benzyl side chain, into *cis*-2 was similarly studied and was found to proceed approximately 1.6 times faster than isomerization of *trans*-1 (Table 2 and Figure S3). The activation enthalpy of  $\Delta H^\ddagger = 125 \text{ kJ mol}^{-1}$  and activation entropy of  $\Delta S^\ddagger = 52 \text{ J K}^{-1} \text{ mol}^{-1}$  for the overall transformation translate into an activation energy of  $E_a = 128 \text{ kJ mol}^{-1}$  (Figure S4). In the  $70$ – $85^\circ\text{C}$  temperature range, the homolysis of the *cis* diastereomers must be at least 2–3 orders of magnitude slower than or even negligible compared to the homolysis of the *trans* diastereomer, that is,  $k_{d(\text{trans})} \gg k_{d(\text{cis})}$  (see below). This allows approximation of the observed rate constants for the isomerization process to the homolysis rate constants of the *trans* diastereomers, that is,  $k_{\text{obs}} \approx k_{d(\text{trans})}$ .

These results are fully supported by a computational investigation performed at the (U)B2PLYP/G3MP2Large//((U)B3LYP/6-31G(d) level in combination with the SMD continuum model for DMSO solution (Figures 6A and S11–S13, Table S8): DKP alkoxyamine *cis*-1 is, in Gibbs free-energy terms,  $12.1 \text{ kJ mol}^{-1}$  more stable than *trans*-1 at  $298.15 \text{ K}$ . The barrier for radical pair formation amounts to  $+120.5 \text{ kJ mol}^{-1}$  for *trans*-1, whereas that for *cis*-1 is higher, as expected, with  $+126.1 \text{ kJ mol}^{-1}$ . The barrier for homolysis of *trans*-1 is slightly higher than the value of  $+109 \text{ kJ mol}^{-1}$  calculated from the experimentally determined activation parameters (Table 2).

Quaternary DKP alkoxyamines have so far remained elusive, and any attempts to isolate them have so far failed. Their formation can be inferred experimentally from successful cyclization reactions that culminate in an approach to asperparaline C.<sup>[27]</sup> To define the reasons for their instability and to draw conclusions that may lead to the design of DKP alkoxyamines that only slowly homolyze at physiological temperatures, quaternary DKP alkoxyamines *trans*-q1 and *cis*-q1 with fully substituted carbon atoms were computationally investigated (Figure 6B) and compared to the isomers of **1** (Figure 6A). On the one hand, both the stereoelectronic and thermodynamic trends are conserved, like those found for **1**. Significant pyramidalization of the N2 atom in *trans*-q1 is observed with a (O)C3–N2–C21–C2 dihedral angle amounting to  $166^\circ$  compared to  $171^\circ$  in *cis*-q1 (Figures S22–S24, Tables S4 and S6). On the other hand, coupling of the transient tertiary DKP radical with persistent 2,2,6,6-tetramethylpiperidin-1-oxyl (TEMPO) becomes endergonic for *trans*-q1, and at the same time, the activation barrier for homolysis is significantly reduced in both isomers, which thus makes DKP-derived quaternary alkoxyamines q1 extremely labile (Figures S25–S27 and Table S9). These results, however, clearly point to opportunities to design DKP alkoxyamines with a defined homolysis range, if the homolysis rate constant of at least the *cis* isomer can be decreased by increasing the strength of the C–O bond through optimizing the substitution pattern at C4.

The assumption that homolysis of the *cis* diastereomers of **1** and **2** is negligible at lower temperatures is additionally supported by a radical reduction experiment (Figure 7A). Heating

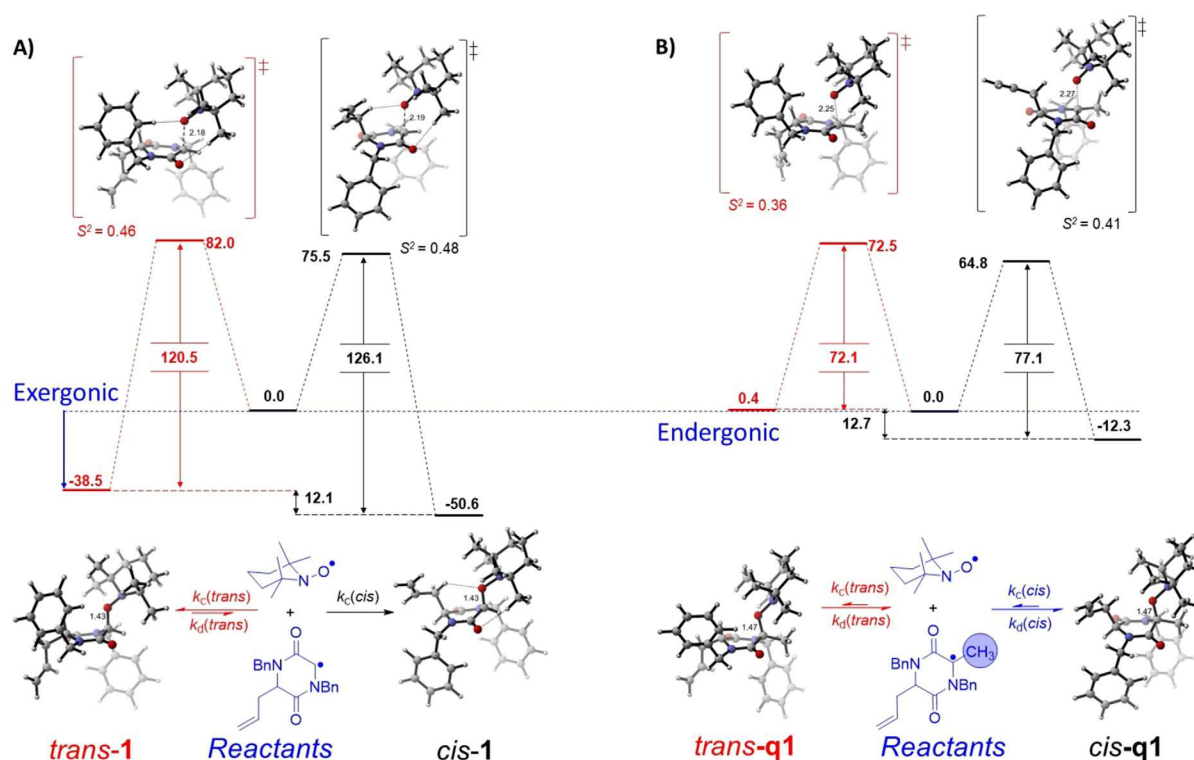


**Figure 6.** Solvation-corrected Gibbs energy ( $\Delta G_{\text{sol-sp}}$  [kJ mol<sup>-1</sup>]) profile for A) *trans*→*cis* isomerization of DKP-alkoxyamine **1** and B) its hypothetical quaternary analogue **q1**, both calculated at the (U)B2PLYP/G3MP2Large//((U)B3LYP/6-31G(d)) level of theory. Single-point solvation energies were calculated for DMSO at the SMD/(U)B3LYP/6-31G(d) level of theory.

the 11:1 *trans/cis*-2 mixture in the presence of an excess amount of thiophenol (13 equiv.) at 70 °C and monitoring by <sup>1</sup>H NMR spectroscopy showed that isomerization into *cis*-2 effectively competed with radical reduction by thiophenol. Moreover, once *trans*-2 was fully consumed, the ratio of *cis*-2 to reduced DKP red-2 was approximately 50:50, and most importantly, it remained essentially constant upon heating for another 3 h. In contrast, heating *cis*-2 with thiophenol under identical conditions, but at 110 °C, led to clean formation of fully reduced DKP red-2 (Figure 7B). Taken together, these experiments convincingly demonstrate that *cis*-2 does not undergo homolysis of the C–O bond at 70 °C.

Knowing the homolysis rate constants,  $k_{\text{isom}} \approx k_{\text{d}(\text{trans})}$ , for the *trans* isomers of **1** and **2** (see Table 2) and that isomerization does not compete upon homolysis of the *cis* isomers because of a clean pseudo-first-order reduction (Figure 7B), the  $k_{\text{d}(\text{cis})}$  values for *cis*-1 and *cis*-2 were obtained by applying the method developed by Edeleva et al.,<sup>[53]</sup> which is based on the thermolysis of alkoxyamines in the presence of an excess amount of PhSH. Clean first-order consumption of *cis*-1 and *cis*-2 took place, and the  $k_{\text{d}(\text{cis})}$  rate constants were obtained in the temperature range of 90 to 115 °C (Table 3, Figure S5). It is noteworthy that under these conditions potential cyclization reactions of both substrates were not observed, showing that the rate of reduction is orders of magnitude faster.<sup>[54–58]</sup> Comparison of these values with the homolysis rate constants for *trans*-2 (see Table 2) shows that homolysis of *cis*-2 at 90 °C is 1.5 times slower than the homolysis of *trans*-2 at 70 °C, where-

as the homolysis of *cis*-1 at 90 °C is 1.8 times slower than that of *trans*-1 at 70 °C. This confirms that the thermodynamic preference for the *cis* configuration is undoubtedly a consequence of a significant difference between the bond-dissociation energies (BDEs) of the C–O bonds of the *trans* and *cis* isomers, as was also confirmed by the computational study.

To determine the relative facility of the isomerization reaction of the isomers of **1** and potential subsequent C–C bond-formation reactions, the cyclization kinetics were determined by thermolysis of pure *cis*-1 in the absence of PhSH at 100, 110, and 115 °C and by monitoring the progress of the reaction by <sup>1</sup>H NMR spectroscopy (Figure S6). A clean first-order decay of the signals corresponding to *cis*-1 and the appearance of signals corresponding to 6-*exo-trig* cyclization products *syn/anti*-**6** and 7-*endo-trig* cyclization product **7** were observed (Figure 8A). The cyclization was slow at 100 °C and required approximately 3 h to reach completion. However, the rate of cyclization increased eightfold at 115 °C. The obtained rate constants for the first-order decay of *cis*-1 were with  $3.7 \times 10^{-4}$ ,  $1.6 \times 10^{-3}$ , and  $2.8 \times 10^{-3}$  s<sup>-1</sup> at 100, 110, and 115 °C, respectively, slightly smaller than those determined for reduction in the presence of thiophenol (see Table 3).

This indicates that the cyclization rates are in the same range as the reduction rates, and therefore, a mechanism for the overall cyclization can be derived: the reaction proceeds by slow homolysis of *cis*-1 followed by a slightly faster radical cyclization step, which is terminated by fast radical coupling of the bicyclic radical intermediates with TEMPO. This is

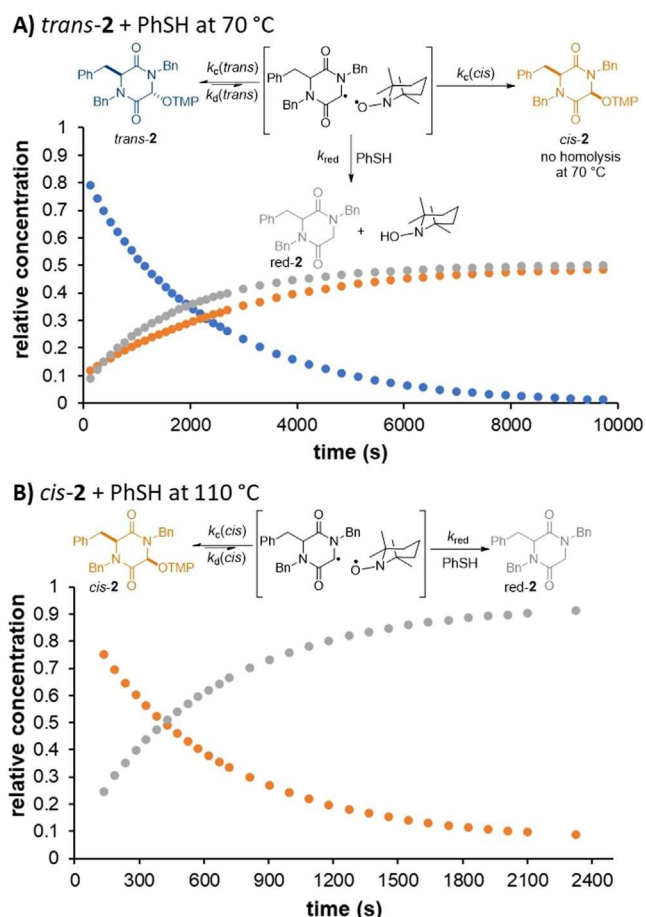


**Figure 7.** Kinetic traces for the thermolysis of *trans*-2 and *cis*-2 in the presence of an excess amount of the radical scavenger PhSH. a) Competitive fast isomerization versus hydrogen abstraction upon thermolysis of *trans*-2 with an excess amount of PhSH at 70 °C. b) Thermolysis of pure *cis*-2 in the presence of PhSH at 110 °C.

supported by calculations at the (U)B2PLYP/G3MP2Large// (U)B3LYP/6-31G(d) level in combination with the SMD continuum model for DMSO (Figures 8B and S14–S20). The Gibbs free-

**Table 3.** Kinetic data for the thermal homolysis of *cis*-1 and *cis*-2 in the presence of an excess amount of PhSH.

<i>cis</i> -1			
<i>T</i> [K]	$k_d$ [ $10^{-4} \text{ s}^{-1}$ ]	$t_{1/2}$ [min]	$\Delta G^\ddagger$ [kJ mol $^{-1}$ ]
363.15	2.8	41.1	114.2
373.15	9.7	12.0	113.7
388.15	47	2.4	113.1
$A^{[a]}$ [ $\text{s}^{-1}$ ]	$E_a$ [kJ mol $^{-1}$ ]	$\Delta H^\ddagger$ [kJ mol $^{-1}$ ]	$\Delta S^\ddagger$ [J K $^{-1}$ mol $^{-1}$ ]
$2.92 \times 10^{15}$	132	129	41
<i>cis</i> -2			
<i>T</i> [K]	$k_d$ [ $10^{-4} \text{ s}^{-1}$ ]	$t_{1/2}$ [min]	$\Delta G^\ddagger$ [kJ mol $^{-1}$ ]
363.15	1.9	62.1	115.9
373.15	4.0	28.6	115.5
383.15	16	7.3	115.2
388.15	30	3.9	115.0
$A^{[a]}$ [ $\text{s}^{-1}$ ]	$E_a$ [kJ mol $^{-1}$ ]	$\Delta H^\ddagger$ [kJ mol $^{-1}$ ]	$\Delta S^\ddagger$ [J K $^{-1}$ mol $^{-1}$ ]
$1.69 \times 10^{15}$	132	129	36

[a] *A* = Arrhenius factor.

energy barrier for 6-*exo* cyclization starting from the corresponding DKP radical derived from *cis*-1 amounts to only 70.5 kJ mol $^{-1}$ , which is thus more than 50 kJ mol $^{-1}$  lower than the barrier for formation of the respective radical pair. The barrier for 7-*endo* cyclization is somewhat higher at +82.8 kJ mol $^{-1}$ , in full agreement with the formation of 6-*exo* products *syn/anti*-6 as the major products under the experimental conditions.<sup>[21]</sup>

## Discussion

The 15–22° deviation of the amide nitrogen atom from planarity in *trans*-DKP alkoxyamines 1–5, which are normal ring-sized lactams, is a significant distortion for an amide bond.<sup>[59]</sup> Nitrogen atom pyramidalization in DKPs has been observed previously, however, only in proline- and pipercolic acid fused DKPs,

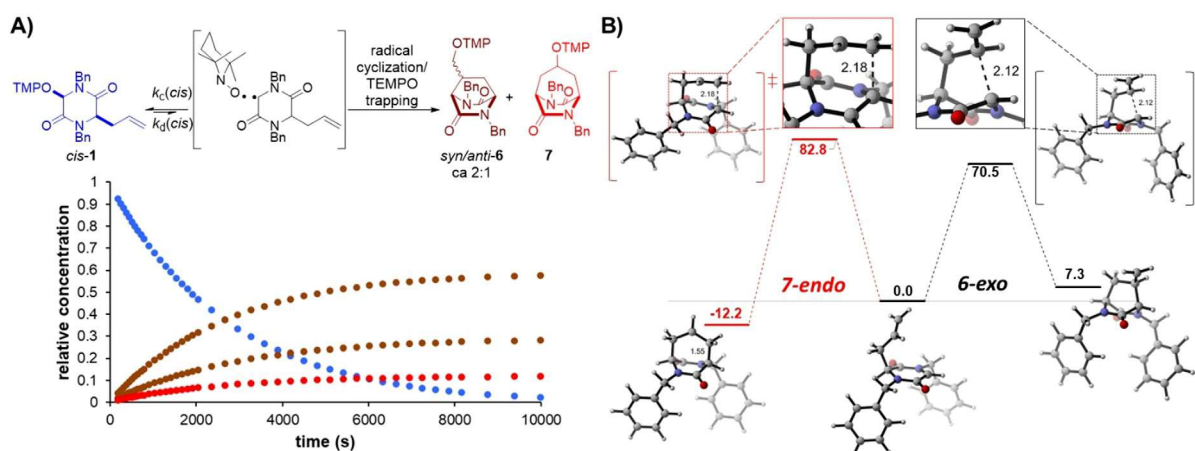


**Figure 8.** Thermal cycloisomerization of *cis*-1 into bridged DKPs *syn/anti*-6 and 7. A) First-order decay of *cis*-1 and formation of cyclization products 6 and 7 at 100 °C. B)  $\Delta G_{\text{sol}}^{\ddagger}$  [kJ mol $^{-1}$ ] profile for the cyclization steps calculated at the (U)B2PLYP/G3MP2Large// (U)B3LYP/6-31G(d) level of theory. Single-point solvation energies were calculated for DMSO at the SMD/(U)B3LYP/6-31G(d) level of theory.

in which it is enforced by the conformation of the pyrrolidine and piperidine rings.<sup>[60,61]</sup> In the monocyclic DKP alkoxyamines reported here, amide pyramidalization is the main reason why homolysis is significantly more facile for the *trans* diastereomers than for the *cis* isomers. Strain release as a result of planarization of the distorted amide bond and concomitant conjugation with the incipient radical center leads to significant lowering of the transition-state energy required for homolytic bond cleavage. It is significant that ground-state destabilization of the amide bond in *trans*-alkoxyamines leads to a decrease in the strength of a bond that is two skeletal bonds away. This C–O bond weakening is conceptually different from the amide-bond-twisting-induced C–N weakening of adjacent nitrogen substituents or the distorted N–C(O) bond itself.<sup>[62,63]</sup> To the best of our knowledge, such a mechanism for adjacent bond activation is very rare.<sup>[64]</sup> A computational investigation of quaternary DKP alkoxyamine analogues shows that substituent effects offer opportunities to modulate significantly the temperature window in which controlled homolysis can occur, thus providing prospect for future theranostic applications.

A second potential prospect is the possibility of temporary information or energy storage by alkoxyamines (Figure 9), as the DKP skeleton *red-A* can be charged by deprotonation and oxygenation under kinetically controlled conditions to provide *trans*-substituted alkoxyamines *trans-A* often with good diastereoselectivity (Figure 9, step a). Thermal isomerization to the strain-free *cis*-diastereomers *cis-A* leads to release (Figure 9, step b), and reductive removal of the alkoxyamine restores the original state *red-A* (Figure 9, step c). In this way, the system might be recycled multiple times. Significantly, this process occurs exclusively by directed configurational switching.

Diastereomeric excess has been previously noted for stereoisomeric alkoxyamines upon reversible homolysis and coupling.<sup>[65,66]</sup> by which an achiral nitroxide radical couples to a chiral carbon-centered radical (Figure 10 A). However, none of the so-far-investigated diastereomeric acyclic alkoxyamines 8–10, described by Marque and Ananchenko,<sup>[67]</sup> Moad and Rizzardo,<sup>[68]</sup> and Georges,<sup>[69]</sup> exhibited large diastereomeric preferences on thermal homolysis/radical coupling reactions. Only sterically very crowded SG1-derived alkoxyamines 9 equilibrated

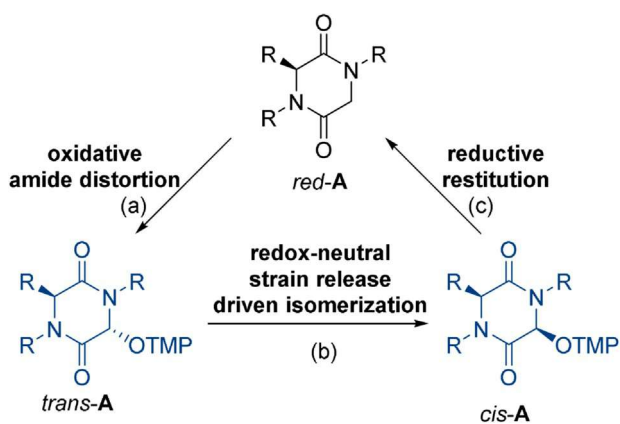
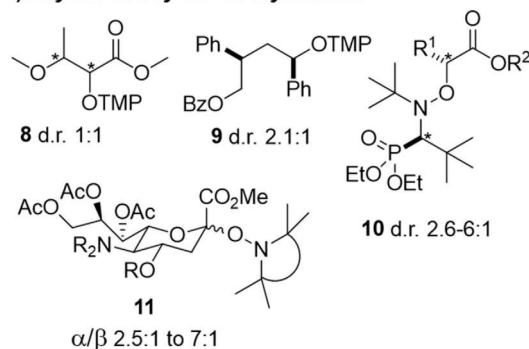


Figure 9. An overall reversible introduction of amide distortion into DKPs, its redox-neutral planarization, and reductive restoration.

#### A) Acyclic and cyclic alkoxyamines:



#### B) Strain-release driven alkoxyamines:

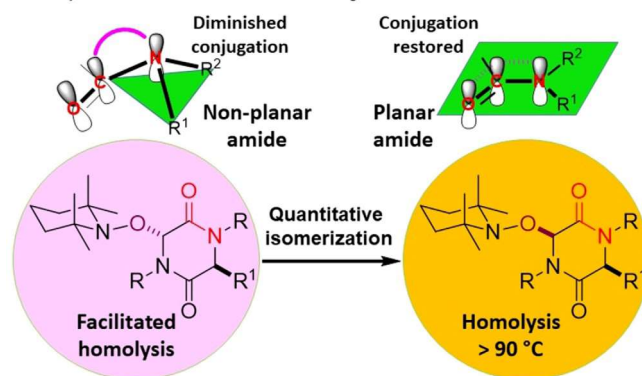


Figure 10. A) Previous thermal isomerization of diastereomeric alkoxyamine motives. B) Irreversible isomerization by strain release in a conformationally constrained cycle.

up to a 6:1 mixture if a 1:1 diastereomeric mixture or the individual diastereomers was heated at 100 °C. The most promising examples for directed isomerizations have so far proven to be cyclic sialic acid derived anomeric alkoxyamines 11, recently reported by Crich, providing a 7:1 ratio of  $\alpha/\beta$  anomers at 90 °C depending on the protecting groups.<sup>[70,71]</sup> Alkoxyamines 11 are also interesting in that the nitroxide unit is attached to a natural product core structure, providing the bias, but it shows that a simple cyclic constraint as in 11 is not sufficient to induce complete isomerization. However, combining the cyclic constraint with the strain induced by amide distortion in DKP alkoxyamines (Figure 10 B) provides the necessary driving force for a unidirectional three-point redox-fueled switching system based on central chirality (see Figure 9).

The here-reported complete thermodynamic preference for the *cis* isomer irrespective of steric and electronic factors is unique for 3,6-disubstituted DKPs. Except for fused proline-derived DKPs,<sup>[72]</sup> such high thermodynamic bias has only been observed for a few *N*-alkyl-*N'*-acyl DKPs because of the specific distal effect of the *N*-acyl carbonyl group.<sup>[73]</sup>

Recently, it was suggested that the additive Winkler–Dunitz parameter ( $\Sigma\tau + \chi_N$ ) describes amide-bond distortions more accurately on the basis of the linear correlation between ( $\Sigma\tau + \chi_N$ ) and N–C(O) bond lengths or differences in N-/O-protonation aptitude.<sup>[74,75]</sup> The maximum possible value for a fully perpendicular amide bond amounts to  $\Sigma\tau + \chi_N = 150^\circ$ . Compared to this value, the total distortion in our most non-

planar DKP *trans*-1 amounts to only 31.2°, and our results thus show that even a small additive amide distortion of one fifth of the maximum value suffices in normal-sized lactams to trigger interesting and unusual reactivity. The here-reported additive distortion values are similar to those found in sterically hindered amides **VIII** reported by Lloyd-Jones and Booker-Milburn<sup>[24]</sup> and in *N*-acylazetidines studied by Ohwada<sup>[76]</sup> and Szostak.<sup>[77]</sup>

## Conclusion

In summary, the first example of a quantitative and stereochemically unidirectional radical *trans*→*cis* isomerization of DKP alkoxyamines was presented. Although radical coupling reactions with nitroxides are generally known to be relatively unselective, the thermodynamic preference for the *cis* configuration was shown to be general and complete for all studied DKP alkoxyamines, irrespective of the electronic and steric nature of the amino-acid side chains and the alkyl groups attached to the DKP nitrogen atoms. Structural studies with the help of X-ray crystallography unambiguously confirmed the stereochemistry of both the kinetic and thermodynamic products, as well as significant distortion of the amide bond from planarity in *trans*-DKP alkoxyamines but to a much lower extent in their *cis* isomers. Kinetic investigations of the isomerization by <sup>1</sup>H NMR spectroscopy revealed the rate constants of homolysis and allowed determination of the activation parameters for both the *trans* isomers and *cis* isomers of two representative alkoxyamine pairs. These studies showed that isomerization of the initial *trans* isomer into the more stable *cis* isomer was faster than any follow-up transformation such as radical reduction or cyclization. Quantum-chemical calculations proved to be very valuable in rationalizing the importance of structural and reactivity parameters governing the isomerization and further transformations. On this basis, they also allowed the prediction of the structure and reactivity of more labile, not isolable quaternary DKP alkoxyamines. The studies reported here have many implications. The generation of the kinetic *trans* isomers having a defined absolute configuration with good selectivity allows energy uptake through significant amide distortion, which can be released by quantitative thermal isomerization; significant are the complete stereoselectivity and stability under ambient conditions. The here-gained knowledge may serve as a foundation for applications of this novel class of amino-acid-derived alkoxyamines for the design of smart and functional small molecules, in polymerization processes to access amino-acid-derived or -terminated polymers, and for the use of these amino-acid-derived alkoxyamines as versatile amino acid surrogates. Studies toward envisioned applications of these alkoxyamines are ongoing in these laboratories and will be reported in due course.

## Acknowledgements

Generous financial support by the Institute of Organic Chemistry and Biochemistry of the Czech Academy of Sciences (RVO:

61388963), the COST action CM1201 “Biomimetic Radical Chemistry”, the Gilead Sciences & IOCB Research Center, and the European Regional Development Fund; OP RDE; Project: Chemical biology for drugging undruggable targets (ChemBio-Drug) (No.CZ.02.1.01/0.0/0.0/16 019/0000729) is gratefully acknowledged. I.C. thanks the Ministry of Education, Youth and Sports of the Czech Republic (MSM0021620857) for financial support.

## Conflict of interest

The authors declare no conflict of interest.

**Keywords:** amides · cleavage reactions · isomerization · persistent radical effect · radicals

- [1] *The Amide Linkage: Structural Significance in Chemistry, Biochemistry and Materials Science* (Eds.: A. Greenberg, C. M. Breneman, J. F. Liebman), Wiley, New York, **2000**.
- [2] J. Clayden, N. Vassiliou, *Org. Biomol. Chem.* **2006**, *4*, 2667.
- [3] B. A. F. Le Bailly, J. Clayden, *Chem. Commun.* **2016**, *52*, 4852.
- [4] S. Z. Vatsadze, Y. D. Loginova, G. dos Passos Gomes, I. V. Alabugin, *Chem. Eur. J.* **2017**, *23*, 3225.
- [5] S. A. Glover, J. M. White, A. A. Rosser, K. M. Digianantonio, *J. Org. Chem.* **2011**, *76*, 9757.
- [6] R. Lukeš, *Collect. Czech. Chem. Commun.* **1938**, *10*, 148.
- [7] H. K. Hall, A. El-Sheikeil, *Chem. Rev.* **1983**, *83*, 549.
- [8] M. Szostak, J. Aube, *Chem. Rev.* **2013**, *113*, 5701.
- [9] K. Tani, B. M. Stoltz, *Nature* **2006**, *441*, 731.
- [10] M. Liniger, D. G. VanderVelde, M. K. Takase, M. Shahgholi, B. M. Stoltz, *J. Am. Chem. Soc.* **2016**, *138*, 969.
- [11] J. Clayden, W. J. Moran, *Angew. Chem. Int. Ed.* **2006**, *45*, 7118; *Angew. Chem.* **2006**, *118*, 7276.
- [12] *The Chemistry of Penicillin* (Eds.: H. T. Clark, J. R. Johnson, R. Robinson), Princeton University Press, Princeton, **1949**.
- [13] S. Adachi, N. Kumagai, M. Shibasaki, *Tetrahedron Lett.* **2018**, *59*, 1147.
- [14] G. Meng, S. Shi, M. Szostak, *Synlett* **2016**, *27*, 2530.
- [15] C. Liu, M. Szostak, *Chem. Eur. J.* **2017**, *23*, 7157.
- [16] J. E. Dander, N. K. Garg, *ACS Catal.* **2017**, *7*, 1413.
- [17] S. Shi, G. Meng, M. Szostak, *Angew. Chem. Int. Ed.* **2016**, *55*, 6959; *Angew. Chem.* **2016**, *128*, 7073.
- [18] Y. Lei, A. D. Wroblewski, J. E. Golden, D. R. Powell, J. Aube, *J. Am. Chem. Soc.* **2005**, *127*, 4552.
- [19] M. Szostak, L. Yao, V. D. Day, D. R. Powell, J. Aube, *J. Am. Chem. Soc.* **2010**, *132*, 8836.
- [20] F. Hu, R. Lalancette, M. Szostak, *Angew. Chem. Int. Ed.* **2016**, *55*, 5062; *Angew. Chem.* **2016**, *128*, 5146.
- [21] F. Hu, P. Nareddy, R. Lalancette, F. Jordan, M. Szostak, *Org. Lett.* **2017**, *19*, 2386.
- [22] K. Weidner, N. Kumagai, M. Shibasaki, *Angew. Chem. Int. Ed.* **2014**, *53*, 6150; *Angew. Chem.* **2014**, *126*, 6264.
- [23] S. Adachi, N. Kumagai, M. Shibasaki, *Chem. Sci.* **2017**, *8*, 85.
- [24] M. Hutchby, C. E. Houlden, M. F. Haddow, S. N. G. Tyler, G. C. Lloyd-Jones, K. I. Booker-Milburn, *Angew. Chem. Int. Ed.* **2012**, *51*, 548; *Angew. Chem.* **2012**, *124*, 563.
- [25] T. Amatov, R. Pohl, I. Cisařová, U. Jahn, *Angew. Chem. Int. Ed.* **2015**, *54*, 12153; *Angew. Chem.* **2015**, *127*, 12321.
- [26] T. Amatov, M. Gebauer, R. Pohl, I. Cisařová, U. Jahn, *Free Radical Res.* **2016**, *50*, S6.
- [27] T. Amatov, R. Pohl, I. Cisařová, U. Jahn, *Org. Lett.* **2017**, *19*, 1152.
- [28] H. Fischer, *Chem. Rev.* **2001**, *101*, 3581.
- [29] A. Studer, *Chem. Eur. J.* **2001**, *7*, 1159.
- [30] A. Studer, *Chem. Soc. Rev.* **2004**, *33*, 267.
- [31] A. Studer, T. Schulte, *Chem. Rec.* **2005**, *5*, 27.
- [32] C. J. Hawker, A. W. Bosman, E. Harth, *Chem. Rev.* **2001**, *101*, 3661.

- [33] J. Nicolas, Y. Guillaneuf, C. Lefay, D. Bertin, D. Gigmes, B. Charleux, *Prog. Polym. Sci.* **2013**, *38*, 63.
- [34] *Encyclopedia of Radicals in Chemistry, Biology, and Materials*, (Eds: C. Chatgililoglu, A. Studer), Wiley, Chichester, **2012**.
- [35] A. Studer, *Angew. Chem. Int. Ed.* **2000**, *39*, 1108; *Angew. Chem.* **2000**, *112*, 1157.
- [36] G. Audran, P. Bremond, S. R. A. Marque, *Chem. Commun.* **2014**, *50*, 7921.
- [37] G. Gryn'ova, D. L. Marshall, S. J. Blanksby, M. L. Coote, *Nat. Chem.* **2013**, *5*, 474.
- [38] G. Gryn'ova, M. L. Coote, *J. Am. Chem. Soc.* **2013**, *135*, 15392.
- [39] D. Moncelet, P. Voisin, N. Koonjoo, V. Bouchaud, P. Massot, E. Parzy, G. Audran, J.-M. Franconi, E. Thiaudiere, S. R. A. Marque, P. Bremond, P. Mellet, *Mol. Pharm.* **2014**, *11*, 2412.
- [40] G. Audran, P. Bremond, J.-M. Franconi, S. R. A. Marque, P. Massot, P. Mellet, E. Parzy, E. Thiaudiere, *Org. Biomol. Chem.* **2014**, *12*, 719.
- [41] A. D. Borthwick, *Chem. Rev.* **2012**, *112*, 3641.
- [42] J. F. González, I. Ortin, E. de La Cuesta, J. C. Menendez, *Chem. Soc. Rev.* **2012**, *41*, 6902.
- [43] T. Amatov, U. Jahn, *Angew. Chem. Int. Ed.* **2014**, *53*, 3312; *Angew. Chem.* **2014**, *126*, 3378.
- [44] Previously characterized by X-ray crystallography, see Ref. 21.
- [45] M. V. Ciriano, H.-G. Korth, W. B. van Scheppingen, P. Mulder, *J. Am. Chem. Soc.* **1999**, *121*, 6375.
- [46] S. Marque, H. Fischer, E. Baier, A. Studer, *J. Org. Chem.* **2001**, *66*, 1146.
- [47] J. L. Hodgson, C. Y. Lin, M. L. Coote, S. R. A. Marque, K. Matyjaszewski, *Macromolecules* **2010**, *43*, 3728.
- [48] K. Molawi, T. Schulte, K. O. Siegenthaler, C. Wetter, A. Studer, *Chem. Eur. J.* **2005**, *11*, 2335.
- [49] A. Gaudel-Siri, D. Siri, P. Tordo, *ChemPhysChem* **2006**, *7*, 430.
- [50] V. Kapras, V. Vyklicky, M. Budesinsky, I. Cisarova, L. Vyklicky, H. Chodounska, U. Jahn, *Org. Lett.* **2018**, *20*, 946.
- [51] U. Jahn, unpublished.
- [52] F. K. Winkler, J. D. Dunitz, *J. Mol. Biol.* **1971**, *59*, 169.
- [53] M. Edeleva, S. R. A. Marque, D. Bertin, D. Gigmes, Y. Guillaneuf, E. Bagryanskaya, *Polymer* **2010**, *2*, 364.
- [54] V. W. Bowry, K. U. Ingold, *J. Am. Chem. Soc.* **1992**, *114*, 4992.
- [55] J. Chateaneuf, J. Lusztyk, K. U. Ingold, *J. Org. Chem.* **1988**, *53*, 1629.
- [56] I. W. C. E. Arends, P. Mulder, K. B. Clark, D. D. M. Wayner, *J. Phys. Chem.* **1995**, *99*, 8182.
- [57] A. L. J. Beckwith, V. W. Bowry, K. U. Ingold, *J. Am. Chem. Soc.* **1992**, *114*, 4983.
- [58] E. G. Bagryanskaya, S. R. A. Marque, *Chem. Rev.* **2014**, *114*, 5011.
- [59] J. D. Dunitz, F. K. Winkler, *Acta. Cryst. Sect. B* **1975**, *31*, 251.
- [60] M. Budesinsky, I. Cisarova, J. Podlaha, F. Borremans, J. C. Martins, M. Waroquier, E. Powels, *Acta Crystallogr. Sect. B* **2010**, *66*, 662.
- [61] M. Budesinsky, I. Cisarova, F. Borremans, J. C. Martins, E. Powels, *Acta Crystallogr. Sect. B* **2017**, *73*, 1179.
- [62] J. Aubé, *Angew. Chem. Int. Ed.* **2012**, *51*, 3063; *Angew. Chem.* **2012**, *124*, 3117.
- [63] G. Meng, S. Shi, R. Lalancette, R. Szostak, M. Szostak, *J. Am. Chem. Soc.* **2018**, *140*, 727 and references therein.
- [64] A conceptually similar situation exists in reactions of strained aniline-derived cyclodecynes: T. Harris, G. P. Gomes, S. Ayad, R. J. Clark, V. V. Lobodin, M. A. Tuscan, K. Hanson, I. V. Alabugin, *Chem* **2017**, *3*, 629.
- [65] R. Braslau, N. Naik, H. Zipse, *J. Am. Chem. Soc.* **2000**, *122*, 8421.
- [66] R. Braslau, L. C. Burrill II, L. K. Mahal, T. Wedeking, *Angew. Chem. Int. Ed. Engl.* **1997**, *36*, 237; *Angew. Chem.* **1997**, *109*, 247.
- [67] G. Ananchenko, S. Marque, D. Gigmes, D. Bertin, P. Tordo, *Org. Biomol. Chem.* **2004**, *2*, 709.
- [68] G. Moad, E. Rizzardo in *Nitroxide Mediated Polymerization: From Fundamentals to Applications in Materials Science* (Ed.: D. Gigmes), RSC, Cambridge, **2015**, pp. 1–44.
- [69] L. Li, G. K. Hamer, M. K. Georges, *Macromolecules* **2006**, *39*, 9201.
- [70] P. K. Kancharla, T. Kato, D. Crich, *J. Am. Chem. Soc.* **2014**, *136*, 5472.
- [71] P. K. Kancharla, C. Navuluri, D. Crich, *Angew. Chem. Int. Ed.* **2012**, *51*, 11105; *Angew. Chem.* **2012**, *124*, 11267.
- [72] C. Eguchi, A. Kakuta, *J. Am. Chem. Soc.* **1974**, *96*, 3985.
- [73] J. Ho, M. L. Coote, C. J. Easton, *J. Org. Chem.* **2011**, *76*, 5907.
- [74] R. Szostak, J. Aube, M. Szostak, *Chem. Commun.* **2015**, *51*, 6395.
- [75] R. Szostak, J. Aube, M. Szostak, *J. Org. Chem.* **2015**, *80*, 7905.
- [76] Y. Otani, O. Nagae, Y. Naruse, S. Inagaki, M. Ohno, K. Yamaguchi, G. Yamamoto, M. Uchiyama, Y. Ohwada, *J. Am. Chem. Soc.* **2003**, *125*, 15191.
- [77] C. Liu, M. Achtenhagen, M. Szostak, *Org. Lett.* **2016**, *18*, 2375.

---

Manuscript received: June 28, 2018  
 Revised manuscript received: August 2, 2018  
 Accepted manuscript online: August 9, 2018  
 Version of record online: September 13, 2018

## 5.1 Supporting Information

### For: Unique Stereoselective Homolytic C-O Bond Activation in Diketopiperazine-Derived Alkoxyamines by Adjacent Amide Pyramidalization

#### 5.1.1 Technical Details

Force field-based calculations: The MacroModel module of Maestro 10.2,<sup>1</sup> was employed for molecular mechanics (MM)-based conformational search using OPLS 2005 force field.

Quantum mechanics calculations: The geometries of all conformers were optimized at the B3LYP/6-31G(d) level of theory in the gas phase.<sup>2</sup> The frequency calculations were performed at the same level of theory and all minima were confirmed with all positive frequencies. Single point calculations were done at double hybrid B2-PLYP/G3MP2Large<sup>3</sup> level. The energies were calculated for a temperature of 298.15 K in the gas phase and the thermal corrections to the enthalpy and Gibb's free energy were obtained at the B3LYP/6-31G(d) level of theory. The solvent correction for  $\Delta G_{\text{sol}}$  was calculated for gas phase optimized geometries using the SMD<sup>4</sup> continuum solvation model and subsequently added to gas phase Gibbs energies ( $\Delta G_{298}$ ) to obtain solution phase Gibbs energies that will be mentioned as single point solvation free energies ( $\Delta G_{\text{sol-sp}}$ ).

Potential energy surface (PES): Geometry optimizations for all stationary points (minima, complexes and TSs) along the PES have been performed at B3LYP/6-31G(d) level under implicit DMSO solvation as implemented in the SMD solvation model. Energy minima, complexes and TSs were confirmed by vibrational frequency calculation with 0, 0 and 1 imaginary frequencies, respectively. All stationary points were checked for wavefunction stability (stable=opt). The nature of transition states was further confirmed by IRC calculations [30 steps in both directions (reverse/forward) with stepsize=3] followed by geometry optimization to a minimum. PES surfaces were re-evaluated at B2-PLYP/G3MP2Large level. Orbital interactions were analyzed using NBO 6.0.<sup>5</sup> All calculations were performed using Gaussian09, Rev. D.01.<sup>6</sup>

#### 5.1.2 Diketopiperazine (DKP)-Derived Alkoxyamine (1)

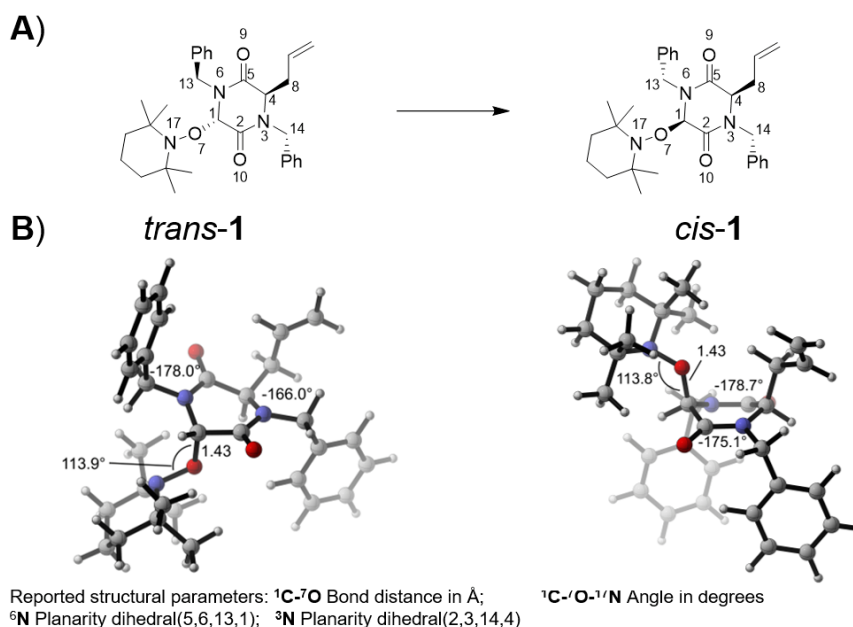


**Figure S5-1.** [Figure S7] (A) An unusual *trans-cis* isomerization of diketopiperazine (DKP)-derived alkoxyamine **1**. (B) Structure of the lowest gas phase Gibbs energy ( $\Delta G_{298}$ ) minima of *trans* and *cis* isomers of **1** obtained at the B3LYP/6-31G(d) level of theory.

For solvation-corrected energies, geometry optimization was performed at the B3LYP/6-31G(d) level of theory in the gas phase, followed by a single point at higher levels of theory for selected

conformers. Gas phase energy values were corrected with DMSO implicit solvation energies ( $\Delta G_{\text{sol}}$ ) calculated using the SMD solvation model at the same level of theory.

### 5.1.2.1 Conformational energetics

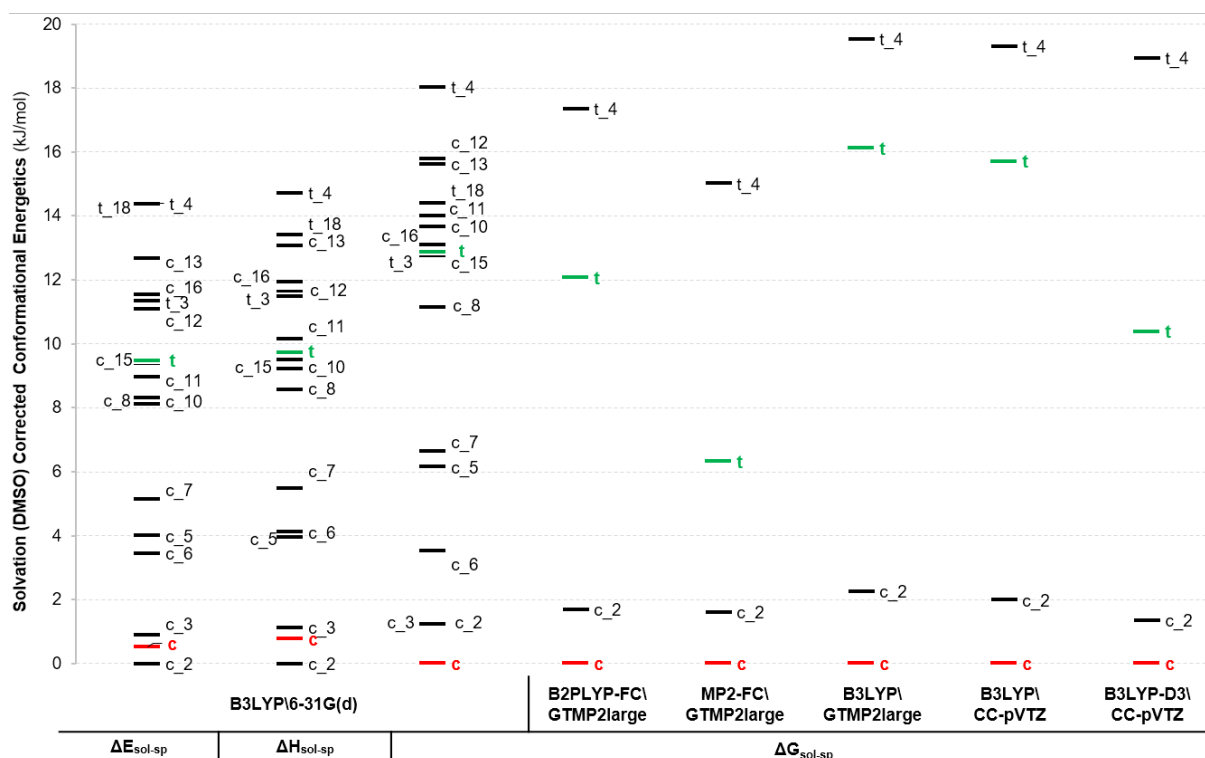


**Figure S5-2.** [Figure S10] Solvation corrected conformational energetics for the *trans(t)-cis(c)* isomerization of DKP-alkoxyamine (**1**) at different levels of theory.

**Table S5-1.** Solvation corrected conformational energetics (kJ/mol) for the *trans(t)-cis(c)* isomerization of DKP-alkoxyamine (**1**) at different levels of theory.

SI	Conformer Marker	B3LYP/6-31G(d)			B2PLYP-FC	MP2-FC	B3LYP	B3LYP	B3LYP-D3
		$\Delta E_{\text{sol-sp}}$	$\Delta H_{\text{sol-sp}}$	$\Delta G_{\text{sol-sp}}$	\G3MP2Large	\G3MP2Large	\G3MP2Large	\cc-pVTZ	\cc-pVTZ
<b>1</b>	<b>c</b>	<b>0.4</b>	<b>0.7</b>	<b>0.0</b>	<b>0.0</b>	<b>0.0</b>	<b>0.0</b>	<b>0.0</b>	<b>0.0</b>
2	c_3	0.8	1.1	1.2	-	-	-	-	-
3	c_6	3.4	4.0	3.5	-	-	-	-	-
4	c_2	0.0	0.0	1.3	1.8	1.7	2.4	2.1	1.5
5	c_7	4.8	5.1	6.4	-	-	-	-	-
6	c_5	3.8	3.8	6.0	-	-	-	-	-
7	c_8	8.7	9.1	11.8	-	-	-	-	-
8	c_16	11.8	12.2	13.4	-	-	-	-	-
9	c_13	12.9	13.3	16.0	-	-	-	-	-
10	c_10	7.8	9.0	13.2	-	-	-	-	-
11	c_11	8.6	9.8	13.7	-	-	-	-	-
12	c_12	10.5	11.0	15.3	-	-	-	-	-
13	c_15	10.7	10.5	14.2	-	-	-	-	-
<b>14</b>	<b>t</b>	<b>9.2</b>	<b>9.5</b>	<b>12.7</b>	<b>11.9</b>	<b>6.1</b>	<b>16.0</b>	<b>15.5</b>	<b>10.2</b>
15	t_18	15.2	14.3	15.3	-	-	-	-	-
16	t_3	10.9	11.0	12.3	-	-	-	-	-
17	t_4	14.2	14.6	18.0	17.3	15.0	19.5	19.3	18.9

Conformers in the energy window of 15 kJ/mol in terms of  $\Delta E_{\text{tot}}$  at B3LYP/6-31G(d) level have been reported.

## 5.1.2.2 Mechanistic investigation

**Table S5-2.** Transition state (TS), reactant complex (RC) and product (P) relative energies (kJ/mol) for the *trans-cis* isomerization, thermal cycloisomerization and radical recombination of DKP-alkoxyamines (**1**) calculated at different levels of theory. (see Figure S5-3 for more information on labels under path name).

Path Name (Label)	FileName	$\Delta G_{\text{sol-sp}}$			$\Delta H_{\text{sol-sp}}$		
		RC	TS	P	RC	TS	P
<b>(U)B3LYP/6-31G(d)</b>							
<b><i>trans-cis</i> isomerization</b>							
ts_cis	cis_6_196	40.5	72.8	-27.3	-6.7	11.9	-93.2
ts_cis	cis_6_7	40.8	78.9	-20.9	-3.8	15.1	-88.5
ts_cis	cis_6_2	35.0	73.0	-26.3	-6.9	11.1	-94.0
ts_trans	trans_6_216	38.6	81.7	-14.7	-7.9	16.9	-84.3
ts_trans	trans_6_4	-	89.6	-9.5	-	26.3	-79.3
<b>Thermal cycloisomerization</b>							
ts_7_endo	rTrans_6_11	-	81.9	-5.6	-	68.8	-16.8
ts_7_endo	rCis_6_10	-	79.4	-12.1	-	67.6	-18.7
ts_6_exo	rCis_6_exo_5	-	72.3	16.8	-	60.9	8.4
ts_6_exo	rCis_6_exo_3	-	74.7	19.1	-	61.2	9.2
ts_6_exo	rCis_6_exo_2	-	69.7	16.4	-	59.2	8.7
ts_6_exo	rCis_6_exo_6	-	69.7	15.7	-	59.5	7.3
ts_6_exo	rCis_6_exo_1	-	68.3	13.0	-	58.3	7.1
ts_6_exo	rCis_6_exo_4	-	78.6	19.3	-	62.8	10.1
<b>Radical recombination</b>							
ts_7e_rb	rCis_Bdg_2	32.2	55.3	-83.4	-22.0	-9.3	-159.0
ts_7e_rb	rCis_Bdg_1	24.9	56.1	-88.2	-26.0	-9.6	-160.3
ts_6e_rb	rCis_6_exo_2_4	53.3	76.0	-49.1	-1.0	3.8	-120.7
ts_6e_rb	rCis_6_exo_2_6	50.9	75.4	-56.9	-0.1	5.8	-125.3
ts_6e_rb	rCis_6_exo_2_3	52.5	82.8	-56.8	-2.2	10.9	-126.1
ts_6e_rb	rCis_6_exo_2_1	52.0	76.5	-56.1	-0.5	5.9	-124.8
ts_6e_rb	rCis_6_exo_2_2	56.0	83.3	-95.3	1.4	-0.1	-164.1
<b>/(U)B2PLYP/G3MP2Large//B3LYP/6-31G(d)</b>							
<b><i>trans-cis</i> isomerization</b>							
ts_cis	cis_6_196	40.1	75.5	-50.6	-7.1	14.7	-116.3
ts_cis	cis_6_7	-	82.4	-	-	18.6	-
ts_cis	cis_6_2	-	76.8	-48.9	-	15.0	-116.6
ts_trans	trans_6_216	35.1	82.0	-38.5	-11.5	17.2	-108.1
ts_trans	trans_6_4	-	91.1	-33.2	-	27.8	-103.0
<b>Thermal cycloisomerization</b>							
ts_7_endo	rTrans_6_11	-	85.1	-5.2	-	72.1	-16.4
ts_7_endo	rCis_6_10	-	82.8	-12.2	-	71.0	-18.8
ts_6_exo	rCis_6_exo_5	-	74.3	11.8	-	62.9	3.4
ts_6_exo	rCis_6_exo_3	-	76.4	14.6	-	62.9	4.6
ts_6_exo	rCis_6_exo_2	-	71.5	11.6	-	61.0	3.9
ts_6_exo	rCis_6_exo_6	-	71.7	9.7	-	61.4	1.3
ts_6_exo	rCis_6_exo_1	-	70.5	7.3	-	60.5	1.4
ts_6_exo	rCis_6_exo_4	-	79.7	14.3	-	64.0	5.1
<b>Radical recombination</b>							
ts_7e_rb	rCis_Bdg_2	29.0	55.0	-104.3	-25.1	-9.5	-179.9
ts_7e_rb	rCis_Bdg_1	22.1	56.9	-108.5	-28.9	-8.8	-180.6
ts_6e_rb	rCis_6_exo_2_4	47.3	72.5	-68.8	-7.0	0.3	-140.4
ts_6e_rb	rCis_6_exo_2_6	-	-	-	-	-	-
ts_6e_rb	rCis_6_exo_2_3	47.9	-	-	-6.7	-	-
ts_6e_rb	rCis_6_exo_2_1	-	-	-	-	-	-
ts_6e_rb	rCis_6_exo_2_2	-	83.9	-115.3	-	0.5	-184.1

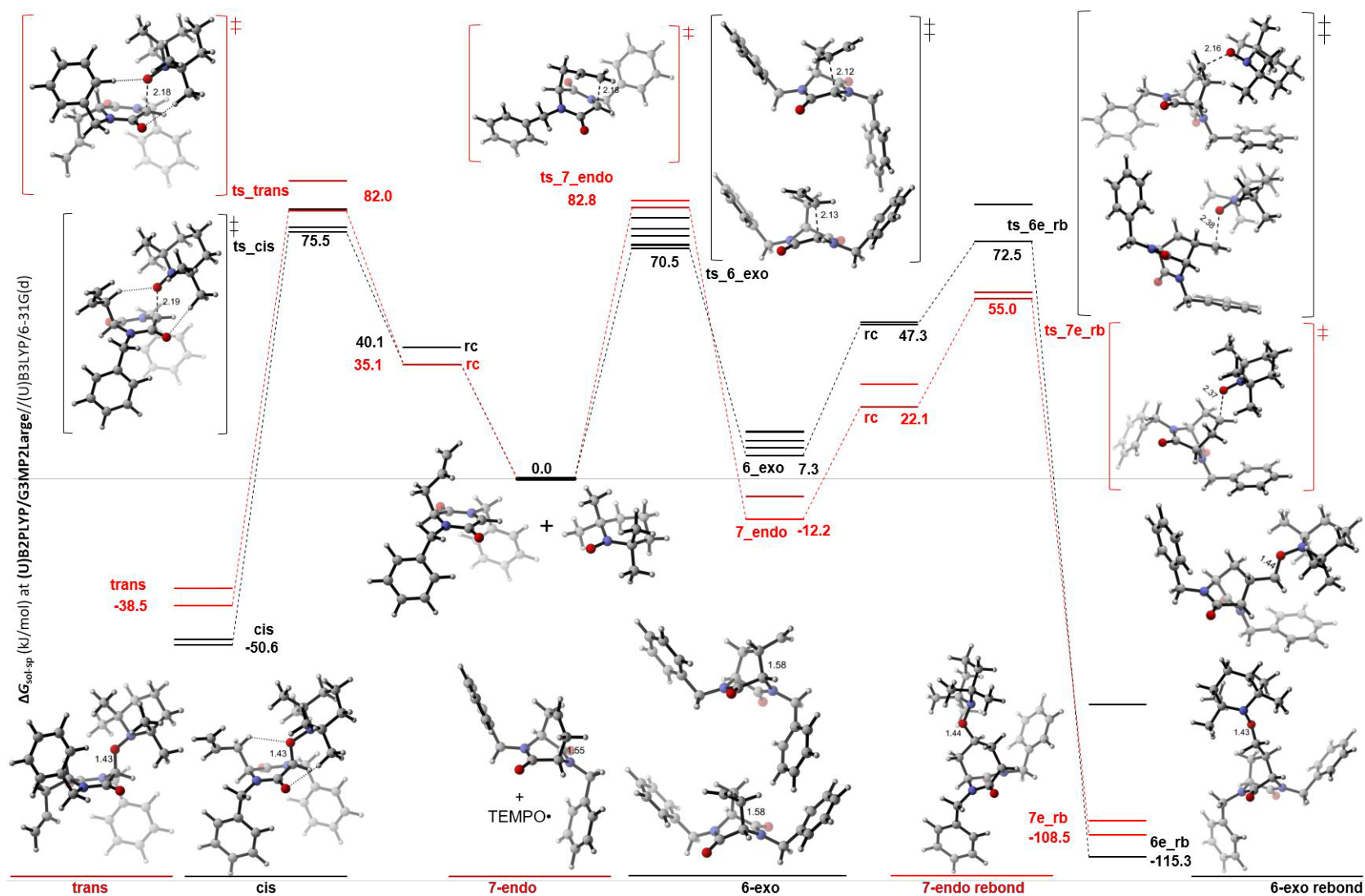


**Figure S5-3.** [Figure S20] Solvation corrected Gibbs energy ( $\Delta G_{\text{sol-sp}}$ ) surface for the *trans-cis* isomerization and reaction diagram for homolysis and radical recombination of DKP-alkoxyamines (1) calculated at (U)B2PLYP/G3MP2Large//((U)B3LYP/6-31G(d) level of theory. A single point solvation correction [ $\Delta G_{\text{sol}}$ , at SMD(DMSO)/(U)B3LYP/6-31G(d)] is added to  $\Delta G_{298}$  [at (U)B2PLYP/G3MP2Large//((U)B3LYP/6-31G(d)].

## 5.1.2.3 NBO analysis

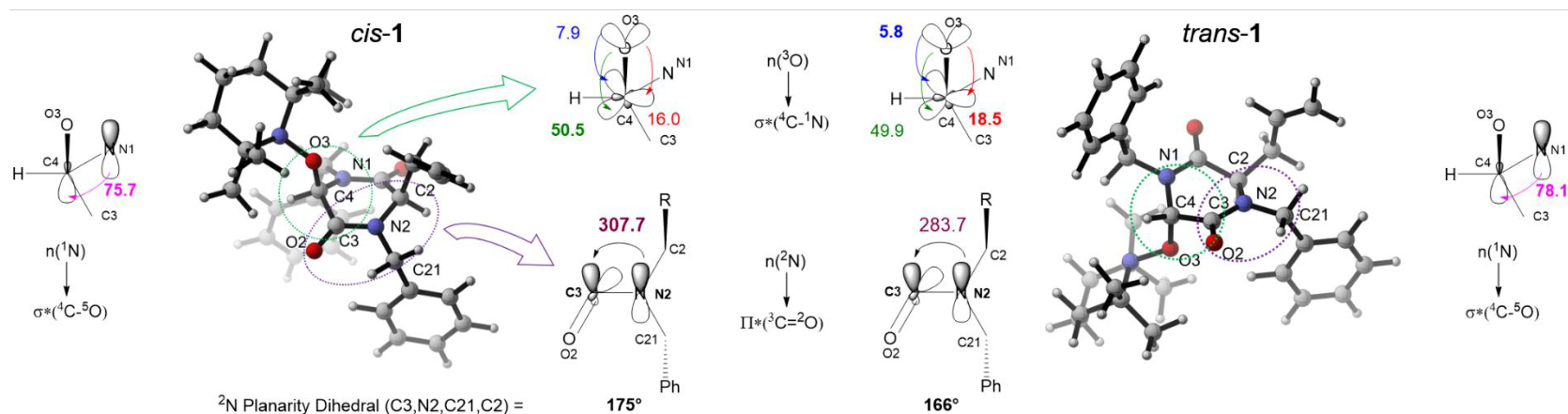


**Figure S5-4.** [Figure S21] Important hyperconjugation interactions (in kJ/mol) in *cis* and *trans* isomers of DKP alkoxyamines **1**.

**Table S5-3.** [Table S3] Important hyperconjugation interactions (in kJ/mol, pop=nbo6) in lowest gas phase Gibbs energy ( $\Delta G_{298}$ ) conformers of *cis* and *trans* isomers of DKP alkoxyamines **1** calculated at the B3LYP/6-31G(d) level of theory.

<i>cis</i> -1						<i>trans</i> -1							
Donor Orbital	Atom 1	→	Acceptor Orbital	Atom 1	Atom 2	E(2) kJ/mol	Donor Orbital	Atom 1	→	Acceptor Orbital	Atom 1	Atom 2	E(2) kJ/mol
LP (2)	O3	→	BD* (1)	C4	N1	50.5	LP (2)	O3	→	BD* (1)	C4	N1	49.9
LP (1)	O3	→	BD* (1)	C4	H	8.5	LP (2)	O3	→	BD* (1)	C4	H6	9.8
LP (2)	O3	→	BD* (1)	C4	H	7.5	LP (1)	O3	→	BD* (1)	C4	H6	8.7
					<b>SUM</b>	<b>16.0</b>						<b>SUM</b>	<b>18.5</b>
LP (1)	O3	→	BD* (1)	C3	C4	2.2	LP (1)	O3	→	BD* (1)	C3	C4	2.4
LP (2)	O3	→	BD* (1)	C3	C4	5.7	LP (2)	O3	→	BD* (1)	C3	C4	3.4
					<b>SUM</b>	<b>7.9</b>						<b>SUM</b>	<b>5.8</b>
LP (1)	N2	→	BD* (2)	C3	O2	307.7	LP (1)	N2	→	BD* (2)	C3	O2	283.7
LP (1)	N1	→	BD* (1)	C4	O3	75.7	LP (1)	N1	→	BD* (1)	C4	O3	78.1

### 5.1.3 Quaternary diketopiperazine (QDKP)-derived alkoxyamines (q1)

#### 5.1.3.1 Conformational energetics

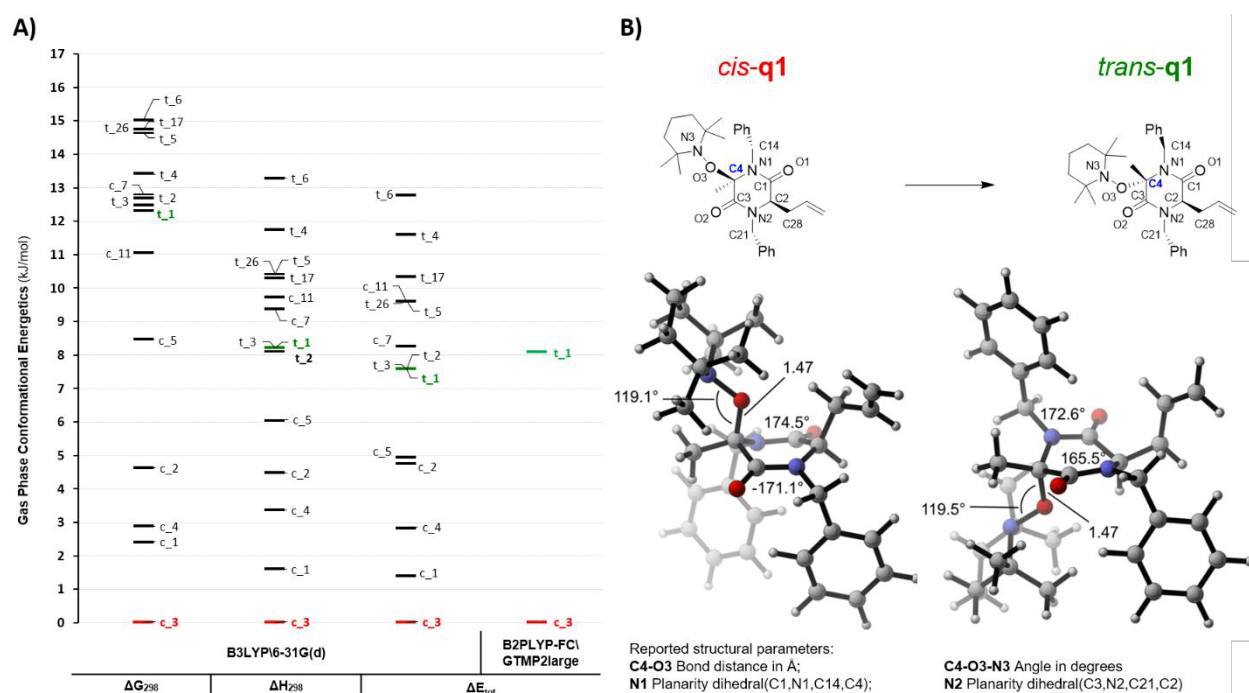


**Figure S5-5.** [Figure S23] (A) Gas phase conformational energetics for *trans*→*cis* isomerization of **q1**. Geometry optimization was performed at the B3LYP/6-31G(d) level of theory in the gas phase, followed by single point calculations at higher levels of theory for selected conformers. (B) Lowest gas phase Gibbs energy ( $\Delta G_{298}$ ) minima in the *trans/cis* isomerization of **q1**.

**Table S5-4.** Gas phase conformational energetics (kJ/mol) for *trans*(t)-*cis*(c) isomerization of **q1** at different levels of theory.

SI	Conf.	B3LYP/6-31G(d)		B2PLYP-FC \G3MP2Large	
		$\Delta G_{\text{sol-sp}}$	$\Delta H_{\text{sol-sp}}$	$\Delta E_{\text{sol-sp}}$	
1	<b>c_3</b>	<b>0.0</b>	<b>0.0</b>	<b>0.0</b>	<b>0.0</b>
2	c_1	2.4	1.6	1.4	
3	c_4	2.9	3.4	2.8	
4	c_2	4.6	4.5	4.8	
5	c_5	8.5	6.0	5.0	
6	c_11	11.0	9.7	9.6	
7	c_7	12.8	9.4	8.3	
8	<b>t_1</b>	<b>12.3</b>	<b>8.2</b>	<b>7.6</b>	<b>8.1</b>
9	t_3	12.5	8.2	7.6	
10	t_2	12.7	8.1	7.6	
11	t_4	13.4	11.8	11.6	
12	t_5	14.6	10.4	9.6	
13	t_26	14.7	10.4	9.6	
14	t_17	14.7	10.3	10.3	
15	t_6	15.0	13.3	12.8	

Only the first 15 conformers in terms of lowest  $\Delta E_{\text{tot}}$  at B3LYP/6-31G(d) level have been reported.

### 5.1.3.2 NBO analysis

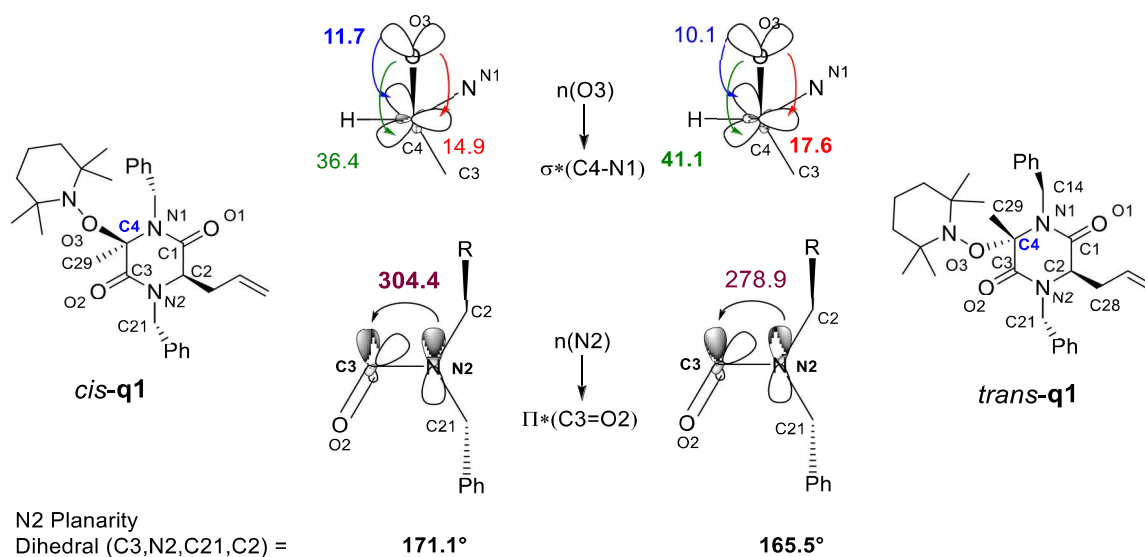


**Figure S5-6.** [Figure S24] Important hyperconjugation interactions (in kJ/mol, pop=nbo6) in *cis* and *trans* isomers of QDKP alkoxyamine **q1** calculated at the B3LYP/6-31G(d) level of theory.

**Table S5-5.** [Table S4] Important hyperconjugation interactions (in kJ/mol, pop=nbo6) in the lowest gas phase Gibbs energy *cis* and *trans* isomers of **q1** calculated at the B3LYP/6-31G(d) level of theory.

<i>cis</i> -q1				<i>trans</i> -q1			
Donor Orbital	→	Acceptor Orbital	E(2) kJ/mol	Donor Orbital	→	Acceptor Orbital	E(2) kJ/mol
LP(2) O3	→	BD*(1) C4 N1	<b>36.4</b>	LP(2) O3	→	BD*(1) C4 N6	<b>41.1</b>
LP(1) O3	→	BD*(1) C4 C29	<b>14.9</b>	LP(2) O3	→	BD*(1) C4 C29	2.8
				LP(1) O3	→	BD*(1) C4 C29	14.8
						<b>SUM</b>	<b>17.6</b>
LP(1) O3	→	BD*(1) C3 C4	<b>11.7</b>	LP(1) O3	→	BD*(1) C3 C4	2.2
				LP(2) O3	→	BD*(1) C3 C4	7.9
						<b>SUM</b>	<b>10.1</b>
LP(1) N2	→	BD*(2) C3 O2	<b>304.4</b>	LP(1) N2	→	BD*(2) C3 O2	<b>278.9</b>

**Table S5-6.** Transition state, and product relative energies (kJ/mol) for the *trans*-*cis* isomerization of **q1** calculated at different levels of theory. (see Figure S5-7 for more information on labels under path name)

Path Name (Label)	Conf. FileName	(U)B3LYP/6-31G(d)		(U)B2PLYP/G3MP2Large //B3LYP/6-31G(d)	
		$\Delta G_{298}$	$\Delta G_{\text{sol-sp}}$	$\Delta G_{298}$	$\Delta G_{\text{sol-sp}}$
<b>Transition state</b>					
ts_cis	ts_qdkp_c6_2	72.1	90.2	67.2	83.9
ts_cis	ts_qdkp_c6_1	74.5	71.7	69.0	64.8
ts_trans	ts_qkdp_t6_4	84.0	83.1	74.8	72.5
<b>Product</b>					
cis-q1	qdkp_c6_3	6.5	23.7	-28.1	-12.3
trans-q1	qdkp_t6_1	18.8	37.8	-15.3	2.3
trans-q1	qdkp_t6_25	23.2	36.7	-11.7	0.4

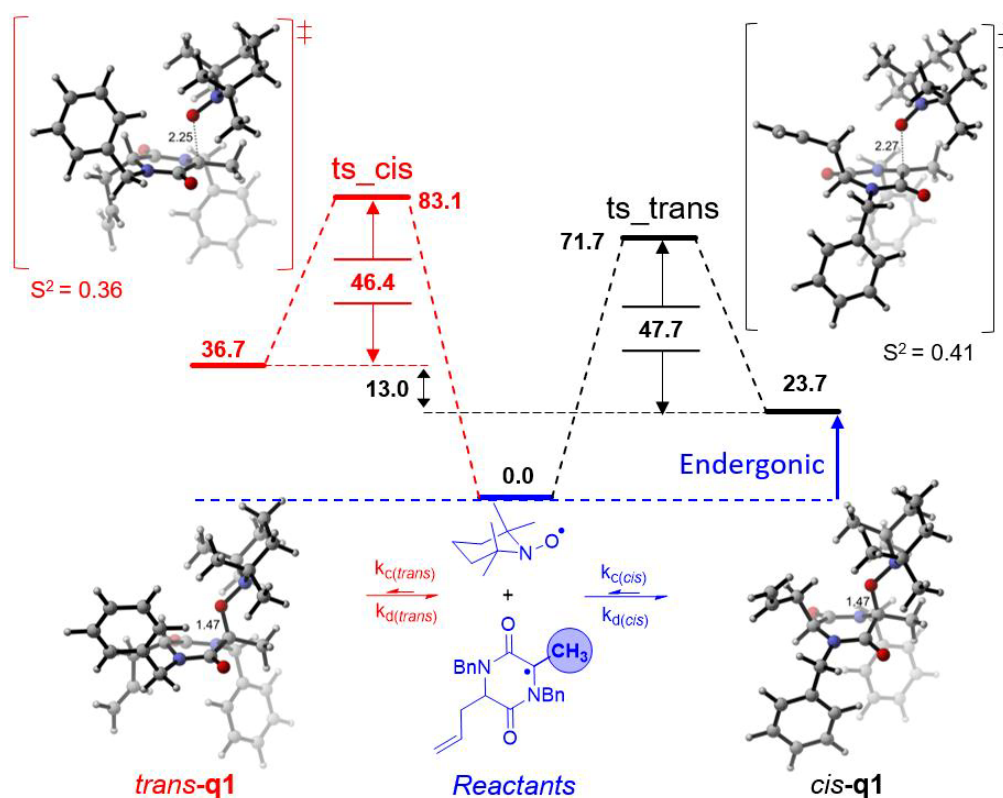


**Figure S5-7.** [Figure S25(B)] Solvation corrected Gibbs energy profiles ( $\Delta G_{\text{sol-sp}}$ , kJ/mol) for *trans-cis* isomerization of QDKP alkoxyamine **q1** calculated at (U)B3LYP/6-31G(d) level of theory. A single point solvation correction calculated for implicit DMSO using SMD solvation model at (U)B3LYP/6-31G(d) level of theory.

#### 5.1.4 References

- (1) *Schrödinger Release 2015–2: MacroModel*, Version 10.8; Schrödinger: LLC, New York, USA, **2015**.
- (2) (a) Hariharan, P. C.; Pople, J. A., *Theor. Chim. Acta* **1973**, *28*, 213-222. (b) Becke, A. D., *J. Chem. Phys.* **1993**, *98*, 5648-5652.
- (3) Graham, D. C.; Menon, A. S.; Goerigk, L.; Grimme, S.; Radom, L., *J. Phys. Chem. A* **2009**, *113*, 9861-9873.
- (4) Marenich, A. V.; Cramer, C. J.; Truhlar, D. G., *J. Phys. Chem. B* **2009**, *113*, 6378-6396.
- (5) Glendening, E. D.; Landis, C. R.; Weinhold, F., *J. Comput. Chem.* **2013**, *34*, 1429-1437.
- (6) Frisch, M. J. T., G. W.; Schlegel, H. B.; Scuseria, G. E.; Robb, M. A.; Cheeseman, J. R.; Scalmani, G.; Barone, V.; Mennucci, B.; Petersson, G. A.; Nakatsuji, H.; Caricato, M.; Li, X.; Hratchian, H. P.; Izmaylov, A. F.; Bloino, J.; Zheng, G.; Sonnenberg, J. L.; Hada, M.; Ehara, M.; Toyota, K.; Fukuda, R.; Hasegawa, J.; Ishida, M.; Nakajima, T.; Honda, Y.; Kitao, O.; Nakai, H.; Vreven, T.; Montgomery, Jr., J. A.; Peralta, J. E.; Ogliaro, F.; Bearpark, M.; Heyd, J. J.; Brothers, E.; Kudin, K. N.; Staroverov, V. N.; Keith, T.; Kobayashi, R.; Normand, J.; Raghavachari, K.; Rendell, A.; Burant, J. C.; Iyengar, S. S.; Tomasi, J.; Cossi, M.; Rega, N.; Millam, J. M.; Klene, M.; Knox, J. E.; Cross, J. B.; Bakken, V.; Adamo, C.; Jaramillo, J.; Gomperts, R.; Stratmann, R. E.; Yazyev, O.; Austin, A. J.; Cammi, R.; Pomelli, C.; Ochterski, J. W.; Martin, R. L.; Morokuma, K.; Zakrzewski, V. G.; Voth, G. A.; Salvador, P.; Dannenberg, J. J.; Dapprich, S.; Daniels, A. D.; Farkas, O.; Foresman, J. B.; Ortiz, J. V.; Cioslowski, J.; Fox, D. J.; *Gaussian 09 Revision D. 01*, Gaussian, Inc., Wallingford CT: **2013**.

## **Chapter 6. A Third Generation of Radical Fluorinating Agents Based on N-Flouro-N-Arylsulfonamides**

Daniel Meyer, Harish Jangra, Fabian Walther, Hendrik Zipse and Philippe Renaud  
*Nat. Commun.* **2018**, *9*, 1-10.

---

### ***Authors contribution***

P.R. proposed the research direction and guided the project. D.M. designed and ran the experimental work with the assistance of F.W. Calculations were designed by H.Z. and H.J., and performed by H.J. The manuscript was jointly written by D.M., P.R., and H.Z.

### ***Copyright***

This research was originally published in the *Nature Communications* with *Open Access* and is reprinted here as the 6<sup>th</sup> chapter of this thesis from *Nat. Commun.* **2018**, 9, 1-10 © The Author(s) 2018.

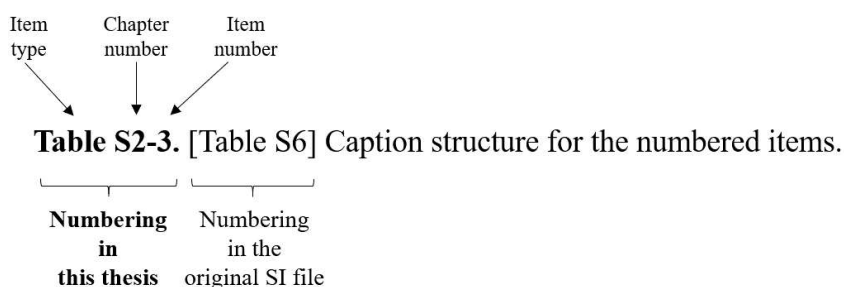
(Link to article: <https://www.nature.com/articles/s41467-018-07196-9>)

Selected supporting material for the computational part of this work is provided at the end of this chapter. For complete supporting information (SI), please follow the link below:

<https://doi.org/10.1038/s41467-018-07196-9>

### ***Additional information***

The accompanying SI is the shorter and altered version of the original content. The items (Tables, Figure, Schemes etc.) may have a different number than what was originally assigned. To make it easier to locate the SI content referred to in the following reprint, the original numbering is also provided in the caption of the numbered items as described below:



ARTICLE

DOI: 10.1038/s41467-018-07196-9

OPEN

# A third generation of radical fluorinating agents based on *N*-fluoro-*N*-arylsulfonamides

Daniel Meyer <sup>1</sup>, Harish Jangra<sup>2</sup>, Fabian Walther<sup>1</sup>, Hendrik Zipse <sup>2</sup> & Philippe Renaud <sup>1</sup>

Radical fluorination has been known for a long time, but synthetic applications were severely limited by the hazardous nature of the first generation of reagents such as F<sub>2</sub> and the strongly electrophilic nature of the second generation of reagents such as *N*-fluorobenzenesulfonimide (NFSI) and Selecfluor<sup>®</sup>. Here, we report the preparation, use and properties of *N*-fluoro-*N*-arylsulfonamides (NFASs), a class of fluorinating reagents suitable for radical fluorination under mild conditions. Their N-F bond dissociation energies (BDE) are 30–45 kJ mol<sup>-1</sup> lower than the N-F BDE of the reagents of the second generation. This favors clean radical fluorination processes over undesired side reactions. The utility of NFASs is demonstrated by a metal-free radical hydrofluorination of alkenes including an efficient remote C-H fluorination via a 1,5-hydrogen atom transfer. NFASs have the potential to become the reagents of choice in many radical fluorination processes.

<sup>1</sup>Department of Chemistry and Biochemistry, University of Bern, Freiestrasse 3, 3012 Bern, Switzerland. <sup>2</sup>Department of Chemistry, LMU München, Butenandtstrasse 5-13, 81377 München, Germany. Correspondence and requests for materials should be addressed to H.Z. (email: [zipse@cup.uni-muenchen.de](mailto:zipse@cup.uni-muenchen.de)) or to P.R. (email: [philippe.renaud@dcb.unibe.ch](mailto:philippe.renaud@dcb.unibe.ch))

The introduction of fluorine atoms into organic molecules significantly changes their physical, chemical, and biological properties, and is therefore very attractive for the preparation of innovative materials, agrochemicals, and pharmaceuticals<sup>1–3</sup>. Moreover, <sup>18</sup>F-labeled organic compounds are of high clinical interest as contrast agents for positron emission tomography (PET)<sup>4–6</sup>. This situation has created a strong demand for efficient fluorination techniques. In the last 30 years, the introduction of fluorine atoms using nucleophilic and electrophilic reagents has led to remarkable advances. Radical fluorination has been known for a long time, but synthetic applications were severely limited by the hazardous nature of the first generation of reagents (Fig. 1a) such as F<sub>2</sub><sup>7</sup>, hypofluorites (ROF)<sup>8</sup>, and XeF<sub>2</sub><sup>9</sup>. Recently, a second generation of reagents, initially developed and optimized for electrophilic fluorination, changed dramatically that picture and radical fluorination is becoming an essential tool for selective fluorination under mild conditions (Fig. 1b)<sup>10–13</sup>. Sammis and co-workers<sup>14</sup> proposed in 2012 that *N*-fluorobenzenesulfonimide (NFSI), Selectfluor<sup>®</sup>, and *N*-fluoropyridinium salts (NFPY), due to their low N–F bond dissociation energies (BDE), may be used for radical fluorination. This hypothesis was confirmed by the description of a radical fluorinative decarboxylation of *tert*-butyl peresters (Fig. 1b)<sup>14</sup> and 2-aryloxy carboxylic acids using NFSI<sup>15</sup> as a source of fluorine atom. NFSI was also used by Zhang et al.<sup>16</sup> for the copper-catalyzed aminofluorination of styrene, by Britton and co-workers<sup>17</sup> for a tetra-*n*-butylammonium decatungstate-catalyzed C(sp<sup>3</sup>)–H bond fluorination, and by Lectka and co-workers<sup>18</sup> for the aminofluorination of cyclopropanes. Following the work of Li on the Ag(I)-catalyzed fluorodecarboxylation with

Selectfluor<sup>®</sup><sup>19,20</sup>, this reagent became the most common reagent for radical fluorination processes<sup>11</sup>. Using this reagent, the decarboxylative fluorination<sup>21–24</sup> has been thoroughly investigated and very recently the fluorination of tertiary alkyl halides was reported<sup>25</sup>. Interestingly, the fluorinative deboronation of alkylpinacolboranes and alkylboronic acids catalyzed by Ag(I) with Selectfluor<sup>®</sup> was reported by Li (Fig. 1b)<sup>26</sup>. Aggarwal and co-workers<sup>27</sup> reported that such a radical process involving Selectfluor<sup>®</sup> was a competing reaction during the electrophilic fluorination of boronate complexes. Boger and Barker<sup>28</sup> developed an Fe(III)/NaBH<sub>4</sub>-mediated free radical Markovnikov hydrofluorination of unactivated alkenes with Selectfluor<sup>®</sup>. A related cobalt-catalyzed hydrofluorination reaction was reported by Hiroya and co-workers<sup>29</sup> using a *N*-fluoropyridine source of atomic fluorine. Groves and co-workers<sup>30,31</sup> developed recently an appealing manganese-catalyzed procedure for C–H fluorination process using the nucleophilic F<sup>–</sup> as the fluorine source.

The second generation of radical fluorinating agents has transformed the field. However, they are often penalized by the necessity to use a transition metal catalyst and by their strong electrophilic/oxidative character. A careful look at the reaction mechanisms shows that they are frequently involved in electron transfer processes and that carbocation intermediates are generated by overoxidation processes. This was clearly demonstrated by Li and co-workers<sup>19</sup> for the non-catalyzed fluorinative decarboxylation of peresters with Selectfluor<sup>®</sup> in the absence of a Ag (I) catalyst. A third generation of reagents designed to work efficiently under mild radical reaction conditions without being involved in electrophilic or electron transfer processes is clearly needed<sup>32,33</sup>. We report here that *N*-fluoro-*N*-arylsulfonamides

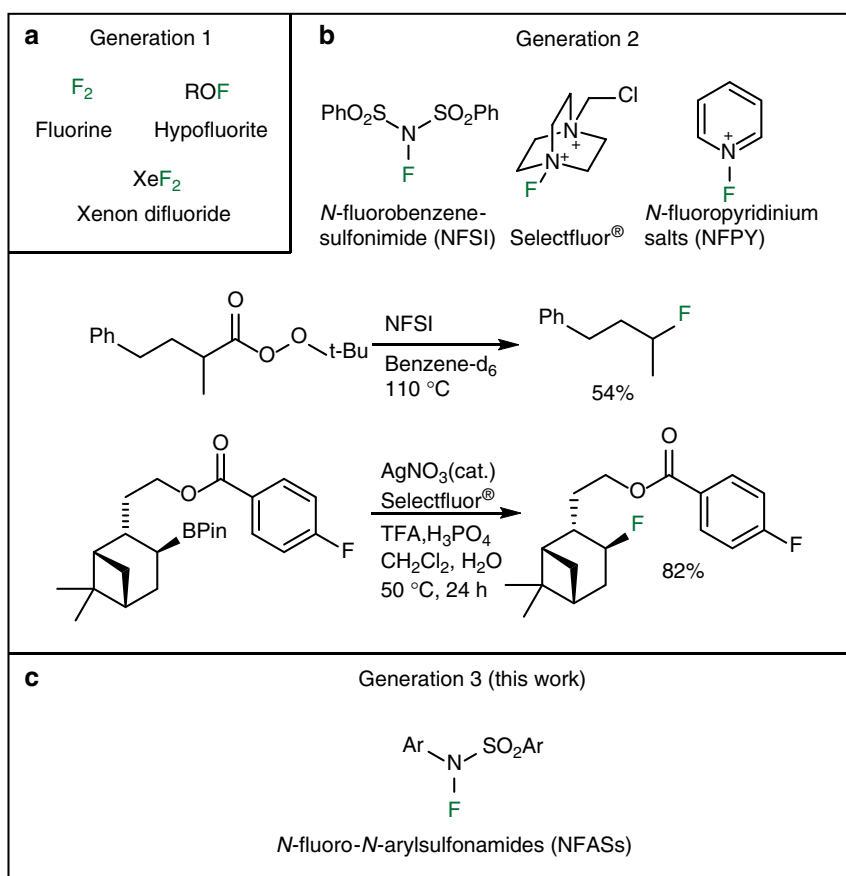


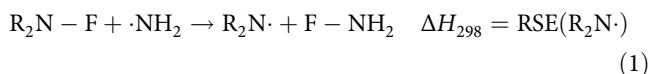
**Fig. 1** The three generations of reagents for radical fluorination. **a** Fluorination reagents of first generation. **b** Example of fluorinative decarboxylation and deboronation reactions using reagents of the second generation. **c** General structure of the *N*-fluoro-*N*-arylsulfonamides (NFASs) described in this work

(NFASs) belong to this third generation of radical fluorinating reagents (Fig. 1c). NFASs have been optimized for the catecholborane-mediated hydrofluorination of alkenes and tested in the fluorinative decarboxylation of preesters.

## Results

**Design of radical fluorinating agents.** Initial investigations of the hydrofluorination of alkenes started with the hydroboration of 1-phenyl-1-cyclohexene **1a** with catecholborane followed by reaction with Selectfluor<sup>®</sup> and NFSI as fluorinating agents (Fig. 2a). Reaction with Selectfluor<sup>®</sup> was highly exothermic and led to decomposition of the intermediate *B*-alkylcatecholborane. No trace of the fluoride **2a** was detected by GC analysis. The reaction with NFSI afforded **2a** in 15% yield. In order to suppress undesired side reactions caused by the electrophilicity of the fluorinating agents, less electrophilic N–F reagents were tested. Benzenesulfonamides **3a–3b** and benzamide **3c** were prepared by fluorination of the corresponding amides<sup>34</sup> and tested, but all three *N*-fluoroamides proved to be inefficient (yields ≤ 4%).

The disappointing results obtained with the *N*-fluoro-*N*-alkylamides **3a–3c** were interpreted as a consequence of a too high BDE of the N–F bonds. In order to put this hypothesis on a quantitative basis, N–F BDEs were calculated for Selectfluor<sup>®</sup>, NFSI, and **3a–3c** in the gas phase and in DMF solution (Fig. 2b). As in previous studies on radical stabilities of *N*-centered radicals, geometry optimizations have been performed at the (U)B3LYP/6–31G(d) level of theory<sup>35</sup>. Thermochemical corrections to 298.15 K have been calculated at the same level of theory using the rigid rotor/harmonic oscillator model. Improved relative energies were obtained using the (RO)B2PLYP/G3MP2Large and G3(MP2)-RAD scheme proposed by Radom and co-workers<sup>36,37</sup>. The stabilities for *N*-centered radicals obtained from fluoramides R<sub>2</sub>N–F have been determined with reference to fluoroamine (H<sub>2</sub>N–F) using the isodesmic fluorine exchange reaction shown in Eq. (1).



$$\text{BDE}(\text{R}_2\text{N}-\text{F}) = \text{RSE}(\text{R}_2\text{N}\cdot) + \text{BDE}(\text{H}_2\text{N}-\text{F}) \quad (2)$$

The reaction enthalpies ( $\Delta H_{298}$ ) obtained from Eq. (1) (commonly referred to as radical stabilization energies of the substrate radicals R<sub>2</sub>N•) can be combined with the reference value for the H<sub>2</sub>N–F parent system (+286.6 kJ mol<sup>-1</sup>)<sup>38</sup> to obtain N–F BDE values of the fluoroamines R<sub>2</sub>N–F as expressed in Eq. (2). The trends in N–F BDE values are very similar at all levels of theory and also in the gas phase and in DMF solution (see Supplementary Figs. 219–221 and Supplementary Tables 4–7). For the sake of brevity we will only discuss the results obtained at the G3(MP2)-RAD level. In DMF solution the N–F BDEs of **3a**, **3b**, and **3c** are calculated to be 263.0, 263.6, and 274.6 kJ mol<sup>-1</sup> (62.9, 63.0, and 65.6 kcal mol<sup>-1</sup>), which is close to the N–F BDE in Selectfluor<sup>®</sup> (265.7 kJ mol<sup>-1</sup>, 63.5 kcal mol<sup>-1</sup>), but slightly higher than in NFSI (259.3 kJ mol<sup>-1</sup>, 62.0 kcal mol<sup>-1</sup>) (Fig. 2b). These results are in line with the fact that such *N*-alkylamidyl radicals are only weakly stabilized<sup>35</sup> and have been used recently for C–H chlorination, bromination, and xanthylation reactions<sup>39–41</sup>.

In order to decrease the N–F BDE while maintaining enough polar effects to favor the fluorination of (nucleophilic) alkyl radicals, *N*-fluoro-*N*-arylsulfonamides (NFASs) **4** were investigated (Fig. 3). A solution phase N–F BDE of 222.3 kJ mol<sup>-1</sup> (53.1 kcal mol<sup>-1</sup>) was calculated for *N*-Fluoro-*N*-(4-(trifluoromethyl)phenyl)benzenesulfonamide **4a**, supporting our assumption that *N*-aryl substituents should lead to lower N–F BDEs due to stabilization of the corresponding amidyl radical by delocalization onto the aromatic ring. Analyzing the impact of electron-withdrawing substituents in the anilide moiety and of electron-donating substituents in the arylsulfonyl moiety of **4a**, we find neither of these to lead to large alterations in the N–F BDE values. In fact, all N–F BDE values calculated for NFASs **4a–4i** cluster in the range from 220.0–226.1 kJ mol<sup>-1</sup> (52.6–54.0 kcal mol<sup>-1</sup>), which is well below that for NFSI (62.0 kcal mol<sup>-1</sup>, this value is in good accordance with the one of 63.4 kcal mol<sup>-1</sup> calculated recently by Xue, Cheng and co-workers<sup>33</sup>).

Attempts to prepare the simple *N*-fluoro-*N*-phenylbenzenesulfonamide were not successful, presumably due to side reactions involving reaction of NFSI with the electron-rich aromatic anilide moiety. After deactivation of the anilide moiety with electron-withdrawing groups (CF<sub>3</sub>, F), the NFASs **4a–4i** were readily prepared by fluorination of the amides upon treatment with Cs<sub>2</sub>CO<sub>3</sub> and NFSI and they could be purified by flash chromatography followed by recrystallization from heptane

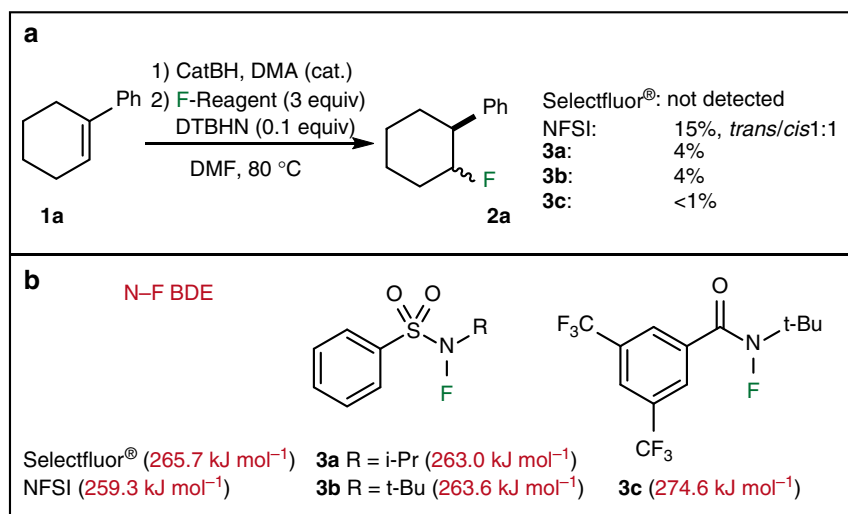


**Fig. 2** Initial attempts of hydrofluorination via formation of *B*-alkylcatecholboranes. **a** Hydrofluorination of 1-phenyl-1-cyclohexene (**1a**) with Selectfluor<sup>®</sup>, NFSI, and *N*-fluoro-*N*-alkylamides **3a–3c**. **b** Solution phase (DMF) N–F bond BDEs ( $\Delta H_{\text{sol}}$ ) calculated at the G3(MP2)-RAD level of theory

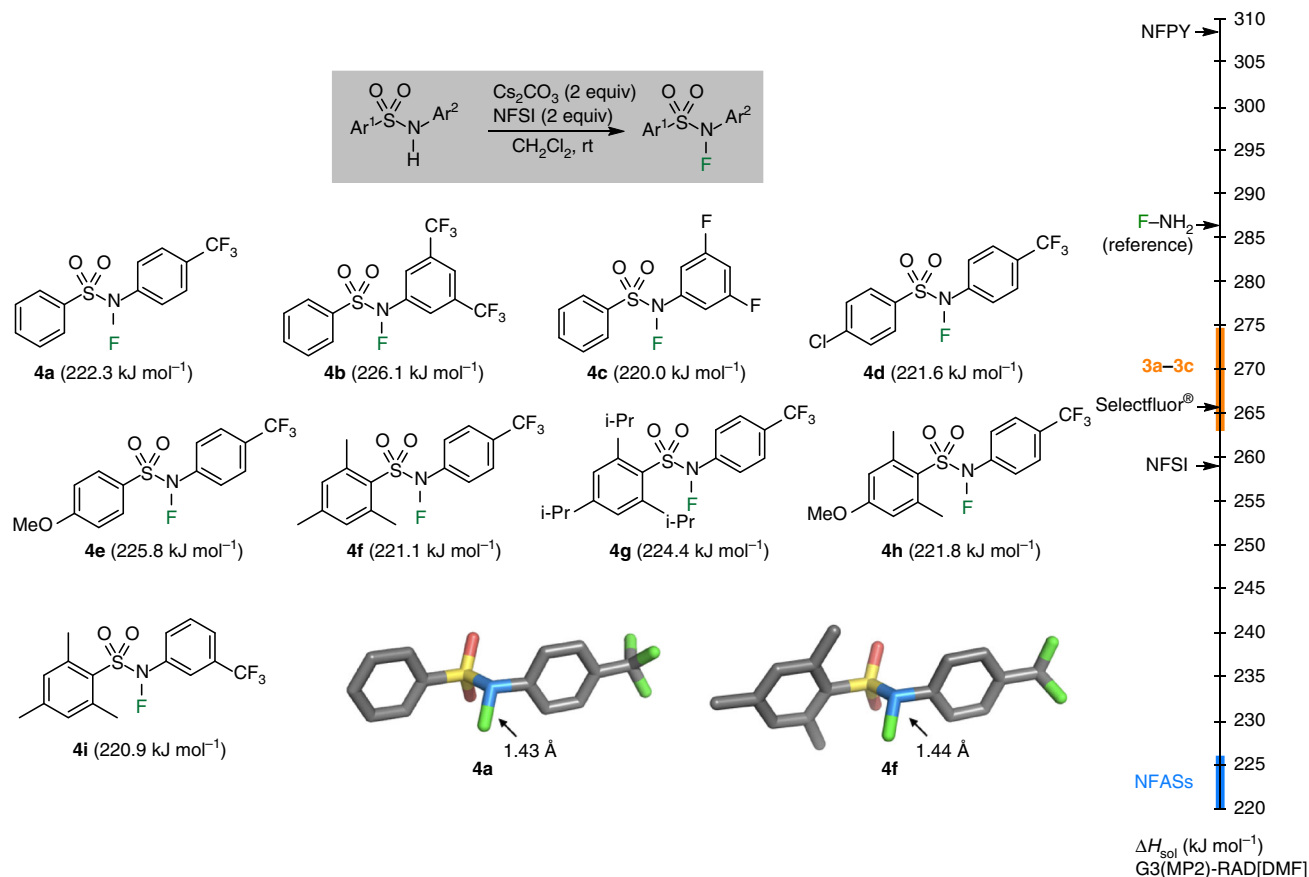
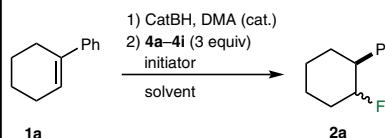


**Fig. 3** Preparation and characterization of NFASs **4a–4i**. X-ray single crystal structure of **4a** and **4f** and solution phase (DMF) N–F BDEs calculated at the G3(MP2)-RAD level of theory

(Fig. 3). The structures of **4a** and **4f** have also been determined by X-ray crystallography and are depicted in Fig. 3. The N–F bond lengths in **4a** and **4f** (1.43 and 1.44 Å, respectively) were found to be marginally longer than the N–F bond length in NFSI (1.42 Å). The structures obtained by X-ray crystallography match well with those calculated at (U)B3LYP/6–31G(d) level (see Supplementary Figs. 1, 2 and 218).

The hydrofluorination of 1-phenyl-1-cyclohexene (**1a**) with NFASs **4a–4i** was examined. Results are summarized in Table 1. The *N*-fluorosulfonamide **4a** was tested first using 0.1 equivalent of DTBHN as the initiator in DMF. The fluorinated product **2a** was obtained in 30% yield together with 8% of phenylcyclohexane and 10% of **1a**. Since DMF is a good hydrogen atom donor, the reaction was tested in benzene and acetonitrile<sup>35</sup>. However, the desired fluoroalkane **2a** was not formed in these less Lewis-basic solvents (Table 1, entries 2–3). Other solvents such as *N*-methylformamide, *N*-methyl-2-pyrrolidone, and hexamethylphosphoramide were also tested, but they provided no improvement over DMF. Using a larger amount of the radical initiator DTBHN led to a slight but reproducible increase of the yield (Table 1, entries 4–5, 45%). The other NFASs **4b–4i** were tested under the optimized reaction conditions of entry 4 (0.5 equivalent DTBHN, DMF at 80 °C). NFASs bearing a second electron-withdrawing group such as **4b–4d** gave lower yields (Table 1, entries 6–8). The other fluorinating agents **4e–4i** provided the desired fluoride **2a** in similar yields (Table 1, entries 9–13, 40–47%). For practical reasons, ease of preparation, and stability, the NFASs **4a** and **4f** were selected for further studies. All the reactions reported in

**Table 1** Hydrofluorination of **1a** with *N*-fluoro-*N*-(aryl)arenesulfonamides **4a–4i**



Entry	F-reagent yield [%] <sup>a</sup>	Initiator (equiv)	Solvent	T (°C)	2a
1	<b>4a</b>	DTBHN (0.1)	DMF	80	30
2	<b>4a</b>	DTBHN (0.1)	Benzene	80	-
3	<b>4a</b>	DTBHN (0.1)	CH <sub>3</sub> CN	80	-
4	<b>4a</b>	DTBHN (0.5)	DMF	80	45
5	<b>4a</b>	DTBHN (1)	DMF	80	45
6	<b>4b</b>	DTBHN (0.5)	DMF	80	9
7	<b>4c</b>	DTBHN (0.5)	DMF	80	23
8	<b>4d</b>	DTBHN (0.5)	DMF	80	30
9	<b>4e</b>	DTBHN (0.5)	DMF	80	41
10	<b>4f</b>	DTBHN (0.5)	DMF	80	47
11	<b>4g</b>	DTBHN (0.5)	DMF	80	43
12	<b>4h</b>	DTBHN (0.5)	DMF	80	41
13	<b>4i</b>	DTBHN (0.5)	DMF	80	40
14	<b>4a</b>	DTBPO (0.5)	DMF	60	47
15	<b>4f</b>	DTBPO (0.5)	DMF	60	51

<sup>a</sup>Yields determined by GC using *n*-undecane as an internal standard

Table 1, except for the bulky **4g** (entry 11), were finished in less than 10 min. Therefore, running the reaction at lower temperature was attempted. At 60 °C, the use of di-*tert*-butyl peroxyoxalate (DTBPO, easily prepared by reacting oxalyl chloride with *tert*-butyl hydroperoxide in the presence of pyridine in DMF) as an initiator<sup>42,43</sup> provided highly reproducible and slightly improved yields of 47% (**4a**) and 51% (**4f**) (Table 1, entries 14 and 15). The reaction is believed to be a chain process involving the reaction of the *N*-arylsulfonamidyl radical with the alkylcatecholborane to provide the desired alkyl radical. By comparison, the yield obtained with NFSI under these optimized conditions was significantly lower (29%). Beside the fluoride **2a**, small amounts of phenylcyclohexane were detected by gas

chromatography in similar quantities with all three fluorinating agents. Interestingly, the presence of the starting alkene **1a** was also observed but in significantly larger proportion with NFSI than with **4a** and **4f** (see Supplementary Table 1 and Supplementary Figs. 3–5). Since the hydroboration process takes place with complete conversion, the formation of the alkene **1a** results from undesired side reactions (see Discussion).

The scope of the metal-free hydrofluorination process was examined with non-terminal alkenes **1a–1i** and NFASs **4a** and **4f** (Fig. 4a). The corresponding secondary and tertiary fluorides **2a–2i** were isolated in 48–68% yields. In many cases, the mesitylenesulfonamide **4f** gave higher yields than the benzene-sulfonamide **4a**. Cyclopentene **1b** was obtained with a good *trans*-

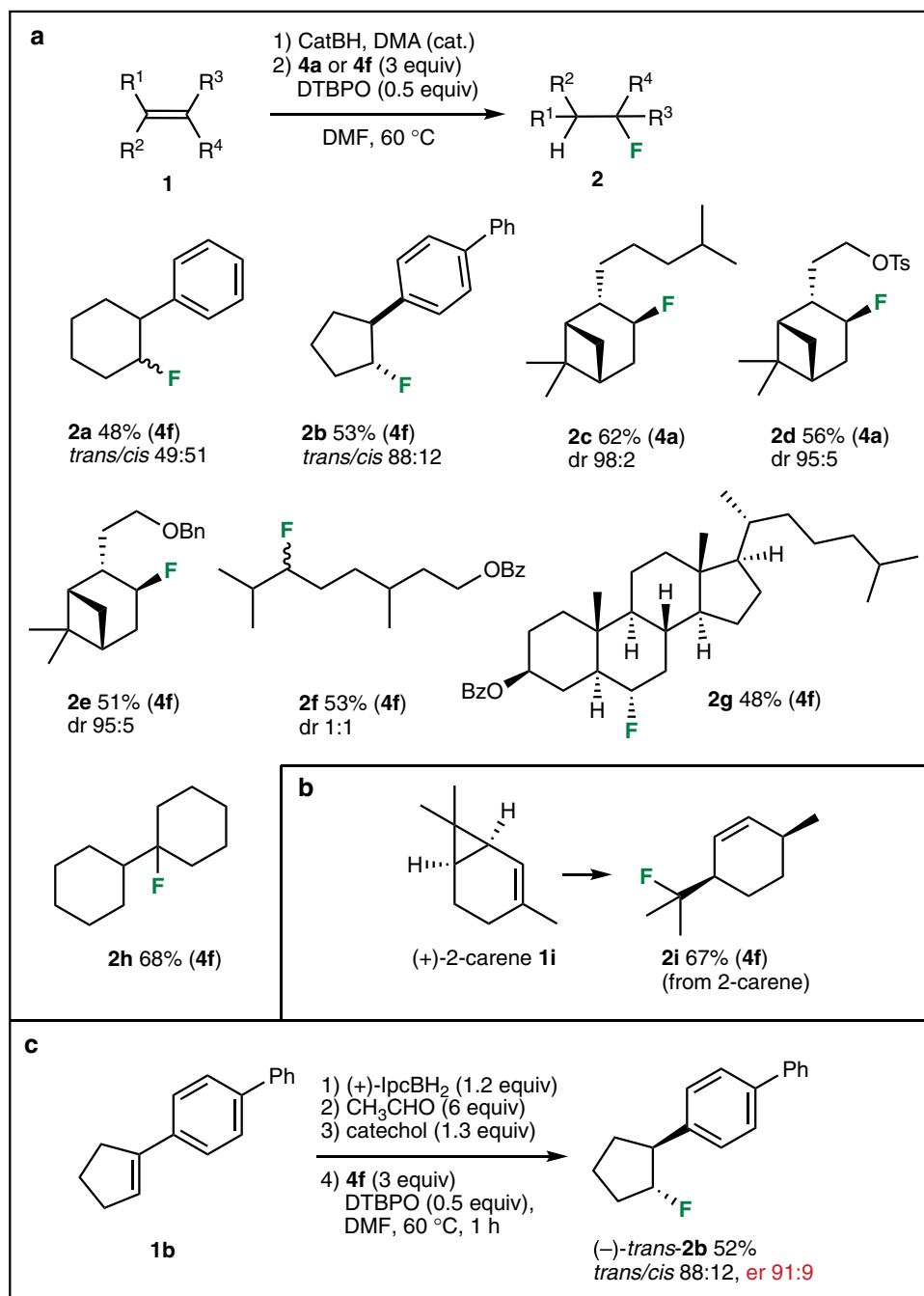


**Fig. 4** Hydrofluorination of non-terminal alkenes. **a** The reaction works efficiently with secondary and tertiary radicals derived from di- and trisubstituted alkenes, respectively. **b** The radical nature of the process is demonstrated by the ring-opening process observed with (+)-2-carene **1i**. **c** Preparation of the enantioenriched fluoride (-)-*trans*-**2b** from alkene **1b** is possible using (+)-isopinocampheylborane in the hydroboration step. Isolated yields are reported

selectivity (*trans/cis* 88:12). The hydrofluorination of the  $\alpha$ -pinene- and nopol-derivatives **1c–1e** afforded **2c–2e** with high diastereoselectivities (*dr*  $\geq$  95:5). The  $\beta$ -citronellyl benzoate **1f** and the cholesteryl benzoate **1g** were successfully hydrofluorinated in 53% and 48% yield, respectively. Preparation of the tertiary fluoride **2h** from 1,1'-bi(cyclohexylidene) (**1h**) worked as expected (68% yield). The presence of a free radical intermediate was demonstrated with (+)-2-carene **1i** that produced the ring-opening product **2i** in 67% yield (Fig. 4b). Finally, based on our recent work on the enantioselective hydroazidation<sup>44</sup>, a one-pot enantioselective hydrofluorination of **1b** was performed (Fig. 4c). This one-pot procedure includes a hydroboration of the alkene with (+)-IpcBH<sub>2</sub>, conversion to the diethyl boronate, transesterification to the *B*-alkylcatecholborane and a final radical fluorination. The fluoride **2b** was isolated in 52% yield and 91:9 enantiomeric ratio.

**Kinetic data.** The rate constants for the fluorine atom transfer process between a secondary alkyl radical and NFSI, **4a** and **4f** were estimated using the cyclooct-1-en-5-yl radical clock<sup>45–47</sup>. The *B*-cyclooct-1-en-5-ylcatecholborane **5** was prepared by hydroboration of 1,5-cyclooctadiene and treated with the three fluorinating agents ([N–F] reagent = 1.2 M, three-fold excess) (Fig. 5a). The reaction with NFSI afforded a 75:25 mixture of the 5-fluorocyclooct-1-ene **6** and 2-fluorobicyclo[3.3.0]octane **7**. Both **4a** and **4f** afforded a nearly equimolar mixture of **6** and **7**. Based on this single concentration experiment and the published rate constant for the cyclization reaction ( $k_c = 3.3 \times 10^4 \text{ s}^{-1}$  at 80 °C)<sup>47</sup>, a rough estimation of the rate constants for fluorine transfer can be made, which for NFSI amounts to  $k_F \approx 10^5 \text{ M}^{-1} \text{ s}^{-1}$  and for the two *N*-fluoro-*N*-aryl (arenesulfonamides) **4a** and **4f** to  $k_F \approx 3 \times 10^4 \text{ M}^{-1} \text{ s}^{-1}$  at 80 °C (Fig. 5b). A preparative reaction was performed with **4f** on 4 mmol scale. It afforded the pure fluorides **6** (31% yield) and **7** (22%) (Fig. 5a).

**Remote fluorination.** The hydrofluorination of terminal alkenes **8a**, **8b**, and **11** was examined next (Fig. 6). The alkene **8a** gave the fluorinated product **9a** in only 7% yield together with 7% of its isomer **9a'** resulting from a radical mediated 1,5-hydrogen shift and 50% of the corresponding alkane **10a**. Running this reaction in DMF-*d*<sub>7</sub> gave **9a** (12%) and **9a'** (11%) together with 29% of the alkane **10a** with less than 5% D-incorporation. The improved

hydrofluorination/reduction ratio demonstrates that the non-deuterated DMF is probably acting as a hydrogen atom donor. However, the absence of deuterium incorporation demonstrates that other sources of hydrogen atoms are also present in the reaction mixture (including the intermediate organoborane and the fluorinating reagent itself). The methylated alkene **8b** was also investigated. The presence of the methyl group was expected to favor the hydrogen atom transfer step. Indeed, product **9b'** (30% yield) became the major fluorinated product. However, a significant amount of alkane **10b** (34%) was still produced. Based on these observations, it became clear that with suitable substrates, the radical hydrofluorination process can be used for efficient remote fluorination via 1,5-hydrogen atom transfer. A related remote fluorination process involving photoredox generated iminyl radicals has been recently reported<sup>24</sup>. This point is demonstrated by the hydrofluorination of the terminal alkene **11** that afforded the fluoride **12** in 68% yield with an excellent *trans* diastereoselectivity.

**Decarboxylative fluorination.** The radical fluorination ability of the NFASs **4a** and **4f** was further tested in the decarboxylative fluorination of *tert*-butyl peresters and compared with NFSI and Selectfluor<sup>®</sup> (Fig. 7). This reaction, due to its non-chain nature, is not expected to be particularly efficient and recent methods have clearly surpassed this procedure<sup>19,23</sup>. However, this simple reaction is very suitable to compare reagents involved in a radical mediated metal-free fluorination process. The decarboxylative fluorination of **13a** using 5 equivalents of NFSI at 110 °C (sealed tube) according to the condition of Sammis, except for the use of benzene instead of benzene-*d*<sub>6</sub>, gave 3-fluoropentadecane **14a** in 5% yield together with a complex mixture of alkenes. This outcome is in line with the result of Li who ran the same reaction in benzene at 110 °C and did not observe the formation of the fluoride **14a**. All subsequent reactions were run in chlorobenzene instead of benzene to avoid the use of a sealed reaction vessel and only 2 equivalents of the fluorinating agent were used. Under these conditions, the reaction was run with NFSI, Selectfluor<sup>®</sup>, and NFASs **4a** and **4f**. NFSI provided the fluoride **14a** in 7% yield, while Selectfluor<sup>®</sup> gave only traces of **14a** (<2%, due to the high polarity of Selectfluor<sup>®</sup>, the reaction was performed in a 1:1 mixture of chlorobenzene and DMPU). Interestingly, both **4a** and **4f** gave the fluoride **14a** in moderate 48% and 47% yield. Similar

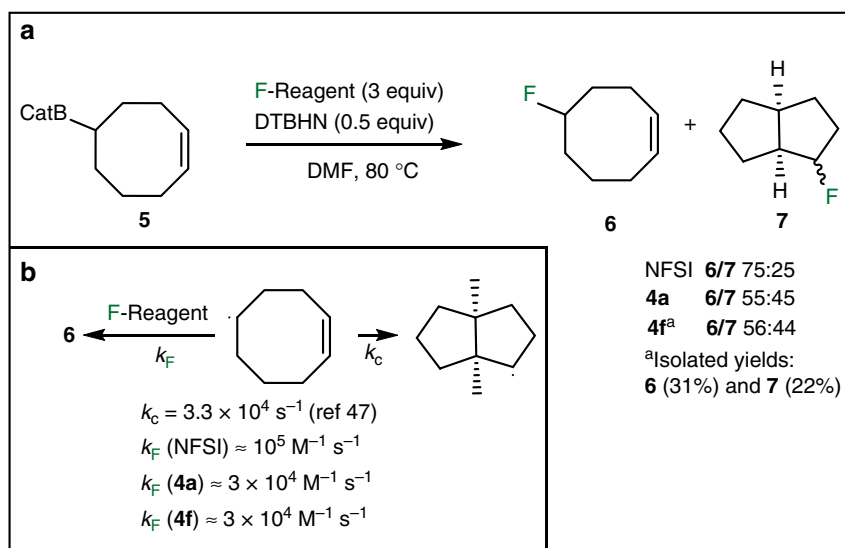


**Fig. 5** Rate constant determination using the (*Z*)-cyclooct-1-en-5-yl radical clock. **a** Fluorination of boronate **5** with NFSI, **4a** and **4f** affords mixtures of mono and bicyclic fluorides **6** and **7**. **b** Estimated rate constants for the radical fluorination

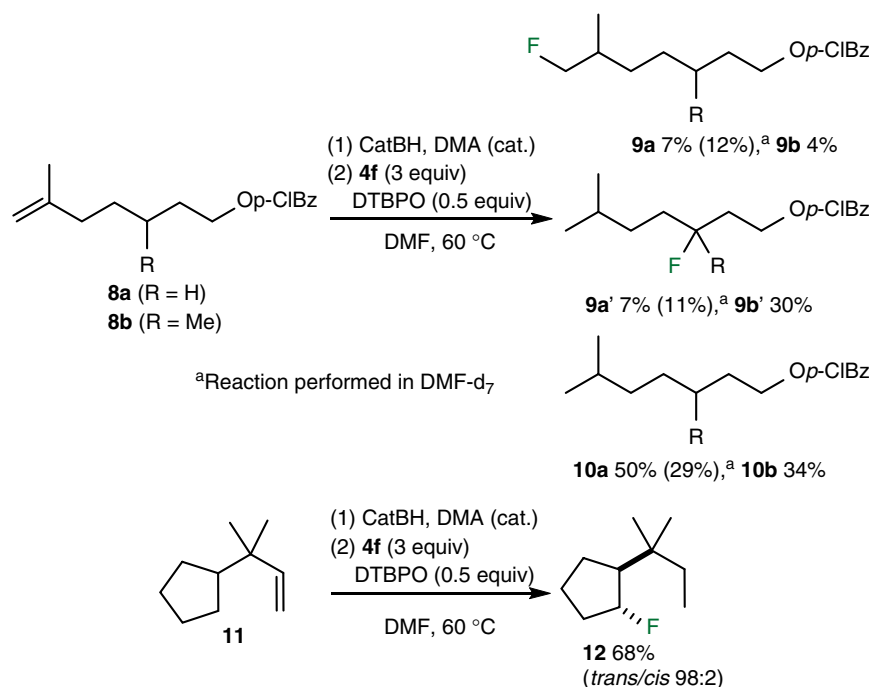


**Fig. 6** Hydrofluorination of terminal alkenes. The lower nucleophilicity of primary alkyl radical slows the direct fluorination and favors hydrogen atom abstraction processes leading to remote fluorination of unactivated C-H bonds (*p*-CIBz = *para*-chlorobenzoyl)

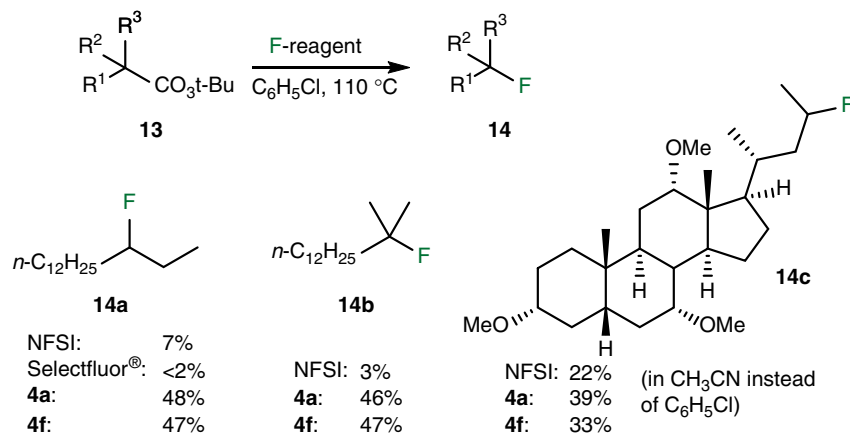


**Fig. 7** Decarboxylative fluorination of *tert*-butyl peresters. The fluorinating reagents of the second generation provide the desired fluorides in significantly lower yield than the one of the third generation due mainly to the formation of alkene side products

results were obtained with the tertiary radical derived from **13b**. Reactions with **4a** and **4f** gave **14b** in 46% and 47% yield accompanied by 35% of the alkenes. NFSI afforded only traces of the product **14b** (3%) together with larger amounts of 2-methyltetradec-2-ene and 2-methyltetradec-1-ene (64%) (see Supplementary Figs. 10 and 11). The cholic acid derivative **13c** was examined next. In that case too, NFSI (22% yield) was inferior to **4a** and **4f** (39% and 33%, respectively). Sammis and co-workers<sup>14</sup> reported a yield of 50% for this reaction when it was performed in deuterated acetonitrile on a 0.05 mmol scale.

**Transition states and discussion.** The higher fluorination rate observed with NFSI relative to the NFASs results is best rationalized by polar effects. The paramount importance of polar effects on the rate of radical reactions is well-established and has

been thoroughly discussed by Giese<sup>48</sup>, Fischer and Radom<sup>49</sup> in their leading review articles. Polar effects have been reported to override thermodynamic effects for radical addition to alkenes<sup>50</sup>. Recently, Xue, Cheng and co-workers have reported that NFSI has a fluorine plus detachment (FPD) value lower than that of *N*-methyl-*N*-fluoro-*p*-toluenesulfonamides by 145.6 kJ mol<sup>-1</sup> (34.8 kcal mol<sup>-1</sup>) in acetonitrile solution. FPD values correlated well with the reactivity of electrophilic fluorinating N-F reagents<sup>32</sup>. The free energy surfaces for the fluorination of the isopropyl radical in DMF solution have therefore been calculated at the (RO)B2PLYP/G3MP2large level for NFSI, **4a**, and **4f**. The calculations show slightly lower barriers for NFSI than for **4a** ( $\Delta G^\ddagger_{298} = +46.1$  vs.  $+51.3$  kJ mol<sup>-1</sup>) and a somewhat higher barrier for **4f** ( $\Delta G^\ddagger_{298} = +56.7$  kJ mol<sup>-1</sup>). The transition states (TSs) for NFSI and **4f** are depicted in Fig. 8a, b, respectively. They are characterized by long C-F (2.32–2.33 Å) and short N-F

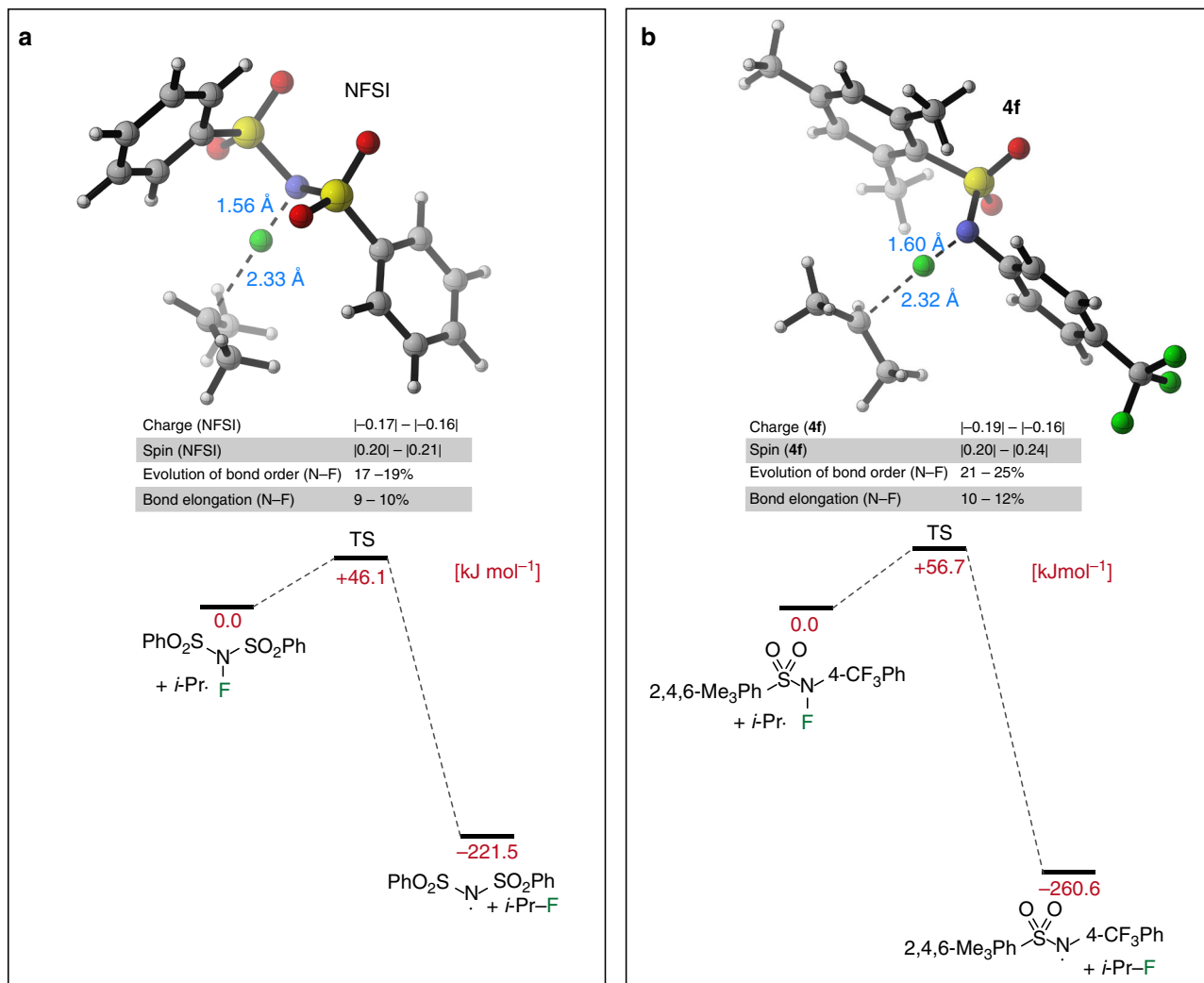


**Fig. 8** Calculated transition states for the fluorination of the isopropyl radical. **a** Free energy surfaces ( $\Delta G_{\text{sol-opt}}$ , in  $\text{kJ mol}^{-1}$ ) in DMF solution for the reaction of isopropyl radical ( $i\text{-Pr}\cdot$ ) with NFSI and **b** **4f** calculated at the (RO)B2PLYP/G3MP2Large level of theory. Distances (in Å), NPA charges and NPA spin distributions have been calculated at the SMD(DMF)/(U)B3LYP/6-31G(d) level of theory. Free energies in solution  $\Delta G_{\text{sol-opt}}$  have been obtained by adding  $\Delta G_{\text{sol}}[(\text{U})\text{B3LYP}/6-31\text{G}(\text{d})/\text{SMD}(\text{DMF})]$  to  $\Delta G_{298}[(\text{RO})\text{B2PLYP}/\text{G3MP2Large}/\text{SMD}(\text{DMF})/(\text{U})\text{B3LYP}/6-31\text{G}(\text{d})]$

(1.56–1.60 Å) distances typical for very early transition states. The transition state charge distribution is very similar for all three fluorination reagents and indicates a charge transfer component of ca. 0.15–0.19e from the radical to the reagent. This charge transfer component is quite important for such an early transition state, where only 20–24% of the spin density has left the substrate isopropyl radical. Interestingly, the most significant difference between the NFSI and NFAS transition states concerns the length of the N–F bond (1.56 Å for NFSI against 1.58–1.60 Å for NFASs). In other words, the more electrophilic NFSI is able to accommodate the extra electron density caused by the charge transfer with less cleavage of the N–F bond relative to the NFASs leading to an extra stabilization of the transition state in full accordance with the polar effects aforementioned.

Both in the hydrofluorination and the decarboxylation processes, NFSI provided the desired fluorinated products in significantly lower yields than NFASs despite the observed higher rate constant for the fluorine atom transfer. For both reactions, the analysis of the crude reaction mixture showed the formation of larger quantities of alkenes for reactions involving NFSI relative to NFASs. The alkenes may result from at least three

competitive processes: a single electron transfer (SET) between the fluorinating agent and the secondary alkyl radical leading to a cation followed by loss of a proton; a post fluorination acid catalyzed HF elimination; a radical cross-disproportionation process involving the alkyl radical and the imidyl radical (NFSI) or the amidyl radicals (NFASs). All these three processes are expected to be more prominent when reactions are run with NFSI relative to NFASs. Indeed, the electrophilic nature of NFSI should favor the SET process (pathway a). The HF elimination (pathway b) was experimentally found to be triggered by HF itself. The presence of HF may result from electrophilic reactions between the fluorinating agents and DMF or *tert*-butanol (hydrofluorination reaction) or traces of water (decarboxylation reaction)<sup>51,52</sup>. Finally, the radical cross-disproportionation process (pathway c) is expected to be favored by the more reactive NFSI-derived imidyl radical over the amidyl radicals derived from NFASs. The difference of reactivity of these radicals is well-illustrated by the calculated N–H BDE for the corresponding amides (H–NFSI: BDE 454.2  $\text{kJ mol}^{-1}$ ; H–**4a** BDE 393.0  $\text{kJ mol}^{-1}$ ; H–**4f** BDE 390.6  $\text{kJ mol}^{-1}$  (see Supplementary Fig. 222 and Supplementary Table 8).

## Discussion

We have developed NFASs, a class of fluorinating reagents suitable for radical fluorination under mild conditions. The bond dissociation energies of the NFASs are 30–45 kJ mol<sup>-1</sup> lower than the one of NFSI and Selectfluor<sup>®</sup>. This favors smooth radical processes over side reactions caused by the electrophilic and oxidant properties of the previous generations of radical fluorinating agents. NFASs were successfully used in a metal-free hydrofluorination method involving hydroboration with catecholborane followed by a radical deborylative fluorination. By using monoisopinocampheylborane (IpcBH<sub>2</sub>) in the hydroboration step, the asymmetric hydrofluorination of trisubstituted alkenes can easily be performed. Remarkably, NFASs also proved to be superior to NFSI in decarboxylative fluorination of *tert*-butyl peresters demonstrating that they are attractive reagents for a broad range of radical mediated fluorination processes. They have the potential to deeply transform the field of radical fluorination by enabling powerful transformations under milder conditions than the former generations of fluorinating agents.

## Methods

**N-Fluoro-N-(4-(trifluoromethyl)phenyl)benzenesulfonamide (4a).** To a solution of *N*-(4-(trifluoromethyl)phenyl)benzenesulfonamide (12.05 g, 40.0 mmol) in DCM (400 mL) was added Cs<sub>2</sub>CO<sub>3</sub> (16.90 g, 52.0 mmol) and stirred at room temperature for 60 min. Then, NFSI (16.40 g, 52.0 mmol) was added and the mixture was allowed to stir at room temperature for 5 h. The mixture was diluted with pentane (400 mL), filtered, and concentrated. The product was purified by rapid column chromatography (heptane/TBME 85:15). Concentration of the collected chromatography fractions to a volume of 100–150 mL promoted the crystallization. The solution was stored for one night at 4 °C to yield **4a** (10.15 g, 80%) as a slightly yellow solid. *R*<sub>f</sub> 0.40 (heptane/TBME 9:1); m.p. 74–75 °C.

**N-Fluoro-2,4,6-trimethyl-N-(4-(trifluoromethyl)phenyl)-benzenesulfonamide (4f).** According to the procedure for **4a**, starting from *N*-(4-(trifluoromethyl)phenyl)-2,4,6-trimethylbenzenesulfonamide (17.17 g, 50.0 mmol). Crystallization at 4 °C yielded **4f** (16.16 g, 89%) as a slightly yellow solid. *R*<sub>f</sub> 0.55 (heptane/TBME 9:1); m.p. 116–117 °C.

**General procedure for the hydrofluorination of alkenes.** To a solution of the alkene (1.0 mmol), *N,N*-dimethylacetamide (14 μL, 0.15 mmol) in dry DCM (1 mL) was added dropwise catecholborane (0.23 mL, 2.2 mmol) at 0 °C. The reaction was allowed to stir at 30 °C for 16 h. The mixture was cooled to 0 °C and *t*-BuOH (0.124 mL, 1.3 mmol) was added. The reaction mixture was stirred at room temperature for 15 min, concentrated under vacuum, and the residue was dissolved in dry DMF (2 mL). DTBPO (117 mg, 0.5 mmol) and **4a** or **4f** (3.0 mmol) were added. The mixture was heated to 60 °C (preheated oil bath was used) and stirred at this temperature for 30–45 min. The crude product was purified by column chromatography.

## Data availability

Data supporting the findings of this work are available within the paper and its Supplementary Information files and from the corresponding authors on request. Source data for Supplementary Tables 9, 16 and 17 are provided as supplementary data. CCDCs 1828679 and 1828684 contain the supplementary crystallographic data for compound **4a** and **4f**, respectively. These data can be obtained free of charge from The Cambridge Crystallographic Data Centre via [http://www.ccdc.cam.ac.uk/data\\_request/cif](http://www.ccdc.cam.ac.uk/data_request/cif)

Received: 6 June 2018 Accepted: 16 October 2018

Published online: 20 November 2018

## References

- Müller, K., Faeh, C. & Diederich, F. Fluorine in pharmaceuticals: looking beyond intuition. *Science* **317**, 1881–1886 (2007).
- Purser, S., Moore, P. R., Swallow, S. & Gouverneur, V. Fluorine in medicinal chemistry. *Chem. Soc. Rev.* **37**, 320–330 (2008).
- O'Hagan, D. Understanding organofluorine chemistry. An introduction to the C–F bond. *Chem. Soc. Rev.* **37**, 308–319 (2008).
- Ametamey, S. M., Honer, M. & Schubiger, P. A. Molecular imaging with PET. *Chem. Rev.* **108**, 1501–1516 (2008).
- Miller, P. W., Long, N. J., Vilar, R. & Gee, A. D. Synthesis of <sup>11</sup>C, <sup>18</sup>F, <sup>15</sup>O, and <sup>13</sup>N radiolabels for positron emission tomography. *Angew. Chem. Int. Ed.* **47**, 8998–9033 (2008).
- Brooks, A. F., Topczewski, J. J., Ichiishi, N., Sanford, M. S. & Scott, P. J. H. Late-stage [18F]fluorination: new solutions to old problems. *Chem. Sci.* **5**, 4545–4553 (2014).
- Rozen, S. Elemental fluorine as a “legitimate” reagent for selective fluorination of organic compounds. *Acc. Chem. Res.* **21**, 307–312 (1988).
- Wang, N. & Rowland, F. S. Trifluoromethyl hypofluorite: a fluorine-donating radical scavenger. *J. Phys. Chem.* **89**, 5154–5155 (1985).
- Patrick, T. B., Khazaali, S., Nadjji, S., Hering-Smith, K. & Reif, D. Mechanistic studies of fluorodecarboxylation with xenon difluoride. *J. Org. Chem.* **58**, 705–708 (1993).
- Sibi, M. P. & Landais, Y. C(sp<sup>3</sup>)–F bond formation: a free-radical approach. *Angew. Chem. Int. Ed.* **52**, 3570–3572 (2013).
- Chatalova-Sazepin, C., Hemelaere, R., Paquin, J.-F. & Sammis, G. M. Recent advances in radical fluorination. *Synthesis* **47**, 2554–2569 (2015).
- Yan, H. & Zhu, C. Recent advances in radical-mediated fluorination through C–H and C–C bond cleavage. *Sci. China Chem.* **60**, 214–222 (2016).
- Lantaño, B. & Postigo, A. Radical fluorination reactions by thermal and photoinduced methods. *Org. Biomol. Chem.* **15**, 9954–9973 (2017).
- Rueda-Becerril, M. et al. Fluorine transfer to alkyl radicals. *J. Am. Chem. Soc.* **134**, 4026–4029 (2012).
- Leung, J. C. T. & Sammis, G. M. Radical decarboxylative fluorination of arylacetic acids using *N*-fluorobenzenesulfonimide and a photosensitizer. *Eur. J. Org. Chem.* **2015**, 2197–2204 (2015).
- Zhang, H., Song, Y., Zhao, J., Zhang, J. & Zhang, Q. Regioselective radical aminofluorination of styrenes. *Angew. Chem. Int. Ed.* **53**, 11079–11083 (2014).
- Halperin, S. D., Fan, H., Chang, S., Martin, R. E. & Britton, R. A convenient photocatalytic fluorination of unactivated C–H bonds. *Angew. Chem. Int. Ed.* **53**, 4690–4693 (2014).
- Pitts, C. R., Ling, B., Snyder, J. A., Bragg, A. E. & Lectka, T. Aminofluorination of cyclopropanes: a multifold approach through a common, catalytically generated intermediate. *J. Am. Chem. Soc.* **138**, 6598–6609 (2016).
- Yin, F., Wang, Z., Li, Z. & Li, C. Silver-catalyzed decarboxylative fluorination of aliphatic carboxylic acids in aqueous solution. *J. Am. Chem. Soc.* **134**, 10401–10404 (2012).
- Patel, N. R. & Flowers, R. A. II Mechanistic study of silver-catalyzed decarboxylative fluorination. *J. Org. Chem.* **80**, 5834–5841 (2015).
- Rueda-Becerril, M. et al. Direct C–F bond formation using photoredox catalysis. *J. Am. Chem. Soc.* **136**, 2637–2641 (2014).
- Leung, J. C. T. et al. Photo-fluorodecarboxylation of 2-aryloxy and 2-aryl carboxylic acids. *Angew. Chem. Int. Ed.* **51**, 10804–10807 (2012).
- Ventre, S., Petronijevic, F. R. & MacMillan, D. W. C. Decarboxylative fluorination of aliphatic carboxylic acids via photoredox catalysis. *J. Am. Chem. Soc.* **137**, 5654–5657 (2015).
- Dauncey, E. M., Morcillo, S. P., Douglas, J. J., Sheikh, N. S. & Leonori, D. Photoinduced remote functionalisations by iminyl radical promoted C–C and C–H bond cleavage cascades. *Angew. Chem. Int. Ed.* **57**, 744–748 (2018).
- Chen, H. et al. Selective radical fluorination of tertiary alkyl halides at room temperature. *Angew. Chem. Int. Ed.* **56**, 15411–15415 (2017).
- Li, Z., Wang, Z., Zhu, L., Tan, X. & Li, C. Silver-catalyzed radical fluorination of alkylboronates in aqueous solution. *J. Am. Chem. Soc.* **136**, 16439–16443 (2014).
- Sandford, C., Rasappan, R. & Aggarwal, V. K. Synthesis of enantioenriched alkylfluorides by the fluorination of boronate complexes. *J. Am. Chem. Soc.* **137**, 10100–10103 (2015).
- Barker, T. J. & Boger, D. L. Fe(III)/NaBH<sub>4</sub>-mediated free radical hydrofluorination of unactivated alkenes. *J. Am. Chem. Soc.* **134**, 13588–13591 (2012).
- Shigehisa, H., Nishi, E., Fujisawa, M. & Hiroya, K. Cobalt-catalyzed hydrofluorination of unactivated olefins: a radical approach of fluorine transfer. *Org. Lett.* **15**, 5158–5161 (2013).
- Liu, W. et al. Oxidative aliphatic C–H fluorination with fluoride ion catalyzed by a manganese porphyrin. *Science* **337**, 1322–1325 (2012).
- Huang, X. et al. Late stage benzylic C–H fluorination with [18F]fluoride for PET imaging. *J. Am. Chem. Soc.* **136**, 6842–6845 (2014).
- Xue, X.-S., Wang, Y., Li, M. & Cheng, J.-P. Comprehensive energetic scale for quantitatively estimating the fluorinating potential of N–F reagents in electrophilic fluorinations. *J. Org. Chem.* **81**, 4280–4289 (2016).
- Yang, J.-D., Wang, Y., Xue, X.-S. & Cheng, J.-P. A systematic evaluation of the N–F bond strength of electrophilic N–F reagents: hints for atomic fluorine donating ability. *J. Org. Chem.* **82**, 4129–4135 (2017).
- Taylor, D. M. & Meier, G. P. A facile transfer fluorination approach to the synthesis of *N*-fluoro sulfonamides. *Tetrahedron Lett.* **41**, 3291–3294 (2000).
- Šakić, D. & Zipse, H. Radical stability as a guideline in C–H Amination reactions. *Adv. Synth. Catal.* **358**, 3983–3991 (2016).

36. Graham, D. C., Menon, A. S., Goerigk, L., Grimme, S. & Radom, L. Optimization and basis-set dependence of a restricted-open-shell form of B2-PLYP double-hybrid density functional theory. *J. Phys. Chem. A* **113**, 9861–9873 (2009).
37. Henry, D. J., Sullivan, M. B. & Radom, L. G3-RAD and G3X-RAD: modified Gaussian-3 (G3) and Gaussian-3X (G3X) procedures for radical thermochemistry. *J. Chem. Phys.* **118**, 4849–4860 (2003).
38. Luo, Y.-R. *Comprehensive Handbook of Chemical Bond Energies* (CRC Press, Boca Raton, FL, 2007).
39. Schmidt, V. A., Quinn, R. K., Brusoe, A. T. & Alexanian, E. J. Site-selective aliphatic C-H bromination using N-bromoamides and visible light. *J. Am. Chem. Soc.* **136**, 14389–14392 (2014).
40. Czaplyski, W. L., Na, C. G. & Alexanian, E. J. C–H xanthylation: a synthetic platform for alkane functionalization. *J. Am. Chem. Soc.* **138**, 13854–13857 (2016).
41. Quinn, R. K. et al. Site-selective aliphatic C–H chlorination using N-chloroamides enables a synthesis of chlorolissoclimide. *J. Am. Chem. Soc.* **138**, 696–702 (2016).
42. Bartlett, P. D., Benzing, E. P. & Pincock, R. E. Peresters. Di-*t*-butylperoxyoxalate. *J. Am. Chem. Soc.* **82**, 1762–1768 (1960).
43. Abdallah, D. et al. Multi-armed, TEMPO-functionalized unimolecular initiators for starburst dendrimer synthesis via stable free radical polymerization. I. Tri azo-functionalized unimer. *Can. J. Chem.* **82**, 1393–1402 (2004).
44. Meyer, D. & Renaud, P. Enantioselective hydroazidation of trisubstituted non-activated alkenes. *Angew. Chem. Int. Ed.* **56**, 10858–10861 (2017).
45. Griller, D. & Ingold, K. U. Free-radical clocks. *Acc. Chem. Res.* **13**, 317–323 (1980).
46. Newcomb, M. in *Radicals in Organic Synthesis* Vol. 1 (eds. Renaud, P. & Sibi, M. P.) Ch. 3.1, 317–336 (Wiley-VCH, 2001).
47. Villa, G., Povie, G. & Renaud, P. Radical chain reduction of alkylboron compounds with catechols. *J. Am. Chem. Soc.* **133**, 5913–5920 (2011).
48. Giese, B. Formation of CC bonds by addition of free radicals to alkenes. *Angew. Chem. Int. Ed.* **22**, 753–764 (1983).
49. Fischer, H. & Radom, L. Factors controlling the addition of carbon-centered radicals to alkenes—an experimental and theoretical perspective. *Angew. Chem. Int. Ed.* **40**, 1340–1371 (2001).
50. Giese, B. & Kretzschmar, G. Phenyleffekte bei radikalischen Additionen an Alkene. *Chem. Ber.* **116**, 3267–3270 (1983).
51. Lal, G. S., Pez, G. P. & Syvret, R. G. Electrophilic NF fluorinating agents. *Chem. Rev.* **96**, 1737–1756 (1996).
52. Zupan, M., Papez, M. & Stavber, S. Reactions of the N-F class of fluorinating reagents with solvents. *J. Fluor. Chem.* **78**, 137–140 (1996).

## Acknowledgements

The Swiss National Science Foundation (Project 200020\_172621) and the University of Bern are gratefully acknowledged for their support. We thank the Leibniz Supercomputing Centre ([www.lrz.de](http://www.lrz.de)) for generous allocation of computational resources. We are very grateful to Lars Gnägi and Michael Hofstetter for their investigation of side reactions and to Konrad Uhlmann for his support in gas chromatography analyses.

## Author contributions

P.R. proposed the research direction and guided the project. D.M. designed and run the experimental work with the assistance of F.W. Calculations were designed by H.Z. and H. J., and performed by H.J. The manuscript was jointly written by D.M., P.R., and H.Z.

## Additional information

**Supplementary Information** accompanies this paper at <https://doi.org/10.1038/s41467-018-07196-9>.

**Competing interests:** The authors declare no competing interests.

**Reprints and permission** information is available online at <http://npg.nature.com/reprintsandpermissions/>

**Publisher's note:** Springer Nature remains neutral with regard to jurisdictional claims in published maps and institutional affiliations.



**Open Access** This article is licensed under a Creative Commons Attribution 4.0 International License, which permits use, sharing, adaptation, distribution and reproduction in any medium or format, as long as you give appropriate credit to the original author(s) and the source, provide a link to the Creative Commons license, and indicate if changes were made. The images or other third party material in this article are included in the article's Creative Commons license, unless indicated otherwise in a credit line to the material. If material is not included in the article's Creative Commons license and your intended use is not permitted by statutory regulation or exceeds the permitted use, you will need to obtain permission directly from the copyright holder. To view a copy of this license, visit <http://creativecommons.org/licenses/by/4.0/>.

© The Author(s) 2018

## 6.1 Supporting Information

### For: A Third Generation of Radical Fluorinating Agents Based on N-Flouro-N-Arylsulfonamides

#### 6.1.1 Methodology

As in previous studies on radical stabilities,<sup>1</sup> geometry optimizations have been performed with a combination of the (U)B3LYP hybrid functional<sup>2</sup> and the 6-31G(d) basis set<sup>3</sup> in the gas phase. Thermochemical corrections (corr.  $\Delta H$  &  $\Delta G$ ) to 298.15 K have been calculated at the same level of theory using the rigid rotor/harmonic oscillator model. Enthalpies ( $\Delta H_{298}$ ) and Gibbs energies ( $\Delta G_{298}$ ) at B3LYP/6-31G(d) level have been obtained through addition of corr.  $\Delta G$  and corr.  $\Delta H$  to  $\Delta E_{\text{tot}}$  respectively. Improved single point total electronic energies ( $\Delta E_{\text{tot}}$ ) are obtained using the (RO)B2PLYP<sup>4</sup>/G3MP2Large and G3(MP2)-RAD scheme proposed by Radom et al.<sup>5</sup> Final enthalpies ( $\Delta H_{298}$ ) and Gibbs energies ( $\Delta G_{298}$ ) have been obtained through a combination of  $\Delta E_{\text{tot}}$  calculated at (RO)B2PLYP/G3MP2Large and G3(MP2)-RAD with the thermochemical corrections (corr.  $\Delta G$  and corr.  $\Delta H$ ) calculated at B3LYP/6-31G(d) level. A scaling factor of 0.9806 has been used for thermal correction to the G3(MP2)-RAD scheme. Single point solvation energies ( $\Delta G_{\text{solv}}$ ) for DMF were calculated for gas phase optimized geometries using the SMD<sup>6</sup> continuum solvation model and subsequently added to gas phase energies to obtain solution phase energies that will be designated solution enthalpies ( $\Delta H_{\text{sol}} = \Delta H_{298} + \Delta G_{\text{solv}}$ ) and solution free energies ( $\Delta G_{\text{sol}} = \Delta G_{298} + \Delta G_{\text{solv}}$ ). In an alternative approach, geometry optimizations were carried out in the presence of the SMD continuum solvation model for DMF at the (U)B3LYP/6-31G(d) level. The Gibbs energies calculated using the implicit DMF optimized geometry are designated as  $\Delta G_{\text{sol-opt}}$ . Radical stabilization energies (RSE) for N-centered radicals generated by N-F homolytic bond cleavage in fluoroamines are measured with reference to fluoramine ( $\text{H}_2\text{N-F}$ ) using the isodesmic fluorine exchange reaction shown in equ. 1a.  $\text{R}_2\text{N-F}$  bond dissociation energies (BDE) can then be derived from the calculated RSE values through the addition of the reference N-F BDE value in  $\text{H}_2\text{N-F}$  (286.6 kJ/mol)<sup>7</sup> as expressed in equ. 1b.



$$\text{BDE}_{\text{R}_2\text{N-F}} = \text{RSE}_{\text{R}_2\text{N-F}} + \text{BDE}_{\text{H}_2\text{N-F}}^{\text{Exp}} \quad (1b)$$

In a completely analogous manner, N-H bond BDE values in the respective amines ( $\text{R}_2\text{N-H}$ ) are calculated using  $\text{NH}_3$  as a reference. BDE values for important reference molecules are listed in Table S1.

**Table S6-1.** [Table S1] Experimental and theoretical BDE values for reference molecules.

(Fluoro)Amine	BDE (kcal/mol)	BDE (kJ/mol)	Methods
F-NH <sub>2</sub>	68.5	<b>286.6*</b>	Derived from $\Delta_f H^0$ (NIST database) <sup>7</sup>
H-NH <sub>2</sub>	107.57 ± 0.06	<b>450.08 ± 0.24*</b>	Photolysis <sup>7,9</sup>
F-NH <sub>2</sub>		291.7	W1w <sup>8</sup>
H-NH <sub>2</sub>		450.3	W1w <sup>8</sup>

\*Value used as a reference.

Potential energy surfaces (PESs): Geometry optimizations for all stationary points (minima, complexes and TS) along the PES have been performed at (U)B3LYP/6-31G(d) level in the gas phase. Energy minima, complexes and TSs were confirmed by vibrational frequency calculation with 0, 0, and 1 imaginary frequencies, respectively. All stationary points were checked for wavefunction stability (stable=opt). The nature of transition states was further confirmed by IRC

calculations [15 steps in both directions (reverse/forward) with stepsize=3] followed by geometry optimization to the next minimum. In cases of very flat PES(s), manual displacement away from the TS(s) followed by geometry optimization was employed. NBO charges were calculated using the NBO6 module.<sup>10</sup> All calculations have been performed with Gaussian 09, revision D. 01.<sup>11</sup>

### 6.1.2 Structural Comparison (X-Ray vs QM)

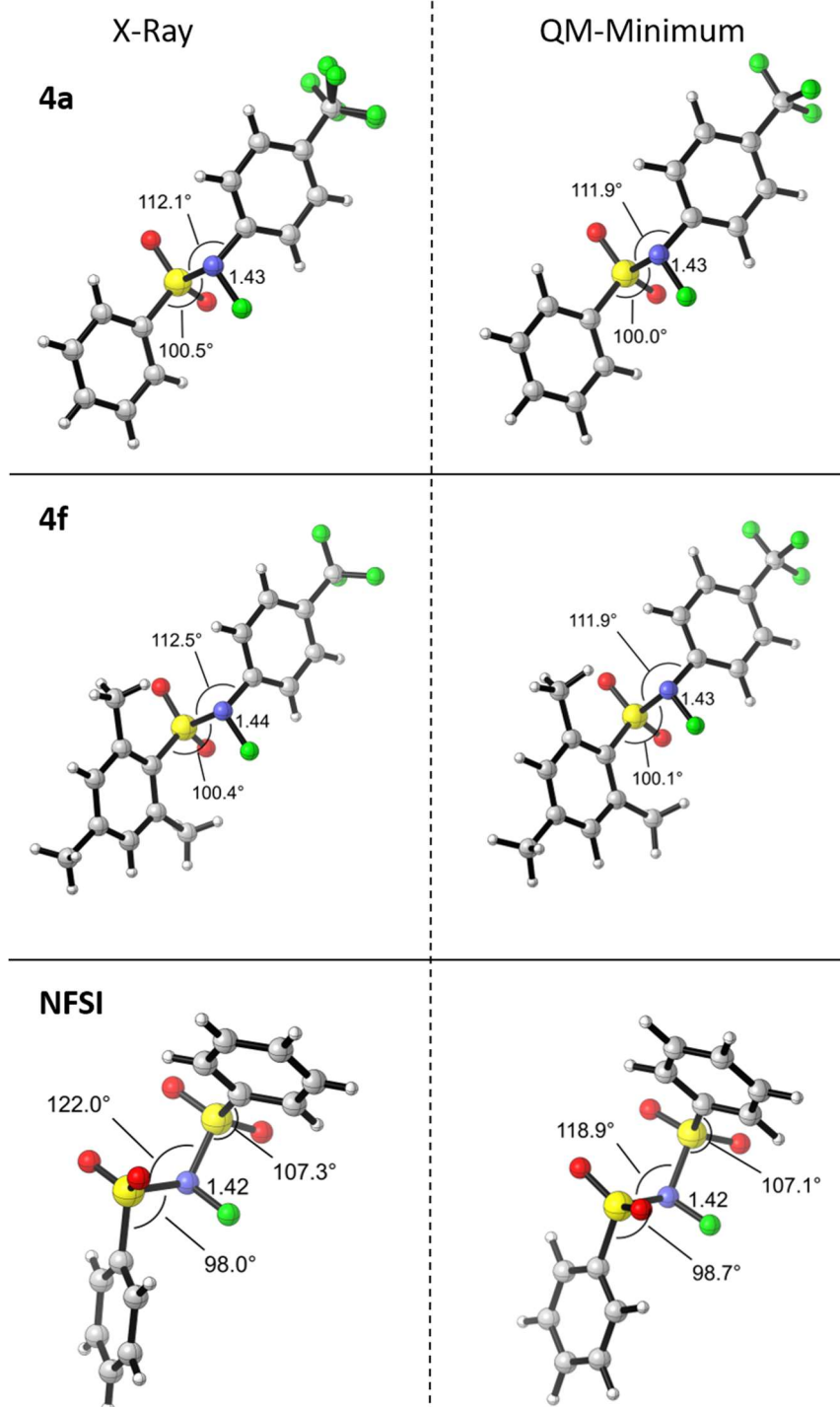


**Figure S6-1.** [Figure S1] Structural comparison between X-ray crystal structures and the corresponding gas phase QM minima obtained at the B3LYP/6-31G(d) level of theory. Distances are given in Å.

6.1.3 Bond Strengths (F—NR<sub>2</sub>)

**Scheme S6-1.** [Scheme S3] Gas phase ( $\Delta H_{298}$ ) and solution phase (DMF,  $\Delta H_{\text{sol}} = \Delta H_{298} + \Delta G_{\text{solv}}$ ) F—NR<sub>2</sub> BDEs and RSEs calculated at the G3(MP2)-RAD level of theory.  $\Delta G_{\text{solv}}$  (single point solvation energy) have been calculated at the SMD(DMF)/(U)B3LYP/6-31G(d)//(U)B3LYP/6-31G(d,p) level of theory.

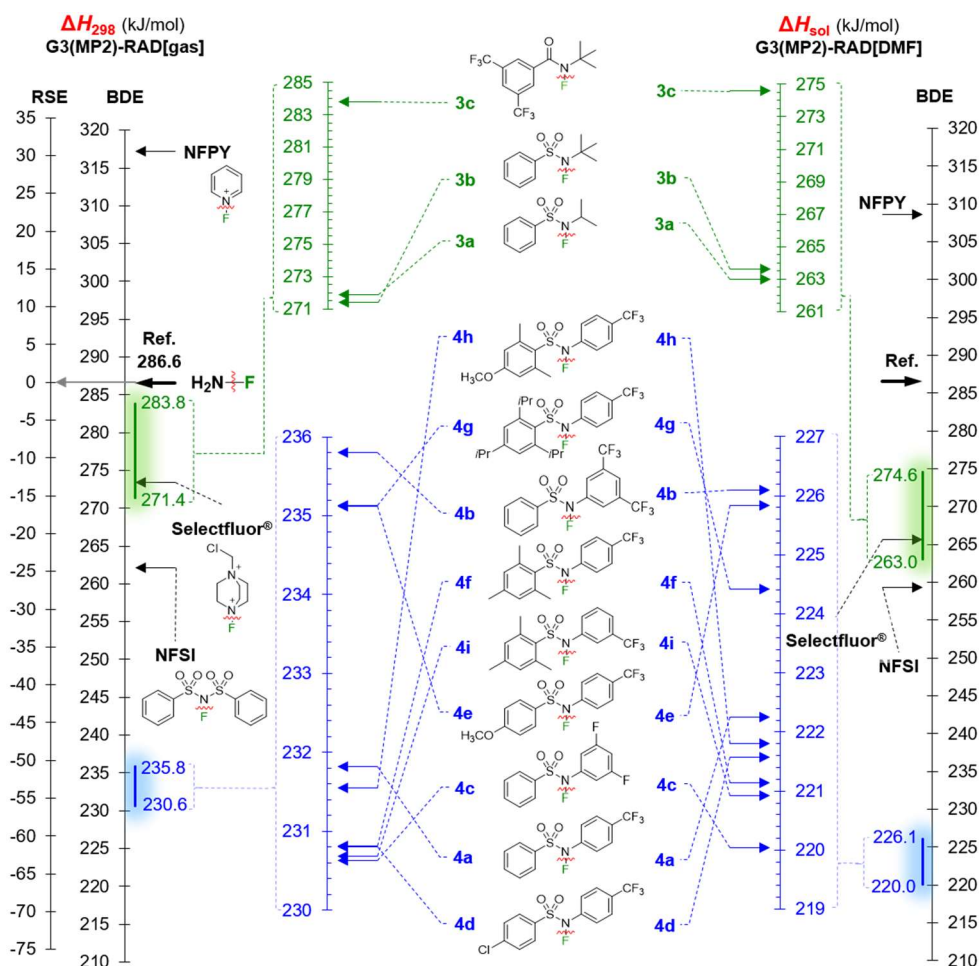
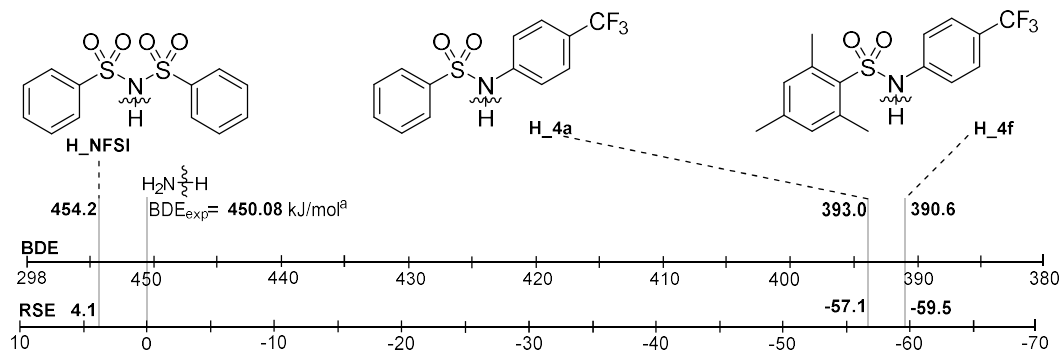


**Table S6-2.** [Table S4] Gas phase ( $\Delta H_{298}$ ) and solution phase (DMF,  $\Delta H_{\text{sol}} = \Delta H_{298} + \Delta G_{\text{solv}}$ ) F—NR<sub>2</sub> BDEs and RSEs calculated at different levels of theory. Ref. [BDE, NH<sub>2</sub>—F = 286.6]

System	(U)B3LYP/6-31G(d)				(RO)B2PLYP/G3MP2Large				G3(MP2)-RAD			
	$\Delta H_{298}$		$\Delta H_{\text{sol}}$		$\Delta H_{298}$		$\Delta H_{\text{sol}}$		$\Delta H_{298}$		$\Delta H_{\text{sol}}$	
	RSE	BDE	RSE	BDE	RSE	BDE	RSE	BDE	RSE	BDE	RSE	BDE
3a	-18.5	268.1	-27.3	259.3	-21.8	264.8	-30.6	256.0	-14.7	271.9	-23.6	263.0
3b	-18.4	268.2	-26.4	260.2	-22.9	263.7	-30.8	255.8	-15.2	271.4	-23.0	263.6
3c	-7.8	278.8	-16.6	270.0	-10.0	276.6	-18.6	268.0	-2.8	283.8	-12.0	274.6
4a	-63.8	222.8	-74.4	212.2	-64.2	222.4	-73.7	212.9	-54.8	231.8	-64.3	222.3
4b	-60.4	226.2	-71.5	215.1	-60.1	226.5	-69.9	216.7	-50.8	235.8	-60.5	226.1
4c	-63.6	223.0	-75.2	211.4	-65.1	221.5	-75.7	210.9	-56.0	230.6	-66.6	220.0
4d	-65.3	221.3	-75.8	210.8	-65.7	220.9	-75.0	211.6	-55.8	230.8	-65.0	221.6
4e	-61.7	224.9	-71.7	214.9	-60.9	225.7	-70.1	216.5	-51.5	235.1	-60.8	225.8
4f	-61.0	225.6	-71.2	215.4	-64.5	222.1	-74.8	211.8	-55.8	230.8	-65.5	221.1
4g	-60.3	226.3	-71.3	215.3	-64.6	222.0	-75.2	211.4	-51.5	235.1	-62.2	224.4
4h	-59.9	226.7	-70.2	216.4	-63.4	223.2	-73.6	213.0	-55.1	231.5	-64.8	221.8
4i	-61.0	225.6	-71.4	215.2	-64.6	222.0	-75.0	211.6	-55.9	230.7	-65.7	220.9
NFSI	-25.6	261.0	-36.3	250.3	-29.5	257.1	-36.9	249.7	-24.5	262.1	-27.3	259.3
Selectfluor®	-23.1	263.5	-30.9	255.7	-25.8	260.8	-33.6	253.0	-13.1	273.5	-20.9	265.7
NFPY	31.2	317.8	22.6	309.2	26.5	313.1	17.9	304.5	30.6	317.2	22.0	308.6

### 6.1.4 Bond Strengths (H—NR<sub>2</sub>)

**Scheme S6-2.** [Scheme S4] Gas phase ( $\Delta H_{298}$ ) H—NR<sub>2</sub> BDEs, (in kJ/mol) and RSEs, (in kJ/mol) relative to the NH<sub>3</sub>/•NH<sub>2</sub> reference system calculated at the G3(MP2)-RAD level of theory.



<sup>a</sup>See Table S6-1.

**Table S6-3.** [Table S6] RSEs (in kJ/mol) relative to the NH<sub>3</sub>/•NH<sub>2</sub> reference for the systems listed in Scheme S4 at different levels of theory.

System	(U)B3LYP/6-31G(d)[gas]			(RO)B2PLYP/G3MP2Large[gas]			G3(MP2)-RAD[gas]		
	$\Delta E_{rot}$	$\Delta H_{298}$	$\Delta G_{298}$	$\Delta E_{rot}$	$\Delta H_{298}$	$\Delta G_{298}$	$\Delta E_{rot}$	$\Delta H_{298}$	$\Delta G_{298}$
<b>H_4a</b>									
Boltzmann Avg.	-79.59	-74.64	-82.05	-68.23	-63.30	-70.96	-61.95	<b>-57.12</b>	-64.75
Best Conf.	-79.01	-74.03	-81.01	-67.90	-62.92	-69.99	-61.64	-56.77	-63.88
<b>H_4f</b>									
Boltzmann Avg.	-83.53	-78.44	-83.02	-72.02	-67.15	-74.10	-64.49	<b>-59.47</b>	-66.74
Best Conf.	-82.57	-77.39	-82.07	-71.19	-66.30	-73.23	-63.81	-59.02	-65.94
<b>H_NFSI</b>									
Boltzmann Avg.	-14.72	-9.06	-15.17	-5.93	-0.26	-5.84	-1.40	<b>4.14</b>	-1.52
Best Conf.	-15.26	-9.60	-15.33	-6.22	-0.56	-6.28	-1.46	4.08	-1.63

### 6.1.5 Mechanistic Investigation

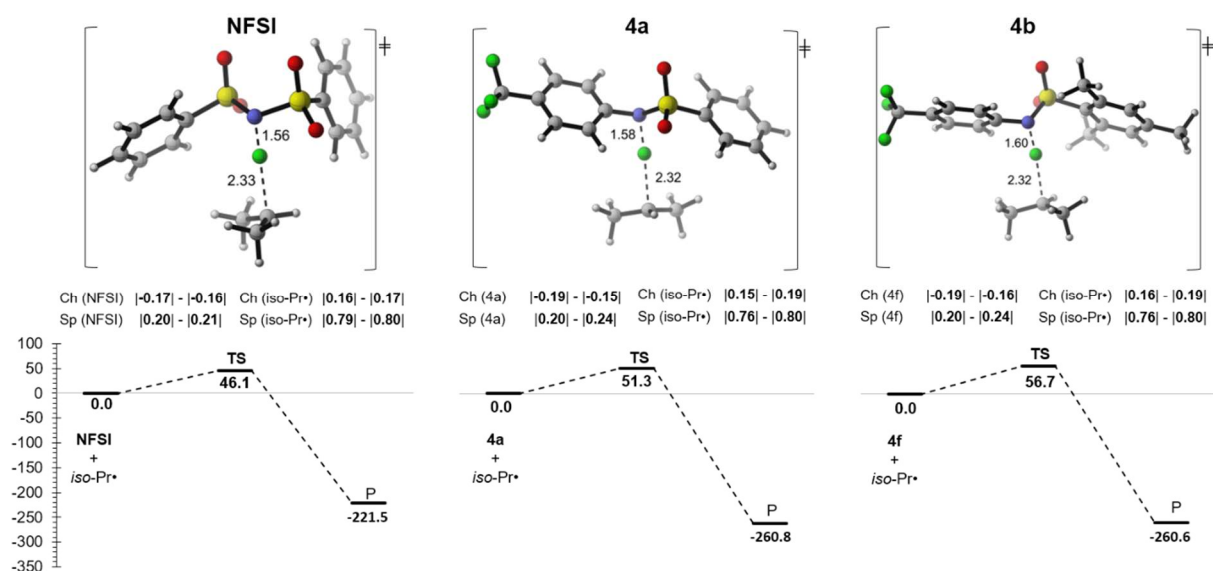


**Figure S6-2.** [Figure S7] Solution phase optimized (DMF,opt) free energy ( $\Delta G_{sol-opt}$ ) surfaces (in kJ/mol) for the fluorine atom transfer process between *iso-Pr*• and NFSI, 4a and 4f calculated at the (RO)B2PLYP/G3MP2Large level of theory. Charge/spin is calculated using the NBO6 module at the SMD(DMF)/(U)B3LYP/6-31G(d) level of theory.

**Table S6-4.** [Table S12] Solvation phase optimized (DMF,opt) free energies ( $\Delta G_{\text{sol-opt}}$ , in kJ/mol) for reactant complexes (RCs), transition states (TSs) and product complexes (PCs) energies relative to separate reactants (ref.) for the fluorine atom transfer process from NFSI, **4a** and **4f** to *iso-Pr* $\bullet$  calculated at different levels of theory.

System (Filename)	(U)B3LYP/6-31G(d)[DMF,opt]			(RO)B2PLYP/G3MP2Large[DMF,opt] <sup>a</sup>		
	RC	TS	PC	RC	TS	PC
<b>NFSI + iso-Pr<math>\bullet</math> (Ref.)</b>						
nfsi_ipr_ts_25	29.4	<b>44.3</b>	-184.4	29.3	<b>46.1</b>	-185.1
nfsi_ipr_ts_32	26.8	47.1	<b>-186.2</b>	30.8	53.6	<b>-190.7</b>
nfsi_ipr_ts_16	27.2	47.2	-184.4	27.4	48.4	-185.1
nfsi_ipr_ts_30	29.4	47.2	-184.4	29.3	48.4	-185.1
nfsi_ipr_ts_20	<b>26.7</b>	49.1	-184.7	<b>26.3</b>	50.5	-185.7
nfsi_ipr_ts_34	28.6	49.3	-183.4	33.5	55.8	-182.1
nfsi_ipr_ts_15	29.8	50.1	-175.1	32.4	54.9	-178.1
nfsi_ipr_ts_23	27.0	50.4	-185.4	30.1	57.0	-184.7
nfsi_ipr_ts_1	29.6	51.8	-174.4	31.5	56.3	-176.4
Separate Product			<b>-216.8</b>			<b>-221.5</b>
<b>4a + iso-Pr<math>\bullet</math> (Ref.)</b>						
a4_ipr_ts_13	26.4	<b>45.3</b>	<b>-226.9</b>	28.4	51.7	<b>-232.1</b>
a4_ipr_ts_16	30.1	45.5	-225.9	32.7	<b>51.3</b>	-228.9
a4_ipr_ts_15	<b>26.0</b>	46.6	-224.4	31.2	52.5	-229.5
a4_ipr_ts_10	34.3	49.4	-222.1	39.1	54.5	-226.1
a4_ipr_ts_2	30.2	50.6	-225.0	28.3	52.0	-226.5
a4_ipr_ts_12	33.2	52.3	-221.8	34.6	56.5	-226.2
a4_ipr_ts_1	30.7	53.4	-212.8	27.1	54.4	-221.7
a4_ipr_ts_9	36.4	54.1	-221.1	41.2	59.0	-225.0
a4_ipr_ts_7	27.9	55.2	-222.9	<b>24.2</b>	56.2	-219.5
Separate Product			<b>-253.1</b>			<b>-260.8</b>
<b>4f + iso-Pr<math>\bullet</math> (Ref.)</b>						
f4_ipr_ts_6	<b>26.6</b>	<b>53.1</b>	-220.2	<b>27.4</b>	<b>56.7</b>	-226.8
f4_ipr_ts_9	-	54.7	-224.3	-	57.2	-229.7
f4_ipr_ts_8	30.9	55.0	<b>-225.2</b>	29.8	57.6	<b>-231.6</b>
f4_ipr_ts_4	32.2	57.2	-224.5	32.6	58.9	-225.8
f4_ipr_ts_15	33.8	66.7	-217.7	30.4	64.3	-222.3
Separate Product			<b>-251.5</b>			<b>-260.6</b>

<sup>a</sup> $\Delta G_{\text{sol-opt}} = \Delta E_{\text{tot}} + \text{corr. } \Delta G + \Delta G_{\text{sol-v}}$ ; corr.  $\Delta G$ , corr.  $\Delta H$ , and  $\Delta G_{\text{sol-v}}$  were calculated at SMD(DMF)/(U)B3LYP/6-31G(d) level.  $\Delta E_{\text{tot}}$  was calculated at (RO)B2PLYP/G3MP2Large// SMD(DMF)/(U)B3LYP/6-31G(d) level

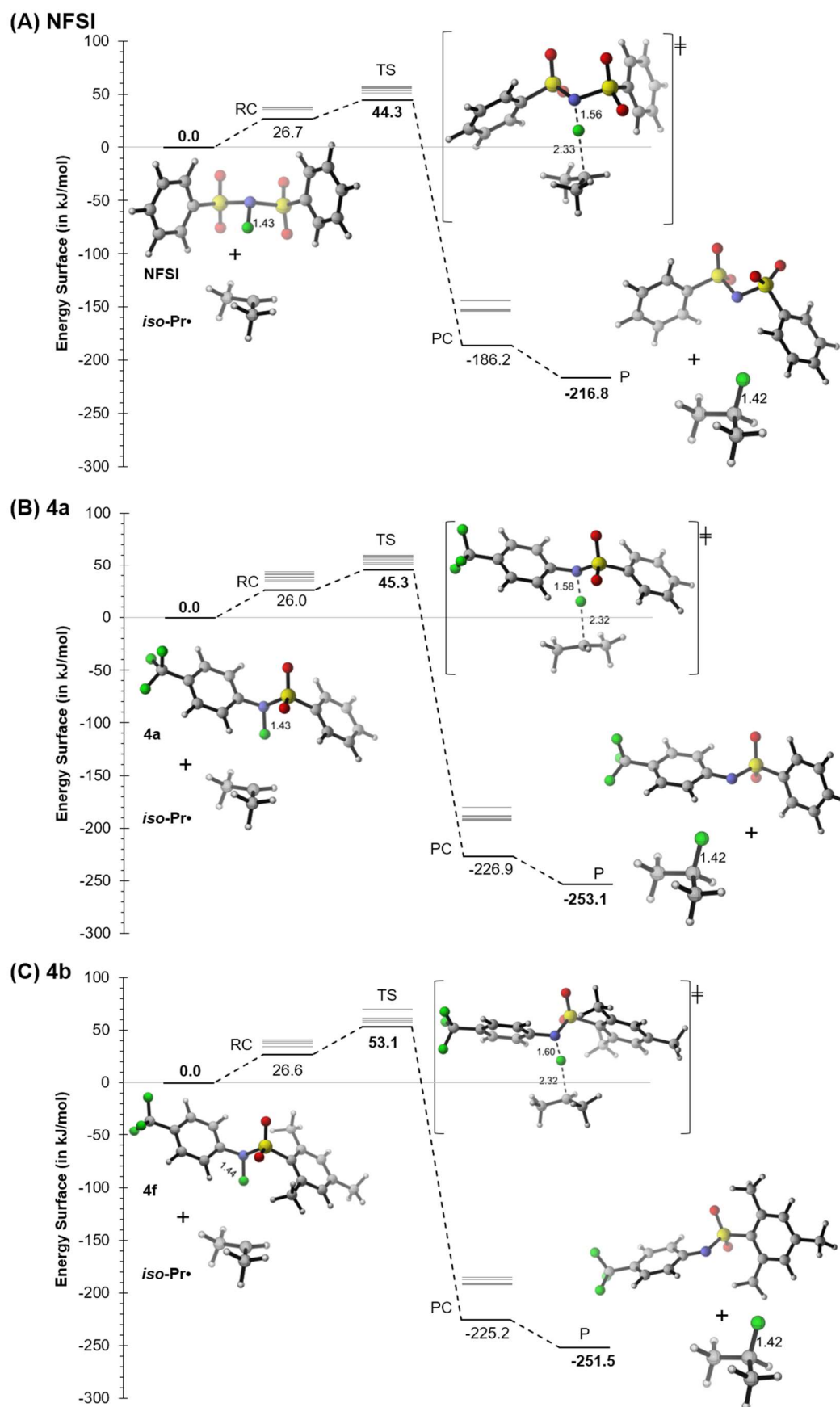
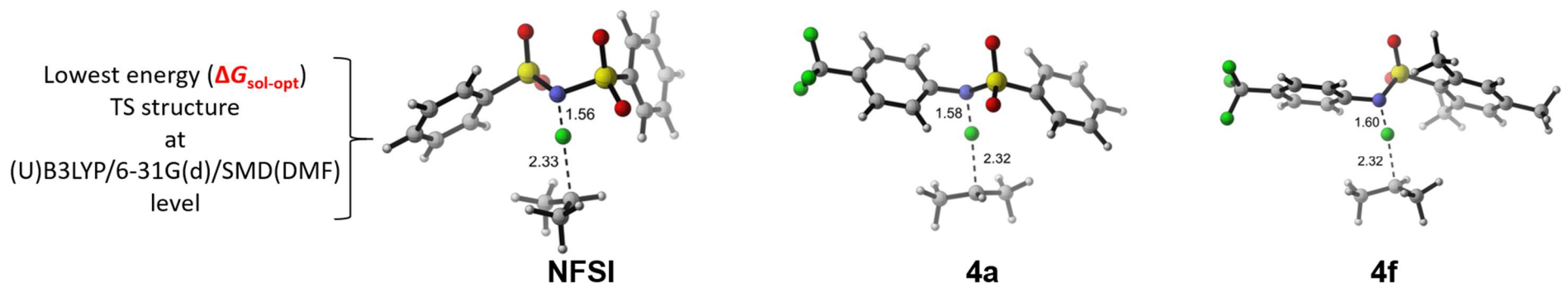


**Figure S6-3.** Solution phase optimized (DMF,opt) free energy ( $\Delta G_{\text{sol-opt}}$ ) surfaces (in kJ/mol) for the fluorine atom transfer process between *iso-Pr*<sup>•</sup> and (A) NFSI, (B) 4a and (C) 4f calculated at SMD(DMF)/(U)B3LYP/6-31G(d) level. Faded bars are used to show the conformational space.

## 6.1.6 Charge and Spin Analysis (Solution Phase Optimized)



<b>N-F Bond</b>			
% Bond Elongation (Distance) <sup>a</sup>	9 - 10%	10 - 11%	10 - 12%
% Evolution of Bond Order (%E <sub>v</sub> ) <sup>b</sup>	17 - 19%	20 - 23%	21 - 25%
<b>C-F Bond</b>			
% Bond Elongation (Distance) <sup>c</sup>	64 - 65%	61 - 64%	61 - 63%
% Evolution of Bond Order (%E <sub>v</sub> ) <sup>d</sup>	82 - 83%	80 - 84%	80 - 83%
<b>Charge on Fluorinating Reagents in TS</b>			
Mulliken-Solvent(DMF)	-0.16  -  -0.15	-0.17  -  -0.14	-0.18  -  -0.14
NBO6-Solvent(DMF)	-0.17  -  -0.16	-0.19  -  -0.15	-0.19  -  -0.16
<b>Spin on Fluorinating Reagents in TS</b>			
Mulliken-Solvent(DMF)	0.19  -  0.20	0.19  -  0.23	0.20  -  0.24
NBO6-Solvent(DMF)	0.20  -  0.21	0.20  -  0.24	0.20  -  0.24

**Figure S6-4.** [Figure S8] TS analysis for spin and charge distribution and % of bond breaking and formation for fluorine atom transfer. This analysis is conducted over implicit solvation optimized geometries at the SMD(DMF)/(U)B3LYP/6-31G(d) level of theory. % Bond elongation is the deviation of bond distance in the TS to the avg. bond distances in reactants<sup>a</sup>/products<sup>c</sup>. % Evolution of bond order (%E<sub>v</sub>) is the ratio of the Wiberg Index (B<sub>i</sub>) of the TS to the avg. B<sub>i</sub> of reactants<sup>b</sup>/products<sup>d</sup>. All properties are provided as a range that is calculated over conformational space (see Table S6-5 for more details). Distances are given in Å.

**Table S6-5.** [Table S13] Transition state analysis for spin and charge distribution and % of bond breaking and formation calculated at the SMD(DMF)/(U)B3LYP/6-31G(d) level of theory. NBO charge/spin is calculated using the NBO6 module.

Molecule	% Bond Elongation (Distance)				% Evolution of Bond Order [Wiberg Index(B <sub>i</sub> )]				Charge		Spin	
	N-F	C-F	%N-F =	% C-F =	N-F	C-F	% N-F =	%C-F =	Mulliken	NBO	Mulliken	NBO
	Dis.[Å]	Dis. [Å]	(TS-R)/R	(TS-P)/P	B <sub>i</sub>	B <sub>i</sub>	100-(B <sub>i</sub> <sup>TS</sup> /B <sub>i</sub> <sup>R</sup> )	100-(B <sub>i</sub> <sup>TS</sup> /B <sub>i</sub> <sup>P</sup> )				
<b>4a</b>												
a4_ipr_ts_1	1.59	2.28	11.2%	60.8%	0.68	0.16	23.4%	80.0%	-0.17	-0.19	0.23	0.24
a4_ipr_ts_10	1.57	2.33	9.9%	64.0%	0.71	0.13	19.9%	83.6%	-0.14	-0.15	0.19	0.20
a4_ipr_ts_12	1.58	2.33	10.1%	64.2%	0.71	0.13	20.2%	83.5%	-0.14	-0.16	0.19	0.20
a4_ipr_ts_13	1.58	2.32	10.6%	63.3%	0.69	0.14	22.2%	82.8%	-0.14	-0.16	0.20	0.21
a4_ipr_ts_15	1.58	2.32	10.7%	63.6%	0.69	0.14	22.3%	83.0%	-0.14	-0.16	0.20	0.20
a4_ipr_ts_16	1.58	2.32	10.7%	63.3%	0.69	0.14	22.4%	82.9%	-0.14	-0.16	0.20	0.21
a4_ipr_ts_2	1.59	2.28	11.1%	60.9%	0.68	0.16	23.1%	80.5%	-0.16	-0.18	0.22	0.23
a4_ipr_ts_7	1.59	2.28	11.2%	60.9%	0.68	0.16	23.5%	80.0%	-0.17	-0.19	0.23	0.24
a4_ipr_ts_9	1.57	2.33	10.0%	63.7%	0.71	0.13	20.0%	83.5%	-0.14	-0.16	0.19	0.20
<b>4f</b>												
f4_ipr_ts_15	1.60	2.28	11.8%	60.6%	0.67	0.16	24.7%	79.6%	-0.18	-0.19	0.24	0.24
f4_ipr_ts_4	1.58	2.31	10.3%	63.0%	0.70	0.14	20.6%	82.9%	-0.14	-0.16	0.20	0.20
f4_ipr_ts_6	1.60	2.32	11.4%	63.0%	0.68	0.14	23.5%	82.2%	-0.15	-0.17	0.21	0.21
f4_ipr_ts_8	1.60	2.32	11.7%	63.3%	0.67	0.15	24.2%	81.6%	-0.16	-0.17	0.21	0.22
f4_ipr_ts_9	1.60	2.32	11.7%	63.2%	0.67	0.15	24.2%	81.5%	-0.16	-0.17	0.21	0.22
<b>NFSI</b>												
nfsi_ipr_ts_1	1.55	2.34	8.9%	64.5%	0.74	0.14	17.6%	82.4%	-0.16	-0.17	0.20	0.21
nfsi_ipr_ts_15	1.55	2.34	8.7%	64.7%	0.75	0.14	17.3%	82.9%	-0.15	-0.17	0.20	0.20
nfsi_ipr_ts_16	1.56	2.33	9.6%	64.3%	0.73	0.14	19.2%	82.3%	-0.15	-0.17	0.20	0.21
nfsi_ipr_ts_20	1.56	2.33	9.6%	63.7%	0.73	0.14	19.4%	81.9%	-0.16	-0.17	0.20	0.21
nfsi_ipr_ts_23	1.55	2.33	8.8%	64.2%	0.75	0.14	17.2%	82.8%	-0.15	-0.16	0.20	0.20
nfsi_ipr_ts_25	1.56	2.33	9.6%	63.9%	0.73	0.14	19.3%	82.1%	-0.15	-0.17	0.20	0.21
nfsi_ipr_ts_30	1.56	2.33	9.6%	64.3%	0.73	0.14	19.2%	82.3%	-0.15	-0.17	0.20	0.21
nfsi_ipr_ts_32	1.55	2.33	8.8%	64.1%	0.75	0.14	17.2%	82.7%	-0.15	-0.17	0.20	0.20
nfsi_ipr_ts_34	1.55	2.33	8.9%	64.2%	0.75	0.14	17.3%	82.7%	-0.15	-0.17	0.20	0.20
<b>Reactant (R)</b>												
N-F Bond:	Dis.[Å]	B <sub>i</sub> <sup>R</sup>	N-F Bond:	Dis.[Å]	B <sub>i</sub> <sup>R</sup>	N-F Bond:	Dis.[Å]	B <sub>i</sub> <sup>R</sup>	<b>Product (P)</b>			
<b>4a</b> <sub>Avg</sub>	<b>1.43</b>	<b>0.89</b>	<b>4f</b> <sub>Avg</sub>	<b>1.43</b>	<b>0.88</b>	<b>NFSI</b> <sub>Avg</sub>	<b>1.42</b>	<b>0.90</b>	<b>iso-Pr</b>	<b>1.42</b>	<b>0.80</b>	
a4_1	1.43	0.88	f4_1	1.43	0.88	nfsi_1	1.42	0.91				
a4_10	1.43	0.89	f4_10	1.43	0.88	nfsi_10	1.42	0.91				
a4_4	1.43	0.88	f4_11	1.44	0.88	nfsi_11	1.43	0.90				
a4_5	1.43	0.89	f4_3	1.43	0.89	nfsi_3	1.42	0.90				
						nfsi_4	1.42	0.90				

### 6.1.7 References

- (1) (a) Hioe, J.; Zipse, H., *Org. Biomol. Chem.* **2010**, *8*, 3609-3617. (b) Hioe, J.; Zipse, H., *Faraday Discuss.* **2010**, *145*, 301-313. (c) Hioe, J.; Savasci, G.; Brand, H.; Zipse, H., *Chem. Eur. J.* **2011**, *17*, 3781-3789. (d) Hioe, J.; Zipse, H., Radical Stability—Thermochemical Aspects. In *Encyclopedia of Radicals in Chemistry, Biology and Materials*, Chrystostomos, C.; Armido, S., Eds. John Wiley & Sons Ltd: Chichester, UK, **2012**; pp 449-476. (e) Hioe, J.; Zipse, H., *Chem. Eur. J.* **2012**, *18*, 16463-16472. (f) Hioe, J.; Mosch, M.; Smith, D. M.; Zipse, H., *RSC Adv.* **2013**, *3*, 12403-12408. (g) Šakić, D.; Zipse, H., *Adv. Synth. Catal.* **2016**, *358*, 3983-3991.
- (2) Becke, A. D., *J. Chem. Phys.* **1993**, *98*, 5648-5652.
- (3) (a) Ditchfield, R.; Hehre, W. J.; Pople, J. A., *J. Chem. Phys.* **1971**, *54*, 724-728. (b) Krishnan, R.; Binkley, J. S.; Seeger, R.; Pople, J. A., *J. Chem. Phys.* **1980**, *72*, 650-654.
- (4) Graham, D. C.; Menon, A. S.; Goerigk, L.; Grimme, S.; Radom, L., *J. Phys. Chem. A* **2009**, *113*, 9861-9873.
- (5) Henry, D. J.; Sullivan, M. B.; Radom, L., *J. Chem. Phys.* **2003**, *118*, 4849-4860.
- (6) Marenich, A. V.; Cramer, C. J.; Truhlar, D. G., *J. Phys. Chem. B* **2009**, *113*, 6378-6396.
- (7) Luo, Y.-R., *Comprehensive Handbook of Chemical Bond Energies*. CRC press: **2007**.
- (8) Chan, B.; Radom, L., *J. Phys. Chem. A* **2012**, *116*, 4975-4986.
- (9) Mordaunt, D. H.; Ashfold, M. N.; Dixon, R. N., *J. Chem. Phys.* **1996**, *104*, 6460-6471.
- (10) Glendenning, E. D.; Landis, C. R.; Weinhold, F., *J. Comput. Chem.* **2013**, *34*, 1429-1437.
- (11) Frisch, M. J. T., G. W.; Schlegel, H. B.; Scuseria, G. E.; Robb, M. A.; Cheeseman, J. R.; Scalmani, G.; Barone, V.; Mennucci, B.; Petersson, G. A.; Nakatsuji, H.; Caricato, M.; Li, X.; Hratchian, H. P.; Izmaylov, A. F.; Bloino, J.; Zheng, G.; Sonnenberg, J. L.; Hada, M.; Ehara, M.; Toyota, K.; Fukuda, R.; Hasegawa, J.; Ishida, M.; Nakajima, T.; Honda, Y.; Kitao, O.; Nakai, H.; Vreven, T.; Montgomery, Jr., J. A.; Peralta, J. E.; Ogliaro, F.; Bearpark, M.; Heyd, J. J.; Brothers, E.; Kudin, K. N.; Staroverov, V. N.; Keith, T.; Kobayashi, R.; Normand, J.; Raghavachari, K.; Rendell, A.; Burant, J. C.; Iyengar, S. S.; Tomasi, J.; Cossi, M.; Rega, N.; Millam, J. M.; Klene, M.; Knox, J. E.; Cross, J. B.; Bakken, V.; Adamo, C.; Jaramillo, J.; Gomperts, R.; Stratmann, R. E.; Yazyev, O.; Austin, A. J.; Cammi, R.; Pomelli, C.; Ochterski, J. W.; Martin, R. L.; Morokuma, K.; Zakrzewski, V. G.; Voth, G. A.; Salvador, P.; Dannenberg, J. J.; Dapprich, S.; Daniels, A. D.; Farkas, O.; Foresman, J. B.; Ortiz, J. V.; Cioslowski, J.; Fox, D. J.; *Gaussian 09 Revision D. 01*, Gaussian, Inc., Wallingford CT: **2013**.



## **Chapter 7. Quantification and Theoretical Analysis of the Electrophilicities of Michael Acceptors**

Dominik S. Allgäuer, Harish Jangra, Haruyasu Asahara, Zhen Li, Quan Chen, Hendrik Zipse, Armin R. Ofial, and Herbert Mayr  
*J. Am. Chem. Soc.* **2017**, *139*, 13318-13329.

---

### ***Authors contribution***

A.R.O., H.Z. and H.M. designed the project. D.S.A., H.A., Z.L. and Q.C. did the experimental work that was designed A.R.O and H.M. H.J. performed theoretical calculations that were designed by him and H.Z.. A.R.O., H.Z. and H.M. jointly wrote the manuscript.

### ***Copyright***

This research was originally published in the *Journal of the American Chemical Society* and reprinted with permission from *J. Am. Chem. Soc.* **2017**, *139*, 13318-13329 © 2017 American Chemical Society as the 7<sup>th</sup> chapter of this thesis.

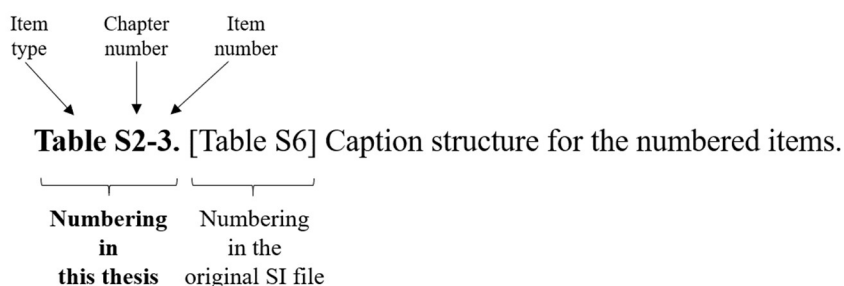
(Link to publication: <https://pubs.acs.org/doi/abs/10.1021/jacs.7b05106>)

Selected supporting material for the computational part of this work is provided at the end of this chapter. For complete supporting information (SI), please follow the link below:

[https://pubs.acs.org/doi/suppl/10.1021/jacs.7b05106/suppl\\_file/ja7b05106\\_si\\_001.pdf](https://pubs.acs.org/doi/suppl/10.1021/jacs.7b05106/suppl_file/ja7b05106_si_001.pdf)

### ***Additional information***

The accompanying SI is the shorter and altered version of the original content. The items (Tables, Figure, Schemes etc.) may have a different number than what was originally assigned. To make it easier to locate the SI content referred to in the following reprint, the original numbering is also provided in the caption of the numbered items as described below:



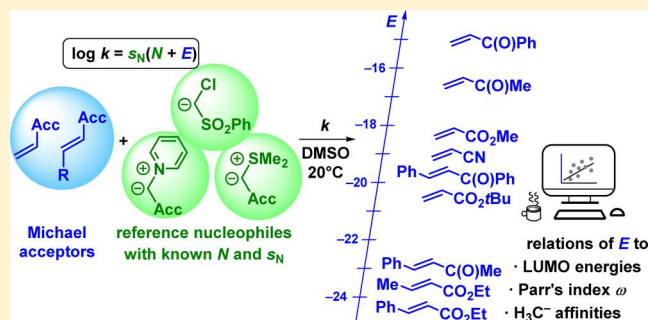
# Quantification and Theoretical Analysis of the Electrophilicities of Michael Acceptors

Dominik S. Allgäuer, Harish Jangra, Haruyasu Asahara,<sup>1b</sup> Zhen Li, Quan Chen, Hendrik Zipse,<sup>\*1b</sup> Armin R. Ofial,<sup>\*1b</sup> and Herbert Mayr<sup>\*1b</sup>

Department Chemie, Ludwig-Maximilians-Universität München, Butenandtstrasse 5-13, 81377 München, Germany

**S** Supporting Information

**ABSTRACT:** In order to quantify the electrophilic reactivities of common Michael acceptors, we measured the kinetics of the reactions of monoacceptor-substituted ethylenes ( $\text{H}_2\text{C}=\text{CH}-\text{Acc}$ , **1**) and styrenes ( $\text{PhCH}=\text{CH}-\text{Acc}$ , **2**) with pyridinium ylides **3**, sulfonium ylide **4**, and sulfonyl-substituted chloromethyl anion **5**. Substitution of the 57 measured second-order rate constants ( $\log k$ ) and the previously reported nucleophile-specific parameters  $N$  and  $s_N$  for **3–5** into the correlation  $\log k = s_N(E + N)$  allowed us to calculate 15 new empirical electrophilicity parameters  $E$  for Michael acceptors **1** and **2**. The use of the same parameters  $s_N$ ,  $N$ , and  $E$  for these different types of reactions shows that all reactions proceed via a common rate-determining step, the nucleophilic attack of **3–5** at the Michael acceptors with formation of acyclic intermediates, which subsequently cyclize to give tetrahydroindolizines (stepwise 1,3-dipolar cycloadditions with **3**) and cyclopropanes (with **4** and **5**), respectively. The electrophilicity parameters  $E$  thus determined can be used to calculate the rates of the reactions of Michael acceptors **1** and **2** with any nucleophile of known  $N$  and  $s_N$ . DFT calculations were performed to confirm the suggested reaction mechanisms and to elucidate the origin of the electrophilic reactivities. While electrophilicities  $E$  correlate poorly with the LUMO energies and with Parr's electrophilicity index  $\omega$ , good correlations were found between the experimentally observed electrophilic reactivities of 44 Michael acceptors and their calculated methyl anion affinities, particularly when solvation by dimethyl sulfoxide was taken into account by applying the SMD continuum solvation model. Because of the large structural variety of Michael acceptors considered for these correlations, which cover a reactivity range of 17 orders of magnitude, we consider the calculation of methyl anion affinities to be the method of choice for a rapid estimate of electrophilic reactivities.



## INTRODUCTION

Michael additions belong to the most important C–C-bond-forming reactions in organic chemistry.<sup>1</sup> Although kinetic investigations of numerous Michael additions have been reported in the past,<sup>1b,2</sup> a general method to predict the corresponding reactivities and selectivities is still missing.

It has been demonstrated that within narrow families of Michael acceptors, relative reactivities correlate with the corresponding LUMO energies.<sup>3</sup> Parr's electrophilicity index, which is defined as "the square of its electronegativity divided by its chemical hardness",<sup>4</sup> has also been reported to be a measure for relative reactivities of structurally related electrophiles.<sup>5–7</sup> In some reaction series, correlations with the local electrophilicity index defined as the product of the global electrophilicity index and the Fukui function at the reaction site<sup>8</sup> have also been analyzed.<sup>9–12</sup>

In systematic investigations, we have shown that rate constants for the reactions of carbenium ions, Michael acceptors, and other  $\text{sp}^2$  hybridized electrophiles with  $n$ - (amines, alkoxides, etc.),  $\pi$ - (alkenes, arenes, resonance stabilized carbanions, etc.), and  $\sigma$ -nucleophiles (hydride donors, alkylzirconocenes, etc.) can be expressed by the correlation

$$\log k_{20^\circ\text{C}} = s_N(E + N) \quad (1)$$

where  $E$  is a nucleophile-independent electrophilicity parameter,  $N$  is an electrophile-independent nucleophilicity parameter, and  $s_N$  is an electrophile-independent nucleophile-specific susceptibility parameter, usually in the range  $0.5 < s_N < 1.2$ .<sup>13</sup>

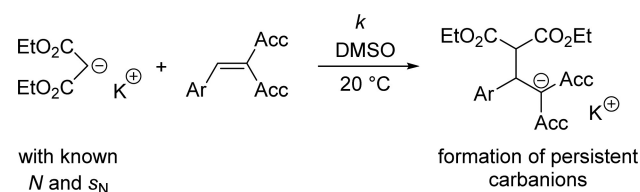
In previous characterizations of electrophilicities of Michael acceptors, we have focused on nitro- and 1,1-diacceptor-substituted ethylenes, which give persistent anions in reactions with stabilized carbanions (reference nucleophiles) in DMSO solution (Scheme 1).<sup>14</sup> The kinetics of these reactions were usually monitored photometrically.

This method, which allowed us to characterize the electrophilicities of a large variety of Michael acceptors, could not be adapted to the investigation of the synthetically most important Michael acceptors, for example, monoacceptor-substituted ethylenes, because the nucleophilic attack of stabilized carbanions at acrylates, acrylonitrile, vinyl ketones, or vinyl sulfones is usually reversible due to the low stabilization

Received: May 17, 2017

Published: September 18, 2017

### Scheme 1. Reference Reactions for the Determination of Electrophilic Reactivities of 1,1-Diacceptor-Substituted Olefins

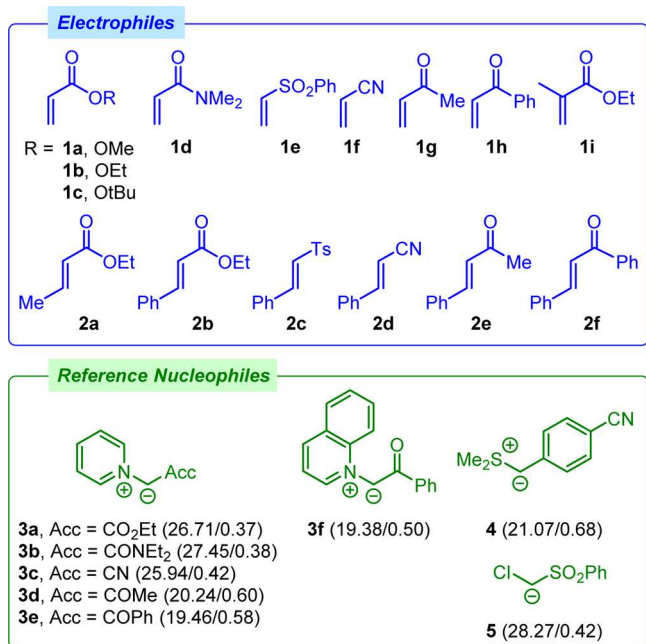


of the resulting carbanions. Other groups have circumvented this problem by performing the kinetic investigations in aqueous or alcoholic solution, where the initially generated carbanions are immediately trapped by proton transfer from the solvent.<sup>15–24</sup>

A method to characterize Michael acceptor reactivities in aprotic solvents (DMSO) has recently been employed for the characterization of 1,2-diacceptor substituted ethylenes. By employing nucleophiles which give adducts that undergo fast subsequent intramolecular reactions, the reversibility of the C–C-bond-forming step could be suppressed.<sup>25</sup>

We now report on the kinetics of the reactions of Michael acceptors **1a–1i** and **2a–2f** with pyridinium ylides **3a–3f**, sulfonium ylide **4**, and the sulfonyl-chloro-substituted methyl anion **5** (Chart 1) and show that all reactions of these structurally diverse nucleophiles with simple Michael acceptors proceed with rate determining formation of one C–C-bond followed by fast cyclization. In addition, we report that the rate constants of all of these reactions follow eq 1, which allowed us to determine the nucleophile-independent electrophilicity parameters  $E$  for Michael acceptors **1a–1i** and **2a–2f**. With

**Chart 1. Electrophilicities of Acceptor-Substituted Olefins 1 and 2 Investigated in This Work by Using Pyridinium Ylides 3a–f, Sulfonium Ylide 4, and Carbanion 5 as Structurally Diverse Reference Nucleophiles<sup>a</sup>**



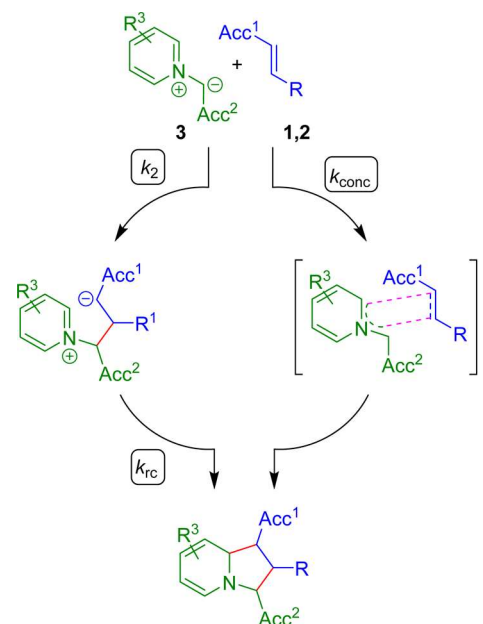
<sup>a</sup>Ts = *p*-tosyl. Reactivity parameters  $N/s_N$  in DMSO are from the following references: for **3a–f**, ref 26; for **4**, ref 27; and for **5**, ref 28.

these electrophilicities  $E$ , the rate constants of the reactions of **1** and **2** with any nucleophile of known  $N$  and  $s_N$  values can be predicted with high reliability. Quantum chemical calculations are then employed to elucidate the origin of the observed electrophilicities.

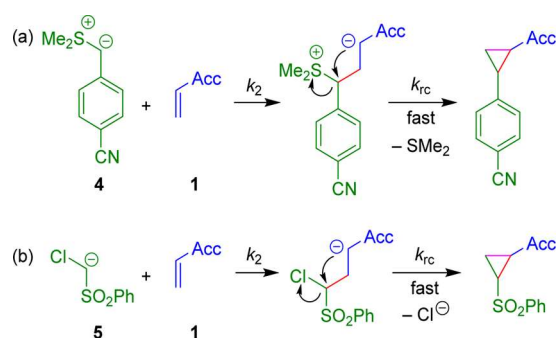
## RESULTS AND DISCUSSION

**General.** Since the (3 + 2)-cycloadditions (Huisgen reactions) of Michael acceptors **1** and **2** with pyridinium ylides

**Scheme 2. Concerted and Stepwise Cycloadditions of Pyridinium Ylides 3 with Acceptor-Substituted Olefins 1 and 2**

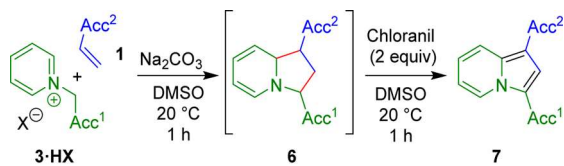


**Scheme 3. Mechanisms for the Reactions of Acceptor-Substituted Olefins 1 with (a) Sulfonium Ylide 4 and (b) Carbanion 5**



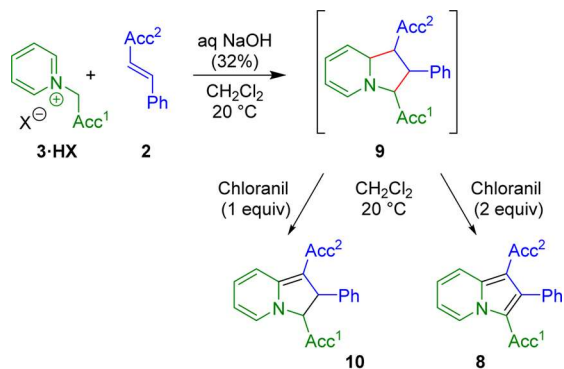
**3** involve 6 electrons ( $[4\pi + 2\pi]$ ), concerted ( $k_{\text{conc}}$ ; Scheme 2, right) or stepwise ( $k_2$ ; Scheme 2, left) mechanisms have to be considered.<sup>29–31</sup> In stepwise processes, intermediate betaines are formed ( $k_2$ ) which cyclize ( $k_{\text{rc}}$ ) to give tetrahydroindolizines (Scheme 2). For other 1,3-dipolar cycloaddition reactions, stepwise mechanisms via diradical intermediates have also been considered.<sup>32–34</sup> A stepwise mechanism via zwitterionic intermediates has recently been reported for the 1,3-dipolar cycloadditions of pyridinium ylides with substituted benzyldiene malononitriles and chalcones.<sup>26</sup>

Scheme 4. Synthesis of the Indolizines 7

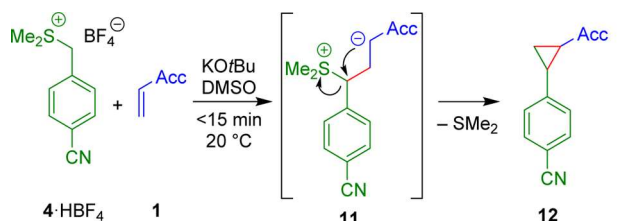


3·HX	Acc <sup>1</sup>	1	Acc <sup>2</sup>	7 (Yield)
3b·HBr	CONEt <sub>2</sub>	1a	CO <sub>2</sub> Me	7a (52%)
3c·HBr	CN	1b	CO <sub>2</sub> Et	7b (58%)
3d·HCl	COMe	1c	CO <sub>2</sub> tBu	7c (96%)
3c·HBr	CN	1d	CONMe <sub>2</sub>	7d (64%)
3d·HCl	COMe	1e	SO <sub>2</sub> Ph	7e (98%)
3a·HBr	CO <sub>2</sub> Et	1f	CN	7f (59%)
3e·HBr	COPh	1g	COMe	7g (74%)
3d·HCl	COMe	1h	COPh	7h (96%)

Scheme 5. Reactions of Michael Acceptors 2 with Pyridinium Ylides 3



3·HX	Acc <sup>1</sup>	2	Acc <sup>2</sup>	10 (Yield)	8 (Yield)
3a·HBr	CO <sub>2</sub> Et	2b	CO <sub>2</sub> Et	10b (89%)	8b (89%)
3c·HBr	CN	2b	CO <sub>2</sub> Et	10c (89%)	8c (85%)
3c·HBr	CN	2b	CO <sub>2</sub> Et		8d (90%)
3c·HBr	CN	2c	Ts		8e (90%)
3a·HBr	CO <sub>2</sub> Et	2d	CN	10e (90%)	8e (90%)
3a·HBr	CO <sub>2</sub> Et	2d	CN		8f (50%)
3c·HBr	CN	2e	COMe		8g (68%)
3d·HCl	COMe	2f	COPh		

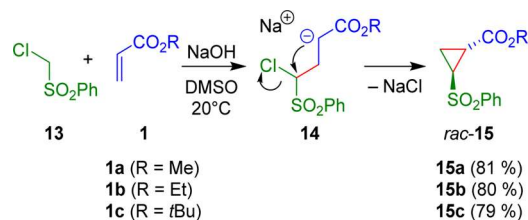
Scheme 6. Cyclopropanations of Michael Acceptors 1 with Sulfonium Ylide 4<sup>a</sup>

1	Acc	12 (Yield)
1a	CO <sub>2</sub> Me	12a (64%)
1b	CO <sub>2</sub> Et	12b (66%)
1c	CO <sub>2</sub> tBu	12c (60%)
1e	SO <sub>2</sub> Ph	12e (92%)
1f	CN	12f (42%)
1g	COMe	12g (67%)
1h	COPh	12h (83%)

<sup>a</sup>For diastereomeric ratios see the Supporting Information.

The reactions of sulfonium ylide 4 and carbanion 5 with Michael acceptors proceed stepwise, with initial irreversible

Scheme 7. Reactions of Chloro(phenylsulfonyl)-Stabilized Carbanion 5 (Generated from 13) with Alkyl Acrylates 1a–c



1a (R = Me)	15a (81%)
1b (R = Et)	15b (80%)
1c (R = tBu)	15c (79%)

Scheme 8. 2:1-Product Formation by the Reaction of Carbanion 5 (Generated by Deprotonation of 13) with Methyl Acrylate 1a (2 equiv)

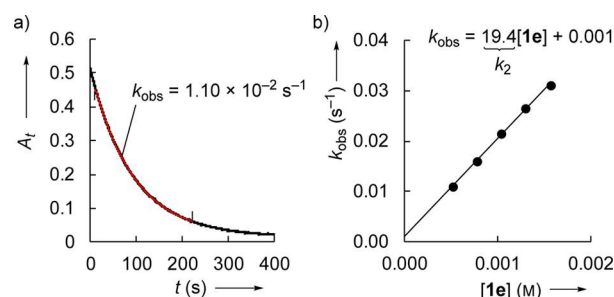
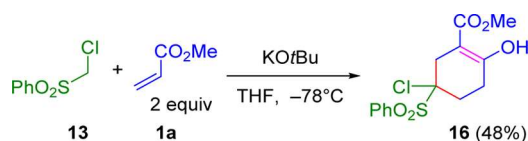


Figure 1. (a) Decay of the absorbance of 3d ( $[3d]_0 = 5 \times 10^{-5}$  M) at 427 nm during the reaction with 1e ( $[1e]_0 = 5.22 \times 10^{-4}$  M) in DMSO at 20 °C. (b) Linear correlation of  $k_{\text{obs}}$  with the concentration of 1e.

formation of intermediate betaines or acceptor-stabilized carbanions, respectively ( $k_2$ ; Scheme 3). The subsequent ring closures ( $k_{\text{rc}}$ ) to cyclopropanes are usually fast processes.<sup>27,28,35–37</sup>

**Products.** The reactions of Michael acceptors 1 with pyridinium ylides 3, generated by deprotonation of their conjugate acids, 3·HX, in DMSO gave tetrahydroindolizines 6 as initial products (Scheme 4). Given that tetrahydroindolizines had been reported to be unstable at ambient temperature,<sup>31</sup> we did not attempt the isolation of 6 but oxidized them with chloranil to the corresponding indolizines 7, which were obtained in 52–98% yield after purification (Scheme 4).

The analogous (3 + 2)-cycloaddition of ethyl methacrylate 1i with pyridinium ylide 3e (generated in situ from 3e·HBr and NEt<sub>3</sub>) and subsequent decarboxylative oxidation with chloranil was reported previously.<sup>38</sup> The reaction of ethyl crotonate (2a) with 3c·HBr under the conditions of the reactions in Scheme 4 furnished 2-methyl-substituted indolizine 8a in 84% yield.



Further 2-substituted indolizines were obtained by a combination of styrene-derived Michael acceptors 2b–f with pyridinium salts 3·HX under biphasic conditions (CH<sub>2</sub>Cl<sub>2</sub>/aqueous NaOH). The initially formed tetrahydroindolizines 9

**Table 1. Experimental and Calculated Second-Order Rate Constants for the Reactions of Michael Acceptors 1 and 2 with Ylides 3 and 4 or Carbanion 5 in DMSO at 20 °C**

Electrophile	Nucleophile	$k_2^{\text{exp}} (\text{M}^{-1} \text{s}^{-1})$	$k_2^{\text{calcd}} (\text{M}^{-1} \text{s}^{-1})^a$	$k_2^{\text{exp}}/k_2^{\text{calcd}}$
<b>1a</b>  $E = -18.84$	<b>3a</b>	$1.09 \times 10^3$	$8.17 \times 10^2$	1.33
	<b>3b</b>	$6.91 \times 10^3$ <sup>b</sup>	$1.87 \times 10^3$	3.69
	<b>3c</b>	$2.02 \times 10^3$	$9.60 \times 10^2$	2.10
	<b>3d</b>	$1.37 \times 10^1$	6.92	1.98
	<b>4</b>	3.26	$3.29 \times 10^1$	0.10
<b>1b</b>  $E = -19.07$	<b>3a</b>	$1.04 \times 10^3$	$6.71 \times 10^2$	1.55
	<b>3c</b>	$1.72 \times 10^3$	$7.68 \times 10^2$	2.24
	<b>3d</b>	$1.12 \times 10^1$	5.03	2.22
	<b>4</b>	3.89	$2.29 \times 10^1$	0.17
	<b>5</b>	$1.25 \times 10^4$	$7.31 \times 10^3$	1.71
<b>1c</b>  $E = -20.22$	<b>3a</b>	$2.61 \times 10^2$	$2.52 \times 10^2$	1.04
	<b>3b</b>	$3.40 \times 10^2$	$5.58 \times 10^2$	0.61
	<b>3c</b>	$2.79 \times 10^2$	$2.52 \times 10^2$	1.11
	<b>3d</b>	2.02	1.03	1.97
	<b>4</b>	1.89	3.77	0.50
<b>1d</b>  $E = -23.54$	<b>3a</b>	$1.12 \times 10^1$	$1.49 \times 10^1$	0.75
	<b>3b</b>	$1.39 \times 10^1$	$3.06 \times 10^1$	0.45
	<b>3c</b>	$2.68 \times 10^1$	$1.02 \times 10^1$	2.63
	<b>3e</b>	$3.82 \times 10^3$	$2.40 \times 10^3$	1.59
	<b>4</b>	1.89	3.77	0.50
<b>1e</b>  $E = -18.36$	<b>3a</b>	$1.59 \times 10^3$	$1.23 \times 10^3$	1.29
	<b>3b</b>	$5.55 \times 10^3$ <sup>b</sup>	$2.86 \times 10^3$	1.94
	<b>3c</b>	$2.56 \times 10^3$	$1.53 \times 10^3$	1.67
	<b>3d</b>	$1.94 \times 10^1$	$1.35 \times 10^1$	1.44
	<b>3e</b>	4.09	4.37	0.94
<b>1f</b>  $E = -19.05$	<b>3a</b>	$1.89 \times 10^3$	$6.81 \times 10^2$	2.78
	<b>3b</b>	$3.80 \times 10^3$	$1.55 \times 10^3$	2.45
	<b>3c</b>	$3.63 \times 10^3$	$7.81 \times 10^2$	4.65
	<b>3d</b>	2.36	5.15	0.46
	<b>3e</b>	2.28	1.72	1.32
<b>1g</b>  $E = -16.76$	<b>3a</b>	$6.80 \times 10^3$	$4.80 \times 10^3$	1.42
	<b>3c</b>	$8.00 \times 10^3$	$7.16 \times 10^3$	1.12
	<b>3d</b>	$1.24 \times 10^2$	$1.22 \times 10^2$	1.02
	<b>3e</b>	$2.67 \times 10^1$	$3.67 \times 10^1$	0.73
	<b>4</b>	$2.36 \times 10^1$	$7.01 \times 10^1$	0.34
<b>1h</b>  $E = -15.25$	<b>3a</b>	$3.47 \times 10^4$	$1.74 \times 10^4$	2.00
	<b>3b</b>	$2.75 \times 10^4$	$4.32 \times 10^4$	0.64
	<b>3c</b>	$4.89 \times 10^4$	$3.09 \times 10^4$	1.58
	<b>3d</b>	$8.10 \times 10^2$	$9.86 \times 10^2$	0.82
	<b>3e</b>	$2.10 \times 10^2$	$2.76 \times 10^2$	0.76
<b>1i</b>  $E = -22.77$	<b>3a</b>	$1.50 \times 10^1$	$2.86 \times 10^1$	0.52
	<b>3c</b>	$3.77 \times 10^1$	$2.14 \times 10^1$	1.77
<b>2a</b>  $E = -23.59$	<b>3a</b>	4.16	$1.43 \times 10^1$	0.29
	<b>3c</b>	$2.87 \times 10^1$	9.70	2.96
<b>2b</b>  $E = -24.52$	<b>3a</b>	2.98	6.47	0.46
	<b>3c</b>	7.82	3.95	1.98
<b>2c</b>  $E = -24.69$	<b>3a</b>	2.35	5.59	0.42
	<b>3c</b>	7.18	3.35	2.14
<b>2d</b>  $E = -24.6$	<b>3a</b>	6.15	identical	–
<b>2e</b>  $E = -23.01$	<b>3a</b>	$1.78 \times 10^1$	$2.34 \times 10^1$	0.76
	<b>3b</b>	$2.55 \times 10^1$	$4.87 \times 10^1$	0.52
	<b>3c</b>	$3.90 \times 10^1$	$1.70 \times 10^1$	2.29
<b>2f</b>  $E = -19.39$ <sup>d</sup>	<b>3a</b>	$3.31 \times 10^2$	$5.11 \times 10^2$	0.65
	<b>3b</b>	$3.20 \times 10^2$	$1.16 \times 10^3$	0.28
	<b>3c</b>	$6.17 \times 10^2$	$5.64 \times 10^2$	1.09
	<b>4</b>	$3.41 \times 10^1$ <sup>e</sup>	$1.39 \times 10^1$	2.46

<sup>a</sup>Calculated by eq 1 from  $N$ ,  $s_N$  (Chart 1), and  $E$  from this table. <sup>b</sup>Bis-exponential decay of the absorbance was observed and only the initial rate was used to determine  $k_2$ . <sup>c</sup>Not used for the determination of  $E$  as the reaction rate may already be enhanced by a partially concerted

**Table 1. continued**

cycloaddition (ref 25). <sup>d</sup>The previously reported electrophilicity value of  $E(2f) = -18.82$  (ref 14g) was derived only from the rate constant for the reaction of 2f with 4 and is revised in this work. <sup>e</sup>Second-order rate constant  $k_2$  from ref 14g.

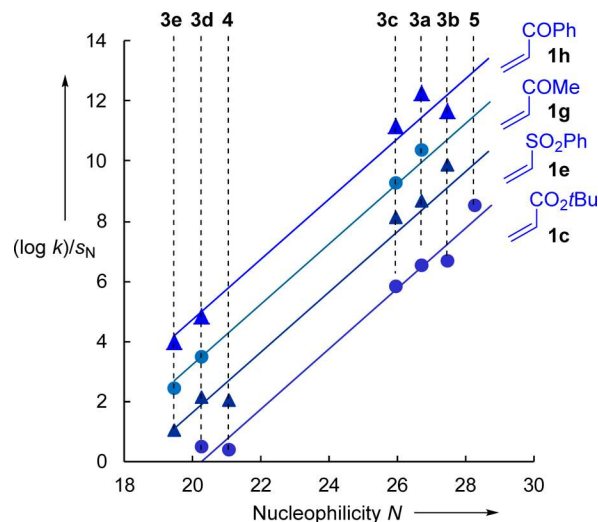


**Figure 2.** Correlation of  $(\log k_2)/s_N$  against the nucleophilicity parameters  $N$  of 3–5 (DMSO, 20 °C). For all correlations, a slope of 1.0 was enforced, as required by eq 1 (individual correlations for all electrophiles investigated are shown in the Supporting Information).

were not isolated but subsequently oxidized with chloranil as displayed in Scheme 5.<sup>26</sup>

When 1 equiv of chloranil was employed, partial oxidation of 9 furnished ester- or cyano-substituted dihydroindolizines 10c and 10e in 89 and 90% yield, respectively. Treatment of tetrahydroindolizines 9 with 2 equiv of chloranil resulted in the formation of indolizines 8 (Scheme 5). The reactions of acceptor-substituted ethylenes 1a–c and 1e–h with sulfonium ylide 4 in DMSO at ambient temperature gave cyclopropanes 12 (42–92% yield) by Michael-initiated ring closure (MIRC) reactions with variable diastereoselectivities (Scheme 6). Cyclopropanes were also obtained by the reactions of carbanion 5 (generated by deprotonation of its conjugate acid 13) with the alkyl acrylates 1a–c in DMSO at ambient temperature (Scheme 7).

When 13 and 1a (2 equiv) were combined at low temperature in THF with potassium *tert*-butoxide as the base, cyclic  $\beta$ -keto ester 16 was formed by a 2-fold Michael addition with subsequent Dieckmann condensation (Scheme 8, for the detailed mechanism see Supporting Information). Analogous 4,4-disubstituted cyclohexane  $\beta$ -keto esters were previously obtained when phenylacetone nitriles or phenylacetates were treated with 1a (2 equiv) under basic conditions (*t*BuOK, THF, rt).<sup>39</sup>

**Kinetic Studies.** The kinetics of the reactions of acceptor-substituted olefins 1 and 2 with pyridinium ylides 3, sulfonium ylide 4, and carbanion 5 in DMSO at 20 °C were monitored photometrically by following the disappearance of the absorbances of nucleophiles 3–5 at or close to their absorption maxima. Due to their low stabilities, nucleophiles 3 and 4 were generated in solution by combining freshly prepared solutions of 3•HX or 4•HBF<sub>4</sub> and KO*t*Bu (typically 1.05 equiv) in

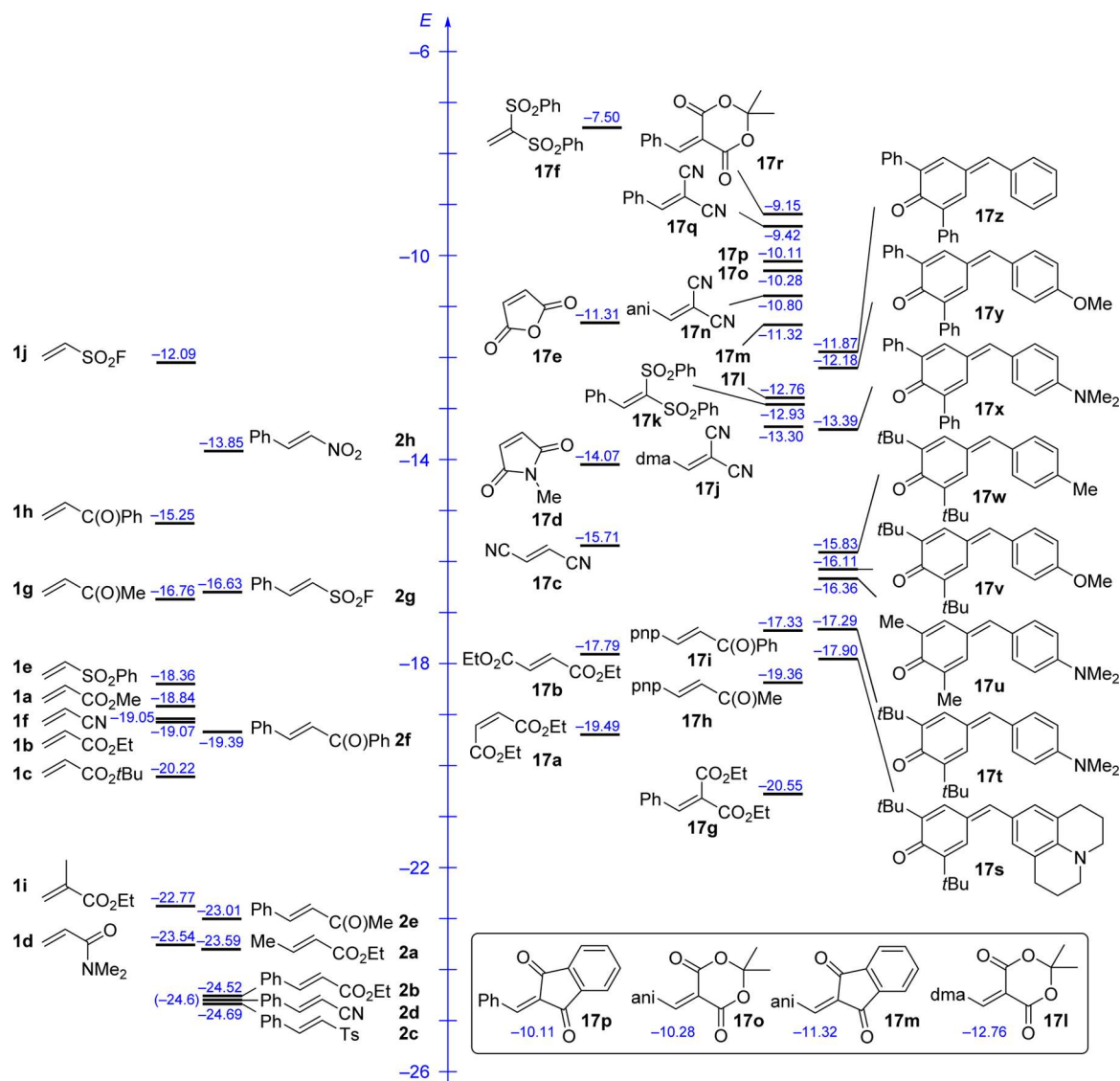


**Figure 3.** Comparison of the electrophilic reactivities of Michael acceptors **1** and **2** with those of structurally diverse Michael acceptors **17a–z** (<sup>13g,14,25</sup>Abbreviations: ani = 4-methoxyphenyl, dma = 4-(dimethylamino)phenyl, pnp = 4-nitrophenyl).

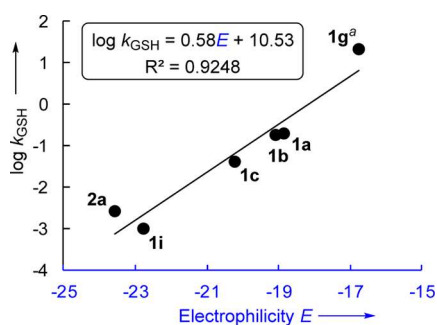


**Figure 4.** Correlation of  $\log k_{\text{GSH}}$  (with  $k_{\text{GSH}}$  in a DMSO/buffer mixture at pH 7.4 from ref <sup>23d</sup>, converted from  $\text{M}^{-1} \text{min}^{-1}$  to  $\text{M}^{-1} \text{s}^{-1}$ ) with the electrophilicity parameters  $E$  for five  $\alpha,\beta$ -unsaturated esters and one enone. <sup>a</sup>The  $\log k_{\text{GSH}}$  for pent-1-en-3-one was used.

DMSO directly before each kinetic experiment. Carbanion **5** was prepared in solution by deprotonation of the corresponding CH acid **13** with KO<sup>t</sup>Bu (1.00–1.05 equiv) in dry THF at  $-78$  °C. Then, small amounts of the thus generated stock solution were dissolved in DMSO at room temperature directly

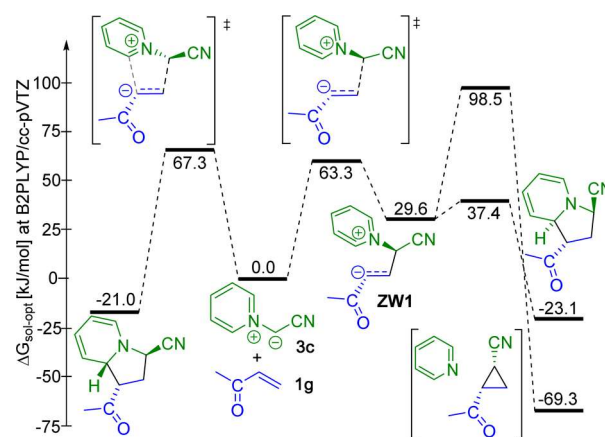


**Figure 5.** Gibbs energy surface for the reaction of methyl vinyl ketone (**1g**) with pyridinium ylide **3c** (SMD(DMSO)/B2PLYP/cc-pVTZ//SMD(DMSO)/B3LYP/6-31G(d,p) level, in  $\text{kJ mol}^{-1}$ ).

before each kinetic experiment. Pseudo-first-order conditions were achieved by using electrophiles **1** and **2** in high excess

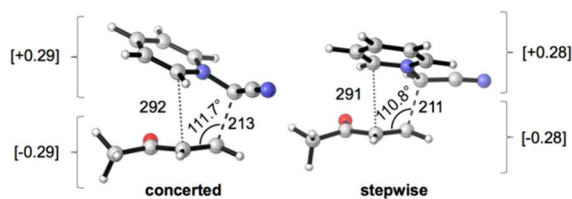


**Figure 6.** Transition states for stepwise and concerted reaction of methyl vinyl ketone (**1g**) with pyridinium ylide **3c** (SMD(DMSO)/B3LYP/6-31G(d,p) structures). Distances are in pm, and angles are in degrees. Charge parameters were obtained by summing Mulliken atomic charges over all centers of the two reactants.

( $\geq 10$  equiv) over nucleophiles **3–5**, which resulted in monoexponential decays of the nucleophiles' UV-vis absorbances. First-order rate constants  $k_{\text{obs}}$  ( $\text{s}^{-1}$ ) were then derived by least-squares fitting of the exponential function  $A_t = A_0 \cdot \exp(-k_{\text{obs}}t) + C$  to the time-dependent absorbances  $A_t$  (Figure 1a). Correlations of  $k_{\text{obs}}$  with the concentrations of Michael acceptors **1** and **2** were linear (Figure 1b). The second-order rate constants  $k_2$  ( $\text{M}^{-1} \text{s}^{-1}$ ) listed in Table 1 were derived from the slopes of the linear  $k_{\text{obs}}$  versus [1] (or [2]) correlations (see Supporting Information for the individual correlations of all investigated reactions).

If the reactions of Michael acceptors **1** and **2** with ylides **3** and **4** proceed stepwise with rate-determining formation of the intermediate betaines, then the measured second-order rate constants equal  $k_2$  as defined in Schemes 2 and 3a. Analogously, the observed rate constants for the reaction of carbanion **5** with Michael acceptors **1a–c** correspond to  $k_2$  (Scheme 3b) if the formation of the carbanionic intermediates **14** (Scheme 7) is rate-determining. As the rates of attack of nucleophiles at electron-deficient  $\pi$ -systems have previously been shown to follow eq 1, this equation may also be suitable to correlate the rate constants listed in Table 1. Figure 2 shows that the correlations of  $(\log k_2)/s_N$  for the reactions of electrophiles **1** and **2** with ylides **3** and **4** as well as with carbanion **5** versus the corresponding nucleophilicity parameters  $N$  are indeed linear with a slope of roughly 1.0 as required by eq 1, indicating a common rate-determining step for these different reactions. Though only two rate constants for the reactions with sulfonium ylide **4** and one rate constant for the reaction with carbanion **5** are shown in Figure 2, the matching of these  $k_2$  values with the correlation lines is quite remarkable, as the  $N$  values of these nucleophiles (abscissa of Figure 2) have been derived from the rates of their reactions with quinone methides and benzhydrylium ions.

Electrophilicity parameters  $E$  for acceptor-substituted olefins **1** and **2** in the first column of Table 1 were determined by least-squares minimization [minimization of  $\Delta^2 = \sum(\log k_2 - s_N(N + E))^2$ ] considering the rate constants of their reactions with pyridinium ylides **3a–e**, sulfonium ylide **4**, and carbanion **5**.

The rate constant for the reaction of acrylonitrile **1f** with quinolinium ylide **3f** (marked by footnote c in Table 1) deviates by a factor of 18 from  $k_2$  predicted by using eq 1, which is still within the limit of confidence of eq 1 (that is, within 2 orders of magnitude) but also might be due to a low degree of concertedness of the reaction. Therefore, this reaction was not considered for the determination of the electrophilicity parameter  $E$  of acrylonitrile **1f**.

All 57 measured rate constants ( $k_2^{\text{exp}}$ ) in Table 1 (except one) agree within 1 order of magnitude with the rate constants ( $k_2^{\text{calcd}}$ ) calculated by eq 1. This indicates that despite the

different reaction products (tetrahydroindolizines **6** and **9** (Schemes 4 and 5) and cyclopropanes **12** and **15** (Schemes 6 and 7)) all investigated reactions proceed via a common rate-determining step: the initial C–C-bond formation to the intermediate betaines or carbanions. It is, therefore, possible to directly compare the electrophilicities of Michael acceptors **1** and **2** derived in this work from stepwise 1,3-dipolar cycloadditions (Huisgen reactions) and cyclopropanations by MIRC reactions with electrophilicities previously derived from the kinetics of carbanion additions as illustrated in Scheme 1. Figure 3 compares the electrophilic reactivities of Michael acceptors determined in this work (**1**, **2**) with previously reported electrophilicities of bis-acceptor-substituted ethylenes (**17**). With  $-24.7 < E < -7.5$ , a reactivity range of 17 orders of magnitude is covered for reactions with nucleophiles of  $s_N = 1$ , corresponding to relative reaction times of 1 s versus 3 billion years. In combination with the reported  $N$  and  $s_N$  parameters of more than 1000 nucleophiles,<sup>13g</sup> eq 1 can now be used to predict rate constants for a large variety of potential reactions of Michael acceptors **1**, **2**, and **17** with nucleophiles and thus define their synthetic potential.

The rates of formation of covalent bonds between nucleophiles and electrophiles have furthermore been discussed to be useful parameters for identifying biological targets<sup>40</sup> and predicting toxicological effects.<sup>23</sup> In this context, Schüürmann and co-workers have determined rate constants  $\log k_{\text{GSH}}$  for the Michael additions of glutathione (GSH) to a set of 58  $\alpha,\beta$ -unsaturated carbonyl compounds.<sup>23d</sup> The fair linear correlation of  $\log k_{\text{GSH}}$  for the reactions with six Michael acceptors, for which  $E$  parameters have been determined in this study (Figure 4), indicates that the electrophilicity parameters  $E$  may also be applicable for quantitative structure–activity relationships.<sup>41–43</sup>

Santelli and co-workers reported linear relationships of Hammett  $\sigma_p$  parameters with the reduction potentials ( $E_{1/2}$ ) and frontier orbital energies of a series of Michael acceptors.<sup>7</sup> In our study, neither  $\log k$  for the reactions with pyridinium ylide **3a** nor electrophilicities  $E$  of monosubstituted ethylenes **1a–1h** correlate well with Hammett's  $\sigma_p$  and  $\sigma_p^-$  constants,<sup>44</sup> respectively (see Supporting Information, Section 4). Whereas  $\text{SO}_2\text{F}$  was found to be the best electron-acceptor substituent in arenes (Hammett constants) as well as in vinylic position (our data), the high electrophilicity of benzoyl substituted ethylenes (and also of benzoyl substituted styrenes) cannot be predicted by Hammett substituent constants, confirming the need of a separate Michael acceptor reactivity scale.

**Quantum Chemical Calculations.** In order to examine the conclusions drawn from the kinetic investigations by an independent method and to characterize the transition states of these reactions more closely, we have investigated the potential energy surfaces (PES) for the reactions of pyridinium ylide **3c** with four Michael acceptors of widely differing electrophilicities (**1d**, **1f**, **1g**, and **2e**) at the SMD(DMSO)/B2PLYP/cc-pVTZ//SMD(DMSO)/B3LYP/6-31G(d,p)<sup>45,46</sup> level of theory. Since the results for all four systems were similar (Figures S25–S29), only the reaction of **3c** with methyl vinyl ketone (**1g**) will now be discussed explicitly. The free energy surface in Figure 5 reveals a stepwise mechanism as the lowest energy pathway (see also Figure S25 for  $\Delta H_{\text{sol-opt}}$  surface and Figure S26 for results at different levels of theory). Nucleophilic attack of **3c** at the terminal position of vinyl ketone **1g** gives zwitterion **ZW1** over a free energy barrier of  $63.3 \text{ kJ mol}^{-1}$ . The barrier for the collapse of this adduct to 5-membered ring adduct **6** is much lower than that for the reverse reaction back to the reactants,

Table 2. Quantum Chemically Calculated Frontier Orbital Energies, Global ( $\omega$ ), and Local ( $\omega_\beta$ ) Electrophilicities As Well As Methyl Anion Affinities (MAAs) of Michael Acceptors

Michael acceptor	$E^a$	$\epsilon_{\text{HOMO}}$ (Hartree) <sup>b</sup>	$\epsilon_{\text{LUMO}}$ (Hartree) <sup>b</sup>	global $\omega$ (eV) <sup>b</sup>	local $\omega_\beta$ (eV) <sup>b</sup>	-MAA (kJ mol <sup>-1</sup> )	
						$\Delta G_{\text{gas}}^c$	$\Delta G_{\text{sol-sp}}^d$
1a	-18.84	-0.27299	-0.04454	1.50	0.62	-205.5	-80.7
1b	-19.07	-0.27018	-0.04291	1.47	0.61	-203.4	-75.1
1c	-20.22	-0.26291	-0.04079	1.41	0.58	-205.7	-71.6
1d	-23.54	-0.23432	-0.03058	1.17	0.49	-187.1	-59.6
1e	-18.36	-0.27133	-0.05219	1.62	0.37	-246.0	-96.8
1f	-19.05	-0.28955	-0.05700	1.76	0.82	-205.1	-109.4
1g	-16.76	-0.24738	-0.05476	1.61	0.60	-222.8	-104.2
1h	-15.25	-0.24946	-0.07147	1.97	0.44	-251.9	-116.7
1i	-22.77	-0.26630	-0.03698	1.36	0.52	-189.9	-51.9
1j	-12.09	-0.32333	-0.06439	1.97	0.98	-295.9	-160.5
2a	-23.59	-0.26444	-0.03391	1.31	0.51	-187.1	-49.8
2b	-24.52	-0.23332	-0.06275	1.75	0.39	-186.9	-36.1
2c	-24.69	-0.23960	-0.06449	1.80	0.36	-219.7	-51.8
2d	-24.60	-0.24292	-0.07488	2.04	0.47	-190.0	-66.1
2e	-23.01	-0.23367	-0.06919	1.90	0.43	-207.7	-60.4
2f	-19.39	-0.23235	-0.07737	2.11	0.42	-231.4	-74.8
2g	-16.63	-0.26113	-0.08298	2.26	0.56	-268.2	-113.3
2h	-13.85	-0.25556	-0.09700	2.67	0.59	-264.6	-123.8
17a	-19.49	-0.26528	-0.05705	1.70	0.60	-246.9	-93.1
17b	-17.79	-0.27664	-0.07861	2.17	0.55	-223.1	-74.2
17c	-15.71	-0.30733	-0.11295	3.09	0.92	-264.1	-132.4
17d	-14.07	-0.27143	-0.09656	2.63	0.59	-260.8	-113.9
17e	-11.31	-0.29924	-0.11734	3.25	0.77	-301.9	-149.8
17f	-7.50	-0.26834	-0.07201	2.01	0.81	-355.3	-174.8
17g	-20.55	-0.23512	-0.06617	1.83	0.46	-284.5	-104.8
17h	-19.36	-0.25831	-0.10948	3.09	0.24	-266.3	-75.2
17i	-17.33	-0.25656	-0.11015	3.12	0.28	-281.9	-86.8
17j	-13.30	-0.21263	-0.08495	2.36	0.70	-290.2	-141.3
17k	-12.93	-0.25143	-0.08056	2.19	0.62	-344.3	-155.9
17l	-12.76	-0.20434	-0.07478	2.05	0.63	-311.2	-135.3
17m	-11.32	-0.22045	-0.08670	2.40	0.65	-318.9	-147.1
17n	-10.80	-0.23815	-0.09709	2.71	0.81	-311.1	-161.9
17o	-10.28	-0.22917	-0.08527	2.34	0.73	-330.7	-154.4
17p	-10.11	-0.23995	-0.09406	2.60	0.70	-331.9	-160.7
17q	-9.42	-0.25994	-0.10707	3.00	0.88	-325.4	-177.4
17r	-9.15	-0.25084	-0.09360	2.57	0.78	-344.7	-169.6
17s	-17.90	-0.18246	-0.07722	2.18	0.54	-295.6	-120.4
17t	-17.29	-0.18808	-0.07918	2.23	0.55	-297.7	-123.2
17u	-16.36	-0.18661	-0.07661	2.14	0.53	-284.6	-130.7
17v	-16.11	-0.20491	-0.08668	2.45	0.61	-312.1	-137.4
17w	-15.83	-0.21214	-0.08977	2.53	0.62	-314.8	-141.3
17x	-13.39	-0.18767	-0.08470	2.45	0.62	-329.6	-147.3
17y	-12.18	-0.20226	-0.09208	2.67	0.68	-344.2	-163.6
17z	-11.87	-0.21015	-0.09719	2.84	0.70	-354.2	-174.6

<sup>a</sup>Empirical electrophilicity parameter as defined in eq 1. <sup>b</sup>Calculated at B3LYP/6-31G(d,p) level in the gas phase. <sup>c</sup>Calculated at B3LYP/6-311++G(3df,2pd)//B3LYP/6-31G(d,p) level in the gas phase. <sup>d</sup>Based on methyl anion affinities ( $\Delta G_{\text{gas}}$ ), which were corrected for solvent effects by adding single point solvation energies calculated at B3LYP/6-31G(d,p) using the SMD (solvent = DMSO) solvation model on gas phase optimized geometries at the same level.

i.e., the formation of the first C–C-bond with formation of **ZW1** is rate-limiting.

A second reaction pathway starting from the same zwitterionic intermediate, **ZW1**, may lead to pyridine elimination and formation of a cyclopropane. In agreement with the much higher barrier calculated for this pathway, cyclopropanes were not detected among the reaction products. The stepwise formation of the 5-membered ring adduct **6** competes with a concerted process, which yields a slightly less

stable diastereoisomer of **6** over a marginally higher barrier (67.3 kJ mol<sup>-1</sup>).<sup>47</sup> The side-by-side comparison of the transition states for the stepwise and the concerted cyclo-additions shown in Figure 6 clearly documents the large similarity of both processes. The angle of attack, the largely different lengths of the forming C–C bonds, and the charge transfer from the attacking nucleophile to the electrophile (0.28 or 0.29 electrons) are almost the same for the transition state of

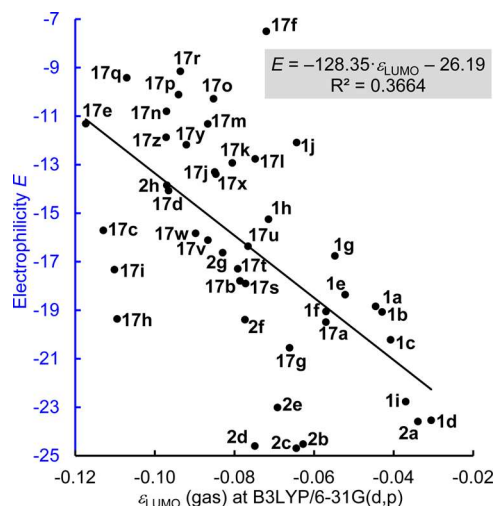


**Figure 7.** Correlation between experimentally determined electrophilicities ( $E$ ) and gas phase lowest unoccupied molecular orbital energies ( $\epsilon_{\text{LUMO}}$ ) calculated at B3LYP/6-31G(d,p) level for the 44 electrophiles listed in Figure 3.

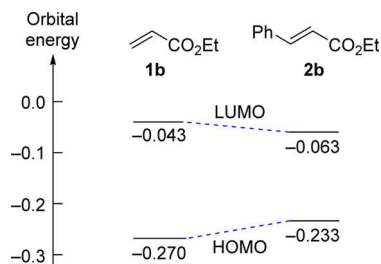


**Figure 8.** Change of gas phase HOMO and LUMO energies (in Hartree) by the introduction of a  $\beta$ -phenyl group at ethyl acrylate (**1b**  $\rightarrow$  **2b**).

the stepwise pathway and the concerted, but very asynchronous cycloaddition reaction.

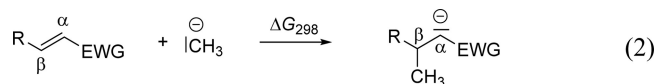
Using the same theoretical approach, the potential and Gibbs energy surfaces in DMSO have also been calculated for the reactions of pyridinium ylide **3c** with Michael acceptors **1d**, **1f**, and **2e** (Figures S27–S29). In all three cases, the barriers for the stepwise and concerted cycloadditions are energetically quite close, with a small preference for the stepwise pathway in the reaction of **2e** and an equally small preference for the concerted pathway in the reactions of **1d** and **1f**. However, in all of these reactions the structural and electronic characteristics of the transition states for concerted pathway share the same asynchronicity as those shown in Figures 5 and 6 for the reaction of vinyl ketone **1g** and thus confirm that all of these (stepwise or concerted) pathways exhibit the reactivity characteristics typical for the nucleophilic addition to Michael acceptors, as derived from the kinetic investigations described above.

Analogous calculations for the reaction of sulfonium ylide **4** with acrylonitrile (**1f**) also showed the rate-determining formation of zwitterion **11**, as suggested in Scheme 6, which expels dimethyl sulfide over a barrier of only  $5.2 \text{ kJ mol}^{-1}$  (Figure S30). A slightly different approach of the two reactants leads to a concerted process with a  $2.3 \text{ kJ mol}^{-1}$  higher Gibbs activation energy, where ring closure and expulsion of dimethyl sulfide start before the initial Michael addition is complete.

Again, the calculated potential energy surface confirms our interpretation of the kinetic data.

In order to elucidate methods for predicting the synthetic potential of Michael acceptors so far not yet experimentally characterized, we investigated correlations of experimentally determined electrophilic reactivities with various quantum chemically calculated properties:

Methyl anion affinities ( $\text{MAA} = -\Delta G_{298}$ ) were calculated as the Gibbs reaction energies for the methyl anion additions shown in eq 2.



Following the methodology used in earlier studies,<sup>48</sup> gas phase MAA values were calculated at B3LYP/6-311++G(3df,2pd)//B3LYP/6-31G(d,p) level<sup>45</sup> (see Supporting Information for details). In addition, solvent effects were probed by additional single-point calculations with the SMD continuum solvation model for dimethyl sulfoxide (DMSO)<sup>46</sup> at B3LYP/6-31G(d,p) level as well as full geometry optimization with this solvation model.

Parr's electrophilicity indices  $\omega$  (eq 3) for 44 Michael acceptors were calculated from the electronic chemical potential  $\mu$  (eq 4) and the chemical hardness  $\eta$  (eq 5).

$$\omega = \mu^2/2\eta \quad (3)$$

$$\mu = \frac{1}{2}(\epsilon_{\text{HOMO}} + \epsilon_{\text{LUMO}}) \quad (4)$$

$$\eta = (\epsilon_{\text{LUMO}} - \epsilon_{\text{HOMO}}) \quad (5)$$

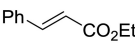
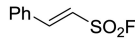
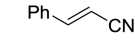
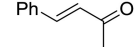
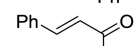
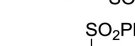
Values for the electronic chemical potential  $\mu$  and the chemical hardness  $\eta$  were derived from orbital energies for the lowest unoccupied molecular orbital ( $\epsilon_{\text{LUMO}}$ ) and the highest occupied molecular orbital ( $\epsilon_{\text{HOMO}}$ ) calculated at gas phase B3LYP/6-31G(d,p) level (in Hartree). Following the practice in ref 5, Parr's electrophilicity index  $\omega$  is then expressed in eV. Local electrophilicity indices  $\omega_{\beta}$  at the  $\beta$ -centers of Michael acceptors (eq 2) were calculated using the nucleophilic Fukui function ( $f_{\text{k}}^+$ ) as defined in eq 6.

$$\omega_{\beta} = \omega f_{\beta}^+ \quad (6)$$

The condensed Fukui function for the nucleophilic attack at the  $\beta$ -atom ( $f_{\beta}^+$ ) in an electrophile was calculated using a procedure from ref 8.

The most relevant calculated properties for the 44 Michael acceptors shown in Figure 3 are listed in Table 2 (for further quantum chemically calculated data, see the Supporting Information).

**Correlation with LUMO Energies and Parr's electrophilicity Index.** Liu and co-workers<sup>49</sup> as well as Yu and co-workers<sup>3</sup> have reported excellent correlations between electrophilic reactivities of benzhydrylium ions and the corresponding LUMO energies. However, Figure 5 in ref 3 shows that Michael acceptors  $\text{ArCH}=\text{C}(\text{Acc})_2$  with different acceptor groups Acc follow separate electrophilicity vs LUMO energy correlations. In line with these observations, Figure 7 in this work shows that LUMO energies are not a useful guide for predicting electrophilic reactivities when a larger variety of Michael acceptors are compared. Even inferior correlations are obtained when using LUMO energies calculated with larger basis sets (such as 6-311++G(3df,2pd),  $R^2 = 0.362$ , Figure S10) or

	Electrophilicity $E$	$\Delta G_{sol-sp}$ (in DMSO) (kJ mol <sup>-1</sup> )	$\epsilon_{LUMO}$ (Hartree)	$\omega$ (eV)	
<b>1b</b>		-19.07	-75.1	-0.0429	1.47
<b>2b</b>		-24.52	-36.1	-0.0628	1.75
	$\Delta E = -5.45$	$\Delta\Delta G_{sol-sp} = 39.0$	$\Delta\epsilon = -0.0199$	$\Delta\omega = 0.28$	
<b>1j</b>		-12.09	-160.5	-0.0644	1.97
<b>2g</b>		-16.63	-113.3	-0.0830	2.26
	$\Delta E = -4.54$	$\Delta\Delta G_{sol-sp} = 47.2$	$\Delta\epsilon = -0.0186$	$\Delta\omega = 0.29$	
<b>1f</b>		-19.05	-109.4	-0.0570	1.76
<b>2d</b>		-24.6	-66.1	-0.0749	2.04
	$\Delta E = -5.5$	$\Delta\Delta G_{sol-sp} = 43.3$	$\Delta\epsilon = -0.0179$	$\Delta\omega = 0.28$	
<b>1g</b>		-16.76	-104.2	-0.0548	1.61
<b>2e</b>		-23.01	-60.4	-0.0692	1.90
	$\Delta E = -6.25$	$\Delta\Delta G_{sol-sp} = 43.8$	$\Delta\epsilon = -0.0144$	$\Delta\omega = 0.29$	
<b>1h</b>		-15.25	-116.7	-0.0715	1.97
<b>2f</b>		-19.39	-74.8	-0.0774	2.11
	$\Delta E = -4.14$	$\Delta\Delta G_{sol-sp} = 41.9$	$\Delta\epsilon = -0.0059$	$\Delta\omega = 0.14$	
<b>17f</b>		-7.50	-174.8	-0.0720	2.01
<b>17k</b>		-12.93	-155.9	-0.0806	2.19
	$\Delta E = -5.43$	$\Delta\Delta G_{sol-sp} = 18.9$	$\Delta\epsilon = -0.0086$	$\Delta\omega = 0.18$	

**Figure 9.**  $\beta$ -Phenyl effect on different descriptors for electrophilic reactivities of Michael acceptors ( $\Delta G_{sol-sp}$  corresponds to the negative values of the methyl anion affinities in DMSO solution, eq 2).

calculated in the presence of the SMD solvation model for DMSO ( $R^2 = 0.351$ , see Supporting Information).

The teams of Contreras, Domingo, Perez, and Chamorro have examined Parr's electrophilicity index  $\omega$  (eq 3) and modifications thereof for rationalizing and predicting electrophilic reactivities.<sup>11,50</sup> Within the series of benzhydrylium ions, good correlations have been found.<sup>50</sup> They furthermore observed good correlations between the electrophilicity parameters of Michael acceptors and Parr's electrophilicity indices within families of closely related Michael acceptors, e.g., benzylidenemalononitriles.<sup>5,11</sup> The good correlations obtained within these families, however, do not allow a generalization. While the authors explicitly predicted that introduction of a phenyl group in  $\beta$ -position of methyl acrylate leads to an increase of electrophilicity, the kinetic data reported in this work show the opposite: Ethyl cinnamate (**2b**) is more than 5 orders of magnitude less electrophilic than ethyl acrylate (**1b**). Figure 8 illustrates the  $\beta$ -phenyl effect on frontier orbital energies.

It is a general phenomenon that conjugation raises HOMO and lowers LUMO energy levels. For that reason, the large reduction of electrophilicity by  $\beta$ -phenyl substitution is not in line with the expectations on the basis of LUMO energies. The same discrepancy arises with all other Michael acceptors as shown in Figure 9. In all cases,  $\beta$ -phenyl substitution lowers LUMO energies and at the same time decreases electrophilicity.

For a similar reason, Parr's electrophilicity index  $\omega$  (eq 3) fails to predict the  $\beta$ -phenyl effect. Due to the simultaneous raising of HOMO and lowering of LUMO, the electronic

potential  $\mu$  (eq 4) is only slightly affected by the phenyl substitution, whereas hardness  $\eta$  (eq 5) decreases and, as a consequence,  $\omega$  increases, in contrast to the experimentally observed decrease of electrophilic reactivity. A certain portion of the decrease of electrophilic reactivity by  $\beta$ -phenyl can certainly be explained by a steric effect. However, whatever the reason, it is obvious that (like LUMO energies) Parr's electrophilicity  $\omega$  is not suitable to predict electrophilic reactivities for a wider range of Michael acceptors, as shown in Figure 10a. When moving from global ( $\omega$ ) to local electrophilicity indices  $\omega_\beta$  (eq 6), the correlations with experimentally determined  $E$  parameters improve, but with  $R^2 = 0.467$  still remain unsatisfactory (Figure 10b). We note in passing that the latter correlation does not improve with other strategies for calculating local electrophilicity parameters (see Supporting Information for details).

Excellent correlations between the electrophilic reactivities of benzhydrylium ions and their Lewis acidities, represented by  $pK_{R^+}$  values or calculated methyl anion affinities have previously been reported.<sup>51,52</sup> While the high qualities of these correlations can be assigned to the constant steric demand of these electrophiles, a fair correlation between electrophilic reactivities and the Lewis acidities  $pK_{R^+}$  has also been observed for carbocations of variable structure.<sup>53</sup> For that reason, it appeared promising to also examine the relationship between electrophilicities and Lewis acidities of the Michael acceptors. Figure 11 shows the correlation between electrophilicities and calculated gas phase methyl anion affinities. Though of moderate quality, this correlation is already much better than

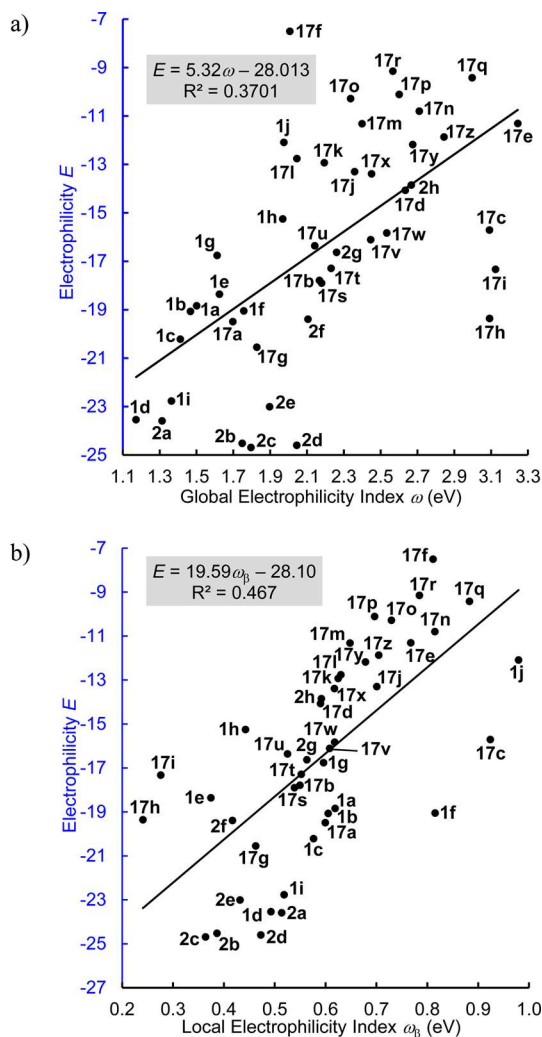


**Figure 10.** Correlation between experimentally determined electrophilicities ( $E$ ) and (a) global electrophilicity index  $\omega$  and (b) local electrophilicity index  $\omega_{\beta}$  calculated at B3LYP/6-31G(d,p) level for the 44 electrophiles listed in Figure 3.

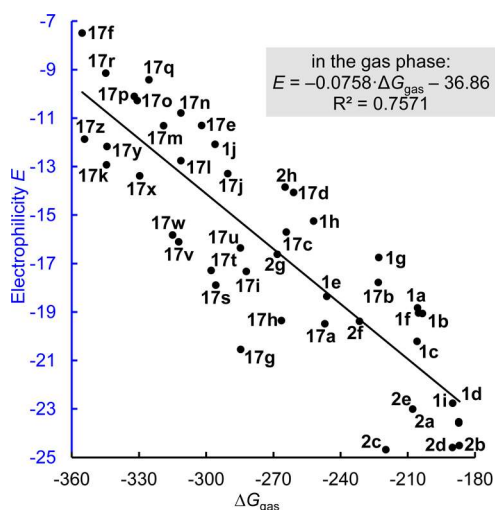


**Figure 11.** Correlation between experimentally determined electrophilicities ( $E$ ) and gas phase methyl anion affinities ( $-\text{MAA} = \Delta G_{\text{gas}}$ ,  $\text{kJ mol}^{-1}$ ) calculated at B3LYP/6-311++G(3df,2pd)//B3LYP/6-31G(d,p) level for the 44 electrophiles listed in Figure 3.

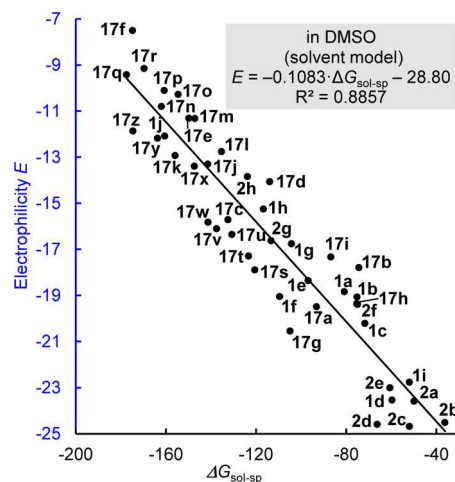


**Figure 12.** Correlation between experimentally determined electrophilicities ( $E$ ) and methyl anion affinities ( $-\text{MAA} = \Delta G_{\text{sol-sp}}$  in  $\text{kJ mol}^{-1}$ ) in DMSO calculated at SMD(DMSO)/B3LYP/6-311++G(3df,2pd)//B3LYP/6-31G(d,p) level for the 44 electrophiles listed in Figure 3.

those related to orbital energies (Figure 7 and Figure S3). A good linear correlation was observed, however, when the empirical electrophilicity parameters  $E$  (derived from kinetic measurements) were plotted against the methyl anion affinities calculated for DMSO solution (Figure 12).

The correlation did not improve significantly when the methyl anion affinities calculated for DMSO-solvated gas-phase optimized structures in Figure 12 were replaced by methyl anion affinities derived from structures, which had been geometrically optimized in DMSO solution ( $R^2 = 0.8867$ , Figure S19). For that reason, our discussion will focus on correlations with the methyl anion affinities calculated for DMSO-solvated gas-phase optimized structures. Let us first compare the different slopes in Figures 11 and 12: The ratio of these slopes ( $0.0758/0.1083 = 0.70$ ) indicates that the differences of the methyl anion affinities in the gas phase are attenuated to 70% in DMSO solution. This information can directly be derived from a plot of methyl anion affinities in DMSO solution versus MAA in the gas phase (Figure S24).

Combination of eq 1 with the Eyring equation leads to

$$\Delta G^{\ddagger} = 2.303RT[\log(k_{\text{B}}T/h) - s_{\text{N}}(E + N)] \quad (7)$$

which can be rewritten as eq 8 for the reaction with a certain nucleophile

$$\Delta G^{\ddagger} = -2.303RTs_{\text{N}}E + \text{const} \quad (8)$$

Insertion of the correlation derived in Figure 12 yields eq 9

$$\Delta G^{\ddagger} = 0.61 \cdot s_{\text{N}} \cdot \Delta G_{\text{sol-sp}} + \text{const}' \quad (9)$$

which shows that in reactions of Michael acceptors with nucleophiles of  $s_{\text{N}} = 0.7$  about 43% of the differences of the Gibbs reaction energies are reflected in the transition states.

Figure 12 illustrates that the experimentally determined  $E$  values deviate on average by  $\pm 1.3$  units from the correlated values, while the maximum deviations are 3 units in  $E$ , corresponding to a deviation of a factor of 100 in rate constants for reactions with nucleophiles having a typical susceptibility factor of  $s_{\text{N}} = 0.7$ . We consider this as an excellent agreement in view of the wide structural variety covered by the Michael

acceptors in this investigation, which span 17 orders of magnitude in electrophilicity  $E$ .

## CONCLUSION

Kinetic investigations show that the reactions of weakly activated Michael acceptors with pyridinium ylides ((3 + 2)-cycloadditions), a sulfonium ylide, and a phenylsulfonyl-substituted chloromethyl anion (cyclopropanations) follow eq 1, indicating stepwise processes with a common rate-determining step. This conclusion, which has been confirmed by potential energy surface calculations, implies that a single set of electrophilicity parameters  $E$  for Michael acceptors can be used to calculate rate constants for ordinary Michael additions (for example, additions of carbanions) as well as for a variety of other reactions which proceed via rate-determining formation of the first C–C  $\sigma$ -bond. By inclusion of these data in our comprehensive electrophilicity scale, the direct comparison of weak and strong electrophiles becomes possible. The electrophilicities of the acceptor-substituted olefins investigated in this work may also broaden the experimental basis for the ongoing developments of the distortion/interaction energy model<sup>54</sup> and the activation strain model.<sup>55</sup>

Quantum chemical calculations show that neither LUMO energies nor Parr's electrophilicity index allow the prediction of relative reactivities of structurally diverse Michael acceptors. In contrast, a good correlation between electrophilic reactivities and quantum chemically calculated methyl anion affinities in DMSO solution was found, which may also be useful for evaluating the toxicological profile of naturally occurring or anthropogenic Michael acceptors. It is thus indicated that the relative reactivities of different families of Michael acceptors cannot be derived from orbital interactions of the reactants but from the thermodynamics of the rate-determining step, as postulated by the Bell–Evans–Polanyi principle.<sup>56</sup>

## ASSOCIATED CONTENT

### Supporting Information

The Supporting Information is available free of charge on the ACS Publications website at DOI: 10.1021/jacs.7b05106.

Detailed experimental procedures and compound characterization data, results of individual kinetic experiments, and details of quantum chemical calculations (PDF)

## AUTHOR INFORMATION

### Corresponding Authors

\*zipse@cup.uni-muenchen.de

\*ofial@lmu.de

\*herbert.mayr@cup.uni-muenchen.de

### ORCID

Haruyasu Asahara: 0000-0002-1808-7373

Hendrik Zipse: 0000-0002-0534-3585

Armin R. Ofial: 0000-0002-9600-2793

Herbert Mayr: 0000-0003-0768-5199

### Present Addresses

D.S.A.: Clariant Produkte (Deutschland) GmbH, 84504 Burgkirchen, Germany.

H.A.: Department of Applied Chemistry, Faculty of Engineering, Osaka University, Osaka 565-0871, Japan.

Q.C.: Institut für Anorganische and Angewandte Chemie, Universität Hamburg, 20148 Hamburg, Germany.

## Notes

The authors declare no competing financial interest.

## ACKNOWLEDGMENTS

We thank the Deutsche Forschungsgemeinschaft for financial support (SFB 749, projects B1 and C6) and the China Scholarship Council for a fellowship to Z. L.

## REFERENCES

- (1) (a) Bergmann, E. D.; Ginsburg, D.; Pappo, R. *Org. React.* **1959**, *10*, 179–556. (b) Patai, S.; Rappoport, Z. In *The Chemistry of Alkenes*; Patai, S., Rappoport, Z., Eds.; Wiley: New York, 1964; pp 469–584. (c) Nagata, W.; Yoshioka, M. *Org. React.* **1977**, *25*, 255–476. (d) Oare, D. A.; Heathcock, C. H. In *Topics in Stereochemistry*; Eliel, E. L., Wilen, S. H., Eds.; Wiley-Interscience: New York, 1989; Vol. 18, pp 227–407. (e) Rappoport, Z. In *Nucleophilicity*; Harris, J. M., McManus, S. P., Eds.; American Chemical Society: Washington, DC, 1987; pp 399–424. (f) Oare, D. A.; Heathcock, C. H. In *Topics in Stereochemistry*; Eliel, E. L., Wilen, S. H., Eds.; Wiley-Interscience: Hoboken, NJ, 1991; Vol. 20, pp 87–170. (g) Perlmutter, P. In *Tetrahedron Organic Chemistry Series*; Baldwin, J. E., Ed.; Pergamon: Oxford, 1992; Vol. 9.
- (2) (a) Bernasconi, C. F. *Tetrahedron* **1989**, *45*, 4017–4090. (b) Rappoport, Z.; Ladkani, D. *Chem. Scripta* **1974**, *5*, 124–133.
- (3) Zhuo, L.-G.; Liao, W.; Yu, Z.-X. *Asian J. Org. Chem.* **2012**, *1*, 336–345.
- (4) Parr, R. G.; Szentpály, L. v.; Liu, S. *J. Am. Chem. Soc.* **1999**, *121*, 1922–1924.
- (5) Domingo, L. R.; Pérez, P.; Contreras, R. *Tetrahedron* **2004**, *60*, 6585–6591.
- (6) Domingo, L. R.; Ríos-Gutiérrez, M.; Pérez, P. *Molecules* **2016**, *21*, 748.
- (7) Moraleda, D.; El Abed, D.; Pellissier, H.; Santelli, M. *J. Mol. Struct.: THEOCHEM* **2006**, *760*, 113–119.
- (8) Contreras, R. R.; Fuentealba, P.; Galván, M.; Pérez, P. *Chem. Phys. Lett.* **1999**, *304*, 405–413.
- (9) (a) Chattaraj, P. K.; Sarkar, U.; Roy, D. R. *Chem. Rev.* **2006**, *106*, 2065–2091. (b) Chattaraj, P. K.; Roy, D. R. *Chem. Rev.* **2007**, *107*, PR46–PR74. (c) Chattaraj, P. K.; Giri, S.; Duley, S. *Chem. Rev.* **2011**, *111*, PR43–PR75.
- (10) Liu, S. In *Chemical Reactivity Theory – A Density Functional View*; Chattaraj, P. K., Ed.; CRC Press: Boca Raton, FL, 2009; Chapter 13, pp 179–192.
- (11) (a) Aizman, A.; Contreras, R.; Pérez, P. *Tetrahedron* **2005**, *61*, 889–895. (b) Pérez, P.; Domingo, L. R.; Aizman, A.; Contreras, R. In *Theoretical Aspects of Chemical Reactivity*; Theoretical and Computational Chemistry series; Toro-Labbé, A., Ed.; Elsevier, Amsterdam, 2007; Vol. 19, Chapter 9, pp 139–201.
- (12) Wondrousch, D.; Böhme, A.; Thaens, D.; Ost, N.; Schüürmann, G. *J. Phys. Chem. Lett.* **2010**, *1*, 1605–1610.
- (13) (a) Mayr, H.; Patz, M. *Angew. Chem., Int. Ed. Engl.* **1994**, *33*, 938–957. (b) Mayr, H.; Bug, T.; Gotta, M. F.; Hering, N.; Irrgang, B.; Janker, B.; Kempf, B.; Loos, R.; Ofial, A. R.; Remennikov, G.; Schimmel, H. *J. Am. Chem. Soc.* **2001**, *123*, 9500–9512. (c) Mayr, H.; Kempf, B.; Ofial, A. R. *Acc. Chem. Res.* **2003**, *36*, 66–77. (d) Mayr, H.; Ofial, A. R. *Pure Appl. Chem.* **2005**, *77*, 1807–1821. (e) Mayr, H.; Ofial, A. R. *J. Phys. Org. Chem.* **2008**, *21*, 584–595. (f) Mayr, H.; Lakhdar, S.; Maji, B.; Ofial, A. R. *Beilstein J. Org. Chem.* **2012**, *8*, 1458–1478. (g) For a comprehensive database of nucleophilicity parameters  $N$ ,  $N_S$ , and electrophilicity parameters  $E$ , see <http://www.cup.lmu.de/oc/mayr/DBintro.html>.
- (14) (a) Lucius, R.; Loos, R.; Mayr, H. *Angew. Chem., Int. Ed.* **2002**, *41*, 91–95. (b) Lemek, T.; Mayr, H. *J. Org. Chem.* **2003**, *68*, 6880–6886. (c) Berger, S. T. A.; Seeliger, F. H.; Hofbauer, F.; Mayr, H. *Org. Biomol. Chem.* **2007**, *5*, 3020–3026. (d) Kaumanns, O.; Lucius, R.; Mayr, H. *Chem. - Eur. J.* **2008**, *14*, 9675–9682. (e) Lakhdar, S.; Tokuyasu, T.; Mayr, H. *Angew. Chem., Int. Ed.* **2008**, *47*, 8723–8726. (f) Kanzian, T.; Nicolini, S.; De Crescentini, L.; Attanasio, O. A.; Ofial,

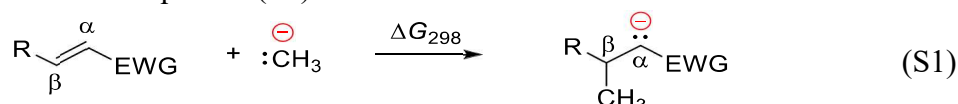
- A. R.; Mayr, H. *Chem. - Eur. J.* **2010**, *16*, 12008–12016. (g) Appel, R.; Mayr, H. *J. Am. Chem. Soc.* **2011**, *133*, 8240–8251. (h) Zenz, I.; Mayr, H. *J. Org. Chem.* **2011**, *76*, 9370–9378. (i) Asahara, H.; Mayr, H. *Chem. - Asian J.* **2012**, *7*, 1401–1407.
- (15) (a) Ogata, Y.; Okano, M.; Furuya, Y.; Tabushi, I. *J. Am. Chem. Soc.* **1956**, *78*, 5426–5428. (b) Finley, K. T.; Call, D. R.; Sovocool, G. W.; Hayles, W. J. *Can. J. Chem.* **1967**, *45*, 571–573.
- (16) (a) Ogata, N.; Asahara, T. *Bull. Chem. Soc. Jpn.* **1966**, *39*, 1486–1490. (b) Šestáková, I.; Horák, V.; Zuman, P. *Collect. Czech. Chem. Commun.* **1966**, *31*, 3889–3902. (c) Dienys, G. J.; Kunskaite, L. J. J.; Vaitkevicius, A. K.; Klimavicius, A. V. *Org. React. (Tartu), Engl. Ed.* **1975**, *12*, 275–282. (d) Adomeniene, O.; Dienys, G.; Stumbreviciute, Z. *Org. React. (Tartu), Engl. Ed.* **1978**, *15*, 38–44.
- (17) (a) Mallik, K. L.; Das, M. N. *Z. Phys. Chem.* **1960**, *25*, 205–216. (b) Sanui, K.; Ogata, N. *Bull. Chem. Soc. Jpn.* **1967**, *40*, 1727. (c) Shenhav, H.; Rappoport, Z.; Patai, S. *J. Chem. Soc. B* **1970**, 469–476. (d) Szczesna, J.; Kostecki, M.; Kinastowski, S. *Rocz. Akad. Roln. Poznaniu* **1988**, *192*, 99–104. (e) Kostecki, M.; Szczesna, J.; Kinastowski, S. *Rocz. Akad. Roln. Poznaniu* **1993**, *256*, 25–32.
- (18) (a) Bunting, J. W.; Toth, A.; Heo, C. K. M.; Moors, R. G. *J. Am. Chem. Soc.* **1990**, *112*, 8878–8885. (b) Heo, C. K. M.; Bunting, J. W. *J. Org. Chem.* **1992**, *57*, 3570–3578.
- (19) (a) Friedman, M.; Wall, J. S. *J. Am. Chem. Soc.* **1964**, *86*, 3735–3741. (b) Friedman, M.; Cavins, J. F.; Wall, J. S. *J. Am. Chem. Soc.* **1965**, *87*, 3672–3682. (c) Friedman, M.; Wall, J. S. *J. Org. Chem.* **1966**, *31*, 2888–2894. (d) Friedman, M.; Romersberger, J. A. *J. Org. Chem.* **1968**, *33*, 154–157.
- (20) (a) Cársky, P.; Zuman, P.; Horák, V. *Collect. Czech. Chem. Commun.* **1965**, *30*, 4316–4336. (b) Feit, B. A.; Pazhenchevsky, R.; Pazhenchevsky, B. *J. Org. Chem.* **1976**, *41*, 3246–3250.
- (21) (a) Ferry, N.; McQuillin, F. J. *J. Chem. Soc.* **1962**, 103–113. (b) Feit, B.-A.; Zilkha, A. *J. Org. Chem.* **1963**, *28*, 406–410. (c) Ring, R. N.; Tesoro, G. C.; Moore, D. R. *J. Org. Chem.* **1967**, *32*, 1091–1094.
- (22) (a) Morton, M.; Landfield, H. *J. Am. Chem. Soc.* **1952**, *74*, 3523–3526. (b) Davies, W. G.; Hardisty, E. W.; Nevell, T. P.; Peters, R. H. *J. Chem. Soc. B* **1970**, 998–1004.
- (23) (a) Roberts, D. W.; Natsch, A. *Chem. Res. Toxicol.* **2009**, *22*, 592–603. (b) Schwöbel, J. A. H.; Wondrousch, D.; Koleva, Y. K.; Madden, J. C.; Cronin, M. T. D.; Schüürmann, G. *Chem. Res. Toxicol.* **2010**, *23*, 1576–1585. (c) Amslinger, S.; Al-Rifai, N.; Winter, K.; Wörmann, K.; Scholz, R.; Baumeister, P.; Wild, M. *Org. Biomol. Chem.* **2013**, *11*, 549–554. (d) Böhme, A.; Laqua, A.; Schüürmann, G. *Chem. Res. Toxicol.* **2016**, *29*, 952–962.
- (24) Petneházy, I.; Clementis, G.; Jászay, Z. M.; Töke, L.; Hall, C. D. *J. Chem. Soc., Perkin Trans. 2* **1996**, 2279–2284.
- (25) Allgäuer, D. S.; Mayr, H. *Eur. J. Org. Chem.* **2014**, 2956–2963.
- (26) Allgäuer, D. S.; Mayer, P.; Mayr, H. *J. Am. Chem. Soc.* **2013**, *135*, 15216–15224.
- (27) Appel, R.; Hartmann, N.; Mayr, H. *J. Am. Chem. Soc.* **2010**, *132*, 17894–17900.
- (28) Li, Z.; Chen, Q.; Mayer, P.; Mayr, H. *J. Org. Chem.* **2017**, *82*, 2011–2017.
- (29) Zugravescu, I.; Petrovanu, M. *N-Ylid Chemistry*; McGraw-Hill: New York, 1976.
- (30) (a) Mikhailovskii, A. G.; Shklyayev, V. S. *Chem. Heterocycl. Compd.* **1997**, *33*, 243–265. (b) Jacobs, J.; Van Hende, E.; Claessens, S.; De Kimpe, N. *Curr. Org. Chem.* **2011**, *15*, 1340–1362. (c) Kakehi, A. *Heterocycles* **2012**, *85*, 1529–1577.
- (31) Tsuge, O.; Kanemasa, S.; Takenaka, S. *Bull. Chem. Soc. Jpn.* **1985**, *58*, 3137–3157.
- (32) Huisgen, R. *J. Org. Chem.* **1976**, *41*, 403–419.
- (33) (a) Firestone, R. A. *J. Org. Chem.* **1968**, *33*, 2285–2290. (b) Firestone, R. A. *J. Org. Chem.* **1972**, *37*, 2181–2191.
- (34) Huisgen, R. *J. Org. Chem.* **1968**, *33*, 2291–2297.
- (35) Li, A.-H.; Dai, L.-X.; Aggarwal, V. K. *Chem. Rev.* **1997**, *97*, 2341–2372.
- (36) Appel, R.; Mayr, H. *Chem. - Eur. J.* **2010**, *16*, 8610–8614.
- (37) Riches, S. L.; Saha, C.; Filgueira, N. F.; Grange, E.; McGarrigle, E. M.; Aggarwal, V. K. *J. Am. Chem. Soc.* **2010**, *132*, 7626–7630.
- (38) Allgäuer, D. S.; Mayr, H. *Eur. J. Org. Chem.* **2013**, 6379–6388.
- (39) DeGraffenreid, M. R.; Bennett, S.; Caille, S.; Gonzalez-Lopez de Turiso, F.; Hungate, R. W.; Julian, L. D.; Kaizerman, J. A.; McMinn, D. L.; Rew, Y.; Sun, D.; Yan, X.; Powers, J. P. *J. Org. Chem.* **2007**, *72*, 7455–7458.
- (40) Gersch, M.; Kreuzer, J.; Sieber, S. A. *Nat. Prod. Rep.* **2012**, *29*, 659–682.
- (41) Mayr, H.; Ofial, A. R. *SAR QSAR Environ. Res.* **2015**, *26*, 619–646.
- (42) At pH 7.4, glutathione (GSH) was shown to react with enones to give S-alkylation, terminal N-alkylation, and adducts of two-fold (S and N) alkylation: Slawik, C.; Rickmeyer, C.; Brehm, M.; Böhme, A.; Schüürmann, G. *Environ. Sci. Technol.* **2017**, *51*, 4018–4026.
- (43) Mulliner, D.; Wondrousch, D.; Schüürmann, G. *Org. Biomol. Chem.* **2011**, *9*, 8400–8412.
- (44) Hansch, C.; Leo, A.; Hoekman, D. *Exploring QSAR – Hydrophobic, Electronic and Steric Constants*; American Chemical Society: Washington, DC, 1995.
- (45) (a) Ditchfield, R.; Hehre, W. J.; Pople, J. A. *J. Chem. Phys.* **1971**, *54*, 724–728. (b) Krishnan, R.; Binkley, J. S.; Seeger, R.; Pople, J. A. *J. Chem. Phys.* **1980**, *72*, 650–654. (c) Clark, T.; Chandrasekhar, J.; Spitznagel, G. W.; Schleyer, P. v. R. *J. Comput. Chem.* **1983**, *4*, 294–301. (d) Dunning, T. H., Jr. *J. Chem. Phys.* **1989**, *90*, 1007–1023. (e) Becke, A. D. *J. Chem. Phys.* **1993**, *98*, 5648–5652. (f) Grimme, S. *J. Chem. Phys.* **2006**, *124*, 034108.
- (46) Marenich, A. V.; Cramer, C. J.; Truhlar, D. G. *J. Phys. Chem. B* **2009**, *113*, 6378–6396.
- (47) As compounds **6** were not isolated but oxidized to give isolated indolizines **7**, the stereochemical course was not investigated.
- (48) Byrne, P. A.; Kobayashi, S.; Würthwein, E.-U.; Ammer, J.; Mayr, H. *J. Am. Chem. Soc.* **2017**, *139*, 1499–1511.
- (49) Wang, C.; Fu, Y.; Guo, Q.-X.; Liu, L. *Chem. - Eur. J.* **2010**, *16*, 2586–2598.
- (50) (a) Chamorro, E.; Duque-Noreña, M.; Pérez, P. *J. Mol. Struct.: THEOCHEM* **2009**, *896*, 73–79. (b) Chamorro, E.; Duque-Noreña, M.; Pérez, P. *J. Mol. Struct.: THEOCHEM* **2009**, *901*, 145–152.
- (51) Schindele, C.; Houk, K. N.; Mayr, H. *J. Am. Chem. Soc.* **2002**, *124*, 11208–11214.
- (52) (a) Mayr, H.; Ammer, J.; Baidya, M.; Maji, B.; Nigst, T. A.; Ofial, A. R.; Singer, T. *J. Am. Chem. Soc.* **2015**, *137*, 2580–2599. (b) Mayr, H.; Ofial, A. R. *Acc. Chem. Res.* **2016**, *49*, 952–965.
- (53) Mayr, H.; Patz, M.; Gotta, M. F.; Ofial, A. R. *Pure Appl. Chem.* **1998**, *70*, 1993–2000.
- (54) (a) Ess, D. H.; Houk, K. N. *J. Am. Chem. Soc.* **2008**, *130*, 10187–10198. (b) Bickelhaupt, F. M.; Houk, K. N. *Angew. Chem., Int. Ed.* **2017**, *56*, 10070–10086.
- (55) (a) van Zeist, W.-J.; Bickelhaupt, F. M. *Org. Biomol. Chem.* **2010**, *8*, 3118–3127. (b) Fernández, I.; Bickelhaupt, F. M. *Chem. Soc. Rev.* **2014**, *43*, 4953–4967.
- (56) (a) Bell, R. P. *Proc. R. Soc. London, Ser. A* **1936**, *154* (882), 414–429. (b) Evans, M. G.; Polanyi, M. *Trans. Faraday Soc.* **1938**, *34*, 11–24.

## 7.1 Supporting Information

For: Quantification and Theoretical Analysis of the Electrophilicities of Michael Acceptors

### 7.1.1 Methodology

Methyl anion affinities (MAA) in the gas phase have been calculated using the same methodology employed successfully in earlier studies<sup>1</sup> as the gas phase free energy at 298.15 K ( $\Delta G_{298}$ ) of the addition reaction shown in equation (S1).



Geometry optimizations have been performed with a combination of the B3LYP hybrid functional<sup>2</sup> and the 6-31G(d,p) basis set.<sup>3</sup> Thermochemical corrections to Gibbs energies (Corr.  $\Delta G$ ) at 298.15 K have been calculated using the rigid rotor/harmonic oscillator model without any scaling. Single point calculations have subsequently been calculated using a combination of the B3LYP hybrid functional and the larger 6-311++G(3df,2pd) basis set.<sup>3-4</sup> Final Gibbs energies ( $\Delta G_{298}$ ) have been obtained through a combination of these single point energies ( $E_{\text{tot}}$ ) with the thermochemical corrections to Gibbs energies (Corr.  $\Delta G$ ) calculated at lower level. In the following these will be designated as  $\Delta G_{\text{gas}}(\text{B3LYP}/6-311++\text{G}(3\text{df},2\text{pd})/\text{B3LYP}/6-31\text{G}(\text{d},\text{p}))$ .

Solvent effects on MAA values have first been estimated by adding single point solvation corrections ( $\Delta G_{\text{Solv}}$ ) to  $\Delta G_{\text{gas}}$  values for eq. (S1).  $\Delta G_{\text{Solv}}$  was calculated for the gas phase optimized geometries using the SMD<sup>5</sup> continuum solvation model and subsequently added to the gas phase Gibbs energies ( $\Delta G_{\text{gas}}$ ) to obtain solution phase Gibbs energies that will be mentioned as single point solvation free energies ( $\Delta G_{\text{sol-sp}}$ ). In another approach geometry optimization is carried out under implicit DMSO (SMD) conditions at B3LYP/6-31G(d,p) level. The Gibbs energies calculated using the implicit DMSO optimized geometry will be designated as  $\Delta G_{\text{sol-opt}}$ .

Electrophilicity indices like the electronic chemical potential ( $\mu$ ), chemical hardness ( $\eta$ ) and global electrophilicity index ( $\omega$ ) were calculated from orbital energies using equations (S2), (S3), and (S4).<sup>6</sup>

$$\mu = \frac{1}{2} (\varepsilon_{\text{HOMO}} + \varepsilon_{\text{LUMO}}) \quad (\text{S2})$$

$$\eta = (\varepsilon_{\text{LUMO}} - \varepsilon_{\text{HOMO}}) \quad (\text{S3})$$

$$\omega = \mu^2 / 2\eta \quad (\text{S4})$$

Local electrophilicity indices at  $\alpha$  ( $\omega_{\alpha}$ ) and  $\beta$  ( $\omega_{\beta}$ ) centers for electrophiles (see eq. S1) were calculated using the nucleophilic Fukui function ( $f_{\beta}^+$ ) as defined in equation (S5).

$$\omega_{\beta} = \omega f_{\beta}^+ \quad (\text{S5})$$

In this work, we calculated the nucleophilic Fukui function ( $f^+$ ) using two different approaches. First, the condensed nucleophilic Fukui function ( $f_{\beta}^+$ ) for atom  $\beta$  was calculated using a procedure described by Contreras and co-workers.<sup>7</sup> The nucleophilic Fukui function ( $f_{\beta}^+$ ) was calculated from the Gaussian 09 output files by the Fukui function program available at <https://github.com/dmsteglenko/Fukui-function-calculation>.

In a second approach we used the Yang and Mortier method<sup>8</sup> where the Fukui function for nucleophilic attack is defined as the change of partial charge  $q_{\beta}$  at a certain atom  $\beta$  by adding an electron to the corresponding molecule, that is:

$$f_{\beta}^+ = q_{\beta}(N+1) - q_{\beta}(N) \quad (\text{S6})$$

with  $N$  = total number of electrons in the neutral molecule. We calculated  $f_{\beta}^+$  as defined in equation (S6) using both Mulliken and NBO charges.

Potential energy surface (PES): Geometry optimizations for all stationary points (minima, complexes and TSs) along the PES have been performed at B3LYP/6-31G(d,p) level under implicit DMSO solvation as implemented in the SMD solvation model. Energy minima, complexes and TSs were confirmed by vibrational frequency calculations with 0, 0, and 1 imaginary frequencies, respectively. All stationary points were checked for wavefunction stability (stable=opt). The nature of transition states was further confirmed by IRC calculations [30 steps in both directions (reverse/forward) with stepsize=3] followed by geometry optimization to the next minimum. In cases of very flat PES(s), manual displacement away from the TS(s) followed by geometry optimization was employed. PES surfaces were re-evaluated at B3LYP/6-311++G(3df,2pd) and B2PLYP/cc-pVTZ levels in combination with implicit DMSO solvation (SMD). All calculations were performed with Gaussian 09, Rev. D.<sup>9</sup>

### 7.1.2 Calculation of HOMO and LUMO Energies and Global and Local Electrophilicity Indices for Michael acceptors

**Table S7-1.** [Table S1] Electrophilicity indices calculated at B3LYP/6-31G(d,p) level for Michael acceptors.

SI	Marker	$E$	$\epsilon_{\text{HOMO}}$ $E_{\text{H}}$ (Hartree)	$\epsilon_{\text{LUMO}}$ $E_{\text{L}}$ (Hartree)	$\mu \approx$ ( $E_{\text{H}} + E_{\text{L}}$ )/2	$\eta \approx$ ( $E_{\text{L}} - E_{\text{H}}$ )	$\omega =$ $\mu^2/2\eta$ (eV)	$f_{\beta}^+$	$f_{\alpha}^+$	$\omega_{\beta} =$ $\omega * f_{\beta}^+$ (eV)	$\omega_{\alpha} =$ $\omega * f_{\alpha}^+$ (eV)
1	<b>1a</b>	-18.84	-0.27299	-0.04454	-0.15877	0.22845	1.50	0.41	0.20	0.62	0.30
2	<b>1b</b>	-19.07	-0.27018	-0.04291	-0.15655	0.22727	1.47	0.41	0.20	0.61	0.29
3	<b>1c</b>	-20.22	-0.26291	-0.04079	-0.15185	0.22212	1.41	0.41	0.20	0.58	0.28
4	<b>1d</b>	-23.54	-0.23432	-0.03058	-0.13245	0.20374	1.17	0.42	0.22	0.49	0.26
5	<b>1e</b>	-18.36	-0.27133	-0.05219	-0.16176	0.21914	1.62	0.23	0.13	0.37	0.21
6	<b>1f</b>	-19.05	-0.28955	-0.05700	-0.17328	0.23255	1.76	0.46	0.27	0.82	0.47
7	<b>1g</b>	-16.76	-0.24738	-0.05476	-0.15107	0.19262	1.61	0.37	0.15	0.60	0.23
8	<b>1h</b>	-15.25	-0.24946	-0.07147	-0.16047	0.17799	1.97	0.22	0.06	0.44	0.12
9	<b>1i</b>	-22.77	-0.26630	-0.03698	-0.15164	0.22932	1.36	0.38	0.18	0.52	0.25
10	<b>1j</b>	-12.09	-0.32333	-0.06439	-0.19386	0.25894	1.97	0.50	0.30	0.98	0.59
11	<b>2a</b>	-23.59	-0.26444	-0.03391	-0.14918	0.23053	1.31	0.39	0.17	0.51	0.23
12	<b>2b</b>	-24.52	-0.23332	-0.06275	-0.14804	0.17057	1.75	0.22	0.19	0.39	0.32
13	<b>2c</b>	-24.69	-0.23960	-0.06449	-0.15205	0.17511	1.80	0.20	0.20	0.36	0.36
14	<b>2d</b>	-24.60	-0.24292	-0.07488	-0.15890	0.16804	2.04	0.23	0.21	0.47	0.44
15	<b>2e</b>	-23.01	-0.23367	-0.06919	-0.15143	0.16448	1.90	0.23	0.16	0.43	0.30
16	<b>2f</b>	-19.39	-0.23235	-0.07737	-0.15486	0.15498	2.11	0.20	0.10	0.42	0.21
17	<b>2g</b>	-16.63	-0.26113	-0.08298	-0.17206	0.17815	2.26	0.25	0.22	0.56	0.50
18	<b>2h</b>	-13.85	-0.25556	-0.09700	-0.17628	0.15856	2.67	0.22	0.10	0.59	0.26
19	<b>17a</b>	-19.49	-0.26528	-0.05705	-0.16117	0.20823	1.70	0.35	0.21	0.60	0.36
20	<b>17b</b>	-17.79	-0.27664	-0.07861	-0.17763	0.19803	2.17	0.25	0.25	0.55	0.55
21	<b>17c</b>	-15.71	-0.30733	-0.11295	-0.21014	0.19438	3.09	0.30	0.30	0.92	0.92
22	<b>17d</b>	-14.07	-0.27143	-0.09656	-0.18400	0.17487	2.63	0.22	0.22	0.59	0.59
23	<b>17e</b>	-11.31	-0.29924	-0.11734	-0.20829	0.18190	3.25	0.24	0.24	0.77	0.77
24	<b>17f</b>	-7.50	-0.26834	-0.07201	-0.17018	0.19633	2.01	0.40	0.20	0.81	0.40
25	<b>17g</b>	-20.55	-0.23512	-0.06617	-0.15065	0.16895	1.83	0.25	0.17	0.46	0.30
26	<b>17h</b>	-19.36	-0.25831	-0.10948	-0.18390	0.14883	3.09	0.08	0.11	0.24	0.35
27	<b>17i</b>	-17.33	-0.25656	-0.11015	-0.18336	0.14641	3.12	0.09	0.11	0.28	0.33
28	<b>17j</b>	-13.30	-0.21263	-0.08495	-0.14879	0.12768	2.36	0.30	0.14	0.70	0.33
29	<b>17k</b>	-12.93	-0.25143	-0.08056	-0.16600	0.17087	2.19	0.28	0.19	0.62	0.42
30	<b>17l</b>	-12.76	-0.20434	-0.07478	-0.13956	0.12956	2.05	0.31	0.10	0.63	0.21
31	<b>17m</b>	-11.32	-0.22045	-0.08670	-0.15358	0.13375	2.40	0.27	0.07	0.65	0.17
32	<b>17n</b>	-10.80	-0.23815	-0.09709	-0.16762	0.14106	2.71	0.30	0.15	0.81	0.41
33	<b>17o</b>	-10.28	-0.22917	-0.08527	-0.15722	0.14390	2.34	0.31	0.11	0.73	0.27
34	<b>17p</b>	-10.11	-0.23995	-0.09406	-0.16701	0.14589	2.60	0.27	0.08	0.70	0.21
35	<b>17q</b>	-9.42	-0.25994	-0.10707	-0.18351	0.15287	3.00	0.29	0.16	0.88	0.48
36	<b>17r</b>	-9.15	-0.25084	-0.09360	-0.17222	0.15724	2.57	0.31	0.13	0.78	0.33

37	<b>17s</b>	-17.90	-0.18246	-0.07722	-0.12984	0.10524	2.18	0.25	0.05	0.54	0.11
38	<b>17t</b>	-17.29	-0.18808	-0.07918	-0.13363	0.10890	2.23	0.25	0.05	0.55	0.11
39	<b>17u</b>	-16.36	-0.18661	-0.07661	-0.13161	0.11000	2.14	0.25	0.05	0.53	0.12
40	<b>17v</b>	-16.11	-0.20491	-0.08668	-0.14580	0.11823	2.45	0.25	0.06	0.61	0.14
41	<b>17w</b>	-15.83	-0.21214	-0.08977	-0.15096	0.12237	2.53	0.24	0.06	0.62	0.15
42	<b>17x</b>	-13.39	-0.18767	-0.08470	-0.13619	0.10297	2.45	0.25	0.05	0.62	0.11
43	<b>17y</b>	-12.18	-0.20226	-0.09208	-0.14717	0.11018	2.67	0.25	0.05	0.68	0.14
44	<b>17z</b>	-11.87	-0.21015	-0.09719	-0.15367	0.11296	2.84	0.25	0.06	0.70	0.16

**Table S7-2.** [Table S2] Local electrophilicity indices calculated at B3LYP/6-31G(d,p) level using both Mulliken and NBO charges (Yang and Mortier method) for Michael acceptors.

SI	Marker	$\omega$	Mulliken Charge ( $\beta$ )				NBO Charge ( $\beta$ )			
			$q_{\beta}(N)$	$q_{\beta}(N+1)$	$f_{\beta}^{+}$	$\omega^{*} f_{\beta}^{+}$	$q_{\beta}(N)$	$q_{\beta}(N+1)$	$f_{\beta}^{+}$	$\omega^{*} f_{\beta}^{+}$
1	<b>1a</b>	1.50	-0.201	-0.322	0.12	0.18	-0.349	-0.624	0.28	0.41
2	<b>1b</b>	1.47	-0.201	-0.322	0.12	0.18	-0.350	-0.624	0.27	0.40
3	<b>1c</b>	1.41	-0.203	-0.321	0.12	0.17	-0.353	-0.619	0.27	0.38
4	<b>1d</b>	1.17	-0.207	-0.327	0.12	0.14	-0.351	-0.617	0.27	0.31
5	<b>1e</b>	1.62	-0.201	-0.279	0.08	0.13	-0.377	-0.542	0.16	0.27
6	<b>1f</b>	1.76	-0.191	-0.321	0.13	0.23	-0.347	-0.652	0.30	0.53
7	<b>1g</b>	1.61	-0.200	-0.321	0.12	0.19	-0.339	-0.607	0.27	0.43
8	<b>1h</b>	1.97	-0.204	-0.284	0.08	0.16	-0.335	-0.518	0.18	0.36
9	<b>1i</b>	1.36	-0.254	-0.383	0.13	0.18	-0.372	-0.633	0.26	0.36
10	<b>1j</b>	1.97	-0.190	-0.330	0.14	0.28	-0.355	-0.663	0.31	0.61
11	<b>2a</b>	1.31	-0.023	-0.118	0.09	0.12	-0.130	-0.377	0.25	0.32
12	<b>2b</b>	1.75	-0.080	-0.141	0.06	0.11	-0.153	-0.273	0.12	0.21
13	<b>2c</b>	1.80	-0.077	-0.127	0.05	0.09	-0.182	-0.284	0.10	0.18
14	<b>2d</b>	2.04	-0.075	-0.135	0.06	0.12	-0.148	-0.271	0.12	0.25
15	<b>2e</b>	1.90	-0.083	-0.152	0.07	0.13	-0.144	-0.277	0.13	0.25
16	<b>2f</b>	2.11	-0.088	-0.152	0.06	0.14	-0.140	-0.273	0.13	0.28
17	<b>2g</b>	2.26	-0.070	-0.134	0.06	0.14	-0.157	-0.290	0.13	0.30
18	<b>2h</b>	2.67	-0.096	-0.166	0.07	0.19	-0.172	-0.322	0.15	0.40
19	<b>17a</b>	1.70	-0.099	-0.206	0.11	0.18	-0.233	-0.444	0.21	0.36
20	<b>17b</b>	2.17	-0.108	-0.176	0.07	0.15	-0.269	-0.419	0.15	0.32
21	<b>17c</b>	3.09	-0.051	-0.169	0.12	0.36	-0.269	-0.469	0.20	0.62
22	<b>17d</b>	2.63	-0.109	-0.184	0.08	0.20	-0.268	-0.419	0.15	0.40
23	<b>17e</b>	3.25	-0.109	-0.192	0.08	0.27	-0.283	-0.448	0.16	0.54
24	<b>17f</b>	2.01	-0.180	-0.280	0.10	0.20	-0.336	-0.531	0.19	0.39
25	<b>17g</b>	1.83	-0.114	-0.192	0.08	0.14	-0.123	-0.262	0.14	0.26
26	<b>17h</b>	3.09	-0.083	-0.117	0.03	0.10	-0.158	-0.205	0.05	0.14
27	<b>17i</b>	3.12	-0.090	-0.126	0.04	0.11	-0.156	-0.216	0.06	0.19
28	<b>17j</b>	2.36	-0.083	-0.157	0.07	0.18	-0.089	-0.247	0.16	0.37
29	<b>17k</b>	2.19	-0.071	-0.151	0.08	0.18	-0.152	-0.301	0.15	0.33
30	<b>17l</b>	2.05	-0.144	-0.238	0.09	0.19	-0.073	-0.239	0.17	0.34
31	<b>17m</b>	2.40	-0.147	-0.232	0.08	0.20	-0.083	-0.238	0.15	0.37
32	<b>17n</b>	2.71	-0.078	-0.155	0.08	0.21	-0.086	-0.246	0.16	0.43
33	<b>17o</b>	2.34	-0.138	-0.235	0.10	0.23	-0.071	-0.240	0.17	0.39
34	<b>17p</b>	2.60	-0.146	-0.231	0.08	0.22	-0.083	-0.236	0.15	0.40
35	<b>17q</b>	3.00	-0.076	-0.153	0.08	0.23	-0.085	-0.241	0.16	0.47
36	<b>17r</b>	2.57	-0.135	-0.230	0.10	0.25	-0.071	-0.236	0.17	0.42
37	<b>17s</b>	2.18	-0.215	-0.280	0.06	0.14	-0.126	-0.265	0.14	0.30
38	<b>17t</b>	2.23	-0.214	-0.280	0.07	0.15	-0.128	-0.268	0.14	0.31
39	<b>17u</b>	2.14	-0.212	-0.281	0.07	0.15	-0.135	-0.279	0.14	0.31
40	<b>17v</b>	2.45	-0.215	-0.281	0.07	0.16	-0.131	-0.273	0.14	0.35
41	<b>17w</b>	2.53	-0.215	-0.281	0.07	0.17	-0.133	-0.271	0.14	0.35
42	<b>17x</b>	2.45	-0.209	-0.272	0.06	0.15	-0.124	-0.257	0.13	0.33
43	<b>17y</b>	2.67	-0.209	-0.273	0.06	0.17	-0.127	-0.262	0.14	0.36
44	<b>17z</b>	2.84	-0.212	-0.275	0.06	0.18	-0.131	-0.263	0.13	0.38

**Table S7-3.** [Table S3] Molecular orbital energies calculated at B3LYP/6-311++G(3df,2pd)//B3LYP/6-31G(d,p) level in the gas phase for Michael acceptors.

Marker	$\epsilon_{\text{HOMO}}$ (Hartree)	$\epsilon_{\text{LUMO}}$ (Hartree)	Marker	$\epsilon_{\text{HOMO}}$ (Hartree)	$\epsilon_{\text{LUMO}}$ (Hartree)	Marker	$\epsilon_{\text{HOMO}}$ (Hartree)	$\epsilon_{\text{LUMO}}$ (Hartree)
1a	-0.28933	-0.06356	17a	-0.28086	-0.07339	17t	-0.19919	-0.08981
1b	-0.28598	-0.06165	17b	-0.29204	-0.09441	17u	-0.21654	-0.09825
1c	-0.27728	-0.05851	17c	-0.31949	-0.12747	17v	-0.22338	-0.10112
1d	-0.24864	-0.05062	17d	-0.28756	-0.11137	17w	-0.19975	-0.09764
1e	-0.28292	-0.07079	17e	-0.31481	-0.13136	17x	-0.21400	-0.10481
1f	-0.30230	-0.07531	17f	-0.27945	-0.08890	17y	-0.22305	-0.11028
1g	-0.26369	-0.07531	17g	-0.24793	-0.08119	17z	-0.19919	-0.08981
1h	-0.26372	-0.08911	17h	-0.27201	-0.12598			
1i	-0.27802	-0.05557	17i	-0.26854	-0.12625			
1j	-0.33587	-0.08172	17j	-0.22481	-0.09848			
			17k	-0.26234	-0.09516			
2a	-0.27640	-0.05063	17l	-0.21684	-0.08897			
2b	-0.24571	-0.07891	17m	-0.23350	-0.10232			
2c	-0.25062	-0.08016	17n	-0.25059	-0.11065			
2d	-0.25529	-0.09075	17o	-0.24198	-0.09951			
2e	-0.24641	-0.08606	17p	-0.25271	-0.10996			
2f	-0.24467	-0.09358	17q	-0.27214	-0.12089			
2g	-0.27262	-0.09797	17r	-0.26341	-0.10820			
2h	-0.26796	-0.11385	17s	-0.19324	-0.08840			

### 7.1.2.1 Correlations of electrophilicity $E$ with HOMO and LUMO energies

Gas phase optimized geometries:

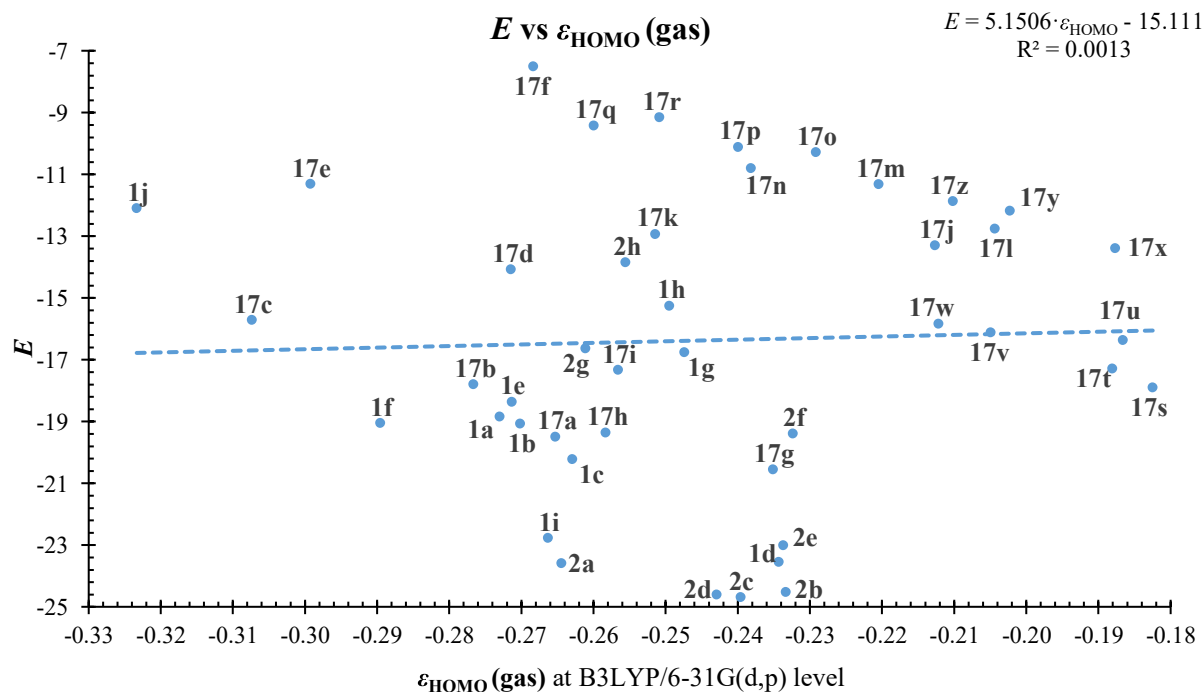


**Figure S7-1.** [Figure S4] Correlation between the empirical electrophilicity  $E$  and the gas phase highest occupied molecular orbital energies ( $\text{HOMO}_E$ , Hartree) calculated at B3LYP/6-31G(d,p) level for Michael acceptors.

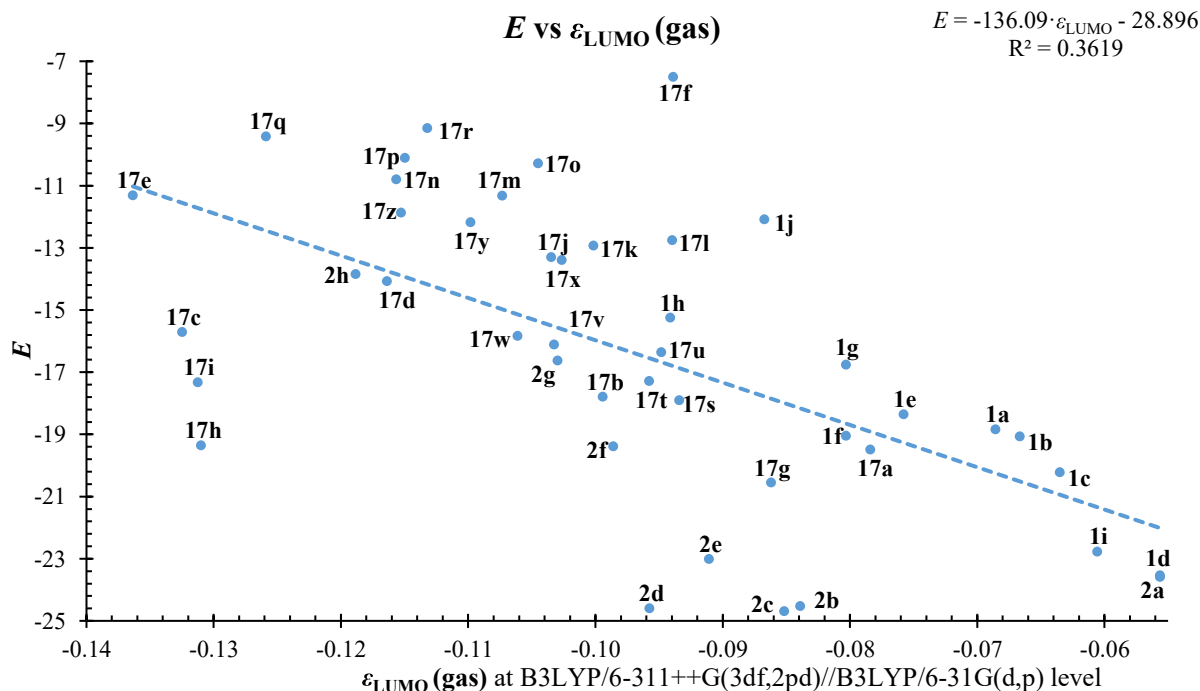


**Figure S7-2.** [Figure S10] Correlation between the empirical electrophilicity  $E$  and gas phase lowest unoccupied molecular orbital energies ( $\text{LUMO}_E$ , Hartree) calculated at B3LYP/6-311++G(3df,2pd)//B3LYP/6-31G(d,p) level for Michael acceptors.

Implicit solvation (DMSO) optimized geometries:

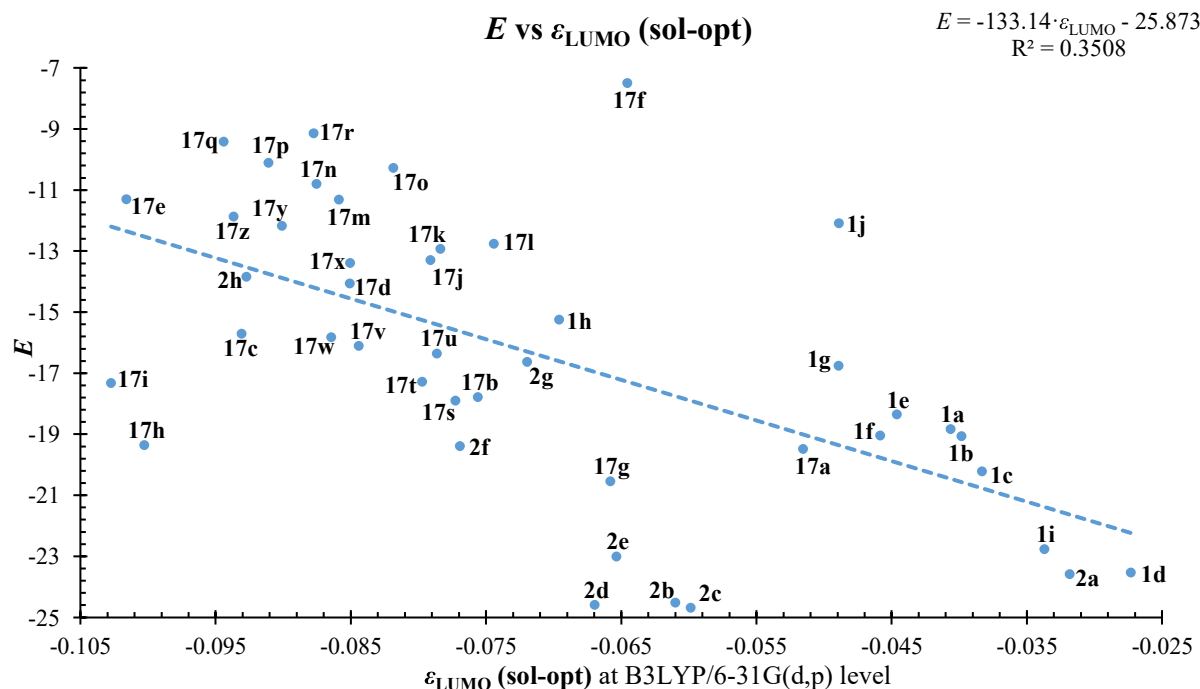


**Figure S7-3.** [Figure S3] Correlation between the empirical electrophilicity  $E$  and implicit solvation (DMSO) optimized lowest unoccupied molecular orbital energies ( $\text{LUMO}_E$ , Hartree) calculated at B3LYP/6-31G(d,p) level for Michael acceptors.



7.1.3 Correlations of the Empirical Electrophilicity  $E$  and the Methyl Anion Affinity (MAA)**Table S7-4.** [Table S4] Methyl anion affinities (MAAs, in terms of  $\Delta G$ , kJ/mol) calculated at different levels of theory for Michael acceptors.

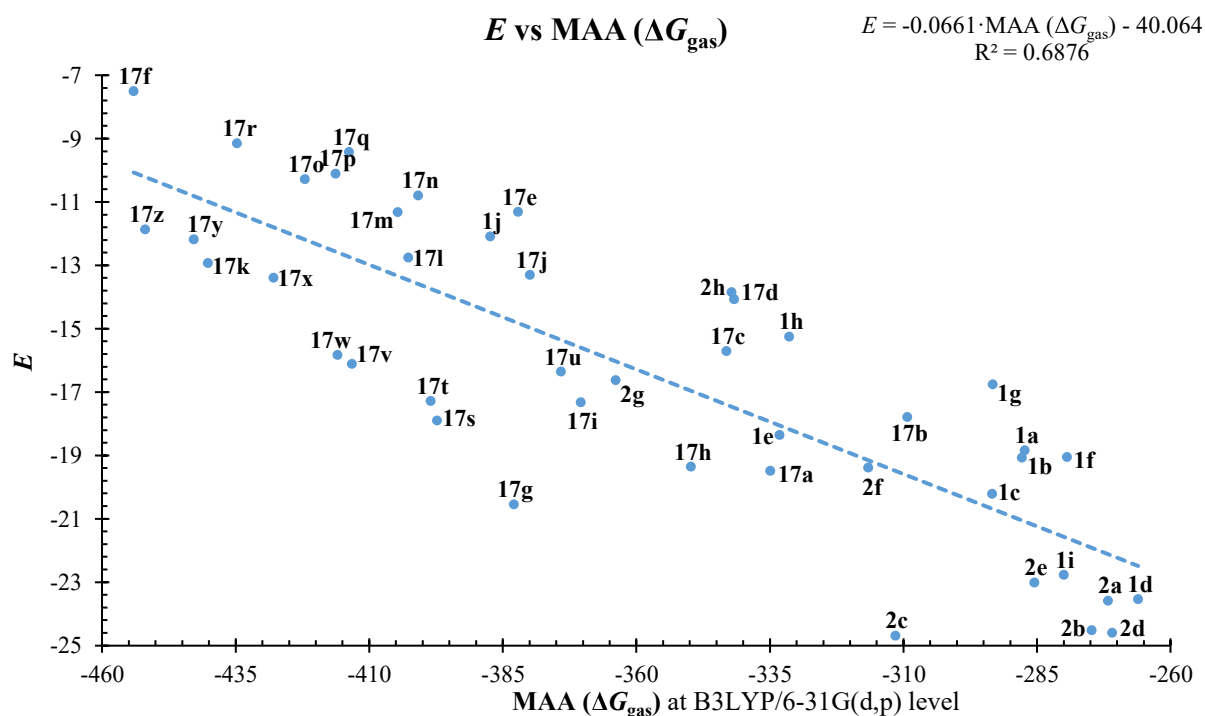
Marker	Gas Phase Optimized		Single Point Implicit Solvation Corrected		Implicit Solvation Optimized	
	MAA( $\Delta G_{\text{gas}}$ ) <sup>a</sup>		MAA ( $\Delta G_{\text{sol-sp}}$ ) <sup>b</sup>		MAA ( $\Delta G_{\text{sol-opt}}$ ) <sup>c</sup>	
	B3LYP		B3LYP		B3LYP	
	6-31G (d,p) <sup>d</sup>	6-311++G (3df,2pd) <sup>d</sup>	6-31G (d,p) <sup>d</sup>	6-311++G (3df,2pd) <sup>d</sup>	6-31G (d,p) <sup>e</sup>	6-311++G (3df,2pd) <sup>e</sup>
<b>1a</b>	-287.3	-205.5	-162.5	-80.7	-163.7	-80.2
<b>1b</b>	-287.8	-203.4	-159.7	-75.1	-167.6	-79.4
<b>1c</b>	-293.4	-205.7	-159.2	-71.6	-158.0	-66.2
<b>1d</b>	-266.1	-187.1	-138.6	-59.6	-138.7	-55.3
<b>1e</b>	-333.2	-246.0	-184.0	-96.8	-184.5	-91.6
<b>1f</b>	-279.4	-205.1	-183.8	-109.4	-185.4	-106.3
<b>1g</b>	-293.3	-222.8	-176.4	-104.2	-179.9	-102.4
<b>1h</b>	-331.4	-251.9	-196.2	-116.7	-197.9	-113.6
<b>1i</b>	-280.0	-189.9	-142.0	-51.9	-144.5	-50.3
<b>1j</b>	-387.4	-295.9	-251.1	-160.5	-251.1	-156.5
<b>2a</b>	-271.7	-187.1	-134.4	-49.8	-133.5	-45.2
<b>2b</b>	-274.7	-186.9	-123.7	-36.1	-131.4	-43.7
<b>2c</b>	-311.5	-219.7	-141.4	-51.8	-144.7	-50.6
<b>2d</b>	-270.9	-190.0	-145.2	-66.1	-151.4	-68.7
<b>2e</b>	-285.5	-207.7	-139.3	-60.4	-141.6	-59.4
<b>2f</b>	-316.6	-231.4	-157.2	-74.8	-160.7	-76.9
<b>2g</b>	-363.9	-268.2	-207.9	-113.3	-214.4	-121.0
<b>2h</b>	-342.1	-264.6	-199.6	-123.8	-202.2	-122.9
<b>17a</b>	-334.9	-246.9	-181.7	-93.1	-187.1	-95.4
<b>17b</b>	-309.3	-223.1	-160.4	-74.2	-164.4	-75.7
<b>17c</b>	-343.1	-264.1	-211.5	-132.4	-214.1	-130.0
<b>17d</b>	-341.7	-260.8	-194.7	-113.9	-196.5	-111.2
<b>17e</b>	-382.2	-301.9	-230.0	-149.8	-230.6	-145.7
<b>17f</b>	-454.1	-355.3	-273.6	-174.8	-268.3	-165.2
<b>17g</b>	-382.9	-284.5	-204.8	-104.8	-205.3	-98.9
<b>17h</b>	-349.8	-266.3	-159.8	-75.2	-160.9	-73.3
<b>17i</b>	-370.4	-281.9	-175.2	-86.8	-180.0	-88.1
<b>17j</b>	-379.9	-290.2	-231.0	-141.3	-232.3	-138.9
<b>17k</b>	-440.2	-344.3	-251.7	-155.9	-255.7	-155.7
<b>17l</b>	-402.7	-311.2	-226.8	-135.3	-231.1	-135.2
<b>17m</b>	-404.7	-318.9	-232.8	-147.1	-233.0	-142.6
<b>17n</b>	-400.8	-311.1	-251.5	-161.9	-255.8	-162.2
<b>17o</b>	-422.0	-330.7	-245.9	-154.4	-247.2	-151.1
<b>17p</b>	-416.3	-331.9	-245.1	-160.7	-245.1	-156.0
<b>17q</b>	-413.7	-325.4	-265.7	-177.4	-270.9	-178.5
<b>17r</b>	-434.8	-344.7	-259.7	-169.6	-261.6	-166.1
<b>17s</b>	-397.3	-295.6	-221.9	-120.4	-222.3	-116.5
<b>17t</b>	-398.5	-297.7	-224.0	-123.2	-224.3	-119.3
<b>17u</b>	-374.1	-284.6	-220.4	-130.7	-217.8	-123.9
<b>17v</b>	-413.2	-312.1	-238.2	-137.4	-241.9	-137.5
<b>17w</b>	-415.9	-314.8	-242.4	-141.3	-241.9	-136.5
<b>17x</b>	-427.9	-329.6	-245.6	-147.3	-249.8	-146.9
<b>17y</b>	-442.8	-344.2	-261.5	-163.6	-262.0	-159.4
<b>17z</b>	-451.9	-354.2	-272.0	-174.6	-272.1	-170.0

<sup>a</sup> MAA( $\Delta G_{\text{gas}}$ ) calculated using  $\Delta G_{298}$  values of gas phase optimized geometries. <sup>b</sup> MAA( $\Delta G_{\text{sol-sp}}$ ) calculated using  $\Delta G_{\text{gas}} + \Delta G_{\text{sol}}$  [single point implicit solvation correction for gas phase geometry (smd, solvent=dms)]. <sup>c</sup> MAA( $\Delta G_{\text{sol-opt}}$ ) calculated using  $\Delta G_{298}$  values for implicit DMSO optimized geometries (SMD). <sup>d</sup> Using gas phase optimized B3LYP/6-31G(d,p) geometries. <sup>e</sup> Using solution phase optimized [smd,solvent=dms,B3LYP/6-31G(d,p)] geometries.

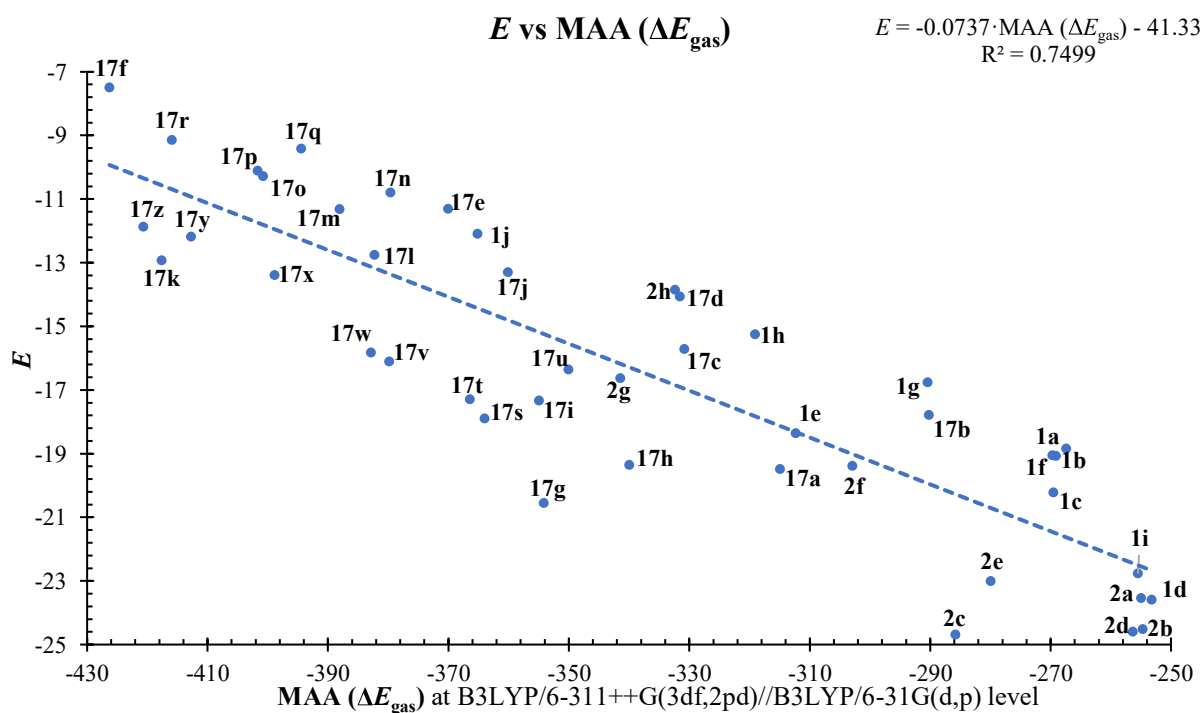
**Table S7-5.** [Table S5] Methyl anion affinities (MAAs, in terms of  $\Delta E$  and  $\Delta H$ , kJ/mol) calculated at different levels of theory for Michael acceptors.

Marker	Gas Phase Optimized B3LYP				Implicit Solvation Optimized B3LYP			
	6-31G (d,p)		6-311++G(3df,2pd) <sup>c</sup>		6-31G (d,p)		6-311++G (3df,2pd) <sup>f</sup>	
	$\Delta E_{\text{gas}}^a$	$\Delta H_{\text{gas}}^b$	$\Delta E_{\text{gas}}^a$	$\Delta H_{\text{gas}}^b$	$\Delta E_{\text{sol-opt}}^c$	$\Delta H_{\text{sol-opt}}^d$	$\Delta E_{\text{sol-opt}}^c$	$\Delta H_{\text{sol-opt}}^d$
<b>1a</b>	-349.2	-267.4	-332.5	-250.7	-225.9	-142.5	-210.5	-127.1
<b>1b</b>	-353.5	-269.1	-336.0	-251.6	-225.2	-137.1	-209.0	-120.5
<b>1c</b>	-357.1	-269.5	-340.1	-252.5	-223.2	-131.4	-207.1	-115.3
<b>1d</b>	-334.0	-255.0	-318.0	-239.0	-206.0	-122.6	-191.1	-107.7
<b>1e</b>	-399.6	-312.3	-380.6	-293.3	-251.0	-158.2	-233.0	-140.2
<b>1f</b>	-344.1	-269.7	-325.6	-251.2	-248.0	-168.9	-230.5	-151.4
<b>1g</b>	-362.0	-290.4	-342.9	-271.7	-243.4	-165.9	-226.1	-148.6
<b>1h</b>	-398.6	-319.1	-378.0	-298.6	-262.5	-178.2	-245.4	-161.1
<b>1i</b>	-345.6	-255.5	-328.6	-238.5	-207.2	-113.3	-188.3	-94.5
<b>1j</b>	-457.8	-365.2	-436.7	-344.1	-320.1	-224.1	-300.3	-204.8
<b>2a</b>	-337.8	-253.2	-321.2	-236.6	-200.8	-112.6	-184.7	-96.6
<b>2b</b>	-344.2	-254.7	-327.3	-238.1	-191.4	-103.1	-176.3	-88.4
<b>2c</b>	-377.6	-285.8	-359.9	-268.1	-211.9	-117.9	-195.5	-101.5
<b>2d</b>	-336.9	-256.3	-320.1	-238.9	-212.1	-129.3	-196.2	-113.4
<b>2e</b>	-357.8	-280.0	-339.7	-261.9	-210.7	-127.2	-191.0	-108.7
<b>2f</b>	-388.0	-302.9	-368.2	-283.2	-227.8	-142.0	-209.9	-124.7
<b>2g</b>	-437.1	-341.5	-417.4	-321.7	-279.4	-186.1	-262.2	-168.7
<b>2h</b>	-414.6	-332.4	-395.4	-313.6	-266.7	-186.2	-249.1	-169.6
<b>17a</b>	-404.4	-314.9	-386.3	-297.0	-250.4	-160.2	-234.3	-144.3
<b>17b</b>	-377.1	-290.2	-359.6	-273.0	-228.7	-141.6	-212.6	-125.4
<b>17c</b>	-409.8	-330.8	-390.7	-311.7	-278.5	-194.4	-261.3	-177.3
<b>17d</b>	-412.4	-331.5	-393.8	-313.0	-264.7	-179.5	-248.1	-162.8
<b>17e</b>	-450.3	-370.0	-430.7	-350.5	-297.2	-212.2	-279.4	-194.5
<b>17f</b>	-525.1	-426.3	-502.7	-403.9	-338.7	-235.6	-317.7	-214.6
<b>17g</b>	-454.6	-354.2	-435.0	-335.5	-274.9	-170.7	-257.9	-153.2
<b>17h</b>	-423.4	-339.9	-404.4	-320.9	-232.4	-143.5	-214.7	-127.0
<b>17i</b>	-443.4	-354.9	-422.7	-334.3	-247.1	-154.7	-231.6	-139.2
<b>17j</b>	-449.8	-360.1	-430.4	-339.8	-301.4	-208.0	-283.1	-189.6
<b>17k</b>	-513.4	-417.6	-492.7	-396.9	-321.3	-221.2	-302.0	-201.9
<b>17l</b>	-473.9	-382.3	-454.7	-363.0	-297.4	-201.1	-280.8	-184.5
<b>17m</b>	-473.8	-388.0	-454.0	-368.2	-301.2	-210.9	-280.4	-190.1
<b>17n</b>	-469.3	-379.6	-448.4	-358.7	-320.6	-227.1	-303.8	-210.2
<b>17o</b>	-492.3	-400.7	-472.2	-380.7	-315.4	-219.1	-298.0	-201.7
<b>17p</b>	-486.0	-401.7	-466.0	-381.7	-313.9	-224.9	-295.6	-206.6
<b>17q</b>	-482.8	-394.4	-461.7	-373.4	-335.3	-242.9	-316.2	-223.8
<b>17r</b>	-506.1	-415.9	-485.7	-395.5	-330.1	-234.7	-312.3	-216.8
<b>17s</b>	-465.6	-364.0	-448.7	-347.1	-289.8	-184.0	-273.8	-168.1
<b>17t</b>	-467.2	-366.4	-450.3	-349.5	-293.5	-188.8	-277.5	-172.8
<b>17u</b>	-439.6	-350.1	-422.0	-332.5	-286.2	-192.2	-269.1	-175.2
<b>17v</b>	-480.9	-379.8	-463.6	-362.5	-306.3	-201.3	-290.4	-185.7
<b>17w</b>	-483.9	-382.8	-466.4	-365.3	-310.9	-205.5	-294.1	-188.7
<b>17x</b>	-497.2	-398.9	-478.9	-380.5	-315.2	-212.6	-298.4	-195.8
<b>17y</b>	-511.3	-412.7	-492.2	-393.6	-329.5	-227.1	-311.8	-209.3
<b>17z</b>	-518.4	-420.6	-499.3	-401.5	-338.5	-236.9	-320.5	-218.8

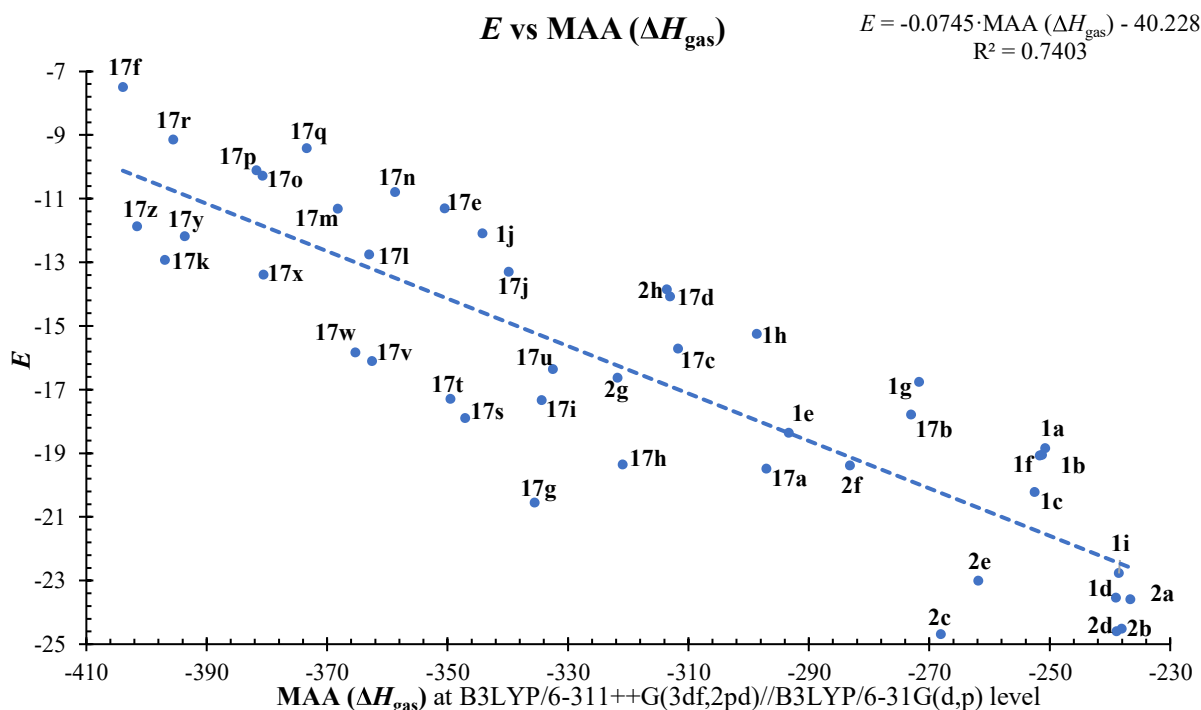
<sup>a</sup> MAA( $\Delta E_{\text{gas}}$ ) calculated using  $\Delta E_{\text{tot}}$  values of gas phase optimized geometries. <sup>b</sup> MAA( $\Delta H_{\text{gas}}$ ) calculated using  $\Delta H_{298}$  values of gas phase optimized geometries. <sup>c</sup> MAA( $\Delta E_{\text{sol-opt}}$ ) calculated using  $\Delta E_{\text{tot}}$  values for implicit DMSO optimized geometries (SMD). <sup>d</sup> MAA( $\Delta H_{\text{sol-opt}}$ ) calculated using  $\Delta H_{298}$  values for an implicit DMSO optimized geometries (SMD). <sup>e</sup> Using gas phase optimized B3LYP/6-31G(d,p) geometries. | <sup>f</sup>Using solution phase optimized [smd,solvent=dmsolvent, B3LYP/6-31G(d,p)] geometries.

7.1.3.1 Empirical electrophilicity ( $E$ ) vs gas phase MAA

**Figure S7-6.** [Figure S12] Correlation between the empirical electrophilicity  $E$  and gas phase MAA values ( $\Delta G_{\text{gas}}$ , kJ/mol) calculated at B3LYP/6-31G(d,p) level for Michael acceptors.

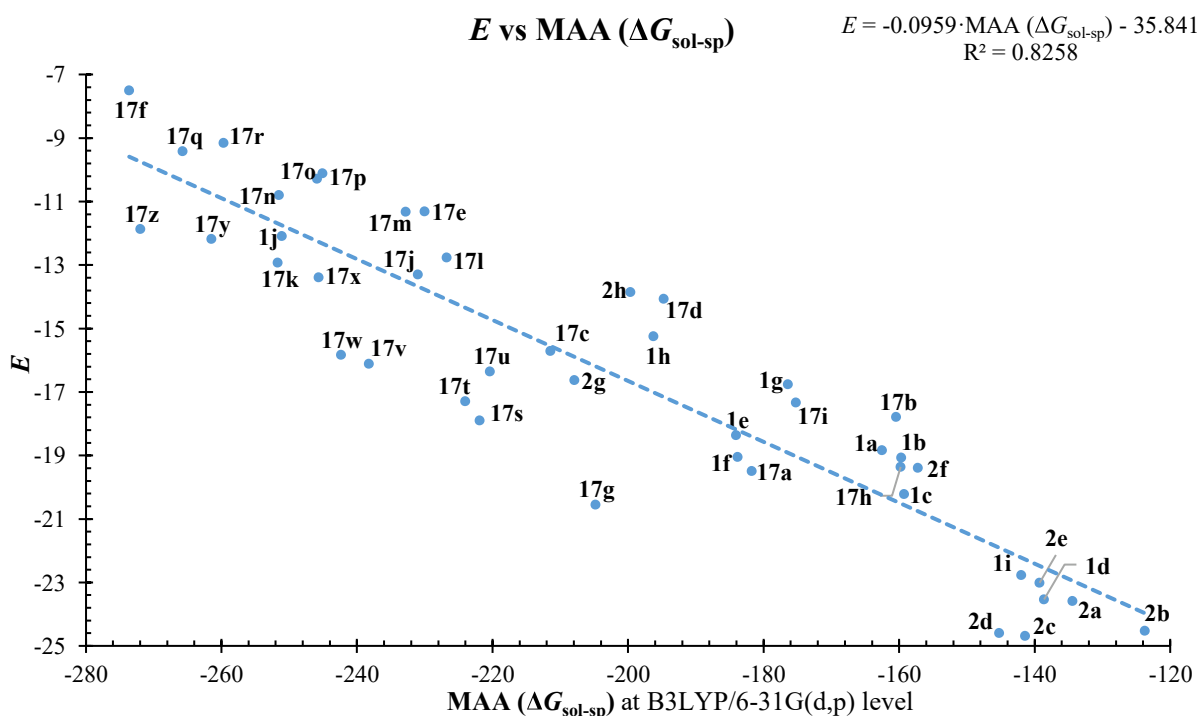


**Figure S7-7.** [Figure S14] Correlation between the empirical electrophilicity  $E$  and gas phase MAA values ( $\Delta E_{\text{gas}}$ , kJ/mol) calculated at B3LYP/6-311++G(3df,2pd)//B3LYP/6-31G(d,p) level for Michael acceptors.

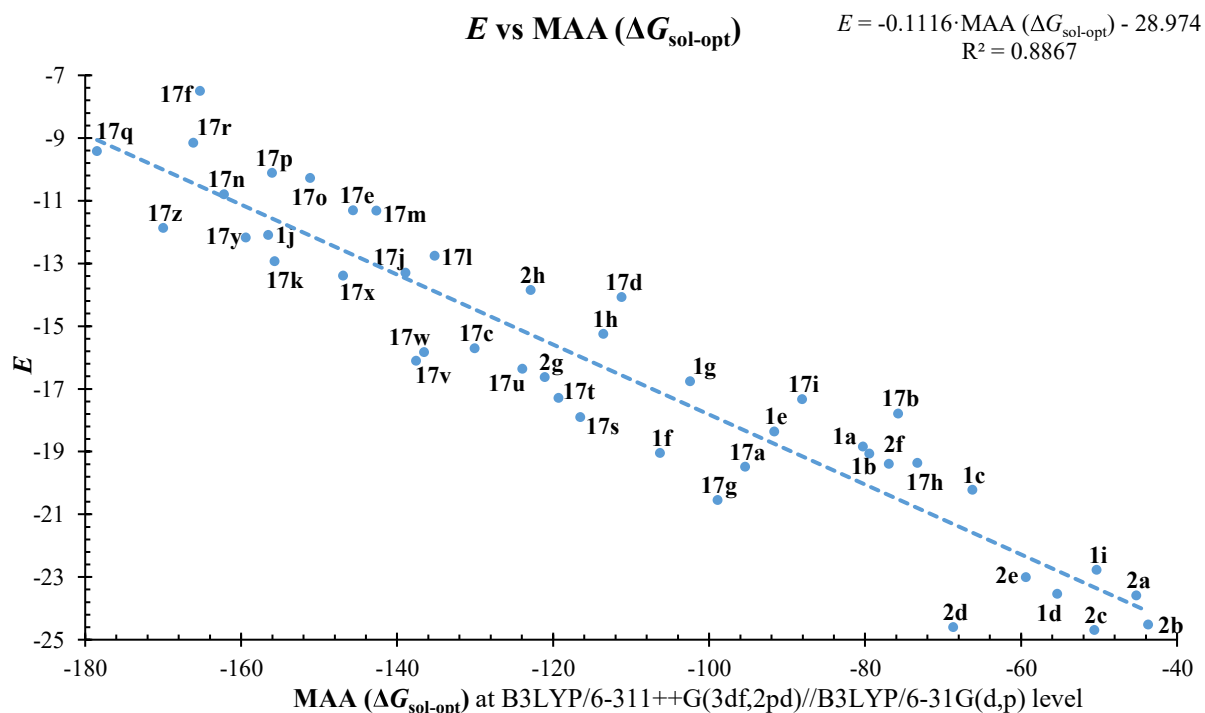


**Figure S7-8.** [Figure S15] Correlation between the empirical electrophilicity  $E$  and gas phase MAA values ( $\Delta H_{\text{gas}}$ , kJ/mol) calculated at B3LYP/6-311++G(3df,2pd)//B3LYP/6-31G(d,p) level for Michael acceptors.

### 7.1.3.2 Empirical electrophilicity ( $E$ ) vs single point implicit-solvation (DMSO) corrected MAA



**Figure S7-9.** [Figure S16] Correlation between the empirical electrophilicity  $E$  and MAA values [ $\Delta G_{\text{sol-sp}}$  ( $\Delta G_{\text{gas}} + \Delta G_{\text{Solv}}$ ), kJ/mol] calculated at B3LYP/6-31G(d,p) level for Michael acceptors.  $\Delta G_{\text{Solv}}$  has been calculated for DMSO using the SMD solvation model.

7.1.3.3 Empirical electrophilicity ( $E$ ) vs implicit-solvation (DMSO) optimized MAA

**Figure S7-10.** [Figure S19] Correlation between the empirical electrophilicity  $E$  and MAA values ( $\Delta G_{\text{sol-opt}}$ , kJ/mol) calculated at B3LYP/6-311++G(3df,2pd) level using B3LYP/6-31G(d,p) optimized geometries under implicit DMSO (SMD) solvation for Michael acceptors.

## 7.1.4 Mechanistic Investigation

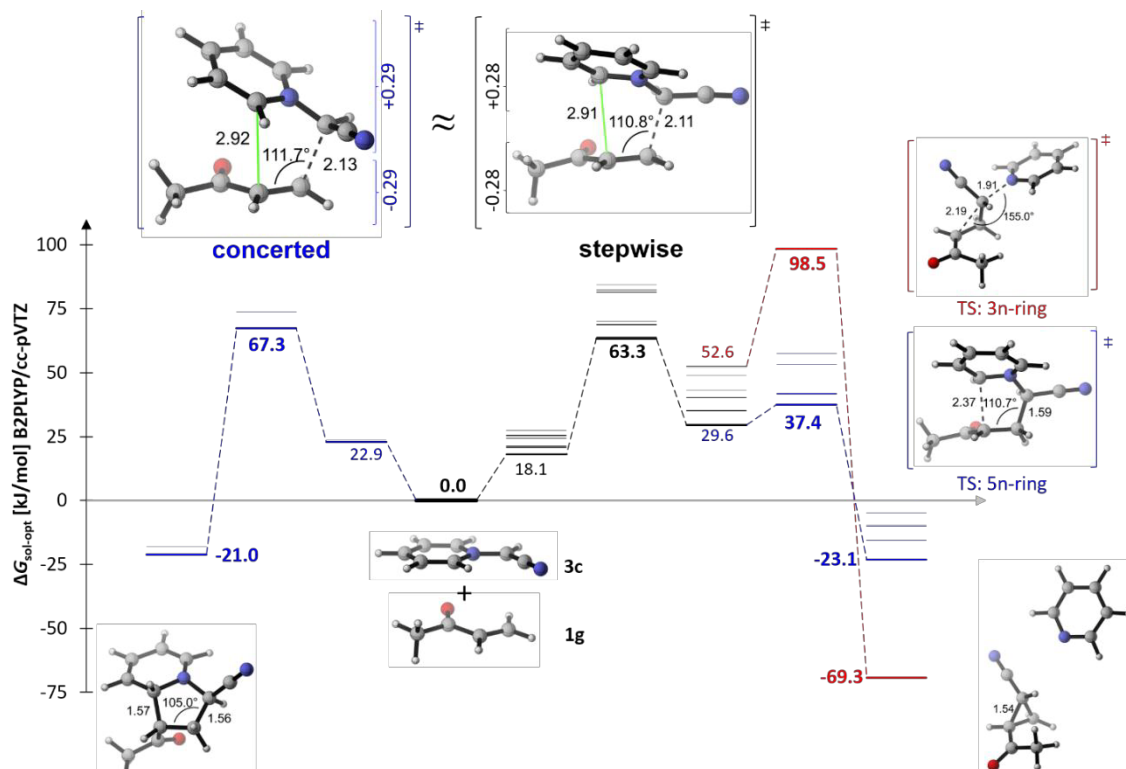


**Figure S7-11.** [Figure S29] Gibbs free energy surface for the reaction of methyl vinyl ketone (**1g**) with pyridinium ylide **3c** calculated at B2PLYP/cc-pVTZ/SMD(DMSO)//B3LYP/6-31G(d,p)/SMD(DMSO) level of theory. Distances (Å), angles (degrees) and charges ( $\Sigma$  Mulliken charges over all atomic centers of the two reactants).

**Table S7-6.** Transition state (TS), reactant complex (RC) and product (P) energies ( $\Delta G_{\text{sol-opt}}$ , kJ/mol) for the reaction of Michael acceptors (**1g**, **1d**, **2e**, and **1f**) with pyridinium ylide **3c** calculated at different levels of theory.

Path	B3LYP/6-31G(d,p) /SMD(DMSO)			B3LYP/6-311++G(3df,2pd) /SMD(DMSO) //B3LYP/6-31G(d,p) /SMD(DMSO)			B2PLYP/cc-pVTZ /SMD(DMSO) //B3LYP/6-31G(d,p) /SMD(DMSO)			
	RC	TS	P	RC	TS	P	RC	TS	P	
<b>1g</b> + <b>3c</b>										
<b>concerted</b>										
TS Con	27.7	79.1	-9.5	32.3	86.3	16.7	23.6	67.3	-21.0	
TS Con	27.1	84.0	-5.6	31.6	90.0	14.9	22.9	73.7	-18.1	
<b>stepwise</b>										
TS Step	27.6	72.3	46.2	32.0	81.0	55.5	24.4	63.3	29.6	
TS Step	25.3	75.3	53.5	29.7	82.8	58.2	21.0	64.0	35.3	
TS Step	25.5	77.8	56.3	30.6	87.1	65.1	21.3	68.4	40.2	
TS Step	31.6	82.1	65.7	33.7	86.4	68.4	25.3	70.0	49.0	
TS Step	23.3	79.3	67.5	24.3	83.4	68.3	18.1	68.8	52.2	
TS Step	26.4	85.4	53.2	34.0	95.8	59.0	27.5	82.5	35.0	
TS Step	26.3	87.8	62.1	35.8	97.5	66.8	25.6	81.4	43.2	
TS Step	25.0	92.7	74.6	25.3	92.7	65.6	20.7	84.5	52.6	
<b>5n-ring</b>										
TS R5	46.2	51.3	-3.1	55.4	66.2	20.0	29.6	37.4	-15.6	
TS R5	53.5	57.9	3.1	58.2	67.2	28.0	35.3	41.4	-9.6	
TS R5	56.3	56.3	-12.5	65.1	67.7	11.4	40.2	41.8	-23.1	
TS R5	65.8	69.8	9.5	68.4	74.8	32.0	49.1	53.3	-4.7	
TS R5	67.1	72.6	4.4	67.0	75.0	24.6	51.2	57.6	-10.0	
<b>3n-ring</b>										
TS R3	74.6	110.0	-65.3	65.6	115.3	-50.6	52.6	98.5	-69.3	
<b>1d</b> + <b>3c</b>										
<b>concerted</b>										
TS Con	25.4	89.8	-7.3	34.5	105.9	18.3	25.4	82.8	-19.6	
TS Con	27.6	96.6	-14.4	32.9	112.0	12.7	22.3	88.4	-24.1	
TS Con	33.3	116.8	-15.1	44.9	130.6	10.5	31.7	107.7	-25.4	
TS Con	35.9	119.4	5.1	37.3	130.6	31.5	30.5	106.5	-8.4	
<b>stepwise</b>										
TS Step	27.7	94.7	85.6	40.2	103.3	96.1	29.7	89.6	70.6	
TS Step	24.2	100.3	84.1	35.7	115.6	95.6	25.8	98.4	69.3	
TS Step	23.5	100.8	85.6	35.3	110.6	96.1	24.9	96.2	70.6	
TS Step	25.0	108.5	96.9	37.8	122.8	108.1	23.9	102.7	80.7	
TS Step	30.0	113.9	107.6	41.6	126.4	116.9	31.2	105.9	93.1	
<b>5n-ring</b>										
TS R5	107.5	113.0	-4.6	116.9	124.4	21.0	93.1	98.8	-16.7	
<b>3n-ring</b>										
TS R3	84.1	114.9	-75.8	95.6	132.5	-54.1	69.3	107.1	-76.2	
TS R3	85.6	118.3	-75.1	96.1	134.9	-50.2	70.6	110.4	-74.1	
TS R3	97.4	124.8	-71.6	100.8	139.0	-49.9	78.7	115.9	-71.9	
<b>2e</b> + <b>3c</b>										
<b>concerted</b>										
TS Con	29.1	115.6	49.0	30.7	119.6	69.6	19.3	90.8	24.7	

TS Con		31.3	119.9	51.4		32.9	124.4	71.6		20.6	95.3	26.3
TS Con		31.2	120.9	36.7		35.1	125.7	55.1		22.2	97.0	13.7
<b>stepwise</b>												
TS Step		29.9	100.9	88.7		35.7	113.0	101.2		23.7	80.5	61.9
TS Step		30.6	106.6	91.7		36.6	115.2	97.6		24.4	83.6	63.3
TS Step		26.4	107.6	100.3		31.0	116.8	109.4		19.4	86.4	74.1
TS Step		31.8	109.9	95.1		37.6	117.7	101.1		24.8	85.8	66.5
TS Step		25.3	115.3	102.7		34.6	124.2	106.9		23.9	97.3	73.6
TS Step		53.4	121.1	91.3		64.5	135.4	106.8		52.8	104.6	65.9
TS Step		56.4	128.3	105.6		66.4	141.8	118.7		52.2	110.7	78.9
TS Step		26.5	129.0	127.8		25.9	127.3	119.6		18.3	104.0	92.8
TS Step		56.9	134.9	124.9		67.3	148.5	132.9		51.4	113.6	91.9
TS Step		48.5	140.9	97.8		58.3	154.1	105.3		49.3	123.7	67.1
TS Step		48.0	141.6	117.9		62.4	155.5	128.7		51.2	123.2	89.7
<b>5n-ring</b>												
TS R5		88.7	102.0	42.1		101.2	120.2	65.8		61.9	77.5	19.3
TS R5		105.6	117.0	-		118.7	137.8	-		79.0	96.1	-
TS R5		124.9	133.1	54.3		132.8	149.2	81.0		91.9	106.7	32.2
<b>3n-ring</b>												
TS R3		106.1	136.0	-44.8		100.2	143.7	-25.7		69.9	112.5	-53.3
TS R3		97.8	143.4	-39.3		105.3	158.7	-19.8		67.1	124.2	-47.9
TS R3		120.4	163.7	-21.2		125.0	178.5	-		88.2	143.6	-
<b>1f</b>												
<b>+</b>												
<b>3c</b>												
<b>concerted</b>												
TS Con		26.9	66.7	-5.4		31.7	76.4	17.3		22.1	59.4	-17.8
TS Con		26.9	68.1	-16.8		31.7	77.3	5.1		22.1	63.2	-27.6
TS Con		28.8	69.4	-17.7		33.6	78.9	5.1		23.7	61.6	-28.9
<b>stepwise</b>												
TS Step		21.8	66.0	49.2		25.5	74.8	57.5		18.5	61.5	41.9
TS Step		19.4	74.3	56.7		21.9	79.9	56.7		17.4	72.3	43.4
TS Step		23.8	78.2	56.8		28.9	85.6	57.4		20.9	76.7	43.6
<b>5n-ring</b>												
TS R5		49.2	53.0	-7.9		57.5	63.0	13.9		41.8	46.0	-19.8
<b>3n-ring</b>												
TS R3		56.7	95.1	-65.7		56.8	107.8	-49.0		43.4	91.6	-68.0
TS R3		56.7	95.9	-64.5		56.8	109.1	-44.8		43.4	92.6	-64.9
TS R3		56.8	96.4	-60.0		57.4	108.7	-42.9		43.7	91.9	-63.1

**Table S7-7.** Transition state (TS), reactant complex (RC) and product (P) energies ( $\Delta H_{\text{sol-opt}}$ , kJ/mol) for the reaction of Michael acceptors (**1g**, **1d**, **2e**, and **1f**) with pyridinium ylide **3c** calculated at different levels of theory.

Path	B3LYP/6-31G(d,p) /SMD(DMSO)			B3LYP/6-311++G(3df,2pd) /SMD(DMSO) //B3LYP/6-31G(d,p) /SMD(DMSO)			B2PLYP/cc-pVTZ /SMD(DMSO) //B3LYP/6-31G(d,p) /SMD(DMSO)			
	RC	TS	P	RC	TS	P	RC	TS	P	
<b>1g</b> + <b>3c</b>										
<b>concerted</b>										
TS Con	-7.9	23.1	-69.4	-3.3	30.4	-43.2	-12.0	11.4	-81.0	
TS Con	-10.1	28.3	-64.5	-5.6	34.4	-44.1	-14.3	18.0	-77.1	
<b>stepwise</b>										
TS Step	-7.9	19.1	-13.0	-3.4	27.7	-3.7	-11.0	10.1	-29.6	
TS Step	-7.5	20.6	-2.9	-3.1	28.1	1.8	-11.8	9.2	-21.1	
TS Step	-8.0	23.3	-2.1	-3.0	32.7	6.7	-12.2	14.0	-18.2	
TS Step	-7.9	25.7	9.3	-5.9	29.9	11.9	-14.3	13.5	-7.5	
TS Step	-7.6	25.6	12.4	-6.5	29.7	13.2	-12.7	15.1	-2.9	
TS Step	-10.2	31.8	-3.3	-2.5	42.2	2.5	-9.1	28.9	-21.5	
TS Step	-9.5	32.6	3.2	0.1	42.3	7.8	-10.1	26.2	-15.8	
TS Step	-5.7	39.4	22.9	-5.4	39.5	14.0	-9.9	31.2	1.0	
<b>5n-ring</b>										
TS R5	-13.0	-8.7	-63.1	-3.7	6.3	-40.0	-29.6	-22.5	-75.6	
TS R5	-2.9	-4.9	-57.9	1.8	4.4	-33.1	-21.1	-21.4	-70.7	
TS R5	-2.1	-4.7	-71.9	6.7	6.7	-48.0	-18.2	-19.2	-82.5	
TS R5	9.3	7.0	-51.7	11.9	11.9	-29.2	-7.5	-9.6	-65.9	
TS R5	11.9	10.0	-56.1	11.8	12.4	-36.0	-3.9	-5.0	-70.5	
<b>3n-ring</b>										
TS R3	22.9	57.9	-99.8	14.0	63.3	-85.1	1.0	46.4	-103.9	
<b>1d</b> + <b>3c</b>										
<b>concerted</b>										
TS Con	-11.9	30.7	-63.9	-2.9	46.8	-38.3	-11.9	23.7	-76.2	
TS Con	-7.5	36.9	-73.8	-2.2	52.4	-46.7	-12.9	28.7	-83.4	
TS Con	-6.4	59.3	-73.4	5.3	73.1	-47.8	-8.0	50.2	-83.7	
TS Con	0.9	60.9	-60.0	2.3	72.1	-33.6	-4.6	47.9	-73.5	
<b>stepwise</b>										
TS Step	-14.9	47.9	28.7	-2.5	56.5	39.2	-12.9	42.8	13.7	
TS Step	-14.0	46.1	27.7	-2.5	61.4	39.2	-12.4	44.2	12.9	
TS Step	-14.3	48.1	28.7	-2.5	58.0	39.2	-12.9	43.6	13.7	
TS Step	-13.5	49.5	37.0	-0.8	63.8	48.2	-14.7	43.6	20.8	
TS Step	-8.0	56.4	50.0	3.6	68.9	59.4	-6.7	48.4	35.6	
<b>5n-ring</b>										
TS R5	50.0	48.1	-64.0	59.4	59.5	-38.5	35.6	33.9	-76.2	
<b>3n-ring</b>										
TS R3	27.7	63.0	-111.8	39.2	80.6	-90.1	12.9	55.2	-112.2	
TS R3	28.7	64.0	-114.6	39.2	80.6	-89.6	13.7	56.1	-113.5	
TS R3	40.9	70.3	-107.8	44.3	84.5	-86.2	22.2	61.5	-108.1	
<b>2e</b> + <b>3c</b>										
<b>concerted</b>										
TS Con	-4.3	57.6	-11.9	-2.6	61.7	8.7	-14.0	32.8	-36.3	

TS Con		-4.2	60.3	-10.7		-2.6	64.8	9.6	-14.8	35.7	-35.7
TS Con		-6.7	63.8	-23.3		-2.8	68.6	-4.9	-15.7	39.9	-46.2
<b>stepwise</b>											
TS Step		-6.4	42.4	28.6		-0.7	54.4	41.0	-12.7	22.0	1.7
TS Step		-6.0	47.4	37.3		0.0	56.1	43.2	-12.1	24.5	8.9
TS Step		-6.5	51.3	42.6		-1.8	60.5	51.6	-13.5	30.1	16.4
TS Step		-6.4	51.3	40.5		-0.7	59.1	46.6	-13.4	27.2	11.9
TS Step		-9.0	58.0	45.2		0.3	66.9	49.3	-10.4	40.0	16.1
TS Step		16.4	64.4	29.7		27.4	78.7	45.2	15.7	47.9	4.3
TS Step		18.0	70.5	44.3		28.0	84.1	57.4	13.8	53.0	17.6
TS Step		-2.5	74.9	71.8		-3.0	73.1	63.7	-10.7	49.8	36.9
TS Step		17.1	73.0	65.8		27.5	86.6	73.8	11.6	51.7	32.8
TS Step		16.6	82.8	40.7		26.5	96.0	48.2	17.5	65.6	10.0
TS Step		13.4	83.0	59.2		27.8	96.9	70.0	16.7	64.6	31.1
<b>5n-ring</b>											
TS R5		28.6	37.7	-18.5		41.1	55.9	5.2	1.7	13.2	-41.2
TS R5		44.3	52.3			57.4	73.1		17.6	31.3	
TS R5		65.8	69.6	-5.9		73.8	85.7	20.7	32.8	43.2	-28.0
<b>3n-ring</b>											
TS R3		50.8	84.2	-76.7		45.0	91.9	-57.6	14.7	60.7	-85.2
TS R3		40.7	92.5	-71.3		48.2	107.8	-51.8	10.0	73.3	-79.9
TS R3		62.6	110.6	-57.6		67.2	125.4		30.4	90.5	
<b>1f</b>											
+											
<b>3c</b>											
<b>concerted</b>											
TS Con		-9.2	12.7	-63.3		-4.4	22.4	-40.5	-14.0	5.4	-75.6
TS Con		-9.2	16.6	-73.2		-4.4	25.8	-51.3	-14.0	11.8	-84.0
TS Con		-8.8	14.5	-72.1		-3.9	24.0	-49.2	-13.9	6.7	-83.2
<b>stepwise</b>											
TS Step		-7.9	14.2	-2.5		-4.1	23.0	5.8	-11.2	9.7	-9.9
TS Step		-5.9	26.1	7.5		-3.5	31.7	7.5	-8.0	24.1	-5.8
TS Step		-7.6	27.5	8.4		-2.5	35.0	9.0	-10.4	26.1	-4.7
<b>5n-ring</b>											
TS R5		-2.5	-4.9	-65.3		5.8	5.2	-43.5	-9.9	-11.9	-77.2
<b>3n-ring</b>											
TS R3		7.5	47.7	-95.3		7.5	60.4	-78.6	-5.8	44.2	-97.6
TS R3		7.5	48.0	-101.3		7.5	61.2	-81.6	-5.8	44.7	-101.7
TS R3		8.4	48.1	-93.4		9.0	60.5	-76.4	-4.7	43.7	-96.6

### 7.1.5 References

- (1) (a) Mayr, H.; Ammer, J.; Baidya, M.; Maji, B.; Nigst, T. A.; Ofial, A. R.; Singer, T., *J. Am. Chem. Soc.* **2015**, *137*, 2580-2599. (b) Byrne, P. A.; Kobayashi, S.; Würthwein, E.-U.; Ammer, J.; Mayr, H., *J. Am. Chem. Soc.* **2017**, *139*, 1499-1511.
- (2) Becke, A. D., *J. Chem. Phys.* **1993**, *98*, 5648-5652.
- (3) (a) Ditchfield, R.; Hehre, W. J.; Pople, J. A., *J. Chem. Phys.* **1971**, *54*, 724-728. (b) Krishnan, R.; Binkley, J. S.; Seeger, R.; Pople, J. A., *J. Chem. Phys.* **1980**, *72*, 650-654.
- (4) Clark, T.; Chandrasekhar, J.; Spitznagel, G. W.; Schleyer, P. V. R., *J. Comput. Chem.* **1983**, *4*, 294-301.
- (5) Marenich, A. V.; Cramer, C. J.; Truhlar, D. G., *J. Phys. Chem. B* **2009**, *113*, 6378-6396.
- (6) (a) Parr, R. G.; Yang, W., *Density-Functional Theory of Atoms and Molecules*, vol. 16 of *International Series of Monographs on Chemistry*. Oxford University Press, New York: **1989**. (b) Parr, R. G.; Szentpaly, L. v.; Liu, S., *J. Am. Chem. Soc.* **1999**, *121*, 1922-1924. (c) Domingo, L. R.; Pérez, P.; Contreras, R., *Tetrahedron* **2004**, *60*, 6585-6591.
- (7) Contreras, R. R.; Fuentealba, P.; Galván, M.; Pérez, P., *Chem. Phys. Lett.* **1999**, *304*, 405-413.
- (8) Yang, W.; Mortier, W. J., *J. Am. Chem. Soc.* **1986**, *108*, 5708-5711.
- (9) Frisch, M. J. T., G. W.; Schlegel, H. B.; Scuseria, G. E.; Robb, M. A.; Cheeseman, J. R.; Scalmani, G.; Barone, V.; Mennucci, B.; Petersson, G. A.; Nakatsuji, H.; Caricato, M.; Li, X.; Hratchian, H. P.; Izmaylov, A. F.; Bloino, J.; Zheng, G.; Sonnenberg, J. L.; Hada, M.; Ehara, M.; Toyota, K.; Fukuda, R.; Hasegawa, J.; Ishida, M.; Nakajima, T.; Honda, Y.; Kitao, O.; Nakai, H.; Vreven, T.; Montgomery, Jr., J. A.; Peralta, J. E.; Ogliaro, F.; Bearpark, M.; Heyd, J. J.; Brothers, E.; Kudin, K. N.; Staroverov, V. N.; Keith, T.; Kobayashi, R.; Normand, J.; Raghavachari, K.; Rendell, A.; Burant, J. C.; Iyengar, S. S.; Tomasi, J.; Cossi, M.; Rega, N.; Millam, J. M.; Klene, M.; Knox, J. E.; Cross, J. B.; Bakken, V.; Adamo, C.; Jaramillo, J.; Gomperts, R.; Stratmann, R. E.; Yazyev, O.; Austin, A. J.; Cammi, R.; Pomelli, C.; Ochterski, J. W.; Martin, R. L.; Morokuma, K.; Zakrzewski, V. G.; Voth, G. A.; Salvador, P.; Dannenberg, J. J.; Dapprich, S.; Daniels, A. D.; Farkas, O.; Foresman, J. B.; Ortiz, J. V.; Cioslowski, J.; Fox, D. J.; *Gaussian 09 Revision D. 01*, Gaussian, Inc., Wallingford CT: **2013**.

## **Chapter 8. Kinetics and Mechanism of Oxirane-Formation by Darzens Condensation of Ketones: Quantification of the Electrophilicities of Ketones**

Zhen Li, Harish Jangra, Quan Chen, Peter Mayer, Armin R. Ofial, Hendrik Zipse, and Herbert Mayr

*J. Am. Chem. Soc.* **2018**, *140*, 5500–5515.

---

### ***Authors contribution***

A.R.O., H.Z. and H.M. designed the project. Z.L. and Q.C. did the experimental work that was designed by A.R.O and H.M. The X-ray crystallography was done by P.M.. H.J. performed theoretical calculations that were designed by him and H.Z.. A.R.O., H.Z. and H.M. jointly wrote the manuscript.

### ***Copyright***

This research was originally published in the *Journal of the American Chemical Society* and reprinted with permission from *J. Am. Chem. Soc.* **2018**, *140*, 5500–5515 © 2018 American Chemical Society as the 8<sup>th</sup> chapter of this thesis.

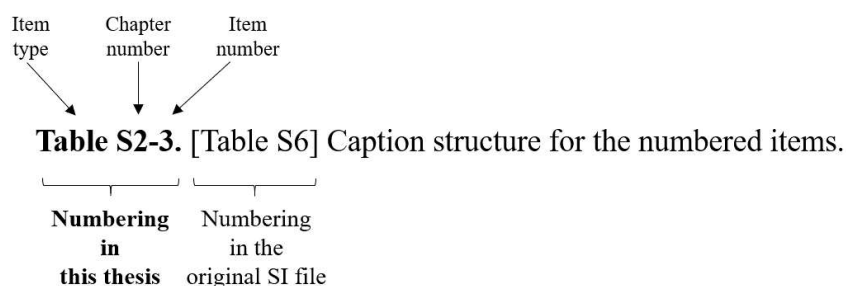
(Link to publication: <https://pubs.acs.org/doi/abs/10.1021/jacs.8b01657>)

Selected supporting material for the computational part of this work is provided at the end of this chapter. For complete supporting information (SI), please follow the link below:

<https://pubs.acs.org/doi/suppl/10.1021/jacs.8b01657>

### ***Additional information***

The accompanying SI is the shorter and altered version of the original content. The items (Tables, Figure, Schemes etc.) may have a different number than what was originally assigned. To make it easier to locate the SI content referred to in the following reprint, the original numbering is also provided in the caption of the numbered items as described below:



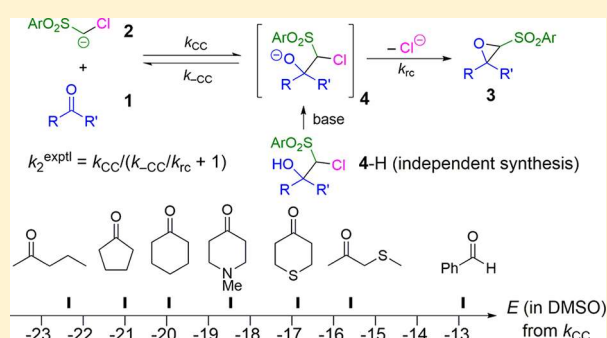
# Kinetics and Mechanism of Oxirane Formation by Darzens Condensation of Ketones: Quantification of the Electrophilicities of Ketones

Zhen Li, Harish Jangra, Quan Chen, Peter Mayer, Armin R. Ofial,\*<sup>1b</sup> Hendrik Zipse,\*<sup>1b</sup> and Herbert Mayr\*<sup>1b</sup>

Department Chemie, Ludwig-Maximilians-Universität München, Butenandtstrasse 5-13, 81377 München, Germany

**S** Supporting Information

**ABSTRACT:** The kinetics of epoxide formation by Darzens condensation of aliphatic ketones **1** with arylsulfonyl-substituted chloromethyl anions **2** ( $\text{ArSO}_2\text{CHCl}^-$ ) have been determined photometrically in DMSO solution at 20 °C. The reactions proceed via nucleophilic attack of the carbanions at the carbonyl group to give intermediate halohydrin anions **4**, which subsequently cyclize with formation of the oxiranes **3**. Protonation of the reaction mixture obtained in THF solution at low temperature allowed the intermediates to be trapped and the corresponding halohydrins **4-H** to be isolated. Crossover experiments, i.e., deprotonation of the halohydrins **4-H** in the presence of a trapping reagent for the regenerated arylsulfonyl-substituted chloromethyl anions **2**, provided the relative rates of backward ( $k_{-CC}$ ) and ring closure ( $k_{rc}$ ) reactions of the intermediates. Combination of the kinetic data ( $k_2^{\text{exptl}}$ ) with the splitting ratio ( $k_{-CC}/k_{rc}$ ) gave the second-order rate constants  $k_{CC}$  for the attack of the carbanions **2** at the ketones **1**. These  $k_{CC}$  values and the previously reported reactivity parameters  $N$  and  $s_N$  for the arylsulfonyl-substituted chloromethyl anions **2** allowed us to use the linear free energy relationship  $\log k_2(20^\circ\text{C}) = s_N(N + E)$  for deriving the electrophilicity parameters  $E$  of the ketones **1** and thus predict potential nucleophilic reaction partners. Density functional theory calculations of the intrinsic reaction pathways showed that the reactions of the ketones **1** with the chloromethyl anions **2** yield two rotational isomers of the intermediate halohydrin anions **4**, only one of which can cyclize while the other undergoes retroaddition because the barrier for rotation is higher than that for reversal to the reactants **1** and **2**. The electrophilicity parameters  $E$  correlate moderately with the lowest unoccupied molecular orbital energies of the carbonyl groups, very poorly with Parr's electrophilicity indices, and best with the methyl anion affinities calculated for DMSO solution.



## INTRODUCTION

Combinations of electrophiles with nucleophiles are the most important reactions in organic synthesis. To predict the scope and selectivities of such reactions, we have developed scales of nucleophilicity and electrophilicity on the basis of eq 1, which characterizes electrophiles by one parameter,  $E$  (electrophilicity), and nucleophiles by two solvent-dependent parameters,  $N$  (nucleophilicity) and  $s_N$  (susceptibility).<sup>1</sup>

$$\log k_2(20^\circ\text{C}) = s_N(N + E) \quad (1)$$

Though carbonyl compounds belong to the most frequently employed electrophiles in organic synthesis, there has been only one previous attempt to integrate aldehydes in these scales.<sup>2</sup> The major problem for the quantitative determination of the electrophilic reactivities of carbonyl compounds is the fact that the nucleophilic attack at the carbonyl group is often a reversible process, which is followed by an irreversible rate-determining step.<sup>3</sup>

In the late 1950s, kinetic investigations of the reactions of ketones and aldehydes with sodium borohydride in protic

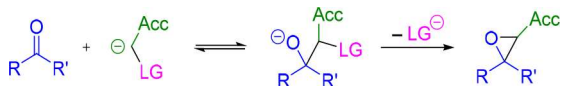
solvents were reported by H. C. Brown.<sup>4</sup> Geneste and associates studied the kinetics of the reactions of ketones with  $\text{BH}_4^-$ ,<sup>5a</sup>  $\text{CN}^-$ ,<sup>5b</sup>  $\text{SO}_3^{2-}$ ,<sup>5b,c</sup>  $\text{NH}_2\text{OH}$ ,<sup>5b,d</sup> and  $\text{RS}^-$ <sup>5e</sup> in water and reported linear correlations<sup>5f</sup> between the different sets of data. Thermodynamics accounts for the fact that ordinary acceptor-stabilized carbanions (e.g., malonate anions), which have previously been used as reference nucleophiles for the quantification of electrophilic reactivities,<sup>1b,6</sup> are not suitable for the determination of the  $E$  parameters of carbonyl compounds in aprotic solvents: Due to the high basicity of the initially formed alkoxide anions ( $\text{p}K_{\text{aH}} = 29.0$  for  $\text{MeO}^-$  in DMSO),<sup>7</sup> additions of weakly basic carbanions ( $\text{p}K_{\text{aH}} \approx 16$  for dimethyl malonate in DMSO)<sup>8</sup> to ordinary ketones and aldehydes are highly endergonic in aprotic solvents and only proceed in the presence of a suitable proton source. For that reason, reference nucleophiles are needed, which yield intermediates that undergo fast subsequent irreversible

Received: February 9, 2018

Published: April 16, 2018

reactions to form stable products. One possibility is to use carbanions carrying a leaving group (LG) in the  $\alpha$ -position, since the resulting intermediates may undergo cyclization with formation of epoxides (Scheme 1).

### Scheme 1. Epoxides from Carbonyl Compounds



For LG = Hal, the reaction depicted in Scheme 1 corresponds to the Darzens condensation,<sup>9,10</sup> which has mechanistically been investigated by Ballester<sup>11</sup> and others.<sup>3a,12</sup>

Whereas early work has preferentially been performed with  $\alpha$ -halogen-substituted esters, ketones, and aldehydes (Acc = CO<sub>2</sub>R or COR), Vogt and Tavares reported that  $\alpha$ -halo-substituted sulfones (Acc = ArSO<sub>2</sub>) also undergo the reaction sequence shown in Scheme 1 to give sulfonyl-substituted epoxides.<sup>3b</sup> For LG = R<sub>2</sub>S<sup>+</sup>, the nucleophile in Scheme 1 is a sulfonium ylide, and the sequence depicted in Scheme 1 then corresponds to the Corey–Chaykovsky epoxidation.<sup>13,14</sup>

In previous work, we have determined the nucleophile-specific reactivity parameters for acceptor-substituted sulfonium ylides<sup>15</sup> and for arylsulfonyl-substituted chloromethyl anions.<sup>16</sup> Since acceptor-substituted sulfonium ylides are not sufficiently nucleophilic to react with typical ketones, we have employed anions **2** (Scheme 2) as reference nucleophiles to quantify the electrophilicities of ketones.

## RESULTS

**Product Study.** The reactions of the ketones **1a–l** with the carbanions **2a,b** in anhydrous DMSO proceeded smoothly at room temperature (Scheme 2) and gave the epoxides **3** in good yields. The asymmetric ketones **1i–l** generally reacted with low diastereoselectivity. Only in the reaction of **1l** with **2b**, the formation of the diastereomer with ArSO<sub>2</sub> and CF<sub>3</sub> *trans* to each other is highly preferred (de = 88%) (Scheme 2). The different stereoselectivities of **2a** and **2b** in reactions with **1l** have been observed in numerous experiments where **1l** was used as a trapping reagent in crossover experiments (see below). As shown in the Supporting Information, **2a** always gave 2/1 mixtures of two diastereomers, while **2b** gave one diastereomer almost exclusively, possibly because **1l** reacts with **2a**, but not with **2b**, under diffusion control.<sup>17</sup>

**Kinetic Investigations.** All kinetic investigations were performed in anhydrous DMSO solution at 20 °C by following the disappearance of the UV/vis absorptions of the carbanion **2a** (320 nm) or **2b** (405 nm) under pseudo-first-order conditions ( $[1]_0/[2]_0 > 10$ ). As the carbanions **2a,b** decompose on the minute time scale at 20 °C (depending on the method of preparation), they were generated by treatment of their conjugate CH acids with 1.00–1.05 equiv of *t*-BuOK in dry THF at –78 °C. Small amounts of these solutions were dissolved in DMSO at 20 °C immediately before the ketones **1** were added. The first-order rate constants  $k_{\text{obsd}}$  were obtained by least-squares fitting of the exponential function  $A = A_0 \exp(-k_{\text{obsd}}t) + C$  to the observed time-dependent absorbances  $A$  of **2** (Figure 1a). The slopes of the linear correlations between  $k_{\text{obsd}}$  and the different concentrations of **1a–j** (Figure

### Scheme 2. Reactions of Carbanions **2** with Ketones **1** and Corresponding Gross Second-Order Rate Constants $k_2^{\text{exptl}}$

Ketones <b>1</b>	X	$k_2^{\text{exptl}}$ (M <sup>-1</sup> s <sup>-1</sup> ) <sup>b</sup>	Oxiranes <b>3</b> (yield)	
 <b>1a</b> $n = 1$ <b>1b</b> $n = 2$ <b>1c</b> $n = 3$ <b>1d</b> $n = 4$	<b>2b</b> CN	$7.05 \times 10^3$	<b>3ab</b> (80%) <sup>c</sup>	
	<b>2a</b> H		<b>3ba</b> (87%) <sup>d</sup>	
	<b>2b</b> CN	$1.31 \times 10^2$	<b>3bb</b> (73%) <sup>d</sup>	
	<b>2a</b> H	$2.98 \times 10^3$	<b>3ca</b> (95%) <sup>c</sup>	
	<b>2b</b> CN	$2.61 \times 10^2$	<b>3cb</b> (75%) <sup>c</sup>	
	<b>2a</b> H	$8.49 \times 10^1$	<b>3da</b> (90%) <sup>c</sup>	
	 <b>1e</b> X = NMe <b>1f</b> X = O <b>1g</b> X = S	<b>2a</b> H	$1.77 \times 10^4$	<b>3ea</b> (90%) <sup>c</sup>
		<b>2b</b> CN	$1.82 \times 10^3$	<b>3eb</b> (90%) <sup>c</sup>
<b>2b</b> CN		$7.62 \times 10^3$	<b>3fb</b> (70%) <sup>c</sup>	
<b>2a</b> H		very fast <sup>e</sup>	<b>3ga</b> (95%) <sup>c</sup>	
 <b>1h</b>	<b>2a</b> H	$2.12 \times 10^4$	<b>3ha</b> (80%) <sup>c</sup>	
	<b>2b</b> CN	$3.00 \times 10^3$	<b>3hb</b> (75%) <sup>c</sup>	
 <b>1i</b> X = CH <sub>2</sub> <b>1j</b> X = S <b>1k</b> X = O	<b>2a</b> H	$7.42 \times 10^1$	<b>3ia</b> (90%, rel-2S,3S/rel-2R,3S = 2.6) <sup>c</sup>	
	<b>2b</b> CN	$3.21 \times 10^4$	<b>3jb</b> (80%, rel-2S,3S/rel-2R,3S = 2.2) <sup>d</sup>	
	<b>2b</b> CN	very fast <sup>e</sup>	<b>3kb</b> (89%, rel-2R,3R/rel-2R,3S = 2.3) <sup>c</sup>	
 <b>1l</b>	<b>2a</b> H	very fast <sup>e</sup>	<b>3la</b> (90%, rel-2R,3R/rel-2R,3S = 2.0) <sup>c</sup>	
	<b>2b</b> CN	very fast <sup>e</sup>	<b>3lb</b> (80%, rel-2S,3S/rel-2R,3S > 15) <sup>c</sup>	

<sup>a</sup>Counterion: K<sup>+</sup> for kinetics, Na<sup>+</sup> for product studies. <sup>b</sup>Carbanions **2a,b** generated by treatment of (**2a,b**)-H with *t*-BuOK, as described in the section “Kinetic Investigations”. <sup>c</sup>Isolated yield obtained after chromatographic purification. <sup>d</sup>Yield determined by <sup>1</sup>H NMR spectroscopy using *m*-xylene as an internal standard. <sup>e</sup>Too fast to be measured by the stopped-flow technique.

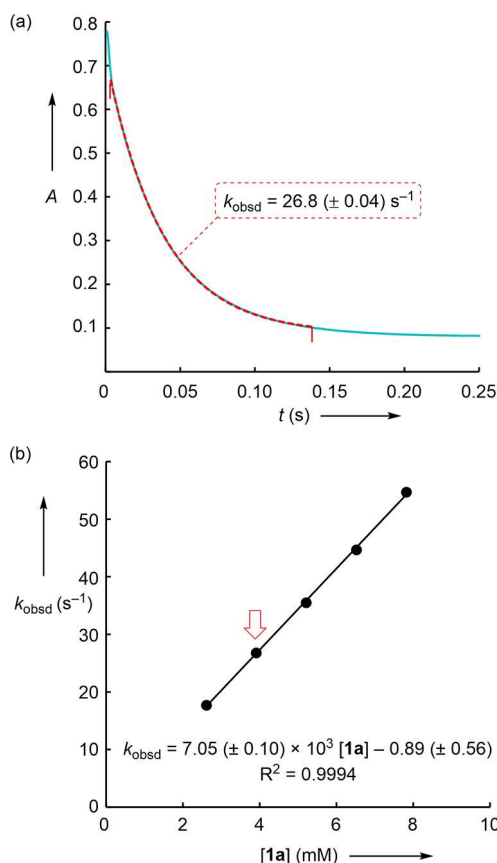


**Figure 1.** (a) Monoexponential decay of the absorbance  $A$  of **2b** (at 405 nm) during the reaction of **1a** ( $3.91 \times 10^{-3} \text{ mol L}^{-1}$ ) with **2b** ( $2.50 \times 10^{-4} \text{ mol L}^{-1}$ ) in DMSO at  $20^\circ\text{C}$  (the remaining absorbance is due to products generated by degradation of carbanion **2b**). (b)  $k_{\text{obsd}}$  for the reaction of **1a** with **2b** versus the concentration of **1a**.

1b) correspond to the second-order rate constants  $k_2^{\text{exptl}}$  listed in Scheme 2.

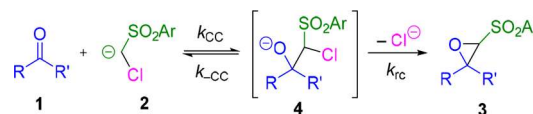
Table 1 shows the role of counterions on the reaction kinetics. Neither addition of 18-crown-6 ether to the potassium salts of **2a** or **2b** nor exchange of *t*-BuOK by Schwesinger's base  $\text{P}_4\text{-}^t\text{Bu}^{18}$  for the generation of **2b** from its conjugate acid had a significant effect on the second-order rate constants  $k_2^{\text{exptl}}$ .

**Determination of the Rate-Limiting Step.** As shown in Scheme 3, nucleophilic attack of **2** at the ketone **1** yields the intermediate alkoxide anion **4**, which either cyclizes with formation of the epoxide **3** or undergoes retroaddition with regeneration of ketone **1** and carbanion **2**.

The time-dependent concentrations of **2**, **4**, and **3** can be expressed by eqs 2–4.

$$d[\mathbf{2}]/dt = -k_{\text{CC}}[\mathbf{1}][\mathbf{2}] + k_{-\text{CC}}[\mathbf{4}] \quad (2)$$

### Scheme 3. Mechanism of the Reactions of Arylsulfonyl-Substituted Chloromethyl Anions with Ketones



$$d[\mathbf{4}]/dt = k_{\text{CC}}[\mathbf{1}][\mathbf{2}] - k_{-\text{CC}}[\mathbf{4}] - k_{\text{rc}}[\mathbf{4}] \quad (3)$$

$$d[\mathbf{3}]/dt = k_{\text{rc}}[\mathbf{4}] \quad (4)$$

As the intermediate  $\beta$ -chloroalkoxide anion **4** is formed as a short-lived species, the Bodenstein approximation holds ( $d[\mathbf{4}]/dt = 0$ ), and the concentration of **4** is given by eq 5. Substitution into eq 4 yields eq 6, and  $k_2^{\text{exptl}}$  is a function of  $k_{\text{CC}}$ ,  $k_{-\text{CC}}$ , and  $k_{\text{rc}}$  as shown by eq 7.

$$[\mathbf{4}] = k_{\text{CC}}[\mathbf{1}][\mathbf{2}]/(k_{-\text{CC}} + k_{\text{rc}}) \quad (5)$$

$$\Rightarrow d[\mathbf{3}]/dt = -d[\mathbf{2}]/dt = k_{\text{CC}}k_{\text{rc}}[\mathbf{1}][\mathbf{2}]/(k_{-\text{CC}} + k_{\text{rc}}) \quad (6)$$

$$\Rightarrow k_2^{\text{exptl}} = k_{\text{CC}}/(k_{-\text{CC}}/k_{\text{rc}} + 1) \quad (7)$$

According to eq 7, the rate of the attack of **2** at the carbonyl group ( $k_{\text{CC}}$ ) can be derived from the measured rate constant  $k_2^{\text{exptl}}$  (Scheme 2) if the ratio  $k_{-\text{CC}}/k_{\text{rc}}$  is known. To determine  $k_{-\text{CC}}/k_{\text{rc}}$  we have developed an independent access to the intermediate **4**.

**Synthesis of the Halohydrins 4-H.** Whereas treatment of **2-H** with base in the presence of ketones **1** at ambient temperature led to the formation of the epoxides **3** (Scheme 2), the reactions of **2a-H** with BuLi or of **2b-H** with lithium diisopropylamide (LDA) in THF at  $-78^\circ\text{C}$ , followed by addition of the ketones **1a–j**, and subsequent acidification at low temperature yielded the halohydrins **4-H** in good yields (Scheme 4).<sup>19</sup> In the case of the acyclic ketones **1i** and **1j**, two diastereomeric compounds were formed, which were separated by column chromatography on silica gel and fully characterized. The structure of **4ca-H** was confirmed by single-crystal X-ray crystallography and showed a conformer with chlorine *gauche* to the hydroxyl group (Figure 2).

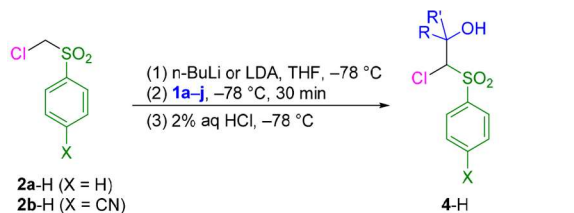
**Examination of the Reversibility of the Attack of 2 at the Ketones 1.** To examine whether the intermediates **4**, generated by treatment of the halohydrins **4-H** with base, undergo ring closure with formation of **3** ( $k_{\text{rc}}$ , Scheme 3) or retroaddition with regeneration of **1** and **2** ( $k_{-\text{CC}}$ , Scheme 3), it was necessary to find a trapping reagent which rapidly intercepts **2** after its generation from **4**. In view of their high reaction rates (Scheme 2), ketones **1g**, **1j**, **1k**, and **1l** were considered to be suitable trapping agents. Ketone **1j** was then eliminated from this series because the resulting oxirane **3jb** turned out not to be stable at  $20^\circ\text{C}$ .

**Table 1.** Second-Order Rate Constants  $k_2^{\text{exptl}}$  ( $\text{M}^{-1} \text{s}^{-1}$ ) for the Reactions of the Ketones **1** with Carbanions **2** under Various Conditions

ketone	nucleophile	$k_2^{\text{exptl}, a}$	$k_2^{\text{exptl}(18\text{-crown-6})}^b$	$k_2^{\text{exptl}(\text{P}_4\text{-}^t\text{Bu})}$
<b>1e</b>	<b>2a</b>	$(1.77 \pm 0.13) \times 10^4$	$(1.79 \pm 0.11) \times 10^4$	
<b>1f</b>	<b>2b</b>	$(7.62 \pm 0.35) \times 10^3$	$(7.65 \pm 0.47) \times 10^3$	
<b>1g</b>	<b>2b</b>	$(1.81 \pm 0.07) \times 10^4$	$(1.71 \pm 0.04) \times 10^4$	$(1.66 \pm 0.05) \times 10^4$
<b>1j</b>	<b>2b</b>	$(3.21 \pm 0.55) \times 10^4$	$(3.59 \pm 0.33) \times 10^4$	

<sup>a</sup>Data from Scheme 2. <sup>b</sup>18-Crown-6 (2.0–2.5 equiv) was added to the potassium salts of **2a,b**.

Scheme 4. Synthesis of the Halohydrins 4-H



ketone	nucleophile	product (yield)
1a	2b	4ab-H (90%)
1b	2b	4bb-H (85%)
1c	2a	4ca-H (90%)
	2b	4cb-H (85%)
1d	2a	4da-H (85%)
1e	2a	4ea-H (75%)
	2b	4eb-H (95%)
1f	2b	4fb-H (80%)
1g	2b	4gb-H (70%)
1h	2a	4ha-H (70%)
	2b	4hb-H (95%)
1i	2a	4ia-H (93%, dr 1.8/1)
1j	2b	4jb-H (83%, dr 1.1/1)

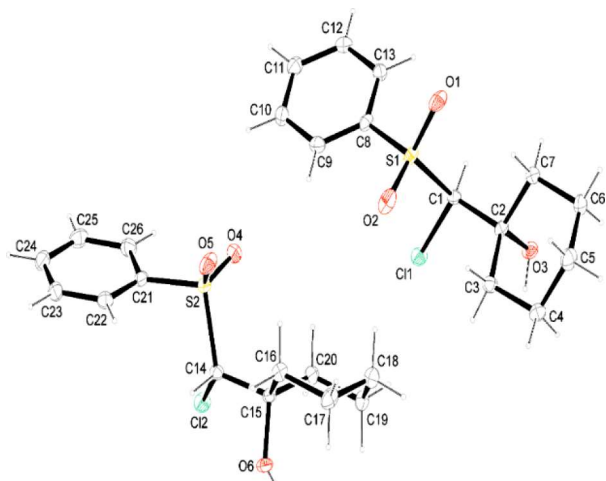
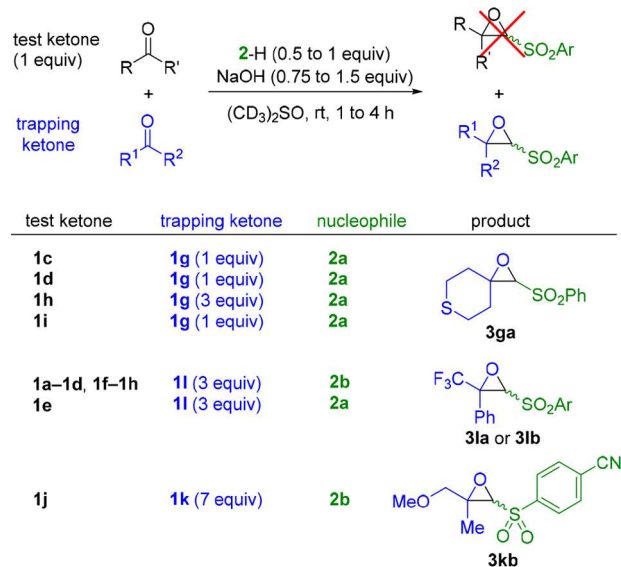


Figure 2. ORTEP drawing of the crystal structure of 4ca-H (the ellipsoid probability level is 50%).

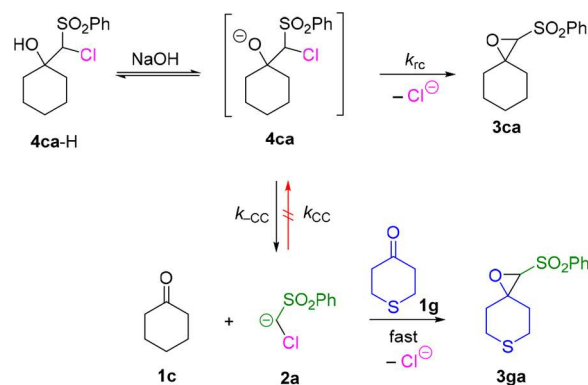
When 1/1 mixtures of **1g** on one side and of **1c**, **1d**, or **1i** on the other were combined with 0.5 equiv of the carbanion **2a**, the oxiranes derived from **1g** (i.e., **3ga**) were formed exclusively (Scheme 5). Since **1g** is only 6 times more reactive than **1h**, 3 equiv of **1g** was employed to obtain **3ga** exclusively from a mixture of **1h** and **1g**.

The oxiranes **3la** and **3lb** were the only products obtained from the reactions of 3/1 mixtures of **1l** and **1a–h** with **2** (1 equiv with respect to **1a–h**). Since the product obtained by treatment of a mixture of **1j** and **1l** with **2b** was difficult to analyze, **1k** was used as a trapping agent, and treatment of a 7/1 mixture of **1k** and **1j** with 1 equiv of **2b** gave the oxirane **3kb** exclusively.

The principle of the crossover experiments is illustrated in Scheme 6. When the independently synthesized halohydrin **4ca-H** is treated with NaOH in the presence of the highly reactive ketone **1g**, the generated intermediate **4ca** has the choice of undergoing either ring closure with formation of the epoxide **3ca** or retroaddition with regeneration of **1c** and **2a**. As **1g** is considerably more reactive and present in higher

Scheme 5. Competition Reactions To Examine the Suitability of Ketones **1g,k,l** as Trapping Agents

Scheme 6. Crossover Reaction of the Cyclohexanone Adduct 4ca-H



concentration than **1c**, any regenerated carbanion **2a** will exclusively be converted into the crossover product **3ga**, and the ratio  $[3ga]/[3ca]$  equals the ratio  $k_{-CC}/k_{rc}$ .

Scheme 7 shows that in all crossover experiments at least 3 equiv of trapping agents was employed to ensure that they will quantitatively intercept the regenerated carbanions **2**. In Scheme 7, one can furthermore see that, in most cases investigated, ring closure ( $k_{rc}$ ) is up to 8 times faster than retroaddition. Entries 5–7 show, however, that the intermediates generated from cycloheptanone (**1d**) undergo retroaddition 3–4 times faster than ring closure. Comparison of entry 5 with entry 7 and of entry 13 with entry 14 indicates that almost the same  $k_{-CC}/k_{rc}$  ratio is obtained with different trapping agents, and entries 5/6 and 8/9 show that the nature of the counterion ( $K^+$  vs  $Na^+$ ) has only a small influence on this ratio. The similarity of  $k_{-CC}/k_{rc}$  in entries 3/4, 8/10, and 13/15 implies that the ratio of retroaddition vs ring closure is almost independent of the substituents at the arylsulfonyl groups. Entries 16/17 as well as 18/19 show that the two diastereomeric halohydrins obtained from the asymmetric ketones **1i** and **1j** react with significantly different  $k_{-CC}/k_{rc}$  ratios.

## Scheme 7. Crossover Reactions of 4-H

entry	halohydrin	trapping ketone	$P_{-CC}/P_{rc} = k_{-CC}/k_{rc}^a$
1	4ab-H	1l (4 equiv)	0.89
2	4bb-H	1l (4 equiv)	0.63
3	4ca-H	1g (3 equiv) <sup>b</sup>	0.60
4	4cb-H	1l (4 equiv) <sup>b</sup>	0.86
5	4da-H	1g (3 equiv) <sup>b</sup>	3.5
6		1g (3 equiv) <sup>c</sup>	3.3
7		1l (3 equiv)	4.1
8	4ea-H	1l (4 equiv)	0.37
9		1l (4 equiv) <sup>c</sup>	0.29
10	4eb-H	1l (4 equiv)	0.33
11	4fb-H	1l (4 equiv)	0.13
12	4gb-H	1l (4 equiv)	0.57
13	4ha-H	1g (4 equiv)	0.19
14		1l (4 equiv)	0.24
15	4hb-H	1l (4 equiv)	0.21
16	4ia'-H	1g (3 equiv) <sup>b</sup>	2.2
17	4ia''-H	1g (3 equiv)	6.9
18	4jb'-H	1k (8 equiv)	2.2
19	4jb''-H	1k (8 equiv)	5.1

<sup>a</sup>Determined by <sup>1</sup>H NMR spectroscopic analysis of the crude product.

<sup>b</sup>Product yields determined by using 1,3,5-trimethoxybenzene as an internal standard (Supporting Information). <sup>c</sup>KOH was used as the base instead of NaOH.

Combination of the  $k_{-CC}/k_{rc}$  ratios from Scheme 7 with  $k_2^{\text{exptl}}$  from Scheme 2 according to eq 7 yields the rate constants for nucleophilic attack of **2** at the ketones **1** ( $k_{CC}$ ), which are listed in Table 2. While this procedure is straightforward for the reactions with symmetrical ketones, the situation is more complex for unsymmetrical ketones because their reactions with the carbanions **2** yield mixtures of diastereomeric halohydrins **4-H**, as specified for **1i** and **1j** in the last two entries of Table 2.

The stereospecificity of ring closure has exemplarily been studied for the reaction of **2a** with pentan-2-one (**1i**). The diastereomeric halohydrins **4ia'**-H and **4ia''**-H undergo either stereospecific ring closure with formation of epoxides or retroaddition with regeneration of **1i** and **2a**. Figure 3a shows

the <sup>1</sup>H NMR spectrum of **3ga**, the product formed by trapping the regenerated carbanion **2a** with the ketone **1g**. Treatment of ketone **1i** with anion **2a** yielded a mixture of the diastereomeric epoxides **3ia'** and **3ia''** (Figure 3b). Since the ring protons A' and A'' of the epoxides **3ia'** and **3ia''** have similar chemical shifts, their ratio was derived from the <sup>1</sup>H NMR signals of the methyl groups B'/B'' and C'/C''. Nuclear Overhauser effect (NOE) experiments show that the methyl resonances at lower field (B' and C'') arise from the groups *cis* to the phenylsulfonyl substituent.<sup>20</sup> Parts c and d of Figure 3 reveal that the epoxides **3ia'** and **3ia''** are formed stereospecifically from the diastereomeric halohydrins **4ia'**-H and **4ia''**-H, respectively. When **4ia'**-H is treated with NaOH in the presence of **1g**, epoxides **3ia'** and **3ga** are formed in the ratio 1/2.2, as derived from the integrals of protons A' and A in Figure 3c. Since there are no peaks at  $\delta$  1.32 and 0.93, the chemical shifts of the methyl protons (B'' and C'') of the diastereomer **3ia''**, we can conclude that **4ia'** either cyclizes with formation of **3ia'** or fragments with formation of **1i** and **2a**, the latter of which is subsequently trapped by **1g** to give **3ga**.

Analogously, treatment of the other diastereomer (**4ia''**-H) with NaOH in the presence of **1g** yields the epoxides **3ia''** and **3ga** in a ratio of 1/6.9 (from integrals A'' and A, Figure 3d). The stereospecificity of this cyclization, i.e., the exclusive formation of **3ia''** from **4ia''**-H, can be derived from the absence of **3ia'** in the product mixture, which would be detectable by a <sup>1</sup>H NMR signal for the methyl group B' at  $\delta$  1.63 and less clearly by the methyl triplet at  $\delta$  0.80 for C'.

With the product ratio **3ia'**/**3ia''** = 2.6 given in Scheme 2, we can split the measured gross second-order rate constant  $k_2^{\text{exptl}} = 74.2 \text{ M}^{-1} \text{ s}^{-1}$  for the reaction of **1i** with **2a** (Scheme 2) into the partial rate constants  $k_2'^{\text{(exptl)}} = 53.6 \text{ M}^{-1} \text{ s}^{-1}$  and  $k_2''^{\text{(exptl)}} = 20.6 \text{ M}^{-1} \text{ s}^{-1}$  for the formation of **3ia'** and **3ia''**, respectively. The ratio of these partial rate constants corresponds to the observed product ratio (eq 8) given in Scheme 2, and their sum corresponds to the measured rate constants ( $k_2^{\text{exptl}}$  in Scheme 2, eq 9).

$$k_2'^{\text{(exptl)}}/k_2''^{\text{(exptl)}} = 2.6 \quad (8)$$

$$k_2'^{\text{(exptl)}} + k_2''^{\text{(exptl)}} = k_2^{\text{exptl}} = 74.2 \text{ M}^{-1} \text{ s}^{-1} \quad (9)$$

Table 2. Determination of Second-Order Rate Constants  $k_{CC}$  from Measured Rate Constants  $k_2^{\text{exptl}}$  and Ratios  $k_{-CC}/k_{rc}$

ketone	nucleophile	$k_2^{\text{exptl}, a}$ ( $\text{M}^{-1} \text{ s}^{-1}$ )	$(k_{-CC}/k_{rc}) + 1^b$	$k_{CC}$ ( $\text{M}^{-1} \text{ s}^{-1}$ )	<i>E</i>	$k^{\text{calcd}}/k_{CC}$
1a	2b	$7.05 \times 10^3$	1.89	$1.33 \times 10^4$	-17.5	identical
1b	2b	$1.31 \times 10^2$	1.63	$2.14 \times 10^2$	-21.0	identical
1c	2a	$2.98 \times 10^3$	1.60	$4.77 \times 10^3$	-19.9 <sup>c</sup>	0.69
	2b	$2.61 \times 10^2$	1.86	$4.85 \times 10^2$		1.6
1d	2a	$8.49 \times 10^1$	4.5	$3.8 \times 10^2$	-22.1	identical
1e	2a	$1.77 \times 10^4$	1.37	$2.42 \times 10^4$	-18.4 <sup>c</sup>	0.58
	2b	$1.82 \times 10^3$	1.33	$2.42 \times 10^3$		1.9
1f	2b	$7.62 \times 10^3$	1.13	$8.61 \times 10^3$	-17.9	identical
1g	2b	$1.81 \times 10^4$	1.57	$2.84 \times 10^4$	-16.9	identical
1h	2a	$2.12 \times 10^4$	1.19	$2.52 \times 10^4$	-18.2 <sup>c</sup>	0.67
	2b	$3.00 \times 10^3$	1.21	$3.63 \times 10^3$		1.6
1i	2a	$7.42 \times 10^1$	3.2 <sup>d</sup>	$3.3 \times 10^{2e}$	-22.3	identical
			7.9 <sup>d</sup>			
1j	2b	$3.21 \times 10^4$	3.2 <sup>d</sup>	$1.3 \times 10^{5e}$	-15.6	identical
			6.1 <sup>d</sup>			identical

<sup>a</sup>From Scheme 2. <sup>b</sup>From Scheme 7. <sup>c</sup>Calculated by averaging the individual *E* parameters. <sup>d</sup>Ratios ( $k_{-CC}/k_{rc}$ ) for the individual halohydrin diastereoisomers. <sup>e</sup> $k_{CC} = k'_{CC} + k''_{CC}$  (see the text for the calculation).

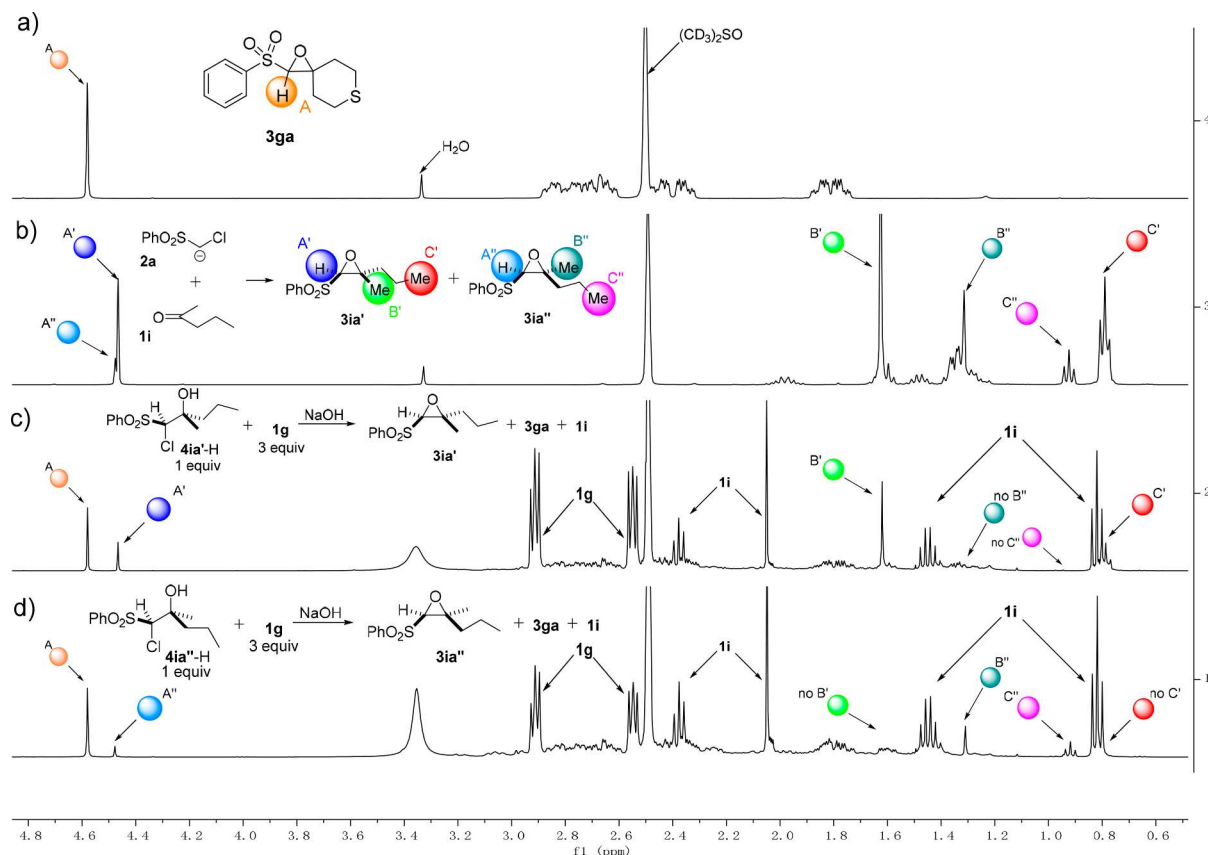


**Figure 3.** Examination of the stereospecificity of ring closure of the diastereomeric halohydrins **4ia'**-H and **4ia''**-H by  $^1\text{H}$  NMR spectroscopy: (a) independently synthesized trapping product of regenerated **2a**, (b) mixture of **3ia'** and **3ia''** obtained from the reaction of **2a** with **1i**, (c) exclusive formation of **3ia'** and **3ga** ( $1/2.2 = k'_{\text{rc}}/k'_{\text{-CC}}$ ) by treatment of **4ia'**-H with NaOH in the presence of **1g**, (d) exclusive formation of **3ia''** and **3ga** ( $1/6.9 = k''_{\text{rc}}/k''_{\text{-CC}}$ ) by treatment of **4ia''**-H with NaOH in the presence of **1g**.

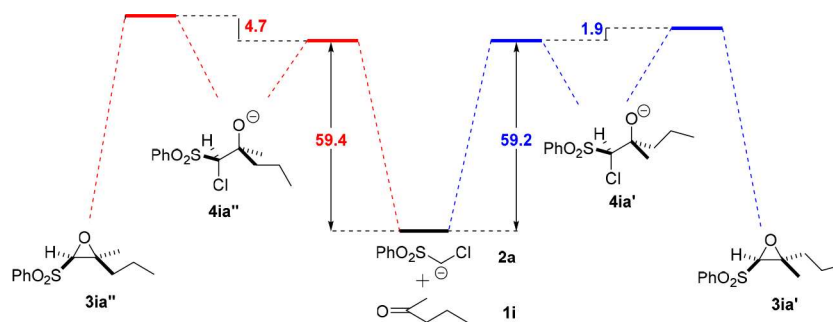


**Figure 4.** Gibbs energy profile ( $\text{kJ mol}^{-1}$ ) for the reaction of carbanion **2a** with pentan-2-one (**1i**) at  $20^\circ\text{C}$  in DMSO derived from rate measurements (Scheme 2) and crossover experiments (Figure 3, Table 2).

With application of eq 7 to the two parallel reactions with  $k'_{\text{-CC}}/k'_{\text{rc}} = 2.2$  (Figure 3c and Scheme 7, entry 16) and  $k''_{\text{-CC}}/k''_{\text{rc}} = 6.9$  (Figure 3d and Scheme 7, entry 17), we obtain  $k'_{\text{CC}} = (2.2 + 1) \times 53.6 \text{ M}^{-1} \text{ s}^{-1} = 1.7 \times 10^2 \text{ M}^{-1} \text{ s}^{-1}$  and  $k''_{\text{CC}} = (6.9 + 1) \times 20.6 \text{ M}^{-1} \text{ s}^{-1} = 1.6 \times 10^2 \text{ M}^{-1} \text{ s}^{-1}$ , i.e., both halohydrins are formed with similar rates, and the stereoselectivity originates from the different rates of cyclization as illustrated in Figure 4. In contrast, in THF at  $-78^\circ\text{C}$ , **4ia'**-Li is formed 1.8 times faster than **4ia''**-Li (Scheme 4).

An analogous calculation gave  $k'_{\text{CC}} = 7.1 \times 10^4 \text{ M}^{-1} \text{ s}^{-1}$  and  $k''_{\text{CC}} = 6.1 \times 10^4 \text{ M}^{-1} \text{ s}^{-1}$  for the reaction of **2b** with the unsymmetrical ketone **1j**.

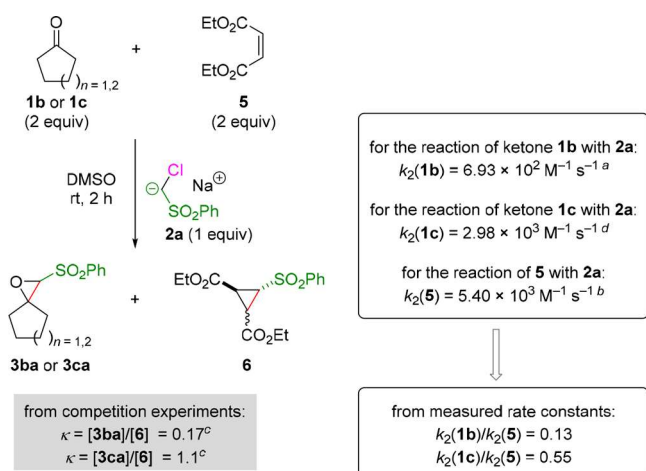
Substitution of  $k_{\text{CC}}$  and the published parameters  $N$  and  $s_N$  for **2a,b** into eq 1 yielded the electrophilicity parameters  $E$  of

the ketones **1**. In cases where the electrophilicity parameters  $E$  are derived from reactions with **2a** and **2b**, both rate constants should ideally give the same value of  $E$ . As this is not the case, the  $E$  values derived from different reactions were averaged and listed in Table 2. The last column of Table 2, which compares the rate constants calculated by eq 1 with the directly determined rate constants, shows that, in this series, eq 1 reproduces the rate constants  $k_{\text{CC}}$  within a factor of 2.

A confirmation for the ketone reactivities derived in this way was obtained by competition experiments. When a mixture of diethyl maleate (**5**) ( $E = -19.49$ ) and cycloalkanone **1b** or **1c** was treated with **2a** (in situ generated from **2a**-H and NaOH), mixtures of the epoxides **3** and the cyclopropane **6** were obtained. Their ratio was determined by  $^1\text{H}$  NMR spectroscopy

and used to calculate the ratio  $k_2^{\text{exptl}}(\mathbf{1})/k_2^{\text{exptl}}(\mathbf{5})$  given in Scheme 8. The ratios of direct rate measurements,  $k_2(\mathbf{1})/k_2(\mathbf{5})$ ,

### Scheme 8. Examination of the *E* Parameters of Ketones 1



<sup>a</sup>Equation 1 gives  $k_{\text{CC}} = 1.13 \times 10^3 \text{ M}^{-1} \text{ s}^{-1}$ , which was corrected for reversibility by applying eq 7 with  $k_{-\text{CC}}/k_{\text{CC}} = 0.63$ . <sup>b</sup>This work (Table S20, Supporting Information). <sup>c</sup>For the calculation, see the Supporting Information. <sup>d</sup>From Scheme 2.

agree with product ratios from competition experiments,  $\kappa = [\mathbf{3}]/[\mathbf{6}]$ , within a factor of 2. This suggests that diethyl maleate (**5**) and cyclohexanone (**1c**) have similar electrophilicities *E*, one order of magnitude greater than the electrophilic reactivity of cyclopentanone (**1b**).

**Intrinsic Reaction Pathway Calculations.** The mechanistic picture derived from the kinetic studies was subsequently complemented by reaction path calculations. Geometry optimizations and calculations of intrinsic reaction pathways have been performed at the B3LYP<sup>21</sup>-D3<sup>22</sup>/6-31+G(d,p)<sup>23</sup> level of theory in combination with the polarizable continuum model (PCM)<sup>24</sup> for DMSO as the solvent and UA0 radii. Improved energies for ground and transition states have been calculated at the PCM(DMSO,UA0)/B2PLYP<sup>25</sup>-D3/def2TZVPP<sup>26</sup> level. Combination of energies with thermochemical corrections obtained at a lower level then yields the reaction Gibbs energies reported in the Supporting Information and summarized in Figures 5–7.

For the reaction of carbanion **2a** with cyclohexanone (**1c**) (a ketone of intermediate electrophilicity,  $E = -19.9$ ), the Gibbs energy surface is shown in Figure 5. Two distinct pathways have been identified for the addition of anion **2a** to the C=O double bond in ketone **1c**, which differ by the relative orientation of the two reactants. The energies shown are those of the energetically best conformers for each pathway (for full details, see the Supporting Information). The blue, energetically less favorable reaction pathway ( $\Delta G^\ddagger = +61.5 \text{ kJ mol}^{-1}$ ) directly yields an adduct with the C–Cl bond *anti* to the C–O bond. Chloride expulsion through epoxide ring closure is possible from this adduct with a barrier of +44.8  $\text{kJ mol}^{-1}$  (relative to separate reactants). A second, red reaction pathway ( $\Delta G^\ddagger = +47.4 \text{ kJ mol}^{-1}$ ) leads to a primary adduct where the C–Cl bond assumes a *gauche* orientation relative to the C–O bond. Epoxide ring closure from this adduct is not immediately possible, but requires rotation around the newly formed C–C bond such that the C–Cl and C–O bonds attain the *anti* orientation required for cyclization. The barrier for this

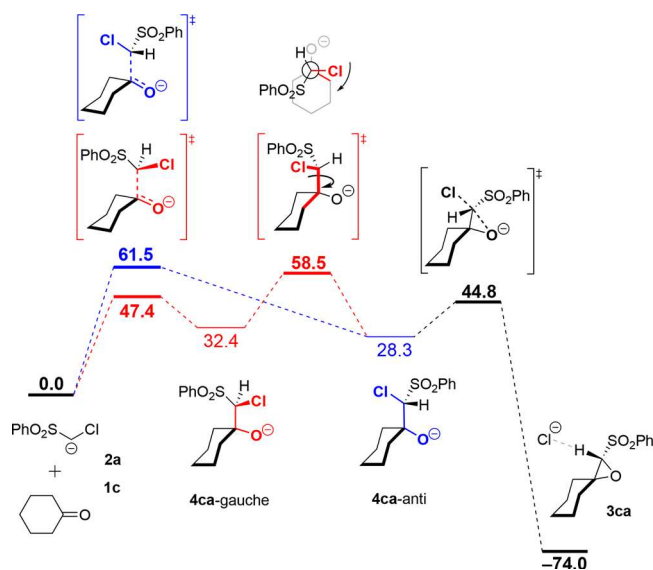


**Figure 5.** Gibbs energy surface (25 °C) for the reaction of **1c** with **2a** [at the PCM(DMSO,UA0)/B2PLYP-D3/def2TZVPP//PCM-(DMSO,UA0)/B3LYP-D3/6-31+G(d,p) level,  $\text{kJ mol}^{-1}$ ].

rotation is higher ( $\Delta G^\ddagger = +58.5 \text{ kJ mol}^{-1}$  relative to separate reactants) than the barrier for the reversal to the separate reactants **2a** and **1c**. The comparable heights of the barriers for initial nucleophilic addition and conformational reorientation are in line with the results derived from the crossover experiments with halohydrin **4ca-H** described in Scheme 7. Guided by the conformational analysis of halohydrin **4ca-H** and its deprotonated form **4ca**, we assume that **4ca-H** exists as a mixture of conformers in solution, from which only that with the C–Cl and C–O bonds in *gauche* conformation had crystallized (see Figure 2 and Figure S15 in the Supporting Information). Deprotonation of **4ca-H** will give both adduct conformers shown in Figure 5. While the adduct **4ca** with *gauche* C–Cl and C–O bonds will revert back to reactants, the conformer with *anti* C–Cl/C–O orientation will cyclize to epoxide **3ca**.

The reaction of anion **2a** with the more reactive ketone **1g** ( $E = -16.9$ ) has been studied analogously. The resulting Gibbs energy surface in Figure 6 shows that the nucleophilic addition can also lead to intermediates **4ga** with C–Cl/C–O *gauche* or *anti* orientation, and the rotational barrier for their interconversion ( $\Delta G^\ddagger = +41.4 \text{ kJ mol}^{-1}$  relative to separate reactants) is again comparable to the barriers of the reverse reaction. The barrier for epoxide ring closure is, in comparison, lower at  $\Delta G^\ddagger = +30.0 \text{ kJ mol}^{-1}$ , which again implies that adducts with C–Cl/C–O *anti* orientation will move forward to epoxide product rather than revert to separate reactants. In agreement with the larger *E* value of ketone **1g** as compared to **1c** ( $-16.9$  vs  $-19.9$ ), the calculated overall Gibbs energy barrier for reaction with anion **2a** is much lower for **1g** than for **1c** ( $+41.6$  vs  $+58.5 \text{ kJ mol}^{-1}$ ).

To test whether the mechanistic picture obtained for the ketone addition reaction is comparable to that for addition to electron-poor alkenes (Michael acceptors), the reaction of anion **2a** with dimethyl maleate (**5\***), as a model for the experimentally studied diethyl maleate (**5**), was also treated computationally (Figure 7). While the same sequence of initial nucleophilic addition, *gauche/anti* reorientation, and ring closure was also found for this system, the relative barriers

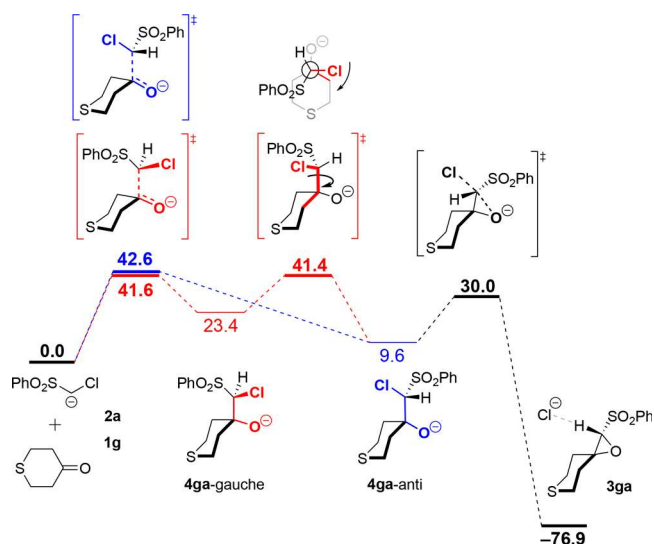


**Figure 6.** Gibbs energy surface (25 °C) for the reaction of **1g** with **2a** [at the PCM(DMSO,UA0)/B2PLYP-D3/def2TZVPP//PCM(DMSO,UA0)/B3LYP-D3/6-31+G(d,p) level, kJ mol<sup>-1</sup>].

for the individual steps differ significantly from those found for the ketones: While the barrier for the initial addition step ( $\Delta G^\ddagger = +46.2$  kJ mol<sup>-1</sup>) is similar to that for ketone **1c** (in line with the kinetic measurements described above), the barriers for rotation and cyclopropane ring closure are much lower than the barrier for the reverse reaction. This implies that the initial addition step of anion **2a** to alkene **5\*** is practically irreversible, irrespective of the *gauche*/*anti* orientation in the initial addition step.

**Electrophilicities of Benzaldehydes.** According to Table 2, most of the ketones characterized in this work have *E* parameters similar to that previously reported for benzaldehyde

(**1m**;  $E = -19.5$ ),<sup>2</sup> in contrast to common experience that aldehydes are generally more electrophilic than ordinary ketones. How can this discrepancy be explained?

On the basis of Aggarwal's report that the independently synthesized *anti*-betaine **8a**, formed from sulfonium ylide **7a** and benzaldehyde (**1m**), does not undergo retroaddition but rapidly cyclizes with formation of *trans*-stilbene oxide (**9a**) (Scheme 9),<sup>3c</sup> we had extrapolated that the same was true for the betaine generated from benzaldehyde (**1m**) and *p*-cyano-substituted sulfonium ylide **7b**.<sup>2</sup>

**Scheme 9.** Aggarwal's Mechanism Accounting for the High *trans* Selectivity in the Epoxidation Reaction of Benzaldehyde with Semistabilized Sulfur Ylide **7a**

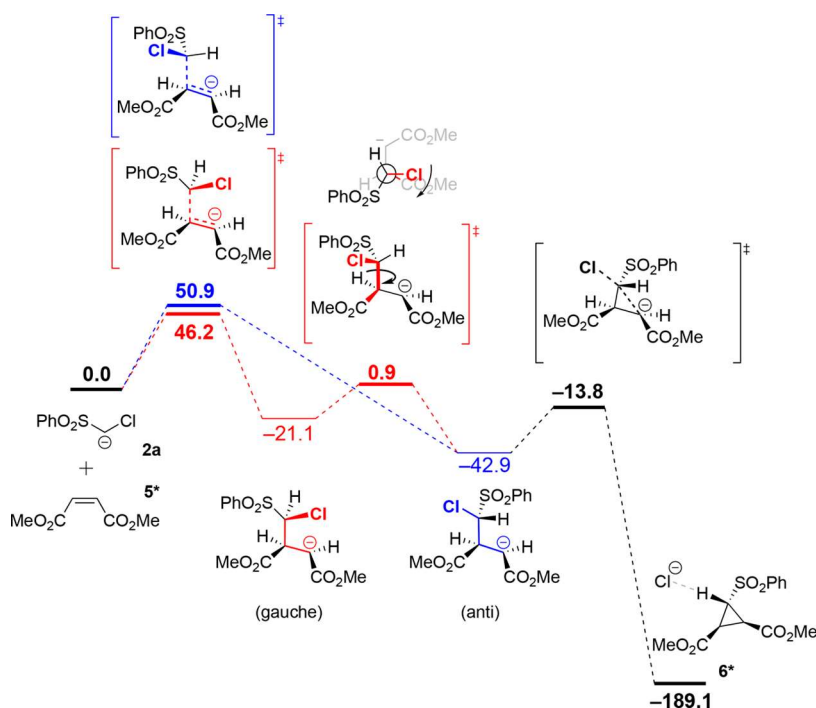
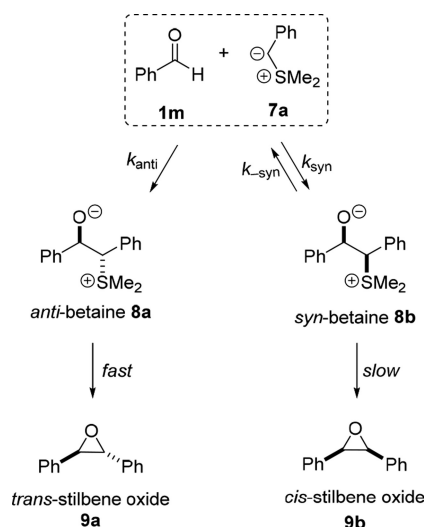
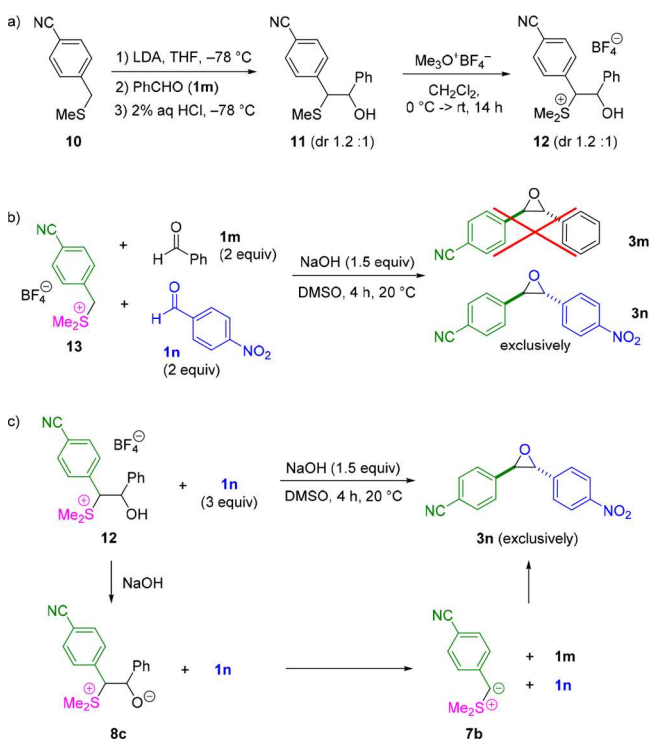


**Figure 7.** Gibbs energy surface (25 °C) for the reaction of **5\*** with **2a** [at the PCM(DMSO,UA0)/B2PLYP-D3/def2TZVPP//PCM(DMSO,UA0)/B3LYP-D3/6-31+G(d,p) level, kJ mol<sup>-1</sup>]. Dimethyl maleate (**5\***) is used as a model substrate for diethyl maleate (**5**).

This conclusion was obviously incorrect as shown by the following experiments. Treatment of the benzyl thioether **10** with LDA and benzaldehyde (**1m**) yielded the  $\beta$ -thio-substituted alcohol **11**, which was converted into the sulfonium tetrafluoroborate **12** by treatment with trimethyloxonium tetrafluoroborate (Scheme 10a). As shown in Scheme 10b,

### Scheme 10. Synthesis of Sulfonium Tetrafluoroborate **12** and Crossover Experiment To Elucidate the Rate-Determining Step in the Epoxidation of Benzaldehyde with the Sulfonium Ylide **7b**



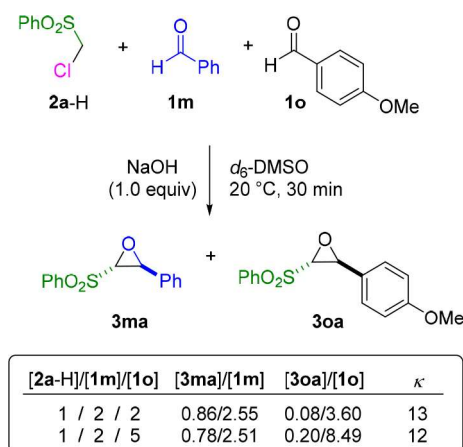
the sulfonium ylide generated by treatment of the sulfonium ion **13** with NaOH in the presence of *p*-nitrobenzaldehyde (**1n**) and benzaldehyde (**1m**) reacts exclusively with the former to yield the epoxide **3n**. As expected, *p*-nitrobenzaldehyde (**1n**) is much more reactive than the parent benzaldehyde (**1m**).

The crossover experiment in Scheme 10c shows the exclusive formation of the epoxide **3n** when **12** is treated with base in the presence of *p*-nitrobenzaldehyde (**1n**). This observation implies that the betaine **8c**, which is formed by deprotonation of **12**, does not cyclize, but rather undergoes retroaddition with regeneration of benzaldehyde (**1m**) and the sulfonium ylide **7b**, which is quantitatively intercepted by *p*-nitrobenzaldehyde (**1n**). The rate-determining step for the reaction of the sulfonium ylide **7b** with benzaldehyde (**1m**) thus is the cyclization and not the nucleophilic attack of the ylide at the carbonyl group, as assumed for the derivation of the electrophilic reactivity of benzaldehyde (**1m**) in ref 2. The electrophilicity parameters of aldehydes reported in ref 2 thus do not refer to the initial attack of nucleophiles at the carbonyl group but describe the gross rate constants for the reactions of carbonyl groups with the sulfonium ylide **7b**.

How can the rate of the initial nucleophilic attack at aldehydes be determined? Are the chloro-substituted carbanions **2a,b** suitable reference nucleophiles, because the corresponding intermediates cyclize with lower barriers than

the intermediates formed from sulfur ylides? In line with the expected higher electrophilic reactivity of benzaldehyde (**1m**), its reactions with the carbanions **2a,b** were found to be too fast for direct measurements with our stopped-flow techniques. We succeeded, however, to measure the rate of the reaction of **2b** with the less electrophilic *p*-methoxybenzaldehyde (**1o**) in the same way as described above for the corresponding reactions with ketones and obtained the second-order rate constant  $k_2^{\text{exptl}} = 2.69 \times 10^4\text{ M}^{-1}\text{ s}^{-1}$ , which will be used in Table 3. Subsequently, the relative reactivities of benzaldehyde (**1m**) and *p*-methoxybenzaldehyde (**1o**) toward **2a** were determined by the competition experiment illustrated in Scheme 11.<sup>27</sup>

### Scheme 11. Competition Experiments for Determining the Relative Reactivities of Benzaldehyde (**1m**) and *p*-Methoxybenzaldehyde (**1o**) toward **2a**



From the composition of the reaction mixtures given in Scheme 11, we derived the competition constant  $\kappa$  using eq 10,<sup>28</sup> which is applicable when the competing reagents are not used in high excess and the ratio of their concentrations changes during the reaction.

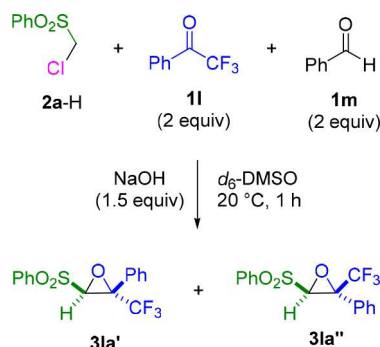
$$\kappa = \frac{k_2^{\text{exptl}}(\mathbf{1m})}{k_2^{\text{exptl}}(\mathbf{1o})} = \frac{\log\left(\frac{[\mathbf{1m}]_0}{[\mathbf{1m}]_t}\right)}{\log\left(\frac{[\mathbf{1o}]_0}{[\mathbf{1o}]_t}\right)} = \frac{\log\left(1 + \frac{[\mathbf{3ma}]_t}{[\mathbf{1m}]_t}\right)}{\log\left(1 + \frac{[\mathbf{3oa}]_t}{[\mathbf{1o}]_t}\right)} \quad (10)$$

From the directly measured rate constant for the reaction of **2b** with **1o** and the competition constant  $\kappa$  (Scheme 11), one can calculate the rate constant  $k_2^{\text{exptl}}$  for the reaction of **2b** with benzaldehyde (**1m**) according to eq 11.

$$k_2^{\text{exptl}}(\mathbf{1m}) = \kappa k_2^{\text{exptl}}(\mathbf{1o}) \quad (11)$$

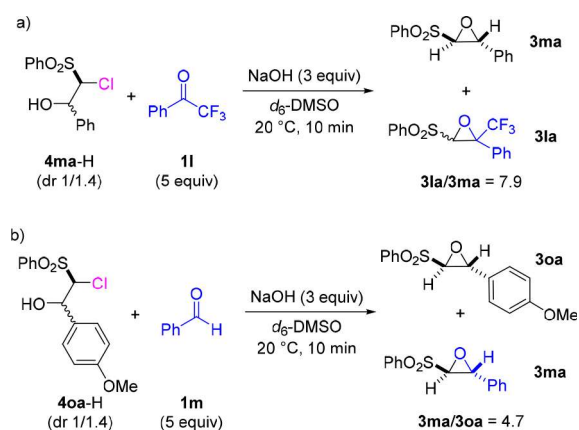
As described in Scheme 3 and eqs 2–7, the rate constants  $k_2^{\text{exptl}}$  thus obtained refer to the rates of the overall reactions. To derive the rate of attack of the anions **2** at the carbonyl groups of the aldehydes **1m** and **1o** ( $k_{\text{CC}}$ ), we must know the degree of reversibility of the initial addition step, which again was determined by crossover experiments. For their design, it was necessary to identify trapping agents which can quantitatively intercept the carbanions **2** generated by reverse addition of the halohydrin anions. As shown in Scheme 12, the epoxides **3la'** and **3la''** are formed exclusively when a 1/1 mixture of benzaldehyde (**1m**) and trifluoroacetophenone (**11**) is treated with 0.5 equiv of **2a**, indicating that the fluorinated ketone **11** is much more electrophilic than benzaldehyde (**1m**).

### Scheme 12. Competition Experiment To Demonstrate the Much Higher Reactivity of Ketone **11** Compared to Benzaldehyde (**1m**)



In analogy to the procedure described in Scheme 4, the chlorohydrins **4ma-H** and **4oa-H** (Scheme 13) were synthe-

### Scheme 13. Crossover Reactions of Aldehydes **1m** and **1o**



sized in THF at  $-78$  °C by the reaction of **2a-Li** with the aldehydes **1m** and **1o**, respectively, and subsequent acidification. As illustrated in Scheme 13, treatment of a 1/5 mixture of **4ma-H** and **11** gave the crossover product **31a** in addition to **3ma**, the cyclization product of **4ma**, in a ratio of 7.9/1. Since **11** is much more electrophilic than **1m** (Scheme 12), we can conclude that **3ma** is exclusively formed by direct cyclization of the deprotonated chlorohydrin **4ma**, whereas the carbanion **2a**, which is formed by reversal of **4ma**, is quantitatively converted into **31a**. The ratio  $[31a]/[3ma] = 7.9$  (Scheme 13a) thus reflects the ratio  $k_{-CC}/k_{rc}$  given in Table 3.

Since the competition experiment in Scheme 11 showed **1m** to be 12 times more reactive than **1o**, benzaldehyde (**1m**) could be used as a trapping reagent for the crossover experiment in Scheme 13b, and the ratio  $[3ma]/[3oa] = 4.7$  (Scheme 13b) again reflects the ratio  $k_{-CC}/k_{rc}$  given in Table 3.

**Table 3. Derivation of the Rate Constants  $k_{CC}$  for Nucleophilic Attack of **2b** at the Aldehydes **1o** and **1m** and the Resulting  $E$  Parameters**

aldehyde	nucleophile	$k_2^{\text{exptl}}$ ( $M^{-1} s^{-1}$ )	$k_{-CC}/k_{rc}^a$	$k_{CC}^b$ ( $M^{-1} s^{-1}$ )	approximate $E$
<b>1m</b>	<b>2b</b>	$3.36 \times 10^{5c}$	7.9	$3.0 \times 10^6$	-12.9
<b>1o</b>	<b>2b</b>	$2.69 \times 10^{4d}$	4.7	$1.5 \times 10^5$	-15.4

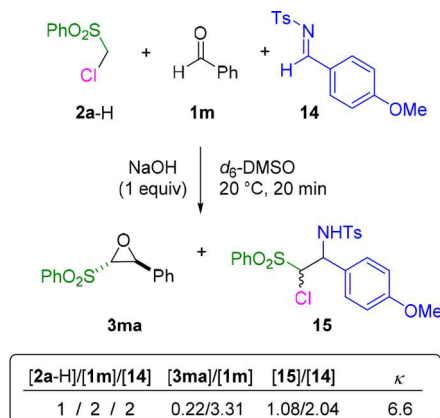
<sup>a</sup>From Scheme 13. <sup>b</sup>From eq 7. <sup>c</sup>From eq 11 using the averaged  $\kappa$  from Scheme 11,  $k_2^{\text{exptl}} = 12.5 \times (2.69 \times 10^4 M^{-1} s^{-1})$ . <sup>d</sup>Direct rate measurement.

Equation 7 was then used to calculate the rate constants  $k_{CC}$  for the nucleophilic attack of **2b** at the aldehydes **1o,m** from the gross rate constants  $k_2^{\text{exptl}}$  listed in Table 3 and the  $k_{-CC}/k_{rc}$  ratios from Scheme 13. Substitution into eq 1 with the  $N$  and  $s_N$  parameters of **2b** eventually yielded the electrophilicity parameters  $E$  of the aldehydes **1m** and **1o** in the last column of Table 3. It should be admitted, however, that there are two uncertainties in this derivation. First, the mixtures of diastereomers of the chlorohydrins **4ma-H** and **4oa-H**, which are used for the crossover experiments in Scheme 13, are formed by the reactions with the lithiated nucleophiles **2a-Li** in THF at  $-78$  °C and may differ somewhat from the diastereomeric ratios of the halohydrins generated under the conditions of the kinetic experiments. Second, we had to use the  $k_{-CC}/k_{rc}$  ratios for the adducts of **2a** for the calculation of  $k_{CC}$  in Table 3 because the epoxides obtained from **2b** were not stable. The plausibility of this assumption is based on the comparison of entries 3/4, 8/10, and 13/15 in Scheme 7, which indicated that the ratio of retroaddition vs ring closure ( $k_{-CC}/k_{rc}$ ) is almost independent of the substituents at the arylsulfonyl groups.

These uncertainties prompted us to examine the  $E$  value for benzaldehyde thus derived by an independent experiment. Substitution of the  $E$  values for **1m** and **14** and of the  $N$  and  $s_N$  parameters for **2a** into eq 1 gives  $k_{CC}$ , the rate constant for the initial nucleophilic attack of **2a** at these electrophiles. Since the attack of **2a** at **1m** (in contrast to the attack at **14**) is reversible,  $k_{CC}$  was corrected by the splitting ratio  $k_{-CC}/k_{rc}$  according to eq 7 to obtain the overall rate constant  $k_2^{\text{exptl}}$  for the formation of the epoxide **3ma**.

In the competition experiment described in Scheme 14, which compares the electrophilic reactivity of benzaldehyde

### Scheme 14. Competition Experiment To Determine the Relative Reactivities of Benzaldehyde (**1m**) and Imine **14**



(**1m**) with that of the *N*-tosyl imine **14**, we observed the ratios  $[3ma]/[1m] = 0.22/3.31$  and  $[15]/[14] = 1.08/2.04$  from which the reactivity ratio  $\kappa = k(14)/k(1m) = 6.6$  was derived by

**Table 4. Comparison of the Relative Reactivities of Benzaldehyde (1m) and Imine 14 toward 2a Derived from Rate Measurements and Competition Studies**

electrophile	$E$	$k_{\text{CC}}^{\text{a}}$ ( $\text{M}^{-1} \text{s}^{-1}$ )	$k_2^{\text{expl}}$ ( $\text{M}^{-1} \text{s}^{-1}$ )	$k_{\text{rel}}(\text{rates})$	$k_{\text{rel}}(\text{competition})$
<b>1m</b>	-12.9	$2.85 \times 10^6$	$3.20 \times 10^{5b}$	1	1
<b>14</b>	-13.05 <sup>c</sup>	$2.47 \times 10^6$	$2.47 \times 10^6$	7.7	6.6 <sup>d</sup>

<sup>a</sup>From eq 1 with  $E$  from this table and  $N = 28.27$  and  $s_N = 0.42$  for **2a**. <sup>b</sup>Calculated with eq 7 using  $k_{\text{-CC}}/k_{\text{rc}} = 7.9$  from Table 3. <sup>c</sup>Reference 2. <sup>d</sup>From Scheme 14; for a competition experiment with  $[\mathbf{2a-H}]/[\mathbf{1m}]/[\mathbf{14}] = 1/5/2$ , a  $\kappa = 6.65$  was obtained (see the Supporting Information).

**Table 5. Quantum Chemically Calculated Frontier Orbital Energies (hartrees), Global ( $\omega$ ) and Local ( $\omega_C$ ) Parr Electrophilicity Indices (eV), and Methyl Anion Affinities (MAAs;  $\text{kJ mol}^{-1}$ ) of Ketones and Aldehydes**

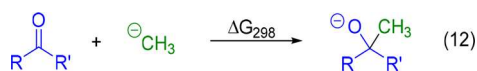
electrophile	$E^{\text{a}}$	$\epsilon_{\text{HOMO}}^{\text{b}}$	$\epsilon_{\text{LUMO}}^{\text{b}}$	global $\omega^{\text{b}}$	local $\omega_C^{\text{b}}$	$\Delta G_{\text{gas}}(-\text{MAA})^{\text{c}}$	$\Delta G_{\text{sol-sp}}(-\text{MAA})^{\text{d}}$
<b>1a</b>	-17.5	-0.24245	-0.02117	1.07	0.16	-131.6	-8.0
<b>1b</b>	-21.0	-0.23597	-0.01449	0.96	0.15	-114.2	14.6
<b>1c</b>	-19.9	-0.23443	-0.01201	0.93	0.15	-126.7	11.7
<b>1d</b>	-22.1	-0.23483	-0.01104	0.92	0.14	-116.3	26.8
<b>1e</b>	-18.4	-0.22444	-0.01456	0.93	0.15	-136.2	2.9
<b>1f</b>	-17.9	-0.24378	-0.02071	1.07	0.18	-147.3	-1.4
<b>1g</b>	-16.9	-0.23250	-0.02310	1.06	0.19	-158.3	-4.1
<b>1h</b>	-18.2	-0.23481	-0.01233	0.93	0.15	-138.5	5.3
<b>1i</b>	-22.3	-0.24272	-0.00948	0.93	0.15	-114.3	16.4
<b>1j</b>	-15.6	-0.22563	-0.02762	1.10	0.14	-144.4	-5.9
<b>1m</b>	(-12.9) <sup>e</sup>	-0.25521	-0.06342	1.80	0.22	-155.2	-27.8
<b>1o</b>	(-15.4) <sup>e</sup>	-0.23442	-0.05149	1.52	0.18	-143.7	-13.2

<sup>a</sup>Empirical electrophilicity parameters from Tables 2 and 3, as defined in eq 1. <sup>b</sup>Calculated at the B3LYP/6-31G(d,p) level in the gas phase. <sup>c</sup>Calculated at the B3LYP/6-311+G(3df,2pd)<sup>32</sup>//B3LYP/6-31G(d,p) level in the gas phase. <sup>d</sup>Based on methyl anion affinities ( $\Delta G_{\text{gas}}$ ), which were corrected for solvent effects by adding single-point solvation energies calculated at B3LYP/6-31G(d,p) using the solvation model based on density (SMD)<sup>33</sup> (solvent = DMSO) on gas-phase optimized geometries at the same level. <sup>e</sup>Approximate electrophilicities  $E$  of aldehydes (see text and Table 3).

eq 10 as summarized in Table 4. The fair agreement between the relative reactivities of **1m** and **14** and the rate constants calculated by eq 1 confirms the electrophilicity parameter of benzaldehyde (**1m**) derived above.

**Correlation Analysis.** To elucidate the origin of the corresponding electrophilic reactivities, we have determined various properties of the investigated carbonyl compounds by quantum chemical calculations (Table 5). As specified in Table 5 and Table S25 (Supporting Information), the computational methods used in these calculations differ from those employed in the reaction path calculations (see above) to make them strictly comparable to our earlier work on nucleophilic additions to Michael acceptors and carbenium ions.<sup>29</sup>

Methyl anion affinities (MAAs) have been calculated as the negative of the reaction Gibbs energies for the addition of methyl anion to ketones and aldehydes (eq 12). In addition, we



calculated Parr electrophilicity indices  $\omega$  (eq 13) for 12 carbonyl compounds<sup>30</sup> from the chemical hardness  $\eta$  (eq 14) and the electronic chemical potential  $\mu$  (eq 15). The values of  $\eta$  and  $\mu$  have been calculated from the energies of the lowest unoccupied molecular orbital ( $\epsilon_{\text{LUMO}}$ ) and the highest occupied molecular orbital ( $\epsilon_{\text{HOMO}}$ ), which were derived at the gas-phase B3LYP/6-31G(d,p) level. As in previous studies, the Parr electrophilicity indices are expressed in electronvolts (eV).

$$\omega = \mu^2/2\eta \quad (13)$$

$$\eta = \epsilon_{\text{LUMO}} - \epsilon_{\text{HOMO}} \quad (14)$$

$$\mu = 1/2(\epsilon_{\text{LUMO}} + \epsilon_{\text{HOMO}}) \quad (15)$$

$$\omega_C = \omega f_k^+ \quad (16)$$

The local electrophilicity indices  $\omega_C$  at the carbonyl carbon were calculated as the product of Parr's electrophilicity index  $\omega$  and the nucleophilic Fukui function ( $f_k^+$ ) according to eq 16. The Fukui function for nucleophilic attack is defined as the change of the partial charge  $q$  at a certain atom  $k$  by adding an electron to the corresponding compound; that is,  $f_k^+ = q(k, N+1) - q(k, N)$  with  $N =$  total number of electrons.<sup>31</sup>

Previously, good correlations between the electrophilicities of benzhydrylium ions and their LUMO energies were reported by Liu<sup>34a</sup> and Yu.<sup>34b</sup> Figure 8 shows a moderate correlation between the electrophilicity parameters  $E$  of ketones and their LUMO energies in the gas phase. This correlation improves slightly when the correlation with LUMO energies in DMSO solution is considered (as depicted in Figure S29B, Supporting Information). Though the correlation between the electrophilicity parameters  $E$  and LUMO energies of Michael acceptors has been reported to be very poor,<sup>29a</sup> Figure 8 shows that ketones are generally more electrophilic than Michael acceptors of equal LUMO energies.

Whereas Figure 9 shows a moderate correlation between electrophilicities  $E$  and Parr's global electrophilicity index  $\omega$ , a plot of  $E$  vs the local electrophilicity index  $\omega_C$  (Figure S33A, Supporting Information) has a correlation coefficient of  $R^2 = 0.30$  (!); i.e.,  $\omega_C$  is inadequate to predict electrophilic reactivities of ketones.<sup>35</sup>

As in our previous investigation of the electrophilic reactivities of Michael acceptors,<sup>29a</sup> the electrophilicities  $E$  of the ketones **1a–1j** correlate fairly with the calculated gas-phase methyl anion affinities ( $R^2 = 0.77$ ; Figure S17B, Supporting

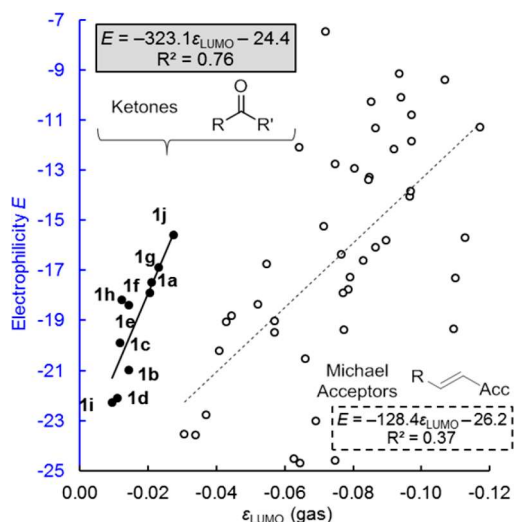


**Figure 8.** Correlation of the electrophilicities ( $E$ ) of ketones with their gas-phase lowest unoccupied molecular orbital energies ( $\epsilon_{\text{LUMO}}$ ) calculated at the B3LYP/6-31G(d,p) level of theory compared with the corresponding correlation for Michael acceptors.

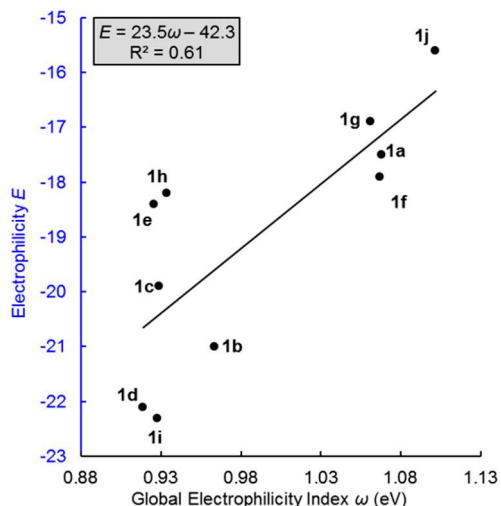


**Figure 9.** Correlation between electrophilicities ( $E$ ) of ketones **1a–1j** and Parr's global electrophilicity index ( $\omega$ ) calculated at the B3LYP/6-31G(d,p) level of theory.

Information),<sup>21,23,32,36</sup> and this correlation improves further when solvation is included in the calculated methyl anion affinities (Figure 10). Obviously, the solvation energy of the methyl anion is overestimated by this model, since negative MAAs were calculated for several additions. Though the data for the benzaldehydes **1m** and **1o** were not used for the correlation because of the uncertainty of the experimental  $E$  parameters, they also are on this best fit line, thus justifying the approximations made for the derivation of their  $E$  parameters.

When the plots of  $E$  vs MAA for carbonyl compounds and Michael acceptors are drawn in the same graph (Figure 11), one can clearly see two correlation lines, which differ in two aspects. First, the slope for the ketones is significantly larger than that for Michael acceptors. As pointed out previously, the slope of the Michael acceptor correlation implies that in reactions with a nucleophile of  $s_{\text{N}} = 0.7$  (see eq 1) about 43% of the differences of the Gibbs reaction energies are reflected in the Gibbs activation energies.<sup>29a</sup> A significantly higher

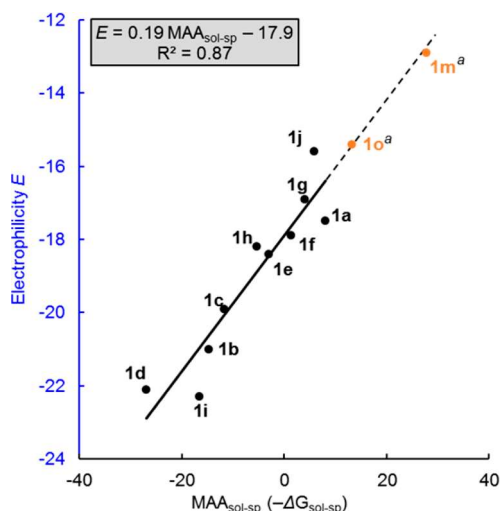


**Figure 10.** Correlation between electrophilicities ( $E$ ) of ketones and their  $\text{MAA}_{\text{sol-sp}}$  values ( $-\Delta G_{\text{sol-sp}}$ ,  $\text{kJ mol}^{-1}$ ) calculated at the SMD(DMSO)/B3LYP/6-311++G(3df,2pd)//B3LYP/6-31G(d,p) level of theory. A superscript  $a$  indicates the data point was not used for the construction of the correlation line.

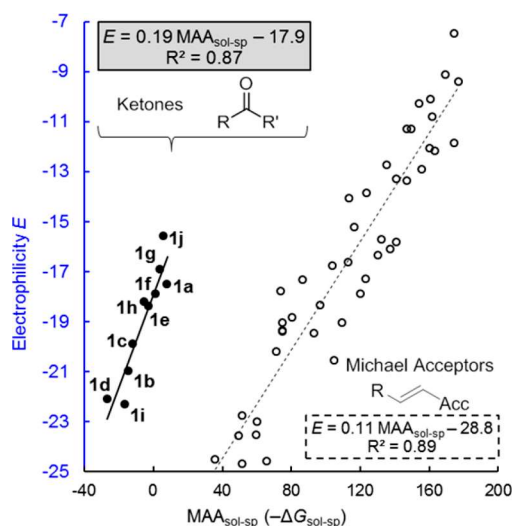


**Figure 11.** Correlation between the empirical electrophilicities ( $E$ , eq 1) and MAA ( $-\Delta G_{\text{sol-sp}}$ ,  $\text{kJ mol}^{-1}$ ) values calculated at the SMD(DMSO)/B3LYP/6-311++G(3df,2pd)//B3LYP/6-31G(d,p) level of theory for ketones and Michael acceptors.

percentage (75%) of the Gibbs reaction energies is mirrored by the activation energies of the additions of nucleophiles with the typical value  $s_{\text{N}} = 0.7$  to carbonyl compounds.<sup>37</sup> Second, the different positions of the two correlation lines imply that additions to carbonyl compounds are significantly faster than Michael additions of equal thermodynamic driving force ( $\Delta_r G^\circ$ ). In Marcus terminology,<sup>38a–c</sup> this means that Michael additions proceed with significantly higher reorganization energies than nucleophilic additions to carbonyl groups, which can be explained by the much greater movements of electrons and structural changes occurring in Michael additions (Scheme 15).<sup>38f</sup>

**Structure–Reactivity Relationships.** As shown in Table 6, the reactivity order cyclobutanone (**1a**) > cyclohexanone (**1c**) > cyclopentanone (**1b**) > cycloheptanone (**1d**), which we found for reactions with carbanions **2a,b**, had previously been

**Scheme 15. Less Movement of Electrons and Nuclei Required in Nucleophilic Additions to Carbonyl Groups Than to Michael Acceptors**

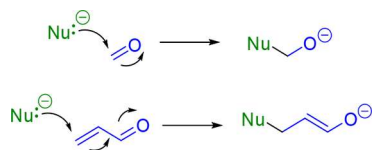


**Table 6. Comparison of the Reactivities of the Cycloalkanones 1a–d toward Different Nucleophiles**

	$k_{CC}(2b)^a$ ( $M^{-1} s^{-1}$ )	$k_2(NaBH_4)^b$ ( $M^{-1} s^{-1}$ )	$k_{rel}(2b)^a$	$k_{rel}(NaBH_4)^b$	$k_{rel}(Nu)^c$
1a	$1.33 \times 10^4$	$2.66 \times 10^{-2}$	27	1.6	1.2
1b	$2.14 \times 10^2$	$7.01 \times 10^{-4}$	0.44	0.044	0.066
1c	$4.85 \times 10^2$	$1.61 \times 10^{-2}$	1	1	1
1d	$3.88 \times 10^{1d}$	$1.02 \times 10^{-4}$	0.080	0.0063	0.11

<sup>a</sup>In DMSO, 20 °C, from Table 2. <sup>b</sup>In *i*PrOH, 0 °C, from ref 4c. <sup>c</sup>Averaged value derived from reactions with  $NH_2OH$ ,  $SO_3^{2-}$ ,  $CN^-$ ,  $BH_4^-$ , and  $HOC_2H_4S^-$  in aqueous solution;  $k_{rel}(Nu) = 10^B$  calculated from Geneste's *B* values defined by the relation  $\log k = A \log k_0 + B$  in ref 5f. <sup>d</sup>From the rate constant with 2a (Table 2) divided by 9.8, the reactivity ratio 2a/2b toward cyclohexanone (1c).

observed in reactions with other nucleophiles, though the relative reactivities of the different cycloalkanones depend on the reaction partner and conditions.<sup>39</sup> The uniformly higher electrophilic reactivity of cyclobutanone (1a) can partially be explained by the higher release of ring strain during conversion of the  $sp^2$  carbon in the four-membered ring into an  $sp^3$  carbon. Table 5 shows, however, that the gas-phase methyl anion affinity of 1a is only 5  $\text{kJ mol}^{-1}$  higher than that of cyclohexanone (1c), indicating that release of strain can only account for part of the reactivity difference of 1a and 1c. Since the MAA of 1a is almost 20  $\text{kJ mol}^{-1}$  higher than that of 1c in DMSO solution, we must conclude that differences of solvation are the major reason for the higher reactivity of cyclobutanone (1a) toward 2b in solution. Let us analyze the origin of the solvation effect in the following comparison of cyclohexanone with cyclopentanone.

H. C. Brown rationalized the 23 times faster reaction of  $NaBH_4$  with cyclohexanone compared to cyclopentanone by a change of torsional strain: As the hybridization of the carbonyl carbon changes from  $sp^2$  to  $sp^3$ , the torsional strain increases in the five-membered ring (eclipsed bonds), but decreases in the six-membered ring because the equatorial hydrogens are nearly eclipsed with carbonyl oxygen in cyclohexanone and attain staggered arrangements in the chair conformation of cyclohexanol.<sup>40</sup> Since the opposite rehybridization takes place in the rate-determining step of  $S_N1$  reactions of cycloalkyl halides, differences in torsional strain were analogously used to explain the much larger solvolysis rates of cyclopentyl halides compared to cyclohexyl halides.<sup>40</sup> We had already doubted that the change from  $C_{sp^3}$  to  $C_{sp^2}$  is the major contribution to this difference of the  $S_N1$  reactivities because methylenecyclopentane was found to react 50 times faster with benzhydrylium ions than methylenecyclohexane though the rate-determining step does not involve rehybridization of a ring carbon.<sup>41</sup>

The 12.5  $\text{kJ mol}^{-1}$  higher gas-phase methyl anion affinity of cyclohexanone (1c) compared to cyclopentanone (1b) in Table 5 supports the torsional strain argument. However, the difference between the MAAs of 1c and 1b shrinks to 2.9  $\text{kJ}$

$\text{mol}^{-1}$  in DMSO solution. As discussed in detail in Figures S24 and S25 (Supporting Information), this change is due to the fact that the cyclohexanolate conformer with oxygen in the axial position, which is most stable in the gas phase, is less efficiently solvated and becomes even less stable in DMSO solution than the conformer with equatorial oxygen. Thus, the overall poorer solvation of the cyclohexanolate ion accounts for the fact that the MAA of cyclohexanone, which is much higher than that of cyclopentanone in the gas phase, is only slightly higher in solution. The poor solvation of the cyclohexanolate anion with oxygen in the axial position analogously accounts for the finding (Table 5) that the MAAs of cyclobutanone and cyclohexanone differ only slightly in the gas phase (5  $\text{kJ mol}^{-1}$ ) but strongly in solution (20  $\text{kJ mol}^{-1}$ ).

As shown in Table 7, the introduction of electronegative elements in the 4-position of cyclohexanone leads to an

**Table 7. Influence of Heteroatoms in the  $\gamma$ -Position on the Reactivities of Cyclic Ketones**

ketone 1	$k_{rel}(2b)^a$	$k_{rel}(BH_4)^b$
1c (X = CH <sub>2</sub> )	1.0	1.0
1e (X = NMe)	5.0	9.9
1f (X = O)	18	
1g (X = S)	59	11.2

<sup>a</sup> $k_{CC}$  in DMSO from Table 2. <sup>b</sup>In water/dioxane (1/1) at 25 °C (from ref 5a).

increase of the electrophilic reactivity toward carbanion 2b as well as toward  $BH_4^-$ . Possibly different solvation accounts for the fact that the relative reactivities in the two reaction series correlate only moderately. From the fact that the data for the four six-membered ring ketones 1c, 1e, 1f, and 1g are perfectly on the correlation line of Figure 10, one can conclude that the relative reactivities of these ketones are predominantly controlled by the thermodynamics of the CC-bond-forming step. Though oxygen is more electronegative than sulfur, tetrahydrothiopyranone (1g) is more electrophilic than tetrahydropyranone (1f), which may be due to through-bond interaction.<sup>42</sup>

When the  $\beta$ -carbon of ketones is replaced by sulfur (1i  $\rightarrow$  1j) or oxygen (1i  $\rightarrow$  1k), the heteroatom effect is larger (by a factor of 400 for S and not measurable for O) than the  $\gamma$ -heteroatom effect shown in Table 7 and follows the electronegativity order  $O \gg S$ .

## CONCLUSIONS

The arylsulfonyl-substituted chloromethyl anions 2a,b are suitable reference nucleophiles for the determination of the electrophilic reactivities of ordinary aliphatic ketones. The rate constants  $k_{CC}$  for the initial nucleophilic attack are accessible by combination of the directly measured gross rate constants ( $k_2^{exptl}$ ) for the formation of the epoxides 3 from the reactants 1 and 2 with the degree of reversibility of the initial step ( $k_{-CC}/k_{CC}$ ). This ratio was derived from crossover experiments with the independently synthesized intermediates 4. Two reaction pathways have been identified for the reactions of the carbanions 2 with the ketones 1: one which yields the intermediate halohydrin anions 4 with the C–Cl and C–O<sup>−</sup> bonds in *anti*-arrangements that can undergo direct cyclization to the epoxides 3 and a second one which gives the halohydrin

anions **4** with C–Cl and C–O<sup>−</sup> in *gauche* orientation. The latter undergo retroaddition with regeneration of the reactants **1** and **2**, because the barrier for reversal is lower than the barrier for rotation to give the *anti* conformer suitable for cyclization. The cyclopropanation of diethyl maleate with **2a** proceeds via an analogous mechanism, with the difference that the initial CC-bond-forming step, which also gives different conformers, is irreversible.

The electrophilicity parameters  $E$  of the ketones **1** were calculated by eq 1 from the rate constants  $k_{CC}$  and the previously reported reactivity parameters  $N$  and  $s_N$  for the carbanions **2**. The  $E$  parameters, which refer to the nucleophilic attack of **2** at the carbonyl groups, correlate moderately with the gas-phase LUMO energies of the ketones ( $R^2 = 0.76$ , Figure 8), poorly with Parr's global electrophilicity index  $\omega$  ( $R^2 = 0.61$ , Figure 9), very poorly with Parr's local electrophilicity index  $\omega_C$  ( $R^2 = 0.30$ , Figure S33A in the Supporting Information), and best with the methyl anion affinities calculated for DMSO solution ( $R^2 = 0.87$ , Figure 10). We thus do not consider Parr's electrophilicity indices suitable measures for electrophilic reactivities, though electrophilic reactivities within a series of structurally closely related Michael acceptors correlate well with Parr's indices.<sup>30</sup>

Comparison of the electrophilicities  $E$  of ketones with those of Michael acceptors shows that ketones are significantly more electrophilic than Michael acceptors of equal methyl anion affinity ( $\hat{=}$  Lewis acidity), indicating that nucleophilic additions to ketones proceed over much lower Marcus intrinsic barriers due to less electronic and geometrical reorganization than in Michael additions.

Crossover experiments showed that the initial attack of the *p*-cyanophenyl sulfonium ylide at aldehydes is reversible (in contrast to previous extrapolations), with the consequence that the previously reported  $E$  parameters for aldehydes correspond to the gross rate constants for these epoxidations and do not reflect the rates of initial attack of nucleophiles at the carbonyl group. By using the carbanions **2** as reference nucleophiles, estimates for the rate of nucleophilic attack at aldehydes have been obtained, showing that the electrophilicity parameter  $E$  of benzaldehyde (**1m**) is approximately 7 units greater than that of cyclohexanone (**1c**).

As illustrated in Figure 12, the electrophilicities of saturated aliphatic ketones are comparable to the C=C bond reactivities of  $\beta$ -phenyl-substituted  $\alpha,\beta$ -unsaturated ketones and much lower than the C=C bond reactivities of terminally unsaturated vinyl ketones. Benzaldehyde, on the other hand, is more electrophilic than the  $\alpha,\beta$ -unsaturated carbonyl compounds depicted in Figure 12, in line with the observation that  $\alpha,\beta$ -unsaturated aldehydes usually undergo 1,2-additions under kinetically controlled conditions. In earlier applications of eq 1, we have shown that in reactions of nucleophiles with carbenium ions and a variety of Michael acceptors the electrophilicity parameters  $E$  can be treated as solvent-independent quantities, with the consequence that all solvent effects are shifted into the nucleophile-specific parameters  $N$  and  $s_N$ . Because of the high basicity of alkoxide ions in aprotic media, this approximation probably does not hold for the electrophilicities of carbonyl compounds, and systematic investigations of solvent effects are now needed to arrive at reliable predictions of carbonyl reactivities in different solvents.

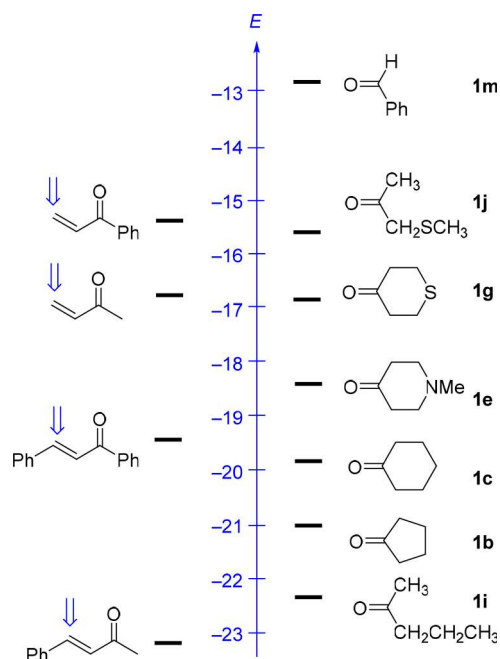


Figure 12. Comparison of the empirical electrophilicities  $E$  of carbonyl groups and Michael acceptors in DMSO.

## ■ ASSOCIATED CONTENT

### Supporting Information

The Supporting Information is available free of charge on the ACS Publications website at DOI: 10.1021/jacs.8b01657.

Details of the product studies, kinetic experiments, NMR spectra of all characterized compounds, single-crystal X-ray structure of **4ca-H**, competition experiments, crossover experiments, and computational analysis (PDF)  
Coordinates of optimized structures (ZIP)  
Crystallographic data for **4ca-H** (CIF)

## ■ AUTHOR INFORMATION

### Corresponding Authors

\*ofial@lmu.de  
\*zipse@cup.uni-muenchen.de  
\*herbert.mayr@cup.uni-muenchen.de

### ORCID

Armin R. Ofial: 0000-0002-9600-2793  
Hendrik Zipse: 0000-0002-0534-3585  
Herbert Mayr: 0000-0003-0768-5199

### Notes

The authors declare no competing financial interest.

## ■ ACKNOWLEDGMENTS

This paper is dedicated to Professor Ernst-Ulrich Würthwein on the occasion of his 70th birthday. We thank the Deutsche Forschungsgemeinschaft (SFB 749, Projects B1 and C6) and the China Scholarship Council (fellowship to Z.L.) for financial support. We are grateful for computing time on the Linux-Cluster at the Leibniz Supercomputing Centre ([www.lrz.de](http://www.lrz.de)) and thank Dr. Peter A. Byrne (University College Cork, Ireland) for helpful discussions.

## REFERENCES

- (1) (a) Mayr, H.; Bug, T.; Gotta, M. F.; Hering, N.; Irrgang, B.; Janker, B.; Kempf, B.; Loos, R.; Ofial, A. R.; Remennikov, G.; Schimmel, H. *J. Am. Chem. Soc.* **2001**, *123*, 9500–9512. (b) Lucius, R.; Loos, R.; Mayr, H. *Angew. Chem., Int. Ed.* **2002**, *41*, 91–95. (c) Mayr, H.; Kempf, B.; Ofial, A. R. *Acc. Chem. Res.* **2003**, *36*, 66–77.
- (2) Appel, R.; Mayr, H. *J. Am. Chem. Soc.* **2011**, *133*, 8240–8251.
- (3) (a) Zimmerman, H. E.; Ahramjian, L. *J. Am. Chem. Soc.* **1960**, *82*, 5459–5466. (b) Vogt, P. F.; Tavares, D. F. *Can. J. Chem.* **1969**, *47*, 2875–2881. (c) Aggarwal, V. K.; Calamai, S.; Ford, J. G. *J. Chem. Soc., Perkin Trans. 1* **1997**, 593–599.
- (4) (a) Brown, H. C.; Mead, E. J.; Rao, B. C. S. *J. Am. Chem. Soc.* **1955**, *77*, 6209–6213. (b) Brown, H. C.; Wheeler, O. H.; Ichikawa, K. *Tetrahedron* **1957**, *1*, 214–220. (c) Brown, H. C.; Ichikawa, K. *Tetrahedron* **1957**, *1*, 221–230. (d) Brown, H. C.; Ichikawa, K. *J. Am. Chem. Soc.* **1962**, *84*, 373–376. (e) Brown, H. C.; Muzzio, J. *J. Am. Chem. Soc.* **1966**, *88*, 2811–2822. (f) Brown, H. C.; Wang, K. K.; Chandrasekharan, J. *J. Am. Chem. Soc.* **1983**, *105*, 2340–2343.
- (5) (a) Geneste, P.; Durand, R.; Hugon, I.; Reminiac, C. *J. Org. Chem.* **1979**, *44*, 1971–1973. (b) Geneste, P.; Lamaty, G.; Moreau, C.; Roque, J. P. *Tetrahedron Lett.* **1970**, *11*, 5011–5014. (c) Geneste, P.; Lamaty, G.; Roque, J. P. *Tetrahedron* **1971**, *27*, 5539–5559. (d) Geneste, P.; Lamaty, G.; Roque, J. P. *Tetrahedron* **1971**, *27*, 5561–5578. (e) Fournier, L.; Lamaty, G.; Natat, A.; Roque, J. P. *Tetrahedron* **1975**, *31*, 1031–1034. (f) Finiels, A.; Geneste, P. *J. Org. Chem.* **1979**, *44*, 1577–1578.
- (6) (a) Zenz, L.; Mayr, H. *J. Org. Chem.* **2011**, *76*, 9370–9378. (b) Kaumanns, O.; Lucius, R.; Mayr, H. *Chem. - Eur. J.* **2008**, *14*, 9675–9682. (c) Lemek, T.; Mayr, H. *J. Org. Chem.* **2003**, *68*, 6880–6886. (d) For a comprehensive database of nucleophilicity parameters  $N$  and  $N_N$  as well as electrophilicity parameters  $E$ , see <http://www.cup.lmu.de/oc/mayr/DBintro.html>.
- (7) (a) Olmstead, W. N.; Margolin, Z.; Bordwell, F. G. *J. Org. Chem.* **1980**, *45*, 3295–3299. (b) Bordwell, F. G. *Acc. Chem. Res.* **1988**, *21*, 456–463.
- (8) (a) Arnett, E. M.; Maroldo, S. G.; Schilling, S. L.; Harrelson, J. A. *J. Am. Chem. Soc.* **1984**, *106*, 6759–6767. (b) For a comprehensive list of  $pK_a$  values, see <http://ibond.nankai.edu.cn/>.
- (9) (a) Darzens, G. *Compt. Rend.* **1904**, *139*, 1214–1217. (b) Darzens, G. *Compt. Rend.* **1905**, *141*, 766–768. (c) Darzens, G. *Compt. Rend.* **1906**, *142*, 214–215. (d) Darzens, G.; Lefébure, P. *Compt. Rend.* **1906**, *142*, 714–715.
- (10) (a) Newman, M. S.; Magerlein, B. *J. Org. React.* **1949**, *5*, 413–440. (b) Rosen, T. Darzens Glycidic Ester Condensation. In *Comprehensive Organic Synthesis*, 1st ed.; Trost, B. M., Fleming, I., Eds.; Pergamon Press: Oxford, U.K., 1991; Vol. 2, pp 409–439. (c) Aggarwal, V. K.; Crimmin, M.; Riches, S. Synthesis of Epoxide by Carbonyl Epoxidation. In *Science of Synthesis*; Forysth, C. J., Jacobsen, E. N., Eds.; Thieme: Stuttgart, Germany, 2008; Vol. 37, pp 321–406. (d) Reutrakul, V.; Pohmakotr, M. Chloromethyl Phenyl Sulfone. In *Encyclopedia of Reagents for Organic Synthesis*, 2nd ed.; Paquette, L. A., Crich, D., Fuchs, P. L., Molander, G. A., Eds.; Wiley: Chichester, U.K., 2009; Vol. 4, pp 2375–2378. (e) Bako, P.; Rapi, Z.; Keglevich, G. *Curr. Org. Synth.* **2014**, *11*, 361–376. For diastereoselective or asymmetric Darzens reactions, see: (f) Liu, Y.; Provencher, B. A.; Bartelson, K. J.; Deng, L. *Chem. Sci.* **2011**, *2*, 1301–1304. (g) Kuang, Y.; Lu, Y.; Tang, Y.; Liu, X.; Lin, L.; Feng, X. *Org. Lett.* **2014**, *16*, 4244–4247. (h) Li, B.; Li, C. *J. Org. Chem.* **2014**, *79*, 8271–8277. (i) Sakowicz, A.; Loska, R.; Mąkosza, M. *Synlett* **2016**, *27*, 2443–2446. (j) Chai, G.-L.; Han, J.-W.; Wong, H. N. C. *Synthesis* **2017**, *49*, 181–187. (k) Chai, G.-L.; Han, J.-W.; Wong, H. N. C. *J. Org. Chem.* **2017**, *82*, 12647–12654.
- (11) Ballester, M. *Chem. Rev.* **1955**, *55*, 283–300.
- (12) (a) Bachelor, F. W.; Bansal, R. K. *J. Org. Chem.* **1969**, *34*, 3600–3604. (b) Sipos, G.; Schöbel, G.; Sirokmán, F. *J. Chem. Soc., Perkin Trans. 2* **1975**, 805–808.
- (13) (a) Corey, E. J.; Chaykovsky, M. *J. Am. Chem. Soc.* **1965**, *87*, 1353–1363. (b) Johnson, A. W.; LaCount, R. B. *J. Am. Chem. Soc.* **1961**, *83*, 417–423.
- (14) (a) Aggarwal, V. K.; Winn, C. L. *Acc. Chem. Res.* **2004**, *37*, 611–620. (b) McGarrigle, E. M.; Myers, E. L.; Illa, O.; Shaw, M. A.; Riches, S. L.; Aggarwal, V. K. *Chem. Rev.* **2007**, *107*, 5841–5883.
- (15) (a) Appel, R.; Mayr, H. *Chem. - Eur. J.* **2010**, *16*, 8610–8614. (b) Appel, R.; Hartmann, N.; Mayr, H. *J. Am. Chem. Soc.* **2010**, *132*, 17894–17900.
- (16) Li, Z.; Chen, Q.; Mayer, P.; Mayr, H. *J. Org. Chem.* **2017**, *82*, 2011–2017.
- (17) Mayr, H.; Ofial, A. R. *Angew. Chem., Int. Ed.* **2006**, *45*, 1844–1854.
- (18) Schwesinger, R.; Schlemper, H.; Hasenfratz, C.; Willaredt, J.; Dambacher, T.; Breuer, T.; Ottaway, C.; Fletschinger, M.; Boele, J.; Fritz, H.; Putzas, D.; Rotter, H. W.; Bordwell, F. G.; Satish, A. V.; Ji, G. Z.; Peters, E. M.; Peters, K.; von Schnering, H. G.; Walz, L. *Liebigs Ann.* **1996**, 1055–1081.
- (19) (a) Durst, T.; Tin, K.-C.; De Reinach-Hirtzbach, F.; Decesare, J. M.; Ryan, M. D. *Can. J. Chem.* **1979**, *57*, 258–266. (b) Reutrakul, V.; Jarussophon, S.; Pohmakotr, M.; Chaiyasut, Y.; U-Thet, S.; Tuchinda, P. *Tetrahedron Lett.* **2002**, *43*, 2285–2288.
- (20) Arai, S.; Shioiri, T. *Tetrahedron* **2002**, *58*, 1407–1413.
- (21) Becke, A. D. *J. Chem. Phys.* **1993**, *98*, 5648–5652.
- (22) (a) Grimme, S. *J. Comput. Chem.* **2006**, *27*, 1787–1799. (b) Grimme, S.; Antony, J.; Ehrlich, S.; Krieg, H. *J. Chem. Phys.* **2010**, *132*, 154104. (c) Wagner, J. P.; Schreiner, P. R. *Angew. Chem., Int. Ed.* **2015**, *54*, 12274–12296.
- (23) (a) Ditchfield, R.; Hehre, W. J.; Pople, J. A. *J. Chem. Phys.* **1971**, *54*, 724–728. (b) Krishnan, R.; Binkley, J. S.; Seeger, R.; Pople, J. A. *J. Chem. Phys.* **1980**, *72*, 650–654.
- (24) (a) Cancès, E.; Mennucci, B.; Tomasi, J. *J. Chem. Phys.* **1997**, *107*, 3032–3041. (b) Tomasi, J.; Mennucci, B.; Cammi, R. *Chem. Rev.* **2005**, *105*, 2999–3094. (c) Mayer, R. J.; Tokuyasu, T.; Mayer, P.; Gomar, J.; Sabelle, S.; Mennucci, B.; Mayr, H.; Ofial, A. R. *Angew. Chem., Int. Ed.* **2017**, *56*, 13279–13282.
- (25) Grimme, S. *J. Chem. Phys.* **2006**, *124*, 034108.
- (26) (a) Weigend, F.; Ahlrichs, R. *Phys. Chem. Chem. Phys.* **2005**, *7*, 3297–3305. (b) Weigend, F. *Phys. Chem. Chem. Phys.* **2006**, *8*, 1057–1065.
- (27) The corresponding competition experiment with **2b** could not be performed because of the low stability of the resulting oxiranes.
- (28) Huisgen, R. *Angew. Chem., Int. Ed. Engl.* **1970**, *9*, 751–762.
- (29) (a) Allgäuer, D. S.; Jangra, H.; Asahara, H.; Li, Z.; Chen, Q.; Zipse, H.; Ofial, A. R.; Mayr, H. *J. Am. Chem. Soc.* **2017**, *139*, 13318–13329. (b) Mayr, H.; Ammer, J.; Baidya, M.; Maji, B.; Nigst, T. A.; Ofial, A. R.; Singer, T. *J. Am. Chem. Soc.* **2015**, *137*, 2580–2599.
- (30) Domingo, L. R.; Pérez, P.; Contreras, R. *Tetrahedron* **2004**, *60*, 6585–6591.
- (31) (a) Contreras, R. R.; Fuentealba, P.; Galván, M.; Pérez, P. *Chem. Phys. Lett.* **1999**, *304*, 405–413. (b) Yang, W.; Mortier, W. J. *J. Am. Chem. Soc.* **1986**, *108*, 5708–5711.
- (32) Clark, T.; Chandrasekhar, J.; Spitznagel, G. W.; Schleyer, P. v. R. *J. Comput. Chem.* **1983**, *4*, 294–301.
- (33) Marenich, A. V.; Cramer, C. J.; Truhlar, D. G. *J. Phys. Chem. B* **2009**, *113*, 6378–6396.
- (34) (a) Wang, C.; Fu, Y.; Guo, Q.-X.; Liu, L. *Chem. - Eur. J.* **2010**, *16*, 2586–2598. (b) Zhuo, L.-G.; Liao, W.; Yu, Z.-X. *Asian J. Org. Chem.* **2012**, *1*, 336–345.
- (35) (a) Aizman, A.; Contreras, R.; Pérez, P. *Tetrahedron* **2005**, *61*, 889–895. (b) Pérez, P.; Domingo, L. R.; Aizman, A.; Contreras, R. In *Theoretical Aspects of Chemical Reactivity*; Toro-Labbé, A., Ed.; Theoretical and Computational Chemistry, Vol. 19; Elsevier: Amsterdam, 2007; Chapter 9, pp 139–201. (c) Chamorro, E.; Duque-Noreña, M.; Pérez, P. *J. Mol. Struct.: THEOCHEM* **2009**, *896*, 73–79. (d) Chamorro, E.; Duque-Noreña, M.; Pérez, P. *J. Mol. Struct.: THEOCHEM* **2009**, *901*, 145–152.
- (36) Byrne, P. A.; Kobayashi, S.; Würthwein, E.-U.; Ammer, J.; Mayr, H. *J. Am. Chem. Soc.* **2017**, *139*, 1499–1511.
- (37)  $\Delta\Delta G^\ddagger = 2.303RT[\Delta(\log k)] = 2.303RT_{S_N} \Delta E$ .
- (38) (a) Marcus, R. A. *J. Chem. Phys.* **1956**, *24*, 966–978. (b) Marcus, R. A. *J. Phys. Chem.* **1968**, *72*, 891–899. (c) Albery, W. J. *Annu. Rev.*

*Phys. Chem.* **1980**, *31*, 227–263. (d) Murdoch, J. R.; Magnoli, D. E. *J. Am. Chem. Soc.* **1982**, *104*, 3792–3800. (e) Chen, M. Y.; Murdoch, J. R. *J. Am. Chem. Soc.* **1984**, *106*, 4735–4743. (f) Hine, J. *Adv. Phys. Org. Chem.* **1977**, *15*, 1–61.

(39) Carey, F. A., Sundberg, R. J. *Advanced Organic Chemistry Part A: Structure and Mechanisms*, 5th ed; Springer: New York, 2007; pp 632–637.

(40) Brown, H. C.; Borkowski, M. J. *Am. Chem. Soc.* **1952**, *74*, 1894–1902.

(41) Roth, M.; Schade, C.; Mayr, H. *J. Org. Chem.* **1994**, *59*, 169–172.

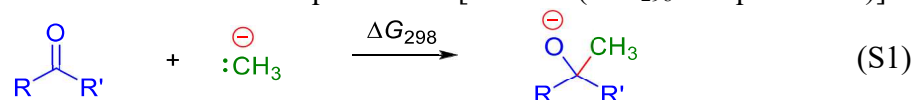
(42) Hoffmann, R. *Acc. Chem. Res.* **1971**, *4*, 1–9.

## 8.1 Supporting Information

### For: Kinetics and Mechanism of Oxirane-Formation by Darzens Condensation of Ketones: Quantification of the Electrophilicities of Ketones

#### 8.1.1 Methodology

Methyl anion affinities (MAA) in the gas phase have been calculated using the same methodology employed successfully in earlier studies<sup>1</sup> as the negative of the gas phase free energy at 298.15 K ( $\Delta G_{298}$ ) for the addition reaction shown in equation S1. [MAA =  $(-\Delta G_{298}$  of equation S1)].



Geometry optimizations have been performed with a combination of the B3LYP hybrid functional<sup>2</sup> and the 6-31G(d,p) basis set.<sup>3</sup> Thermochemical corrections to Gibbs energies (corr.  $\Delta G$ ) at 298.15 K have been calculated using the rigid rotor/harmonic oscillator model without any scaling. Gibbs energies ( $\Delta G_{298}$ ) at B3LYP/6-31G(d,p) level have been obtained through addition of  $\Delta E_{\text{tot}}$  and corr.  $\Delta G$ . Single point total electronic energies ( $\Delta E_{\text{tot}}$ ) have subsequently been calculated using a combination of the B3LYP hybrid functional and the larger 6-311++G(3df,2pd) basis set.<sup>3-4</sup> Final Gibbs energies ( $\Delta G_{298}$ ) have been obtained through a combination of  $\Delta E_{\text{tot}}$  with the thermochemical corrections to Gibbs energies (corr.  $\Delta G$ ) calculated at a lower level. In the following these will be designated as  $\Delta G_{\text{gas}}$  at [B3LYP/6-311++G(3df,2pd)//B3LYP/6-31G(d,p)]. Solvent effects on MAA values have first been estimated by adding single point solvation corrections ( $\Delta G_{\text{Solv}}$ ) to  $\Delta G_{\text{gas}}$  for equation S1.  $\Delta G_{\text{Solv}}$  was calculated for gas phase optimized geometries using the SMD<sup>5</sup> continuum solvation model and subsequently added to gas phase Gibbs energies ( $\Delta G_{\text{gas}}$ ) to obtain solution phase Gibbs energies that will be designated single point solvation free energies ( $\Delta G_{\text{sol-sp}}$ ). In an alternative approached geometry optimization was carried out in the presence of the SMD continuum solvation model for DMSO at B3LYP/6-31G(d,p) level. The Gibbs energies calculated using the implicit DMSO optimized geometry are designated as  $\Delta G_{\text{sol-opt}}$ .

Electrophilicity indices like the electronic chemical potential ( $\mu$ ), the chemical hardness ( $\eta$ ), and the global electrophilicity index ( $\omega$ ) were calculated from orbital energies using eqs. S2, S3, and S4.<sup>6</sup>

$$\mu = \frac{1}{2} (\epsilon_{\text{HOMO}} + \epsilon_{\text{LUMO}}) \quad (\text{S2})$$

$$\eta = (\epsilon_{\text{LUMO}} - \epsilon_{\text{HOMO}}) \quad (\text{S3})$$

$$\omega = \mu^2 / 2\eta \quad (\text{S4})$$

Local electrophilicity indices ( $\omega_c$ ) at the carbonyl carbon atom for electrophiles (see equation S1) were calculated using the nucleophilic Fukui function ( $f_c^+$ ) as defined in eq. S5.

$$\omega_c = \omega f_c^+ \quad (\text{S5})$$

In this work, we calculated the nucleophilic Fukui function ( $f_c^+$ ) using two different approaches. First, the condensed nucleophilic Fukui function ( $f_c^+$ ) for atom  $c$  (carbonyl carbon atom for electrophiles) was calculated using a procedure described by Contreras and co-workers,<sup>7</sup> where  $f_c^+$  was calculated from the Gaussian 09 output files by the Fukui function program available at <https://github.com/dmsteglenko/Fukui-function-calculation>. In a second approach we used the Yang and Mortier method,<sup>8</sup> where the Fukui function for the nucleophilic attack is defined as the change of partial charge  $q$  at a certain atom  $c$  (carbonyl carbon atom for electrophiles) by adding an electron to the corresponding molecule, that is:

$$f_c^+ = q_c(N+1) - q_c(N) \quad (\text{S6})$$

with  $N$  = total number of electrons in the neutral molecule. We calculated  $f_c^+$  as defined in eq. S6 using Mulliken charges.

The methodology used for the calculation of potential energy surfaces (PES) for nucleophilic additions to electrophiles follows suggestions recently made for this type of reaction in ref 9. This includes geometry optimizations for all stationary points (minima, complexes and transition states) along the PES at the PCM(DMSO,UA0)/B3LYP-D3/6-31+G(d,p) level of theory. The PCM variant used here is based on the “Integral Equation Formalism for the Polarizable Continuum Model (IEFPCM)” solvation model employing United Atom Topological Model (UA0) radii derived from the UFF force field [scrf=(iefpcm,read,solvent=dmsol), radii=ua0].<sup>10</sup> The dispersion model is that proposed by Grimme as the "GD3" model [empiricaldispersion=gd3].<sup>11</sup>

All stationary points were confirmed by vibrational frequency calculation with 0, 0, and 1 imaginary frequencies, respectively. All stationary points were checked for wavefunction stability (stable=opt). The nature of transition states was further confirmed by IRC calculations [20 steps in both directions (reverse/forward) with stepsize=3] followed by geometry optimization to the next minima. In cases of very flat PES(s), manual displacement away from the TS(s) followed by geometry optimization was employed. PES surfaces were re-evaluated at PCM(DMSO,UA0)/B2PLYP<sup>12</sup>-D3/Def2TZVPP level of theory.<sup>13</sup> All calculations were performed with Gaussian 09, Rev. D.<sup>14</sup>

## 8.1.2 Mechanistic Investigation

### 8.1.2.1 QM data for reaction profiles

**Table S8-1.** [Table S22] Transition state (TS), reactant complex (RC) and product complex (PC) barriers ( $\Delta G_{\text{sol-opt}}$ , kJ/mol) for the reaction of arylsulfonyl-substituted chloromethyl anions **2a** with electrophiles [ketones (**1c** and **1g**) and dimethyl maleate **5\***] calculated at different levels of theory.

Path	B3LYP-D3/6-31G+(d,p) /PCM(DMSO,UA0)			B3LYP-D3 /6-31G+(d,p)			B2PLYP-D3 /def2TZVPP/PCM(UA0)		
	//B3LYP-D3/6-31G+(d,p)/PCM(DMSO,UA0)								
	RC	TS	PC	RC	TS	PC	RC	TS	PC
<b>1c</b>									
+									
<b>2a</b>									
syn	<b>19.4</b>	<b>46.5</b>	<b>26.8</b>	-23.7	11.9	13.6	<b>16.6</b>	<b>47.4</b>	<b>32.4</b>
syn	26.0	50.8	31.8	-11.0	19.9	19.4	28.0	56.3	39.5
syn	28.1	51.1	42.8	-	-	-	-	55.2	51.6
syn	31.4	52.7	36.9	-	-	-	-	55.5	42.5
syn	27.8	55.1	36.8	-	-	-	-	60.5	42.6
syn	34.0	60.8	36.2	-	-	-	-	66.0	41.2
syn	31.1	62.6	50.0	-	-	-	-	64.0	55.9
syn	30.9	64.2	55.2	-	-	-	-	72.8	66.3
syn	34.4	66.5	55.4	-	-	-	-	74.6	65.9
syn	37.0	72.9	54.9	-	-	-	-	79.3	62.6
syn	40.0	78.7	59.3	-	-	-	-	85.1	66.4
anti	<b>26.4</b>	<b>56.7</b>	32.3	-4.5	28.5	2.8	<b>28.5</b>	<b>61.5</b>	37.7
anti	30.4	63.2	<b>25.1</b>	-3.8	34.2	-6.1	34.4	67.8	<b>28.3</b>
anti	35.7	77.6	51.3	-	-	-	-	80.0	56.6
anti	40.1	79.8	53.8	-	-	-	-	85.3	60.9
anti	41.4	85.8	46.0	-	-	-	-	92.4	50.6
anti	-	87.3	48.7	-	-	-	-	92.4	52.3
cy	<b>25.1</b>	<b>37.7</b>	-89.1	-6.1	10.5	-21.6	<b>28.3</b>	<b>44.8</b>	-66.0
cy	40.9	46.6	<b>-94.0</b>	11.0	17.4	-52.6	47.5	54.5	<b>-74.0</b>
cy	32.3	51.8	-90.2	-	-	-	37.7	60.8	-68.3
cy	45.9	58.7	-76.4	-	-	-	50.6	66.6	-55.0
cy	50.1	59.0	-78.6	-	-	-	52.7	65.6	-57.4
cy	48.7	60.1	-74.1	-	-	-	52.3	67.5	-52.0

cy	51.4	65.2	-72.8	-	-	-	56.6	72.5	-53.0
cy	52.5	65.9	-	-	-	-	60.1	74.2	-
cy	54.7	72.1	-78.6	-	-	-	60.6	81.3	-57.4
cy	53.8	72.1	-76.4	-	-	-	60.9	82.0	-55.0
rot	<b>26.7</b>	<b>52.1</b>	29.1	13.5	37.1	23.4	<b>32.4</b>	<b>58.5</b>	35.1
rot	31.8	60.1	36.8	19.4	45.1	26.2	39.5	68.9	43.7
rot	34.0	61.6	<b>25.1</b>	26.7	45.6	-6.1	41.4	68.2	<b>28.3</b>
rot	42.8	59.6	44.6	-	-	-	51.6	68.2	51.4
rot	53.8	79.7	51.3	-	-	-	58.6	84.5	56.5
rot	55.4	71.0	40.9	-	-	-	65.9	79.9	47.6
rot	59.3	86.0	48.3	-	-	-	66.4	92.9	53.3
rot	63.9	86.8	48.3	-	-	-	67.9	89.2	53.3
rot	71.1	90.3	48.1	-	-	-	72.4	-	51.2
rot	-	59.6	-	-	-	-	-	68.2	-
rot	-	61.6	-	-	-	-	-	-	-
rot	-	62.7	-	-	-	-	-	-	-
rot	-	63.2	-	-	-	-	-	-	-
rot	-	69.6	-	-	-	-	-	-	-
rot	-	75.2	-	-	-	-	-	-	-
rot	-	77.1	-	-	-	-	-	-	-
rot	-	86.0	-	-	-	-	-	-	-
rot	-	86.0	-	-	-	-	-	-	-
rot	-	86.3	-	-	-	-	-	-	-
rot	-	86.3	-	-	-	-	-	-	-
rot	-	88.8	-	-	-	-	-	-	-
rot	-	89.6	-	-	-	-	-	-	-
rot	-	89.9	-	-	-	-	-	-	-
rot	-	90.0	-	-	-	-	-	-	-
<b>1g</b>									
+									
<b>2a</b>									
Path	RC	TS	PC	RC	TS	PC	RC	TS	PC
syn	<b>16.8</b>	<b>36.5</b>	28.1	-28.3	-2.6	9.8	<b>15.9</b>	<b>41.6</b>	37.7
syn	-	36.6	28.1	-	-	-	-	41.7	37.7
syn	22.9	38.7	23.3	-13.4	13.8	31.3	21.5	41.8	29.5
syn	22.8	38.8	23.3	-	-	-	-	41.8	29.5
syn	-	43.2	28.2	-	-	-	-	45.5	34.8
syn	-	49.9	40.0	-	-	-	-	59.0	51.3
syn	28.9	53.5	42.6	-	-	-	-	62.0	53.4
syn	-	55.5	36.0	-	-	-	-	63.0	44.6
syn	-	57.5	38.3	-	-	-	-	64.3	45.8
anti	<b>28.4</b>	<b>39.6</b>	14.0	-	2.7	-21.8	<b>30.3</b>	<b>42.6</b>	18.8
anti	30.0	50.4	<b>6.7</b>	7.0	16.7	-32.5	33.8	53.7	<b>9.6</b>
anti	28.9	55.8	26.1	-	-	-	-	62.8	33.5
anti	31.5	59.0	31.4	-	-	-	-	64.5	38.7
anti	33.7	60.1	34.3	-	-	-	-	66.6	42.2
anti	33.9	66.9	25.0	-	-	-	-	72.9	29.5
anti	33.8	66.9	25.0	-	-	-	-	72.9	29.5
anti	-	67.0	28.4	-	-	-	-	74.8	34.1
anti	-	67.5	28.4	-	-	-	-	75.1	34.1
cy	<b>6.8</b>	<b>22.8</b>	<b>-98.2</b>	-32.4	-8.8	-73.5	<b>9.7</b>	<b>30.0</b>	<b>-76.9</b>
cy	-	32.1	-97.8	-	-	-	-	40.9	-76.8
cy	14.0	38.9	-	-	-	-	-	48.2	-
cy	27.5	42.3	-82.9	-7.4	9.7	-57.4	33.4	51.0	-61.5
cy	25.0	43.2	-72.1	-	-	-	-	51.7	-51.0
cy	34.3	54.3	-83.0	-	-	-	-	65.1	-61.6
cy	31.4	55.3	-74.2	-	-	-	-	65.8	-54.3

rot	28.6	<b>40.3</b>	<b>6.7</b>	3.8	10.9	-32.5	30.2	<b>41.4</b>	<b>9.5</b>
rot	21.3	42.1	14.0	-20.7	2.1	-21.8	23.8	44.0	18.8
rot	<b>16.6</b>	46.9	6.7	1.5	23.2	-32.5	<b>23.4</b>	52.5	9.5
rot	28.0	47.3	29.7	-	-	-	-	56.7	37.5
rot	32.8	51.2	22.2	-	-	-	-	55.8	29.3
rot	28.2	56.2	31.1	-	-	-	-	63.1	39.0
rot	45.6	62.1	25.0	-	-	-	-	65.5	29.5
rot	44.2	64.2	27.0	-	-	-	-	67.3	33.0
rot	39.1	68.0	34.3	-	-	-	-	72.2	42.2
rot	-	47.3	-	-	-	-	-	-	-
rot	-	47.3	-	-	-	-	-	-	-
rot	-	51.5	-	-	-	-	-	-	-
rot	-	54.5	-	-	-	-	-	-	-
rot	-	54.5	-	-	-	-	-	-	-
rot	-	62.1	-	-	-	-	-	-	-
rot	-	63.2	-	-	-	-	-	-	-
rot	-	63.3	-	-	-	-	-	-	-
rot	-	63.7	-	-	-	-	-	-	-
rot	-	64.6	-	-	-	-	-	-	-
rot	-	64.7	-	-	-	-	-	-	-
rot	-	64.7	-	-	-	-	-	-	-
rot	-	64.8	-	-	-	-	-	-	-
rot	-	64.9	-	-	-	-	-	-	-
rot	-	65.2	-	-	-	-	-	-	-
rot	-	67.5	-	-	-	-	-	-	-
rot	-	67.5	-	-	-	-	-	-	-
<b>5*</b>									
+									
<b>2a</b>									
Path	RC	TS	PC	RC	TS	PC	RC	TS	PC
syn	<b>30.4</b>	<b>45.6</b>	<b>-21.7</b>	-	-	-	<b>27.6</b>	<b>46.2</b>	<b>-21.1</b>
syn	32.0	52.7	-0.3	-	-	-	28.3	52.8	0.1
syn	35.1	54.7	-1.8	-	-	-	-	60.1	-0.4
syn	34.6	55.1	-7.5	-	-	-	-	57.5	-8.7
syn	36.4	55.1	-7.5	-	-	-	-	57.6	-8.7
syn	41.5	56.3	-13.1	-	-	-	-	62.6	-10.4
syn	36.7	57.7	-4.6	-	-	-	-	62.5	-3.2
syn	36.0	60.3	-2.5	-	-	-	-	66.2	0.4
anti	32.7	<b>49.3</b>	-15.1	-	-	-	34.2	54.7	-14.0
anti	<b>15.3</b>	49.6	-31.4	-	-	-	<b>15.7</b>	<b>50.9</b>	-28.6
anti	37.9	54.3	-40.5	-	-	-	42.8	58.2	-39.0
cy	<b>-43.8</b>	<b>-22.7</b>	<b>-206.7</b>	-	-	-	<b>-42.9</b>	<b>-13.8</b>	<b>-189.1</b>
cy	-40.6	-17.8	-203.8	-	-	-	-39.0	-8.8	-186.0
cy	-37.2	-5.8	-173.9	-	-	-	-37.1	3.4	-155.5
cy	-34.8	-3.2	-171.4	-	-	-	-34.2	6.1	-153.4
cy	-27.3	-2.9	-188.2	-	-	-	-25.9	6.2	-171.1
cy	-19.2	13.5	-160.4	-	-	-	-18.5	23.5	-142.3
rot	-19.9	<b>-0.7</b>	-31.4	-	-	-	-17.3	<b>0.9</b>	-28.6
rot	-2.6	2.2	-35.8	-	-	-	0.3	2.7	-32.8
rot	-5.5	3.8	-34.8	-	-	-	-7.0	4.9	-32.7
rot	-0.8	5.7	-29.8	-	-	-	0.7	8.0	-25.5

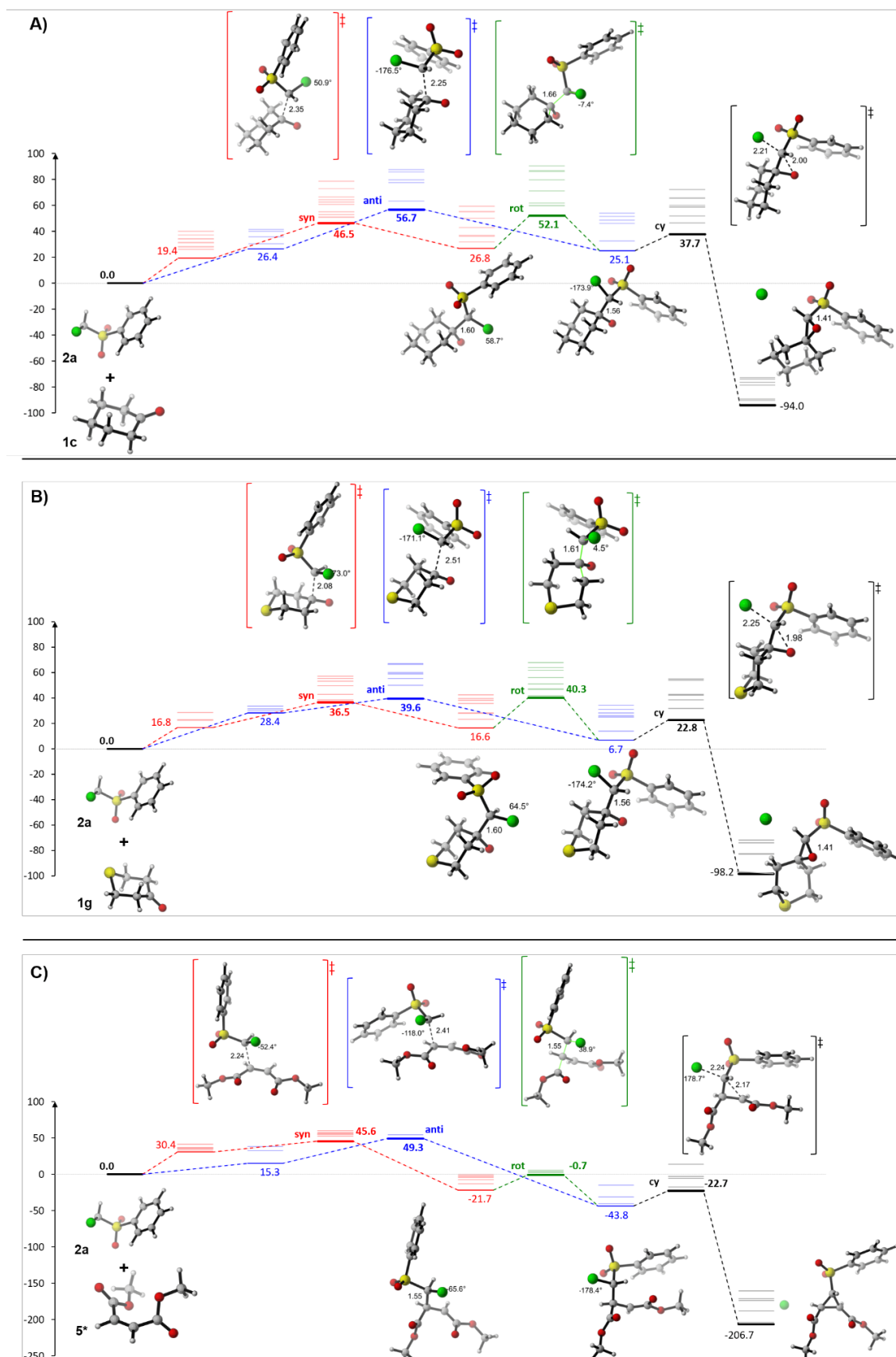


**Figure S8-1.** Reaction profiles ( $\Delta G_{\text{sol-opt}}$ , kJ/mol) for the reaction of **2a** with (A) [Figure S3] **1c**, (B) [Figure S8] **1g** and (C) [Figure S13] **5\*** calculated at the B3LYP-D3/6-31+G(d,p)/PCM(UA0,DMSO) level of theory. Faded bars are used to show the conformational space screened for each point along the profile. Dimethyl maleate **5\*** is used as a model substrate for diethyl maleate **5**.

## 8.1.2.2 Halohydrin conformational distribution

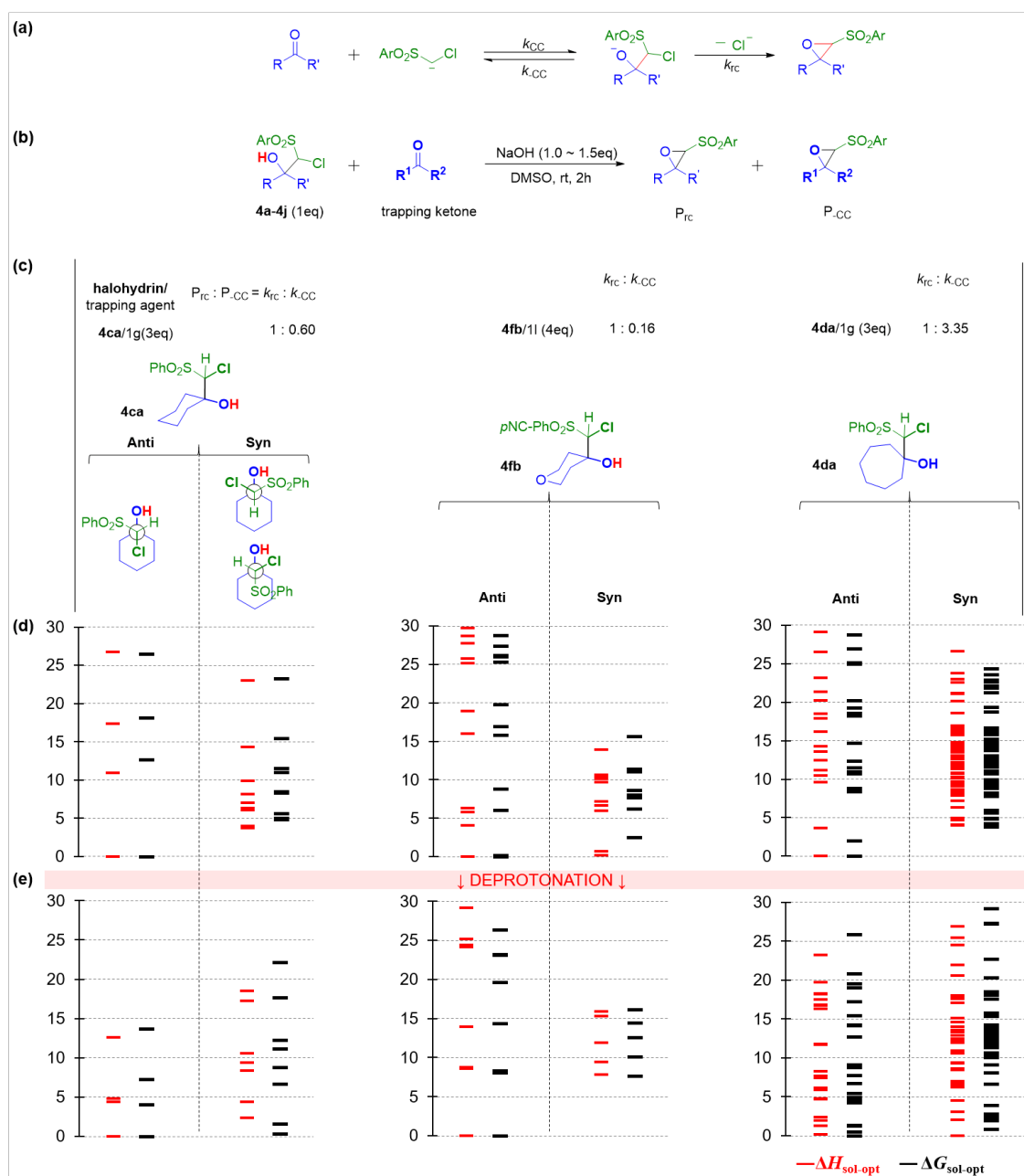


**Figure S8-2.** [Figure S15] (a) The proposed mechanism of the reactions of reference nucleophiles with ketones. (b) Crossover reaction. (c) The experimentally derived ratio of  $k_{rc}/k_{cc}$ . Conformational distribution of halohydrins in (d) neutral and (e) anionic (deprotonated) form calculated at the B3LYP-D3/6-31+G(d,p)/PCM(UA0,DMSO) level of theory. Energies are reported in kJ/mol.

## 8.1.3 Correlations

### 8.1.3.1 Gas phase MAA

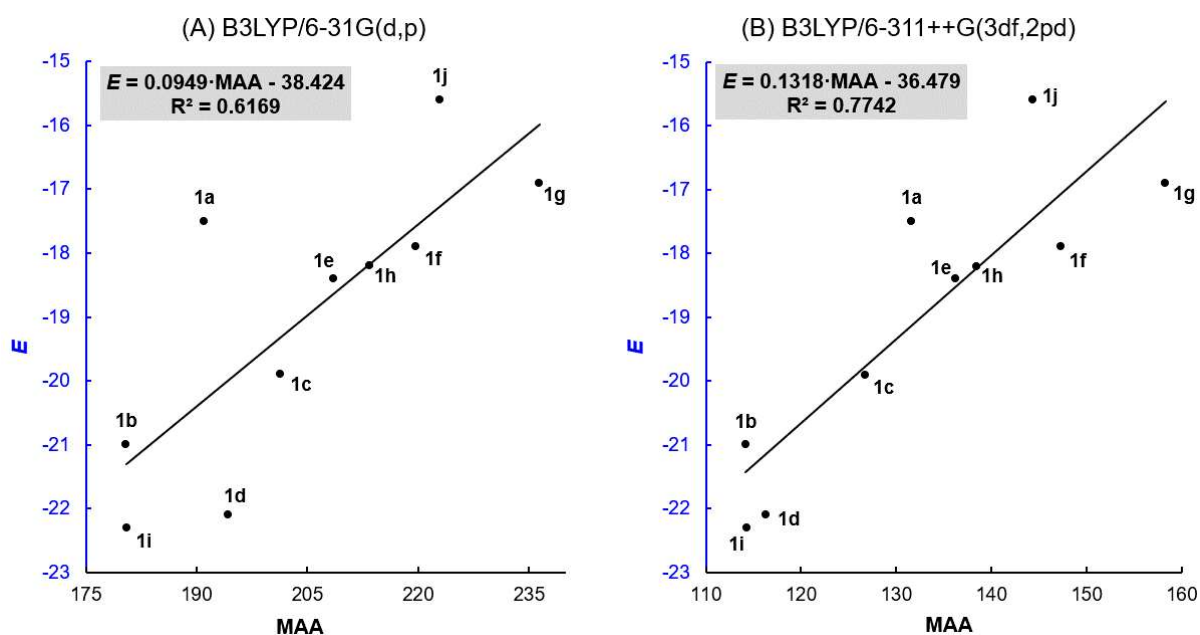


**Figure S8-3.** [Figure S17] Correlation between  $E$  of ketones and their gas phase MAA ( $-\Delta G_{\text{gas}}$ , kJ/mol) calculated at (A) B3LYP/6-31G(d,p) and (B) B3LYP/6-311++G(3df,2pd)//B3LYP/6-31G(d,p) level of theory.

### 8.1.3.2 Single point implicit-solvation (DMSO) corrected MAA

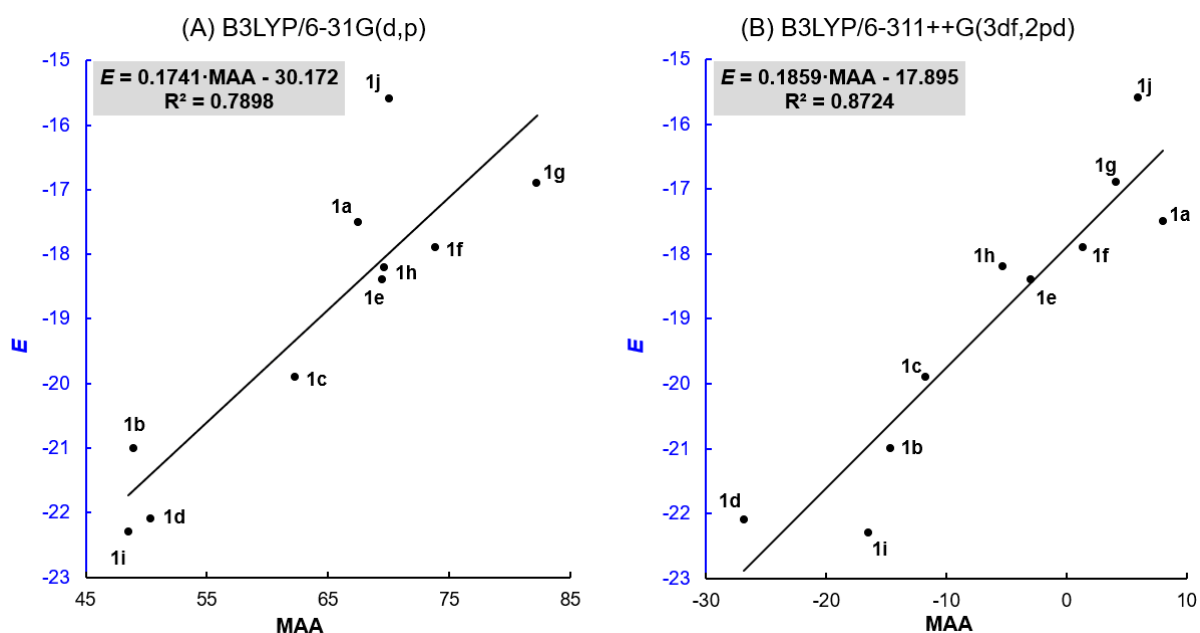


**Figure S8-4.** [Figure S20] Correlation between  $E$  of ketones and their MAA [ $-\Delta G_{\text{sol-sp}} = (\Delta G_{298} + \Delta G_{\text{Solv}})$ , kJ/mol] calculated at (A) B3LYP/6-31G(d,p) and (B) B3LYP/6-311++G(3df,2pd)//B3LYP/6-31G(d,p) levels of theory. (see **Table S8-2**)

**Table S8-2.** [Table S25] Methyl anion affinities ( $-\Delta G$ , in kJ/mol) calculated for ketones and aldehydes at different levels of theory.

Marker	$E$	Gas Phase Optimized		Single Point Implicit Solvation Corrected	
		MAA( $\Delta G_{\text{gas}}$ ) <sup>a</sup>		MAA ( $\Delta G_{\text{sol-sp}}$ ) <sup>b</sup>	
		B3LYP		B3LYP	
		6-31G (d,p) <sup>d</sup>	6-311++G(3df,2pd) <sup>d</sup>	6-31G (d,p) <sup>d</sup>	6-311++G(3df,2pd) <sup>d</sup>
<b>1a</b>	-17.47	191.0	131.6	67.5	8.0
<b>1b</b>	-21.04	180.5	114.2	49.0	-14.6
<b>1c</b>	-19.88	201.3	126.7	62.3	-11.7
<b>1d</b>	-22.16	194.3	116.3	50.4	-26.8
<b>1e</b>	-18.39	208.6	136.2	69.5	-2.9
<b>1f</b>	-17.85	219.7	147.3	73.8	1.4
<b>1g</b>	-16.84	236.4	158.3	82.2	4.1
<b>1h</b>	-18.17	213.5	138.5	69.7	-5.3
<b>1i</b>	-22.24	180.6	114.3	48.5	-16.4
<b>1j</b>	-15.60	222.9	144.4	70.1	5.9
<b>1m*</b>	-13.1	221.9	155.2	94.5	27.8
<b>1o*</b>	-15.4	212.7	143.7	82.2	13.2

<sup>a</sup>MAA( $\Delta G_{\text{gas}}$ ) calculated using  $\Delta G_{298}$  values of gas phase optimized geometries. <sup>b</sup>MAA( $\Delta G_{\text{sol-sp}}$ ) calculated using  $\Delta G_{298}$  of gas phase geometries + single point implicit DMSO solvation energies (SMD) for the same. <sup>c</sup>MAA( $\Delta G_{\text{sol-opt}}$ ) calculated using  $\Delta G_{298}$  values for implicit DMSO optimized geometries (SMD). <sup>d</sup>Using gas phase optimized B3LYP/6-31G(d,p) geometries.

### 8.1.3.3 Effects of solvation energies on conformational selection

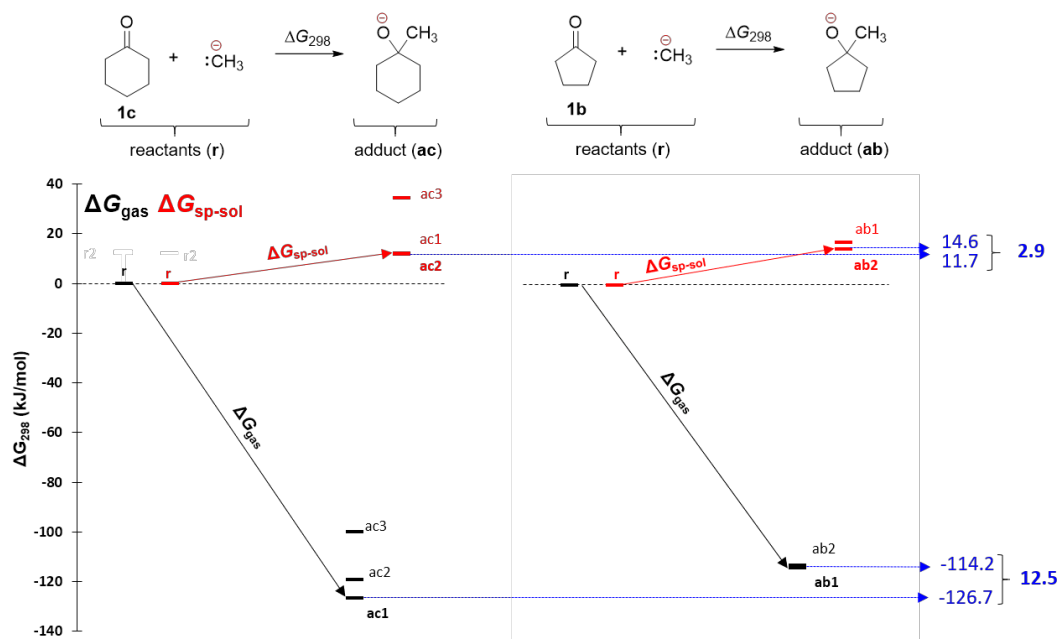


**Figure S8-5.** [Figure S24] Free energies for  $\text{CH}_3^-$  addition to **1c** and **1b** in gas ( $\Delta G_{\text{gas}}$ ) and solution phase ( $\Delta G_{\text{sp-sol}}$ ) calculated at B3LYP/6-311++G(3df,2pd)//B3LYP/6-31G(d,p) and B3LYP/6-311++G(3df,2pd)/SMD(DMSO)//B3LYP/6-31G(d,p) levels of theory, respectively.

The correlation between MAA and  $E$  improves when gas phase values ( $\Delta G_{\text{gas}}$ ) of the former were corrected by solvation energies ( $\Delta G_{\text{solv}}$ ) obtained in single point SMD calculations. It is important to mention that this improvement in the correlation depends heavily on finding the lowest energy conformer both in the gas and solution phase. This observation is illustrated in Figure S8-5 for the example of cyclohexanone **1c**, which has a 12.5 kJ/mol higher MAA than cyclopentanone **1b** in the

gas phase ( $\Delta G_{\text{gas}}$ ), which is reduced to 2.9 kJ/mol in DMSO ( $\Delta G_{\text{sp-sol}}$ ). This 9.6 kJ/mol change results from two important factors. First, a change in conformational preference for the adducts from the gas phase to DMSO and second the differences in the absolute solvation energies of both ketones and their corresponding adducts.

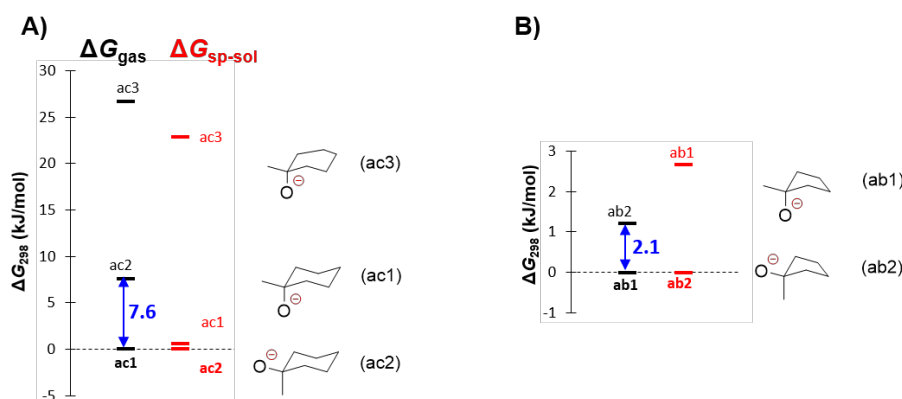


**Figure S8-6.** [Figure S25] Conformational energetics for  $\text{CH}_3^-$  adducts (A) **ac** (of **1c**) and (B) **ab** (of **1b**) in gas ( $\Delta G_{\text{gas}}$ ) and solution phase ( $\Delta G_{\text{sp-sol}}$ ) calculated at B3LYP/6-311++G(3df,2pd)//B3LYP/6-31G(d,p) and B3LYP/6-311++G(3df,2pd)/SMD(DMSO)//B3LYP/6-31G(d,p) levels of theory, respectively.

Conformational preference: ketones **1b** and **1c** prefer conformations where the carbonyl oxygen is equatorially oriented (gas phase and DMSO). Adducts of these ketones have different conformational preferences in the gas phase and in DMSO: **ab1** and **ac1** are preferred in the gas phase, and **ab2** and **ac2** are preferred in DMSO. For cyclohexanone adducts the conformer **ac2** has a 8.2 kJ/mol higher solvation energy than conformer **ac1** and thus becomes the global minimum in DMSO [see Figure S8-6 (A), for solvation energies see column 4 of Table S8-3]. Because of this change, the driving force for  $\text{CH}_3^-$  addition to ketone **1c** is reduced by 7.6 kJ/mol in DMSO relative to the gas phase (**ac2** is 7.6 kJ/mol higher in gas phase). A similar conformational switch can be observed for the reaction of cyclopentanone **1b**, where adduct conformer **ab2** becomes the global minimum in DMSO due to a 3.9 kJ/mol higher solvation energy as compared to conformer **ab1**.

**Table S8-3.** [Table S27] Relative energies (in kJ/mol) for **1b** and **1c** along with their adducts.

Marker	Rel. $\Delta G_{\text{gas}}$	$\Delta G_{\text{sol}}$	Rel. $\Delta G_{\text{sp-sol}}$
	B3LYP /6-311++G(3df,2pd) //B3LYP/6-31G(d,p)	SMD(DMSO)/B3LYP /6-31G(d,p) //B3LYP/6-31G(d,p)	SMD(DMSO)/B3LYP /6-311++G(3df,2pd) //B3LYP/6-31G(d,p)
<b>1b</b>	0.0	-25.9	0.0
<b>ab1</b>	0.0	-224.2	2.7
<b>ab2</b>	1.2	-228.0	0.0
<b>1c</b>	0.0	-26.8	0.0
<b>1c</b>	12.5	-27.1	12.1
<b>ac1</b>	0.0	-217.5	0.6
<b>ac2</b>	7.6	-225.7	0.0
<b>ac3</b>	26.7	-221.9	22.9

Taken together this change in conformational preference leads to a loss of 1.2 kJ/mol driving force for  $\text{CH}_3^-$  addition to **1b** in DMSO relative to the gas phase. Overall, because of the changes in conformation preferences, it becomes 6.4 (7.6-1.2) kJ/mol more difficult to add  $\text{CH}_3^-$  to **1c** in DMSO relative to the gas phase when comparing it with **1b**. The absolute solvation free energy of ketone **1c** (-26.8 kJ/mol) is 0.9 kJ/mol higher than that for **1b** (-25.9 kJ/mol), while for the methyl anion adducts **ab2** (-228.0 kJ/mol) is 2.3 kJ/mol better solvated than **ac2** (-225.7 kJ/mol). [see column 4

of Table S8-3]. Taking these solvation effects into account, the  $\text{CH}_3^-$  addition to **1c** is reduced relative to **1b** by 3.2 kJ/mol in DMSO solution. Combination of both factors (change in conformational preference with 6.4 kJ/mol, and difference in absolute solvation energies of 3.2 kJ/mol) results in a 9.6 kJ/mol reduction of  $\text{CH}_3^-$  addition reaction energy for **1c** relative to **1b** in DMSO when compared to the gas phase.

### 8.1.3.4 $E$ vs Frontier Molecular Orbital Energies (FMO<sub>E</sub>)

**Table S8-4.** [Table S28]  $\epsilon_{\text{HOMO}}$  and  $\epsilon_{\text{LUMO}}$  energies (Hartree) for ketones and aldehydes at different levels of theory.

Marker	B3LYP/6-31G(d,p)		B3LYP/6-31G(d,p)/SMD(DMSO) //B3LYP/6-31G(d,p)		B3LYP/6-311++G(3df,2pd) //B3LYP/6-31G(d,p)	
	$\epsilon_{\text{HOMO}}$ ( $E_{\text{H}}$ )	$\epsilon_{\text{LUMO}}$ ( $E_{\text{L}}$ )	$\epsilon_{\text{HOMO}}$	$\epsilon_{\text{LUMO}}$	$\epsilon_{\text{HOMO}}$	$\epsilon_{\text{LUMO}}$
<b>1a</b>	-0.24245	-0.02117	-0.23629	-0.01179	-0.25743	-0.03994
<b>1b</b>	-0.23597	-0.01449	-0.23076	-0.00600	-0.25073	-0.03336
<b>1c</b>	-0.23443	-0.01201	-0.22980	-0.00432	-0.24879	-0.03383
<b>1d</b>	-0.23483	-0.01104	-0.23104	-0.00427	-0.24950	-0.03153
<b>1e</b>	-0.22444	-0.01456	-0.21284	-0.00768	-0.23805	-0.03542
<b>1f</b>	-0.24378	-0.02071	-0.23565	-0.00941	-0.25848	-0.04045
<b>1g</b>	-0.23250	-0.02310	-0.22327	-0.01134	-0.24075	-0.04213
<b>1h</b>	-0.23481	-0.01233	-0.23238	-0.00757	-0.24970	-0.03238
<b>1i</b>	-0.24272	-0.00948	-0.23665	-0.00012	-0.25646	-0.02730
<b>1j</b>	-0.22563	-0.02762	-0.22018	-0.01957	-0.23476	-0.04346
<b>1m*</b>	-0.25521	-0.06342	-0.25209	-0.05735	-0.26952	-0.08083
<b>1o*</b>	-0.23442	-0.05149	-0.22737	-0.04826	-0.24806	-0.06825

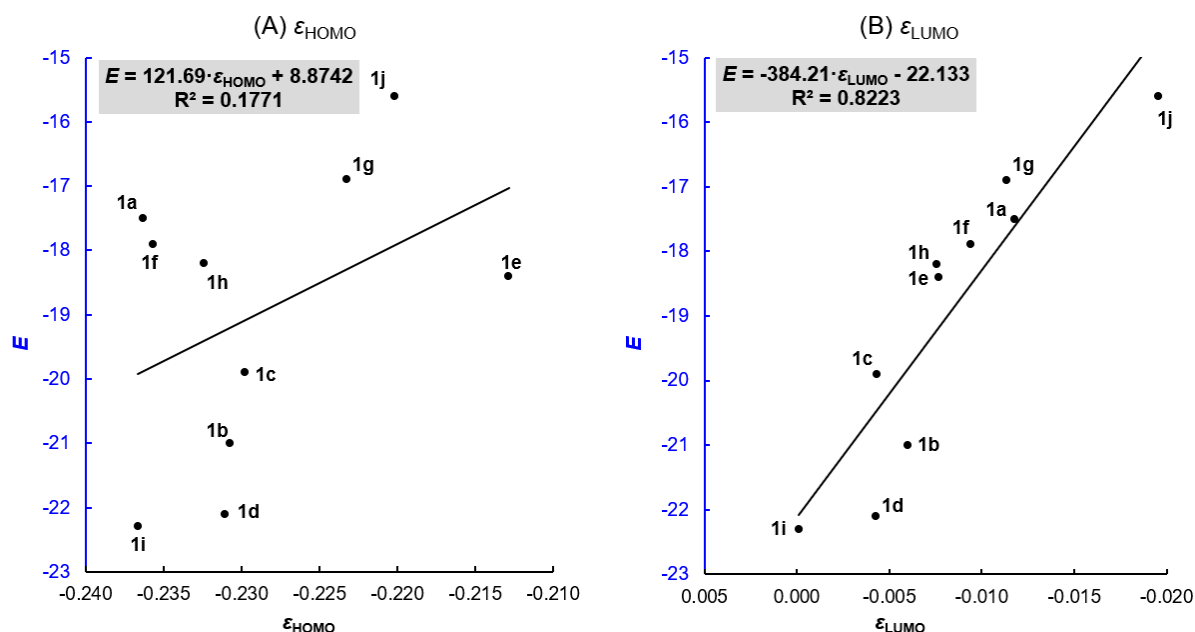


**Figure S8-7.** [Figure S29] Correlation between  $E$  and frontier molecular orbital energies of ketones electrophiles (A)  $\epsilon_{\text{HOMO}}$  and (B)  $\epsilon_{\text{LUMO}}$  calculated at the B3LYP/6-31G(d,p)/SMD(DMSO) //B3LYP/6-31G(d,p) level of theory. FMO energies are reported in Hartree.

8.1.3.5  $E$  vs Electrophilicity Indices**Table S8-5.** [Table S29] Electrophilicity indices for ketones and aldehydes calculated at B3LYP/6-31G(d,p) level of theory. Global ( $\omega$ ) and local ( $\omega_c$ ) Parr electrophilicity indices (eV).

Marker	Chemical Potential $\mu \approx$ ( $E_H + E_L$ )/2	Chemical Hardness $\eta \approx$ ( $E_L - E_H$ )	Global Electrophilicity Index $\omega = \mu^2 / 2\eta$	Local Electrophilicity ( $\omega_c$ ), Yang and Mortier				$\omega_c$ Contreras	
				$q_c$ (N)	$q_c$ (N+1)	$f_c^+$	$\omega_c$ ( $\omega^* f_c^+$ )	$f_c^+$	$\omega_c$ ( $\omega^* f_c^+$ )
1a	-0.13181	0.22128	1.07	0.395103	0.242452	0.15	0.16	0.48	0.51
1b	-0.12523	0.22148	0.96	0.416329	0.260839	0.16	0.15	0.50	0.48
1c	-0.12322	0.22242	0.93	0.426145	0.261355	0.16	0.15	0.50	0.47
1d	-0.12294	0.22379	0.92	0.421597	0.271794	0.15	0.14	0.51	0.47
1e	-0.11950	0.20988	0.93	0.415529	0.252644	0.16	0.15	0.50	0.46
1f	-0.13225	0.22307	1.07	0.413215	0.241469	0.17	0.18	0.50	0.53
1g	-0.12780	0.20940	1.06	0.429222	0.251864	0.18	0.19	0.51	0.54
1h	-0.12357	0.22248	0.93	0.422973	0.257594	0.17	0.15	0.51	0.47
1i	-0.12610	0.23324	0.93	0.420833	0.254655	0.17	0.15	0.53	0.49
1j	-0.12663	0.19801	1.10	0.431925	0.305401	0.13	0.14	0.46	0.51
1m*	-0.15932	0.19179	1.80	0.258182	0.137644	0.12	0.22	0.26	0.48
1o*	-0.14296	0.18293	1.52	0.253321	0.132615	0.12	0.18	0.28	0.42

For the Yang and Mortier method:  $f_c^+ = |q_c(N+1) - q_c(N)|$ , where,  $q_c$  is partial charge at atom  $c$  (carbonyl carbon atom for electrophiles) and  $N$  is a number of electrons in the neutral system.

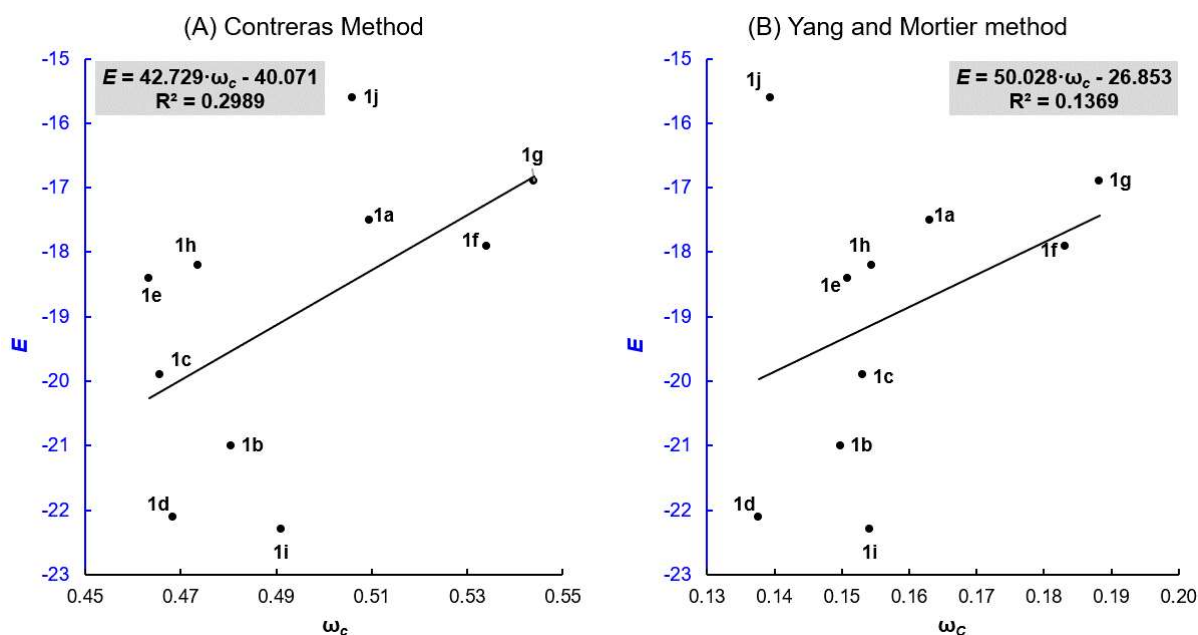


**Figure S8-8.** [Figure S33] Correlation between  $E$  and gas phase local electrophilicity index ( $\omega_c$ , in eV) calculated at B3LYP/6-31G(d,p) level of theory for ketones using (A) The Contreras method and (B) The Yang and Mortier method. The Fukui function for nucleophilic attack ( $f_c^+$ ) has been calculated using Mulliken charges for the Yang and Mortier method.

### 8.1.4 References

- (1) (a) Mayr, H.; Ammer, J.; Baidya, M.; Maji, B.; Nigst, T. A.; Ofial, A. R.; Singer, T., *J. Am. Chem. Soc.* **2015**, *137*, 2580-2599. (b) Allgäuer, D. S.; Jangra, H.; Asahara, H.; Li, Z.; Chen, Q.; Zipse, H.; Ofial, A. R.; Mayr, H., *J. Am. Chem. Soc.* **2017**, *139*, 13318-13329. (c) Byrne, P. A.; Kobayashi, S.; Würthwein, E.-U.; Ammer, J.; Mayr, H., *J. Am. Chem. Soc.* **2017**, *139*, 1499-1511.
- (2) Becke, A. D., *J. Chem. Phys.* **1993**, *98*, 5648-5652.
- (3) (a) Ditchfield, R.; Hehre, W. J.; Pople, J. A., *J. Chem. Phys.* **1971**, *54*, 724-728. (b) Krishnan, R.; Binkley, J. S.; Seeger, R.; Pople, J. A., *J. Chem. Phys.* **1980**, *72*, 650-654.
- (4) Clark, T.; Chandrasekhar, J.; Spitznagel, G. W.; Schleyer, P. V. R., *J. Comput. Chem.* **1983**, *4*, 294-301.
- (5) Marenich, A. V.; Cramer, C. J.; Truhlar, D. G., *J. Phys. Chem. B* **2009**, *113*, 6378-6396.
- (6) (a) Parr, R. G.; Yang, W., *Density-Functional Theory of Atoms and Molecules*, vol. 16 of *International Series of Monographs on Chemistry*. Oxford University Press, New York: **1989**. (b) Parr, R. G.; Szentpaly, L. v.; Liu, S., *J. Am. Chem. Soc.* **1999**, *121*, 1922-1924. (c) Domingo, L. R.; Pérez, P.; Contreras, R., *Tetrahedron* **2004**, *60*, 6585-6591.
- (7) Contreras, R. R.; Fuentealba, P.; Galván, M.; Pérez, P., *Chem. Phys. Lett.* **1999**, *304*, 405-413.
- (8) Yang, W.; Mortier, W. J., *J. Am. Chem. Soc.* **1986**, *108*, 5708-5711.
- (9) Mayer, R. J.; Tokuyasu, T.; Mayer, P.; Gomar, J.; Sabelle, S.; Mennucci, B.; Mayr, H.; Ofial, A. R., *Angew. Chem. Int. Ed.* **2017**, *56*, 13279-13282.
- (10) (a) Cancès, E.; Mennucci, B.; Tomasi, J., *J. Chem. Phys.* **1997**, *107*, 3032-3041. (b) Tomasi, J.; Mennucci, B.; Cammi, R., *Chem. Rev.* **2005**, *105*, 2999-3094.
- (11) (a) Grimme, S., *J. Comput. Chem.* **2006**, *27*, 1787-1799. (b) Grimme, S.; Antony, J.; Ehrlich, S.; Krieg, H., *J. Chem. Phys.* **2010**, *132*, 154104.
- (12) Grimme, S., *J. Chem. Phys.* **2006**, *124*, 034108.
- (13) (a) Weigend, F.; Ahlrichs, R., *Phys. Chem. Chem. Phys.* **2005**, *7*, 3297-3305. (b) Weigend, F., *Phys. Chem. Chem. Phys.* **2006**, *8*, 1057-1065.
- (14) Frisch, M. J. T., G. W.; Schlegel, H. B.; Scuseria, G. E.; Robb, M. A.; Cheeseman, J. R.; Scalmani, G.; Barone, V.; Mennucci, B.; Petersson, G. A.; Nakatsuji, H.; Caricato, M.; Li, X.; Hratchian, H. P.; Izmaylov, A. F.; Bloino, J.; Zheng, G.; Sonnenberg, J. L.; Hada, M.; Ehara, M.; Toyota, K.; Fukuda, R.; Hasegawa, J.; Ishida, M.; Nakajima, T.; Honda, Y.; Kitao, O.; Nakai, H.; Vreven, T.; Montgomery, Jr., J. A.; Peralta, J. E.; Ogliaro, F.; Bearpark, M.; Heyd, J. J.; Brothers, E.; Kudin, K. N.; Staroverov, V. N.; Keith, T.; Kobayashi, R.; Normand, J.; Raghavachari, K.; Rendell, A.; Burant, J. C.; Iyengar, S. S.; Tomasi, J.; Cossi, M.; Rega, N.; Millam, J. M.; Klene, M.; Knox, J. E.; Cross, J. B.; Bakken, V.; Adamo, C.; Jaramillo, J.; Gomperts, R.; Stratmann, R. E.; Yazyev, O.; Austin, A. J.; Cammi, R.; Pomelli, C.; Ochterski, J. W.; Martin, R. L.; Morokuma, K.; Zakrzewski, V. G.; Voth, G. A.; Salvador, P.; Dannenberg, J. J.; Dapprich, S.; Daniels, A. D.; Farkas, O.; Foresman, J. B.; Ortiz, J. V.; Cioslowski, J.; Fox, D. J.; *Gaussian 09 Revision D. 01*, Gaussian, Inc., Wallingford CT: **2013**.

## **Chapter 9. Nucleophilicity and Electrophilicity Parameters for Predicting Absolute Rate Constants of Highly Asynchronous 1,3-Dipolar Cycloadditions of Aryldiazomethanes**

Harish Jangra, Quan Chen, Elina Fuks, Ivo Zenz, Peter Mayer, Armin R. Ofial, Hendrik Zipse, and Herbert Mayr  
*J. Am. Chem. Soc.* **2018**, *140*, 16758–16772.

---

### ***Authors contribution***

A.R.O., H.Z. and H.M. designed the project. H.J. and Q.C. contributed equally to this work. Experimental work was designed by H.M. and A.R.O and carried out by Q.C. with the help of E.F. and I.Z.. The X-ray crystallography was done by P.M.. H.J. performed theoretical calculations that were designed by him and H.Z.. H.J., Q.C., A.R.O., H.Z. and H.M. jointly wrote the manuscript.

### ***Copyright***

This research was originally published in the *Journal of the American Chemical Society* and reprinted with permission from *J. Am. Chem. Soc.* **2018**, *140*, 16758–16772 © 2018 American Chemical Society as the 9<sup>th</sup> chapter of this thesis.

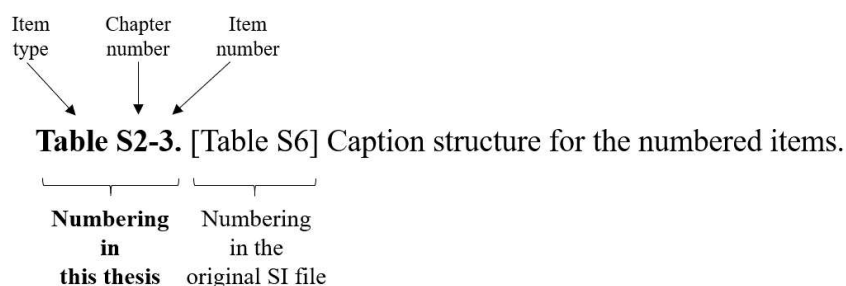
(Link to publication: <https://pubs.acs.org/doi/abs/10.1021/jacs.8b09995>)

Selected supporting material for the computational part of this work is provided at the end of this chapter. For complete supporting information (SI), please follow the link below:

<https://pubs.acs.org/doi/suppl/10.1021/jacs.8b09995>

### ***Additional information***

The accompanying SI is the shorter and altered version of the original content. The items (Tables, Figure, Schemes etc.) may have a different number than what was originally assigned. To make it easier to locate the SI content referred to in the following reprint, the original numbering is also provided in the caption of the numbered items as described below:



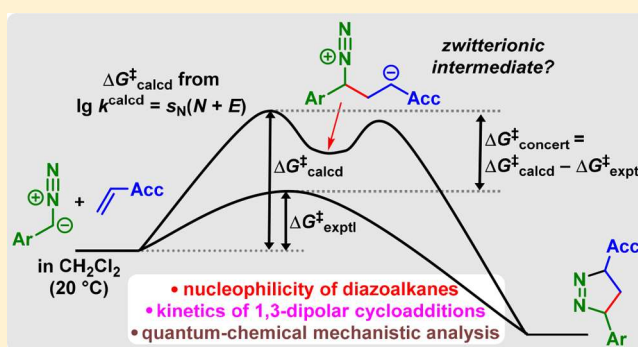
# Nucleophilicity and Electrophilicity Parameters for Predicting Absolute Rate Constants of Highly Asynchronous 1,3-Dipolar Cycloadditions of Aryldiazomethanes

Harish Jangra,<sup>†</sup> Quan Chen,<sup>†,‡</sup> Elina Fuks, Ivo Zenz,<sup>§</sup> Peter Mayer, Armin R. Ofial,<sup>\*†</sup> Hendrik Zipse,<sup>\*†</sup> and Herbert Mayr<sup>\*†</sup>

Department Chemie, Ludwig-Maximilians-Universität München, Butenandtstr. 5-13, 81377 München, Germany

Supporting Information

**ABSTRACT:** Kinetics of the reactions of aryldiazomethanes ( $\text{ArCHN}_2$ ) with benzhydrylium ions ( $\text{Ar}_2\text{CH}^+$ ) have been measured photometrically in dichloromethane. The resulting second-order rate constants correlate linearly with the electrophilicities  $E$  of the benzhydrylium ions which allowed us to use the correlation  $\lg k = s_N(N + E)$  (eq 1) for determining the nucleophile-specific parameters  $N$  and  $s_N$  of the diazo compounds. UV–vis spectroscopy was analogously employed to measure the rates of the 1,3-dipolar cycloadditions of these aryldiazomethanes with acceptor-substituted ethylenes of known electrophilicities  $E$ . The measured rate constants for the reactions of the diazoalkanes with highly electrophilic Michael acceptors ( $E > -11$ , for example 2-benzylidene Meldrum's acid or 1,1-bis(phenylsulfonyl)ethylene) agreed with those calculated by eq 1 from the one-bond nucleophilicities  $N$  and  $s_N$  of the diazo compounds and the one-bond electrophilicities of the dipolarophiles, indicating that the incremental approach of eq 1 may also be applied to predict the rates of highly asynchronous cycloadditions. Weaker electrophiles, e.g., methyl acrylate, react faster than calculated from  $E$ ,  $N$ , and  $s_N$ , and the ratio of experimental to calculated rate constants was suggested to be a measure for the energy of concert  $\Delta G_{\text{concert}}^\ddagger = RT \ln(k_2^{\text{exptl}}/k_2^{\text{calcd}})$ . Quantum chemical calculations indicated that all products isolated from the reactions of the aryldiazomethanes with acceptor substituted ethylenes ( $\Delta^2$ -pyrazolines, cyclopropanes, and substituted ethylenes) arise from intermediate  $\Delta^1$ -pyrazolines, which are formed through concerted 1,3-dipolar cycloadditions with transition states, in which the C–N bond formation lags behind the C–C bond formation. The Gibbs activation energies for these cycloadditions calculated at the PCM(UAO, $\text{CH}_2\text{Cl}_2$ )/(U)B3LYP-D3/6-31+G(d,p) level of theory agree within 5  $\text{kJ mol}^{-1}$  with the experimental numbers showing the suitability of the applied polarizable continuum model (PCM) for considering solvation.



## INTRODUCTION

1,3-Dipolar cycloadditions (Huisgen reactions) represent the most general approach to 5-membered heterocycles.<sup>1</sup> They have been used for the total synthesis of natural products<sup>2</sup> and for the preparation of organic functional materials.<sup>3</sup> The copper-catalyzed reaction of azides ( $\text{R-N}_3$ ) with alkynes has become the most generally applicable click reaction.<sup>4</sup> Although a concerted mechanism with a cyclic transition state has been well established for most Huisgen reactions,<sup>5–7</sup> evidence for a stepwise course via diradical or zwitterionic intermediates has been reported in several cases.<sup>6,8</sup> Since the late 1970s, reactivities and regioselectivities of cycloaddition reactions have commonly been interpreted on the basis of perturbational molecular orbital theory.<sup>7,9</sup> Recently, the groups of Houk and Bickelhaupt have shown that detailed insight in the mechanisms of these reactions can be obtained by the “distortion/interaction energy” or “activation strain” model, respectively.<sup>10–12</sup> We now report a novel approach to

predicting and analyzing cycloaddition reactivities on the basis of linear-free-energy relationships.

Equation 1, in which nucleophiles are characterized by two solvent-dependent parameters,  $N$  and  $s_N$ , and electrophiles are characterized by one parameter,  $E$ , has been demonstrated to predict rate constants of a large variety of electrophile-nucleophile combinations if one or both reaction centers are carbon.<sup>13,14</sup>

$$\lg k_{20^\circ\text{C}} = s_N(N + E) \quad (1)$$

While the electrophilicity parameter  $E$  of a certain electrophile is derived from the rate constants of its reactions with a series of C-centered nucleophiles, the  $N$  and  $s_N$  parameters of a certain nucleophile are derived from the rates of its reactions with a series of C-centered reference electrophiles. Since

Received: September 14, 2018

Published: November 16, 2018

reactions, in which *one* and only *one* new bond is formed in the rate-determining step, were used for the derivation of the reactivity parameters  $E$ ,  $N$ , and  $s_N$ , eq 1 cannot be expected to be applicable to multicenter processes. However, we now report that the relative reactivities of Michael acceptors toward aryldiazomethanes<sup>15</sup> correlate well with the electrophilicities  $E$  of Michael acceptors, which have previously been derived from the one-bond reactivities of the electron-deficient  $\pi$ -systems toward carbanions and ylides.<sup>16</sup> We will furthermore show that eq 1 can even be used to predict absolute rate constants for the reactions of highly electrophilic dipolarophiles with aryldiazomethanes, whereas less electrophilic dipolarophiles react faster than predicted by eq 1 due to the concerted formation of two new  $\sigma$ -bonds. In the latter cases, deviations of the measured cycloaddition rate constants from those calculated by eq 1 can be considered to be a measure for the energy of concert  $\Delta G_{\text{concert}}^\ddagger$  as defined in eq 2.<sup>17</sup>

$$\Delta G_{\text{concert}}^\ddagger = RT \ln(k_2^{\text{exptl}}/k_2^{\text{calcd}}) \quad (2)$$

## RESULTS AND DISCUSSION

Phenyldiazomethane **1a** and its *para*-substituted derivatives **1b–d**, which have UV absorption maxima between 290 and 380 nm, were employed for this study (Chart 1). For the

Chart 1. Aryldiazomethanes (**1**) and Benzhydrylium Tetrafluoroborates (**2-BF<sub>4</sub>**) Used in This Work

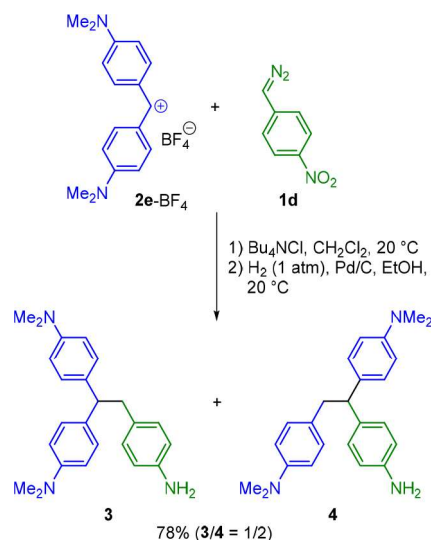
Nucleophiles	Reference Electrophiles
Aryldiazomethanes	Benzhydrylium Tetrafluoroborates
<b>1a</b> (X = H) $\lambda_{\text{max}} = 295$ nm	<b>2a</b> Y = N(Ph)(CH <sub>2</sub> CF <sub>3</sub> ) $E = -3.14$
<b>1b</b> (X = Br) $\lambda_{\text{max}} = 290$ nm	<b>2b</b> Y = NPh <sub>2</sub> $E = -4.72$
<b>1c</b> (X = CN) $\lambda_{\text{max}} = 320$ nm	<b>2c</b> Y = N(CH <sub>2</sub> CH <sub>2</sub> ) <sub>2</sub> O $E = -5.53$
<b>1d</b> (X = NO <sub>2</sub> ) $\lambda_{\text{max}} = 380$ nm	<b>2d</b> Y = N(Me)(Ph) $E = -5.89$
	<b>2e</b> Y = NMe <sub>2</sub> $E = -7.02$
	<b>2f</b> Y = N(CH <sub>2</sub> ) <sub>4</sub> $E = -7.69$
	<b>2g</b> $E = -9.45$

determination of the reactivity parameters  $N$  and  $s_N$  for **1a–d** the rates of their reactions with a set of colored benzhydrylium ions of known electrophilicities  $E^{13a,h}$  (**2a–g** in Chart 1) were measured.

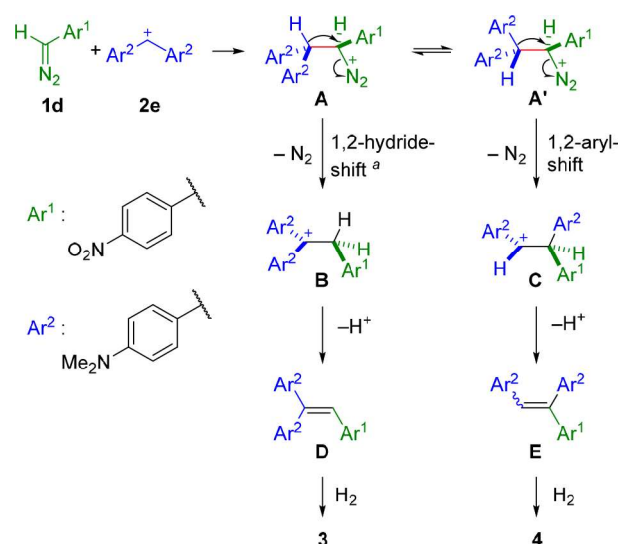
**Determination of Nucleophile-Specific Parameters  $N$  and  $s_N$  for Aryldiazomethanes **1b–d**.**<sup>18</sup> *Product Studies.* The reaction of **1d** with **2e** gave a mixture of (*E*)- and (*Z*)-configured ethylenes, which was hydrogenated to furnish **3** and **4** in a 1:2 ratio and 78% yield of isolated products (Scheme 1).

The mechanism for their formation is rationalized in Scheme 2. The reaction between **1d** and **2e** yields a diazonium ion **A**, which spontaneously loses N<sub>2</sub> accompanied by a hydride shift, leading to carbenium ion **B**, or an aryl shift, leading to carbenium ion **C**. Deprotonation yields the olefins **D** and **E**, respectively, the precursors of the isolated products **3** and **4**. Alternatively, the nonrearranged olefin **D** may be formed by concerted proton and N<sub>2</sub> elimination from diazonium ion **A**. From the 3/4 ratio one can derive that the aryl shift is faster than the competing processes. Concerted N<sub>2</sub> departure and 1,2-shifts have previously been observed from diazonium ions

Scheme 1. Reaction of Aryldiazomethane **1d** with Benzhydrylium Tetrafluoroborate **2e-BF<sub>4</sub>**



Scheme 2. Proposed Mechanism for the Formation of **3** and **4**



<sup>a</sup>Formal hydride shift, which may include further intermediates.

generated by diazotation of primary amines<sup>19</sup> as well as in acid-catalyzed Schmidt reactions of alkyl azides.<sup>20</sup>

*Kinetics.* The rates of the reactions of the diazomethanes **1** with the benzhydrylium ions **2** were followed photometrically under pseudo-first-order conditions by monitoring the decay of the UV–vis absorbance of **2** in the presence of a large excess of **1**, following the procedure reported previously.<sup>18</sup> The resulting second-order rate constants  $k_2$  for the reactions between aryldiazomethanes **1** and benzhydrylium ions **2**, which correspond to the slopes of the plots of the pseudo-first-order rate constants  $k_{\text{obs}}$  vs  $[1]$ , are listed in Table 1. Linear correlations between  $\lg k_2$  and the electrophilicity parameters  $E$  of **2** (Figure 1) indicate the applicability of eq 1. The slopes of the correlation lines and the negative intercepts on the abscissa correspond to the nucleophilicity parameters  $s_N$  and  $N$ , respectively, of **1** (Table 1).

The second-order rate constants for the reactions of **2e-BF<sub>4</sub>** with the aryldiazomethanes listed in Table 1 correlate linearly

**Table 1. Second-Order Rate Constants  $k_2^{\text{exptl}}$  for the Reactions of the Aryldiazomethanes **1** with Benzhydrylium Tetrafluoroborates **2**-BF<sub>4</sub> in Dichloromethane at 20 °C**

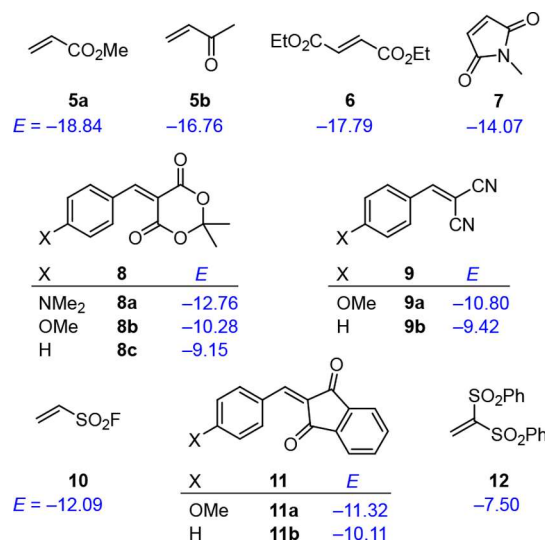
ArCHN <sub>2</sub>	<i>N</i> ( <i>s<sub>N</sub></i> )	electrophile	$k_2^{\text{exptl}}$ (M <sup>-1</sup> s <sup>-1</sup> )
<b>1a</b> (X = H) <sup>a</sup>	9.35 (0.83)	<b>2g</b>	$7.56 \times 10^{-1}$
		<b>2e</b>	$1.19 \times 10^2$
		<b>2d</b>	$5.80 \times 10^2$
		<b>2b</b>	$6.85 \times 10^3$
		<b>2a</b>	$1.45 \times 10^5$
		<b>2f</b>	8.46
<b>1b</b> (X = Br)	8.87 (0.82)	<b>2e</b>	$3.66 \times 10^1$
		<b>2d</b>	$3.02 \times 10^2$
		<b>2c</b>	$4.59 \times 10^2$
		<b>2b</b>	$2.51 \times 10^3$
		<b>2f</b>	$6.21 \times 10^{-1}$
		<b>2e</b>	4.55
<b>1c</b> (X = CN)	7.66 (0.80)	<b>2c</b>	$4.85 \times 10^1$
		<b>2b</b>	$3.38 \times 10^2$
		<b>2a</b>	$2.93 \times 10^3$
		<b>2e</b>	1.51
		<b>2d</b>	9.49
		<b>2c</b>	$2.16 \times 10^1$
<b>1d</b> (X = NO <sub>2</sub> )	7.17 (0.83)	<b>2e</b>	1.26
		<b>2d</b>	1.26
		<b>2c</b>	$2.16 \times 10^1$
		<b>2b</b>	$1.26 \times 10^2$

<sup>a</sup>Data from ref 18.

with the Hammett substituent constants  $\sigma_p$  ( $r^2 = 0.9909$ ).<sup>21</sup> The resulting Hammett reaction constant of  $\rho = -2.34$  will be discussed in the context of the kinetics of reactions of **1a–d** with Michael acceptors (see below).

**Products of the Reactions of Aryldiazomethanes **1** with Michael Acceptors.** The reactions of the aryldiazomethanes **1a–d** with the Michael acceptors **5–12** (Chart 2) give either pyrazolines (from **5–7** and **10**) or nitrogen-free products (from **8–9** and **11–12**). As shown in Table 2, phenyldiazomethane (**1a**) reacts smoothly with methyl acrylate (**5a**)<sup>22</sup> and methyl vinyl ketone (**5b**) at room temperature, affording the 5-phenyl- $\Delta^2$ -pyrazolines **13a** and **13b** in 98% and

**Chart 2. Michael Acceptors **5–12** and Their Electrophilicity Parameters  $E^a$**



<sup>a</sup>Electrophilicities  $E$  from refs 16 and 23.

68% isolated yield, respectively, via tautomerization of the initially formed  $\Delta^1$ -pyrazolines.

Under similar conditions, diethyl fumarate (**6**) undergoes 1,3-dipolar cycloadditions with aryldiazomethanes **1a** and **1b** to give  $\Delta^1$ -pyrazolines, which tautomerize with formation of 5-aryl- $\Delta^2$ -pyrazolines **14a** as a single diastereomer or **14b** as a mixture of *cis/trans*-isomers.<sup>24</sup> The  $\Delta^1$ -pyrazoline initially formed from maleimide **7** and aryldiazomethane **1b** tautomerizes to give the  $\Delta^2$ -pyrazoline **16** (63%) with the aryl group in conjugation to the double bond. Ethenesulfonyl fluoride (ESF, **10**), employed as a second generation click reagent by Sharpless,<sup>23d,25</sup> also undergoes smooth 1,3-dipolar cycloadditions with aryldiazomethanes **1a**, **1c**, and **1d** and yields the 5-aryl- $\Delta^2$ -pyrazolines **15a–d** by subsequent

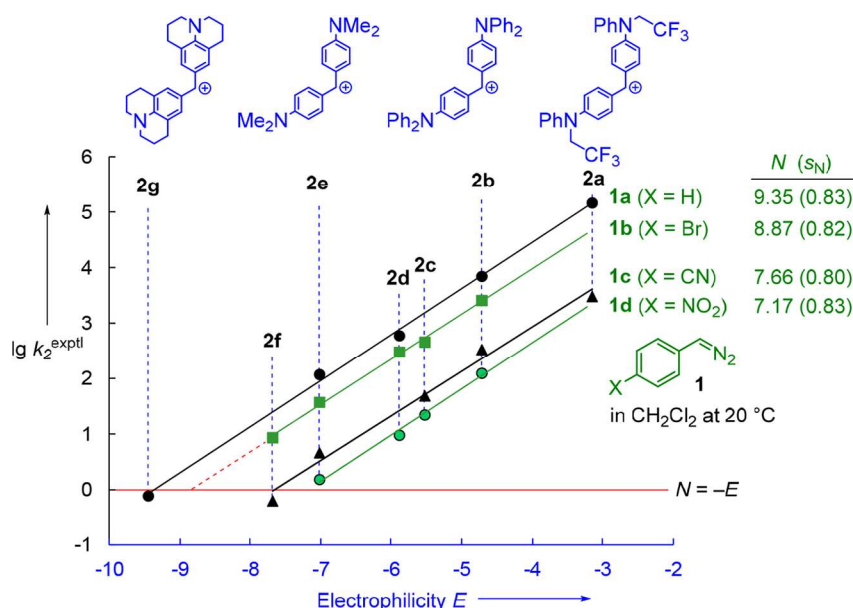
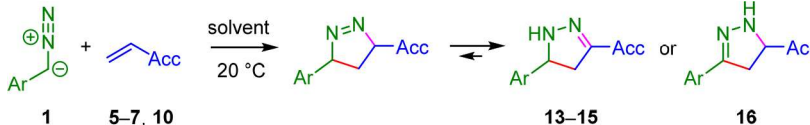


**Figure 1.** Plots of  $\lg k_2^{\text{exptl}}$  for the reactions of the aryldiazomethanes **1a–d** with the reference electrophiles **2a–g** (in CH<sub>2</sub>Cl<sub>2</sub> at 20 °C) versus their electrophilicity parameters  $E$ .

Table 2. Pyrazolines 13–16 Formed by Reactions of the Aryldiazomethanes 1a–d with the Dipolarophiles 5–7 and 10



1	Electrophile	Solvent	Products	Yield (%) <sup>a</sup>
1a	5a	toluene	(±)-13a	98
1a	5b	toluene	(±)-13b	68
1a	6	CH <sub>2</sub> Cl <sub>2</sub>	(±)- <i>trans</i> -14a	48
1b	6	Et <sub>2</sub> O	(±)- <i>trans</i> -14b + (±)- <i>cis</i> -14b	57 + 21
1b	7	CH <sub>2</sub> Cl <sub>2</sub>	(±)-16	63
			X =	
1a	10	toluene	(±)-15a	93
1c	10	toluene	(±)-15c	79
1d	10	toluene	(±)-15d	99

<sup>a</sup>Yield of isolated products.

tautomerization. X-ray crystallography confirmed the structure of 15d (Figure 2).<sup>26</sup>

The reaction of benzylidene Meldrum's acid derivative 8a with 2.5 equiv of phenyldiazomethane (1a) in dichloromethane at 0 °C furnished the cyclopropane (±)-17 in 62% yield (Scheme 3). It is likely that the 1,3-dipolar cycloaddition of 1a with 8a initially leads to pyrazoline F, in analogy to the reactions in Table 2. Subsequent migration of the electron-rich *p*-(dimethylamino)phenyl group and extrusion of molecular nitrogen generates the Michael acceptor G, which undergoes another cycloaddition with a second equivalent of diazoalkane 1a to deliver pyrazoline H. Finally, loss of N<sub>2</sub> from H generates the spirocycle (±)-17, which was purified by column chromatography and isolated as a racemate of a single diastereomer, which was identified by X-ray single crystal structure analysis (Figure 3). We did not search for other diastereomers in the mother liquors and have not explored the origin of the high stereoselectivity of the reaction of G with 1a.

Styrene derivatives 18a,c were obtained through the reactions of 1a,c with bis(phenylsulfonyl)ethene 12 (Figure 4a). Monitoring the reaction of 1c with 12 in CDCl<sub>3</sub> at ambient temperature by <sup>1</sup>H NMR spectroscopy shows the initial formation of 5-aryl-Δ<sup>1</sup>-pyrazoline 19 within several seconds (Figure 4b).<sup>27</sup> The rate of this reaction is too fast to be followed by NMR spectroscopy, but could be determined

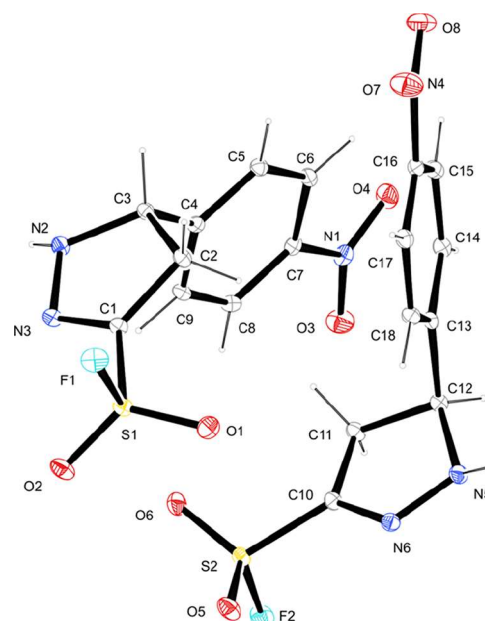
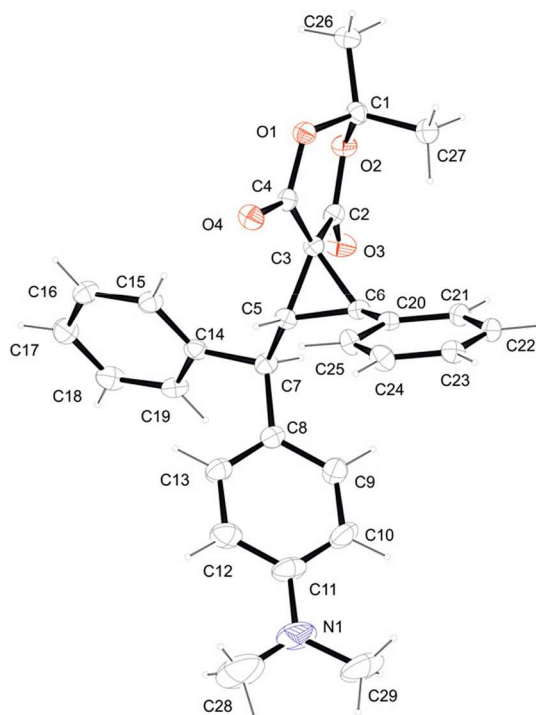
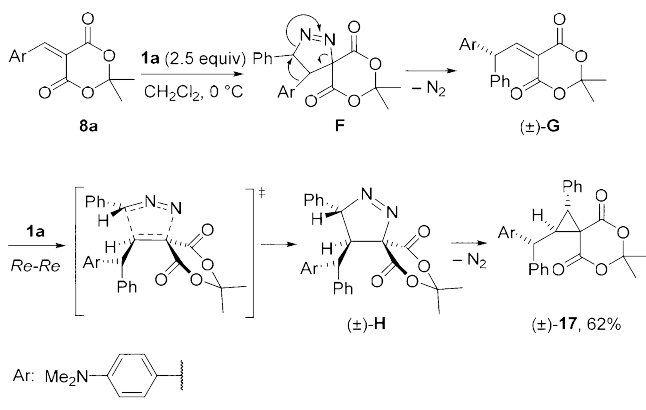


Figure 2. Crystal structure of (±)-15d (ellipsoids are shown on 50% probability level at *T* = 100 K).

**Scheme 3. Reaction of Arylidene Meldrum's Acid 8a with Phenyl diazomethane 1a and Proposed Mechanism for the Formation of (±)-17**



**Figure 3.** Crystal structure of (±)-17 (ellipsoids are shown on 50% probability level at  $T = 100$  K).

by UV-vis spectrometry (see below). As shown by the  $^1\text{H}$  NMR spectra in Figure 4b, **19** undergoes a quick  $\text{N}_2$  elimination accompanied by hydrogen shift<sup>28</sup> and is completely converted into the 1,1-(bis-sulfonyl)-3-aryl-propene **20** within 2 h.<sup>29</sup> On a longer time scale, hydrogen migration converts **20** into **18c**, which was characterized by single crystal X-ray crystallography (Figure 4c).

Benzylidenemalononitrile (**9b**) reacts with phenyl diazomethane (**1a**) in dichloromethane with formation of *trans*-2,3-diphenylcyclopropane **21**<sup>30</sup> (Scheme 4). The *trans*-configuration (that is, the  $C_2$  symmetry) of **22**, which was obtained from **1a** and benzylidene-indane-1,3-dione (**11b**), was derived from the identical  $^{13}\text{C}$  NMR chemical shifts of the carbonyl groups and the AA'BB' system in the  $^1\text{H}$  NMR spectrum for the four aromatic protons of the indan-1,3-dione moiety. Though Schuster and co-workers observed the formation of  $\Delta^1$ -pyrazolines by the reactions of diazomethane

with **9b** or **11b** in diethyl ether at  $-45$  and  $-10$  °C, respectively,<sup>31</sup> it is not certain that **21** and **22** are also formed through initial 1,3-dipolar cycloadditions, because the  $\Delta^1$ -pyrazoline from **9b** with phenyl diazomethane (**1a**) was calculated to be an endergonic species (see below).

**Kinetics of the Reactions of Aryldiazomethanes with Michael Acceptors.** The kinetics of the reactions of aryl diazomethanes **1a–d** with various Michael acceptors from Chart 2 were followed by UV-vis spectroscopy using the methods described previously.<sup>16</sup> Generally, pseudo-first-order conditions were employed. In most cases the dipolarophiles were used in excess ( $>10$  equiv) over **1** and the kinetics were measured by following the decay of the absorbances of the phenyl diazomethanes **1** (295–380 nm, Chart 1). In the reactions with the colored electrophiles **8**, **9**, and **11**, compounds **1** were used in excess, however. The rates of the latter reactions were derived from the time-dependent absorbances of the styrene-chromophore in **8**, **9**, and **11**.

As illustrated for the reaction of **1b** with **10** in Figure 5, the pseudo-first order rate constants  $k_{\text{obs}}$  were obtained by least-squares fitting of the exponential function  $A_t = A_0 \exp(-k_{\text{obs}}t) + C$  to the time-dependent absorbance  $A_t$  of the minor compound. The pseudo-first-order rate constants  $k_{\text{obs}}$  were proportional to the concentrations of the major compounds as shown by the inset of Figure 5, and the slopes of the correlations  $k_{\text{obs}}$  ( $\text{s}^{-1}$ ) vs the concentrations of the excess compounds gave the second-order rate constants  $k_2^{\text{exptl}}$  ( $\text{M}^{-1} \text{s}^{-1}$ ) listed in Table 3.

If the reactions of the phenyl diazomethanes **1** with the acceptor substituted ethylenes **5–12** would proceed stepwise, with rate-determining formation of zwitterionic intermediates, as illustrated in Scheme 5, the observed rate constants should equal those calculated by eq 1 because only one new bond is formed in the rate-determining step, as in the reactions used for deriving the reactivity parameters  $E$ ,  $N$ , and  $s_N$ .<sup>13</sup>

To examine this possibility, we have used eq 1 to calculate the second-order rate constants  $k_2^{\text{calcd}}$  for the formation of the zwitterionic intermediates depicted in Scheme 5 from the one-bond nucleophilicities  $N$  and  $s_N$  of the diazoalkanes **1** (Table 1) and the one-bond electrophilicities  $E$  of the Michael acceptors **5–12** (Chart 2). Table 3 shows that all rate constants  $k_2^{\text{exptl}}$  measured for the reactions of **1a–d** with **8b,c**, **9a**, **11a,b**, and **12** differ by less than a factor of 50 from the rate constants  $k_2^{\text{calcd}}$  calculated by eq 1, while  $k_2^{\text{exptl}}$  is much larger than  $k_2^{\text{calcd}}$  for reactions of **1a–c** with **5a**, **5b**, and **6**.

A graphical illustration of these relationships is presented in Figure 6, where the blue line represents  $k_2^{\text{calcd}}$ , calculated by eq 1 for the formation of zwitterions from **1a** ( $N = 9.35$ ,  $s_N = 0.83$ ) and the electrophiles **5–12** ( $E$  from Chart 2). The shaded area of Figure 6 shows that a fair agreement between  $k_2^{\text{exptl}}$  and  $k_2^{\text{calcd}}$  (deviation  $<$  factor 50) holds for all reactions of phenyl diazomethane (**1a**) with Michael acceptors of  $E > -11$ . The kinetic data thus indicate that the strongest electrophiles of this series either react via zwitterionic intermediates or via nonsynchronous concerted reactions with transition states resembling zwitterions. Table 3 and Figure 6 furthermore show that the deviations between  $k_2^{\text{exptl}}$  and  $k_2^{\text{calcd}}$  increase with decreasing electrophilicities of the Michael acceptors. Whereas the small deviations ( $<$  factor 100) between  $k_2^{\text{exptl}}$  and  $k_2^{\text{calcd}}$  in the right part of Figure 6 cannot reliably be interpreted,<sup>32</sup> the large deviations on the left indicate the operation of a concerted mechanism, and the term  $RT \ln(k_2^{\text{exptl}}/k_2^{\text{calcd}})$  can be considered as a measure for the

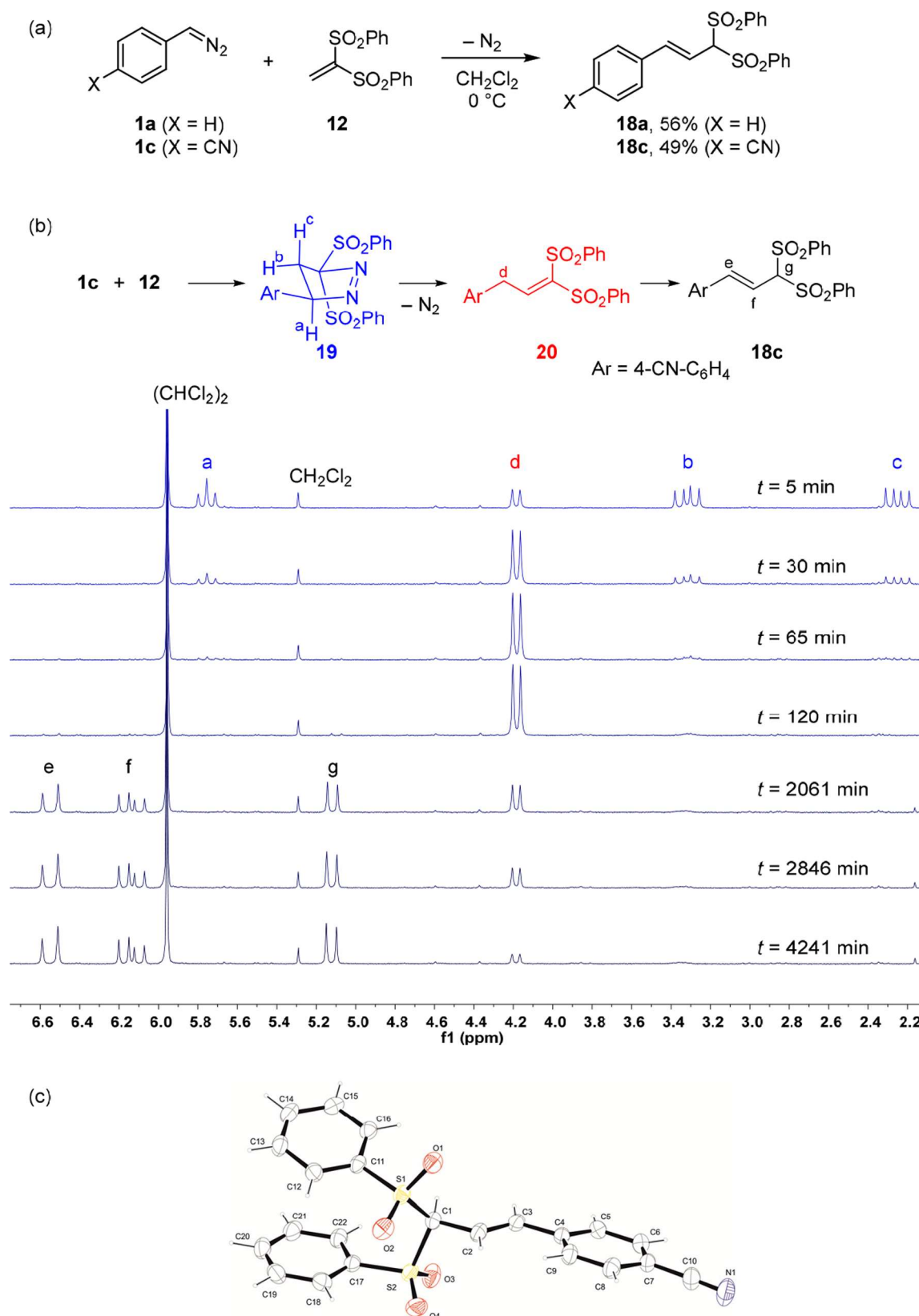
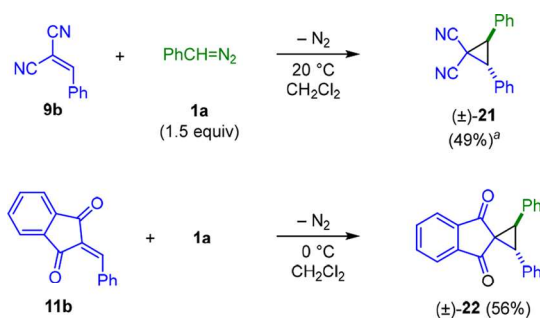


**Figure 4.** (a) Reactions of aryldiazomethanes **1a** and **1c** with bisulfonylene **12**. (b) Mechanism for the formation of **18c** monitored by <sup>1</sup>H NMR spectroscopy (200 MHz) of the reaction mixture [reaction of **1c** (0.10 M) with **12** (0.10 M) in CDCl<sub>3</sub> at 20 °C using 1,1,2,2-tetrachloroethane (0.1 M) as an internal standard]. (c) Crystal structure of **18c** (ellipsoids are shown on 50% probability level at  $T = 173$  K).

## Scheme 4. Reactions of 9b and 11b with Phenyl diazomethane 1a



<sup>a</sup>Determined by <sup>1</sup>H NMR spectroscopy (with 1,1,2,2-tetrachloroethane as an internal standard).

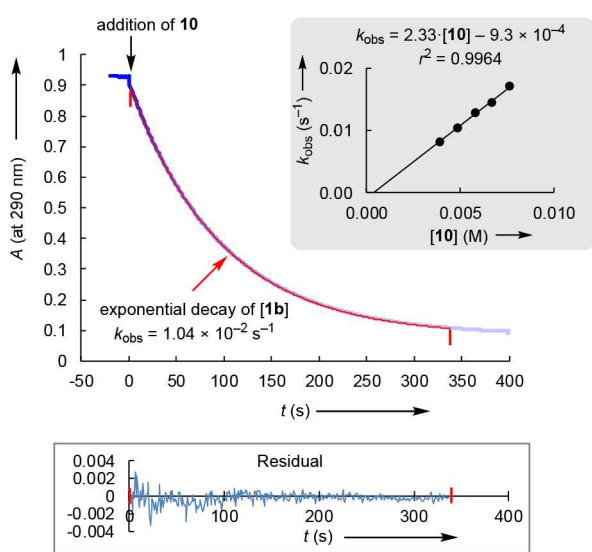


**Figure 5.** Monoexponential decay of the absorbance *A* (at 290 nm) vs time for the reaction of **10** (4.86 × 10<sup>-3</sup> M) with **1b** (8.63 × 10<sup>-5</sup> M) in CH<sub>2</sub>Cl<sub>2</sub> at 20 °C. Inset: Correlation of  $k_{\text{obs}}$  vs the concentration of **10**.

energy of concert (eq 2) due to the stabilization of the transition state by the simultaneous formation of two new bonds (Figure 7).

In line with these interpretations, variation of the nucleophilic reactivities of the diazomethanes **1** affects the rates of the cycloadditions with the highly electrophilic Michael acceptors **12** and **10** to the same degree as the one-bond reactivities toward carbenium ion **2e** (Figure 8a). Comparable charge flows in the transition states of these reactions are thus indicated. The smaller dependence of the rate constants for the reactions with diethyl fumarate (**6**) on the nucleophilicities of the diazomethanes **1** is in accord with a high degree of concertedness of these reactions.

The same conclusion can also be drawn from the Hammett correlations shown in Figure 8b. The Hammett reaction constants for **12** ( $\rho = -2.42$ ) and **10** ( $\rho = -2.61$ ) are of similar magnitude as  $\rho$  for the reactions of **1** with the one-bond electrophile **2e** ( $\rho = -2.34$ ). The reactions of aryldiazomethanes with diethyl fumarate (**6**) in dichloromethane at 20 °C, on the other hand, show a significantly less negative reaction constant ( $\rho = -1.58$ ) indicating a smaller degree of negative charge transfer in the transition states. A similar

Hammett reaction constant of  $\rho = -1.30$ <sup>33</sup> can be derived from the rate constants which Huisgen and Geittner reported for the reactions of eight ring-substituted aryldiazomethanes with ethyl acrylate in DMF at 25 °C.<sup>22a</sup>

The dependence of rate constants on solvent polarity has often been used as a criterion to differentiate concerted cycloadditions from cycloadditions through zwitterionic intermediates.<sup>22b,34</sup> Whereas [2 + 2] cycloadditions of tetracyanoethylene with enol ethers, which proceed via zwitterionic intermediates, are 3–4 orders of magnitude faster in acetonitrile than in cyclohexane,<sup>34,35</sup> the solvent dependence of various Diels–Alder reactions of tetracyanoethylene is so small that there are no significant correlations with any of the known solvent polarity parameters.<sup>36</sup>

Solvent dependences of the rates of 1,3-dipolar cycloadditions were reported to be generally rather small. While the rate constants for the reactions of phenyl diazomethane (**1a**) with ethyl acrylate increased by a factor of 2.4 from cyclohexane to acetonitrile at 25 °C and correlated fairly with Reichardt's  $E_T$  values,<sup>37</sup> the rates of the corresponding reactions with norbornene were almost independent of solvent polarity.<sup>22b</sup>

Table 4 shows that the reactions of phenyl diazomethane (**1a**) with the Michael acceptors **6** and **9–12** proceed slightly faster in the polar solvents acetonitrile and DMSO than in dichloromethane or THF. Though **12**, the strongest electrophile of the investigated Michael acceptors, showed the largest, and **6**, the weakest among the investigated electrophiles, showed the smallest solvent dependence, Table 4 does not reveal a clear correlation between electrophilicity of the dipolarophile and the magnitude of the solvent effect.

**Quantum Chemical Calculations of the Cycloadditions.** Details of the reaction pathways for the reactions of phenyl diazomethane (**1a**) with selected electrophiles have been calculated using the same quantum chemical methods as in our recent quantitative analysis of ketone reactivity.<sup>38</sup> This involves geometry optimizations at the (U)B3LYP<sup>39</sup>-D3<sup>40</sup>/6-31+G(d,p)<sup>41</sup> level of theory in combination with the polarizable continuum model (PCM) for dichloromethane and UA0 radii.<sup>42</sup> Thermochemical corrections to Gibbs energies (Corr.  $\Delta G$ ) and enthalpy (Corr.  $\Delta H$ ) at 298.15 K have been calculated using the rigid rotor/harmonic oscillator model without any scaling. Single point calculations have also been performed for all stationary points at the PCM-(CH<sub>2</sub>Cl<sub>2</sub>,UA0)/(U)B2PLYP<sup>43</sup>-D3/def2TZVPP<sup>44</sup> level in order to verify the validity of all mechanistic conclusions (see the Supporting Information). Given the slightly better agreement between experimentally measured Gibbs activation energies with those calculated at the PCM(CH<sub>2</sub>Cl<sub>2</sub>,UA0)/(U)B3LYP-D3/6-31+G(d,p) level used for geometry optimization, only the latter results will be discussed in the following.

Figure 9 compares the Gibbs energy profiles for the reactions of phenyl diazomethane (**1a**) with five representative electrophiles. The initially formed encounter complexes, which are minima in potential energy, are omitted in these energy profiles, as they are endergonic species ( $\Delta_r G^0 > 0$ ) and do not affect the kinetics. In all five cases, concerted (3 + 2)-cycloadditions are calculated to be the minimum energy pathways with Gibbs energies of activation, which agree within 5 kJ mol<sup>-1</sup> with the experimental  $\Delta G^\ddagger$  obtained by applying the experimental rate constants  $k_2$  from Table 3 in the Eyring equation. The direct formation of the thermodynamically

**Table 3.** Second-Order Rate Constants of Reactions between Aryldiazomethanes (1a–d) and Michael Acceptors (5–12) in Dichloromethane at 20 °C

ArCHN <sub>2</sub>	electrophile	$k_2^{\text{exptl}}$ (M <sup>-1</sup> s <sup>-1</sup> )	$k_2^{\text{calcd}}$ (M <sup>-1</sup> s <sup>-1</sup> ) <sup>a</sup>	$k_2^{\text{exptl}}/k_2^{\text{calcd}}$	$\Delta G_{\text{concert}}^{\ddagger}$ (kJ mol <sup>-1</sup> )
1a	5a	$4.87 \times 10^{-2}$	$1.33 \times 10^{-8}$	$3.7 \times 10^6$	37
	5b	$2.22 \times 10^{-1}$	$7.07 \times 10^{-7}$	$3.1 \times 10^5$	31
	6	$4.05 \times 10^{-1}$	$9.88 \times 10^{-8}$	$4.1 \times 10^6$	37
	8a	$3.33 \times 10^{-1}$	$1.48 \times 10^{-3}$	$2.3 \times 10^2$	– <sup>b</sup>
	8b	7.58	$1.69 \times 10^{-1}$	$4.5 \times 10^1$	– <sup>b</sup>
	8c	$4.80 \times 10^1$	1.47	$3.3 \times 10^1$	– <sup>b</sup>
	9a	$1.51 \times 10^{-2}$	$6.26 \times 10^{-2}$	$2.4 \times 10^{-1}$	– <sup>b</sup>
	10	6.81	$5.32 \times 10^{-3}$	$1.3 \times 10^3$	17
	11a	$2.38 \times 10^{-1}$	$2.32 \times 10^{-2}$	$1.0 \times 10^1$	– <sup>b</sup>
	11b	1.45	$2.34 \times 10^{-1}$	6.2	– <sup>b</sup>
	12	$1.48 \times 10^3$	$3.43 \times 10^1$	$4.3 \times 10^1$	– <sup>b</sup>
1b	6	$2.34 \times 10^{-1}$	$4.85 \times 10^{-8}$	$4.8 \times 10^6$	37
	7	$8.46 \times 10^{-1c}$	$5.45 \times 10^{-5}$	$1.6 \times 10^4$	24
	10	2.33	$2.29 \times 10^{-3}$	$1.0 \times 10^3$	17
1c	12	$6.59 \times 10^2$	$1.33 \times 10^1$	$5.0 \times 10^1$	– <sup>b</sup>
	6	$3.87 \times 10^{-2}$	$7.87 \times 10^{-9}$	$4.9 \times 10^6$	38
	10	$1.83 \times 10^{-1}$	$2.86 \times 10^{-4}$	$6.4 \times 10^2$	16
1d	12	$4.56 \times 10^1$	1.34	$3.4 \times 10^1$	– <sup>b</sup>
	7	$1.74 \times 10^{-2}$	$1.87 \times 10^{-6}$	$9.3 \times 10^3$	22
	10	$5.82 \times 10^{-2}$	$8.25 \times 10^{-5}$	$7.1 \times 10^2$	16
12	12	$2.16 \times 10^1$	$5.32 \times 10^{-1}$	$4.1 \times 10^1$	– <sup>b</sup>

<sup>a</sup>Calculated by eq 1 with  $N$  and  $s_N$  from Table 1 and  $E$  from Chart 2. <sup>b</sup>Too small to be significant (see text). <sup>c</sup>Determined by <sup>1</sup>H NMR spectroscopy.

### Scheme 5. Stepwise 1,3-Dipolar Cycloadditions of Aryldiazomethanes with Acceptor-Substituted Ethylenes

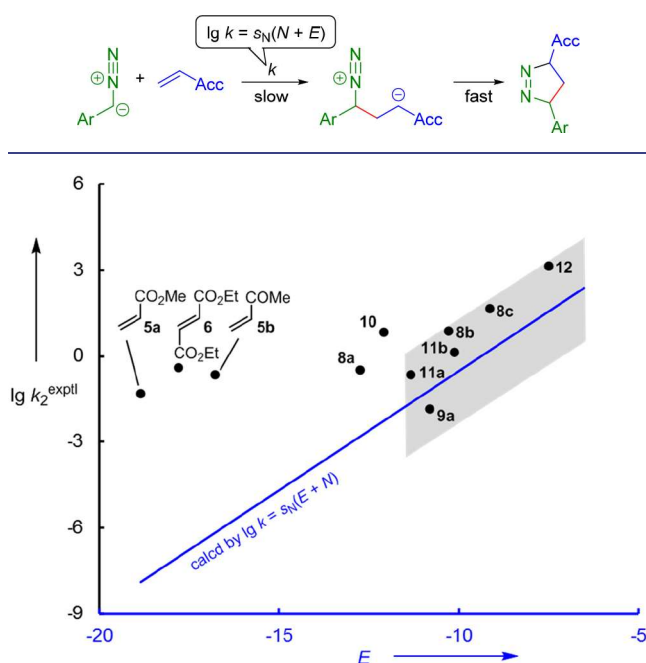


**Figure 6.** Correlation of  $\lg k_2^{\text{exptl}}$  for the reactions between the Michael acceptors 5–12 and phenyldiazomethane (1a) versus the electrophilicity parameters  $E$  of the Michael acceptors.

favored cyclopropanes (+ N<sub>2</sub>) from the reactants generally requires higher activation energies. This suggests that also in those reactions listed in Table 3, where pyrazoline formation was not observed as in the reactions with 5a, 10, and 12,  $\Delta^1$ -pyrazolines are the initially formed products, which may undergo subsequent reactions.

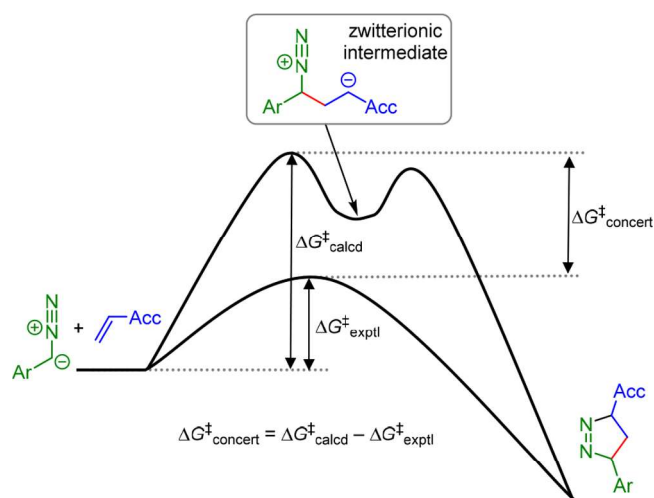


**Figure 7.** Comparison of measured activation Gibbs energies  $\Delta G_{\text{exptl}}^{\ddagger}$  with  $\Delta G_{\text{calcd}}^{\ddagger}$  calculated for the formation of zwitterions from  $E$ ,  $N$ , and  $s_N$  by eq 1.

The calculated high Gibbs energy of the  $\Delta^1$ -pyrazoline from 1a and 9a indicates, however, that in this case conversion of the cycloadduct into the isolated cyclopropane and not the 1,3-dipolar cycloaddition may be rate-determining. This interpretation is supported by the observation that 9a is the only Michael acceptor which is below the calculated line in Figure 6. The excellent agreement between the measured rate constants for the reaction of 1a with 9a and that calculated for the 1,3-dipolar cycloaddition in Figure 9 indicates, on the other hand, that the barrier for nitrogen expulsion from the corresponding  $\Delta^1$ -pyrazoline cannot be much higher than that for retroaddition.

As shown by the geometrical parameters in Figure 10, the development of the new C–N bond lags far behind that of the

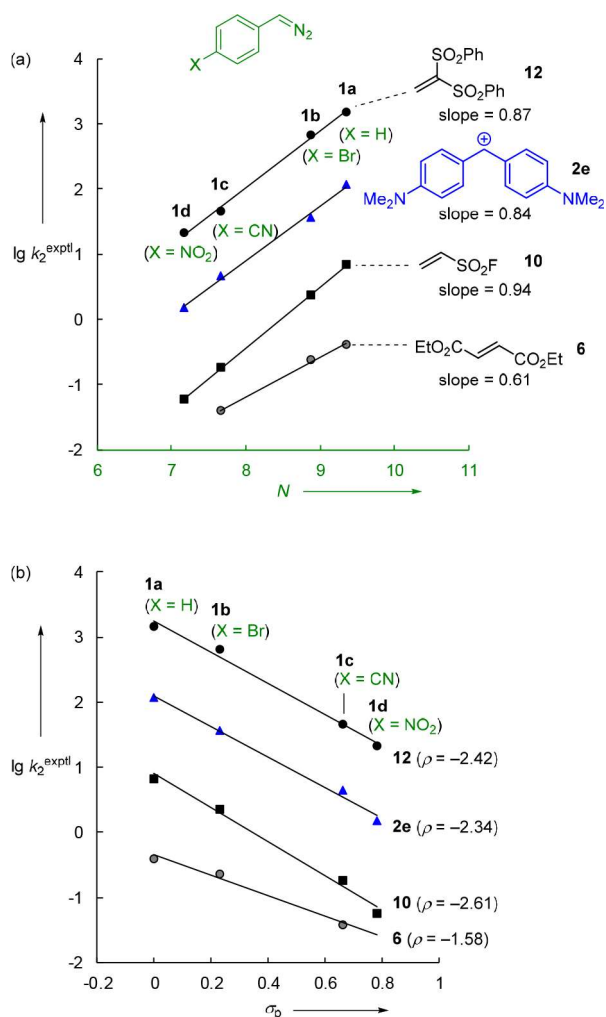


**Figure 8.** Correlation of  $\lg k_2^{\text{exptl}}$  for the reactions of the electrophiles 2e, 6, 10, and 12 with the aryl diazomethanes 1a–d (from Tables 1 and 3) versus (a) the nucleophilicity parameters  $N$  of aryl diazomethanes (from Table 1) and (b) Hammett substituent constants  $\sigma_p$  (from ref 21) for 1a–d.

new C–C bond in all transition states, whereas both bonds have almost equal lengths in the resulting  $\Delta^1$ -pyrazolines. Figure 10 furthermore shows that the atomic distances in the two developing new bonds differ much more in the transition states of the highly electrophilic dipolarophiles ( $\Delta = 0.5\text{--}0.7$  Å for  $E > -11$ ) than in the transition state for the reaction with methyl acrylate (5a,  $\Delta = 0.3$  Å) for which a high degree of concertedness was derived from the kinetic data in Figure 6. This conclusion is confirmed by the relative bond orders (%  $E_V$ ) and the amount of charge transfer from nucleophilic

diazomethane to electrophilic dipolarophile in the transition states (Figure 10). The latter parameter increases from  $-0.2$  e in the transition state of 5a to  $-0.43$  e in the most asynchronous transition state for 8c.

Though the data in Figure 10 are in line with highly unsymmetrical transition states in the reactions of phenyldiazomethane (1a) with highly electrophilic dipolarophiles, the question arises, how the concerted 1,3-dipolar cycloaddition mechanisms, derived from the quantum chemical calculations, concur with the zwitterion-like transition states derived from the kinetic data in Figure 6. Figure 9 shows that, on their way to cyclopropanes, the reactions of 1a with 8c ( $E = -9.15$ ) or 12 ( $E = -7.50$ ) initially yield zwitterions over barriers which are only 7 and 17 kJ mol<sup>-1</sup> higher than the barriers for the concerted reactions, indicating that in the case of strong electrophiles ( $E > -11$ ) concerted and stepwise cycloadditions proceed over comparable barriers. Obviously the interaction between the reaction centers at the “long” new bonds is so weak that the energy of the transition state is hardly affected. As a consequence, the one-bond nucleophilicities of the diazomethanes ( $N$ ,  $s_N$ ) and the one-bond-electrophilicities of the dipolarophiles ( $E$ ) are suitable to calculate the rates of such cycloadditions by eq 1.

Following the distortion interaction analysis of 1,3-dipolar cycloadditions by Houk et al. and by Bickelhaupt et al.,<sup>10</sup> we dissected the reaction barriers of the five reactions in Figure 9 into the distortion energies for deforming the two reactants into their transition state geometries and the interaction energies of the two distorted reactants when brought together into the transition state structure. As this procedure is based on single point energy calculations in the absence of thermal corrections, the resulting reaction barriers given in Figure 11 are much lower than the Gibbs energies reported in Figure 9. In agreement with earlier results by Houk and Ess for the reaction of methyl acrylate (5a) with diazomethane,<sup>10b</sup> we found that, in the highly concerted cycloaddition of 1a with 5a ( $E = -18.84$ ), the electrophile distortion energy is much smaller (27 kJ mol<sup>-1</sup>) than that for the diazoalkane (69 kJ mol<sup>-1</sup>). As the transition states become more unsymmetrical, the distortion energies of the electrophilic alkene grow and the distortion energies of the nucleophilic 1,3-dipole shrink with the consequence that, for the four highly unsymmetrical cycloadditions in Figure 11, the 1,3-dipole distortion energies are only slightly larger (in the case of 8c even smaller) than the dipolarophile distortion energies. According to this treatment, the higher reactivities of the more electrophilic dipolarophiles are predominantly due to the higher interaction energies.

**Quantum Chemical Analysis of the Subsequent Reactions of the  $\Delta^1$ -Pyrazolines.** As described in the subsection “Products of the Reactions of Aryldiazomethanes 1 with Michael Acceptors”, the initially generated  $\Delta^1$ -pyrazolines

**Table 4.** Second-Order Rate Constants  $k_2^{\text{exptl}}$  of the Reactions between Phenyldiazomethane (1a) and Michael Acceptors (6, 9–12) in Different Solvents at 20 °C

solvent	$\epsilon_r^a$	$E_T(30)^a$	$k_2^{\text{exptl}}$ (M <sup>-1</sup> s <sup>-1</sup> )				
			6 ( $E = -17.79$ )	10 ( $E = -12.09$ )	9a ( $E = -10.80$ )	11b ( $E = -10.11$ )	12 ( $E = -7.50$ )
DMSO	46.45	45.1	2.16	32.0	$1.16 \times 10^{-1}$	7.63	$8.00 \times 10^3$
CH <sub>3</sub> CN	35.94	45.6		13.5	$5.27 \times 10^{-2}$	3.18	
CH <sub>2</sub> Cl <sub>2</sub>	8.93	40.7	$4.05 \times 10^{-1}$	6.81	$1.51 \times 10^{-2}$	1.45	$1.48 \times 10^3$
THF	7.58	37.4	$4.08 \times 10^{-1}$	3.03		1.00	$6.21 \times 10^2$

<sup>a</sup>Relative permittivity ( $\epsilon_r$ ) and  $E_T(30)$  were taken from ref 37.

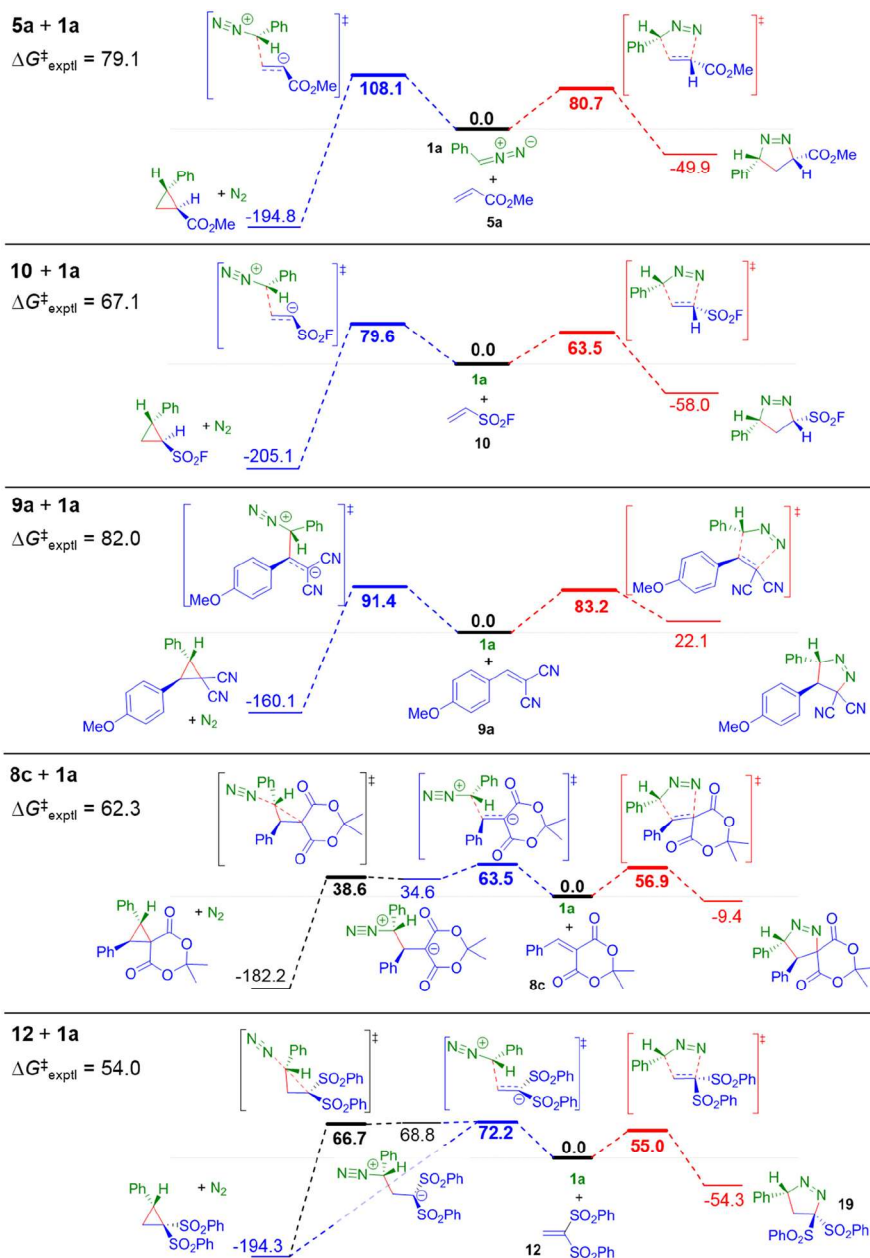


**Figure 9.** Energy profiles ( $\Delta G_{\text{sol}}^{\ddagger}$  in  $\text{kJ mol}^{-1}$ ) for the reactions of **5a**, **10**, **9a**, **8c**, and **12** with **1a** calculated at the PCM(UA0,CH<sub>2</sub>Cl<sub>2</sub>)/(U)B3LYP-D3/6-31+G(d,p) level of theory.

were never isolated from the reactions of the aryldiazomethanes **1** with the Michael acceptors **5–12**. The isolated products were either  $\Delta^2$ -pyrazolines or nitrogen-free products.

Calculation of the relative stabilities of the pyrazoline tautomers obtained from **1a** and methyl acrylate (**5a**) and ESF (**10**) showed that the  $\Delta^1$ -pyrazolines are, indeed, the least stable tautomers (Scheme 6). However, according to Table 2, generally not the most stable tautomers with phenyl in conjugation with the endocyclic double bond were isolated but the tautomers with the acceptor group in conjugation with the double bond (exception: the bicyclic cycloadduct from maleimide **7**). Obviously, it is the higher acidity of the proton in  $\alpha$ -position to the acceptor group that controls the mode of tautomerization.

As discussed above, according to Figure 9,  $\Delta^1$ -pyrazolines should be the initial reaction products in all investigated cases.

The formation of the cyclopropanes **21** and **22** (described in Scheme 4) may, therefore, proceed via retroaddition of the initially formed  $\Delta^1$ -pyrazolines to give the starting materials, which subsequently proceed to the cyclopropanes over the higher barriers on the left side of Figure 9. This pathway appears feasible, in particular for the reaction of **1a** with **9a**, since in this case the corresponding  $\Delta^1$ -pyrazoline is an endergonic adduct according to Figure 9.

Alternatively, the cyclopropanes may be formed through the direct conversion of the  $\Delta^1$ -pyrazolines. Figure 12 shows a possible transition state for such a transformation and also rationalizes the transformation of the  $\Delta^1$ -pyrazoline **19** into the bisulfonylekene **20**. Elongation of both C–N bonds leads to an activated complex ( $\Delta G^{\ddagger} = 75.3 \text{ kJ mol}^{-1}$ ) on a flat surface, which may transform into N<sub>2</sub> complexes of a 1,3-zwitterion, an oxathiolane, or a cyclopropane, which are minima on the

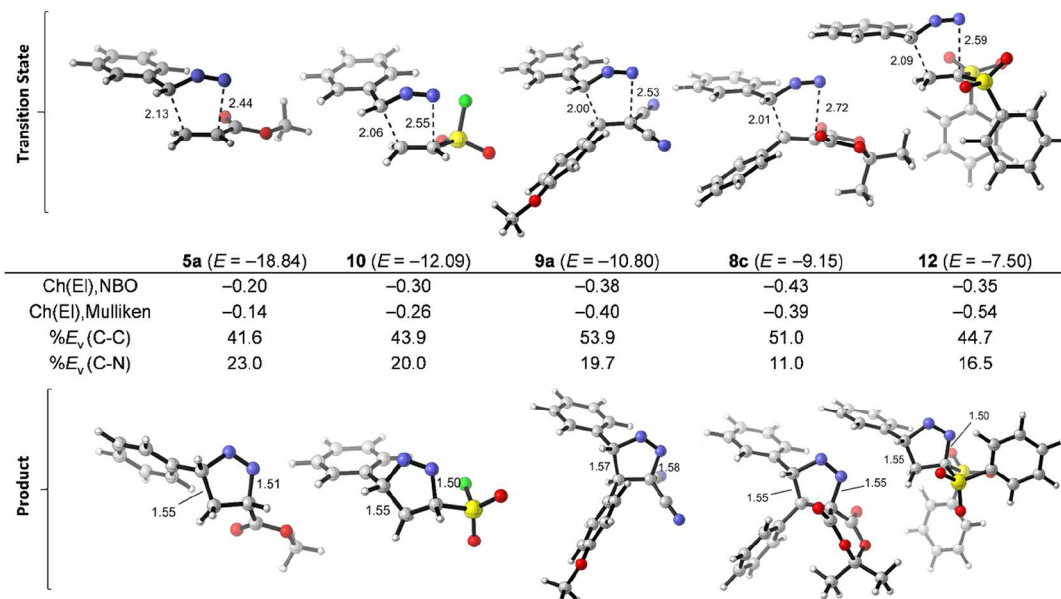


**Figure 10.** Charge on electrophilic dipolarophile [Ch(El)] and percentage of evolution of the bond order (% $E_v$ ) in the transition states for the reactions of phenyldiazomethane (1a) with the electrophiles 5a, 10, 9a, 8c, and 12. Charges (NBO6 and Mulliken) and % $E_v$  (Wiberg indices) are calculated at the PCM(UA0,CH<sub>2</sub>Cl<sub>2</sub>)/(U)B3LYP-D3/6-31+G(d,p) level of theory. Distances are shown in Å.

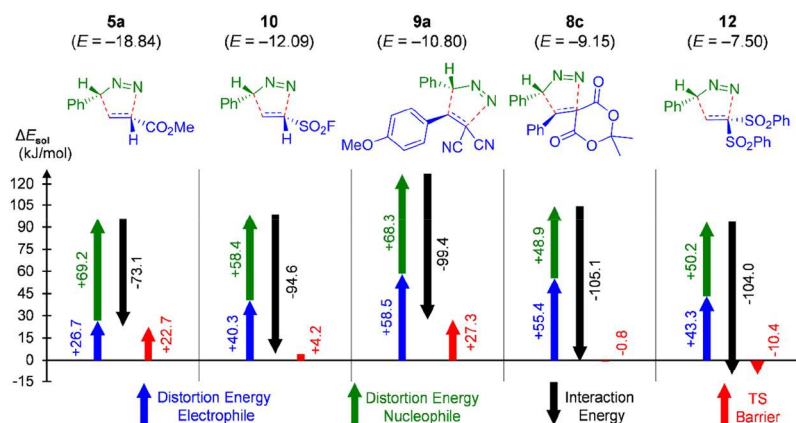
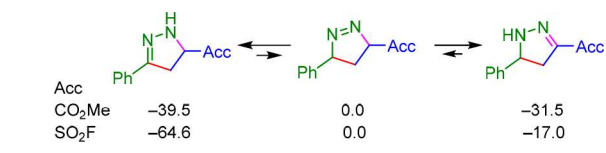


**Figure 11.** Distortion-interaction analysis (DIA,  $\Delta E_{sol}$ , kJ mol<sup>-1</sup>) for the reactions of phenyldiazomethane (1a) with the electrophiles 5a, 10, 9a, 8c, and 12. DIA is performed at the PCM(UA0,CH<sub>2</sub>Cl<sub>2</sub>)/(U)B3LYP-D3/6-31+G(d,p) level of theory.

**Scheme 6. Relative Stabilities ( $\Delta G_{sol}$ , in kJ mol<sup>-1</sup>) of the Tautomers Obtained from Reactions of Phenyldiazomethane (1a) with Methyl Acrylate (5a) or ESF (10) Calculated at the PCM(UA0,CH<sub>2</sub>Cl<sub>2</sub>)/(U)B3LYP-D3/6-31+G(d,p) Level of Theory**



potential energy surface but not on the Gibbs energy surface and, therefore, immediately lose N<sub>2</sub>. According to Figure 12, the barriers for the conversion of the oxathiolane (+78.6 kJ mol<sup>-1</sup>) as well as of the cyclopropane intermediate (+163 kJ mol<sup>-1</sup>) into 20 are higher than the barrier to form these intermediates from 19. Since we did not observe any intermediates during conversion of 19 into 20 (Figure 4), we have to conclude that the alkene 20 is exclusively formed via the 1,3-zwitterion route shown in red in Figure 12. The

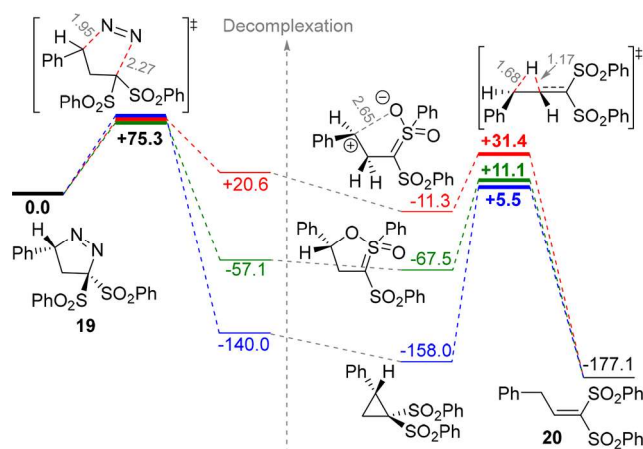


**Figure 12.** Energy profiles ( $\Delta G_{sol}$ , kJ mol<sup>-1</sup>) for the conversion of 19 into 20 (N<sub>2</sub> elimination accompanied by H shift) calculated at the PCM(UA0,CH<sub>2</sub>Cl<sub>2</sub>)/(U)B3LYP-D3/6-31+G(d,p) level of theory. Distances are shown in Å.

untypically high barrier for 1,2-hydride migration in the intermediate 1,3-zwitterion to give **20** can be assigned to the nonbonding interactions of the formal carbocation center with one of the sulfonyl oxygen atoms.

An analogous concerted extrusion of N<sub>2</sub> may account for the formation of the cyclopropanes **21** and **22** from **9b** and **11b**, respectively (Scheme 4).

## CONCLUSION

The differentiation between concerted and stepwise processes has intrigued chemists for many years. In 1962, Doering and Roth used the term “No-mechanism” for so-called “thermoreorganization” reactions like the Diels–Alder and Cope and Claisen rearrangements, in which no involvement of intermediates was detectable.<sup>45</sup> A common rationale for such pericyclic reactions was provided in 1969 by Woodward and Hoffman’s orbital symmetry rules.<sup>46</sup> In his seminal 1984 article entitled “Multibond Reactions Cannot Normally Be Synchronous”, Dewar argued that even concerted cycloadditions proceed via transition states resembling intermediate biradicals or zwitterions.<sup>47</sup> Alabugin and co-workers demonstrated that the diradical/zwitterion dichotomy also applies to cycloaromatization reactions.<sup>48</sup> In this Article, we have introduced a linear free energy approach to measure the energy of concert, i.e., the difference between the activation energies of concerted 1,3-dipolar cycloadditions and of the corresponding stepwise processes via zwitterions.

We have shown that aryldiazomethanes undergo concerted, nonsynchronous 1,3-dipolar cycloadditions with electron-deficient CC-double bonds to give  $\Delta^1$ -pyrazolines, which are subsequently transformed into  $\Delta^2$ -pyrazolines, cyclopropanes, or substituted ethylenes. The direct formation of cyclopropanes from the reactants involves higher barriers and does not usually take place. Though the transformation of the  $\Delta^1$ -pyrazolines into cyclopropanes may proceed via nitrogen extrusion from the  $\Delta^1$ -pyrazolines and formation of intermediate 1,3-zwitterions, as illustrated in Figure 12, retroaddition with regeneration of the reactants and subsequent reaction over the higher barriers as shown on the left side of Figure 9 cannot generally be excluded.

The excellent agreement between experimental activation energies and quantum-chemically calculated values at the PCM(UA0,CH<sub>2</sub>Cl<sub>2</sub>)/(U)B3LYP-D3/6-31+G(d,p) level of theory for the cycloadditions shown in Figure 9 confirms the high reliability of the employed polarizable continuum model (PCM) to consider solvation. Charge densities and geometrical parameters of the transition states depicted in Figure 10 indicate that the nonsynchronicity of the cycloadditions increases with increasing electrophilicity of the acceptor-substituted ethylenes. Figure 6 shows that the measured rate constants for the cycloadditions of phenyldiazomethane (**1a**) with highly reactive Michael acceptors ( $E > -11$  in Chart 2) are almost identical to those calculated by eq 1 from the one-bond nucleophilicities  $N$  and  $s_N$  of **1a** (Table 1) and the one-bond electrophilicities  $E$  of **5–12** (compiled with many other  $E$  parameters in a freely accessible online database<sup>14</sup>). This agreement indicates that the Gibbs activation energies for the concerted nonsynchronous cycloadditions of the highly electrophilic dipolarophiles closely resemble those for hypothetical stepwise cycloadditions via zwitterionic intermediates and that in these cases the formation of the new C–N bond cannot contribute significantly to the stabilization of the transition state of the concerted processes. The last two

examples in Figure 9 confirm the similar magnitude of the Gibbs activation energies for the concerted cycloadditions and the formation of zwitterions from the strong electrophiles **8c** and **12**. On the other hand, Figure 6 illustrates that less electrophilic dipolarophiles (such as, for example, methyl acrylate **5a**) react much faster with phenyldiazomethane (**1a**) than calculated by eq 1, and the ratio  $k_2^{\text{exptl}}/k_2^{\text{calcd}}$  is suggested as a measure for concertedness (eq 2, Figure 7).

Correlations between measured rate constants and LUMO energies exist only for narrow subgroups of Michael acceptors sharing structural similarity at the site of nucleophilic attack. This is seen for the terminally unsubstituted electrophiles (**5a**, **5b**, **10**, and **12**) or for the aryldiene Meldrum’s acid derivatives (**8a–8c**) in Figure 13a. For a larger set of electrophiles,

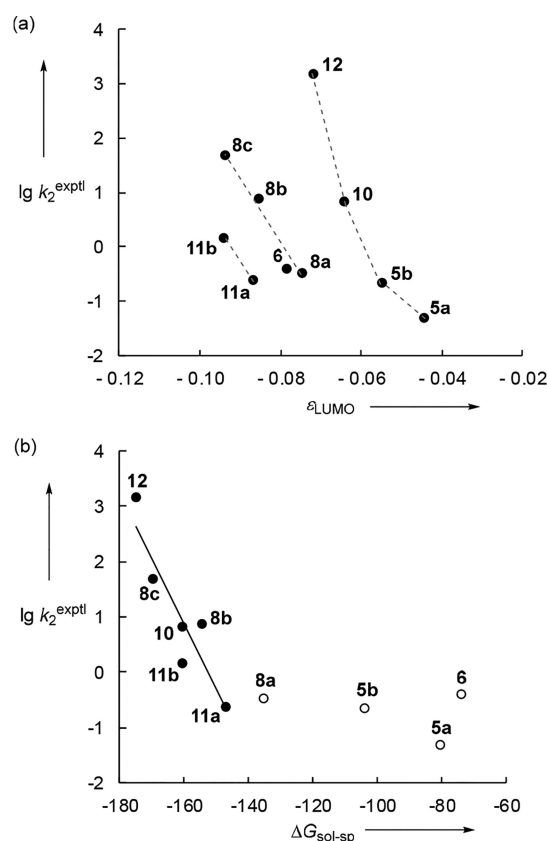


**Figure 13.** Second-order rate constants  $\lg k_2^{\text{exptl}}$  for the reactions of **1a** with diverse electrophiles (from Table 3) correlated with (a) quantum-chemically calculated LUMO energies ( $\epsilon_{\text{LUMO}}$  in Hartree, from ref 16) and (b) methyl anion affinities  $\Delta G_{\text{sol-sp}}$  (in kJ mol<sup>-1</sup>, from ref 16, correlation line refers to electrophiles of  $E > -11$  in Chart 2. Data for **9a** excluded because formation of the  $\Delta^1$ -pyrazoline is not rate-determining, see main text.

however, neither the LUMO energies (Figure 13a) nor the global ( $\omega$ ) or the local ( $\omega_{\beta}$ ) Parr electrophilicity index serve as reliable descriptors of their reactivities (see the Supporting Information).

Figure 13b shows, however, that the cycloaddition rate constants of the highly electrophilic Michael acceptors (that is, those with  $E > -11$  in Chart 2) correlate with their quantum-chemically calculated methyl anion affinities ( $\Delta G_{\text{sol-sp}}$ ). This is a consequence of the correlation between cycloaddition rate constants and electrophilicities  $E$  of these Michael acceptors shown in Figure 6 and the previously reported linear

correlation between the electrophilicities  $E$  of a large variety of Michael acceptors and their calculated methyl anion affinities.<sup>16</sup> As the correlation between the rate constants for the 1,3-dipolar cycloadditions and electrophilicities  $E$  breaks down for weaker electrophiles (that is, **8a**, **5b**, **5a**, and **6** with  $E < -11$ , Figure 6) the cycloaddition rate constants for these electrophiles also do not correlate with the corresponding methyl anion affinities (Figure 13b). While the methyl anion affinities of **8a**, **5b**, **5a**, and **6** cover a range of 70 kJ mol<sup>-1</sup>, the rate constants for the (3 + 2)-cycloadditions with **1a** vary only within 1 order of magnitude, in line with the smaller amount of charge transfer in the transition states of these reactions.

Though the empirical electrophilicity parameters  $E$  (according to eq 1) thus do not allow to rank cycloaddition rates of less electrophilic dipolarophiles, the possibility to predict absolute rate constants for highly asynchronous 1,3-dipolar cycloadditions from the reactivity parameters  $E$ ,  $N$ , and  $s_N$  represents a new tool, and we are currently investigating the applicability of this approach to other types of 1,3-dipolar cycloadditions.

## ■ ASSOCIATED CONTENT

### 📄 Supporting Information

The Supporting Information is available free of charge on the ACS Publications website at DOI: 10.1021/jacs.8b09995.

Details of the product studies, X-ray structures of **15d**, **17**, and **18c**, kinetic experiments, computational analysis, and NMR spectra of all characterized compounds (PDF)

Coordinates of optimized structures (ZIP)

Crystallographic data for **15d** (tv444), **17** (vv089), and **18c** (uo090) (CIF)

## ■ AUTHOR INFORMATION

### Corresponding Authors

\*ofial@lmu.de

\*zipse@cup.uni-muenchen.de

\*herbert.mayr@cup.uni-muenchen.de

### ORCID

Armin R. Ofial: 0000-0002-9600-2793

Hendrik Zipse: 0000-0002-0534-3585

Herbert Mayr: 0000-0003-0768-5199

### Present Addresses

‡Q.C.: Novalde GmbH, 01307 Dresden, Germany.

§I.Z.: Merck KGaA, 64293 Darmstadt, Germany.

### Author Contributions

†H.J. and Q.C. contributed equally to this work.

### Notes

The authors declare no competing financial interest.

## ■ ACKNOWLEDGMENTS

Dedicated to Professor Kendall N. Houk on the occasion of his 75th birthday. We thank the Deutsche Forschungsgemeinschaft (SFB 749, Projects B1 and C6) for financial support and the Leibniz Supercomputing Centre ([www.lrz.de](http://www.lrz.de)) for generous allocation of computational resources.

## ■ REFERENCES

(1) (a) Huisgen, R. 1,3-Dipolar Cycloadditions. Past and Future. *Angew. Chem., Int. Ed. Engl.* **1963**, *2*, 565–598. (b) Huisgen, R. 1,3-Dipolar Cycloadditions – Introduction, Survey, Mechanism. In *1,3-*

*Dipolar Cycloaddition Chemistry* Vol. 1; Padwa, A., Ed.; Wiley: New York, 1984; Chapter 1, pp 1–176. (c) Wang, L.-J.; Tang, Y. Intermolecular 1,3-dipolar cycloadditions of alkenes, alkynes, and allenes. In *Comprehensive Organic Synthesis*, 2nd ed.; Knochel, P., Molander, G. A., Eds.; Elsevier: Amsterdam, 2014; Vol. 4, pp 1342–1383. (d) Menon, R. S.; Nair, V. Intramolecular 1,3-dipolar cycloadditions of alkenes, alkynes, and allenes. In *Comprehensive Organic Synthesis*, 2nd ed.; Knochel, P., Molander, G. A., Eds.; Elsevier: Amsterdam, 2014; Vol. 4, pp 1281–1341. (e) Huisgen, R. Steric course and mechanism of 1,3-dipolar cycloadditions. *Adv. Cycloaddit.* **1988**, *1*, 1–31. (f) Singh, M. S.; Chowdhury, S.; Koley, S. Progress in 1,3-dipolar cycloadditions in the recent decade: an update to strategic development towards the arsenal of organic synthesis. *Tetrahedron* **2016**, *72*, 1603–1644. (g) Hashimoto, T.; Maruoka, K. Recent Advances of Catalytic Asymmetric 1,3-Dipolar Cycloadditions. *Chem. Rev.* **2015**, *115*, 5366–5412. (h) Pellissier, H. Asymmetric 1,3-dipolar cycloadditions. *Tetrahedron* **2007**, *63*, 3235–3285.

(2) (a) Gothelf, K. V.; Jørgensen, K. A. Asymmetric 1,3-Dipolar Cycloaddition Reactions. *Chem. Rev.* **1998**, *98*, 863–910. (b) Chen, S.; Bacuau, V.; Knecht, T.; Mercado, B. Q.; Bergman, R. G.; Ellman, J. A. New Regio- and Stereoselective Cascades via Unstabilized Azomethine Ylide Cycloadditions for the Synthesis of Highly Substituted Tropane and Indolizidine Frameworks. *J. Am. Chem. Soc.* **2016**, *138*, 12664–12670. (c) Mulzer, J. Natural Product Synthesis via 1,3-Dipolar Cycloadditions. In *Organic Synthesis Highlights*; Mulzer, J., Altenbach, H.-J., Braun, M., Krohn, K., Reissig, H.-U., Eds.; VCH: Weinheim, 1991; pp 77–95. (d) Döndas, H. A.; de Gracia Retamosa, M.; Sansano, J. M. Current Trends towards the Synthesis of Bioactive Heterocycles and Natural Products Using 1,3-Dipolar Cycloadditions with Azomethine Ylides. *Synthesis* **2017**, *49*, 2819–2851. (e) Mulzer, J. Selected diastereoselective reactions. Diastereoselective intra- and intermolecular 1,3-dipolar cycloadditions in natural product synthesis. In *Comprehensive Chirality*; Carreira, E. M., Yamamoto, H., Eds.; Elsevier: Amsterdam, 2012; Vol. 2, pp 525–562. (f) Padwa, A. Use of nitrogen and oxygen dipole ylides for alkaloid synthesis. *ARKIVOC* **2018**, 23–49.

(3) (a) Maggini, M.; Scorrano, G.; Prato, M. Addition of Azomethine Ylides to C<sub>60</sub>: Synthesis, Characterization, and Functionalization of Fullerene Pyrrolidines. *J. Am. Chem. Soc.* **1993**, *115*, 9798–9799. (b) Hummelen, J. C.; Knight, B. W.; LePeg, F.; Wudl, F.; Yao, J.; Wilkins, C. L. Preparation and Characterization of Fulleroid and Methanofullerene Derivatives. *J. Org. Chem.* **1995**, *60*, 532–538. (c) Guldi, D. M.; Maggini, M.; Scorrano, G.; Prato, M. Intramolecular Electron Transfer in Fullerene/Ferrocene Based Donor-Bridge-Acceptor Dyads. *J. Am. Chem. Soc.* **1997**, *119*, 974–980. (d) Lutz, J.-F. 1,3-Dipolar Cycloadditions of Azides and Alkynes: A Universal Ligation Tool in Polymer and Materials Science. *Angew. Chem., Int. Ed.* **2007**, *46*, 1018–1025.

(4) (a) Kolb, H. C.; Finn, M. G.; Sharpless, K. B. Click Chemistry: Diverse Chemical Function from a Few Good Reactions. *Angew. Chem., Int. Ed.* **2001**, *40*, 2004–2021. (b) Kolb, H. C.; Sharpless, K. B. The growing impact of click chemistry on drug discovery. *Drug Discovery Today* **2003**, *8*, 1128–1137. (c) Amblard, F.; Cho, J. H.; Schinazi, R. F. Cu(I)-Catalyzed Huisgen Azide–Alkyne 1,3-Dipolar Cycloaddition Reaction in Nucleoside, Nucleotide, and Oligonucleotide Chemistry. *Chem. Rev.* **2009**, *109*, 4207–4220. (d) Kacprzak, K.; Skiera, I.; Piasecka, M.; Paryzek, Z. Alkaloids and Isoprenoids Modification by Copper(I)-Catalyzed Huisgen 1,3-Dipolar Cycloaddition (Click Chemistry): Toward New Functions and Molecular Architectures. *Chem. Rev.* **2016**, *116*, 5689–5743. (e) Belkheira, M.; El Abed, D.; Pons, J.-M.; Bressy, C. Chemoselective Organoclick–Click Sequence. *Synthesis* **2018**, *50*, 4254–4262.

(5) (a) Huisgen, R. On the Mechanism of 1,3-Dipolar Cycloadditions. A Reply. *J. Org. Chem.* **1968**, *33*, 2291–2297. (b) Houk, K. N.; Firestone, R. A.; Munchausen, L. L.; Mueller, P. H.; Arison, B. H.; Garcia, L. A. Stereospecificity of 1,3-Dipolar Cycloadditions of *p*-Nitrobenzoxitrile Oxide to *cis*- and *trans*-Dideuterioethylene. *J. Am. Chem. Soc.* **1985**, *107*, 7227–7228.

(6) For an alternative diradical pathway, see: Firestone, R. A. On the Mechanism of 1,3-Dipolar Cycloadditions. *J. Org. Chem.* **1968**, *33*, 2285–2290.

(7) Theories of 1,3-dipolar cycloaddition: (a) Sustmann, R. A simple model for substituent effects in cycloaddition reactions. I. 1,3-dipolar cycloadditions. *Tetrahedron Lett.* **1971**, *12*, 2717–2720. (b) Sustmann, R.; Trill, H. Substituent Effects in 1,3-Dipolar Cycloadditions of Phenyl Azide. *Angew. Chem., Int. Ed. Engl.* **1972**, *11*, 838–840. (c) Houk, K. N.; Yamaguchi, K. Theory of 1,3-Dipolar Cycloadditions. In *1,3-Dipolar Cycloaddition Chemistry*; Padwa, A., Ed.; Wiley: New York, 1984; Vol. 2; Chapter 13, pp 407–450.

(8) (a) Huisgen, R.; Mloston, G.; Langhals, E. The first two-step 1,3-dipolar cycloadditions: non-stereospecificity. *J. Am. Chem. Soc.* **1986**, *108*, 6401–6402. (b) Huisgen, R.; Mloston, G.; Langhals, E. The first two-step 1,3-dipolar cycloadditions: interception of intermediate. *J. Org. Chem.* **1986**, *51*, 4085–4087. (c) Baran, J.; Mayr, H. The First [4 + 3] Cycloaddition of a 1,3-Dipole with a 1,3-Diene. *J. Am. Chem. Soc.* **1987**, *109*, 6519–6521. (d) Baran, J.; Mayr, H. Mechanistic Impact of Oxime Formation Accompanying 1,3-Dipolar Cycloadditions of Nitrile Oxides. *J. Org. Chem.* **1989**, *54*, 5012–5016. (e) Baran, J.; Mayr, H. Competing [2 + 3] and [4 + 3] Cycloadditions of C,N-Diphenylnitron with 1,3-Dienes. Evidence for Thermally Non-equilibrated Intermediates. *J. Org. Chem.* **1989**, *54*, 5774–5783.

(9) (a) Houk, K. N. The Frontier Molecular Orbital Theory of Cycloaddition Reactions. *Acc. Chem. Res.* **1975**, *8*, 361–369. (b) Fleming, I. *Molecular Orbitals and Organic Chemical Reactions* (Student ed.); Wiley: Chichester, UK, 2009; pp 242–252. (c) Carey, F. A.; Sundberg, R. J. *Advanced Organic Chemistry—Part A: Structure and Mechanisms*, 5th ed.; Springer: New York, 2007; pp 873–883.

(10) (a) Ess, D. H.; Houk, K. N. Distortion/Interaction Energy Control of 1,3-Dipolar Cycloaddition Reactivity. *J. Am. Chem. Soc.* **2007**, *129*, 10646–10647. (b) Ess, D. H.; Houk, K. N. Theory of 1,3-Dipolar Cycloadditions: Distortion/Interaction and Frontier Molecular Orbital Models. *J. Am. Chem. Soc.* **2008**, *130*, 10187–10198. (c) Lan, Y.; Zou, L.; Cao, Y.; Houk, K. N. Computational Methods to Calculate Accurate Activation and Reaction Energies of 1,3-Dipolar Cycloadditions of 24 1,3-Dipoles. *J. Phys. Chem. A* **2011**, *115*, 13906–13920. (d) Bickelhaupt, F. M.; Houk, K. N. Analyzing Reaction Rates with the Distortion/Interaction-Activation Strain Model. *Angew. Chem., Int. Ed.* **2017**, *56*, 10070–10086.

(11) (a) van Zeist, W.-J.; Bickelhaupt, F. M. The activation strain model of chemical reactivity. *Org. Biomol. Chem.* **2010**, *8*, 3118–3127. (b) Fernández, I.; Bickelhaupt, F. M. The activation strain model and molecular orbital theory: understanding and designing chemical reactions. *Chem. Soc. Rev.* **2014**, *43*, 4953–4967.

(12) (a) Engels, B.; Christl, M. What Controls the Reactivity of 1,3-Dipolar Cycloadditions? *Angew. Chem., Int. Ed.* **2009**, *48*, 7968–7970. (b) Breugst, M.; Huisgen, R.; Reissig, H.-U. Regioselective 1,3-Dipolar Cycloaddition of Diazoalkanes with Heteroatom-Substituted Alkynes: Theory and Experiment. *Eur. J. Org. Chem.* **2018**, 2477–2485.

(13) (a) Mayr, H.; Bug, T.; Gotta, M. F.; Hering, N.; Irrgang, B.; Janker, B.; Kempf, B.; Loos, R.; Ofial, A. R.; Remennikov, G.; Schimmel, H. Reference Scales for the Characterization of Cationic Electrophiles and Neutral Nucleophiles. *J. Am. Chem. Soc.* **2001**, *123*, 9500–9512. (b) Lucius, R.; Loos, R.; Mayr, H. Kinetics of Carbocation Carbanion Combinations: Key to a General Concept of Polar Organic Reactivity. *Angew. Chem., Int. Ed.* **2002**, *41*, 91–95. (c) Mayr, H.; Kempf, B.; Ofial, A. R.  $\pi$ -Nucleophilicity in Carbon-Carbon Bond-Forming Reactions. *Acc. Chem. Res.* **2003**, *36*, 66–77. (d) Mayr, H.; Ofial, A. R. Kinetics of Electrophile-Nucleophile Combinations: A General Approach to Polar Organic Reactivity. *Pure Appl. Chem.* **2005**, *77*, 1807–1821. (e) Richter, D.; Hampel, N.; Singer, T.; Ofial, A. R.; Mayr, H. Synthesis and Characterization of Novel Quinone Methides: Reference Electrophiles for the Construction of Nucleophilicity Scales. *Eur. J. Org. Chem.* **2009**, 3203–3211. (f) Mayr, H.; Lakhdar, S.; Maji, B.; Ofial, A. R. A quantitative approach to nucleophilic organocatalysis. *Beilstein J. Org. Chem.* **2012**, *8*, 1458–1478. (g) Mayr, H. Reactivity Scales for Quantifying Polar

Organic Reactivity: The Benzhydrylium Methodology. *Tetrahedron* **2015**, *71*, S095–S111. (h) Mayer, R. J.; Hampel, N.; Mayer, P.; Ofial, A. R.; Mayr, H. Synthesis, Structure and Properties of Amino-Substituted Benzhydrylium Ions – a Link Between Ordinary Carbocations and Neutral Electrophiles. *Eur. J. Org. Chem.* **2018**, DOI: 10.1002/ejoc.201800835.

(14) For a listing of nucleophilicity parameters  $N$ ,  $s_N$ , and electrophilicity parameters  $E$ , see: <http://www.cup.uni-muenchen.de/oc/mayr/DBintro.html>.

(15) (a) Regitz, M. Diazoalkanes. In *1,3-Dipolar Cycloaddition Chemistry*; Padwa, A., Ed.; Wiley: New York, 1984; Vol. 1; Chapter 4, pp 393–558. (b) Aronoff, M. R.; Gold, B.; Raines, R. T. 1,3-Dipolar Cycloadditions of Diazo Compounds in the Presence of Azides. *Org. Lett.* **2016**, *18*, 1538–1541. (c) Gold, B.; Aronoff, M. R.; Raines, R. T. Decreasing Distortion Energies without Strain: Diazo-Selective 1,3-Dipolar Cycloadditions. *J. Org. Chem.* **2016**, *81*, 5998–6006.

(16) Allgäuer, D. S.; Jangra, H.; Asahara, H.; Li, Z.; Chen, Q.; Zipse, H.; Ofial, A. R.; Mayr, H. Quantification and Theoretical Analysis of the Electrophilicities of Michael Acceptors. *J. Am. Chem. Soc.* **2017**, *139*, 13318–13329.

(17) (a) Doering, W. v. E.; Roth, W. R.; Breuckmann, R.; Figge, L.; Lennartz, H.-W.; Fessner, W.-D.; Prinzbach, H. Verbotene Reaktionen. – [2 + 2]-Cycloreversion starrer Cyclobutane. *Chem. Ber.* **1988**, *121*, 1–9. (b) Hartnagel, M.; Grimm, K.; Mayr, H. Addition and Cycloaddition Reactions of Arenediazonium Ions with 1,3-Dienes: A Shift from a Concerted to a Stepwise Mechanism. *Liebigs Ann./Recueil* **1997**, 71–80. (c) Mayr, H.; Henninger, J. Kinetics of the [2<sup>+</sup>+4]-Cycloaddition Reactions of [1,3]-Dithian-2-ylidene Ions with 1,3-Dienes. *Eur. J. Org. Chem.* **1998**, 1919–1922. (d) Mayr, H.; Ofial, A. R.; Sauer, J.; Schmied, B. [2<sup>+</sup>+4] Cycloadditions of Iminium Ions - Concerted or Stepwise Mechanism of Aza Diels-Alder Reactions? *Eur. J. Org. Chem.* **2000**, 2013–2020. (e) Fichtner, C.; Mayr, H. Diels-Alder reactions of 1,1,3-triaryllallyl cations: Determination of the free energy of concert. *J. Chem. Soc., Perkin Trans. 2* **2002**, 1441–1444. (f) Kanzian, T.; Mayr, H. Electrophilic Reactivities of Azodicarboxylates. *Chem. - Eur. J.* **2010**, *16*, 11670–11677.

(18) Phenyl diazomethane (**1a**) has been characterized previously: Bug, T.; Hartnagel, M.; Schlierf, C.; Mayr, H. How Nucleophilic are Diazo Compounds? *Chem. - Eur. J.* **2003**, *9*, 4068–4076.

(19) (a) Streitwieser, A., Jr An Interpretation of the Reaction of Aliphatic Primary Amines with Nitrous Acid. *J. Org. Chem.* **1957**, *22*, 861–869. (b) Friedman, L. Carbonium Ion Formation From Diazonium Ions. In *Carbonium Ions Vol. II*; Olah, G. A., Schleyer, P. v. R., Eds.; Wiley-Interscience: New York, 1970; Chapter 16, pp 655–713. (c) Zollinger, H. *Diazo Chemistry II*; VCH: Weinheim, 1995; Chapter 7, pp 241–304.

(20) (a) Katz, C. E.; Ribelin, T.; Withrow, D.; Basseri, Y.; Manukyan, A. K.; Bermudez, A.; Nuera, C. G.; Day, V. W.; Powell, D. R.; Poutsma, J. L.; Aubé, J. Nonbonded, Attractive Cation– $\pi$  Interactions in Azide-Mediated Asymmetric Ring Expansion Reactions. *J. Org. Chem.* **2008**, *73*, 3318–3327. (b) Gutierrez, O.; Aubé, J.; Tantillo, D. J. Mechanism of the Acid-Promoted Intramolecular Schmidt Reaction: Theoretical Assessment of the Importance of Lone Pair–Cation, Cation– $\pi$ , and Steric Effects in Controlling Regioselectivity. *J. Org. Chem.* **2012**, *77*, 640–647.

(21) Hansch, C.; Leo, A.; Hoekman, D. *Exploring QSAR: Hydrophobic, Electronic, and Steric Constants*; American Chemical Society: Washington, DC, 1995.

(22) (a) Huisgen, R.; Geittner, J. Kinetics of 1,3-Dipolar Cycloaddition Reactions of Aryl- and Diaryldiazomethanes. *Heterocycles* **1978**, *11*, 105–108. (b) Geittner, J.; Huisgen, R.; Reissig, H.-U. Solvent Dependence of Cycloaddition Rates of Phenyl diazomethane and Activation Parameters. *Heterocycles* **1978**, *11*, 109–112.

(23) (a) Allgäuer, D. S.; Mayr, H. Electrophilicities of 1,2-Disubstituted Ethylenes. *Eur. J. Org. Chem.* **2014**, 2956–2963. (b) Kaumanns, O.; Mayr, H. Electrophilicity Parameters of 5-Benzylidene-2,2-dimethyl-[1,3]dioxane-4,6-diones (Benzylidene Meldrum's Acids). *J. Org. Chem.* **2008**, *73*, 2738–2745. (c) Lemek, T.;

- Mayr, H. Electrophilicity Parameters for Benzyldenemalononitriles. *J. Org. Chem.* **2003**, *68*, 6880–6886. (d) Chen, Q.; Mayer, P.; Mayr, H. Ethenesulfonyl Fluoride (ESF): The Most Perfect Michael Acceptor Ever Found? *Angew. Chem., Int. Ed.* **2016**, *55*, 12664–12667. (e) Berger, S. T. A.; Seeliger, F. H.; Hofbauer, F.; Mayr, H. Electrophilicity Parameters for 2-Benzylidene-indan-1,3-diones - a systematic extension of the benzhydrylium based electrophilicity scale. *Org. Biomol. Chem.* **2007**, *5*, 3020–3026. (f) Asahara, H.; Mayr, H. Electrophilicities of Bissulfonyl Ethylenes. *Chem. - Asian J.* **2012**, *7*, 1401–1407.
- (24) The relative configurations of **14a** and **14b** were determined by NMR spectroscopy. See the [Supporting Information](#).
- (25) (a) Krutak, J. J.; Burpitt, R. D.; Moore, W. H.; Hyatt, J. A. Chemistry of ethenesulfonyl fluoride. Fluorosulfonylethylation of organic compounds. *J. Org. Chem.* **1979**, *44*, 3847–3858. (b) Dong, J.; Krasnova, L.; Finn, M. G.; Sharpless, K. B. Sulfur(VI) Fluoride Exchange (SuFEx): Another Good Reaction for Click Chemistry. *Angew. Chem., Int. Ed.* **2014**, *53*, 9430–9448. (c) Zheng, Q.; Dong, J.; Sharpless, K. B. Ethenesulfonyl Fluoride (ESF): An On-Water Procedure for the Kilogram-Scale Preparation. *J. Org. Chem.* **2016**, *81*, 11360–11362.
- (26) Crystallographic data have been deposited with the Cambridge Crystallographic Data Centre [CCDC 1862870 (**15d**), 1862871 (**17**), 1862872 (**18c**)]. These supplementary crystallographic data can be obtained free of charge from The Cambridge Crystallographic Data Centre via [www.ccdc.cam.ac.uk/data\\_request/cif](http://www.ccdc.cam.ac.uk/data_request/cif).
- (27) Yoshimatsu, M.; Kawahigashi, M.; Honda, E.; Kataoka, T. A convenient synthesis of alkynylpyrazoles. *J. Chem. Soc., Perkin Trans. 1* **1997**, 695–700.
- (28) (a) McGreer, D. E.; Wu, W. S. Pyrazolines. VII. Concerning the formation of olefins from the pyrolysis of pyrazolines. *Can. J. Chem.* **1967**, *45*, 461–468. (b) McGreer, D. E.; Masters, I. M. E. Pyrazolines X. Kinetics for the pyrolysis of some deuterated 1-pyrazolines in solution. *Can. J. Chem.* **1969**, *47*, 3975–3978.
- (29) The vinylic proton of **20** (not shown in [Figure 4b](#)) resonates as a triplet ( $J = 7.9$  Hz) at  $\delta$  7.82 ppm (see [Supporting Information](#)).
- (30) The relative configuration of **21** was determined based on its reported NMR spectra and crystal structure, see: Lin, S.; Li, M.; Dong, Z.; Liang, F.; Zhang, J. Hypervalent iodine(III)-mediated cyclopropa(e)nation of alkenes/alkynes under mild conditions. *Org. Biomol. Chem.* **2014**, *12*, 1341–1350.
- (31) Kisch, H.; Polansky, O. E.; Schuster, P. Thermisch instabile  $\Delta^1$ -Pyrazoline durch Reaktion von Diazomethan mit Olefinen bei tiefen Temperaturen. *Tetrahedron Lett.* **1969**, *10*, 805–808.
- (32) Since the three-parameter [eq 1](#), which covers a reactivity range of approximately 40 orders of magnitude, provides rate constants only with an accuracy of a factor of 100, deviations of this order of magnitude cannot reliably be interpreted. See also: Mayr, H. Reply to T.W. Bentley: Limitations of the  $s(E+N)$  and Related Equations. *Angew. Chem., Int. Ed.* **2011**, *50*, 3612–3618.
- (33) Calculated from rate constants in Table 1 of ref [22a](#) and Hammett  $\sigma$ -parameters from ref [21](#).
- (34) See ref [1b](#), pp 76–90.
- (35) (a) Steiner, G.; Huisgen, R. Tetracyanoethylene and Enol Ethers. Dependence of Cycloaddition Rate on Solvent Polarity. *J. Am. Chem. Soc.* **1973**, *95*, 5056–5058. (b) Huisgen, R. Tetracyanoethylene and Enol Ethers. A Model for 2 + 2 Cycloadditions via Zwitterionic Intermediates. *Acc. Chem. Res.* **1977**, *10*, 117–124.
- (36) (a) Brown, P.; Cookson, R. C. Kinetics of Addition of Tetracyanoethylene to Anthracene and Bicyclo[2,2,1]heptadiene. *Tetrahedron* **1965**, *21*, 1977–1991. (b) Kononov, A. I.; Breus, J. P.; Sharagin, I. A.; Kiselev, V. D. Solvation Effects in the Diels-Alder Reactions of 4-Phenyl-1,2,4-triazoline-3,5-dione with Anthracene and trans,trans-1,4-Diphenyl-1,3-butadiene. *J. Org. Chem. USSR* **1979**, *15*, 315–320. (c) Sauer, J.; Sustmann, R. Mechanistic Aspects of Diels-Alder Reactions: A Critical Survey. *Angew. Chem., Int. Ed. Engl.* **1980**, *19*, 779–807.
- (37) Reichardt, C.; Welton, T. *Solvents and Solvent Effects in Organic Chemistry*, Fourth ed.; Wiley-VCH: Weinheim, 2011; pp 455–461.
- (38) Li, Z.; Jangra, H.; Chen, Q.; Mayer, P.; Ofial, A. R.; Zipse, H.; Mayr, H. Kinetics and Mechanism of Oxirane Formation by Darzens Condensation of Ketones: Quantification of the Electrophilicities of Ketones. *J. Am. Chem. Soc.* **2018**, *140*, 5500–5515.
- (39) Becke, A. D. Density-functional thermochemistry. III. The role of exact exchange. *J. Chem. Phys.* **1993**, *98*, 5648–5652.
- (40) (a) Grimme, S. Semiempirical GGA-Type Density Functional Constructed with a Long-Range Dispersion Correction. *J. Comput. Chem.* **2006**, *27*, 1787–1799. (b) Grimme, S.; Antony, J.; Ehrlich, S.; Krieg, H. A consistent and accurate ab initio parametrization of density functional dispersion correction (DFT-D) for the 94 elements H-Pu. *J. Chem. Phys.* **2010**, *132*, 154104. (c) Wagner, J. P.; Schreiner, P. R. London Dispersion in Molecular Chemistry—Reconsidering Steric Effects. *Angew. Chem., Int. Ed.* **2015**, *54*, 12274–12296.
- (41) (a) Ditchfield, R.; Hehre, W. J.; Pople, J. A. Self-Consistent Molecular-Orbital Methods. IX. An Extended Gaussian-Type Basis for Molecular-Orbital Studies of Organic Molecules. *J. Chem. Phys.* **1971**, *54*, 724–728. (b) Krishnan, R.; Binkley, J. S.; Seeger, R.; Pople, J. A. Self-consistent molecular orbital methods. XX. A basis set for correlated wave functions. *J. Chem. Phys.* **1980**, *72*, 650–654.
- (42) (a) Cancès, E.; Mennucci, B.; Tomasi, J. A new integral equation formalism for the polarizable continuum model: Theoretical background and applications to isotropic and anisotropic dielectrics. *J. Chem. Phys.* **1997**, *107*, 3032–3041. (b) Tomasi, J.; Mennucci, B.; Cammi, R. Quantum Mechanical Continuum Solvation Models. *Chem. Rev.* **2005**, *105*, 2999–3094. (c) Mayer, R. J.; Tokuyasu, T.; Mayer, P.; Gomar, J.; Sabelle, S.; Mennucci, B.; Mayr, H.; Ofial, A. R. Solvation Accounts for the Counter-Intuitive Nucleophilicity Ordering of Peroxide Anions. *Angew. Chem., Int. Ed.* **2017**, *56*, 13279–13282.
- (43) Grimme, S. Semiempirical hybrid density functional with perturbative second-order correlation. *J. Chem. Phys.* **2006**, *124*, 034108.
- (44) (a) Weigend, F.; Ahlrichs, R. Balanced basis sets of split valence, triple zeta valence and quadruple zeta valence quality for H to Rn: Design and assessment of accuracy. *Phys. Chem. Chem. Phys.* **2005**, *7*, 3297–3305. (b) Weigend, F. Accurate Coulomb-fitting basis sets for H to Rn. *Phys. Chem. Chem. Phys.* **2006**, *8*, 1057–1065.
- (45) Doering, W. v. E.; Roth, W. R. The Overlap of Two Allyl Radicals or a Four-Centered Transition State in the Cope Rearrangement. *Tetrahedron* **1962**, *18*, 67–74.
- (46) Woodward, R. B.; Hoffmann, R. The Conservation of Orbital Symmetry. *Angew. Chem., Int. Ed. Engl.* **1969**, *8*, 781–853.
- (47) Dewar, M. J. S. Multibond Reactions Cannot Normally Be Synchronous. *J. Am. Chem. Soc.* **1984**, *106*, 209–219.
- (48) (a) Peterson, P. W.; Mohamed, R. K.; Alabugin, I. V. How to Lose a Bond in Two Ways – The Diradical/Zwitterion Dichotomy in Cycloaromatization Reactions. *Eur. J. Org. Chem.* **2013**, 2505–2527. (b) dos Passos Gomes, G.; Alabugin, I. V. Drawing Catalytic Power from Charge Separation: Stereoelectronic and Zwitterionic Assistance in the Au(I)-Catalyzed Bergman Cyclization. *J. Am. Chem. Soc.* **2017**, *139*, 3406–3416.

## 9.1 Supporting Information

For: Nucleophilicity and Electrophilicity Parameters for Predicting Absolute Rate Constants of Highly Asynchronous 1,3-Dipolar Cycloadditions of Aryldiazomethanes

---

### 9.1.1 Methodology

Frontier orbital energies (HOMO/LUMO), global ( $\omega$ ) and local ( $\omega_\beta$ ) electrophilicities as well as methyl anion affinities (MAAs) for the Michael acceptors discussed in this work are taken from ref. 1.

The methodology used for the calculation of potential energy surfaces (PES) for nucleophilic additions to electrophiles follows suggestions recently made by Mayer et al. for this type of reaction.<sup>2</sup> This includes geometry optimizations for all stationary points (minima, complexes and transition states) along the PES at the PCM(CH<sub>2</sub>Cl<sub>2</sub>,UA0)/B3LYP<sup>3</sup>-D3<sup>4</sup>/6-31+G(d,p)<sup>5</sup> level of theory. Thermochemical corrections to Gibbs energies (corr.  $\Delta G$ ) and enthalpy (corr.  $\Delta H$ ) at 298.15 K have been calculated using the rigid rotor/harmonic oscillator model without any scaling. The PCM variant used here is based on the Integral Equation Formalism for the Polarizable Continuum Model (IEFPCM) solvation model employing United Atom Topological Model (UA0) radii derived from the UFF force field [scrf=(iefpcm, read, solvent=dmsol, radii=ua0)].<sup>6</sup> The dispersion model is that proposed by Grimme as the "GD3" model [empiricaldispersion=gd3].<sup>4</sup>

All stationary points (minima, complexes and transition states) were confirmed by vibrational frequency calculation (with 0, 0, and 1 imaginary frequencies, respectively). All stationary points were checked for wavefunction stability (stable=opt). The nature of transition states was further confirmed by IRC calculations [15 steps in both directions (reverse/forward) with stepsize=3] followed by geometry optimization to the next minima. In cases of very flat PES(s), manual displacement away from the TS(s) followed by geometry optimization was employed. PES surfaces were re-evaluated at the B2PLYP<sup>7</sup>-D3/Def2TZVPP<sup>8</sup> level of theory with or without the PCM(CH<sub>2</sub>Cl<sub>2</sub>,UA0) solvation model. The Wiberg bond index ( $B_i$ ) has been calculated using NBO6.<sup>9</sup> All calculations were performed with Gaussian 09, Rev. D.<sup>10</sup>

Gibbs energies ( $\Delta G_{\text{sol}}$ ) at PCM(CH<sub>2</sub>Cl<sub>2</sub>,UA0)/(U)B3LYP-D3/6-31+G(d,p) level have been obtained through addition of the total electronic energy ( $\Delta E_{\text{tot}}$ ) and corr.  $\Delta G$  obtained at the same level of theory.  $\Delta G_{\text{sol}}$  at PCM(CH<sub>2</sub>Cl<sub>2</sub>,UA0)/(U)B2PLYP-D3/Def2TZVPP//PCM(CH<sub>2</sub>Cl<sub>2</sub>,UA0)/(U)B3LYP-D3/6-31+G(d,p) level have been obtained by combination of  $\Delta E_{\text{tot}}$  at a higher level [PCM(CH<sub>2</sub>Cl<sub>2</sub>,UA0)/(U)B2PLYP-D3/Def2TZVPP] with corr.  $\Delta G$  obtained at the level of optimization [PCM(CH<sub>2</sub>Cl<sub>2</sub>,UA0)/(U)B3LYP-D3/6-31+G(d,p)]. Similarly, the gas phase Gibbs energies ( $\Delta G_{\text{gas}}$ ) at (U)B2PLYP-D3/Def2TZVPP//PCM(CH<sub>2</sub>Cl<sub>2</sub>,UA0)/(U)B3LYP-D3/6-31+G(d,p) level have been calculated by adding corr.  $\Delta G$  obtained at the level of optimization to  $\Delta E_{\text{tot}}$  at a higher level.  $\Delta G_{\text{sol}+}$  values at (U)B2PLYP-D3/Def2TZVPP+PCM(CH<sub>2</sub>Cl<sub>2</sub>,UA0)/(U)B3LYP-D3/6-31+G(d,p) level have been calculated by adding single point solvation energies ( $\Delta G_{\text{solv}}$ ) and corr.  $\Delta G$  obtained at the level of optimization to the  $\Delta E_{\text{tot}}$  at a higher level.

## 9.1.2 Correlation analysis

**Table S9-1.** [Table S1] Quantum chemically calculated frontier orbital energies, global ( $\omega$ ) and local ( $\omega_\beta$ ) electrophilicities as well as methyl anion affinities (MAAs) of Michael acceptors. (reported in ref. 1).

Michael acceptor		$E^a$	# lg $k_2^{\text{exptl}}$	$\epsilon_{\text{HOMO}}^b$ (Hartree)	$\epsilon_{\text{LUMO}}^b$ (Hartree)	Global $\omega^b$ (eV)	Local $\omega_\beta^b$ (eV)	MAA (kJ mol <sup>-1</sup> )	
Lable	ref 2.							$-\Delta G_{\text{gas}}^c$	$-\Delta G_{\text{sol-sp}}^d$
<b>5a</b>	<b>1a</b>	-18.84	-1.31	-0.27299	-0.04454	1.50	0.62	205.5	80.7
<b>5b</b>	<b>1g</b>	-16.76	-0.65	-0.24738	-0.05476	1.61	0.60	222.8	104.2
<b>6</b>	<b>17b</b>	-17.79	-0.39	-0.27664	-0.07861	2.17	0.55	223.1	74.2
<b>7</b>	<b>17d</b>	-14.07	-	-0.27143	-0.09656	2.63	0.59	260.8	113.9
<b>8a</b>	<b>17l</b>	-12.76	-0.48	-0.20434	-0.07478	2.05	0.63	311.2	135.3
<b>8b</b>	<b>17o</b>	-10.28	0.88	-0.22917	-0.08527	2.34	0.73	330.7	154.4
<b>8c</b>	<b>17r</b>	-9.15	1.68	-0.25084	-0.09360	2.57	0.78	344.7	169.6
<b>9a</b>	<b>17n</b>	-10.80	-1.82	-0.23815	-0.09709	2.71	0.81	311.1	161.9
<b>9b</b>	<b>17q</b>	-9.42	-	-0.25994	-0.10707	3.00	0.88	325.4	177.4
<b>10</b>	<b>1j</b>	-12.09	0.83	-0.22333	-0.06439	1.97	0.98	295.9	160.5
<b>11a</b>	<b>17m</b>	-11.32	-0.62	-0.22045	-0.08670	2.40	0.65	318.9	147.1
<b>11b</b>	<b>17p</b>	-10.11	0.16	-0.23995	-0.09406	2.60	0.70	331.9	160.7
<b>12</b>	<b>17f</b>	-7.50	3.17	-0.26834	-0.07201	2.01	0.81	355.3	174.8

<sup>a</sup> Empirical electrophilicity parameters as defined in equation [ $\lg k_{20^\circ\text{C}} = s_N(N + E)$ ]. <sup>b</sup> Calculated at B3LYP/6-31G(d,p) level in the gas phase. <sup>c</sup> Calculated at B3LYP/6-311++G(3df,2pd)//B3LYP/6-31G(d,p) level in the gas phase. <sup>d</sup> Based on methyl anion affinities  $\Delta G_{\text{gas}}$  which were corrected for solvent effects by adding single point solvation energies calculated at B3LYP/6-31G(d,p) level using the SMD (solvent=dms) solvation model on gas phase optimized geometries at the same level. <sup>#</sup> Calculated from second-order rate constants of reactions between aryldiazomethane **1a** and Michael acceptors (**5–12**) in dichloromethane at 20 °C (Table 3 in the manuscript)

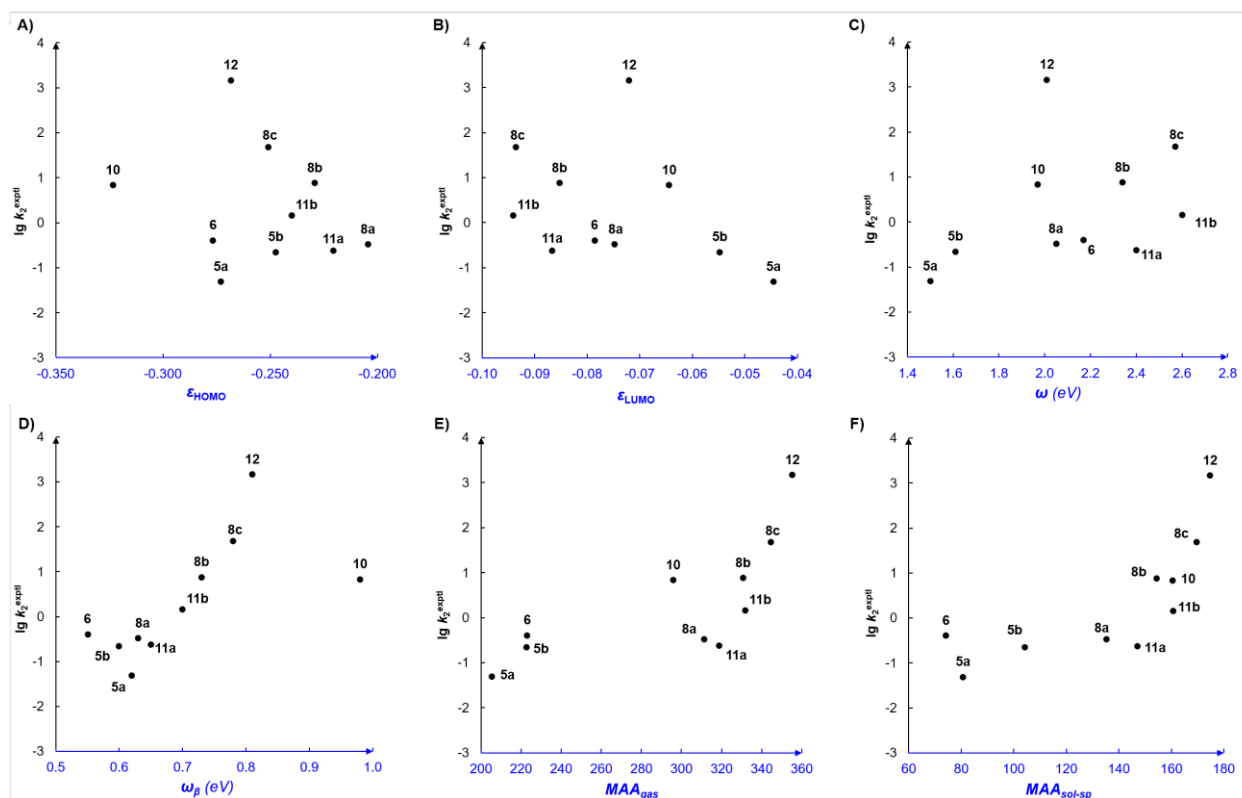


**Figure S9-1.** [Figure S2] Correlation analysis of second order rate constants  $\lg k_2^{\text{exptl}}$  (for the reactions of **1a** with diverse electrophiles) with **A**) HOMO energies ( $\epsilon_{\text{HOMO}}$ ), **B**) LUMO energies ( $\epsilon_{\text{LUMO}}$ ), **C**) global electrophilicities ( $\omega$ ), **D**) local electrophilicities ( $\omega_\beta$ ) calculated at B3LYP/6-

31G(d,p) level in the gas phase. **E)** Correlation with gas phase methyl anion affinities ( $MAA_{\text{gas}}$ ) and **F)** solvation corrected methyl anion affinities ( $MAA_{\text{sol-sp}}$ ) for Michael acceptors listed in Table S9-1. **9a** is excluded from the correlation analysis because of its mechanistic diversion.

### 9.1.3 Mechanistic Investigation

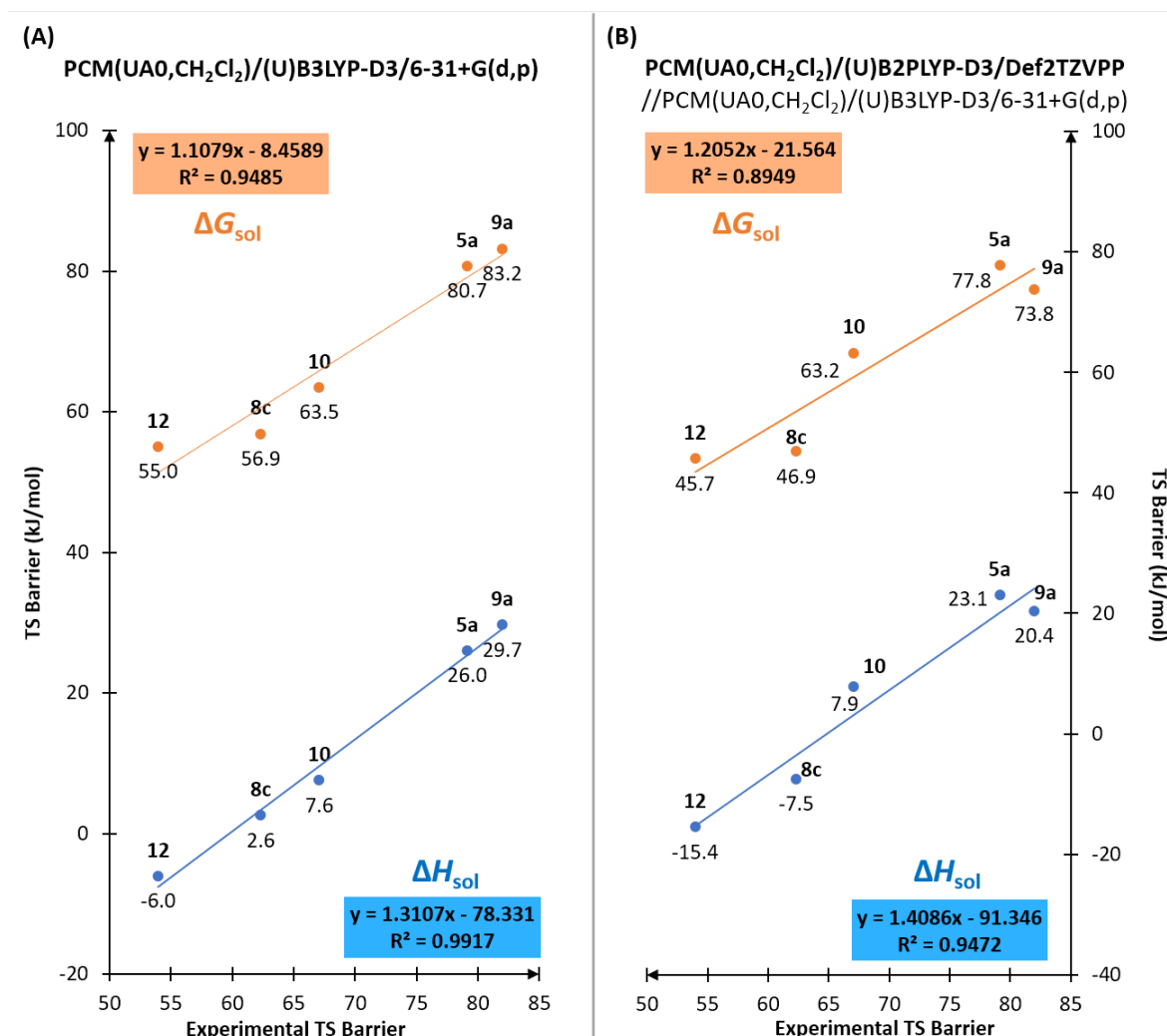


**Figure S9-2.** [Figure S5] Correlation between experimental and theoretically calculated reaction barriers for the reaction of **5a**, **10**, **9a**, **8c** and **12** with **1a** calculated at **(A)** PCM(UA0,CH<sub>2</sub>Cl<sub>2</sub>)/(U)B3LYP-D3/6-31+G(d,p) and **(B)** PCM(UA0,CH<sub>2</sub>Cl<sub>2</sub>)/(U)B2PLYP-D3/Def2TZVPP//PCM(UA0,CH<sub>2</sub>Cl<sub>2</sub>)/(U)B3LYP-D3/6-31+G(d,p) levels of theory.

**Table S 9-2.** [Table S2] Experimental and theoretically calculated reaction barriers for the reaction of **5a**, **10**, **9a**, **8c** and **12** with **1a**.

System	Experimental Data		PCM(UA0,CH <sub>2</sub> Cl <sub>2</sub> )/(U)B3LYP-D3/6-31+G(d,p)		PCM(UA0,CH <sub>2</sub> Cl <sub>2</sub> )/(U)B2PLYP-D3/Def2TZVPP // PCM(UA0,CH <sub>2</sub> Cl <sub>2</sub> )/(U)B3LYP-D3/6-31+G(d,p)	
	$k_2^{\text{exptl}}$ (M <sup>-1</sup> s <sup>-1</sup> )	$\Delta G_{\text{exptl}}^{\ddagger}$	$\Delta H_{\text{sol}}^{\ddagger}$	$\Delta G_{\text{sol}}^{\ddagger}$	$\Delta H_{\text{sol}}^{\ddagger}$	$\Delta G_{\text{sol}}^{\ddagger}$
<b>5a + 1a</b>	0.04870	79.1	26.0	80.7	23.1	77.8
<b>10 + 1a</b>	6.81	67.1	7.6	63.5	7.9	63.2
<b>9a + 1a</b>	0.0151	82.0	29.7	83.2	20.4	73.8
<b>8c + 1a</b>	48.0	62.3	2.6	56.9	-7.5	46.9
<b>12 + 1a</b>	1480	54.0	-6.0	55.0	-15.4	45.7

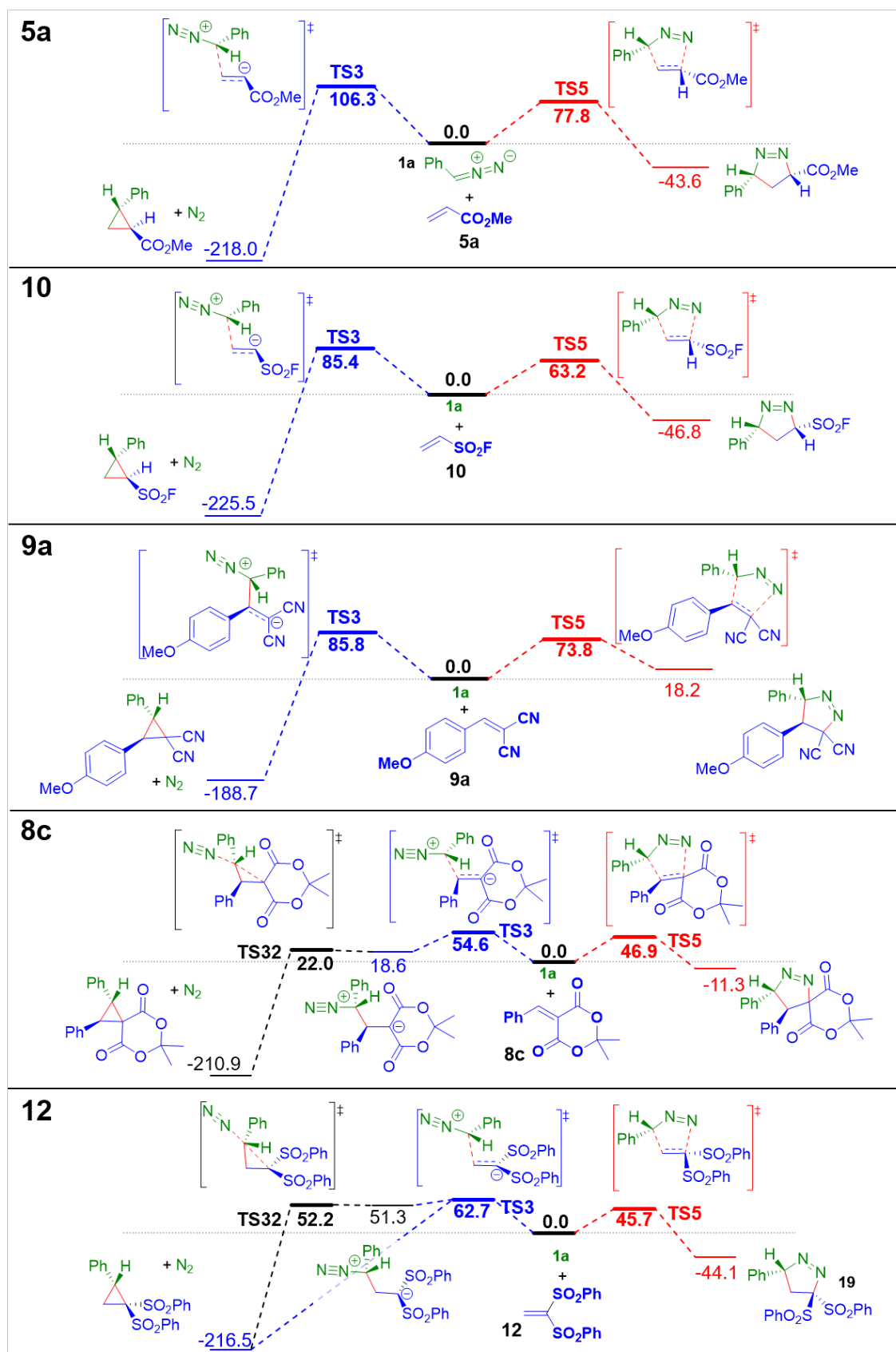


**Figure S9-3.** [Figure S7] Reaction profiles ( $\Delta G_{\text{sol}}$ , kJ/mol) for the reaction of 5a, 10, 9a, 8c and 12 with 1a calculated at the PCM(UA0,CH<sub>2</sub>Cl<sub>2</sub>)/(U)B2PLYP-D3/Def2TZVPP//PCM(UA0,CH<sub>2</sub>Cl<sub>2</sub>)/(U)B3LYP-D3/6-31+G(d,p) level of theory.

## 9.1.3.1 5a with 1a

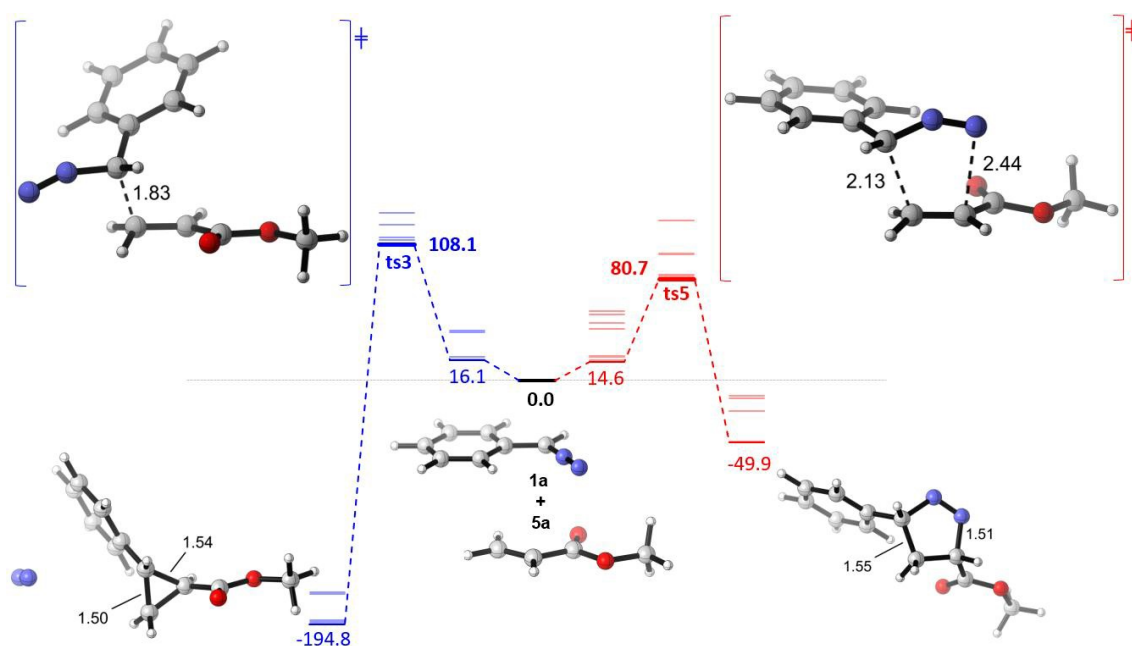


**Figure S9-4.** [Figure S13A] Reaction profiles ( $\Delta G_{\text{sol}}$ , in kJ/mol) for the reaction of Michael acceptor **5a** with phenyl diazomethane **1a** calculated at the PCM(UA0,CH<sub>2</sub>Cl<sub>2</sub>)/(U)B3LYP-D3/6-31+G(d,p) level of theory. Faded bars are used to show the conformational space screened for each point along PES.

## 9.1.3.2 10 with 1a

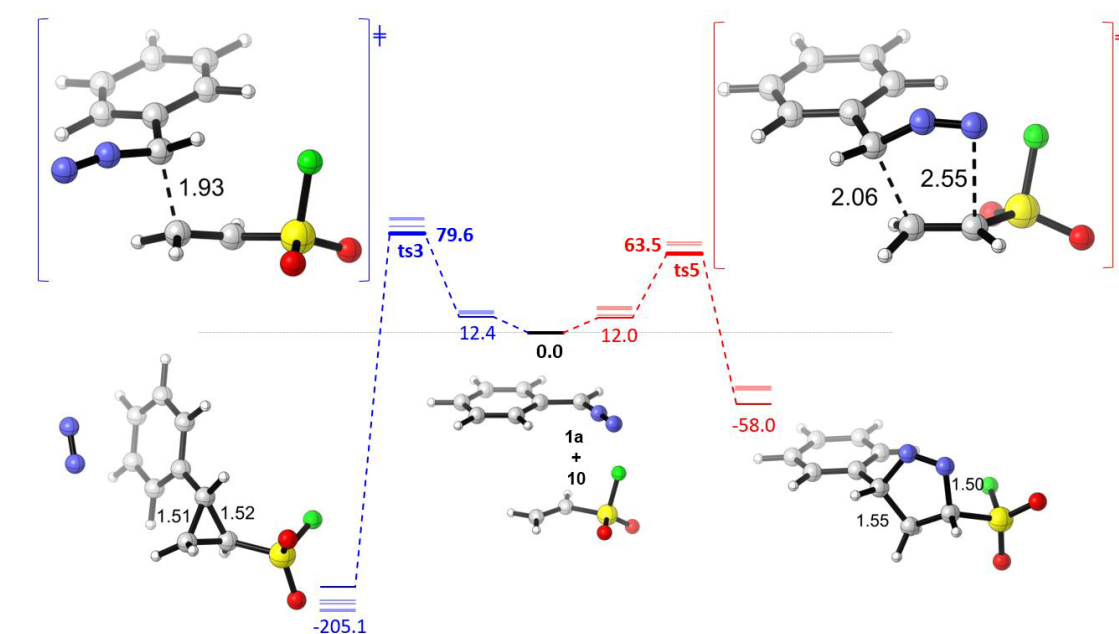


**Figure S9-5.** [Figure S18A] Reaction profiles ( $\Delta G_{\text{sol}}$ , in kJ/mol) for the reaction of Michael acceptor **10** with phenyl diazomethane **1a** calculated at the PCM(UA0,CH<sub>2</sub>Cl<sub>2</sub>)/(U)B3LYP-D3/6-31+G(d,p) level of theory.

### 9.1.3.3 9a with 1a

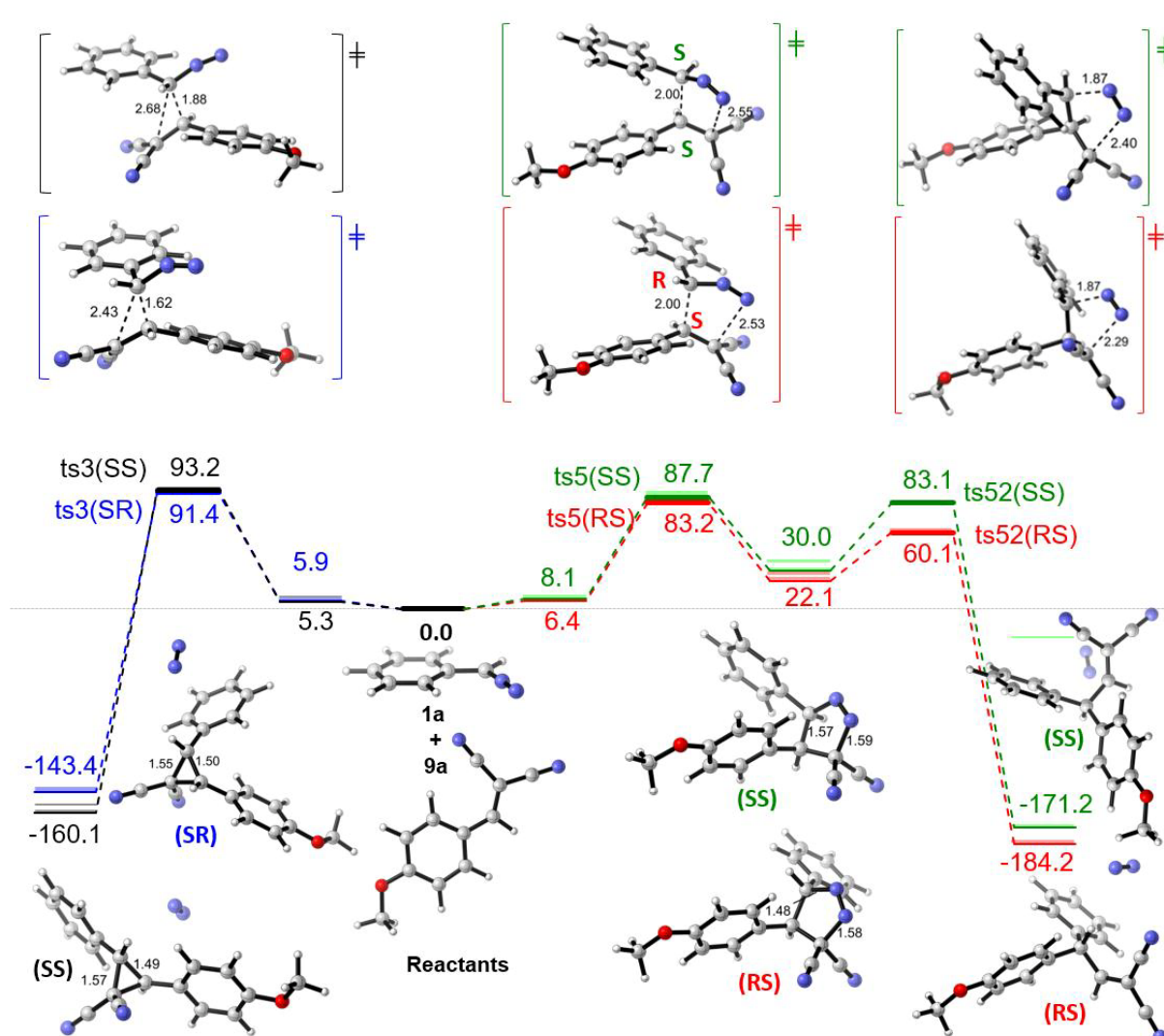


**Figure S9-6.** [Figure S23A] Reaction profiles ( $\Delta G_{\text{sol}}$ , in kJ/mol) for the reaction of Michael acceptor **9a** with phenyl diazomethane **1a** calculated at the PCM(UA0,CH<sub>2</sub>Cl<sub>2</sub>)/(U)B3LYP-D3/6-31+G(d,p) level of theory.

## 9.1.3.4 8c with 1a

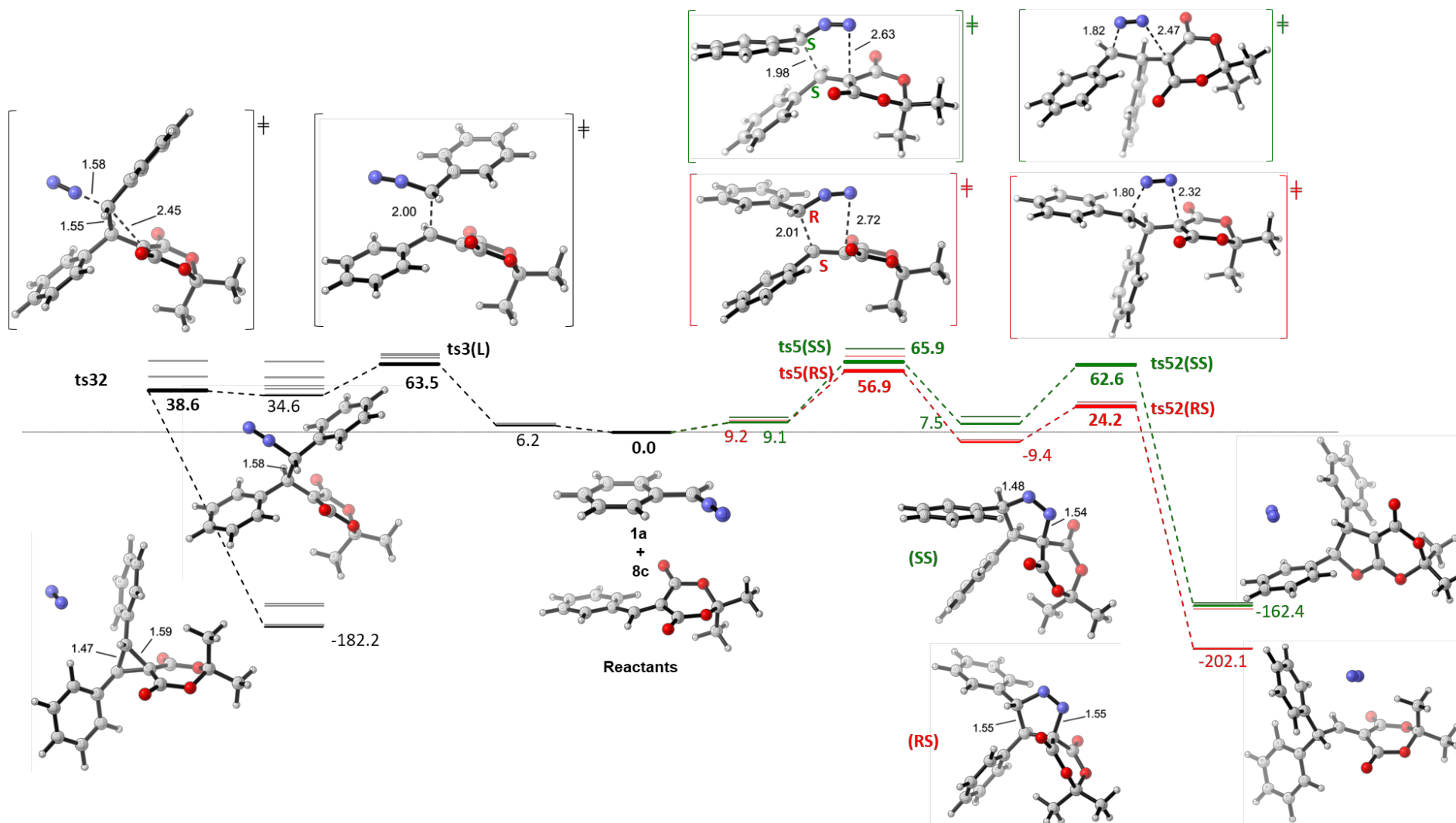


**Figure S9-7.** [Figure S26] Reaction profiles (ΔG<sub>sol</sub>, in kJ/mol) for the reaction of Michael acceptor **8c** with phenyl diazomethane **1a** calculated at the PCM(UA0,CH<sub>2</sub>Cl<sub>2</sub>)/(U)B3LYP-D3/6-31+G(d,p) level of theory.

## 9.1.3.5 12 with 1a

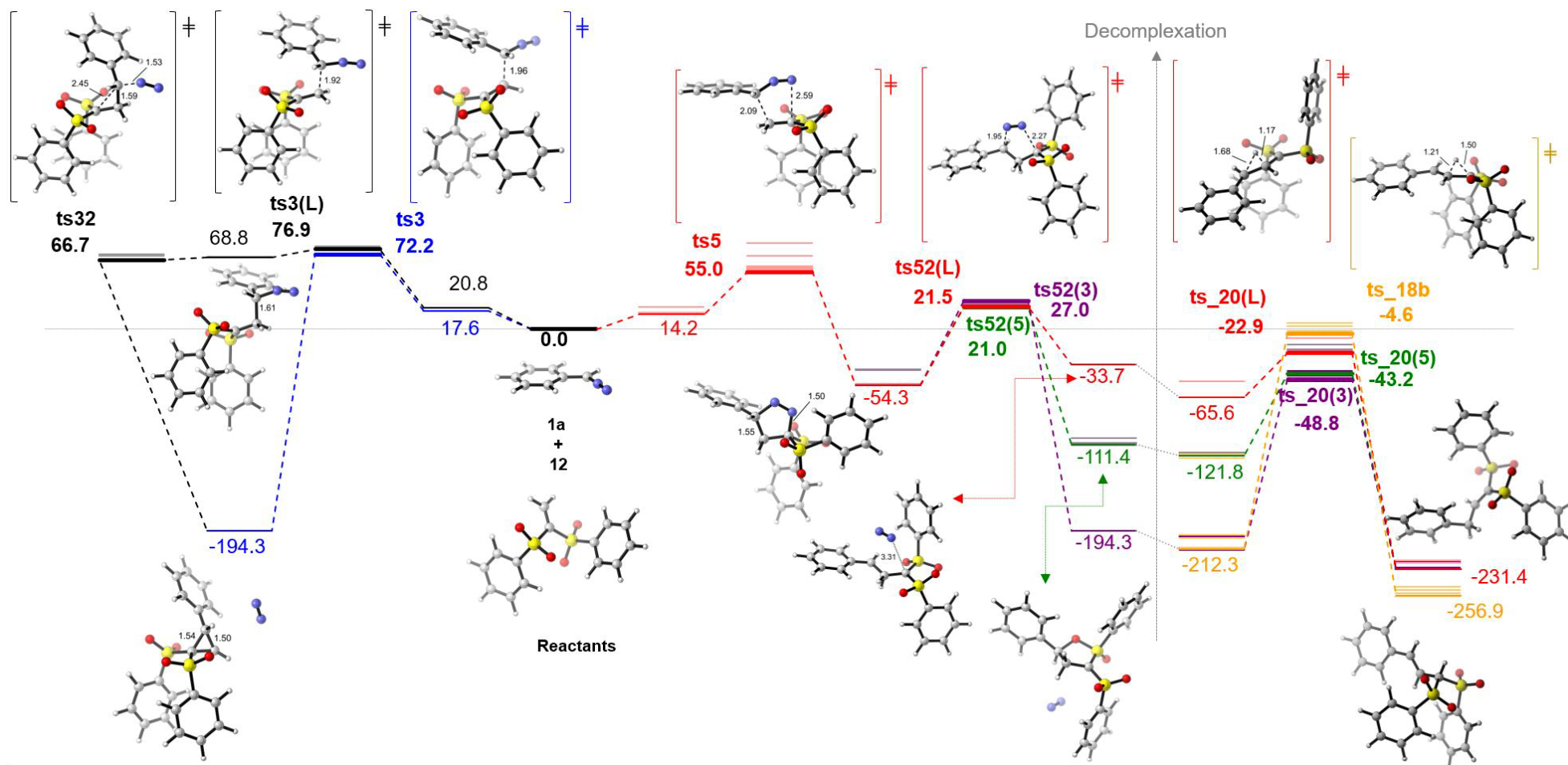


**Figure S9-8.** [Figure S31] Reaction profiles ( $\Delta G_{\text{sol}}$ , in kJ/mol) for the reaction of Michael acceptor **12** with phenyl diazomethane **1a** calculated at the PCM(UA0,CH<sub>2</sub>Cl<sub>2</sub>)/(U)B3LYP-D3/6-31+G(d,p) level of theory.

## 9.1.4 Tautomerisation

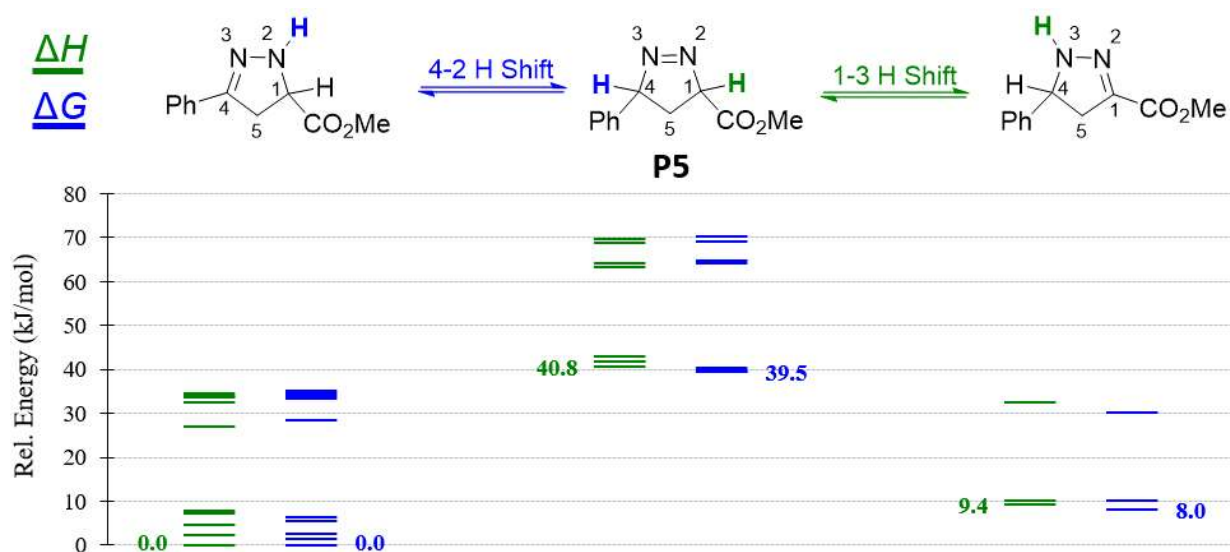


**Figure S9-9.** [Figure S17A] Tautomerisation and conformational space for product **P5** initially formed in the 1,3-dipolar cycloaddition of **1a** with **5a** calculated at the PCM(UA0,CH<sub>2</sub>Cl<sub>2</sub>)/(U)B3LYP-D3/6-31+G(d,p) level of theory.

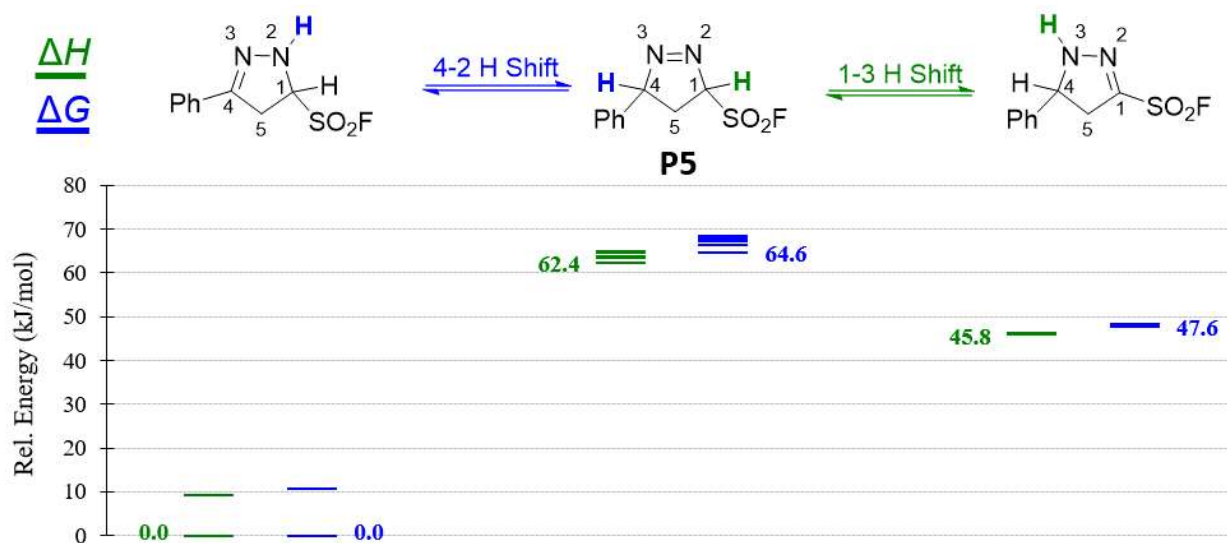


**Figure S9-10.** [Figure S22A] Tautomerisation and conformational space for product **P5** initially formed in the 1,3-dipolar cycloaddition of **1a** with **10** calculated at the PCM(UA0,CH<sub>2</sub>Cl<sub>2</sub>)/(U)B3LYP-D3/6-31+G(d,p) level of theory.

**Table S9-3.** [Table S3] Tautomerisation and conformational space for product **P5** initially formed in the 1,3-dipolar cycloaddition of **1a** with **5a** and **10** calculated at the PCM(UA0,CH<sub>2</sub>Cl<sub>2</sub>)/(U)B3LYP-D3/6-31+G(d,p) level of theory.

P5 (5a + 1a)					P5 (10 + 1a)				
FileName	Tautomer	$\Delta E_{\text{sol}}$	$\Delta H_{\text{sol}}$	$\Delta G_{\text{sol}}$	FileName	Tautomer	$\Delta E_{\text{sol}}$	$\Delta H_{\text{sol}}$	$\Delta G_{\text{sol}}$
a5_26	4-2 H Shift	0.0	0.0	0.0	a10_11	4-2 H Shift	0.0	0.0	0.0
a5_28	4-2 H Shift	2.2	2.2	1.5	a10_12	4-2 H Shift	8.5	9.1	10.8
a5_29	4-2 H Shift	4.7	4.6	2.5					
a5_31	4-2 H Shift	7.5	7.1	6.2	a10_6	1-3 H Shift	44.0	45.8	47.6
a5_30	4-2 H Shift	7.7	7.9	5.6	a10_4	1-3 H Shift	44.6	46.3	48.2
a5_16	4-2 H Shift	27.0	26.9	28.4					
a5_18	4-2 H Shift	32.6	32.4	33.4	a10_20		62.2	62.4	64.6
a5_20	4-2 H Shift	33.7	33.6	33.9	a10_21		63.3	63.6	67.3
a5_17	4-2 H Shift	34.1	34.0	35.1	a10_19		63.5	63.5	67.5
a5_21	4-2 H Shift	34.9	34.6	34.6	a10_3		64.8	64.5	68.0
					a10_1		64.9	64.6	66.4
a5_11	1-3 H Shift	9.9	9.4	8.0	a10_2		65.1	64.9	68.3
a5_12	1-3 H Shift	10.6	10.0	10.1					
a5_13	1-3 H Shift	33.6	32.6	30.0					
a5_2		42.1	40.8	39.5					
a5_1		43.3	41.9	39.6					
a5_6		43.8	41.9	39.7					
a5_7		44.9	43.0	40.3					
a5_4		64.9	63.4	64.3					
a5_9		66.0	64.0	64.8					
a5_5		70.2	68.8	70.4					
a5_10		71.9	69.8	69.1					

## 9.1.5 QM Data

### 9.1.5.1 Distortion-interaction analysis (DIA)

**Table S9-4.** [Table S5] Distortion-interaction analysis (DIA,  $\Delta E_{\text{sol}}$ , kJ/mol) for the concerted transition states (**ts5**) and the step-wise transition states (**ts3**) in the reaction of **5a**, **9a**, **10**, **8c** and **12** with **1a** calculated at different levels of theory.

	PCM(UA0,CH <sub>2</sub> Cl <sub>2</sub> )/(U)B3LYP-D3/6-31+G(d,p)				PCM(UA0,CH <sub>2</sub> Cl <sub>2</sub> )/(U)B2PLYP-D3/Def2TZVPP //PCM(UA0,CH <sub>2</sub> Cl <sub>2</sub> )/(U)B3LYP-D3/6-31+G(d,p)			
	Distortion Electrophile	Distortion Nucleophile	TS Barrier	Interaction Energy	Distortion Electrophile	Distortion Nucleophile	TS Barrier	Interaction Energy
<b>ts5</b>								
<b>5a</b>	26.7	69.2	22.7	-73.1	28.3	68.5	19.8	-77.0
<b>10</b>	40.3	58.4	4.2	-94.6	45.1	56.8	4.5	-97.5
<b>9a</b>	58.5	68.3	27.3	-99.4	59.5	66.0	18.0	-107.5
<b>8c</b>	55.4	48.9	-0.8	-105.1	58.4	45.6	-10.9	-114.8
<b>12</b>	43.3	50.2	-10.4	-104.0	42.1	48.1	-19.8	-110.0
<b>ts3</b>								
<b>5a</b>	54.2	50.8	56.5	-48.4	56.5	46.6	54.7	-48.4
<b>10</b>	65.8	32.3	24.2	-73.8	74.7	27.1	29.9	-71.8
<b>9a</b>	111.1	103.7	32.7	-182.1	113.0	98.6	27.1	-184.5
<b>8c</b>	65.4	27.8	2.8	-90.4	69.6	22.5	-6.1	-98.3
<b>12</b>	59.3	29.0	8.0	-80.3	58.2	24.0	-1.5	-83.7

### 9.1.5.2 Charge distribution and % of evaluation of the bond order

**Table S9-5.** [Table S7] Charge on electrophiles [NBO and Mulliken], percentage of evolution of the bond order (% $E_V$ ) for the concerted transition states (**ts5**) and the step-wise transition states (**ts3**) in the reaction of **5a**, **9a**, **10**, **8c** and **12** with **1a** calculated at PCM(UA0,CH<sub>2</sub>Cl<sub>2</sub>)/(U)B3LYP-D3/6-31+G(d,p) level of theory. % $E_V = (B_i^{TS}/B_i^P)*100$ , where  $B_i$  is the Wiberg bond index of the  $i^{\text{th}}$  bond and superscripts “TS” and “P” refer to the transition states and products, respectively.  $B_i$  is calculated using nbo6 at the PCM(UA0,CH<sub>2</sub>Cl<sub>2</sub>)/(U)B3LYP-D3/6-31+G(d,p) level of theory.

	C-C Bond			C-N Bond			Charge on Electrophile	
	Product (B <sub>i</sub> <sup>P</sup> )	TS (B <sub>i</sub> <sup>TS</sup> )	% $E_V = (B_i^{TS}/B_i^P)*100$	Product (B <sub>i</sub> <sup>P</sup> )	TS (B <sub>i</sub> <sup>TS</sup> )	% $E_V = (B_i^{TS}/B_i^P)*100$	NBO (nbo6)	Mulliken
<b>ts5</b>								
<b>5a</b>	0.98	0.41	41.6 %	0.95	0.22	23.0 %	-0.20	-0.14
<b>10</b>	0.98	0.43	43.9 %	0.97	0.19	20.0 %	-0.30	-0.26
<b>9a</b>	0.94	0.51	53.9 %	0.87	0.17	19.7 %	-0.38	-0.40
<b>8c</b>	0.95	0.48	51.0 %	0.91	0.10	11.0 %	-0.43	-0.39
<b>12</b>	0.97	0.43	44.7 %	0.97	0.16	16.5 %	-0.35	-0.54
<b>ts3</b>								
<b>5a</b>	0.98	0.59	60.5 %	0.90	0.03	3.6 %	-0.31	-0.25
<b>10</b>	0.97	0.52	53.8 %	0.93	0.04	4.1 %	-0.42	-0.43
<b>9a</b>	0.98	0.85	86.4 %	0.87	0.07	8.6 %	-0.57	-0.48
<b>8c</b>	0.90	0.48	53.6 %	0.02	0.02	-	-0.46	-0.19
<b>12</b>	1.00	0.50	49.7 %	0.92	0.04	4.4 %	-0.41	-0.53

### 9.1.5.3 Mechanistic Investigation

**Table S9-6.** [Table S8] Transition state (TS), reactant complex (RC) and product complex (PC) energies ( $\Delta G_{\text{sol}}$ , kJ/mol) for the reaction of Michael acceptors (**5a**, **9a**, **10**, **8c** and **12**) with phenyl diazomethane **1a** calculated at different levels of theory.

System	PCM(UA0,CH <sub>2</sub> Cl <sub>2</sub> )/(U)B3LYP-D3/6-31+G(d,p)					PCM(UA0,CH <sub>2</sub> Cl <sub>2</sub> )/(U)B2PLYP-D3/Def2TZVPP //PCM(UA0,CH <sub>2</sub> Cl <sub>2</sub> )/(U)B3LYP-D3/6-31+G(d,p)		
	Filename	Path	RC	TS	PC	RC	TS	PC
<b>5a</b> + <b>1a</b>	a5_ts5_2	ts5	18.5	<b>80.7</b>	-49.9	17.1	<b>77.8</b>	-43.1
	a5_ts5_12	ts5	<b>14.6</b>	81.1	-49.7	<b>13.0</b>	78.3	<b>-43.6</b>
	a5_ts5_4	ts5	18.8	82.6	<b>-49.9</b>	18.0	80.3	-42.5
	a5_ts5_13	ts5	15.3	84.0	-49.1	13.9	81.6	-42.6
	a5_ts5_19	ts5	40.6	99.7	-24.6	39.8	97.0	-18.2
	a5_ts5_10	ts5	45.4	101.0	-25.2	44.6	98.1	-18.1
	a5_ts5_23	ts5	54.5	126.8	-12.8	54.4	125.9	-4.4
	a5_ts5_11	ts5	52.2	126.9	-14.9	52.9	126.5	-6.9
	a5_ts3_4	ts3		<b>108.1</b>	<b>-194.8</b>		<b>106.3</b>	<b>-218.0</b>
	a5_ts3_13	ts3	<b>16.1</b>	111.5	-193.0	<b>15.1</b>	110.2	-215.5
	a5_ts3_11	ts3	18.3	113.7	-191.6	16.9	111.6	-214.3
a5_ts3_1	ts3	39.6	124.0	-169.5	38.9	122.2	-192.3	
a5_ts3_2	ts3	37.9	133.2	-170.9	37.4	131.0	-193.9	

<b>10 +</b> <b>1a</b>	Filename	Path	RC	TS	PC	RC	TS	PC
	a10_ts5_f_3	ts5	18.8	<b>63.5</b>	<b>-58.0</b>	20.1	63.8	<b>-46.8</b>
	a10_ts5_e_1	ts5	18.0	63.8	-56.1	18.7	<b>63.2</b>	-46.0
	a10_ts5_e_4	ts5	<b>12.0</b>	69.7	-54.6	<b>13.2</b>	70.4	-44.4
	a10_ts5_f_5	ts5	17.9	70.9	-55.0	18.4	72.2	-44.8
	a10_ts3_f_14	ts3	<b>12.4</b>	<b>79.6</b>	<b>-205.1</b>	<b>12.3</b>	<b>85.4</b>	<b>-225.5</b>
	a10_ts3_f_12	ts3	15.3	81.8	-204.7	16.5	85.5	-224.6
	a10_ts3_f_2	ts3	17.3	86.9	-197.1	16.8	90.7	-216.6
	a10_ts3_e_5	ts3	14.0	88.7	-201.2	14.9	92.4	-219.9
<b>9a +</b> <b>1a</b>	Filename	Path	RC	TS	PC	RC	TS	PC
	a9_ts5_2	ts5(RS)	<b>6.4</b>	<b>83.2</b>	<b>26.4</b>	<b>2.0</b>	<b>73.8</b>	<b>22.6</b>
	a9_ts5_1	ts5(RS)	8.8	83.6	27.7	4.5	74.4	24.0
	a9_ts5_4	ts5(SS)	8.3	87.7	30.0	4.0	77.4	24.5
	a9_ts5_6	ts5(SS)	8.8	88.7	37.0	4.2	77.6	32.0
	a9_ts5_3	ts5(SS)	8.1	90.5	36.0	3.9	79.3	31.1
	a9_ts32_f_1	ts3(SR)	5.9	<b>91.4</b>	-143.4	2.7	<b>85.8</b>	-172.6
	a9_ts32_f_2	ts3(SR)	6.8	92.7	-141.5	3.2	87.1	-170.1
	a9_ts3_3	ts3(SS)	8.1	93.2	<b>-160.1</b>	4.0	86.0	<b>-188.7</b>
	a9_ts3_6	ts3(SS)	<b>5.3</b>	94.1	-154.9	<b>1.1</b>	86.7	-183.4
	a9_ts52_e_2	ts52(RS)	23.0	<b>60.1</b>	<b>-184.2</b>	19.1	<b>54.3</b>	<b>-211.0</b>
	a9_ts52_e_1	ts52(RS)	<b>22.1</b>	61.1	-183.8	<b>18.2</b>	55.6	-210.8
	a9_ts52_f_1	ts52(SS)	36.0	83.1	-23.8	31.1	78.4	-28.3
	a9_ts52_f_2	ts52(SS)	37.0	83.6	-171.2	32.0	78.7	-198.6
<b>8c +</b> <b>1a</b>	Filename	Path	RC	TS	PC	RC	TS	PC
	c8_ts5_e_2	ts5(RS)	9.2	<b>56.9</b>	<b>-9.4</b>	5.6	<b>46.9</b>	<b>-11.3</b>
	c8_ts5_e_3	ts5(RS)	11.0	70.7	-7.8	8.7	61.9	-10.1
	c8_ts5_f_1	ts5(SS)	<b>9.1</b>	65.9	7.5	<b>5.3</b>	54.2	5.6
	c8_ts5_f_3	ts5(SS)	13.5	77.5	14.4	9.7	67.8	12.2
	c8_ts3_e_1	ts3(L)	7.5	<b>63.5</b>	<b>40.4</b>	5.1	<b>54.6</b>	<b>24.4</b>
	c8_ts3_e_4	ts3(L)	7.6	69.4	50.6	6.6	60.4	34.5
	c8_ts3_f_1	ts3(L)	<b>6.2</b>	71.2	65.7	<b>4.1</b>	61.2	52.9
	c8_ts3_e_2	ts3(L)	7.8	72.9	43.0	5.8	67.2	26.7
	c8_ts5_e_10	ts3(L)	7.6	69.4	50.6	6.6	60.5	34.5
	c8_ts32_e_1	ts32		<b>38.6</b>	-180.2		22.0	-209.1
	c8_ts33_e_6	ts32	<b>34.6</b>	38.6	-180.2	<b>18.6</b>	<b>22.0</b>	-209.1
	c8_ts32_e_2	ts32	43.0	40.1	<b>-182.2</b>	26.7	23.0	<b>-210.9</b>
	c8_ts34_e_6	ts32*	50.8	51.8	-160.4	34.6	38.2	-188.5
	c8_ts32_f_1	ts32	65.7	66.5	-162.7	52.9	54.1	-191.2
	c8_ts52_e_2	ts52(RS)	-9.4	<b>24.2</b>		<b>-11.3</b>	<b>15.9</b>	
	c8_ts52_e_1	ts52(RS)	<b>-9.4</b>	24.2	-165.8	-11.3	15.9	-192.4
	c8_ts52_e_3	ts52(RS)	-7.8	27.9	<b>-202.1</b>	-10.1	19.9	<b>-227.7</b>
	c8_ts52_e_2	ts52(RS)	7.7	62.6	-162.4	5.7	55.3	-189.2
	c8_ts52_e_1	ts52(RS)	14.4	63.3	-159.9	12.2	55.9	-186.8

<b>12 + 1a</b>	Filename	Path	RC	TS	PC	RC	TS	PC
	a12_ts5_2	ts5	21.1	<b>55.0</b>	-39.0	17.6	<b>45.7</b>	-28.3
	a12_ts5_14	ts5	<b>14.2</b>	57.0	<b>-54.3</b>	12.1	50.9	-42.3
	a12_ts5_5	ts5	21.1	57.0	-39.0	17.6	48.4	-28.3
	a12_ts5_3	ts5	21.5	58.5	-38.9	17.3	48.6	-28.5
	a12_ts5_4	ts5	16.0	59.0	-53.0	14.7	52.2	-40.7
	a12_ts5_15	ts5	16.1	60.3	-53.0	14.8	55.6	-40.7
	a12_ts5_7	ts5	15.7	71.0	-53.9	<b>12.0</b>	64.7	<b>-44.1</b>
	a12_ts5_17	ts5		82.8	-52.1		77.7	-44.1
	a12_ts3_21	ts3	17.6	<b>72.2</b>	<b>-194.3</b>	13.9	<b>62.7</b>	<b>-216.5</b>
	a12_ts3_22	ts3	<b>17.6</b>	72.6	-194.3	<b>13.9</b>	63.0	-216.5
	a12_ts3_24	ts3(L)		<b>76.9</b>	<b>68.8</b>		<b>66.6</b>	55.9
	a12_ts3_16	ts3(L)	<b>20.8</b>	79.7	70.1	<b>17.2</b>	69.0	<b>51.6</b>
	a12_ts32_24	ts32	<b>68.8</b>	<b>66.7</b>	<b>-190.9</b>	55.8	54.0	<b>-210.8</b>
	a12_ts53_2	ts32	69.8	71.0	-112.4	<b>51.3</b>	<b>52.2</b>	-128.9
	a12_ts32_4	ts32	69.4	71.3	-110.0	52.5	53.3	-126.4
	a12_ts32_1	ts32	70.1	72.2	-110.1	51.6	53.3	-126.6
	a12_ts52_15	ts52(5)	-53.0	<b>21.0</b>	-110.2	-40.7	18.4	-124.1
	a12_ts53_5	ts52(5)	-53.1	22.6	-109.3	-40.8	20.2	-123.2
	a12_ts5c_5	ts52(5)	-39.0	23.4	-109.5	-28.3	<b>16.8</b>	-125.4
	a12_ts52_17	ts52(5)	-53.0	23.4	<b>-111.4</b>	-40.7	20.8	-125.4
	a12_ts52_2	ts52(5)	-39.0	24.9	-110.1	-28.3	18.0	<b>-126.1</b>
	a12_ts5c_7	ts52(5)	-38.7	25.6	-109.3	-28.3	19.3	-125.2
	a12_ts52_7	ts52(5)	<b>-53.8</b>	28.4	-104.8	<b>-44.1</b>	26.3	-120.4
	a12_ts53_4	ts52(L)	<b>-54.2</b>	<b>21.5</b>	<b>-33.7</b>	<b>-42.2</b>	<b>19.5</b>	<b>-41.8</b>
	a12_ts52_3	ts52(3)	<b>-38.9</b>	<b>27.0</b>	<b>-187.9</b>	<b>-28.5</b>	<b>20.6</b>	<b>-211.1</b>
	a12_TS_20_2	ts_20(3)	-210.1	<b>-48.8</b>	-229.3	-229.5	-62.1	-249.8
	a12_TS_20_5	ts_20(3)	-199.1	-47.1	-225.0	-222.2	<b>-63.1</b>	-246.8
	a12_TS_20_3	ts_20(3)	<b>-212.3</b>	-45.0	<b>-231.2</b>	<b>-231.9</b>	-58.0	<b>-251.1</b>
	a12_TS_20_7	ts_20(3)	-199.5	-40.1	-223.9	-220.6	-55.0	-244.5
	a12_TS_20_9	ts_20(5)	-120.4	<b>-43.2</b>	-223.6	<b>-137.3</b>	<b>-59.5</b>	-246.2
	a12_TS20a_11	ts_20(5)	-120.3	-42.3	-224.2	-137.1	-58.7	-246.6
	a12_TS20a_19	ts_20(5)	<b>-121.8</b>	-20.0	<b>-231.4</b>	-136.6	-37.4	<b>-251.7</b>
	a12_TS20a_21	ts_20(5)	-118.7	-19.8	-222.2	-135.9	-38.1	-244.0
	a12_TS20a_23	ts_20(5)	-118.7	-14.4	-223.9	-135.9	-34.3	-245.1
	a12_TS20a_18	ts_20(L)	<b>-65.6</b>	<b>-22.9</b>	-222.8	<b>-76.8</b>	<b>-38.7</b>	-244.0
	a12_TS20a_22	ts_20(L)	-50.2	-9.0	<b>-225.0</b>	-58.9	-25.1	<b>-247.3</b>
	a12_ts52_27	ts_18b	-197.8	<b>-4.6</b>	-256.8	-221.9	<b>-30.4</b>	-270.9
	a12_ts52_28	ts_18b	<b>-210.4</b>	-2.0	-254.1	<b>-230.3</b>	-23.3	-267.5
	a12_ts52_32	ts_18b	-120.3	2.9	<b>-256.9</b>	-137.3	-21.5	<b>-270.9</b>
	a12_ts52_24	ts_18b	-123.9	6.0	-248.2	-141.2	-16.9	-265.4
	a12_ts52_26	ts_18b	-201.3	6.3	-250.8	-224.9	-18.8	-266.8

**Table S9-7.** [Table S9] Transition state (TS), reactant complex (RC) and product complex (PC) energies ( $\Delta H_{\text{sol}}$ , kJ/mol) for the reaction of Michael acceptors (**5a**, **9a**, **10**, **8c** and **12**) with phenyl diazomethane **1a** calculated at different levels of theory.

System	PCM(UA0,CH <sub>2</sub> Cl <sub>2</sub> )/(U)B3LYP-D3/6-31+G(d,p)					PCM(UA0,CH <sub>2</sub> Cl <sub>2</sub> )/(U)B2PLYP-D3/Def2TZVPP //PCM(UA0,CH <sub>2</sub> Cl <sub>2</sub> )/(U)B3LYP-D3/6-31+G(d,p)		
	Filename	Path	RC	TS	PC	RC	TS	PC
<b>5a</b> + <b>1a</b>	a5_ts5_2	ts5	-21.2	26.0	-107.9	-22.5	23.1	-101.1
	a5_ts5_12	ts5	-20.0	27.6	-106.7	-21.6	24.8	-100.6
	a5_ts5_4	ts5	-19.9	28.1	-106.8	-20.7	25.9	-99.4
	a5_ts5_13	ts5	-17.0	30.6	-105.6	-18.5	28.2	-99.1
	a5_ts5_19	ts5	0.1	45.2	-84.6	-0.7	42.5	-78.2
	a5_ts5_10	ts5	3.3	44.1	-85.3	2.5	41.2	-78.2
	a5_ts5_23	ts5	17.3	71.1	-71.8	17.2	70.2	-63.4
	a5_ts5_11	ts5	14.1	70.8	-73.9	14.7	70.4	-65.9
	a5_ts3_4	ts3		58.9	-227.6		57.1	-250.8
	a5_ts3_13	ts3	-22.1	62.4	-223.5	-23.1	61.1	-246.1
	a5_ts3_11	ts3	-26.9	59.9	-216.3	-28.2	57.7	-239.0
	a5_ts3_1	ts3	-4.1	71.8	-204.4	-4.8	70.0	-227.3
	a5_ts3_2	ts3	0.9	80.0	-197.3	0.3	77.8	-220.3
	<b>10</b> + <b>1a</b>	Filename	Path	RC	TS	PC	RC	TS
a10_ts5_f_3		ts5	-24.3	7.6	-115.8	-23.0	7.9	-104.7
a10_ts5_e_1		ts5	-22.0	10.6	-113.7	-21.3	9.9	-103.5
a10_ts5_e_4		ts5	-27.0	18.0	-113.7	-25.8	18.6	-103.5
a10_ts5_f_5		ts5	-23.2	15.3	-114.7	-22.7	16.6	-104.5
a10_ts3_f_14		ts3	-24.2	27.6	-238.8	-24.4	33.4	-259.2
a10_ts3_f_12		ts3	-23.0	31.2	-239.3	-21.9	34.9	-259.2
a10_ts3_f_2		ts3	-19.8	35.4	-231.8	-20.4	39.2	-251.3
a10_ts3_e_5	ts3	-21.5	35.4	-231.6	-20.6	39.0	-250.3	
<b>9a</b> + <b>1a</b>	Filename	Path	RC	TS	PC	RC	TS	PC
	a9_ts5_2	ts5(RS)	-35.5	29.7	-32.3	-39.9	20.4	-36.1
	a9_ts5_1	ts5(RS)	-34.6	29.7	-32.1	-38.9	20.5	-35.9
	a9_ts5_4	ts5(SS)	-38.9	30.7	-31.6	-43.2	20.4	-37.1
	a9_ts5_6	ts5(SS)	-36.1	34.2	-27.4	-40.6	23.1	-32.3
	a9_ts5_3	ts5(SS)	-38.3	33.7	-27.6	-42.6	22.5	-32.5
	a9_ts32_f_1	ts3(SR)	-35.1	35.7	-180.1	-38.4	30.1	-209.2
	a9_ts32_f_2	ts3(SR)	-35.4	35.7	-179.5	-39.0	30.1	-208.1
	a9_ts3_3	ts3(SS)	-37.2	39.0	-189.8	-41.3	31.8	-218.5
	a9_ts3_6	ts3(SS)	-38.6	39.0	-190.0	-42.8	31.6	-218.5
	a9_ts52_e_2	ts52(RS)	-37.7	3.6	-213.1	-41.7	-2.2	-239.8
	a9_ts52_e_1	ts52(RS)	-37.7	3.5	-213.6	-41.6	-2.0	-240.5
a9_ts52_f_1	ts52(SS)	-27.6	25.0	-54.9	-32.5	20.3	-59.5	
a9_ts52_f_2	ts52(SS)	-27.4	25.1	-203.6	-32.3	20.2	-230.9	

<b>8c +</b> <b>1a</b>	Filename	Path	RC	TS	PC	RC	TS	PC
	c8_ts5_e_2	ts5(RS)	-38.8	2.6	-73.2	-42.4	-7.5	-75.1
	c8_ts5_e_3	ts5(RS)	-33.4	16.5	-69.3	-35.8	7.7	-71.6
	c8_ts5_f_1	ts5(SS)	-38.8	6.0	-58.1	-42.7	-5.7	-60.1
	c8_ts5_f_3	ts5(SS)	-34.0	19.6	-49.4	-37.7	10.0	-51.6
	c8_ts3_e_1	ts3(L)	-37.8	6.0	-13.3	-40.2	-2.9	-29.3
	c8_ts3_e_4	ts3(L)	-32.9	12.1	-8.1	-33.9	3.2	-24.2
	c8_ts3_f_1	ts3(L)	-39.5	10.8	8.8	-41.6	0.8	-4.0
	c8_ts3_e_2	ts3(L)	-36.4	17.3	-13.7	-38.4	11.6	-30.1
	c8_ts5_e_10	ts3(L)	-32.9	12.1	-8.1	-33.9	3.2	-24.2
	c8_ts32_e_1	ts32		-15.7	-215.9		-32.4	-244.8
	c8_ts33_e_6	ts32	-13.2	-15.7	-215.9	-29.2	-32.4	-244.8
	c8_ts32_e_2	ts32	-13.7	-15.4	-216.4	-30.1	-32.5	-245.1
	c8_ts34_e_6	ts32*	-7.9	-4.3	-199.5	-24.1	-17.9	-227.6
	c8_ts32_f_1	ts32	8.8	7.4	-202.4	-4.0	-5.0	-230.9
	c8_ts52_e_2	ts52(RS)	-73.2	-34.4		-75.1	-42.7	
	c8_ts52_e_1	ts52(RS)	-73.2	-34.4	-205.6	-75.1	-42.7	-232.2
	c8_ts52_e_3	ts52(RS)	-69.3	-31.7	-233.5	-71.6	-39.7	-259.0
	c8_ts52_e_2	ts52(RS)	-58.1	3.9	-204.9	-60.0	-3.5	-231.7
	c8_ts52_e_1	ts52(RS)	-49.4	2.4	-203.4	-51.6	-5.0	-230.4
<b>12 +</b> <b>1a</b>	Filename	Path	RC	TS	PC	RC	TS	PC
	a12_ts5_2	ts5	-29.7	-6.0	-109.4	-33.2	-15.4	-98.7
	a12_ts5_14	ts5	-34.0	-5.4	-123.4	-36.1	-11.5	-111.5
	a12_ts5_5	ts5	-29.7	-5.9	-109.4	-33.2	-14.6	-98.7
	a12_ts5_3	ts5	-29.8	-4.2	-106.8	-34.0	-14.0	-96.5
	a12_ts5_4	ts5	-31.8	-2.6	-121.4	-33.0	-9.4	-109.1
	a12_ts5_15	ts5	-31.8	-2.7	-121.4	-33.0	-7.4	-109.1
	a12_ts5_7	ts5	-37.9	4.2	-124.5	-41.6	-2.1	-114.7
	a12_ts5_17	ts5		18.4	-121.1		13.2	-113.1
	a12_ts3_21	ts3	-32.5	12.5	-235.3	-36.1	2.9	-257.5
	a12_ts3_22	ts3	-32.5	12.5	-235.3	-36.1	2.9	-257.5
	a12_ts3_24	ts3(L)		13.0	7.2		2.7	-5.7
	a12_ts3_16	ts3(L)	-28.1	15.9	8.6	-31.8	5.2	-9.9
	a12_ts32_24	ts32	7.2	4.2	-233.0	-5.7	-8.5	-252.9
	a12_ts53_2	ts32	8.6	9.6	-149.3	-9.9	-9.3	-165.7
	a12_ts32_4	ts32	5.9	9.0	-149.4	-11.0	-8.9	-165.8
	a12_ts32_1	ts32	8.6	10.5	-149.4	-9.9	-8.4	-165.8
	a12_ts52_15	ts52(5)	-121.4	-39.6	-153.4	-109.1	-42.2	-167.3
	a12_ts53_5	ts52(5)	-121.4	-40.5	-153.4	-109.1	-43.0	-167.3
	a12_ts5c_5	ts52(5)	-109.4	-40.4	-154.0	-98.7	-47.0	-169.9
	a12_ts52_17	ts52(5)	-121.4	-39.6	-152.9	-109.1	-42.2	-166.8
	a12_ts52_2	ts52(5)	-109.4	-39.4	-154.0	-98.7	-46.2	-170.0
	a12_ts5c_7	ts52(5)	-106.8	-39.5	-154.0	-96.4	-45.7	-169.9
	a12_ts52_7	ts52(5)	-124.5	-35.8	-155.6	-114.7	-37.8	-171.1
	a12_ts53_4	ts52(L)	-123.4	-40.3	-77.3	-111.4	-42.3	-85.4
	a12_ts52_3	ts52(3)	-106.8	-38.5	-232.6	-96.5	-44.8	-255.8

a12_TS_20_2	ts_20(3)	-228.7	-61.5	-244.1	-248.0	-74.8	-264.5
a12_TS_20_5	ts_20(3)	-221.4	-65.1	-245.7	-244.5	-81.1	-267.5
a12_TS_20_3	ts_20(3)	-234.8	-58.3	-242.7	-254.4	-71.3	-262.6
a12_TS_20_7	ts_20(3)	-222.8	-59.0	-240.3	-243.9	-73.9	-261.0
a12_TS_20_9	ts_20(5)	-140.4	-58.5	-242.3	-157.4	-74.8	-265.0
a12_TS20a_11	ts_20(5)	-141.2	-58.5	-242.8	-158.0	-74.9	-265.2
a12_TS20a_19	ts_20(5)	-139.2	-35.6	-242.7	-154.0	-53.0	-263.1
a12_TS20a_21	ts_20(5)	-137.1	-39.8	-238.2	-154.3	-58.2	-260.0
a12_TS20a_23	ts_20(5)	-137.1	-34.3	-240.3	-154.3	-54.1	-261.5
a12_TS20a_18	ts_20(L)	-80.6	-40.8	-239.1	-91.7	-56.6	-260.3
a12_TS20a_22	ts_20(L)	-72.2	-31.6	-245.7	-81.0	-47.7	-268.0
a12_ts52_27	ts_18b	-220.3	-23.4	-271.8	-244.4	-49.2	-285.8
a12_ts52_28	ts_18b	-234.3	-10.1	-268.3	-254.2	-31.4	-281.7
a12_ts52_32	ts_18b	-140.4	-13.1	-271.8	-157.4	-37.5	-285.8
a12_ts52_24	ts_18b	-139.8	-9.6	-260.9	-157.1	-32.6	-278.1
a12_ts52_26	ts_18b	-223.2	-9.3	-262.8	-246.8	-34.3	-278.7

### 9.1.6 References

- (1) Allgäuer, D. S.; Jangra, H.; Asahara, H.; Li, Z.; Chen, Q.; Zipse, H.; Ofial, A. R.; Mayr, H., *J. Am. Chem. Soc.* **2017**, *139*, 13318-13329.
- (2) Mayer, R. J.; Tokuyasu, T.; Mayer, P.; Gomar, J.; Sabelle, S.; Mennucci, B.; Mayr, H.; Ofial, A. R., *Angew. Chem. Int. Ed.* **2017**, *56*, 13279-13282.
- (3) Becke, A. D., *J. Chem. Phys.* **1993**, *98*, 5648-5652.
- (4) (a) Grimme, S., *J. Comput. Chem.* **2006**, *27*, 1787-1799. (b) Grimme, S.; Antony, J.; Ehrlich, S.; Krieg, H., *J. Chem. Phys.* **2010**, *132*, 154104.
- (5) (a) Ditchfield, R.; Hehre, W. J.; Pople, J. A., *J. Chem. Phys.* **1971**, *54*, 724-728. (b) Krishnan, R.; Binkley, J. S.; Seeger, R.; Pople, J. A., *J. Chem. Phys.* **1980**, *72*, 650-654.
- (6) (a) Cancès, E.; Mennucci, B.; Tomasi, J., *J. Chem. Phys.* **1997**, *107*, 3032-3041. (b) Tomasi, J.; Mennucci, B.; Cammi, R., *Chem. Rev.* **2005**, *105*, 2999-3094.
- (7) Grimme, S., *J. Chem. Phys.* **2006**, *124*, 034108.
- (8) (a) Weigend, F.; Ahlrichs, R., *Phys. Chem. Chem. Phys.* **2005**, *7*, 3297-3305. (b) Weigend, F., *Phys. Chem. Chem. Phys.* **2006**, *8*, 1057-1065.
- (9) Glendening, E. D.; Landis, C. R.; Weinhold, F., *J. Comput. Chem.* **2013**, *34*, 1429-1437.
- (10) Frisch, M. J. T., G. W.; Schlegel, H. B.; Scuseria, G. E.; Robb, M. A.; Cheeseman, J. R.; Scalmani, G.; Barone, V.; Mennucci, B.; Petersson, G. A.; Nakatsuji, H.; Caricato, M.; Li, X.; Hratchian, H. P.; Izmaylov, A. F.; Bloino, J.; Zheng, G.; Sonnenberg, J. L.; Hada, M.; Ehara, M.; Toyota, K.; Fukuda, R.; Hasegawa, J.; Ishida, M.; Nakajima, T.; Honda, Y.; Kitao, O.; Nakai, H.; Vreven, T.; Montgomery, Jr., J. A.; Peralta, J. E.; Ogliaro, F.; Bearpark, M.; Heyd, J. J.; Brothers, E.; Kudin, K. N.; Staroverov, V. N.; Keith, T.; Kobayashi, R.; Normand, J.; Raghavachari, K.; Rendell, A.; Burant, J. C.; Iyengar, S. S.; Tomasi, J.; Cossi, M.; Rega, N.; Millam, J. M.; Klene, M.; Knox, J. E.; Cross, J. B.; Bakken, V.; Adamo, C.; Jaramillo, J.; Gomperts, R.; Stratmann, R. E.; Yazyev, O.; Austin, A. J.; Cammi, R.; Pomelli, C.; Ochterski, J. W.; Martin, R. L.; Morokuma, K.; Zakrzewski, V. G.; Voth, G. A.; Salvador, P.; Dannenberg, J. J.; Dapprich, S.; Daniels, A. D.; Farkas, O.; Foresman, J. B.; Ortiz, J. V.; Cioslowski, J.; Fox, D. J.; *Gaussian 09 Revision D. 01*, Gaussian, Inc., Wallingford CT: **2013**.

---

## Curriculum Vitae

---



## HARISH

**Ph.D. at Ludwig-Maximilians-Universität (LMU) Munich, Germany**

Contact: App. No. 13, Platanenstrasse 56, 81377 Munich, Germany

📞 +4915163041924(M), +4989218077741(O) | ✉ ch.harish.jangra@gmail.com

DOB: 4<sup>th</sup> Jan. 1985      Nationality: Indian

🌐 [www.linkedin.com/in/harish-jangra-55239429](http://www.linkedin.com/in/harish-jangra-55239429)

### EXPERIENCE

**Computational Chemist and Cheminformatician**  
2010-Present

> 7-Years of Experience (Various Roles in Research Projects)

- Main Researcher
- Computational Support to Experiments
- Scientific Programmer
- Co-supervising Master's Project
- Teaching "Introductory Programming" and "Applied Theoretical Chemistry"

**Linux System Administrator**  
2013-Present

Zipse Group, Dept. of Chemistry, LMU Munich, Germany

- Installation and Troubleshooting Linux Systems and Scientific Software.
- Procuring Highly Customized IT Products for Computational Chemistry.

### EDUCATION

**Ph.D.**  
2013-2019

Dept. of Chemistry, LMU, Munich, Germany.

Topic: "Structure and Stability of Radicals and Quantification of Electrophilic Reactivity" | Adviser: Prof. Dr. Hendrik Zipse

**Master of Science Pharmacoinformatics**  
2010-2012

Dept. of Pharmacoinformatics, National Institute of Pharmaceutical Education and Research S.A.S. Nagar (NIPER), Punjab, India. **Grade: 9.54/10**

Topic: "Defining the Fragment-Based Reactivity Descriptors and Development of a Software Tool for the Prediction of Site of Metabolism"

Adviser: Prof. Dr. Prasad V. Bharatam

**Bachelor of Pharmacy**  
2007-2010

Rajendra Institute of Technology Sciences  
Sirsa, Haryana, India.

**Grade: 74%**

**Diploma in Pharmacy**  
2005-2007

Delhi Institute of Pharmaceutical Sciences And Research  
Delhi University, New Delhi, India.

**Grade: 75%**

### IT COURSES

2017-2018

"Introduction to Augmented Reality and ARCore" by Google AR & VR | "Neural Networks and Deep Learning" by Deeplearning.ai | "Machine Learning" by Stanford University | on Coursera.

"Fundamentals of Deep Learning for Computer Vision" by the NVIDIA Deep Learning Institute at Leibniz-Rechenzentrum (LRZ), Garching, Germany.

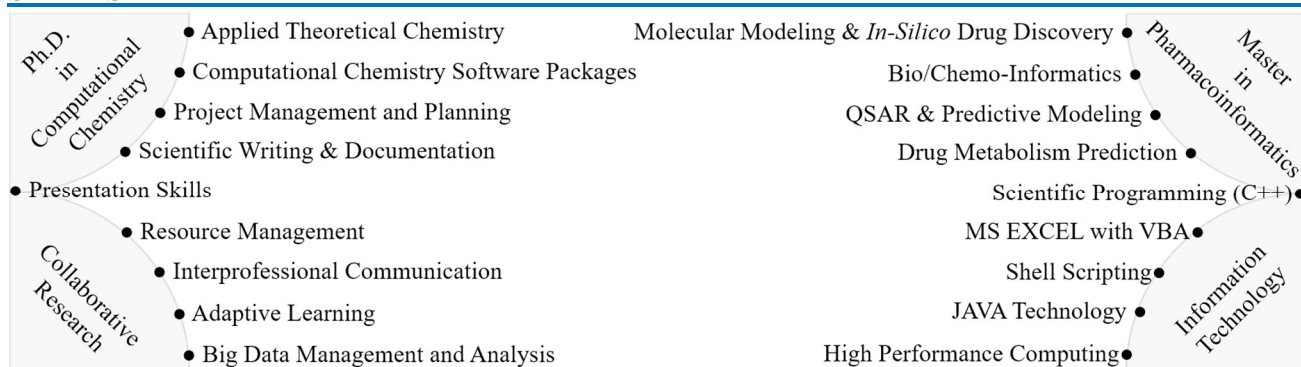
2015-2016

"Programming Mobile Applications for Android Handheld Systems" by University of Maryland, College Park on Coursera.

2012-2013

"Diploma in Java Technology" & "Basics of SQL/PLSQL Oracle 9i" by Micro-Tech Academy of Computer Studies (MACS), Mohali, Punjab-160062, India.

### SKILLS MAP



## LIST OF PUBLICATIONS

15. **H. Jangra**, Q. Chen, E. Fuks, I. Zenz, P. Mayer, A. R. Ofial, H. Zipse, H. Mayr “Nucleophilicity and Electrophilicity Parameters for Predicting Absolute Rate Constants of Highly Asynchronous 1,3-Dipolar Cycloadditions of Aryldiazomethanes” *J. Am. Chem. Soc.* **2018**, *140*, 16758–16772.
14. D. Meyer, **H. Jangra**, F. Walther, H. Zipse, P. Renaud, “A Third Generation of Radical Fluorinating Agents Based on *N*-Fluoro-*N*-Arylsulfonamides” *Nat. Commun.* **2018**, *9*, 1-10.
13. **H. Jangra**, H. Zipse, “Electrostatic Effects on The Stability of Peptide Radicals” *J. Phys. Chem. B* **2018**, *122*, 8880–8890.
12. T. Amatov, **H. Jangra**, R. Pohl, I. Cisarova, H. Zipse, U. Jahn, “Unique Stereoselective Homolytic C-O Bond Activation in Diketopiperazine-Derived Alkoxyamines via Adjacent Amide Pyramidalization” *Chem. Eur. J.* **2018**, *24*, 15336-15345. (*Selected as Very Important Paper*)
11. Z. Li, **H. Jangra**, Q. Chen, P. Mayer, A. R. Ofial, H. Zipse, H. Mayr, “Kinetics and Mechanism of Oxirane Formation by Darzens Condensation of Ketones: Quantification of the Electrophilicities of Ketones” *J. Am. Chem. Soc.* **2018**, *140*, 5500-5515. (*Selected for JACS Spotlight*)
10. D. S. Allgäuer, **H. Jangra**, H. Asahara, Z. Li, Q. Chen, H. Zipse, A. R. Ofial, H. Mayr, “Quantification and Theoretical Analysis of the Electrophilicities of Michael Acceptors” *J. Am. Chem. Soc.* **2017**, *139*, 13318-13329.
9. S. Gaur, .. **H. Jangra**, .. N. G. Sastry, “Assessing Therapeutic Potential of Molecules: Molecular Property Diagnostic Suite for Tuberculosis (MPDS<sup>TB</sup>)”. *J. Chem. Sci.* **2017**, *129*, 515-531. (total 50 authors)
8. N. Khatri, **H. Jangra**, A. Madan, “Path Pendeccentric Connectivity Indices: Detour Matrix Based Molecular Descriptors for QSAR/QSPR Studies, Part 1: Development and Evaluation” *IJQSPR* **2017**, *2*, 62-74.
7. **H. Jangra**, M. H. Haindl, F. Achraimer, J. Hioe, R. M. Gschwind, H. Zipse, “Conformational Preferences in Small Peptide Models: The Relevance of *cis/trans*-Conformations” *Chem. Eur. J.* **2016**, *22*, 13328-13335.
6. R. K. Marwaha, **H. Jangra**, K. C. Das, P. Bharatam, A. Madan, “Path Eccentricity Based Highly Discriminating Molecular Descriptors for QSAR/QSPR Part I: Development and Evaluation” *Int. J. Chem. Model.* **2014**, *6*, 531-556.
5. M. Gupta, **H. Jangra**, P. V Bharatam, A. K Madan, “Detour Cum Distance Matrix Based Topological Descriptors for QSAR/QSPR Part-I: Development and Evaluation” *Lett. Drug Des. Discov.* **2014**, *11*, 844-863.
4. M. Gupta, **H. Jangra**, P. Bharatam, A. Madan, “Relative Eccentric Distance Sum/Product Indices for QSAR/QSPR: Development, Evaluation, and Application” *ACS Comb. Sci.* **2014**, *16*, 101-112.
3. M. Singh, **H. Jangra**, P. Bharatam, A. Madan, “Detour Matrix-based Adjacent Path Eccentric Distance Sum Indices for QSAR/QSPR. Part I: Development and Evaluation” *IJCBD* **2014**, *7*, 295-318.
2. S. Bhatia, V. A Dixit, **H. Jangra**, P. V Bharatam, “Formation/Fate of Reactive Metabolites from General Anesthetics and A Comparison of Toxic and Non-Toxic Analogues: A DFT Study” *Drug Metab. Lett.* **2012**, *6*, 221-234.
1. R. K. Marwaha, **H. Jangra**, K. C. Das, P. Bharatam, A. Madan, “Fourth Generation Detour Matrix-Based Topological Indices for QSAR/QSPR–Part-1: Development and Evaluation” *IJCBD* **2012**, *5*, 335-360.

## COLLABORATIONS MAP

• **Alcohol Autoxidation.**  
BASF SE, Ludwigshafen.

• **Electrophilic Reactivity of Michael Acceptors and Ketones.**  
Prof. H. Mayr, LMU Munich.

• ***N*-Fluoro-*N*-Arylsulfonamides: A Third Generation of Radical Fluorinating Agents.**  
Prof. P. Renaud, Uni. Bern, Bern.

• **An Unusual Radical Trans-Cis Isomerization of Diketopiperazine Derived Alkoxyamines.**  
Prof. U. Jahn, CAS, Prague.

• **The Design and Development of Topological Descriptors for QSAR/QSPR.**  
Prof. A.K. Madan, Uni. of Health Sci., Rohtak.

• **Molecular Property Diagnostic Suite for Tuberculosis.**  
Prof. P.V. Bharatam, NIPER S.A.S. Nagar.

## FELLOWSHIPS & PROJECT GRANTS

2017-Present	Industrial project on “Alcohol Autoxidation”, sponsored by BASF SE.
2013-Present	“Radicals in Enzymatic Catalysis” sponsored by SonderForschungsBereich 749.
2013	SRF sponsored CSIR Open Source Drug Discovery Initiative at NIPER.
2013-2012	Senior Research Fellowship (SRF) by Dept. of Medicinal Chemistry, NIPER.
2012-2010	Fellowship for M.S. (Pharm.) Pharmacoinformatics by Ministry of Chemicals and Fertilizers, Govt. of India. (After qualifying NIPER JEE-2010 & GPAT-2010)

## IMPORTANT SCIENTIFIC EVENTS

Contributed as: Volunteer (👤) | Speaker (🗣️) | Poster presentation (📄)

2018	👤	<p>“WeAreDevelopers World Congress 2018” Vienna, Austria</p> <p>“Optimizing Writing Strategies in English (Natural Sciences)” workshop by Graduate Center LMU Munich, Germany.</p> <p>“Introduction to LRZ Machine Learning Tools” and “Using R at LRZ” workshop by LRZ Garching, Germany.</p>
2017	🗣️   📄	<p>“Molecular Modeling with Schrödinger-Suite Workshop”, LRZ Garching, Germany.</p> <p>8<sup>th</sup> SFB 749 workshop at Kloster Irsee, Allgäu, Germany: “Concertedness in (3+2)-Cycloadditions of Diazoalkanes -Theory and Experiment” (Shared with Dr. A. Ofial)   “Electrostatic Effects on The Stability of Peptide Radicals”.</p>
	👤   📄	<p>11<sup>th</sup> Triennial Congress of the World Association of Theoretical and Computational Chemist, LMU Munich, Germany: “Quantification and Theoretical Analysis of the Electrophilicities of Michael Acceptors”.</p>
	📄	<p>2<sup>nd</sup> International Conference on Hydrogen Atom Transfer, Monteporzio Catone, Italy: “Electrostatic Effects on The Stability of Peptide Radicals”.</p>
	📄	<p>5<sup>th</sup> Modeling of Chemical and Biological (Re)Activity (MCBR), Chennai, India.</p>
2016	📄	<p>7<sup>th</sup> SFB 749 workshop at Kloster Irsee, Allgäu, Germany: “Stability of Peptide Radicals: Thermodynamic vs Kinetics”.</p>
2015	📄	<p>Tokyo-LMU Symposium, Innovation Center for Biotechnology, Munich, Germany.</p> <p>4<sup>th</sup> MCBR, Winterschool and Meeting, Heidelberg, Germany: “Conformational Preferences in Small Peptide Models - the Relevance of Cis/Trans Conformational Isomers”.</p>
2014		<p>SFB 749 Intermediates of Molecular Transformations Conference at Venice International University, San Servolo, Italy.</p>
2013		<p>“Open Source Drug Discovery MPDS<sup>TM</sup>” Galaxy workshop, CSIR-Fourth Paradigm Institute, Bangalore India.</p>
	👤   🗣️	<p>3<sup>rd</sup> MCBR, NIPER S.A.S. Nagar, Punjab, India: “Predictor P450: A Site of Metabolism Prediction Tool using Fragment-Based Descriptors (FBDs) for Cytochrome P450 3A4 and 2D6 Substrates”.</p>
2012	👤   🗣️   📄	<p>4<sup>th</sup> International Symposium on “Drug Metabolism and Pharmacokinetics, NIPER S.A.S. Nagar, Punjab, India: “New Descriptors for Metabolism Prediction of P450 2D6 Substrates”.</p>

## REFERENCES

### Prof. Dr. Hendrik Zipse

Ludwig-Maximilians-Universität München  
 Department of Chemistry, Butenandtstrasse 5-13,  
 D-81377, München, Germany.  
 Ph.: +4989218077737, Fax.: +4989218077738  
 Email: zipse@cup.uni-muenchen.de

### Prof. Dr. Prasad V. Bharatam

Department of Medicinal Chemistry,  
 National Institute of Pharmaceutical Education and  
 Research, S.A.S. Nagar, 160062, Punjab, India.  
 Ph.: +911722292018, Fax.: +911722214692  
 Email: pvbharatam@niper.ac.in

Date: 12<sup>th</sup> Feb. 2019

Place: Munich, Germany

**HARISH**